AFWAL-TR-86-3056

ADA 182109

PANDA2 - PROGRAM FOR MINIMUM WEIGHT DESIGN OF
          STIFFENED, COMPOSITE, LOCALLY BUCKLED PANELS

David Bushnell
Department 93-30/Bldg. 255
Lockheed Palo Alto Research Lab
3251 Hanover Street
Palo Alto, CA 94304

September 1986

Final Report for Period January 1981 - September 1986

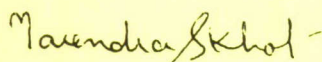Approved for public release; distribution is unlimited

FLIGHT DYNAMICS LABORATORY
AIR FORCE WRIGHT AERONAUTICAL LABORATORIES
AIR FORCE SYSTEMS COMMAND
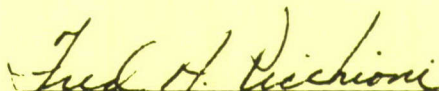WRIGHT-PATTERSON AIR FORCE BASE, OHIO 45433-6553

NOTICE

When Government drawings, specifications, or other data are used for any purpose
other than in connection with a definitely related Government procurement operation,
the United States Government thereby incurs no responsibility nor any obligation
whatsoever; and the fact that the government may have formulated, furnished, or in
any way supplied the said drawings, specifications, or other data, is not to be re-
garded by implication or otherwise as in any manner licensing the holder or any
other person or corporation, or conveying any rights or permission to manufacture
use, or sell any patented invention that may in any way be related thereto.

This report has been reviewed by the Office of Public Affairs (ASD/PA) and is
releasable to the National Technical Information Service (NTIS). At NTIS, it will
be available to the general public, including foreign nations.

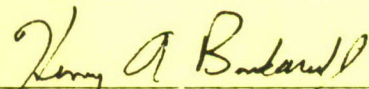This technical report has been reviewed and is approved for publication.

NARENDRA S. KHOT
Project Engineer
Design & Analysis Methods Group

FREDERICK A. PICCHIONI, Lt Col, USAF
Chief, Analysis & Optimization Branch

FOR THE COMMANDER

HENRY A. BONDARUK, JR., Col, USAF
Chief, Structures Division

REPORT DOCUMENTATION PAGE

1a. REPORT SECURITY CLASSIFICATION	1b. RESTRICTIVE MARKINGS
UNCLASSIFIED	

2a. SECURITY CLASSIFICATION AUTHORITY	3. DISTRIBUTION/AVAILABILITY OF REPORT
2b. DECLASSIFICATION/DOWNGRADING SCHEDULE	Approved for public release; distribution is authorized

4. PERFORMING ORGANIZATION REPORT NUMBER(S)	5. MONITORING ORGANIZATION REPORT NUMBER(S)
LMSC D067175	AFWAL-TR-86-3056

6a. NAME OF PERFORMING ORGANIZATION	6b. OFFICE SYMBOL (If applicable)	7a. NAME OF MONITORING ORGANIZATION
Lockheed Palo Alto Research Lab		Flight Dynamics Laboratory (AFWAL/FIBRA) Air Force Wright Aeronautical Lab

6c. ADDRESS (City, State and ZIP Code)	7b. ADDRESS (City, State and ZIP Code)
3251 Hanover Street Palo Alto, CA 94304	Wright-Patterson AFB, OHIO 45433-6553

8a. NAME OF FUNDING/SPONSORING ORGANIZATION	8b. OFFICE SYMBOL (If applicable)	9. PROCUREMENT INSTRUMENT IDENTIFICATION NUMBER
	AFWAL/FIBRA	F33615-81-C-3222

8c. ADDRESS (City, State and ZIP Code)	10. SOURCE OF FUNDING NOS.			
	PROGRAM ELEMENT NO.	PROJECT NO.	TASK NO.	WORK UNIT NO.
	62201F	2401	02	48

11. TITLE (Include Security Classification)
See reverse

12. PERSONAL AUTHOR(S)
David Bushnell

13a. TYPE OF REPORT	13b. TIME COVERED	14. DATE OF REPORT (Yr., Mo., Day)	15. PAGE COUNT
Final	FROM 8101 TO 8609	September, 1986	317

16. SUPPLEMENTARY NOTATION

17	COSATI CODES		18. SUBJECT TERMS (Continue on reverse if necessary and identify by block number)
FIELD	GROUP	SUB. GR.	Panel, Optimization, Stiffened, Composite, Cylindrical, Buckling, Postbuckling, Nonlinear

19. ABSTRACT (Continue on reverse if necessary and identify by block number)

PANDA2 finds minimum weight designs of laminated composite flat or curved cylindrical panels or cylindrical shells with stiffeners in one or two orthogonal directions. The panels or shells can be loaded by as many as five combinations of in-plane loads and normal pressure. The axial load can vary across the panel. The presence of overall (bowing) imperfections as well as local imperfections in the form of the local buckling mode are included. Constraints on the design include crippling, local and general buckling, maximum tensile or compressive stress along the fibers and normal to the fibers in each lamina, and maximum in-plane shear stress in each lamina. Local and general buckling loads are calculated with use of either closed-form expressions or with use of discretized models of panel cross sections. An analysis branch exists in which local post buckling of the panel skin is accounted for. In this branch a constraint condition that prevents stiffener popoff is introduced into the optimization calculations. Part of this paper represents a tutorial run through the PANDA2 processors for a hat-stiffened panel under combined axial compression, in-plane shear and normal pressure. Examples follow in which results from PANDA2 are compared with those in the literature and those obtained with the STAGS and EAL computer programs. Results of an extensive study are given for an optimized, blade-stiffened panel designed so that it buckles locally at about 10 per cent of the design load. The axially stiffened panel is subjected to pure axial compression, pure normal pressure, combined axial compression and normal pressure, and combined axial compression and residual stresses and deformations that arise from a simulated curing process. An example is provided of a design process applied to a ring and stringer stiffened cylindrical shell similar in geometry and loading to the 2/3 interstage of the ARIANE 4 booster. PANDA2 predicts nonlinear global-local buckling modal interaction phenomena explored by Koiter, Thompson, Tvergaard, Hutchinson and others in the early 1970's, and accounts for these phemonena during optimization.

20. DISTRIBUTION/AVAILABILITY OF ABSTRACT	21. ABSTRACT SECURITY CLASSIFICATION
UNCLASSIFIED/UNLIMITED ☒ SAME AS RPT. ☐ DTIC USERS ☐	UNCLASSIFIED

22a. NAME OF RESPONSIBLE INDIVIDUAL	22b. TELEPHONE NUMBER (Include Area Code)	22c. OFFICE SYMBOL
N. Khot	513/255-6992	AFWAL/FIBRA

DD FORM 1473, 83 APR   EDITION OF 1 JAN 73 IS OBSOLETE.

11. Title (UNCLASSIFIED):

PANDA2 - Program for Minimum Weight Design of Stiffened, Composite, Locally Buckled Panels

FOREWORD

TABLE OF CONTENTS

TABLE OF CONTENTS (continued)

TABLE OF CONTENTS (continued)

TABLE OF CONTENTS (continued)

TABLE OF CONTENTS (continued)

LIST OF TABLES AND FIGURES

other harder end plates were fabricated from 6061T6 aluminum stock, which had a 56 ksi yield stress.

prediction of 319 lb/in.. The difference is due to the axial restraint at the loaded end of the panel, present in the local bifurcation buckling problem in the STAGS model but absent in the local bifurcation buckling problem in the PANDA2 model.

by heating or cooling the panel skin relative to the stringers, which in this example are kept at ambient temperature (T=0).

upon lower and upper bounds supplied by the user and certain strategies used by CONMIN.

in the previous figure. In (b) and (c) the mode shapes vary as $\sin(M\pi x/L)$ along the axis of the panel, where L is the ring spacing.

load factor. The mode shapes vary as $\sin(M\pi x/L)$ along the axis of the panel, where L is the ring spacing.

Fig. 100 (a) Multi-segment, branched BOSOR4 model of the optimized panel gener-   243
ated by the PANEL processor (local buckling NOT permitted, and (b,c,d,e,f) buckling
modes corresponding to Load Set 1. All five buckling modes represent panel buck-
ling between rings in which stringers and panel skin participate. The load factors are
close to that predicted from the PANDA-type model for buckling between rings with
smeared stringers. The mode shapes vary as $\sin(\pi x/L)$ along the axis of the panel,
where L is the ring spacing.

1.0 PURPOSE OF PANDA2

The purpose of PANDA2 is to find the minimum weight design of a stiffened flat or curved, perfect or imperfect, panel or complete cylindrical shell made of laminated composite material. Of course, simple isotropic panels and cylindrical shells can also be designed.

1.1 DEFINITION OF "PANEL"

A panel is defined here as a structure that is either flat or is part of a cylinder. In most cases the user will probably want to analyze a flat panel or a panel that spans less than about 45 degrees of circumference. However, in PANDA2 complete cylindrical shells can be treated by the user's setting up a model of a panel that spans 180 degrees. The buckling loads given by PANDA2 for half of a cylindrical shell are the same as those given in the literature for a complete cylindrical shell because:

1. the panel is assumed by PANDA2 to be simply supported along its straight edges, and

2. a deep cylindrical panel spanning 180 degrees of circumference with simple supports along the generators at 0 and at 180 degrees behaves in the same way as a complete cylindrical shell: The number of circumferential half-waves in the 180-degree panel in the critical general instability buckling pattern is the same as the number of full circumferential waves in the 360-degree cylindrical shell.

Later an example is given in which a complete cylindrical shell with a single set of axial and shear loads that vary around the circumference is analyzed as a curved panel spanning 45 degrees and subjected to multiple sets of uniform loads. The panel is optimized for two combinations of in-plane loads: that corresponding to maximum axial compression and that corresponding to maximum in-plane shear. It is usually best to treat complete cylindrical shells in this way rather than try to set up a model for the entire cylinder, because buckling is usually local and concentrated in the areas of maximum load and because PANDA2 was really intended to treat panels, not complete cylindrical shells. Therefore, it is best applied to panels.

In PANDA2 the curved edges of a cylindrical panel lie in the plane of the screen (axial coordinate $x = 0$) and parallel to the plane of the screen (axial coordinate $x = L$, where L is the length of the panel). The axial coordinate direction x is normal to the plane of the screen and pointing out of the screen. Thus, an axial load on the panel is normal to the screen, with axial tension pointing out of the screen.

The width of the panel is the arc length along the curved edge. For example, the width of a deep cylindrical panel spanning 180 degrees is πR, where R is the radius of curvature. The coordinate in the width direction is called y. In the following, this direction is referred to with use of the words "circumferential" or "hoop" or "transverse".

The properties of the panel are assumed to be uniform in the axial (x) direction and periodic in the circumferential (y) direction. The panel may be unstiffened, stiffened by stringers alone, stiffened by rings alone, or stiffened by both rings and stringers. Stiffeners referred to as "stringers" are always normal to the screen; stiffeners referred to as "rings" always lie in the plane of the screen or parallel to the plane of the screen. Both stringers

1

and rings must be uniformly spaced. All stringers must be the same. All rings must be the same. The rings can be different from the stringers.

1.2 TYPES OF STIFFENERS

PANDA2 can handle panels with stringers and/or rings with the following cross sections:
   1. T-shaped
   2. J-shaped (angle with flange away from skin)
   3. Rectangular (blade stiffeners)
   4. Hat-shaped or corrugated stiffeners

The portion of the panel skin near the stiffeners can have different properties than those of the panel skin away from the stiffeners. For example, optimum designs of panels with T-shaped stringers have thickened bases under the stringers that help to prevent fracture or delamination along the attachment line of the stringer to the skin. Figures 1 and 2 show an example of a flat panel with T-shaped stringers.

1.3 BOUNDARY CONDITIONS

In the PANDA2 system the panel is assumed to be simply supported along the two edges normal to the plane of the screen (at $y = 0$ and at $y = $ panel width). The panel can be either simply supported or clamped along the other two boundaries (at $x = 0$ and $x = L$), but the conditions must be the same at both of these two boundaries. The PANDA2 analysis is always performed for simple support on all four edges. However, experience has shown that clamping at $x = 0$ and at $x = L$ can be simulated by the analysis of a shorter simply supported panel: A panel clamped at $x = 0$ and $x = L$ has general instability loads approximately equal to those of a panel simply supported at $x = 0$ and $x = L/3.85^{1/2}$. Therefore, in PANDA2, clamping at $x = 0$ and $x = L$ is simulated by calculation of general instability or wide column instability of a simply supported panel with length equal to $L/3.85^{1/2}$.

In PANDA2 local buckling behavior and local stress concentrations near stiffeners are assumed to be independent of the boundary conditions along the four panel edges. This is a good assumption if there are more than two or three halfwaves in the local buckling pattern over the length and width of the entire panel.

1.4 LOADING

The panel can be loaded by up to five independent sets of in-plane loads, N_x, N_y, and N_{xy}, and normal pressure p. Buckling loads, postbuckling behavior, and maximum stresses are calculated for each of the five load sets applied by itself. Optimization is global, that is, PANDA2 determines the best design that is capable of surviving all of the five load sets when each set is applied separately, as it would be during different phases of a panel's lifetime or over different areas of a large, uniform structure such as a complete cylindrical shell. Associated with each of the five independent load sets, there can be two load subsets, Load Set A and Load Set B. Load Set A consists of what are termed in the PANDA2 output as "eigenvalue loads": These are loads that are to be multiplied by the critical buckling

2

load factor (eigenvalue). Load Set B consists of loads that are not multiplied by the critical buckling load factor. Stated mathematically, the critical load is given by

$$N_{cr} = N(\text{load set B}) + (\text{buckling load factor}) \, N(\text{load set A}) \qquad (1.1)$$

The following table lists the components and properties of the loading in PANDA2:

```
              LOADS ON A PANEL PERMITTED BY PANDA2
==================================================================
  NAME OF    LOAD SET      DEFINITION AND          PROPERTIES
   LOAD      A OR B      [EXAMPLE OF UNITS]
------------------------------------------------------------------
    N1         A         axial in-plane load     uniform or linearly
                         [lb/(in. of circ. arc)] varying across panel
                         negative for compression width; uniform along
                                                 panel length.

    N2         A         hoop  in-plane load     uniform along panel
                         [lb/(in. of axial length)] length and width

   N12         A         in-plane shear load     uniform along panel
                         [lb/(in. axial or circ.)] length and width

   N10         B         axial in-plane load     uniform along panel
                         [lb/(in. of circ. arc)] length and width

   N20         B         hoop  in-plane load     uniform along panel
                         [lb/(in. of axial length)] length and width

   N120        B         in-plane shear load     must be zero
                         [lb/(in. axial or circ.)]

    p          B           normal pressure       uniform over panel
                               [psi]

  THERMAL      B         temperature that        uniform in each
                         simulates curing        panel module segment
                         of composite panel      (see Fig. 1)
==================================================================
```

1.5 TYPES OF ANALYSIS

PANDA2 performs the following analyses:

1. CONSTITUTIVE LAW:

   a. PANDA2 obtains the integrated constitutive law [the 6x6 matrix $C(i,j)$] for each segment of a panel module (Figs. 1 and 2).

3

b. It obtains thermal resultants and strains from curing for each segment of a panel module.

c. It obtains the integrated constitutive law [the 6x6 matrix $C_s(i,j)$] for the panel with either and both sets of stiffeners "smeared out". ("Smearing out" the stiffeners means averaging their properties over the entire area of the panel. See Eqs. (40) of Ref. [8], for example.)

d. It obtains the thermal forces and moments and residual deformations of a panel in which skin and stiffeners have been cocured.

e. It obtains the tangent stiffness $C_{TAN}(i,j)$ of the panel skin in its locally post-buckled state, if applicable.

f. It obtains the tangent stiffness $C_{STAN}(i,j)$ of the panel with smeared stiffeners, using $C_{TAN}(i,j)$ for the stiffness of the panel skin.

2. EQUILIBRIUM:

a. PANDA2 obtains bowing of the panel due to curing.

b. It obtains static response of the panel to uniform normal pressure, using nonlinear theory. Two problems are solved:

  i. overall static response of entire panel with smeared stiffeners, and
  ii. local static response of a single panel module with a discretized cross section (Fig. 1).

c. Average strain and resultant distribution in all of the panel parts (Fig. 1) are determined for:

  i. the panel loaded by all loads except normal pressure. The effect of bowing of the panel due to both curing and normal pressure is included.
  ii. the panel loaded by normal pressure.

d. Stresses in material coordinates in each layer in each laminate of the panel module (Fig. 1) are calculated either for the post-locally buckled panel, or for the unbuckled panel, whichever is applicable. The effect of a local imperfection in the form of the local buckling mode is included.

e. Tensile forces in parts of the stiffener web(s) that tend to pull the web from the panel skin are calculated, and these forces are compared to a maximum allowable "peel force" that the user has previously obtained from peel tests on sample coupons that bear some similarity to the concept for which he or she is seeking an optimum design.

3. BUCKLING:

a. PANDA2 obtains buckling load factors from a PANDA-type of analysis (closed form, see Refs. [1] and [8]) for general instability, local buckling, crippling, rolling of stiffeners.

b. It obtains the load factor for local skin buckling from a BOSOR4-type [2] of analysis in which the cross section of a single panel module is discretized [Figs. 1, 2, 20(a,b), 22(a,b)].

4

c. It obtains a load factor for wide column buckling from a BOSOR4-type of analysis of a discretized single panel module [Figs. 2, 20(c), 22(c)].

d. It obtains a load factor for general instability from a BOSOR4-type of analysis of the entire panel with smeared stiffeners. The width of the panel is discretized.

e. It generates an elaborate discretized model of the entire panel width with stringer parts treated as flexible shell branches. This model can be used directly as input to BOSOR4. (See Fig. 21).

1.6 PHILOSOPHY OF PANDA2

PANDA2 represents a more detailed treatment of certain behavior not handled by PANDA [1]. In particular, optimum designs can be obtained for imperfect panels, for panels with locally post–buckled skin and for panels with hat stiffeners. In addition, PANDA2 will handle nonlinear static response to normal pressure and panels with nonuniform axial loading. Also, PANDA2 optimizes panels for multiple sets of loads.

Optimization is carried out based on several independently treated structural models of the panel. These might be classified into three model types, as follows:

1.6.1 Model type 1

Included are PANDA–type models [1] for general, local, and panel buckling, crippling of stiffener parts, and rolling of stiffeners with and without participation of the panel skin. Buckling load factors are calculated from closed-form equations rather than from discretized models. The formulas are given in [1]. (See Table 1 and Figs. 1–4 of [1].) (Numbers [i] refer to references given below.)

1.6.2 Model type 2

Buckling load factors and post–local buckling behavior are calculated for what is termed in PANDA2 a "panel module." Such a module is depicted in Figs. 1 and 2. A module includes the cross section of a stiffener plus the panel skin of width equal to the spacing between stiffeners. In this model the panel module cross section is divided into segments, each of which is discretized and analyzed via the finite difference energy method [2]. Variation of deflection in the axial direction is assumed to be harmonic[$\sin(nx)$ or $\cos(nx)$]. This one–dimensional discretization is similar to that used in the BOSOR programs for the analysis of shells of revolution [2]. In fact, many of the subroutines for buckling and vibration analysis are taken from BOSOR4 and modified slightly. The modification is necessary to handle prismatic structures instead of shells of revolution.

Both local and wide–column instability can be handled with the same discretized structural model. Symmetry conditions are applied at the left and right edges of the single module model, that is, symmetry conditions are applied midway between stringers.

The single module model gives a good approximation to the local skin buckling mode if there are more than three or four equally spaced stringers in the panel. What goes on locally between interior stringers in a panel, stringers which are rotating about their axes only, not bending, is only weakly affected by the boundary conditions at panel edges that may be several bays away.

5

The wide column buckling model in PANDA2 is applied to an axial length of panel between adjacent rings, or if there are no rings, to the entire axial length of the panel, L. The wide–column buckling load predicted from the single panel module is always lower and usually reasonably close to the general instability load of the entire width of the panel between rings because the axial bending stiffness of a stringer–stiffened panel is usually much, much greater than the transverse bending stiffness of the portion of the panel between adjacent rings. Hence, the strain energy in the buckled panel, and therefore the buckling behavior, is only weakly dependent on bending of the panel transverse to the stringers. Therefore, the boundary conditions along the edges of the panel parallel to the stringers are not important. On the other hand, local bending of the skin and local deformation of the stringer parts in the wide column buckling mode may significantly affect the wide column buckling load. These effects are not included in the closed–form PANDA-type model of general instability, but they are included in the single panel module model of wide column buckling. (Note that buckling modal interaction between local and general buckling that is due to initial local imperfections in the panel skin is included in PANDA2.)

1.6.3 Model type 3

Also included in the PANDA2 collection of models is a discretized model of the entire width of the panel, treated in this case with stiffeners smeared out. This model is introduced only if the axial load varies across the width of the panel or if there exists normal pressure.

1.6.4 Overall Philosophy of PANDA2

The overall philosophy of PANDA2 is to use several separate relatively simple models to capture different phenomena, rather than use a single multi-dimensionally discretized finite element model with a large number of degrees of freedom. The aim is to produce a program that can yield optimum designs of rather sophisticated panels that experience very complex and very nonlinear behavior, and to do this without the use of large, general-purpose programs and their elaborate data base management systems.

For example, PANDA-type models (Model type 1) are used in PANDA2 to obtain quick, preliminary designs which one can then use as starting designs in optimization analyses based on the more elaborate discretized panel module model. Also, PANDA-type models are used to obtain buckling load factors in cases for which the discretized panel module model is not applicable, to obtain knockdown factors for the effect of in-plane shear loading, to obtain preliminary estimates of how much growth in any initial panel bowing to expect under compressive in–plane loads, and to check if it is likely that a curved panel with uniform external pressure will collapse under the pressure acting by itself.

Models of type 2 (single discretized module) and type 3 (discretization of entire width with smeared stiffeners) are used in tandem to obtain from nonlinear theory the complex behavior of a stiffened plate or shell loaded by normal pressure. Model type 3 is the only one that is valid if the axial load varies across the width of the panel.

In the panels designed by PANDA2 the skin between stringers and the stringer parts will deform if they are locally imperfect, and even if they are perfect they may buckle well before failure of the panel. The maximum stress components and therefore stress constraints in the optimization analysis are computed including local prebuckling deformation and local post buckling growth and modification of the local skin buckling mode as predicted by a modified form of a theory formulated by Koiter in 1946 [4]. Model type 2 (single discretized module) is the only model in PANDA2 valid for these analyses.

After the optimum design is obtained, the user can, if no in-plane shear load is applied, check the accuracy of the general instability load predicted from the single-module model by running a multi-module model with BOSOR4 [2]. The input data file for this multi-module model is generated automatically by the PANDA2 system.

1.7 ARCHITECTURE OF THE PANDA2 SYSTEM

As with PANDA, the program PANDA2 consists of several independently executable processors which share a common data base. In the processor BEGIN the user supplies a starting design (perhaps a design produced by PANDA). In DECIDE he or she chooses decision variables for the optimization analysis and their upper and lower bounds, linking variables and their factors of proportionality, and "escape" variables (explained in DECIDE). In MAINSETUP the user chooses up to five sets of combined in-plane loads and normal pressure; factors of safety for general instability, local instability, and material failure; strategy parameters such as number and range of axial half-waves in the local buckling mode; and number of design iterations in the optimization problem. The command PANDAOPT initiates a batch run of the PANDA2 mainprocessor, which consists of two main branches: in one branch the structural analyses (stress, buckling and post- buckling) are performed and in the other new designs are produced by the optimizer CONMIN, written by Vanderplaats [3].

2.0 HOW TO OPERATE THE PANDA2 SYSTEM OF PROGRAMS

To operate PANDA2 you must have the BOSOR4 program system on a subdirectory with the name BOSOR4. The PANDA2 system uses many of the libraries from the BOSOR4 system. and certain commands (for example PANEL followed by BOSORALL) use BOSOR4 processors directly.

You first activate PANDA2 commands via the command PANDA2LOG. This command must be given before you do any PANDA2 work.

You then prepare input data interactively via the BEGIN command. These data establish a starting design, material properties, and temperature rise pertaining to residual stresses from curing. The data that you provide interactively are stored on a file NAME.BEG, which you will find very useful in future analyses of the same design concept. (NAME is a name that you choose and retain for the entire case.)

You next type the command SETUP. As a result of SETUP, a BOSOR4-type of input data file is created. Following SETUP, you type the command BOSMODEL. This launches a batch run of a BOSOR4-type preprocessor which is almost identical to BOSORREAD (see HELP4 PROGRAMS in the BOSOR4 subdirectory and Ref. [2], last citation).

The BOSMODEL processor creates a discretized model of a single module of the panel (see Fig. 1) and a discretized model of the entire panel with smeared stiffeners. When the BOSMODEL batch run is finished, you can either type the command DECIDE or the command MAINSETUP. If you choose DECIDE, you will be asked to pick decision variables and their upper and lower bounds, linked variables and linking constants, and escape variables. If you choose MAINSETUP, you will be asked to provide loads, factors of safety, and strategy parameters for a simple buckling analysis of a fixed design.

Suppose you choose DECIDE. This choice means that you intend to do an optimization analysis. After picking decision variables and other optimization parameters in DECIDE, you type the command MAINSETUP. Now you provide up to five sets of combined in-plane loads, normal pressure, and factors of safety for general instability, local instability, and material failure, and you establish certain strategy parameters for the buckling and optimization analyses.

You then type the command PANDAOPT, which launches a batch run of the PANDA2 mainprocessor. Simple buckling analyses require up to several minutes on the VAX 11/780, and 6 to 10 design iterations in an optimization analysis require about 3 to 60 minutes of CPU time. The results of the PANDAOPT run are stored in a file called NAME.OPM.

After inspecting the NAME.OPM file, you may wish to do more design iterations. If you feel that the loads, factors of safety, and strategy parameters established in MAIN-SETUP are still good, simply type the command PANDAOPT again. Look at the new NAME.OPM file. Keep repeating this cycle until you think you have an optimum design. If along the way you want to change the strategy parameters, type MAINSETUP again. If you want to change which parameters are decision variables or upper or lower bounds, or if you want to change the linking variables or linking constants of proportionality, type DECIDE again.

When you are satisfied that you have a good design, you will probably want plots of the cross section and buckling modes. You must first give the command MAINSETUP again and set up a case in which you are analyzing a given design (no optimization). When the system asks if you want plots, answer Y. After you finish with MAINSETUP, give the command PLOTTER.

All the analysis up to this point is for a single panel module or the complete panel in which the stiffeners are smeared out. You may want to check the accuracy of the simplified models for general instability. (By "simplified models for general instability" is meant PANDA–type or discretized models in which the stiffeners are smeared out and a wide–column discrete model which covers only a single panel module). You can check the PANDA2 results by obtaining the general instability load factor for a multi–module discretized model that represents the entire panel, not just a single module of the panel. You type the commands PANEL, BOSOR4LOG, BOSORALL, and BOSORPLOT, in that order. PANEL is analogous to SETUP: It sets up an input data file, NAME.ALL, for a multi–module discretized panel. This file is a regular BOSOR4 input data file. The command BOSOR4LOG activates the BOSOR4 command set, and the command BOSORALL initiates a batch run of the BOSOR4 pre–, main–, and postprocessors. BOSORPLOT gets plots of the discretized multi–module panel and of the buckling modes. The PANEL processor should not be used if there exist multiple load sets. If there exists significant in–plane applied shear load, N_{xy}, you will have to multiply the load factor obtained as just described by a knockdown factor generated by PANDA2 because the BOSOR4 buckling analysis does not include in-plane shear. BOSOR4 works for prismatic structures, such as an axially stiffened flat panel, through a "trick" described in Chapter 7 of Ref. [30]. Figure 22 gives an example.

2.1 SAMPLE RUNSTREAM WITH PANDA2

PANDA2LOG	(you activate PANDA2 commands. Please note that you must insert the following four statements in your LOGIN.COM:
	$ASSIGN DISK:[USERNAME.PANDA2] PANDA2
	$PANDA2LOG :== @DISK:[USERNAME.PANDA2]PANDA2
	$ASSIGN DISK:[USERNAME.BOSOR4] BOSOR4
	$BOSOR4LOG :== @DISK:[USERNAME.BOSOR4]BOSOR4
BEGIN	(you establish a starting design)
SETUP	(system sets up a BOSOR4–type of input file)
BOSMODEL	(system generates BOSOR4–type discrete models)
DECIDE	(you establish optimization parameters)
MAINSETUP	(you provide loads and set up PANDA2 analysis strategy)
PANDAOPT	(system performs PANDA2 analysis)
MAINSETUP	(you provide new strategy: no optimization, yes plots)
PLOTTER	(you launch a batch run to generate plots)
PANEL	(system sets up a BOSOR4 input file for multi–module panel.
BOSOR4LOG	(you activate BOSOR4 command set)
BOSORALL	(you run BOSOR4 to get general bifurcation buckling)
BOSORPLOT	(BOSOR4 system generates a multi–module panel plot file)

3.0 PURPOSE OF BEGIN AND AN EXAMPLE

3.1 PURPOSE OF BEGIN

The purpose of BEGIN is to permit you to provide a starting design in an interactive mode. You give starting dimensions, material properties, allowables. The interactive session is stored on a file called NAME.BEG, in which NAME is a name that you have chosen for the case. (NAME must remain the same for all the PANDA2 processors.) In future runs of the same or of a slightly modified case, you will find it convenient to use the file NAME.BEG as input. Rather than answer all the questions interactively, you can use NAME.BEG or an edited version of NAME.BEG as input to BEGIN. BEGIN also generates an output file called NAME.OPB. OPB lists a summary of the case, and if you choose the tutorial option, the questions, helps, and your answers for each input datum.

3.2 EXAMPLE: A HAT-STIFFENED PANEL

Now you start to provide input data. You will be prompted by short questions. If you need help, just type H as an answer to the prompt instead of the datum called for. In most instances you will then be given more information on the datum you must provide. It may be a good idea to run the tutorial option if you are a new user of PANDA2.

Overall panel dimensions:

1. length normal to the plane of the screen, L1
2. length in the plane of the screen, L2

$Panel length normal to the plane of the screen, L1=H
This is the axial length of the panel. For a cylindrical panel, this is the length of the generator of the panel.

$Panel length normal to the plane of the screen, L1=30

$Panel length in the plane of the screen, L2=H
For a cylindrical panel, this is the arc length along the circumference of the entire panel. A complete cylindrical shell can be modelled by using $L2 = \pi \times$ radius. Then the number of half-waves over this circumferential length is the same as the number of full waves around the complete 360 degree circumference. When analyzing a complete cylindrical shell with loads that vary around the circumference, it is often best to divide the cylindrical shell into panels, each with uniform loading. Then the optimum design of the complete cylindrical shell can be obtained by optimizing one of the panels as if it were subjected to multiple load sets, each set consisting of uniform loads.

$Panel length in the plane of the screen, L2=24

$Identify type of stiffener along L1 (N, T, J, R, A)= H
N = No stiffeners along L1 at all
T = T-shaped cross section
J = J-shaped cross section (angle section with flange away from skin)
R = Rectangular cross section (blade stiffener)
A = A hat-shaped or trapezoidal cross section (enclosing area)

$Identify type of stiffener along L1 (N, T, J, R, A)=A
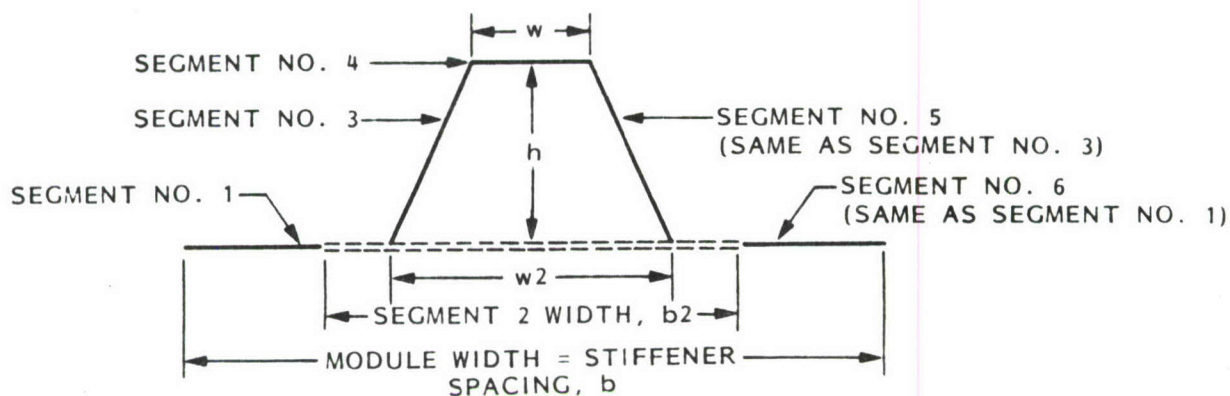
Fig. 3   Panel module with hat-shaped stiffener.

$stiffener spacing, b=8

$width of stiffener base, b2 (must be > 0, see Help)=H

Width b2 must be greater than zero. In fact, it should always be greater than a tenth of the module width, b. This segment of the module is considered by PANDA2 to consist of the skin plus the faying flange, if any, of the stiffener. In the PANDA2 model b2 must be greater than about a tenth of the total module width, b, because the section of width b2 is considered to be a separate segment which is discretized. If you make b2 too small, numerical difficulties might occur.

$width of stiffener base, b2 (must be > 0, see Help)=2.5

$height of stiffener (type H to see sketch), h=H

The height of the stiffener is measured from the surface of the stiffener base to the middle surface of the stiffener flange, as shown in Fig. 4.
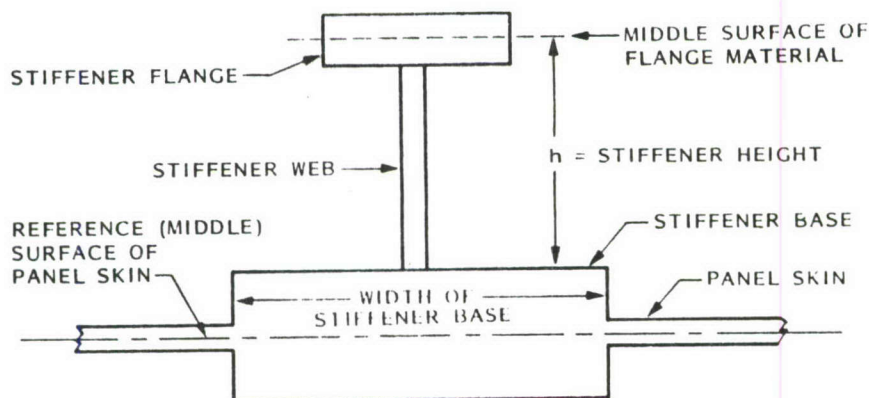
Fig. 4   Height of the stiffener is measured from the top of the stiffener base to the middle surface of the flange.

$width of outer flange of stiffener, w=0.8

11

$width of hat base, w2=1.0

$Are the stringers cocured with the skin?=H

Stringers and skin may be cured separately, then glued together at room temperature, or they may be cocured. Which method is used very much affects the residual stresses and residual deformations of the panel. The residual stresses and deformations in cocured panels are caused by the different thermal expansion properties of the stringers and skin as the panel cools down from the curing temperature to room temperature. If this is not a composite panel, the answer here should probably be N, unless you are simulating the effect of a thermal gradient through the thickness of a stiffened panel.

$Are the stringers cocured with the skin?=Y

$What force/(axial length) will cause web peel-off?=H

Wanted here is the force–per–axial–length of stringer required to peel half of each stringer web and faying flange away from the panel skin. "Half the stringer web" means half of the thickness. It is assumed that each half of the stringer web consists of layers that start as part or all of the faying flange on either side of the stiffener. These layers "turn a corner" to become the stringer web. Tensile forces in the plane of the web, normal to the stringer axis, will therefore tend to peel the web halves from the faying flanges from which they derive. In the post–local buckling regime, such forces develop in each stringer web. These are calculated by PANDA2, and a constraint condition is formulated that indicates whether or not stringer popoff will occur because of web–peel–off caused by post–local buckling deformations. The force required here depends on what sort of adhesive is used between stringers and skin and its thickness. You will probably have to consult peel test data for this input datum. Units required are force/length. A typical value for graphite epoxy is in the range 40–100 lb/in. Figures 5, 6, and 7 show an example.

Figure 5(a) shows a T-stiffened panel module in its locally postbuckled state. The stiffener web bends because the flange, being deep, resists bending in its plane. Tensile forces develop in layers 1 and 2 of the web. These are maximum near the root of the web, and they tend to peel the web away from the panel skin. Figure 6(c) shows a schematic of a peel–test specimen, and Fig. 7 shows a graphite–epoxy peel–test specimen after failure. The force, F_p, per length of specimen normal to the plane of the paper is what is called for here.

$What force/(axial length) will cause web peel–off?=50

Now you will be asked to provide properties for the panel module on a segment–by–segment basis, starting with the skin, which is Segment 1, as shown in Fig. 3. In each segment of the module, the wall is considered to be divided into groups of layers. There are two types of groups:

1. default groups (12 layers, [90,45,0,–45,0,90]s, all of the same material and initially all of the same thickness. Winding angles cannot be chosen as decision variables in this option. Thicknesses can be decision variables. The notation [90, 45, 0, –45, 0, 90]s means [90, 45, 0, –45, 0, 90, 90, 0, –45, 0, 45, 90].)

12

2. just plain groups (any number of layers, any winding angles, any variety of material types and any variety of thickness. Winding angles can be chosen as decision variables.)

For each default group (group type 1) you will be asked to give:

1. the thickness of one of the layers;
2. the material type.

For each "just plain group" (group type 2) you must provide:

1. the number of layers through the thickness of the group
2. whether the winding angles can ever be decision variables
3. layer indices for each layer
4. whether the layer is a new type of layer
5. if it is a new type of layer: thickness, winding angle, and material type corresponding to that layer index.

\$Is the next group of layers to be a "default group"?=H

N means that you will provide a group of layers one–by–one. (This is the answer you will probably most often give.)

Y means that a group of layers will be generated each of which initially has the same thickness and material type. You will be asked to provide this single layer thickness and this material type indicator. A "default group" has 12 layers of initially equal thickness with winding angles in the sequence: [90,45,0,-45,0,90]s.

Note that the thicknesses of the individual layers, which are initially the same in a default group, can become different during optimization iterations. However, the winding angles cannot be decision variables.

\$Is the next group of layers to be a "default group"?=N

\$number of layers in the next group in Segment no.(1)=2

\$Can winding (layup) angles ever be decision variables?=H

Use with caution. Please note that weight does not change with layup angle, so that if you plan to optimize something and allow layup angles to be decision variables, you must also allow the thickness of at least one layer also to be a decision variable. Also, any decision variable that is zero or that becomes zero during design iterations is dropped by PANDA2 from the list of decision variables: It ceases being a decision variable from that moment on. Hence, if you specify that the layup angle of a layer is a decision variable, and if you also specify that the layup angle of this layer is zero, this layer layup angle will not be a decision variable during optimization cycles. If you really want the layer layup angle to be a decision variable, set it initially to 5 or 10 degrees or use CHANGE to change it from zero to 5 or 10 degrees.

\$Can winding (layup) angles ever be decision variables?=N

\$layer index (1,2,...), for layer no.(1)=H

A layer index implies the following "bundle" of properties:

1. thickness of the layer

2. layup angle of the layer (degrees between the normal to the screen and the direction in which the modulus E1 (fiber direction) is measured)
3. material type of the layer

The three properties just listed are identical in two different layers if both of these layers have the same layer index.

$layer index (1,2,...), for layer no.(1)=1

$Is this a new layer type?=Y

thickness, layup angle, material for layer index 1:

$thickness for layer index no.(1)=.006

$layup angle (deg.) for layer index no.(1)=H

The definition of layup angle is: the angle in degrees measured from the normal to the screen to the direction in which the fiber modulus E1 is measured.

$layup angle (deg.) for layer index no.(1)=45

$material index (1,2,...) for layer index no.(1)=2

$layer index (1,2,...), for layer no.(2)=2

$Is this a new layer type?=Y

thickness, layup angle, material for layer index 2:

- - - MUCH MORE INTERACTIVE INPUT NOT SHOWN HERE - - -

3.3 FILE GENERATED DURING THE INTERACTIVE SESSION WITH BEGIN

An annotated file of this input is stored on HAT.BEG, which for this case is as follows:

```
N        $ Do you want a tutorial session and tutorial output?
   30    $ Panel length normal to the plane of the screen, L1
   24    $ Panel length in the plane of the screen, L2
A        $ Identify type of stiffener along L1 (N, T, J, R, A)
    8    $ stiffener spacing, b
  2.5    $ width of stiffener base, b2 (must be > 0, see Help)
  1.3    $ height of stiffener, h
 0.80    $ width of outer flange of stiffener, w
    1    $ width of hat base, w2
Y        $ Are the stringers cocured with the skin?
  50.    $ What force/(axial length) will cause web peel-off?
N        $ Is the next group of layers a ''default group''?
    2    $ number of layers in the next group in Seg. no.(1)
N        $ Can winding (layup) angles ever be decision variables?
    1    $ layer index (1,2,...), for layer no.(1)
Y        $ Is this a new layer type?
0.006    $ thickness for layer index no.(1)
   45    $ layup angle (deg.) for layer index no.(1)
    2    $ material index (1,2,...) for layer index no.(1)
    2    $ layer index (1,2,...), for layer no.(2)
Y        $ Is this a new layer type?
0.006    $ thickness for layer index no.(2)
```

```
  -45     $ layup angle (deg.) for layer index no.(2)
    2     $ material index (1,2,...) for layer index no.(2)
Y         $ Any more layers or groups of layers in Seg. no.(1)
Y         $ Is the next group of layers a ''default group''?
N         $ Is this default group identical to previous group?
.0052     $ thickness of each layer of the default group
    1     $ material type in the default group
Y         $ Any more layers or groups of layers in Seg.(1)
N         $ Is the next group of layers a ''default group''?
    2     $ number of layers in the next group in Seg. no.(1)
N         $ Can winding (layup) angles ever be decision variables?
    2     $ layer index (1,2,...), for layer no.(15)
N         $ Is this a new layer type?
    1     $ layer index (1,2,...), for layer no.(16)
N         $ Is this a new layer type?
N         $ Any more layers or groups of layers in Seg. no.(1)
N         $ Is the next group of layers a ''default group''?
    5     $ number of layers in the next group in Seg. no.(2)
N         $ Can winding (layup) angles ever be decision variables?
    1     $ layer index (1,2,...), for layer no.(1)
N         $ Is this a new layer type?
    2     $ layer index (1,2,...), for layer no.(2)
N         $ Is this a new layer type?
    9     $ layer index (1,2,...), for layer no.(3)
Y         $ Is this a new layer type?
.0208     $ thickness for layer index no.(9)
    0     $ layup angle (deg.) for layer index no.(9)
    1     $ material index (1,2,...) for layer index no.(9)
   10     $ layer index (1,2,...), for layer no.(4)
Y         $ Is this a new layer type?
.0052     $ thickness for layer index no.(10)
   90     $ layup angle (deg.) for layer index no.(10)
    1     $ material index (1,2,...) for layer index no.(10)
    9     $ layer index (1,2,...), for layer no.(5)
N         $ Is this a new layer type?
Y         $ Any more layers or groups of layers in Seg. no.(2)
Y         $ Is the next group of layers a ''default group''?
Y         $ Is this default group identical to previous group?
    1     $ Which module seg. is the previous group in?
    1     $ Which default group in that segment is the same?
Y         $ Any more layers or groups of layers in Seg. no.(2)
N         $ Is the next group of layers a ''default group''?
    5     $ number of layers in the next group in Seg. no.(2)
N         $ Can winding (layup) angles ever be decision variables?
    9     $ layer index (1,2,...), for layer no.(18)
N         $ Is this a new layer type?
   10     $ layer index (1,2,...), for layer no.(19)
N         $ Is this a new layer type?
```

```
    9   $ layer index (1,2,....), for layer no.(20)
N       $ Is this a new layer type?
    2   $ layer index (1,2,....), for layer no.(21)
N       $ Is this a new layer type?
    1   $ layer index (1,2,....), for layer no.(22)
N       $ Is this a new layer type?
N       $ Any more layers or groups of layers in Seg. no.(2)
N       $ Is the next group of layers a ''default group''?
    4   $ number of layers in the next group in Seg. no.(3)
N       $ Can winding (layup) angles ever be decision variables?
    1   $ layer index (1,2,....), for layer no.(1)
N       $ Is this a new layer type?
    2   $ layer index (1,2,....), for layer no.(2)
N       $ Is this a new layer type?
    2   $ layer index (1,2,....), for layer no.(3)
N       $ Is this a new layer type?
    1   $ layer index (1,2,....), for layer no.(4)
N       $ Is this a new layer type?
N       $ Any more layers or groups of layers in Seg. no.(3)
N       $ Is the next group of layers a ''default group''?
   15   $ number of layers in the next group in Seg. no.(4)
N       $ Can winding (layup) angles ever be decision variables?
    1   $ layer index (1,2,....), for layer no.(1)
N       $ Is this a new layer type?
    2   $ layer index (1,2,....), for layer no.(2)
N       $ Is this a new layer type?
   11   $ layer index (1,2,....), for layer no.(3)
Y       $ Is this a new layer type?
.0208   $ thickness for layer index no.(11)
    0   $ layup angle (deg.) for layer index no.(11)
    1   $ material index (1,2,...) for layer index no.(11)
   10   $ layer index (1,2,....), for layer no.(4)
N       $ Is this a new layer type?
   11   $ layer index (1,2,....), for layer no.(5)
N       $ Is this a new layer type?
   10   $ layer index (1,2,....), for layer no.(6)
N       $ Is this a new layer type?
   11   $ layer index (1,2,....), for layer no.(7)
N       $ Is this a new layer type?
   10   $ layer index (1,2,....), for layer no.(8)
N       $ Is this a new layer type?
   11   $ layer index (1,2,....), for layer no.(9)
N       $ Is this a new layer type?
   10   $ layer index (1,2,....), for layer no.(10)
N       $ Is this a new layer type?
   11   $ layer index (1,2,....), for layer no.(11)
N       $ Is this a new layer type?
   10   $ layer index (1,2,....), for layer no.(12)
```

```
N        $ Is this a new layer type?
   11    $ layer index (1,2,...), for layer no.(13)
N        $ Is this a new layer type?
    2    $ layer index (1,2,...), for layer no.(14)
N        $ Is this a new layer type?
    1    $ layer index (1,2,...), for layer no.(15)
N        $ Is this a new layer type?
N        $ Any more layers or groups of layers in Seg. no.(4)
    1    $ choose external (0) or internal (1) stiffeners
N        $ Identify type of stiffener along L2 (N, T, J, R, A)
Y        $ Is the panel curved in the plane of the screen ?
  194    $ Radius of curvature (cylinder radius), R
N        $ Is panel curved normal to plane of screen? (ans. N)
N        $ Is this material isotropic (Y or N)?
 2.E7    $ modulus in the fiber direction,        E1(1)
14.E5    $ modulus transverse to fibers,          E2(1)
 7.E5    $ in-plane shear modulus,                G(1)
.0203    $ small Poisson's ratio,                 NU(1)
 7.E5    $ out-of-plane shear modulus,            G13(1)
 4.E5    $ out-of-plane shear modulus,            G23(1)
 0.500E-07  $ thermal expansion along fibers, A1(1)
 0.160E-04  $ transverse thermal expansion,   A2(1)
270.     $ residual stress temperature (positive),TEMPTUR(1)
N        $ Want to specify  maximum effective stress (N)?
190000.  $ maximum tensile stress along fibers, matl(1)
182800.  $ max compressive stress along fibers, matl(1)
9800     $ max tensile stress normal to fibers, matl(1)
25060    $ max compress stress normal to fibers,matl(1)
10000    $ maximum  shear  stress  in  material type(1)
0.056    $ weight density (greater than 0!) of mat'l type(1)
Y        $ Is this unidirectional composite material (tape) ?
0.0052   $ Thickness of a single lamina of matl type(1)
Y     $ Does max. allowable stress decrease for more layers?
O     $ Degradation(%) in max. sig1(tension) for n layers, n=(2)
O     $ Degradation(%) in max. sig1(comp.)   for n layers, n=(2)
20    $ Degradation(%) in max. sig2(tension) for n layers, n=(2)
O     $ Degradation(%) in max. sig2(comp.)   for n layers, n=(2)
O     $ Degradation(%) in max. sig12         for n layers, n=(2)
Y     $ Any further Degradation with more layers of matl type(1)
O     $ Degradation(%) in max. sig1(tension) for n layers, n=(3)
O     $ Degradation(%) in max. sig1(comp.)   for n layers, n=(3)
30    $ Degradation(%) in max. sig2(tension) for n layers, n=(3)
O     $ Degradation(%) in max. sig2(comp.)   for n layers, n=(3)
O     $ Degradation(%) in max. sig12         for n layers, n=(3)
Y     $ Any further Degradation with more layers of matl type(1)
O     $ Degradation(%) in max. sig1(tension) for n layers, n=(4)
O     $ Degradation(%) in max. sig1(comp.)   for n layers, n=(4)
37    $ Degradation(%) in max. sig2(tension) for n layers, n=(4)
```

```
O    $ Degradation(%) in max. sig2(comp.)   for n layers, n=(4)
O    $ Degradation(%) in max. sig12          for n layers, n=(4)
N    $ Any further Degradation with more layers of matl type(1)
N       $ Is this material isotropic (Y or N)?
1.05E7 $ modulus in the fiber direction,      E1(2)
1.05E7 $ modulus transverse to fibers,        E2(2)
 7.E5  $ in-plane shear modulus,               G(2)
0.077  $ small Poisson's ratio,               NU(2)
 7.E5  $ out-of-plane shear modulus,         G13(2)
 4.E5  $ out-of-plane shear modulus,         G23(2)
  0.150E-05  $ thermal expansion along fibers, A1(2)
  0.150E-05  $ transverse thermal expansion,   A2(2)
270.  $ residual stress temperature (positive),TEMPTUR(2)
N     $ Want to specify  maximum effective stress (N)?
91035  $ maximum tensile stress along fibers, matl(2)
103845 $ max compressive stress along fibers, matl(2)
89880  $ max tensile stress normal to fibers, matl(2)
105000 $ max compress stress normal to fibers,matl(2)
 7000  $ maximum  shear  stress  in  material type(2)
0.056  $ weight density (greater than 0!), mat'l type(2)
N      $ Is this unidirectional composite material (tape) ?
   1   $ Choose 0=simple support or 1=clamping
- - - - - - - - END OF HAT.BEG FILE - - - - - - - -
```

4.0 GENERATING BOSOR4-TYPE DISCRETIZED MODELS

Next, the commands

$ SETUP

$ BOSMODEL

are given by the user. These cause templates of the stiffness and load–geometric matrices to be set up for the buckling problems involving:

1. a single panel module (Fig. 3), which is used for:
   a.   local buckling and postbuckling analysis,
   b.   wide column buckling analysis, and
   c.   the nonlinear local static response of an axially stiffened panel to uniform normal pressure.

2. the entire panel with smeared stiffeners, which is used for:
   a.   general instability for a panel with an axial load that varies across the span of the panel, and
   b.   the nonlinear overall static response of a stiffened panel to uniform normal pressure.

Much of the BOSOR4 preprocessor software is used to do this. Therefore, in order to use PANDA2 you must have available to you the most recent version of BOSOR4.

5.0 PURPOSE OF DECIDE AND AN EXAMPLE

5.1 PURPOSE OF DECIDE

In DECIDE you provide, in a conversationally interactive mode, strategy parameters for PANDA2 optimization. You choose which of the problem parameters are to be decision variables (allowed to change) during optimization and their lower and upper bounds. You also choose linked parameters, that is parameters that are not decision variables but vary in proportion with designated decision variables, and you assign factors of proportionality. Finally, you choose "escape" variables, that is variables that should be increased during any design iteration in which CONMIN fails to change the design. You should choose only thicknesses as escape variables. There is a default option for "escape" variables in which only decision variables that are thicknesses are chosen. You should use the default option.

To repeat, there are three types of variables you choose in DECIDE:

1. DECISION VARIABLES . . . .These variables change independently of each other during optimization.

2. LINKED VARIABLES . . . . .Each of these variables is proportional to one of the decision variables. You choose which one and you choose the factor of proportionality.

3. ESCAPE VARIABLES . . . . .These are variables that, when increased, drive the design toward the feasible region. An escape variable must be a decision variable and should be a thickness. You can choose thickness variables by choosing the default option.

Your interactive input is saved on a file, NAME.DEC, in which NAME is the same name you used for BEGIN, SETUP, etc. In future runs of this or a similar case, you can edit the file NAME.DEC, then give the command DECIDE, and tell the system that you are using an existing file. If you err part way through a case, you can do a CONTROL Y, edit the NAME.DEC file, and re-issue the command DECIDE, telling the system that you are adding to an existing file. The system will answer all the questions up to your error in a "batch" mode, then return control to you. You can then complete the interactive input. (All of the PANDA2 interactive processors have this feature.)

Output from the PANDA2 processor DECIDE is stored in a file with the name NAME.OPD. You should print this file and inspect it to make sure that the case is as you intend it to be.

5.2 EXAMPLE OF USE OF DECIDE IN A RUNSTREAM:

BEGIN	(you establish a starting design)
SETUP	(system sets up an input file for BOSOR4)
BOSMODEL	(system sets up BOSOR4–type discrete models)
DECIDE	(you establish optimization parameters)
MAINSETUP	(you set up loads and analysis strategy to be used by PANDAOPT)
PANDAOPT	(system performs PANDA2 optimization)

5.3 EXAMPLE: A HAT-STIFFENED PANEL

$Want to use default for thickness decision variables?=H

N means you choose thickness decision variables one-by-one.

Y means that for a certain range of layer index types, to be specified by you, the following will happen:

1. the thickness of any layer type for which the winding (layup) angle is either 0 or 90 deg. will be a decision variable.

2. the thickness of any layer type will be a decision variable, regardless of winding (layup) angle, if the layup angle of any previous layer type within the given range of layer types is not equal to minus the layup angle of the current layer type.

3. If the current layup angle is minus some previous layup angle within the given range of layer types, the current thickness will be linked to that previous thickness, and the linking constant C will be 1.0.

$Want to use default for thickness decision variables?=Y

```
LAYER INDEX TYPES FROM WHICH A RANGE MUST NOW BE CHOSEN
```

VAR. NO.	STR/ RNG	SEG. NO.	LAYER NO.	CURRENT VALUE	DEFINITION
6	STR	1	1	6.0E-03	thickness for layer index no.(1)
7	STR	1	2	6.0E-03	thickness for layer index no.(2)
8	STR	1	3	5.2E-03	thickness for layer index no.(3)
9	STR	1	4	5.2E-03	thickness for layer index no.(4)
10	STR	1	5	5.2E-03	thickness for layer index no.(5)
11	STR	1	6	5.2E-03	thickness for layer index no.(6)
12	STR	1	7	5.2E-03	thickness for layer index no.(7)
13	STR	1	8	5.2E-03	thickness for layer index no.(8)
14	STR	2	3	2.08E-02	thickness for layer index no.(9)
15	STR	2	4	5.2E-03	thickness for layer index no.(10)
16	STR	4	3	2.08E-02	thickness for layer index no.(11)

$Lowest layer index for default decision variable=H

Choose a number from the right-hand side of the screen.

You are now specifying a range of layer indices for which you want PANDA2 to set up the decision variables. (These decision variables will be thicknesses only, not winding angles.) What is wanted now is the lowest layer index number for which you want PANDA2 to establish decision variables.

$Lowest layer index for default decision variable=3

$Highest layer index for default decision variable=8

```
          DECISION VARIABLES CHOSEN SO FAR
```

VAR. NO.	STR/ RNG	SEG. NO.	LAYER NO.	CURRENT VALUE	DEFINITION
8	STR	1	3	5.2E-03	thickness for layer index no.(3)

```
 9   STR   1    4    5.2E-03   thickness for layer index no.(4 )
10   STR   1    5    5.2E-03   thickness for layer index no.(5 )
12   STR   1    7    5.2E-03   thickness for layer index no.(7 )
13   STR   1    8    5.2E-03   thickness for layer index no.(8 )


PARAMETERS FROM WHICH A DECISION VAR. MUST NOW BE CHOSEN
VAR. STR/ SEG. LAYER   CURRENT
NO.  RNG  NO.   NO.     VALUE              DEFINITION
 1   STR   0    0    8.0E+00   stiffener spacing, b
 2   STR   0    0    2.5E+00   width of stiffener base, b2
 3   STR   0    0    1.3E+00   height of stiffener, h
 4   STR   0    0    8.0E-01   width of flange of stiffener, w
 5   STR   0    0    1.0E+00   width of hat base, w2
 6   STR   1    1    6.0E-03   thickness for layer index no.(1 )
 7   STR   1    2    6.0E-03   thickness for layer index no.(2 )
14   STR   2    3    2.08E-02  thickness for layer index no.(9 )
15   STR   2    4    5.2E-03   thickness for layer index no.(10)
16   STR   4    3    2.08E-02  thickness for layer index no.(11)
```

$Any more ranges of layer types for default decision variables? = N

$Any more decision variables (Y or N) ?=Y

```
              DECISION VARIABLES CHOSEN SO FAR
VAR. STR/ SEG. LAYER   CURRENT
NO.  RNG  NO.   NO.     VALUE              DEFINITION
 8   STR   1    3    5.2E-03   thickness for layer index no.(3 )
 9   STR   1    4    5.2E-03   thickness for layer index no.(4 )
10   STR   1    5    5.2E-03   thickness for layer index no.(5 )
12   STR   1    7    5.2E-03   thickness for layer index no.(7 )
13   STR   1    8    5.2E-03   thickness for layer index no.(8 )


PARAMETERS FROM WHICH A DECISION VAR. MUST NOW BE CHOSEN
VAR. STR/ SEG. LAYER   CURRENT
NO.  RNG  NO.   NO.     VALUE              DEFINITION
 1   STR   0    0    8.0E+00   stiffener spacing, b
 2   STR   0    0    2.5E+00   width of stiffener base, b2
 3   STR   0    0    1.3E+00   height of stiffener, h
 4   STR   0    0    8.0E-01   width of flange of stiffener, w
 5   STR   0    0    1.0E+00   width of hat base, w2
 6   STR   1    1    6.0E-03   thickness for layer index no.(1 )
 7   STR   1    2    6.0E-03   thickness for layer index no.(2 )
14   STR   2    3    2.08E-02  thickness for layer index no.(9 )
15   STR   2    4    5.2E-03   thickness for layer index no.(10)
16   STR   4    3    2.08E-02  thickness for layer index no.(11)
```

Use an index from the left-hand column of the table above.

$Choose a decision variable (1,2,3,....)=2

$Lower bound of variable no.(2)=1.5

$Upper bound of variable no.(2)=2.5

$Any more decision variables (Y or N) ?=Y

```
            DECISION VARIABLES CHOSEN SO FAR
VAR. STR/ SEG. LAYER  CURRENT
NO.  RNG  NO.  NO.    VALUE        DEFINITION
 2   STR   O    O    2.5E+OO  width of stiffener base, b2
 8   STR   1    3    5.2E-03  thickness for layer index no.(3 )
 9   STR   1    4    5.2E-03  thickness for layer index no.(4 )
10   STR   1    5    5.2E-03  thickness for layer index no.(5 )
12   STR   1    7    5.2E-03  thickness for layer index no.(7 )
13   STR   1    8    5.2E-03  thickness for layer index no.(8 )

PARAMETERS FROM WHICH A DECISION VAR. MUST NOW BE CHOSEN
VAR. STR/ SEG. LAYER  CURRENT
NO.  RNG  NO.  NO.    VALUE        DEFINITION
 1   STR   O    O    8.0E+OO  stiffener spacing, b
 3   STR   O    O    1.3E+OO  height of stiffener, h
 4   STR   O    O    8.0E-01  width of flange of stiffener, w
 5   STR   O    O    1.0E+OO  width of hat base, w2
 6   STR   1    1    6.0E-03  thickness for layer index no.(1 )
 7   STR   1    2    6.0E-03  thickness for layer index no.(2 )
14   STR   2    3    2.08E-02 thickness for layer index no.(9 )
15   STR   2    4    5.2E-03  thickness for layer index no.(10)
16   STR   4    3    2.08E-02 thickness for layer index no.(11)
```

$Choose a decision variable (1,2,3,...)=3

$Lower bound of variable no.(3)=0.8

$Upper bound of variable no.(3)=1.5

$Any more decision variables (Y or N) ?=Y

```
            DECISION VARIABLES CHOSEN SO FAR
VAR. STR/ SEG. LAYER  CURRENT
NO.  RNG  NO.  NO.    VALUE        DEFINITION
 2   STR   O    O    2.5E+OO  width of stiffener base, b2
 3   STR   O    O    1.3E+OO  height of stiffener, h
 8   STR   1    3    5.2E-03  thickness for layer index no.(3 )
 9   STR   1    4    5.2E-03  thickness for layer index no.(4 )
10   STR   1    5    5.2E-03  thickness for layer index no.(5 )
12   STR   1    7    5.2E-03  thickness for layer index no.(7 )
13   STR   1    8    5.2E-03  thickness for layer index no.(8 )

PARAMETERS FROM WHICH A DECISION VAR. MUST NOW BE CHOSEN
VAR. STR/ SEG. LAYER  CURRENT
NO.  RNG  NO.  NO.    VALUE        DEFINITION
 1   STR   O    O    8.0E+OO  stiffener spacing, b
 5   STR   O    O    1.0E+OO  width of hat base, w2
```

```
 4    STR   0   0   8.0E-01   width of flange of stiffener, w
 6    STR   1   1   6.0E-03   thickness for layer index no.(1 )
 7    STR   1   2   6.0E-03   thickness for layer index no.(2 )
14    STR   2   3   2.08E-02  thickness for layer index no.(9 )
15    STR   2   4   5.2E-03   thickness for layer index no.(10)
16    STR   4   3   2.08E-02  thickness for layer index no.(11)
```

- - -MORE DECISION VARIABLES CHOSEN IN THIS SAMPLE CASE- - -

$Any linked variables (Y or N) ?=H

A linked variable is a variable that is not a decision variable, but is proportional to one of the decision variables, thus:

$$(\text{linked variable}) = C * (\text{decision variable})$$

in which C is a constant. For example, material layers with $+ALPHA$ degree orientation are usually matched with layers with $-ALPHA$ degree orientation. Suppose for a certain layer with layup angle $+ALPHA$, this layup angle is chosen as a decision variable. You want another layer in the same laminate to have the layup angle $-ALPHA$. Then, for this other layer

$$(\text{layup angle}) = \text{-1.0} * (\text{layup angle of the layer with } +ALPHA)$$

The layup angle on the left–hand–side of the above equation is called a linked variable because its value is linked to that of the first mentioned layer. The linking constant $C = \text{-1.0}$ in this example.

$Any linked variables (Y or N) ?=Y

```
                 LINKED VARIABLES CHOSEN SO FAR
VAR. STR/ SEG. LAYER  CURRENT
NO.  RNG  NO.   NO.    VALUE           DEFINITION
11   STR   1    6    5.2E-03   thickness for layer index no.(6 )


PARAMETERS FROM WHICH A LINKED VARIABLE MUST NOW BE CHOSEN
VAR. STR/ SEG. LAYER  CURRENT
NO.  RNG  NO.   NO.    VALUE           DEFINITION
 1   STR   0    0    8.0E+00   stiffener spacing, b
 4   STR   0    0    8.0E-01   width of flange of stiffener, w
 7   STR   1    2    6.0E-03   thickness for layer index no.(2 )
15   STR   2    4    5.2E-03   thickness for layer index no.(10)
```

$Choose a linked variable (1,2,3,...)=4

```
LINKED VARIABLE MUST BE LINKED TO ONE OF THE DEC. VAR.
VAR. STR/ SEG. LAYER  CURRENT
NO.  RNG  NO.   NO.    VALUE           DEFINITION
 2   STR   0    0    2.5E+00   width of stiffener base, b2
 3   STR   0    0    1.3E+00   height of stiffener, h
 5   STR   0    0    1.0E+00   width of hat base, w2
```

23

```
  6    STR    1    1    6.0E-03   thickness for layer index no.(1 )
  8    STR    1    3    5.2E-03   thickness for layer index no.(3 )
  9    STR    1    4    5.2E-03   thickness for layer index no.(4 )
 10    STR    1    5    5.2E-03   thickness for layer index no.(5 )
 12    STR    1    7    5.2E-03   thickness for layer index no.(7 )
 13    STR    1    8    5.2E-03   thickness for layer index no.(8 )
 14    STR    2    3    2.08E-02  thickness for layer index no.(9 )
 16    STR    4    3    2.08E-02  thickness for layer index no.(11)
```

$To which variable is this variable linked?=5

$Assign a value to the linking constant, C(4)=0.8

- - - - - - ANOTHER LINKED VARIABLE IS CHOSEN - - - - - -

$Any more linked variables (Y or N) ?=N

```
             LINKED VARIABLES FOR THE OPTIMIZATION PROBLEM
  VAR. STR/ SEG. LAYER  CURRENT
  NO.  RNG  NO.   NO.    VALUE           DEFINITION
   4   STR   0    0    8.0E-01   width of flange of stiffener, w
   7   STR   1    2    6.0E-03   thickness for layer index no.(2 )
  11   STR   1    6    5.2E-03   thickness for layer index no.(6 )
```

$Any escape variables (Y or N) ?=H

> An escape variable is a variable that when increased drives the design toward the feasible region. For example, in designs which are buckling–critical, local and general instability represent two constraint conditions that bound the feasible region. Increasing the thicknesses of any parts while keeping all other dimensions the same drives the design toward the feasible region (makes buckling less critical). Hence, a thickness should always be chosen as an escape variable. Other variables, such as layup angles, should not be used as escape variables, since their increase might well result in a decrease in the buckling load, hence driving the design toward the infeasible region.

$Any escape variables (Y or N) ?=Y

$Want to have escape variables chosen by default?=H

> Generally answer Y. PANDA2 will then automatically choose as escape variables all of the thicknesses that are decision variables. This is usually the best strategy and use of the default option saves you the trouble of doing it interactively.

$Want to have escape variables chosen by default?=Y

```
             ESCAPE VARIABLES FOR THE OPTIMIZATION PROBLEM
  VAR. STR/ SEG. LAYER  CURRENT
  NO.  RNG  NO.   NO.    VALUE           DEFINITION
   6   STR   1    1    6.0E-03   thickness for layer index no.(1 )
   8   STR   1    3    5.2E-03   thickness for layer index no.(3 )
   9   STR   1    4    5.2E-03   thickness for layer index no.(4 )
  10   STR   1    5    5.2E-03   thickness for layer index no.(5 )
  12   STR   1    7    5.2E-03   thickness for layer index no.(7 )
```

24

```
13   STR   1   8   5.2E-03  thickness for layer index no.(8 )
14   STR   2   3   2.08E-02 thickness for layer index no.(9 )
16   STR   4   3   2.08E-02 thickness for layer index no.(11)
```

5.4 FILE PRODUCED DURING INTERACTIVE SESSION IN DECIDE

The interactive session in DECIDE generates the following input file for future runs of DECIDE. This file is called HAT.DEC:

```
Y         $ Do you want a tutorial session and tutorial output?
Y         $ Want to use default for thickness decs. variables?
    3     $ Lowest layer index for default decision variable
    8     $ Highest layer index for default decision variable
N         $ Any more ranges of layer types for defalt dec.var.?
Y         $ Any more decision variables (Y or N) ?
    2     $ Choose a decision variable (1,2,3,...)
  1.5     $ Lower bound of variable no.(2)
  2.5     $ Upper bound of variable no.(2)
Y         $ Any more decision variables (Y or N) ?
    3     $ Choose a decision variable (1,2,3,...)
 0.80     $ Lower bound of variable no.(3)
  1.5     $ Upper bound of variable no.(3)
Y         $ Any more decision variables (Y or N) ?
    5     $ Choose a decision variable (1,2,3,...)
 0.80     $ Lower bound of variable no.(5)
    2     $ Upper bound of variable no.(5)
Y         $ Any more decision variables (Y or N) ?
    6     $ Choose a decision variable (1,2,3,...)
0.006     $ Lower bound of variable no.(6)
0.012     $ Upper bound of variable no.(6)
Y         $ Any more decision variables (Y or N) ?
   14     $ Choose a decision variable (1,2,3,...)
.0052     $ Lower bound of variable no.(14)
.0260     $ Upper bound of variable no.(14)
Y         $ Any more decision variables (Y or N) ?
   16     $ Choose a decision variable (1,2,3,...)
.0052     $ Lower bound of variable no.(16)
.0260     $ Upper bound of variable no.(16)
N         $ Any more decision variables (Y or N) ?
Y         $ Any linked variables (Y or N) ?
    4     $ Choose a linked variable (1,2,3,...)
    5     $ To which variable is this variable linked?
 0.80     $ Assign a value to the linking constant, C(4)
Y         $ Any more linked variables (Y or N) ?
    7     $ Choose a linked variable (1,2,3,...)
    6     $ To which variable is this variable linked?
    1     $ Assign a value to the linking constant, C(7)
N         $ Any more linked variables (Y or N) ?
```

```
Y        $ Any escape variables (Y or N) ?
Y        $ Want to have escape variables chosen by default?
- - - - - - - - - END OF HAT.DEC FILE - - - - - - - - -
```

5.5 OUTPUT FILE PRODUCED BY DECIDE

The following is a partial listing of the file HAT.OPD...

SUMMARY OF INFORMATION FOR OPTIMIZATION ANALYSIS

VAR. NO.	DEC. VAR.	ESCAPE VAR.	LINK. VAR.	LINKED TO	LINKING CONSTANT	LOWER BOUND	CURRENT VALUE	UPPER BOUND	DEFINITION
1	N	N	N	0	0.00E+00	0.00E+00	8.0000E+00	0.00E+00	stiffener spacing, b
2	Y	N	N	0	0.00E+00	1.50E+00	2.5000E+00	2.50E+00	width of stiffener base, b2
3	Y	N	N	0	0.00E+00	8.00E-01	1.3000E+00	1.50E+00	height of stiffener, h
4	N	N	Y	5	8.00E-01	0.00E+00	8.0000E-01	0.00E+00	width of outer flange of stiffener, w
5	Y	N	N	0	0.00E+00	8.00E-01	1.0000E+00	2.00E+00	width of hat base, w2
6	Y	Y	N	0	0.00E+00	6.00E-03	6.0000E-03	1.20E-02	thickness for layer index no.(1)
7	N	N	Y	6	1.00E+00	0.00E+00	6.0000E-03	0.00E+00	thickness for layer index no.(2)
8	Y	Y	N	0	0.00E+00	5.20E-05	5.2000E-03	5.20E-01	thickness for layer index no.(3)
9	Y	Y	N	0	0.00E+00	5.20E-05	5.2000E-03	5.20E-01	thickness for layer index no.(4)
10	Y	Y	N	0	0.00E+00	5.20E-05	5.2000E-03	5.20E-01	thickness for layer index no.(5)
11	N	N	Y	9	1.00E+00	0.00E+00	5.2000E-03	0.00E+00	thickness for layer index no.(6)
12	Y	Y	N	0	0.00E+00	5.20E-05	5.2000E-03	5.20E-01	thickness for layer index no.(7)
13	Y	Y	N	0	0.00E+00	5.20E-05	5.2000E-03	5.20E-01	thickness for layer index no.(8)
14	Y	Y	N	0	0.00E+00	5.20E-03	2.0800E-02	2.60E-02	thickness for layer index no.(9)
15	N	N	N	0	0.00E+00	0.00E+00	5.2000E-03	0.00E+00	thickness for layer index no.(10)
16	Y	Y	N	0	0.00E+00	5.20E-03	2.0800E-02	2.60E-02	thickness for layer index no.(11)

- - - - - - - END OF DECIDE PROCESSING - - - - - - -

6.0 ESTABLISHING LOADS AND STRATEGY IN PANDA2

6.1 INTRODUCTION

Following execution of DECIDE, the user gives the command MAINSETUP. The following is a list of the interactive session that the command MAINSETUP invokes. In this particular session, the user has decided to use the tutorial option for a fixed design (no optimization).

6.2 EXAMPLE: A HAT–STIFFENED PANEL

$MAINSETUP (User establishes loading, type of analysis, and strategy.)

$Do you want a tutorial session and tutorial output? Y

Next, provide in–plane loads, (N_1, N_2, N_{12}) and (N_{10}, N_{20}), which are considered to be applied to the panel edges. These are stress resultants in units, for example, of lb/in.

(N_1, N_2, N_{12}) constitute Load Set A (eigenvalue loads);
(N_{10}, N_{20}) are part of Load Set B (fixed and uniform loads).

In the absence of normal pressure, the loads corresponding to general instability bifurcation buckling are given by:

$$N_x(crit) = N_{10} + \text{eigenvalue} \times \text{Factor-of-safety} \times N_1$$
$$N_y(crit) = N_{20} + \text{eigenvalue} \times \text{Factor-of-safety} \times N_2$$
$$N_{xy}(crit) = \text{eigenvalue} \times \text{Factor-of-safety} \times N_{12}.$$

Also, provide uniform normal pressure, p. In the presence of normal pressure, the loads corresponding to general instability bifurcation buckling are given by:

$$N_x(crit) = N_{10} + N_{10}(p) + \text{eigenvalue} \times \text{Factor-of-safety} \times N_1$$
$$N_y(crit) = N_{20} + N_{20}(p) + \text{eigenvalue} \times \text{Factor-of-safety} \times N_2$$
$$N_{xy}(crit) = \text{eigenvalue} \times \text{Factor-of-safety} \times N_{12}.$$

in which $N_{10}(p)$ and $N_{20}(p)$ are stress resultants induced by the normal pressure.

You are allowed to provide up to 5 load and imperfection sets, that is, up to 5 sets of $(N_1, N_2, N_{12}, N_{10}, N_{20}, p, W_{imp})$. ($W_{imp}$ is a global bowing imperfection, treated as part of the load set because you may want to optimize in the presence of bowing with both positive and negative sign). PANDA2 will generate buckling and stress or strain constraints corresponding to each of the load and imperfection sets that you provide. The resulting design will be the best that PANDA2 can find that is subjected during its mission to all of the load sets and that has bowing imperfections with the signs and amplitudes that you supply.

For each combination (N_1, N_2, N_{12}) you will have to provide two "factors of safety," FSGEN and FSLOC, for general and local buckling. The purpose of these factors is to compensate for initial imperfections. These factors depend on the geometry and loading, and there is a huge literature on the difficult subject of "imperfection sensitivity." A recent survey is contained in the book, COMPUTERIZED BUCKLING ANALYSIS OF SHELLS by David Bushnell, published by Nijhoff and Co., The Netherlands, in 1985 [30].

27

Now, please provide the first Load Set A $(N_1,\ N_2,\ N_{12})$...

$Resultant (e.g.lb/in) normal to the plane of screen,$N_1(1)$=H

What is wanted is the applied line load in the L1 (axial) direction in units of force/length. Negative for compression. If this axial load varies in the L2 (circumferential) direction, use the largest compressive value applied to that edge of the panel. What is wanted now is the axial load in Load Set A, that is, the eigenvalue load: the load to be multiplied by the critical load factor (the eigenvalue) in computations of the critical applied load.

$Resultant (e.g. lb/in) normal to the plane of screen, $N_1(1) = -3000$

$Resultant (e.g. lb/in) in the plane of the screen, $N_2(1)$=H

What is wanted is the applied resultant, N_2, in the L2 (circumferential) direction (units of force/length). Negative for compression. This circumferential load is assumed to be uniform over the entire panel. Again, what is wanted here is the Load Set A (eigenvalue parameter) circumferential stress resultant, N_2.

$Resultant (e.g. lb/in) in the plane of the screen,$N_2(1)$=0

$In–plane shear in load set A, $N_{12}(1)$=H

Positive sense is the same as for the PANDA program. (See Fig. 2 of "PANDA–interactive program...," Computers and Structures, Vol 16, No. 1–4, pp 167–185, 1983). Units are force/length. The in–plane shear is assumed to be uniform over the entire panel. Please note that no fixed in–plane shear component is permitted (N_{120} = 0.)

$In–plane shear in load set A, $N_{12}(1)$=1000

$Does the axial load vary in the L2 direction?=H

The L2 direction is in the plane of the screen (circumferential). If you answer Y you will next be asked to provide values of N_x at the beginning and end of the panel edge which lies in the plane of the screen. PANDA2 assumes that N_x varies linearly across this edge and is uniform in the direction normal to the plane of the screen. If you answer N the axial load will be uniform over the entire panel.

$Does the axial load vary in the L2 direction?=N

$Factor of safety for general instability, FSGEN(1)=H

This factor should account for unknown initial imperfections and the approximate manner in which the general instability load factor is calculated in PANDA2. Panels that buckle locally at loads far below the design load are not particularly sensitive to initial imperfections. For such panels, use

$$1.0 <\quad FSGEN\quad < 1.4$$

Panels designed so that local and general instability loads are nearly equal are somewhat sensitive to initial imperfections, and FSGEN should be about 1.4 even if the panel is flat. Axially stiffened cylinders under axial compression should usually have FSGEN = 2.

Axially compressed monocoque cylinders under axial compression should have FSGEN = 4 if $r/t > 300$; FSGEN= 2 if $r/t < 100$. Cylinders under uniform external pressure

should have FSGEN = 1.4. Cylinders under uniform torsion (in–plane shear) should have FSGEN = 1.3.

NOTE: The above are general guidelines only. For more details, consult the extensive NASA literature, ASME Code Case N–284, and run PANDA with the option to get interaction curves for imperfect shells. Also see COMPUTERIZED BUCKLING ANALYSIS OF SHELLS by David Bushnell, Nijhoff and Co., The Netherlands, 1985 [30].

$Factor of safety for general instability, FSGEN(1)=1

$Factor of safety for local instability, FSLOC(1)=H

By "local" is meant buckling between stringers and rings. Usually, the stringers are closely spaced, so that the portion of shell between them is very flat. In such cases, the structure is stable in the locally post–buckled range and FSLOC should be 1.0.

If your stringers are spaced far apart, so that the panel between them subtends a fairly large angle (greater than 20 degrees, say, then the panel starts to become sensitive to initial imperfections, and FSLOC should be larger than unity. You should consult the literature on this, in particular the book entitled COMPUTERIZED BUCKLING ANALYSIS OF SHELLS by David Bushnell, published by Nijhoff, The Netherlands, 1985 [30].

$Factor of safety for local instability, FSLOC(1)=1

Next, please provide the fixed stress resultants, N_{10} and N_{20}. These are part of the in–plane loads in Load Set B. Note that no fixed in–plane shear resultant, N_{120}, is permitted. The fixed stress resultants, N_{10} and N_{20}, are not multiplied by the eigenvalue (eigenvalue = load factor determined in bifurcation buckling analyses). The critical general instability load can be calculated from:

$$N_x(crit) = N_{10} + N_{10}(p) + \text{eigenvalue} \times \text{Factor-of-safety} \times N_1$$
$$N_y(crit) = N_{20} + N_{20}(p) + \text{eigenvalue} \times \text{Factor-of-safety} \times N_2$$
$$N_{xy}(crit) = \text{eigenvalue} \times \text{Factor-of-safety} \times N_{12}.$$

Note that the fixed loads are added to any stress resultants that are generated by thermal curing of a composite panel. The loads that you are now asked to provide are fixed applied loads. They would arise, for example, in the case of an internally pressurized aircraft fuselage, in which the (N_{10}, N_{20}) from the internal pressure, p $(N_{10} = pr/2; \quad N_{20} = pr)$, are known, fixed quantities acting in addition to unknown (N_1, N_2, N_{12}) generated for example by gust loads.

$Resultant (e.g. lb/in) normal to plane of screen,$N_{10}(1)$=H
Same sign convention as for N_1: positive for tension. This is a Load Set B quantity.

$Resultant (e.g. lb/in) normal to plane of screen,$N_{10}(1)$=0

$Resultant (e.g. lb/in) in the plane of the screen,$N_{20}(1)$=H
Same sign convention as for N_2: positive for tension. This is a Load Set B quantity.

$Resultant (e.g. lb/in) in the plane of the screen,$N_{20}(1)$=0

$Eccentricity of axial loads (usually zero!), $Ecc(1)$**=H**

    Ordinarily, axial loads N_x and N_{xo} act at the neutral surface in the x-direction (axial direction). However, there may be occasions on which you want to specify some other location. The axial load eccentricity is measured from the neutral surface and is positive in the same sense as the coordinate z for the panel module skin segments (segments 1 and 2), that is, positive if the plane of axial load application lies below that of the neutral surface in the x-direction. (SEE FIG. 9).

$Eccentricity of axial loads (usually zero!), $Ecc(1) = 0$

$Uniform applied pressure (positive upward), $p(1)$**=H**

    This pressure p is generally part of Load Set B (fixed loads). Positive pressure always pushes upward. (Please refer to the sketches of the panel module for physical picture of what "upward" means. See Figs. 1, 2, and 8.) If the panel is curved and if stringers are external, positive pressure is inside the cylinder. If the panel is curved and if stringers are internal, positive pressure is outside the cylinder. If there are no stringers, positive pressure is inside the cylinder. Figure 8 shows the sign convention for pressure and curvature.

    Note that this pressure is used primarily for determination of nonlinear bending-stretching of the panel module and of the entire panel. The pressure should not be used to calculate linear, uniform, statically determinate, fixed in–plane resultants, such as $N_{xo} = pr/2$ and $N_{yo} = pr$ for a hydrostatically internally pressurized complete cylindrical shell.

$Uniform applied pressure (positive upward), $p(1)$**=1.0**

$Is the pressure part of Load Set B (generally answer Y!)?=H

    PANDA2 was originally designed in such a way that the pressure is regarded as part of Load Set B (not an eigenvalue parameter). However, it sometimes happens that this leads to negative eigenvalues (negative buckling load factors). In such cases, you will want to make the pressure part of Load Set A, which you do by answering the above question N. However, you should first try the case by answering Y, resorting later to N if negative eigenvalues create a problem or if the following paragraph applies.

    If you are designing decking which is loaded by uniform pressure, you will probably want to make the pressure part of Load Set A, that is, you will probably want to answer Y.

$Is the pressure part of Load Set B (generally answer Y!)?=Y

$Initial bowing imperfection amplitude (type H for sign), $W_{imp}(1) = $ **H**

    Positive W_{imp} is downward in Fig. 9. The imperfection varies as $\sin(\pi x/L)$ in the axial coordinate direction. A positive W_{imp} causes the bottom skin surface to be convex. (The bottom surface is the surface of the skin opposite to that to which the stringers are attached). There is no prestress, either membrane or bending, associated with this bowing imperfection. It is hard to make a general statement whether positive or negative W_{imp} will lead to earlier failure: Positive W_{imp} combined with axial compression tends to cause greater compressive loads in the stringer web and flange and therefore tends to cause earlier buckling and rolling of these parts of the structure;

Negative W_{imp} combined with axial compression tends to cause greater compression in the panel skin and therefore earlier local buckling and higher local bending stresses in the postbuckling regime. It may be a good idea to set up two load cases, both with the same mechanical loads, the first with a positive W_{imp} and the second with a negative W_{imp}. Then the optimized design will be good no matter what the sign of the bowing imperfection is.

$Initial bowing imperfection amplitude, $W_{imp}(1) = 0$.

$Want to provide another load set $(N_1, N_2, N_{12}, N_{10}, N_{20}, p, W_{imp})$?=H
You can provide up to 5 sets of $(N_1, N_2, N_{12}, N_{10}, N_{20}, p, W_{imp})$.

$Want to provide another load set $(N_1, N_2, N_{12}, N_{10}, N_{20}, p, W_{imp})$?=N

$Want to include effect of transverse shear deformation?=H
If you answer Y reduction factors are computed for various kinds of general, semi-general, and local instability and crippling. These factors reduce the eigenvalues computed from classical "normals–remain–normal" shell theory. The reduction factors are based on Timoshenko beam theory. (See pp 132–136 of Timoshenko and Goodier, 2nd edition.) That is, a typical reduction factor has the form:

$$k = 1/[1 + nN_x\lambda/(tG_{13})]$$

in which n is a shape factor (1.2 is now used); N_x is the local stress resultant (lb/in, for example); λ is the critical eigenvalue computed from "normals–remain–normal" theory; t is the local effective thickness of the wall; and G_{13} is the local effective transverse shear stiffness.

$Want to include effect of transverse shear deformation?=Y

$IQUICK = quick analysis indicator (0 or 1)=H
IQUICK = 0 means discrete BOSOR4–type model will be treated.
IQUICK = 1 means only closed–form types of models will be included.
It may be best to start out with IQUICK = 1 and to refine the design later with the longer IQUICK = 0 type of analysis. In any case, before you are done with a case, you must definitely use the IQUICK = 0 option.

$IQUICK = quick analysis indicator (0 or 1)=0

$NPRINT= output index (1=good, 2=debug, 3=too much)=H
Usually use 1. NPRINT = 3 really gets alot of output. NPRINT = 2 yields the C(i,j) matrices, the evolution of eigenvalues during inverse power iterations, local buckling modal displacements, and redistributed loads due to bowing and local postbuckling behavior. Do not use 2 if you are doing an optimization analysis.

$NPRINT= output index (1=good, 2=debug, 3=too much)=1

$Choose type of analysis (1=opt., 2=fixed design)=H
1 means an optimization analysis will be performed. Note that you must have previously chosen decision variables in a DECIDE run!

2 means PANDA2 will perform a buckling analysis of a fixed design.

$Choose type of analysis (1=opt., 2=fixed design)=2

$Do you want plots (Y or N) ?=Y

$Do you want to vary N for minimum local buckling load?=H
> N is the number of axial half-waves in the local buckling mode. Computer time can be saved if you are confident that the number of axial halfwaves N that you next choose is truly the critical value for local skin buckling. Generally answer Y.

$Do you want to vary N for minimum local buckling load?=Y

$Do you want to choose a starting N for local buckling?=H
> N is the number of axial halfwaves between adjacent rings, or if no rings are present, along the entire axial length of the panel. PANDA2 starts with N calculated from the formula:

$$N = (C(5,5)/C(4,4)) \times (\text{axial length between rings})/$$
$$(\text{stringer spacing - stringer base width}) + 2$$

> which is based on experimental observations that local buckles of uniformly axially compressed long, narrow, isotropic plates are almost square. However, from previous experience on this and other similar cases, you may wish to use a different starting value for N. Generally you should answer this question N for "no".

$Do you want to choose a starting N for local buckling?=N

$Factor of safety for stress, FSSTR=H
> This factor should account for the fact that the theory used to calculate stress, expecially if local buckling of the skin occurs well below the design load, is approximate. The failure criterion is also approximate. Use

$$1.0 < FSSTR < 1.5$$

$Factor of safety for stress, FSSTR=1

$Do you want to allow local buckling of the skin?=H
> A panel can be designed so that the skin between stiffeners buckles locally at loads well below the design allowable. If you wish to permit local buckling in the design, answer Y. The analysis will then account for the effect of local skin buckling on the overall stiffness of the panel and will calculate stresses in the locally postbuckled skin. The buckling load factor corresponding to local buckling will NOT constrain the design.
>
> If you answer N, local skin deformations and stresses, as well as effective stiffnesses of locally deformed skin, will still be calculated, but the buckling load factor corresponding to local buckling between stringers WILL constrain the design.

$Do you want to allow local buckling of the skin?=Y

$Do you want wide-column buckling to constrain the design?=H
> If the panel is flat you should probably answer Y. If the panel is cylindrical (curvature in the plane of the screen) the wide-column buckling load may be too conservative, leading to unnecessarily heavy designs. If, for a curved panel, you answer Y, then you will not have to worry as much about the effect of initial imperfections as you would

if you answer N, because the wide-column buckling load is not sensitive to initial geomtrical imperfections if there is little or no interaction between local and general buckling. This is a difficult and not very well understood area in the field of shell buckling. Actually, I recommend that you design a panel first with use of the wide-column model of general instability and then without this model. In any case, check your general instability load when you finish optimizing by running PANEL, which sets up a discretized model of the entire panel width with stringers treated as shell branches. If this PANEL model has a load factor corresponding to general instability less than unity, you need either to include the wide-column model as a constraint or increase the factor of safety.

$Do you want wide-column buckling to constrain the design?=Y

$Want to include curvature in local buckling analysis (N)?=H

It is safest to answer N. If the stringers on a cylindrical shell are spaced rather far apart, you may want to try a run in which the curvature is included in the local buckling analysis. However, if you are designing something it is best to neglect this curvature. The post-local buckling analysis does not account for it. You would have to provide a more severe knockdown factor if you answer this question Y than you would if you answer this question N. Please be careful!

$Want to include curvature in local buckling analysis (N)?=N

$Initial local imperfection amplitude (must be positive), W_{loc}=H

In PANDA2 the local imperfection is assumed to have the same shape as the local buckling mode. Use a positive number for the amplitude, W_{loc}. If you use zero, an amplitude equal to one-tenth of the panel thickness will be assumed.

$Initial local imperfection amplitude (must be positive), W_{loc} = 0.00001

- - - END OF INTERACTIVE SESSION FOR MAINSETUP - - -

6.3 FILE GENERATED DURING THE INTERACTIVE SESSION IN MAINSETUP

The interactive session just completed yields the following file, which is called HAT.OPT:

```
    Y        $ Do you want a tutorial session and tutorial output?
 -3000       $ Resultant (e.g. lb/in) normal to the plane of screen, N1( 1)
    0        $ Resultant (e.g. lb/in) in the plane of the screen,    N2( 1)
 1000        $ In-plane shear in load set A,                         N12( 1)
    N        $ Does the axial load vary in the L2 direction?
   1.0       $ Factor of safety for general instability, FSGEN( 1)
    1        $ Factor of safety for local instability, FSLOC( 1)
    0        $ Resultant (e.g. lb/in) normal to the plane of screen, N10( 1)
    0        $ Resultant (e.g. lb/in) in the plane of the screen,    N20( 1)
    0        $ Eccentricity of axial loads (usually zero!), Ecc( 1)
   1.0       $ Uniform applied pressure (positive upward), p( 1)
    Y        $ Is the pressure part of Load Set B (generally answer Y!)?
   0.0       $ Initial bowing imperfection amplitude, Wimp( 1)
    N        $ Want to provide another set(N1, N2, N12, N10, N20, p, Wimp)?
```

```
Y        $ Want to include effect of transverse shear deformation?
0        $ IQUICK = quick analysis indicator (0 or 1)
1        $ NPRINT= output index (1=good, 2=debug, 3=too much)
2        $ Choose type of analysis (1=opt., 2=fixed design)
Y        $ Do you want plots (Y or N) ?
Y        $ Do you want to vary N for minimum local buckling load?
N        $ Do you want to choose a starting N for local buckling?
1        $ Factor of safety for stress, FSSTR
Y        $ Do you want to allow local buckling of the skin?
Y        $ Do you want wide-column buckling to constrain the design?
N        $ Want to include curvature in local buckling analysis (N)?
0.00001 $ Initial local imperfection amplitude (positive), Wloc
```

- - - - END OF PROCESSING BY MAINSETUP - - - - - - -

7.0 PANDA2 MAINPROCESSOR FLOW OF CALCULATIONS

7.1 INTRODUCTION

Next, the user launches a batch run of the PANDA2 mainprocessor by typing the command PANDAOPT. The following is a modified list of the file HAT.OPM, which contains the results of this tutorial run. Please note that these results correspond to a hat–stiffened panel that had been optimized in previous runs. The starting design is given in the section on BEGIN and the final design is given in the following. The tutorial output has been modified to make it more suitable for presentation in a paper (introduction of section numbers, etc.).

```
BEGINNING OF TUTORIAL RUN....

*********** LOAD SET NO. 1  **************
APPLIED LOADS IN LOAD SET A ("eigenvalue" loads):
    Applied      axial       stress resultant, N1= -3.0000E+03
    Applied circumferential stress resultant, N2= -3.1623E+00
    Applied    in-plane      shear  resultant,N12=  1.0000E+03

APPLIED LOADS IN LOAD SET B ( fixed uniform loads):
    Applied      axial       stress resultant,N10=  0.0000E+00
    Applied circumferential stress resultant,N20=  0.0000E+00
    Applied    in-plane      shear  resultant,N120=  0.0000E+00
    Applied pressure (positive for internal), P =  1.0000E+00
```

The following calculations are performed for each of up to five sets of user–supplied in-plane loads, N_x, N_y, and N_{xy}, and pressure, p. These calculations are performed in SUBROUTINE STRUCT, which is the structural analyzer in the PANDA2 mainprocessor.

7.2 SIGN CONVENTIONS FOR VARIOUS TYPES OF PANEL ANALYSIS PERFORMED BY PANDA2

It is important to document the sign conventions used for stress resultants; moments; strains; changes in curvature; panel curvature; normal displacement; coordinate, z, normal to the reference surface of each segment of the panel module cross section; coordinate, x, along the panel axis (normal to the screen); coordinate y (in the plane of the screen); and coordinate, s, along the reference surface of each segment in the panel module cross section. These sign conventions are defined here. Also defined here is the convention for numbering the layers in each segment of the panel module cross section. A typical panel module is depicted in Figs. 9 and 10.

The PANDA2 system consists of elements of three analyses, each of which has slightly different sign conventions:

(1) BOSOR4–type models of discretized panel modules
(2) PANDA–type models (closed form buckling formulas)
(3) BOSOR4–type model of discretized entire panel span with smeared stiffeners

33

Figures 9 and 10 show a typical panel module. For analysis type (1), BOSOR4–type models of discretized panel modules, the sign convention is described below the figures.

SEGMENT NO. 4
(FLANGE)

SEGMENT NO. 3
(WEB)

z COORDINATE

SEGMENT NO. 2
(BASE)

SEGMENT NO. 1
(SKIN)

SEGMENT NO. 5
(SAME AS SEGMENT NO. 1)

b2

MODULE WIDTH = STIFFENER SPACING, b

s COORDINATE (MEASURED ALONG THE REFERENCE
SURFACE OF EACH SEGMENT)

y COORDINATE ← (MEASURED FROM STRINGER WEB
LINE OF ATTACHMENT, OR IN
CASE OF HAT, FROM THE STRINGER
CENTERLINE. USED IN PANDA
TYPE ANALYSIS.)

z COORDINATE (z IS MEASURED FROM MIDDLE SURFACE OF EACH
SEGMENT IN THE PANEL MODULE CROSS SECTION
AND IS POSITIVE AS SHOWN)

x COORDINATE IS NORMAL TO SCREEN AND POSITIVE OUT OF
THE SCREEN

Fig. 9 Typical panel module cross section, coordinates, segments, nomenclature.

The (s, x, z) coordinate system is local to each panel module segment and forms a right-handed system in each module segment. The (x, y, z) coordinate system is used in the PANDA–type of analysis. It is shown in the paper, "PANDA– interactive program for minimum weight design of stiffened cylindrical panels and shells." Computers and Structures, Vol. 16, No. 1–4, pp 167–185, 1983.
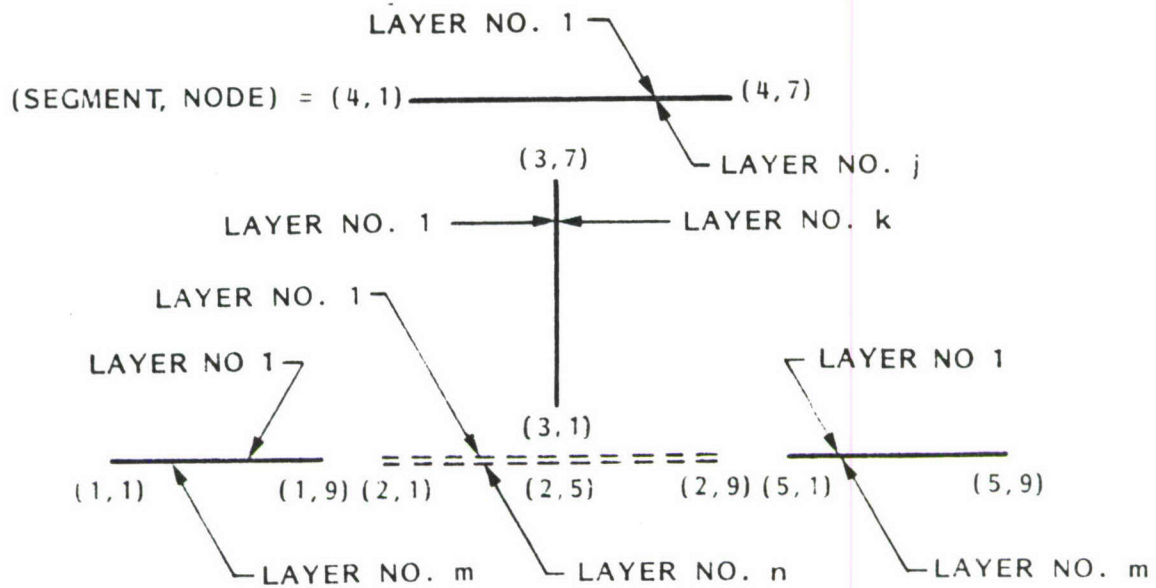
Fig. 10 Exploded view, showing layers and (Segment, Node) numbers.

Positive pressure pushes up on the panel module shown in Fig. 9. The pressure acts only on the skin (Segments 1, 2, and 5 in Fig. 10. Figure 8 shows the sign convention for pressure. The axial load, N_x, is normal to the plane of the screen and positive for tension. Units of this load are force/(length of s coordinate). The hoop or circumferential load, N_y, acts parallel to the plane of the screen and is positive for tension. The units of this load are force/(length of x coordinate) Positive N_{xy} is shown in Fig. 2 of the paper: D. Bushnell, "PANDA–interactive program for minimum weight design of stiffened cylindrical panels and shells", Computers and Structures, Vol. 16, No. 1–4, pp. 167–185, 1983 [1]. It is also shown in Fig. 11, below, along with x and y coordinates and positive winding angle. Positive reference surface strains, e_x and e_y, are tensile. Positive e_{xy} follows from positive N_{xy}. Positive axial moment, M_x, causes compression in the fibers normal to the screen at the bottom of Fig. 9 and tension in the fibers at the top of Fig. 9 That is, the bottom surface of the panel module becomes concave under positive M_x.

Positive change in axial curvature, k_x, has the same effect as positive axial moment, M_x. The bottom surface becomes concave. Positive hoop (circumferential) moment, M_y, causes compression in the fibers parallel to the plane of the screen at the bottom of Fig. 9 and tension in the fibers at the top of Fig. 9. That is, the bottom surface of the panel module sketched in Fig. 9 becomes concave under positive M_y. Positive change in hoop (circumferential) curvature has the same effect as positive hoop moment, M_y.

Positive twisting moment, M_{xy}, tends to force the left side of Fig. 9 downward and the right side of Fig. 9 upward. The twisting angle increases anticlockwise as we proceed

35

out of the screen, that is along the increasing x coordinate. Positive twist, k_{xy}, has the same effect as positive M_{xy}.
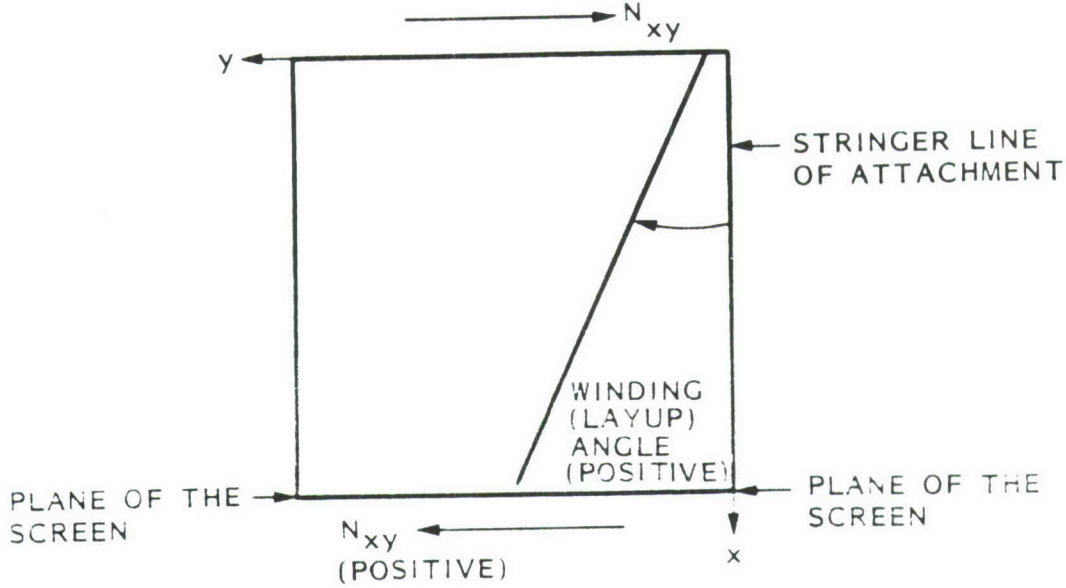
Fig. 11 Positive in-plane shear, winding (layup) angle.

For the discretized panel module model the following kinematic expressions hold:

$$\text{axial change in curvature,} \quad k_x = w_{,xx}$$
$$\text{hoop change in curvature,} \quad k_y = w_{,yy} \tag{7.1}$$
$$\text{twist,} \quad k_{xy} = -2w_{,xy}$$

Strains anywhere in the module cross section are given by:

$$e_x(z) = e_x(\text{ref. surf.}) - zk_x(\text{ref. surf.})$$
$$e_y(z) = e_y(\text{ref. surf.}) - zk_y(\text{ref. surf.}) \tag{7.2}$$
$$e_{xy}(z) = e_{xy}(\text{ref. surf.}) + zk_{xy}(\text{ref. surf.})$$

For cylindrical panels, positive curvature means that the panel skin in the module shown in Fig. 9 is concave downward, that is, Segments 1, 2, and 5 in Fig. 9 are concave downward. The generators of the cylinder are normal to the screen. Figure 8 shows the sign convention for curvature and pressure. The user always supplies a positive number for radius of curvature, and the sign of the curvature in the PANDA2 model depends upon whether the user specifies "external" or "internal" for stringers. If there are no stringers, the curvature is positive.

Positive normal deflection in each panel module segment is in the same direction as positive z. Positive u is in the same direction as positive s. These two displacment

36

components lie in the plane of the screen or parallel to the plane of the screen. Positive axial displacement v is normal to the screen, and is out of the screen (toward the viewer), in the same direction as positive x. The kinematic expressions for each panel module segment are analogous to Eqs. (7.1) and (7.2). The coordinate y is replaced by the coordinate s (Fig. 9).

In PANDA2 the layers of the panel skin (Segments 1, 2, and 5 in Fig. 10) are numbered from the top to the bottom. In all segments of the panel module, layer no. 1 is the leftmost layer as we face in the direction of increasing s coordinate, and layer no. NLAYERS is the rightmost layer.

In the analysis of the entire panel with smeared stiffeners and discretized span (span refers to the length of panel edge in the plane of the screen), a positively curved cylindrical panel is again concave downward, with the curved edges being the edge that lies in the plane of the screen at $x = 0$ and the opposite edge at $x = L$, where L is the length of the panel in the direction of the generators of the cylinder, which is normal to the screen.

7.3 SUMMARY OF COMPUTATIONS REQUIRED FOR EACH DESIGN MODIFICATION

The following is a list of computations which must be performed for each load combination every time the panel design is modified and when design sensitivities (gradients of design constraint conditions and objective function) are being generated:

1. calculation of residual state of the panel after cure and before application of any load.

2. calculation of the prebuckled state of the panel after application of the load. The goal of this step is to determine the distribution of stress resultants over the cross section of the panel module. For each of up to five combinations of $(N_x, N_y, N_{xy}, \text{and } p)$, there may exist two load sets: Load Set A, which includes all loads associated with eigenvalues (load factors for buckling), and Load Set B, which includes all constant (non–eigenvalue) loads. The static response to uniform normal pressure, p, is calculated from nonlinear geometric theory (moderately large rotations).

3. calculation of local buckling (minimization with respect to axial wave number n is required). Two ranges of number of axial waves are checked, a high–n range and a low–n range.

4. calculation of local post buckling behavior from Koiter theory.

5. calculation of stress components in material coordinates and establishment of minimum stress margins (5 margins required for each material type: tension and compression parallel and perpendicular to the fibers and in–plane shear).

6. calculation of general buckling, including the deleterious effect of locally post-buckled skin (reduced tangent stiffness) and nonuniformity of stress resultants distributed over the cross section of the panel.

7. calculation of crippling load factors for the stiffener parts.

8. calculation of the current weight of the panel.

37

8.0 CALCULATION OF CONSTITUTIVE MATRICES C(i,j) FOR EACH PANEL MODULE SEGMENT AND $C_s(i,j)$ FOR THE PANEL WITH SMEARED STIFFENERS

8.1 CALCULATION OF $C(i,j)$ AND THERMAL RESULTANTS IN EACH MODULE SEGMENT

First, calculate the integrated constitutive coefficients, $C(i,j)$, for each segment of the panel module $(i,j = 1,2,..6)$; ("panel module" is defined in Figs. 12 and 13). Calculate thermal resultants, THERM(i), i=1,2,..6, for each segment of the panel module; calculate $C_s(i,j)$, THERMS(i,j) for the panel with smeared stiffeners. Calculate local and general thermal strains. (first call to SUBROUTINE GETCIJ in SUBROUTINE STRUCT)

The stiffened panel is considered to be divided into several identical modules, as follows:
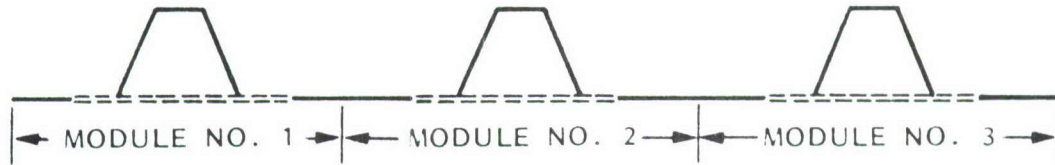
Fig. 12 Panel with three hat modules.

THIS ANALYSIS IS FOR A MODULE WITH HAT SHAPED (TRAPEZOIDAL) STIFFENER...
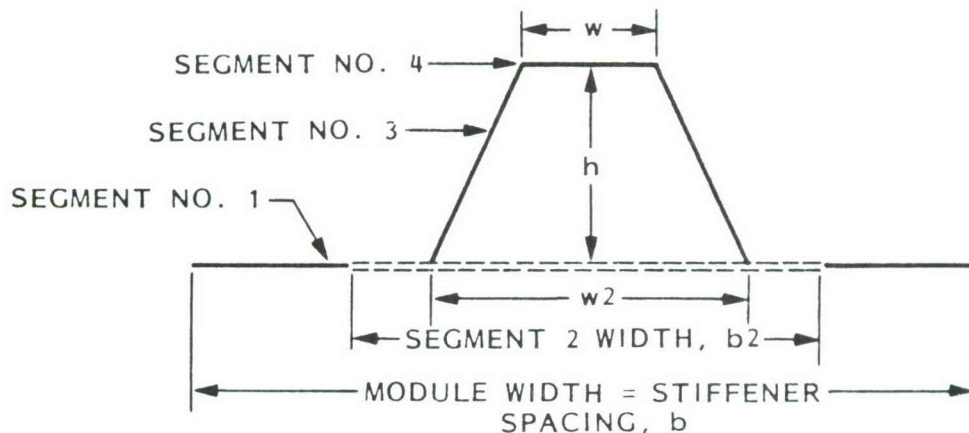
Fig. 13 Single panel module with hat stiffener.

The constitutive law used in PANDA2 for all segments is based on the principle of shell theory in which the stress–strain relationship is integrated through the thickness. In SUBROUTINE GETCIJ we seek the 6x6 matrix $C(i,j)$ and the 6–component vector

$N_T(i)$, which for each segment of the single panel module occur in the thickness–integrated stress–strain relationship thus:

$$
\begin{Bmatrix} N_x \\ N_s \\ N_{xs} \\ M_x \\ M_s \\ M_{xs} \end{Bmatrix} = \begin{bmatrix} C_{11} & C_{12} & C_{13} & C_{14} & C_{15} & C_{16} \\ C_{21} & C_{22} & C_{23} & C_{24} & C_{25} & C_{26} \\ C_{31} & C_{32} & C_{33} & C_{34} & C_{35} & C_{36} \\ C_{41} & C_{42} & C_{43} & C_{44} & C_{45} & C_{46} \\ C_{51} & C_{52} & C_{53} & C_{54} & C_{55} & C_{56} \\ C_{61} & C_{62} & C_{63} & C_{64} & C_{65} & C_{66} \end{bmatrix} \begin{Bmatrix} e_x \\ e_s \\ e_{xs} \\ k_x \\ k_s \\ k_{xs} \end{Bmatrix} - \begin{Bmatrix} N_{tx} \\ N_{ts} \\ N_{txs} \\ M_{tx} \\ M_{ts} \\ M_{txs} \end{Bmatrix} \tag{8.1}
$$

in which $N = N_x, N_s, N_{xs}, M_x, M_s, M_{xs}$ are the stress and moment resultants in any panel module segment; $[C]$ is the 6x6 integrated constitutive law; $E = e_x, e_s, e_{xs}, k_x, k_s, k_{xs}$ are the strains and changes in curvature of the reference surface of the corresponding panel module segment; and $N_T = N_{tx}, N_{ts}, N_{txs}, M_{tx}, M_{ts}, M_{txs}$ are the thermal stress and moment resultants due to curing the composite material panel.

For all panel module segments PANDA2 uses the middle surface of each segment wall as the reference surface for that segment. The same reference surface is used for all segments that comprise the panel skin.

We also need the thermal strains and changes in curvature E_T that would occur if each segment of the panel module were free to strain and warp after curing by itself. These 6 quantities are derived from the constitutive law above by setting $N = N_x, N_s, N_{xs}, M_x, M_s, M_{xs}$ equal to zero and solving for $E_T = e_x, e_s, e_{xs}, k_x, k_s, k_{xs}$:

$$
E_T = [C]^{-1} N_T \tag{8.2}
$$

If the panel is stiffened by both stringers and rings, then $[C], N_T$, and E_T are calculated for two panel module configurations: (1) the panel module that represents a cross section normal to the x–axis and, (2) the panel module that represents a cross section normal to the y–axis.

In addition to the integrated constitutive matrix $[C]$, thermal loads N_T, and thermal deformations E_T for each segment of each panel module, the PANDA2 analysis requires analogous quantities $[C_s], N_{Ts}$, and E_{Ts}, for the panel with smeared stiffeners. These quantities are also computed in SUBROUTINE GETCIJ. Quantities are calculated for the panel with stringers smeared (between rings); for the panel with rings smeared (between stringers); and for the panel with both stringers and rings smeared. The panel deformations E_{Ts} caused by curing are calculated in SUBROUTINE STRTHM, which is called by SUBROUTINE GETCIJ. These calculations are described in Section 8.4.

8.2 REDUCTION FACTORS FOR TRANSVERSE SHEAR DEFORMATION

In order to determine appropriate knockdown factors for the weakening effect of transverse shear deformation, integrated stiffnesses for transverse shear deformation are required. These coefficients are calculated in SUBROUTINE GETCIJ. It is assumed that the reduction factor for a plate is the same as it is for a Timoshenko beam. The equation for the reduction or knockdown factor, given by Timoshenko and Goodier, 2nd edition, pp. 132–135, is:

Reduction factor for axially compressed wide column =

$$K = 1/[1 + nN(\text{EULER})/(t_{eff}G_{eff})] \tag{8.3}$$

in which n is a shape factor (1.2 for homogeneous sheet); $N(\text{EULER})$ is the critical axial stress resultant from Kirchoff theory; T_{eff} is the effective wall thickness (simply the total wall thickness in our case); and G_{eff} is the effective transverse shear stiffness.

For a layered medium, G_{eff} is assumed to be given by:

$$G_{eff} = \frac{T_{eff}}{\sum_{i=1}^{nlayers}[t(i)/G_{13}(i)]} \tag{8.4}$$

in which $t(i)$ is the thickness of the ith layer and $G_{13}(i)$ is the transverse shear stiffness of the ith layer measured in the axial-circumferential (panel) coordinate system rather than in the material coordinate system.

For biaxial loading with or without in-plane shear loading, the "effective" knockdown factor, KSTAR, is derived assuming that the interaction relation between the three in-plane loading components N_x, N_y, N_{xy}, is given by:

$$(N_x/N_{xcr})^2 + (N_y/N_{ycr})^2 + (N_{xy}/N_{xycr})^2 = 1 \tag{8.5}$$

We assume that the "effective" knockdown factor for transverse shear deformation weakening, KSTAR, can by derived from:

$$(1 - KSTAR)^2 = (1 - K_x)^2 + (1 - K_y)^2 + (1 - K_{xy})^2 \tag{8.6}$$

in which K_x is the transverse shear deformation weakening knockdown factor for compression in the x-direction (axial compression); K_y is the knockdown factor for compression in the y-direction; and K_{xy} is the knockdown factor for in-plane shear.

The computations for G_{eff} and T_{eff} occur in SUBROUTINE GETCIJ. The computations for KSTAR occur in SUBROUTINE SHRRED, which is called by subroutines that calculate bifurcation buckling loads neglecting transverse shear deformation effects (GENSTB and LOCAL).

40

8.3 EXAMPLE: THE $C(i,j)$ FOR THE SEGMENTS IN THE HAT–STIFFENED MODULE SHOWN IN FIG. 13

CONSTITUTIVE MATRIX C(i,j) FOR SKIN-STRINGER MODULE   THERMAL {NT} ETHERM {ET}

UNIQUE SKIN-STRINGER MODULE SEGMENT NO. 1:   PANEL SKIN   THERMAL {NT} ETHERM {ET}

```
  7.2450E+05   2.3621E+05  -9.1024E-05  -1.2207E-03  -2.4414E-04   2.3668E-06     -3.3247E+02  -3.1369E-04
  2.3621E+05   6.2738E+05  -1.1978E-02  -2.4414E-04  -9.7656E-04  -1.3759E-05     -3.5351E+02  -4.4537E-04
 -9.1024E-05  -1.1978E-02   2.5017E+05   2.3668E-06  -1.3759E-05  -1.2207E-04      0.0000E+00  -2.1438E-11
 -1.2207E-03  -2.4414E-04   2.3668E-06   2.6910E+02   1.8285E+02   9.2078E+00      3.5763E-07  -3.2733E-10
 -2.4414E-04  -9.7656E-04  -1.3759E-05   1.8285E+02   3.7425E+02   9.2078E+00      3.5763E-07  -2.5126E-10
  2.3668E-06  -1.3759E-05  -1.2207E-04   9.2078E+00   9.2078E+00   1.8411E+02      0.0000E+00  -3.1429E-13
```

UNIQUE SKIN-STRINGER MODULE SEGMENT NO. 2: STRINGER BASE   THERMAL {NT} ETHERM {ET}

```
  1.9945E+06   2.6594E+05  -1.8197E-04  -4.1504E-03  -7.3242E-04   6.6235E-06     -5.2284E+02  -1.5941E-04
  2.6594E+05   9.2449E+05  -2.0046E-02  -7.3242E-04  -3.6621E-03  -2.0709E-06     -7.5466E+02  -7.7045E-04
 -1.8197E-04  -2.0046E-02   3.0113E+05   6.6235E-06  -2.0709E-06  -1.4648E-03      0.0000E+00  -5.1385E-11
 -4.1504E-03  -7.3242E-04   6.6235E-06   3.8020E+03   7.1145E+02   9.2078E+00      4.0531E-06   6.1046E-10
 -7.3242E-04  -3.6621E-03  -2.0709E-06   7.1145E+02   1.6262E+03   9.2078E+00      4.5300E-06   7.1182E-10
  6.6235E-06  -2.0709E-06  -1.4648E-03   9.2078E+00   9.2078E+00   7.5111E+02      0.0000E+00  -1.6928E-11
```

UNIQUE SKIN-STRINGER MODULE SEGMENT NO. 3: STRINGER WEB   THERMAL {NT} ETHERM {ET}

```
  1.5331E+05   1.1971E+05   0.0000E+00   2.4414E-04   1.8311E-04   0.0000E+00     -1.1057E+02  -4.0500E-04
  1.1971E+05   1.5331E+05   0.0000E+00   1.8311E-04   2.4414E-04   0.0000E+00     -1.1057E+02  -4.0500E-04
  0.0000E+00   0.0000E+00   1.1699E+05   0.0000E+00   0.0000E+00   1.8311E-04      0.0000E+00   0.0000E+00
  2.4414E-04   1.8311E-04   0.0000E+00   7.3589E+00   5.7461E+00   0.0000E+00     -1.4901E-07   1.8331E-09
  1.8311E-04   2.4414E-04   0.0000E+00   5.7461E+00   7.3589E+00   0.0000E+00     -1.4901E-07   1.8331E-09
  0.0000E+00   0.0000E+00   1.8311E-04   0.0000E+00   0.0000E+00   5.6156E+00      0.0000E+00   0.0000E+00
```

UNIQUE SKIN-STRINGER MODULE SEGMENT NO. 4: STRINGER FLANGE   THERMAL {NT} ETHERM {ET}

```
  1.4453E+06   1.5581E+05  -4.5473E-04  -9.8877E-03  -1.7090E-03   2.5011E-12     -3.9594E+02  -2.0172E-04
  1.5581E+05   7.6427E+05  -2.0809E-02  -1.7090E-03  -4.5166E-03   1.1642E-10     -5.4348E+02  -6.6999E-04
 -4.5473E-04  -2.0809E-02   1.7887E+05   2.5011E-12   1.1642E-10  -1.4648E-03      0.0000E+00  -7.8457E-11
 -9.8877E-03  -1.7090E-03   2.5011E-12   1.3085E+03   3.2662E+02  -2.2235E-07      2.3842E-06  -2.5881E-10
 -1.7090E-03  -4.5166E-03   1.1642E-10   3.2662E+02   7.0713E+02  -1.0175E-05      2.3842E-06  -1.2757E-09
  2.5011E-12   1.1642E-10  -1.4648E-03  -2.2235E-07  -1.0175E-05   3.3652E+02      0.0000E+00  -1.4698E-16
```

8.4 SMEARING THE STIFFENER BASES AND STIFFENERS

Calculations now proceed inside SUBROUTINE GETCIJ, just before the first of three calls to SUBROUTINE SMRCIJ: In the first call to SUBROUTINE SMRCIJ the stringers are smeared out, and $[C]$, N_T, E_T, T_{eff}, and G_{eff} are computed as if the panel had no transverse stiffeners (rings). The smeared–stringer quantities are stored in arrays and vectors according to the following:

$[C]$ is stored in CX(i,j,5)

N_T is stored in THERMX(i,5)

E_T is stored in ETHRMX(i,5)

T_{eff} is stored in TEFF(1)

G_{eff} is stored in GTX(m,5); m=1 for G_{13}, m=2 for G_{23}

41

In the second call to SUBROUTINE SMRCIJ the rings are smeared out, and $[C]$, N_T, E_T, T_{eff}, and G_{eff} are computed as if the panel had no axial stiffeners (stringers). The smeared–ring quantities are stored in arrays and vectors according to the following:

$[C]$ is stored in CY(i,j,5)

N_T is stored in THERMY(i,5)

E_T is stored in ETHRMY(i,5)

T_{eff} is stored in TEFF(2)

G_{eff} is stored in GTY(m,5); m=1 for G_{13}, m=2 for G_{23}

In the third call to SUBROUTINE SMRCIJ both stringers and rings are smeared out, and $[C]$, N_T, E_T, T_{eff}, and G_{eff} are stored in arrays and vectors according to the following:

$[C]$ is stored in CS(i,j)

N_T is stored in THERMS(i)

E_T is stored in ETHRMS(i)

G_{eff} is stored in GTS(m); m=1 for G_{13}, m=2 for G_{23}

The smearing process is based upon the following assumptions:

(1) No in–plane shear load is carried by stiffener webs or flanges that stand out from the panel skin wall. No in–plane transverse load is carried by these segments either; they carry load only along their axes. (Note that this entire discussion about the $C(i,j)$ holds only for the models in which the stiffeners are smeared out, not for the discretized, branched single module models. Also, it holds only for the phase of the problem in which the skin between stringers is unbuckled.)

(2) The in–plane shear resultant is constant throughout the panel skin, both in the thin and in the thick parts of this skin.

(3) The axial membrane strain component, e_x, is the same in the thin part of the skin and in the part where the stringer bases exist. (This statement of course does not apply when Koiter post–local–buckling theory is being discussed. We are dealing in SUB-ROUTINE GETCIJ only with the unbuckled panel stiffnesses. However, it is always true that the end shortening is the same in the thin part of the skin and in the part where the stringer bases exit.)

(4) The change in axial curvature, k_x, is the same in the unbuckled thin part of the skin and in the part where the stringer bases exist.

(5) The circumferential membrane strain component, e_y, is the same in the unbuckled thin part of the skin and in the part where the ring bases exist.

(6) The circumferential change in curvature, k_y, is the same in the unbuckled thin part of the skin and in the part where the ring bases exist.

(7) Transverse shear stiffness is governed by panel module segment no. 1 (thin part of skin) and stiffener segments 3 and 4: The effect of transverse shear deformation weakening

on the thickened areas under the stiffeners (segment 2) is assumed to be the same as that in segment 1.

(8) For hat stiffeners, the torsional rigidity calculated from the enclosed–area shear flow formula, valid only if there is no local deformation of the hat cross section in the buckling mode, is "knocked down" by a factor $\phi = 0.3$. This factor was established as being reasonable during buckling analysis and tests of aluminum semi–sandwich corrugated cylindrical shells. The work is documented in the JOURNAL OF SPACECRAFT AND ROCKETS (AIAA): "Local and general buckling of axially compressed, semi–sandwich, corrugated, ring- stiffened cylinders", David Bushnell, J. Spacecraft and Rockets, Vol. 9, No. 5, pp 357–363, May 1972.

The following derivation refers to a "panel module". A "panel module" is defined in Fig. 12 and 13. If stiffeners run both ways there are two modules:

   (1) the module whose cross section is perpendicular to the x axis,
   (2) the module whose cross section is perpendicular to the y axis.

In the plan view shown in Fig. 14, both "x" and "y" modules appear. The horizontal dimension of the figure is the stringer spacing and the vertical dimension is the ring spacing.

The starting point for derivation of the constitutive law for the panel module with stringers and rings with thickened bases is the mathematical expression of equilibrium of resultants N_x and N_y [Equations (8.7) and (8.8) below] and of moments M_x and M_y [Equations (8.9) and (8.10) below]. These equilibria are written in terms of the forces and moments in the various panel module parts:

   Part (1) = panel skin,
   Part (2) = stringer base and stringer web(s) and flange,
   Part (3) = ring base and ring web(s) and flange, and
   Part (4) = the region where ring and stringer bases overlap.

A plan view of the panel module with stringer and ring bases is depicted in Fig. 14.

We know that if we "cut" along the lower horizontal edge of the panel module sketched in Fig. 14, the average axial resultant will be equal to the applied axial resultant, N_x. The left–hand side of Eq.(8.7) below expresses this average axial resultant.

Similarly, along the same edge the average moment resultant is equal to the applied moment resultant, M_x. The left–hand side of Eq.(8.9) below expresses this average moment resultant, M_x.

Also, if we "cut" horizontally along the y axis in Fig. 14, the average axial resultant must again be equal to the applied resultant, N_x, and the average moment must be equal to the applied moment, M_x. These average loads are expressed in the right–hand sides of Eqs.(8.7) and (8.9), respectively.

Now we can express analogous relationships for vertical "cuts" along the left–hand side of the figure above and along the x–axis. The average stress resultant along both vertical "cuts" must equal the applied hoop resultant, N_y; the average moment resultant

43

along both vertical "cuts" must equal the applied moment resultant, M_y. Equations (8.8) and (8.10) below express these force and moment equilibria (continuity).
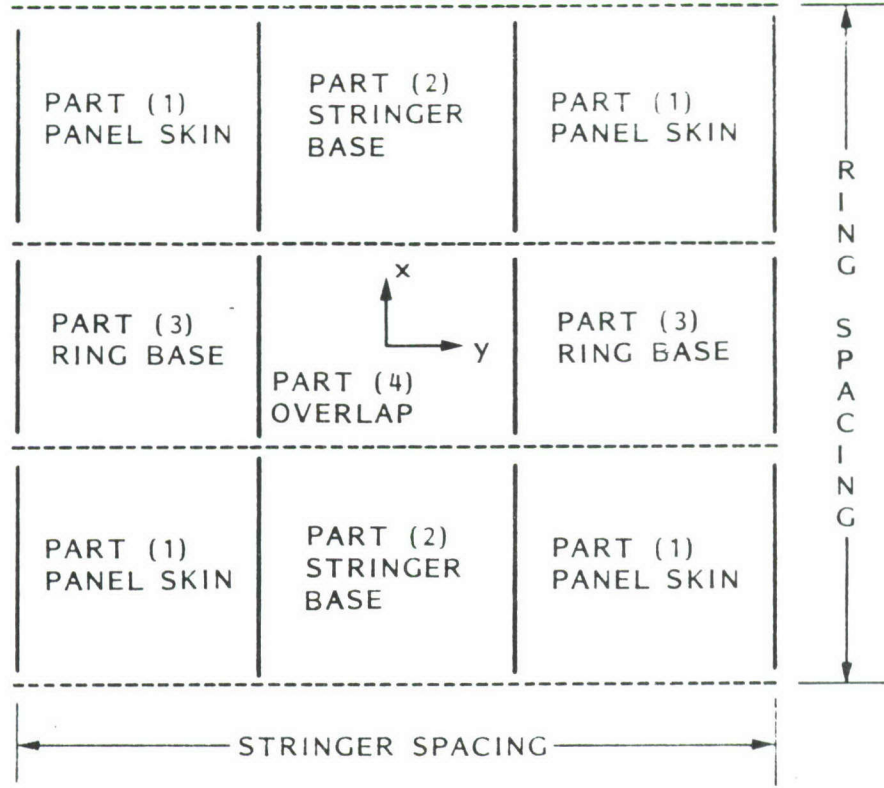
Fig. 14 **Plan view of a single panel module used in the development of the integrated constitutive law C_{ij} for the panel with smeared stringers and rings.**

The four equations expressing continuity of forces and moments are as follows:

$$B_{11}N_x(1) + B_{12}N_x(2) + N_{stringer}(2) = B_{11}N_x(3) + B_{12}N_x(4) + N_{stringer}(3) \quad (8.7)$$

$$B_{22}N_y(1) + B_{21}N_y(3) + N_{ring}(3) = B_{22}N_y(2) + B_{21}N_y(4) + N_{ring}(2) \quad (8.8)$$

$$B_{11}M_x(1) + B_{12}M_x(2) + M_{stringer}(2) = B_{11}M_x(3) + B_{12}M_x(4) + M_{stringer}(3) \quad (8.9)$$

$$B_{22}M_y(1) + B_{21}M_y(3) + M_{ring}(3) = B_{22}M_y(2) + B_{21}M_y(4) + M_{ring}(2) \quad (8.10)$$

The numbers in parentheses, $N_x(1)$ for example, refer to the part or region of the panel illustrated in Fig. 14. The coefficients, $B_{11}, B_{12}, B_{21}, B_{22}$ are given by:

B_{11} = (stringer spacing - stringer base width) /(stringer spacing)

B_{12} = (stringer base width)/(stringer spacing)

B_{21} = (ring base width)/(ring spacing)

B_{22} = (ring spacing - ring base width)/(ring spacing)

$\qquad (8.11)$

For Parts (1), (2), and (3) the resultants and moments in terms of the strains and changes in curvature are given by:

$$N_x(i) = C_{11}(i)e_x(i) + C_{12}(i)e_y(i) + C_{14}(i)k_x(i) + C_{15}(i)k_y(i) - N_{tx}(i) \quad (8.12)$$

$$N_y(i) = C_{12}(i)e_x(i) + C_{22}(i)e_y(i) + C_{24}(i)k_x(i) + C_{25}(i)k_y(i) - N_{ty}(i) \quad (8.13)$$

$$M_x(i) = C_{14}(i)e_x(i) + C_{24}(i)e_y(i) + C_{44}(i)k_x(i) + C_{45}(i)k_y(i) - M_{tx}(i) \quad (8.14)$$

$$M_y(i) = C_{15}(i)e_x(i) + C_{25}(i)e_y(i) + C_{45}(i)k_x(i) + C_{55}(i)k_y(i) - M_{ty}(i) \quad (8.15)$$

in which (i) refers to the part number (region) of the panel and

$e_x(i)$ is the axial (x-dir.) reference surface strain

$e_y(i)$ is the transverse (y-dir.) reference surface strain

$k_x(i)$ is the change in axial curvature of the reference surface

$k_y(i)$ is the change in hoop curvature of the reference surface

(8.16)

The constitutive law for Part (4), the region where the stiffener bases overlap, is:

$$N_x(4) = C_{11}(4)e_x(3) + C_{12}(4)e_y(2) + C_{14}(4)k_x(3) + C_{15}(4)k_y(2) - N_{tx}(4) \quad (8.17)$$

$$N_y(4) = C_{12}(4)e_x(3) + C_{22}(4)e_y(2) + C_{24}(4)k_x(3) + C_{25}(4)k_y(2) - N_{ty}(4) \quad (8.18)$$

$$M_x(4) = C_{14}(4)e_x(3) + C_{24}(4)e_y(2) + C_{44}(4)k_x(3) + C_{45}(4)k_y(2) - M_{tx}(4) \quad (8.19)$$

$$M_y(4) = C_{15}(4)e_x(3) + C_{25}(4)e_y(2) + C_{45}(4)k_x(3) + C_{55}(4)k_y(2) - M_{ty}(4) \quad (8.20)$$

In Eqs. (8.17 through 8.20) the $C_{ij}(4)$ and $N_{tx}(4)$, $N_{ty}(4)$, $M_{tx}(4)$, $M_{ty}(4)$, are assumed to be the averages of these quantities in regions 2 and 3.

The constitutive law for all stiffeners (stringers and rings) has the form:

$$N_{stringer}(i) = STFL1\, e_x(i) + STFM1\, k_x(i) - STFT1 \quad (8.21)$$

$$N_{ring}(i) = STFL2\, e_y(i) + STFM2\, k_y(i) - STFT2 \quad (8.22)$$

$$M_{stringer}(i) = STFM1\, e_x(i) + STFMM1\, k_x(i) - STFMT1 \quad (8.23)$$

$$M_{ring}(i) = STFM2\, e_y(i) + STFMM2\, k_y(i) - STFMT2 \quad (8.24)$$

in which the coefficients $STFL1, STFL2, STFM1, STFM2, STFT1, STFT2, STFMM1,$ $STFMM2, STFMT1, STFMT2$ are derived in SUBROUTINE CSTIF.

It is assumed that the strains and changes in curvature in the various parts (1), (2) and (3) of the panel module are related to eachother as follows:

$$e_x(\text{overall average}) = B_{22}\, e_x(1) + B_{21}\, e_x(3)$$

$$e_y(\text{overall average}) = B_{11}\, e_y(1) + B_{12}\, e_y(2)$$

$$e_x(2) = e_x(1)$$

$$e_y(3) = e_y(1)$$

(8.25)

and

$$k_x(\text{overall average}) = B_{22}\, k_x(1) + B_{21}\, k_x(3)$$

$$k_y(\text{overall average}) = B_{11}\, k_y(1) + B_{12}k_y(2)$$

$$k_x(2) = k_x(1)$$

$$k_y(3) = k_y(1)$$

(8.26)

The constitutive law for the panel with smeared stiffeners is calculated as follows:

1. Express Eqs. (8.7–8.10) in terms of $e_x(i), e_y(i), k_x(i), k_y(i), i = 1, 2, 3$, through use of Eqs. (8.12–8.24). Coefficients for the resulting equations are derived in SUBROUTINE EQSP67.

2. Eliminate $e_x(1), e_y(1), k_x(1), k_y(1)$ from these equations by use of Eqs. (8.25) and (8.26).

3. Solve Eqs.(8.9) and (8.10), thus expressed, for $k_x(3)$ and $k_y(2)$ in terms of $e_x(3)$, $e_y(2)$, and average strains and changes in curvature, e_x, e_y, k_x, k_y, over the entire panel module. Obtain the coefficients $D_{11}, D_{12}, D_{13}, D_{14}, D_{15}, D_{16}, D_{17}$ and $D_{21}, D_{22}, D_{23}, D_{24}, D_{25}, D_{26}, D_{27}$, which occur in the relationships:

$$
\begin{aligned}
k_x(3) &= D_{11} + D_{12}e_x(3) + D_{13}e_y(2) + D_{14}e_x + D_{15}e_y + D_{16}k_x + D_{17}k_y \\
k_y(2) &= D_{21} + D_{22}e_x(3) + D_{23}e_y(2) + D_{24}e_x + D_{25}e_y + D_{26}k_y + D_{27}k_y
\end{aligned}
\tag{8.27}
$$

4. Solve Eqs. (8.7) and (8.8) for $e_x(3)$ and $e_y(2)$ in terms of the average panel module strains and changes in curvature, e_x, e_y, k_x, k_y, thus obtaining the coefficients $F_{11}, F_{12}, F_{13}, F_{14}, F_{15}$ and $F_{21}, F_{22}, F_{23}, F_{24}, F_{25}$ which occur in the relationships:

$$
\begin{aligned}
e_x(3) &= F_{11} + F_{12}e_x + F_{13}e_y + F_{14}k_x + F_{15}k_y \\
e_y(2) &= F_{21} + F_{22}e_x + F_{23}e_y + F_{24}k_x + F_{25}k_y
\end{aligned}
\tag{8.28}
$$

5. Plug the results from step 4 into the expressions for $k_x(3)$ and $k_y(2)$ to yield

$$
\begin{aligned}
k_x(3) &= G_{11} + G_{12}e_x + G_{13}e_y + G_{14}k_x + G_{15}k_y \\
k_y(2) &= G_{21} + G_{22}e_x + G_{23}e_y + G_{24}k_x + G_{25}k_y
\end{aligned}
\tag{8.29}
$$

Steps 2 through 5 are performed in SUBROUTINE EPSKAP.

The constitutive law with smeared stiffeners is then derived starting from the left–hand–sides of Eqs.(8.7)–(8.10) equated to the proper combinations of smeared–stiffener coefficients and average strains and changes in curvature and integrated thermal forces and moments:

$$
\begin{aligned}
B_{11}N_x(1) + B_{12}N_x(2) + N_{stringer}(2) &= C_{11}e_x + C_{12}e_y + C_{14}k_x + C_{15}k_y - N_{tx} & (8.30) \\
B_{22}N_y(1) + B_{21}N_y(3) + N_{ring}(3) &= C_{12}e_x + C_{22}e_y + C_{24}k_x + C_{25}k_y - N_{ty} & (8.31) \\
B_{11}M_x(1) + B_{12}M_x(2) + M_{stringer}(2) &= C_{14}e_x + C_{24}e_y + C_{44}k_x + C_{45}k_y - M_{tx} & (8.32) \\
B_{22}M_y(1) + B_{21}M_y(3) + M_{ring}(3) &= C_{15}e_x + C_{25}e_y + C_{45}k_x + C_{55}k_y - M_{ty} & (8.33)
\end{aligned}
$$

The smeared-stiffener C_{ij} are determined with use of Eqs. (8.5)–(8.26) in Eqs.(8.30)–(8.33) above. Coefficients of e_x, e_y, k_x, k_y on the resulting left–hand–sides are set equal to the corresponding coefficients on the right–hand–sides. This final computation is performed in SUBROUTINE CSMEAR.

Given the C_{ij} and the thermal resultants N_{tx}, N_{ty}, M_{tx}, M_{ty}, the residual thermal strains and changes in curvature, e_{tx}, e_{ty}, e_{txy}, k_{tx}, k_{ty}, k_{txy}, are calculated in SUBROUTINE STRTHM. In this calculation the applied loads, N_x, N_y, N_{xy}, M_x, M_y, M_{xy}, are

46

assumed to be zero, the C_{ij} matrix is inverted, and the system of 6 linear equations is solved for the residual strains and changes in curvature. These quantities play a role in later analyses: the residual strains affect the stress constraints in the optimization analysis; thermal resultants derived from the residual strains affect local instability of the various segments of the panel module, and changes in curvature create a bowing of the panel which increases as compressive loads are applied. An example is given later that demonstrates the complex interactions between thermal residual stresses and deformation (bowing) and local buckling and postbuckling behavior of a blade– stiffened panel.

8.4.1 EXAMPLE: RESULTS FOR THE HAT–STIFFENED PANEL

```
C(i,j) with smeared stringers only...                                    THERMAL {NT}  ETHERM {ET}
Reference surface is at the middle surface of the skin midway between the stringers.
  1.3719E+06   2.4322E+05  -9.1024E-05   3.1942E+05  -2.9173E-04   2.3668E-06    -4.4327E+02  -2.2603E-04
  2.4322E+05   6.9742E+05  -1.1978E-02  -2.0503E-04  -1.2444E-03  -1.3759E-05    -4.4808E+02  -5.6366E-04
 -9.1024E-05  -1.1978E-02   2.5696E+05   2.3668E-06  -1.3759E-05   1.1760E+04     0.0000E+00   2.4975E-10
  3.1942E+05  -2.0503E-04   2.3668E-06   4.1735E+05   2.3291E+02   9.2078E+00    -6.7096E+01   1.2225E-05
 -2.9173E-04  -1.2444E-03  -1.3759E-05   2.3291E+02   4.9282E+02   9.2078E+00     7.7101E-07  -5.7772E-06
  2.3668E-06  -1.3759E-05   1.1760E+04   9.2078E+00   9.2078E+00   1.0328E+04     0.0000E+00  -6.0331E-09
```

8.4.2 RECENT MODIFICATION (AUGUST, 1986)

Changes in the Derivation of $C(i,j)$ for Smeared Stiffeners The integrated constitutive law for smeared stiffeners is derived above. The derivation has been modified as follows:
1.   Equations (8.7) through (8.10) have been replaced by:

$$N_x(1) = N_x(3) \qquad N_y(1) = N_y(2)$$
$$M_x(1) = M_x(3) \qquad M_y(1) = M_y(2) \tag{62}$$

in which the numbers in parentheses refer to the regions (Parts) indicated in Fig. 14. Part (4) no longer enters the calculations. Also, the index (i) in Eqs. (8.21–8.24) no longer appears: The strains and changes in curvature in the stiffener webs and flanges are assumed to be equal to the averages over the entire panel.

8.5 CALCULATE $C(i,j)$ FOR SMEARED STIFFENERS WITH PARTIALLY EFFECTIVE SKIN

Sometimes the wide-column buckling mode calculated with use of the single panel module is characterized by bending of the stringer which is of small amplitude compared to bending of the skin midway between stringers. In PANDA2, if the skin deflects more than 10 times midway between stringers than it does directly under the stringer, then this mode is rejected as indicating wide-column buckling. It is regarded as just another local skin buckling mode, a critical load factor for which is computed elsewhere in PANDA2. Since wide-column buckling is used in PANDA2 as an indication of panel instability (buckling between rings), if the wide-column mode is rejected, then panel instability must be calculated in some other way. In PANDA2 this "other way" is to use PANDA-type closed formulas.

However, panel instability in PANDA is ordinarily calculated by smearing the stringers and treating the skin as if it were undeformed. It is clear that if the skin deforms a great deal in the wide-column buckling mode, only some effective width of it will contribute to panel buckling. The $C(i,j)$ governing panel instability should reflect this reduced effectiveness of the skin.

This is done in PANDA2 by calculation in SUBROUTINE GETCIJ of a constitutive matrix for the panel skin with smeared stringers called $C_{SWIDE}(i,j)$. In the generation of C_{SWIDE}, all $C(i,j)$ of Segment 1 of the panel skin are set equal to 0.2 times their previous values, except $C(4,4)$, $C(5,5)$, and $C(6,6)$, which remain at their previous values.

When the wide-column buckling mode is calculated later in PANDA2, a switch called ISKIN is set equal to 0 if the mode is accepted as a true indication of panel instability and ISKIN is set equal to 1 if the mode is rejected because there is too much relative skin motion in it. Still later in PANDA2, panel instability from the PANDA-type of analysis is calculated with use of the appropriate constitutive matrix:

$C_s(i,j)=$	constitutive matrix with use of the fully effective, undeformed panel skin if the switch ISKIN = 0, if it is known that the skin is not in its postbuckled state, if KOITER = 0, and if IWIDE = 1.
$C_s(i,j)=$	constitutive matrix calculated from Koiter post-buckling theory if the skin is in its post-buckled state, if ISKIN = 0, if KOITER = 1, and if IWIDE = 1.
$C_{SWIDE}(i,j)=$	constitutive matrix calculated with use of the undeformed panel skin, but with $C(i,j)$ of Segment 1 of the panel module reduced as described above if ISKIN = 1 or if IWIDE = 0. and if IQUICK = 0.

IWIDE is a user–determined index that has the following meaning:

IWIDE = 0	means that the user has chosen a strategy in which the wide-column buckling mode does not constrain the design, regardless of the value of ISKIN.
IWIDE = 1	means that the wide-column buckling mode does constrain the design if ISKIN = 0, that is, if PANDA2 does not reject it as a true indication of panel instability.

IWIDE is always set equal to 1 if the run is not an optimization run and if IQUICK = 0. If the run is an optimization run, the user has previously chosen the value of IWIDE during the interactive session in MAINSETUP. If IQUICK = 1 the $C_s(i,j)$ with fully effective skin is always used.

8.5.1 EXAMPLE: THE HAT STIFFENED PANEL. $C_s(i,j)$ WITH REDUCED SKIN EFFECTIVENESS (C_{SWIDE}):

$C(i,j)$ with smeared stringers and reduced stiffness for segment 1 of the panel skin. This C-matrix is called C_{SWIDE}:

```
 4.7498E+05   4.8643E+04  -9.1024E-05   3.1942E+05  -5.8347E-05   2.3668E-06
 4.8643E+04   1.3948E+05  -1.1978E-02  -6.5681E-05  -2.4888E-04  -1.3759E-05
-9.1024E-05  -1.1978E-02   5.1393E+04   2.3668E-06  -1.3759E-05   1.1760E+04
 3.1942E+05  -6.5681E-05   2.3668E-06   4.1740E+05   4.6582E+01   9.2078E+00
-5.8347E-05  -2.4888E-04  -1.3759E-05   4.6582E+01   4.9282E+02   9.2078E+00
 2.3668E-06  -1.3759E-05   1.1760E+04   9.2078E+00   9.2078E+00   1.1021E+04
```

8.6 FIND LOCATION OF NEUTRAL PLANE FOR LOADING IN x-DIRECTION

The starting point is the constitutive law for the panel with smeared stiffeners:

$$N_x = C_s(1,1)\, e_x + C_s(1,2)\, e_y + C_s(1,4)\, k_x + C_s(1,5)\, k_y \qquad (8.34)$$

$$N_y = C_s(1,2)\, e_x + C_s(2,2)\, e_y + C_s(2,4)\, k_x + C_s(2,5)\, k_y \qquad (8.35)$$

$$M_x = -N_x\, d_x = C_s(1,4)\, e_x + C_s(2,4)\, e_y + C_s(4,4)\, k_x + C_s(4,5)\, k_y \qquad (8.36)$$

$$M_y = -N_y\, d_y = C_s(1,5)\, e_x + C_s(2,5)\, e_y + C_s(4,5)\, k_x + C_s(5,5)\, k_y \qquad (8.37)$$

in which dx (same as DNEUTX) is the distance from the middle surface of the thin part of the skin to the neutral plane for axial loading and dy (same as DNEUTY) is the distance from the middle surface of the thin part of the skin to the neutral plane for hoop loading; $C_s(i,j)$ are the coefficients of the constitutive law for the panel with both sets of stiffeners smeared out; and e_x, e_y, k_x, k_y are the average strains and changes in curvature of the reference surface, which in this case is taken to be the middle surface of the thin part of the panel skin.

The objective is to determine d_x and d_y. The procedure used is as follows:

1. Solve Eqs. (8.34) and (8.35) for e_x and e_y.
2. Plug in the resulting expressions for e_x and e_y in Eqs. (8.36) and (8.37)
3. Solve for k_x and k_y in terms of d_x and d_y.
4. Determine what values of d_x and d_y yield $k_x = 0$ and $k_y = 0$.

The calculations are performed in SUBROUTINE NEUTAX, which is called from SUBROUTINE GETCIJ. DNEUTX is first calculated by setting $N_x = 1.0$ and $N_y = 0.0$ and solving for d_x. This is done in the first call to SUBROUTINE NEUTAX. DNEUTY is then calculated by setting $N_x = 0.0$ and $N_y = 1.0$ and solving for d_y. This is done in the second call to SUBROUTINE NEUTAX.

8.7 CALCULATE NEW $C_s(i,j)$ CORRESPONDING TO SHIFTED REFERENCE SURFACE

A constitutive matrix, $C_{NEW}(i,j), i = 1,6, j = 1,6$, is derived given the matrix $C(i,j)$ just calculated and the shift of reference surface, $D = -C(1,4)/C(1,1)$. (The shift D is chosen so that $C_{NEW}(1,4) = 0$.) The new reference surface is close to, but not exactly at, the neutral plane for loading in the x (axial) direction.

Figures 15(a–c) show the nomenclature used in the derivation of $C_{NEW}(i,j)$.

```
                                    skin middle surface, used as the
                                    reference surface for the old
      skin->----------------------- <--constitutive matrix, C.
          -=-=-=-=-=-|-=-=-=-=-=-=-  <---new reference surface,
                 web-->|             located distance D=-C(1,4)/C(1,1)
                      |             below the skin middle surface.
        flange--> =========
```
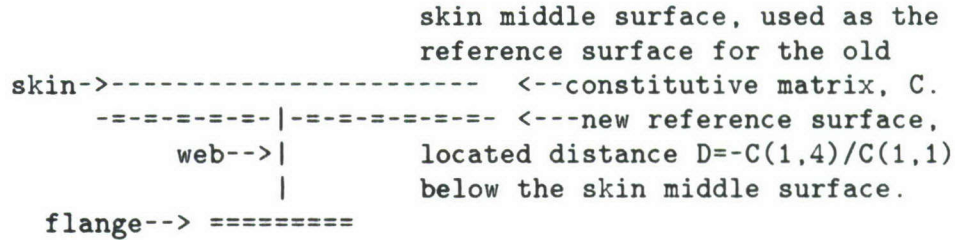
Fig. 15(a) View of panel module cross section, showing old reference
surface located at the skin middle surface, and the new reference
surface located a distance D below the skin middle surface.
(D will be positive in the figure above.)

```
      --> M,k                          --> M',k'
       ^ N,e                            ^ N',e'
       1                          D-->1   1<-
      _1_____                      _1__1_____
      |1|        ||                      |1| 1      ||
      |1|        ||            skin-->|1| 1      ||<--flange
      |1|        ||                      |1| 1      ||
      ~~~\       ||                      ~~~\     <------web
         \~~~~~~~                          \~~~~~~~
```
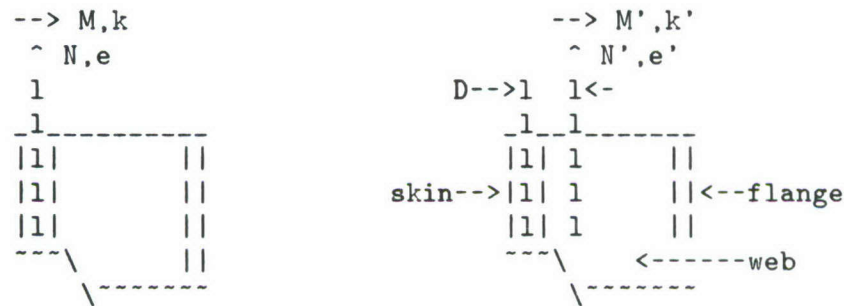
Fig. 15(b) Elevation of panel, showing reference surface at the
skin middle surface, axial resultant N, moment M, strain e, and
curvature change k. (c) Elevation of panel, showing reference
surface near the neutral plane, shift D, axial resultant N',
moment M', strain e', and curvature change k'.

The derivation of the new constitutive matrix C_{NEW} from the old constitutive matrix C and the shift D proceeds as follows: For the original reference surface, shown in (b) above, we have

$$N = C e \tag{8.38}$$

in which N represents the vector of 6 loads

$$N = \{N_x, N_y, N_{xy}, M_x, M_y, M_{xy}\} \tag{8.39}$$

e represents the vector of 6 strains and changes in curvature

$$e = \{e_x, e_y, e_{xy}, k_x, k_y, k_{xy}\} \tag{8.40}$$

50

and C represents the original 6x6 matrix derived for the reference surface located at the middle surface of the part of the panel module skin midway between stiffeners. For the new reference surface, located a distance D from the skin middle surface, we have

$$N' = C_{NEW}\, e' \qquad (8.41)$$

If classical Kirchoff thin shell deformations are assumed (plane sections remain plane, normals remain normal), we can relate the forces N and N' and the strains e and e' as follows:

$$N = \{N'_x,\ N'_y,\ N'_{xy},\ M'_x - N'_x D,\ M'_y - N'_y D,\ M'_{xy} + N'_{xy} D\} \qquad (8.42)$$

$$e = \{e'_x + k'_x D,\ e'_y + k'_y D,\ e'_{xy} - k'_{xy} D,\ k'_x,\ k'_y,\ k'_{xy}\} \qquad (8.43)$$

We now insert the right-hand sides of Eqs. (8.42) and (8.43) into Eq. (8.38), perform the indicated multiplications and additions, and equate coefficients in the result to like terms in Eq. (8.41) in order to obtain the new constitutive matrix C_{NEW}. These computations are performed in SUBROUTINE CSHIFT, which is called near the end of SUBROUTINE GETCIJ.

```
INPUT TO SUBROUTINE CSHIFT...

   C = Old constitutive matrix.
   D = Reference surface shift.

OUTPUT FROM SUBROUTINE CSHIFT...

   CNEW = New constitutive matrix.

FORMULAS FOR NEW C(i,j) IN TERMS OF OLD C(i,j) AND SHIFT, D:

   CNEW(i,j), i = 1,3, j=1,3   are unchanged by reference
                               surface shift, D.

   CNEW(1,4) = C(1,4) + D*C(1,1)
   CNEW(1,5) = C(1,5) + D*C(1,2)
   CNEW(1,6) = C(1,6) - D*C(1,3)

   CNEW(2,4) = C(2,4) + D*C(1,2)
   CNEW(2,5) = C(2,5) + D*C(2,2)
   CNEW(2,6) = C(2,6) - D*C(2,3)

   CNEW(3,4) = C(3,4) + D*C(1,3)
   CNEW(3,5) = C(3,5) + D*C(2,3)
   CNEW(3,6) = C(3,6) - D*C(3,3)

   CNEW(4,4) = C(4,4) + 2.*D*C(1,4) + D*D*C(1,1)
   CNEW(4,5) = C(4,5) + D*(C(2,4)+C(1,5)) + D*D*C(1,2)
   CNEW(4,6) = C(4,6) + D*(C(1,6)-C(3,4)) - D*D*C(1,3)
```

$$(8.44)$$

```
CNEW(5,5) = C(5,5) + 2.*D*C(2,5) + D*D*C(2,2)
CNEW(5,6) = C(5,6) + D*(C(2,6)-C(3,5)) - D*D*C(2,3)

CNEW(6,6) = C(6,6) - 2.*D*C(3,6) + D*D*C(3,3)
```

8.7.1 EXAMPLE: HAT–STIFFENED PANEL: Cs(i,j) WITH SHIFTED REFERENCE SURFACE

For the following, the reference surface is $d = -C_{14}/C_{11}$ from the middle surface of the thin part of the panel skin. In this case $d = $ -2.3283E-01. (Positive d corresponds to a reference surface that lies below the panel skin). Note that the neutral surface is located at DNEUTX = -2.4817E-01

```
 1.3719E+06   2.4322E+05  -9.1024E-05   0.0000E+00  -5.6628E+04  -1.8826E-05
 2.4322E+05   6.9742E+05  -1.1978E-02  -5.6628E+04  -1.6238E+05  -2.8026E-03
-9.1024E-05  -1.1978E-02   2.5696E+05   2.3560E-05   2.7750E-03   7.1588E+04
 0.0000E+00  -5.6628E+04   2.3560E-05   3.4298E+05   1.3417E+04   9.2078E+00
-5.6628E+04  -1.6238E+05   2.7750E-03   1.3417E+04   3.8299E+04   9.2084E+00
-1.8826E-05  -2.8026E-03   7.1588E+04   9.2078E+00   9.2084E+00   2.9734E+04
***** END OF CONSTITUTIVE C(i,j) CALCUL. *****

******** END OF CONSTITUTIVE C(i,j) CALCUL. ********
```

Next, find overall bending of panel (smeared stiffeners) under uniform pressure, $p=$ 1.0000E+00. Nonlinear theory is used...

52

9.0 NONLINEAR STATIC RESPONSE TO UNIFORM NORMAL PRESSURE

9.1 INTRODUCTION

It is well known that monocoque flat plates exhibit a nonlinear stiffening effect under pressure, and that even for rather low design pressures one must account for the membrane stretching that builds up as the plate deflects. Boitnott, Johnson, and Starnes [21] demonstrate that nonlinearities significantly affect the behavior of curved, internally pressurized panels clamped along their straight edges. In this section, which deals with a more complex problem, a stiffened panel, geometric nonlinearities must be included in the model.

Stiffened panels under normal pressure exhibit two types of response, identified here and in the following paragraphs as Problem 1 and Problem 2:

Problem 1.   The panel bends overall. This behavior can be captured with a model in which the stiffeners are smeared out.

Problem 2.   The panel bends locally around each stringer This behavior can be captured with a single module model of the type shown in Fig. 1.

The strategy in PANDA2 is to obtain a reasonably good solution with little computer time by separation of these two behaviors and analysis of each as a nonlinear problem. The total state of the pressurized panel is obtained by adding the results of the two separate analyses.

Immediately one might object that since the problem is nonlinear, one cannot superpose these results. The PANDA2 strategy would be incorrect if it were not for the fact that the membrane stresses obtained from Problem 1, the overall bending model, occur as prestresses in Problem 2, the local "wrap-around" problem. In this way the essential nonlinear contribution of the first problem to the second is included.

9.2 NONLINEAR THEORY USED IN PANDA2

For both the overall (Problem 1) and the local (Problem 2) behavior, the static response to uniform normal pressure is determined from the theory outlined next. The governing equations are derived by minimization of the total potential,

$$P = U - W = \int_{surface} \left[\mathbf{e}^{\mathbf{T}} [\mathbf{C}] \mathbf{e} - \mathbf{W} \right] ds = 0 \tag{9.1}$$

with respect to each of the degrees of freedom q_i of the discretized panel or panel module cross section. Thus, the ith equilibrium equation ($i = 1, 2, 3, \ldots$ N, where N is the number of degrees of freedom in the discretized model of the panel or panel module cross section) is given by:

$$\partial P / \partial q_i = \int_s \left[\mathbf{e}^{\mathbf{T}} [\mathbf{C}] \partial e / \partial q_i - \partial \mathbf{W} / \partial q_i \right] ds = 0 \tag{9.2}$$

53

in which U is the strain energy, W is the work done by external forces, C is the 6 x 6 constitutive law, e is the strain vector consisting of three in–plane reference surface strain components and three reference surface curvature change components, and q_i is the ith degree of freedom. (Most q_i are nodal displacement components, u_i, v_i, w_i. A few of the q_i are Lagrange multipliers corresponding to boundary and juncture constraint conditions.) The quantity ds is an elemental area of the reference surface.

After integration, Eq. (9.2) represents a set of N nonlinear equations which can be solved by the Newton method. The governing linear equation for each Newton iteration is obtained by expanding the terms in Eq. (9.2) in a Taylor series about a given point in $\mathbf{q}$–space. Call this point $\mathbf{q_o}$. Only linear terms in $\triangle\mathbf{q}$ are retained in the Taylor series expansion. The resulting equation for the ith degree of freedom has the form:

$$\sum_{j=1}^{N}\left\{\int_s \left[\mathbf{e^T}[\mathbf{C}]\partial^2\mathbf{e}/\partial q_i\partial q_j + \partial\mathbf{e^T}/\partial q_j\,[\mathbf{C}]\partial\mathbf{e}/\partial q_i\right]ds\right\}\triangle q_j$$

$$= \int_s \left[\partial\mathbf{W}/\partial q_i - \mathbf{e^T}[\mathbf{C}]\partial\mathbf{e}/\partial q_i\right]ds \qquad (9.3)$$

Equation (9.3) represents an integro–differential equation. Before solutions can be obtained, it must be converted into an algebraic equation. This can easily be done, because all quantities are assumed to vary trigonometrically in one coordinate direction and the other coordinate is discretized.

After each Newton iteration, the new equilibrium state is

$$\mathbf{q} = \mathbf{q_o} + \triangle\mathbf{q} \qquad (9.4)$$

in which $\mathbf{q_o}$ is the known state after the previous Newton iteration.

Newton iterations continue until the $\triangle q_i$, $i = 1, 2,..N$ are less than, say, one per cent of the respective q_i for all q_i larger than 10 per cent of the largest nodal degree of freedom. (Lagrange multipliers are not included in this convergence criterion.) Actually, in order to save time, only the largest normal deflection $|w_{max}|$ is monitored for convergence. When $\triangle|w_{max}|$ is less than $0.001\,|w_{max}|$, the Newton iterations are considered converged.

In this analysis the displacement components, U, V, W, are assumed to have the form:

$$U(x, y) = u(y)\sin(\bar{n}x)$$
$$V(x, y) = v(y)\sin(2\bar{n}x) \qquad (9.5)$$
$$W(x, y) = w(y)\sin(\bar{n}x)$$

in which x is the axial coordinate (normal to the plane of the screen) and y is the coordinate along each segment of the panel or panel module cross section (in the plane of the screen). The quantity $\bar{n}$ is given by

$$\bar{n} = \pi/L \qquad (9.6)$$

where L is the axial length presently being considered. (L may be the entire panel length or the length between adjacent rings.)

The strain vector **e** is given by

$$\mathbf{e} = (e_x, e_y, e_{xy}, k_x, k_y, k_{xy}) \qquad (9.7)$$

The in–plane strain components, e_x, e_y, e_{xy}, are given by

$$e_y = (u' + w/R_1)s + 0.5(\chi^2)s^2 + e_{yo}$$
$$e_x = 2\bar{n}vc_2 + (w/R_2)s + 0.5(\psi^2)c^2 + e_{xo} \qquad (9.8)$$
$$e_{xy} = \bar{n}uc + v's_2 + \chi\psi sc$$

and the changes in curvature, k_x and k_y, and twist, k_{xy}, are given by

$$k_y = \chi's$$
$$k_x = -\bar{n}\psi s \qquad (9.9)$$
$$k_{xy} = -4\bar{n}\chi c$$

In Eqs. (9.8) and (9.9) $()' = \partial()/\partial y$, $s = \sin(\bar{n}x)$, $c = \cos(\bar{n}x)$, $s_2 = \sin(2\bar{n}x)$, $c_2 = \cos(2\bar{n}x)$, R_1 and R_2 are the radii of curvature in the plane of the screen and normal to the plane of the screen, respectively, χ is the rotation about an axis normal to the plane of the screen, and ψ is the rotation about an axis in the plane of the screen. These rotations are given by

$$\chi = w' - u/R_1$$
$$\psi = \bar{n}w \qquad (9.10)$$

The total strain vector e consists of a linear part e_L, a nonlinear part e_{NL}, and an initial part e_o. The initial part e_o arises from the thermal curing of the panel and the applied in–plane load sets, N_x, N_y, N_{xy}, and N_{xo}, N_{yo}, N_{xyo}. The radii of curvature, R_1 and R_2, are considered to be the initial curvatures plus any changes due to thermal curing and in–plane loading which is independent of that generated by the uniform normal pressure. Hence, the curvature changes and twist in Eqs. (9.9) do not contain k_{yo} or k_{xo} terms.

The work done by external forces is simply

$$\mathbf{W} = \int_{surface} [pw]\, ds \qquad (9.11)$$

Equation (9.3) is converted into an algebraic equation by use of Eqs. (9.8–9.10), replacement of derivatives $()'$ and $()''$ with appropriate three–point central difference formulas (same as used in BOSOR4), and analytical integration over the axial coordinate x. The calculations are performed in SUBROUTINE BUCKLE. SUBROUTINE BUCKLE calls SUBROUTINE ARRAYS, in which the stiffness matrix and right–hand–side vector are set up, SUBROUTINE FACTR, in which the stiffness matrix is decomposed, and SUBROUTINE SOLVE, in which back–substitution is performed. Newton iterations continue

until the largest nodal displacement converges to within 0.1 per cent. The computational path in SUBROUTINE BUCKLE and SUBROUTINE ARRAYS is identified by a pointer INDIC having the value 3.

If the panel is stiffened, the nonlinear analysis is first performed for the entire panel with smeared stiffeners. In this analysis all four edges are supported such that $u = v = w = 0$ and rotation about each edge is permitted. Warping due to curing is included. If the entire panel is longer in the axial direction than twice the circumferential arc length, or in the case of cylindrical panels, if the axial length is greater than twice the "boundary layer" length, considered to be $2.73 \times$ sqrt(radius x effective thickness), then U, V, W in the panel skin are assumed to be indpendent of x.

Upon convergence of the nonlinear analysis of the entire panel with smeared stiffeners, the nonlinear analysis of a single panel module is begun. Here the segmented model shown in Fig. 13 is used. Symmetry conditions are applied at the two edges of the skin that are normal to the screen. Variations of displacement normal to the screen are assumed to be zero in this local branched model. The panel module is considered to be preloaded by the computed resultants due to curing, the prescribed in-plane Load Set A (N_x, N_y, N_{xy}), the prescribed Load Set B (N_{xo}, N_{yo}), and whatever average in-plane loads are predicted by the just–completed nonlinear analysis of the entire panel with smeared stiffeners.

The strains and stress resultants arising from this nonlinear analysis for static response to uniform normal pressure are evaluated only at the panel or panel module cross section midway along the x–coordinate, that is, at the symmetry plane parallel to the screen at $x = L/2$.

9.3 OVERALL RESPONSE FROM SMEARED STIFFENER DISCRETIZED MODEL OF THE ENTIRE PANEL

The following analysis obtains the nonlinear static response of the entire panel to uniform normal pressure. Both stringers and rings, if any, are assumed to be smeared out in this analysis.

The panel edge in the plane of the screen is discretized. All edges are supported such that $u = v = w = 0$ and the rotation about each edge is permitted. The panel is preloaded by prescribed in-plane resultants resultants N_x, N_y, N_{xy} from Load Set A and prescribed in-plane resultants N_{xo} and N_{yo} from Load Set B.

9.3.1 STABILITY CHECK

First, an analysis is performed to see if curvature should be neglected in the global static nonlinear response to uniform pressure. This branch is entered only if PANDA2 senses the presence of pressure applied to the convex surface of the panel. Some results follow...

```
General instability load factor          EIGPRS=  1.2887E+01
Uniform normal pressure (positive upward)    p=  1.0000E+00
Radius of curvature  (positive down)         R= -1.9400E+02
Resultants in Load Set A: (includes p*R)    Nx=   0
                                            Ny= -1.9400E+02
```

```
Wave numbers in critical buckling pattern:axial = 1
                                           circ. = 8
```

If the general instability load factor, EIGPRS, is less than unity, and if the number of half waves in the circumferential direction is greater than one, then the curvature, $1/R$, is neglected in the following nonlinear static analysis of the entire panel and the hoop tension generated by the deformation of the flat panel is set equal to zero in subsequent analyses of this panel.

9.3.2 NONLINEAR ANALYSIS FOR OVERALL STATIC RESPONSE

```
OVERALL PANEL DEFORMATION UNDER NORMAL PRESSURE HAS CONVERGED.
    Newton iterations required              =    3
    Last increment in normal displacement
            midway between stiffeners, DW =   -2.0614E-07
    Final  value  for normal displacement
            midway between stiffeners,  W =   -1.9376E-02
```
At this point we have reached the end of nonlinear equilibrium calculations for the entire panel with smeared stiffeners under uniform normal pressure, $p = 1.0000E+00$.

9.3.3 RECENT MODIFICATION: SHEAR BUCKLING OF WEB DUE TO NORMAL PRESSURE

When a stiffened panel is loaded by uniform normal pressure considerable in-plane shear develops in the stiffener webs. These webs can buckle because of this shear. The web shear bucklingfailure mode is now included in PANDA2. Prebuckling shear in each web of the hat is 48.3 lb/in.

9.4 NONLINEAR ANALYSIS FOR LOCAL STATIC RESPONSE

Next, find bending of a single panel module under uniform normal pressure, $p = 1.0000E+00$. Nonlinear theory is used.

The following analysis obtains the nonlinear static response of a single panel module to uniform normal pressure. Symmetry conditions are applied at the generators midway between stringers. If the panel module is longer than it is wide, axial bending in the skin is ignored.

```
LOCAL PANEL DEFORMATION UNDER NORMAL PRESSURE HAS CONVERGED.
            Newton iterations required     =    3
    Last Increment in normal displacement
            midway between stiffeners, DW =   -4.2100E-06
    Final   value  for normal displacement
            midway between stiffeners,  W =   -1.1206E-02
```
At this point we have reached the end of nonlinear equilibrium calculations for a single panel module with uniform normal pressure, $p = 1.0000E+00$. The rather complex, two-phase nonlinear analysis for the static response of the stiffened panel to uniform normal pressure has been completed.

10.0 CALCULATION OF AVERAGE STRAIN AND FORCE DISTRIBUTIONS IN VARIOUS PARTS OF THE PANEL

10.1 PRELIMINARY GENERAL INSTABILITY CALC. FOR BOWING GROWTH

First, calculate general instability load factor from a PANDA- type of analysis. Neglect any postbuckling effects in this preliminary calculation, the purpose of which is to obtain a rough estimate of the critical load to be used next when the additional bowing of the cured and pressurized, therefore warped panel under the applied load set, N_x, N_y, and N_{xy}, is computed. (This calculation occurs in the first call to SUBROUTINE BUCPAN in SUBROUTINE STRUCT, immediately following CALL GETCIJ).

We are now in SUBROUTINE GENSTB, which is called from SUBROUTINE BUCPAN. PANDA-type "closed form" analysis is performed. In this particular call to SUBROUTINE GENSTB we obtain a buckling load factor for buckling of the following type: General buckling (simple support at all boundaries).

```
DIMENSIONS, LOADS, C(i,i), AND TRANSVERSE SHEAR
PROPERTIES OF THE PORTION OF THE PANEL NOW BEING ANALYZED:
   Axial, circumferential lengths, this buckling model=  1.5289E+01  2.4000E+01
   Eigenvalue in-plane loads/length of edge, Nx,Ny,Nxy= -3.0000E+03  0.0000E+00  1.0000E+03
   Fixed       in-plane loads/length of edge, Nxo, Nyo =  5.2143E+01 -4.9619E+01
   Constitutive matrix diagonal, [C(i,i), i=1,6]       =  4.7498E+05  1.3948E+05  5.1393E+04  4.1740E+05  4.9282E+02  1.1021E+04
   Effective thickness, x-face, transverse shearing    =  1.4370E+00
   Effective thickness, y-face, transverse shearing    =  8.1209E-02
   Transverse shear stiffness components, G13, G23     =  3.3717E+04  3.4235E+05
   Is transverse shear deformation weakening included?=  YES


Buckling load factors and no. of halfwaves (M = axial, N = circumferential):
   Neglecting transverse shear deformation weakening= 2.9809E+00 (M = 1, N = 1) halfwaves. Nodal line slope=  7.0000E-02
   Including  transverse shear deformation weakening= 2.3424E+00 (M = 1, N = 1) halfwaves. Nodal line slope=  7.0000E-02
   *********************************************************************
```

```
GENERAL INSTABILTY EIGENVALUE (PANDA)           =   2.3424
GROWTH FACTOR OF PANEL CURING BOW DUE TO LOAD   =   1.7449
```

10.2 STRAIN AND FORCE DISTRIBUTIONS FROM ALL LOADS EXCEPT PRESSURE

```
POSITIONS OF STIFFENER SEGMENT CENTROIDS BELOW THE REFERENCE SURFACE OF THE PANEL SKIN...
   STRINGER PARTS...ZPARTX(I), I=1,4=      0.0000E+00  0.0000E+00 -6.9870E-01 -1.3204E+00
   RING     PARTS...ZPARTY(I), I=1,4=      0.0000E+00  0.0000E+00  0.0000E+00  0.0000E+00
BOWING AMPLITUDES DUE TO INITIAL IMPERFECTION, CURING AND PRESSURE...
   AXIAL BOWING DUE TO INITIAL IMPERFECTION  =   0.0000E+00
   AXIAL BOWING DUE TO CURING                =  -1.1147E-03
   CIRCUMFERENTIAL BOWING DUE TO CURING      =   3.3717E-04
   BOWING, ENTIRE PANEL UNDER EXT. PRESSURE  =  -1.9376E-02
   BOWING, PANEL MODULE UNDER EXT. PRESSURE  =   0.0000E+00
   LOCAL IMPERFECTION IN PANEL SKIN, WIMPloc =   1.0000E-05
===========================================================================
APPLIED RESULTANTS: AXIAL, Nx = -3.0000E+03, CIRC., Ny = 0.0000E+00,  IN-PLANE SHEAR, Nxy = 1.0000E+03 (LOAD SET A)
```

APPLIED RESULTANTS: AXIAL, Nxo= 0.0000E+00, CIRC., Nyo= 0.0000E+00, IN-PLANE SHEAR, Nxyo= 0.0000E+00 (LOAD SET B)
REDUCTION FACTOR FOR AXIAL LENGTH OF PANEL (LESS THAN 1.0 ONLY IF PANEL IS CLAMPED) = 5.0965E-01
DISTANCE FROM MIDDLE SURFACE OF PANEL MODULE SEGMENT 1 (SKIN) TO NEUTRAL SURFACES (positive as for z in Fig. 9):
         X-DIRECTION :   DNEUTX = -2.4817E-01   Y-DIRECTION :   DNEUTY = 1.8234E-09
ECCENTRICITY OF AXIAL LOAD (DISTANCE FROM X-DIRECTION NEUTRAL SURFACE TO WHERE Nx AND Nxo ARE APPLIED (pos. as for z in Fig.9):
     AXIAL LOAD ECCENTRICITY, ECC = 0.0000E+00

REFERENCE SURFACE (SKIN MIDDLE SURFACE) STRAINS, CHANGES IN CURVATURE, AND TWIST CAUSED BY APPLIED IN-PLANE LOADS, Nx, Ny, Nxy
AND Nxo, Nyo, Nxyo AND CAUSED BY THERMAL CURING

| REFERENCE | CAUSED BY APPLIED LOADS, Nx,Ny,Nxy | | | CAUSED BY APPLIED LOADS, Nxo,Nxo,Nxyo | | | CAUSED BY THERMAL CURING | | |
| SURFACE | (LOAD SET A) | | | (LOAD SET B) | | | (Considered part of load set B) | | |
QUANTITIES	SKIN	STRINGER BASE	RING BASE	SKIN	STRINGER BASE	RING BASE	SKIN	STRINGER BASE	RING BASE
AXIAL STRAIN	-2.410E-03	-2.410E-03	0.000E+00	0.000E+00	0.000E+00	0.000E+00	-2.260E-04	-2.260E-04	0.000E+00
TRAN. STRAIN	9.072E-04	6.932E-04	0.000E+00	0.000E+00	0.000E+00	0.000E+00	-4.784E-04	-7.513E-04	0.000E+00
SHEAR STRAIN	3.997E-03	3.321E-03	0.000E+00	0.000E+00	0.000E+00	0.000E+00	2.497E-10	2.497E-10	0.000E+00
AXIAL KAPPA	3.174E-04	3.174E-04	0.000E+00	0.000E+00	0.000E+00	0.000E+00	1.222E-05	1.222E-05	0.000E+00
TRAN. KAPPA	-4.007E-05	-1.124E-04	0.000E+00	0.000E+00	0.000E+00	0.000E+00	-5.973E-06	-5.347E-06	0.000E+00
TWIST	-4.675E-03	-4.675E-03	0.000E+00	0.000E+00	0.000E+00	0.000E+00	-6.033E-09	-6.033E-09	0.000E+00

==

               CAUSED BY ALL LOADS EXCEPT NORMAL PRESSURE
      S T R A I N S   I N   V A R I O U S   P A R T S   O F   T H E   P A N E L   S K I N   A N D   S T I F F E N E R S

| ITEM | CAUSED BY APPLIED LOADS, Nx,Ny,Nxy | | | CAUSED BY APPLIED LOADS, Nxo,Nxo,Nxyo | | | CAUSED BY THERMAL CURING | | |
| | (LOAD SET A) | | | (LOAD SET B) | | | (Considered part of load set B) | | |
	SKIN	STRINGER	RING	SKIN	STRINGER	RING	SKIN	STRINGER	RING
SKIN AXIAL	-2.410E-03	-	-	0.000E+00	-	-	-2.260E-04	-	-
SKIN CIRC.	9.072E-04	-	-	0.000E+00	-	-	-4.784E-04	-	-
SKIN SHEAR	3.997E-03	-	-	0.000E+00	-	-	0.000E+00	-	-
		STRINGER	RING		STRINGER	RING		STRINGER	RING
STIFFENER BASE ALONG AXIS	-2.410E-03	9.072E-04		0.000E+00	0.000E+00		-2.260E-04	0.000E+00	
STIFFENER BASE TRANSVERSE	6.932E-04	-2.410E-03		0.000E+00	0.000E+00		-7.513E-04	0.000E+00	
STIFFENER BASE SHEAR	3.321E-03	-3.997E-03		0.000E+00	0.000E+00		0.000E+00	0.000E+00	
ALONG STIFFENER WEB AXIS	-2.188E-03	0.000E+00		0.000E+00	0.000E+00		-2.175E-04	0.000E+00	
TRANSVERSE TO WEB AXIS	1.708E-03	0.000E+00		0.000E+00	0.000E+00		-5.514E-04	0.000E+00	
IN-PLANE SHEARING OF WEB	0.000E+00	0.000E+00		0.000E+00	0.000E+00		0.000E+00	0.000E+00	
ALONG STIFF. FLANGE AXIS	-1.990E-03	0.000E+00		0.000E+00	0.000E+00		-2.099E-04	0.000E+00	
TRANSVERSE TO FLANGE AX.	4.058E-04	0.000E+00		0.000E+00	0.000E+00		-6.683E-04	0.000E+00	
IN-PLANE SHEAR OF FLANGE	0.000E+00	0.000E+00		0.000E+00	0.000E+00		0.000E+00	0.000E+00	

==

               CAUSED BY ALL LOADS EXCEPT NORMAL PRESSURE
      R E S U L T A N T S   I N   V A R I O U S   P A R T S   O F   T H E   P A N E L   S K I N   A N D   S T I F F E N E R S

| ITEM | CAUSED BY APPLIED LOADS, Nx,Ny,Nxy | | | CAUSED BY APPLIED LOADS, Nxo,Nxo,Nxyo | | | CAUSED BY THERMAL CURING | | |
| | (LOAD SET A) | | | (LOAD SET B) | | | (Considered part of load set B) | | |
	SKIN	STRINGER	RING	SKIN	STRINGER	RING	SKIN	STRINGER	RING
SKIN AXIAL	-1.531E+03	-	-	0.000E+00	-	-	5.572E+01	-	-
SKIN CIRC.	1.318E-05	-	-	0.000E+00	-	-	-3.052E-05	-	-
SKIN SHEAR	1.000E+03	-	-	0.000E+00	-	-	0.000E+00	-	-
		STRINGER	RING		STRINGER	RING		STRINGER	RING
STIFFENER BASE ALONG AXIS	-4.622E+03	0.000E+00		0.000E+00	0.000E+00		-1.278E+02	0.000E+00	
STIFFENER BASE TRANSVERSE	-6.638E-05	0.000E+00		0.000E+00	0.000E+00		0.000E+00	0.000E+00	
STIFFENER BASE SHEAR	1.000E+03	0.000E+00		0.000E+00	0.000E+00		0.000E+00	0.000E+00	

ALONG STIFFENER WEB AXIS	-1.309E+02	0.000E+00	0.000E+00	0.000E+00	1.122E+01	0.000E+00
TRANSVERSE TO WEB AXIS	0.000E+00	0.000E+00	0.000E+00	0.000E+00	0.000E+00	0.000E+00
IN-PLANE SHEARING OF WEB	0.000E+00	0.000E+00	0.000E+00	0.000E+00	0.000E+00	0.000E+00
ALONG STIFF. FLANGE AXIS	-2.814E+03	0.000E+00	0.000E+00	0.000E+00	-1.155E+01	0.000E+00
TRANSVERSE TO FLANGE AX.	0.000E+00	0.000E+00	0.000E+00	0.000E+00	0.000E+00	0.000E+00
IN-PLANE SHEAR OF FLANGE	0.000E+00	0.000E+00	0.000E+00	0.000E+00	0.000E+00	0.000E+00

==

CAUSED BY ALL LOADS EXCEPT NORMAL PRESSURE

E Q U I L I B R I U M   O F   R E S U L T A N T S   F R O M   A P P L I E D   L O A D S   A N D   C U R I N G

ITEM	CAUSED BY APPLIED LOADS, Nx,Ny,Nxy (LOAD SET A)			CAUSED BY APPLIED LOADS, Nxo,Nxo,Nxyo (LOAD SET B)			CAUSED BY THERMAL CURING (Considered part of load set B)		
	Nx	Ny	Nxy	Nx	Ny	Nxy	Nx	Ny	Nxy
DERIVED	-3.000E+03	1.318E-05	1.000E+03	0.000E+00	0.000E+00	0.000E+00	-5.448E-05	-3.052E-05	0.000E+00
APPLIED	-3.000E+03	0.000E+00	1.000E+03	0.000E+00	0.000E+00	0.000E+00	0.000E+00	0.000E+00	0.000E+00
ERROR	-2.441E-04	1.318E-05	0.000E+00	0.000E+00	0.000E+00	0.000E+00	-5.448E-05	-3.052E-05	0.000E+00

==
==

10.3 STRAIN AND FORCE DISTRIBUTIONS FROM UNIFORM NORMAL PRESSURE

APPLIED UNIFORM NORMAL PRESSURE, P= 1.0000E+00

IN-PLANE RESULTANTS DEVELOPED FROM MODEL OF ENTIRE PANEL WITH SMEARED STIFFENERS (considered part of Load Set B):

Nx(created by normal pressure) = 5.7501E+01

Ny(created by normal pressure) = -3.4202E+01

Nxy(created by normal pressure) = 0.0000E+00

IN-PLANE RESULTANTS DEVELOPED FROM MODEL OF PANEL MODULE WITH BRANCHED STRINGER (considered part of Load Set B):

Nx(created by normal pressure) = -5.3587E+00

Ny(created by normal pressure) = -1.5417E+01

Nxy(created by normal pressure) = 0.0000E+00

REFERENCE SURFACE (skin middle surface) STRAINS, CHANGES IN CURVATURE, AND TWIST CAUSED BY UNIFORM NORMAL PRESSURE

(entire panel, smeared stiffener model)

REFERENCE SURFACE QUANTITIES	CAUSED BY UNIFORM NORMAL PRESSURE, P (considered part of Load Set B)		
	SKIN	STRINGER BASE	RING
AXIAL STRAIN	1.212E-06	1.212E-06	0.000E+00
TRAN. STRAIN	-5.497E-05	-3.734E-05	0.000E+00
SHEAR STRAIN	0.000E+00	0.000E+00	0.000E+00
AXIAL KAPPA	2.125E-04	2.125E-04	0.000E+00
TRAN. KAPPA	1.136E-04	-4.293E-05	0.000E+00
TWIST	0.000E+00	0.000E+00	0.000E+00

==

CAUSED BY UNIFORM PRESSURE

S T R A I N S   I N   V A R I O U S   P A R T S   O F   T H E   P A N E L   S K I N   A N D   S T I F F E N E R S

ITEM	FROM MODEL OF ENTIRE PANEL(smeared) (LOAD SET B)			FROM MODEL OF PANEL MODULE(branched) (LOAD SET B)			SUM OF STRAINS FROM BOTH MODELS (Considered part of load set B)		
	SKIN	STRINGER	RING	SKIN	STRINGER	RING	SKIN	STRINGER	RING
SKIN AXIAL	1.212E-06	-	-	1.370E-07	-	-	1.349E-06	-	-
SKIN CIRC.	-5.497E-05	-	-	-2.463E-05	-	-	-7.960E-05	-	-

60

SKIN SHEAR	0 000E+00	–	–	0 000E+00	–	–	0.000E+00	–	–
	STRINGER	RING		STRINGER	RING		STRINGER	RING	
STIFFENER BASE ALONG AXIS	1.212E-06	-5.497E-05		-5 041E-25	0.000E+00		1.212E-06	-5 497E-05	
STIFFENER BASE TRANSVERSE	-3.734E-05	1.212E-06		-1 660E-05	0.000E+00		-5.395E-05	1 212E-06	
STIFFENER BASE SHEAR	0.000E+00	0.000E+00		0 000E+00	0.000E+00		0.000E+00	0.000E+00	
ALONG STIFFENER WEB AXIS	1.497E-04	0.000E+00		1.096E-10	0.000E+00		1.497E-04	0.000E+00	
TRANSVERSE TO WEB AXIS	-1.169E-04	0.000E+00		-1.299E-06	0.000E+00		-1.182E-04	0.000E+00	
IN-PLANE SHEARING OF WEB	0.000E+00	0.000E+00		0 000E+00	0.000E+00		0.000E+00	0.000E+00	
ALONG STIFF. FLANGE AXIS	2.818E-04	0.000E+00		2.111E-09	0.000E+00		2.818E-04	0.000E+00	
TRANSVERSE TO FLANGE AX.	-5.744E-05	0.000E+00		9.030E-09	0.000E+00		-5.744E-05	0.000E+00	
IN-PLANE SHEAR OF FLANGE	0.000E+00	0.000E+00		0.000E+00	0.000E+00		0.000E+00	0.000E+00	

==

CAUSED BY UNIFORM PRESSURE

R E S U L T A N T S   I N   V A R I O U S   P A R T S   O F   T H E   P A N E L   S K I N   A N D   S T I F F E N E R S

ITEM   FROM MODEL OF ENTIRE PANEL(smeared)   FROM MODEL OF PANEL MODULE(branched)   SUM OF RESULTANTS FROM BOTH MOD-ELS

	(LOAD SET B)			(LOAD SET B)			(Considered part of load set B)		
	SKIN	STRINGER	RING	SKIN	STRINGER	RING	SKIN	STRINGER	RING
SKIN AXIAL	-1.211E+01	–	–	-5.717E+00	–	–	-1.782E+01	–	–
SKIN CIRC.	-3.420E+01	–	–	-1.542E+01	–	–	-4.962E+01	–	–
SKIN SHEAR	0.000E+00	–	–	0.000E+00	–	–	0.000E+00	–	–
	STRINGER	RING		STRINGER	RING		STRINGER	RING	
STIFFENER BASE ALONG AXIS	-7.514E+00	0.000E+00		-4.416E+00	0.000E+00		-1.193E+01	0.000E+00	
STIFFENER BASE TRANSVERSE	-3.420E+01	0.000E+00		-1.535E+01	0.000E+00		-4.955E+01	0.000E+00	
STIFFENER BASE SHEAR	0.000E+00	0.000E+00		0.000E+00	0.000E+00		0.000E+00	0.000E+00	
ALONG STIFFENER WEB AXIS	8.956E+00	0.000E+00		-1.555E-01	0.000E+00		8.800E+00	0.000E+00	
TRANSVERSE TO WEB AXIS	0.000E+00	0.000E+00		-1.992E-01	0.000E+00		-1.992E-01	0.000E+00	
IN-PLANE SHEARING OF WEB	4.825E+01	0.000E+00		0.000E+00	0.000E+00		4.825E+01	0.000E+00	
ALONG STIFF. FLANGE AXIS	3.983E+02	0.000E+00		4.459E-03	0.000E+00		3.983E+02	0.000E+00	
TRANSVERSE TO FLANGE AX.	0.000E+00	0.000E+00		7.230E-03	0.000E+00		7.230E-03	0.000E+00	
IN-PLANE SHEAR OF FLANGE	0.000E+00	0.000E+00		0.000E+00	0.000E+00		0.000E+00	0.000E+00	

==

CAUSED BY UNIFORM PRESSURE

E Q U I L I B R I U M   O F   R E S U L T A N T S   F R O M   A P P L I E D   N O R M A L   P R E S S U R E, P

ITEM   FROM MODEL OF ENTIRE PANEL(smeared)   FROM MODEL OF PANEL MODULE(branched)   SUM OF RESULTANTS FROM BOTH MOD-ELS

	(LOAD SET B)			(LOAD SET B)			(Considered part of load set B)		
	Nx	Ny	Nxy	Nx	Ny	Nxy	Nx	Ny	Nxy
FROM EQUFCE	5.750E+01	-3.420E+01	0.000E+00	-5.359E+00	-1.542E+01	0.000E+00	5.214E+01	-4.962E+01	0.000E+00
FROM EQUILIB	5.750E+01	-3.420E+01	0.000E+00	-5.359E+00	-1.542E+01	0.000E+00	5.214E+01	-4.962E+01	0.000E+00
ERROR	-7.629E-06	0.000E+00	0.000E+00	0.000E+00	0.000E+00	0.000E+00	-7.629E-06	0.000E+00	0.000E+00

==
==

*** END OF CALCS. FOR PREBUCKING FORCE DIST. ***

11.0 CALCULATION OF KNOCKDOWN FACTORS TO ACCOUNT FOR THE EFFECT OF IN–PLANE SHEAR LOAD N_{xy} ON GENERAL AND LOCAL BUCKLING LOAD FACTORS CALCULATED WITH BOSOR4–TYPE OF DISCRETIZED MODELS

11.1 METHOD USED IN PANDA2

Next, PANDA2 calculates knockdown factors for the effect of in–plane shear loads on general buckling, wide column buckling, and on local buckling. These knockdown factors are obtained from PANDA–type analyses in which general, panel, and local buckling load factors are calculated with and without the in–plane shear load, N_{xy}. The knockdown factors are given by:

$$\text{KNOCKDOWN} = \text{EIGENCRIT(with shear)/EIGENCRIT(no shear)} \qquad (11.1)$$

The shear knockdown factor for general instability calculated with the smeared stiffener model is stored in FKNOCK(1); The shear knockdown factor for wide-column instability calculated with the single panel module model is stored in FKNOCK(4); and shear knock-down factors for local instability are stored in FKNOCK(2) and FKNOCK(3). These factors are later applied to critical loads obtained with BOSOR4–type of discretized panel module models because buckling loads for these models are obtained neglecting in–plane shear. FKNOCK(1) is applied to the BOSOR4–type model in which the entire width of the panel with smeared rings and stringers is discretized; FKNOCK(4) is applied to the discretized single panel module model that is used to predict wide–column buckling [See Figs. 20(c) and 22(c)]; FKNOCK(2) is applied to the discretized single panel module model that is used to predict local buckling [See Figs. 20(a) and 22(a)]; and FKNOCK(3) is applied to buckling of the panel skin under a hat stiffener. It is emphasized that these four knockdown factors are for the effect of in–plane shear loading N_{xy} not for transverse shear deformation. The transverse shear deformation knockdown factors are obtained from Timoshenko beam theory, and they are discussed in Section 8.2.

11.2 EXAMPLE: THE HAT–STIFFENED PANEL

Results from the PANDA–type of analysis:

```
    Preliminary general buckling (from PANDA)=   2.3424E+00
     (axial,circ.) waves with shear=(1,1); without shear=(1,1)
    Preliminary local buckling (from PANDA)  =   1.3663E-01
     Simply-supported edges. No. of axial waves, MLOCAL=4
     Slope of local buckling nodal lines, CSLOPE=3.9415E-01
    Knockdown factors to account for the effect of in-plane shear load:
    Knockdown factor for general instabilty =   9.2027E-01
    Knockdown factor for local instabilty   =   7.9088E-01
    Knockdown factor (under hat crippling)  =   1.0000E+00
    Knockdown factor for inter-ring buckling=   9.2027E-01 (wide-column)
```

Resultants in prebuckled panel module segments:	SEG. 1	SEG. 2	SEG. 3	SEG.4	Nave(calc.)	Nave(given)
Axial resultant, Nx =	-1.4936E+03	-4.7615E+03	-1.1089E+02	-2.4269E+03	-2.9479E+03	-2.9479E+03
Circumferential resultant, Ny =	-4.9619E+01	-4.9553E+01	-1.9921E-01	7.2303E-03	-4.9619E+01	-4.9619E+01
In-plane shear resultant, Nxy =	1.0000E+03	1.0000E+03	0.0000E+00	0.0000E+00	1.0000E+03	1.0000E+03

11.3 RECENT MODIFICATION: KNOCKDOWN FACTORS INCLUDE EFFECT OF ANISOTROPY

Buckling Knockdown Factors Now Include the Effect of Anisotropic C(i,j) A shortcut method has just been described for including the effect of in-plane shear loads on general, panel, and local instability predictions obtained with use of BOSOR4-type of discretized models, which do not admit the effect of in-plane shear loads directly. The knockdown factors are obtained with PANDA-type analyses and defined in Eq. (11.1). PANDA2 has since been modified to include the effect of anisotropic C(i,j) in the computation of these knockdown factors. They are now calculated from the ratio

$$\text{KNOCKDOWN} = \frac{\text{EIGENCRIT(with shear and fully populated C(i,j))}}{\text{EIGENCRIT(no shear and BOSOR4-type C(i,j)}} \tag{11.2}$$

The "BOSOR4-type C(i,j)" are the constitutive law with C(1,3), C(1,6), C(2,3), C(2,6), C(3,4), C(3,5), C(4,6), C(5,6), and symmetric (j,i) terms set equal to zero. Hence, there may be knockdown factors less than unity even if there is no in-plane shear loading. Knockdown factors are never permitted to be greater than unity, so that "beneficial" anisotropic effects, if any, are not included in the buckling estimates obtained from BOSOR4-type discretized panel module models. However, the effects of anisotropy are usually deleterious, not beneficial.

12.0 TYPES OF BUCKLING ANALYSES PERFORMED IN PANDA2

12.1 SUMMARY OF TYPES OF BUCKLING ANALYSIS IN PANDA2:

(a) All types of buckling covered by the original PANDA code. These are listed in Table 1 of Ref. [1]. Included are: general instability (rings and stringers participate), local buckling (between adjacent stringers and adjacent rings), panel buckling (between rings with smeared stringers and between stringers with smeared rings), rolling of stiffeners (no web deformation) with skin participation, rolling of stiffeners (with web deformation) without skin participation, and crippling of stiffener parts.

(b) Local buckling predicted from a model in which the cross section of a single panel module is discretized Two modes may be calculated, depending on results: a "high-axial-wavenumber" mode and a "low-axial-wavenumber" mode.The "high-axial-wavenumber" mode corresponds roughly to buckling of the thin part of the skin (part excluding the width b_2 of the faying flange of the stringer). The "low-axial-wavenumber" mode may correspond roughly to local buckling between stringer centerlines or it may correspond to a mode involving sidesway of the stringers between rings. A constraint is introduced into the optimization problem that the "low-axial-wavenumber" mode shall correspond to a load factor that is 20 per cent higher than the load factor corresponding to the "high-axial-wavenumber" mode. This tends to prevent stiffener popoff for panels loaded into the post-local- buckling regime. Local buckling is enforced by introduction of constraints in the stiffness matrix that force the mode to be antisymmetric about the panel module centerline and symmetric midway between stringers. For both "high" and "low"-axial-wavenumber modes, ranges of number of axial halfwaves are searched until minimum buckling load factors are found with respect to the number of axial halfwaves.

(c) wide column buckling predicted from the mode! in which the cross section of a single panel module is discretized. This mode is obtained in the same way as are the local buckling modes in (b), except that wide–column buckling is enforced by introduction of constraints in the stiffness matrix that force the mode to be symmetric about the panel module centerline as well as symmetric midway between stringers. the number of axial half-waves is fixed at n = 1, rather than search being conducted for a critical load factor by varying n, as is done in (b). If there are transverse stiffeners (rings) present, both the local and the wide-column loads correspond to the panel being simply supported along ring centerlines and rings are neglected in the stability phase of the calculations. (Of course the rings are accounted for in the calculations of prebuckling strain and force distributions in the various parts of the panel.)

(d) general instability (rings and stringers smeared out) of the entire panel from a simple discretized model (no branches for stiffeners, since they are smeared out.) The purposes of this model are:

(1) to provide buckling loads in cases for which the axial load varies along the edge of the panel;

(2) to provide a check on both the PANDA calculations for general instability and on the wide column calculation for the case of uniform axial compression.

Such a check is especially useful for the wide column buckling load from (c) because curvature is neglected in the calculation in (c) and included in the calculation in (d). Note, however, that in this general instability calculation:

(1) The stiffeners are smeared out. Hence local stringer cross section deformation is not accounted for, and local skin bending in the general instability mode is not possible.

(2) The actual (spanwise varying) axial load distribution in the post-locally-buckled panel is not used; only the uniform prebuckling axial load distribution determined in SUBROUTINE FORCES is used.

Neglect of (1) yields an unconservative result (buckling load too high); neglect of (2) could cause either plus or minus error.

12.2 LOCAL BUCKLING PREDICTED FROM A DISCRETIZED MODULE

Local buckling as predicted from the discretized model of the single panel module is performed by SUBROUTINE LOCAL. The first call to SUBROUTINE LOCAL corresponds to determination of the "high-axial-wavenumber" local buckling load factor. If panel module local modes have been determined previously in a given run (for example, for a previous design iteration), the starting axial wavenumber and eigenvector are the values corresponding to the previous critical condition.

If the structural analysis is being conducted for a small design perturbation for the purpose of determining gradients of constraint conditions for optimization (IMOD = 1), new buckling load factors may be calculated from Rayleigh's quotient, in which the eigenmode is that corresponding to the unperturbed design. This is what happens if post-local-buckling effects are neglected (KOITER=0). If post-local-buckling effects are included, a new mode is calculated even for each small design perturbation because this mode is used to calculate the changes in post-local-buckling stresses due to the design perturbation. These changes must be computed accounting for changes in the local buckling mode shape in order to obtain accurate stress constraint gradients, and therefore appropriate design modifications during optimization cycles.

Eigenvalues corresponding to local buckling of the skin obtained from the BOSOR4-discretized panel module model are calculated for a range of axial wavenumbers. All four edges of the panel are assumed to be simply supported, even if you indicated "clamped" in your input, and the in-plane loading is assumed to be uniform (N_1, N_2, N_{12}), even if you provided for axial load N_x varying in the L2 (circumferential) direction.

If KOITER=Y (local postbuckling effects wanted), the state of the locally postbuckled panel is determined at the applied load and at the critical axial wavenumber determined from the local bifurcation buckling analysis.

Local buckling load factors from the discretized model of a single panel module for design iteration no. 0, load set no. 1, material iteration no. 0, follow. These load factors include the knockdown factor, 0.791 that accounts for the effect of in-plane shear loading. Resultants are uniform and given by:

LOAD SET A: axial, Nx = -3.00E+03; circ., Ny = 0.00E+00;
    in-plane shear, Nxy = 1.00E+03
LOAD SET B: axial, Nxo= 0.00E+00; circ., Nyo= 0.00E+00;
    in-plane shear, Nxyo= 0.00E+00 (Not from pressure)
LOAD SET B: Uniform normal pressure, P = 1.0000E+00
    Resultants from global (smeared stiffener) model:
        Nxo(p)= 57.5 Nyo(p)= -34.2, Nxyo(p)= 0.0
    Resultants from local (discrete stiffener) model:
        Nxo(p)= -5.36, Nyo(p)= -15.4, Nxyo(p)= 0.0 :

HIGH AXIAL WAVENUMBER LOAD FACTORS FOR LOCAL BIFURCATION BUCKLING

Axial Halfwaves	Eigenvalue	Knockdown Factors: Transverse shear def.	in-plane shear load	Final Value
8	0.480	0.964	0.791	0.366
9	0.490	0.963	"	0.373
7	0.483	0.963	"	0.368

Buckling modal displacements and derivatives of displacements with respect to s, the arc length along the discretized panel module segments, are computed from the eigenvector for the "high-axial-wavenumber" local buckling. These computations are performed by SUBROUTINE MODE, which follows the first call to SUBROUTINE LOCAL. These quantities are used in the post-local buckling stress analysis and for later plotting.

"Low-axial-wavenumber" local panel module buckling is next calculated. In the search for the critical buckling load factor with respect to the number of axial waves, the maximum number of axial waves is restricted to be less than MHIGH - 1, so that computations for the "high axial wavenumber" will not be repeated. The local buckling load factor and mode are determined in the second call to SUBROUTINE LOCAL in SUBROUTINE STRUCT.

LOW AXIAL WAVENUMBER LOAD FACTORS FOR LOCAL BIFURCATION BUCKLING

Axial Halfwaves	Eigenvalue	Knockdown Factors: Transverse shear def.	in-plane shear load	Final Value
1	1.47	0.894	0.791	1.043
2	0.839	0.938	"	0.622
3	0.739	0.945	"	0.552
4	0.631	0.953	"	0.475
5	0.550	0.959	"	0.417
6	0.504	0.962	"	0.384
7	0.483	0.963	"	0.368

13.0 LOCAL POSTBUCKLING ANALYSIS IN PANDA2

13.1 INTRODUCTION

There is a section of code in SUBROUTINE STRUCT identified as the "KOITER BRANCH". In that branch the nonlinear equilibrium state of a perfect or locally imperfect panel is calculated. The theory used in PANDA2 is similar to a theory originally formulated by Koiter in 1946 in Ref. [4]. Please see Appendix A for the most recent version of this implementation in PANDA2, which includes the effect of local initial geometric imperfections in the form of the local bifurcaton buckling mode. The following discussion applies to a perfect panel only.

13.2 LOCAL POSTBUCKLING THEORY USED IN PANDA2

According to this theory the local buckling mode in the skin changes shape during the post-local-buckling loading phase: for applied loads slightly above the bifurcation buckling load corresponding to local buckling, the post-buckling deformation pattern closely resembles the local bifurcation buckling mode. However, as the applied load is further increased, a region develops midway between two adjacent stringers in which there is little curvature change in the transverse (y) direction. Thus, the post-locally-buckled skin has one-half wave between stringers, but the top of the wave is "chopped off" –nearly flat– midway between stringers. This nearly flat region develops only after the load has risen somewhat above the bifurcation buckling load.

In the KOITER branch the following calculations are performed:

(a) The post-local buckling normal deflection, $w(x, y)$, is assumed to have the form:

$$
\begin{aligned}
w(x, y) &= f\left(\phi + a\phi^3\right) \sin[(\pi/L)(x - my)] \\
&= W(y) \sin[(\pi/L)(x - my)]
\end{aligned}
\tag{13.1}
$$

in which ϕ is the bifurcation buckling mode, f and a are undetermined coefficients, L is the half wavelength in the axial direction of the critical bifurcation buckling mode, and m is the slope of the nodal lines of the post-local buckling pattern.

This post-local-buckling pattern differs from that proposed by Koiter in [4]. Koiter assumed that $W(y)$ was constant in a central region away from the stiffeners. He introduced an edge parameter, α, that determined the extent of this region. Energy minimization with respect to α yielded the extent of the flat region.

In other respects, however, (except when initial local imperfections are present) the local postbuckling theory described next is similar to Koiter's 1946 theory.

(b) Certain wave shape parameters, $A_1, A_2, \ldots A_{26}$, are calculated once the bifurcation buckling mode shape ϕ is known. These calculations, involving numerical integration of various products of the buckling modal normal displacement and its first and second derivatives, take place in SUBROUTINE INTEG, which is called from SUBROUTINE MODE.

66

The heart of the Koiter theory is contained in SUBROUTINE KOIT2, in which the post-locally-buckled state of the panel is derived. The following computations occur in KOIT2:

(c) The average in-plane strains in the panel, e_1, e_2, and e_{12}, are obtained in terms of f, a, and m, which appear above in the expression for $w(x, y)$. This calculation occurs in SUBROUTINE EPSAVE, which is called from SUBROUTINE KOIT2.

The purpose of SUBROUTINE EPSAVE is to calculate certain coefficients, G_{11}, G_{12},...G_{16}, and G_{21}, G_{22},...G_{26}, as described next.

The average in-plane strains in the post-buckling range are given by:

$$e_1 = F_{10} + f^2 \left[G_{11} + aG_{12} + a^2 G_{13} + m^2 \left(G_{14} + aG_{15} + a^2 G_{16} \right) \right]$$

$$e_2 = F_{20} + f^2 \left[G_{21} + aG_{22} + a^2 G_{23} + m^2 \left(G_{24} + aG_{25} + a^2 G_{26} \right) \right] \qquad (13.2)$$

$$e_{12} = N_{xy}/C_x(3,3,5) + f^2 \left(G_{31} + aG_{32} + a^2 G_{33} \right)$$

in which $C_x(3,3,5)$ is the shear stiffness identified in Section 8.4; F_{10}, F_{20}, and G_{ij} are derived in EPSAVE; m is the slope of the buckling nodal lines; and a is an as yet undetermined coefficient that appears in the expression for the y-variation of the post-local-buckling pattern:

$$W(y) = f \left(\phi + a\phi^3 \right) \qquad (13.3)$$

where y is the coordinate across the panel, measured from midway between stringers, and ϕ is the normalized buckling mode shape determined by the BOSOR4-type of analysis for the discretized panel module cross section.

The quantity e_1 is the average axial strain in the locally post-buckled panel, $e_{2s} = e_2 + C(y)$, where e_2 is the average circumferential strain in the locally post-buckled panel; $C(y)$ is a nonlinear function of $W(y)$ given in SUBROUTINE EPSAVE; e_{12} is the average in-plane shear strain in the post-buckled panel; f is the amplitude of the local buckling pattern.

The starting point for this derivation is the relation between given applied loads, N_x, N_y, N_{xy}, and average loads in the panel skin, N_1, N_2, N_{12}:

$$N_x = N_1 + N_{stringer}$$

$$N_y = N_2 + N_{ring} \qquad (13.4)$$

$$N_{xy} = N_{12}$$

in which N_1, N_2, N_{12} are given by

$$N_1 = \int_0^{2L} \left\{ \int_0^b \left[A_{11}^i e_x + A_{12}^i e_y + N_{xo}^i \right] dy \right\} dx / (2bL)$$

$$N_2 = \int_0^{2L} \left\{ \int_0^b \left[A_{12}^i e_x + A_{22}^i e_y + N_{yo}^i \right] dy \right\} dx / (2bL) \qquad (13.5)$$

$$N_{12} = \int_0^{2L} \left\{ \int_0^b \left[A_{33}^i e_{xy} \right] dy \right\} dx / (2bL)$$

The coefficients, $A_{11}^i = C_x(1,1,i);$ $A_{12}^i = C_x(1,2,i);$ $A_{22}^i = C_x(2,2,i);$ $A_{33}^i = C_x(3,3,i)$, where C_x are the membrane stiffnesses of the segments of an "x-oriented" panel module; i is the module segment number; e_x, e_y, e_{xy} are the local membrane strains; and N_{xo}^i, N_{yo}^i are the known thermal resultants from curing. L is the half-wavelength of the local buckle pattern, and b is the stringer spacing.

The axial load in each stringer is

$$N_{stringer} = \int_0^L \left\{ \sum_{i=1}^{NSEGS} \left[\int_0^{S_i} (A_{11}^i e_x + A_{12}^i e_y + N_{xo}^i)\,ds \right] \right\} dx/(2bL) \qquad (13.6)$$

in which S_i is the width of the ith stringer segment. The expression for N_{rings} is analogous. "$NSEGS$" above refers to the segments of the stringer cross section (e.g. web, flange).

The local membrane strains, e_x, e_y, e_{xy}, can be expressed in terms of of average strains, e_1, e_2, e_{12} plus nonlinear terms arising from to local buckling deformations:

$$\begin{aligned} e_x &= e_1 + N\,W^2 \\ e_y &= e_2 + C(y) - \nu_{12}\,N\,W^2 \\ e_{xy} &= e_{12} + \text{(local buckling terms)} \end{aligned} \qquad (13.7)$$

in which the parameter N is given by

$$N = [0.5\,\pi\,n/(\text{ring spacing})]^2 \qquad (13.8)$$

(d) The local bifurcation buckling load factor, EKOITR, is calculated in SUBROUTINE EIGKOI. In this calculation the amplitude of the local postbuckling deformations, f, is assumed to be zero, and the flattening of the bifurcation buckling mode shape, a, is assumed to be zero.

The eigenvalue, EKOITR, is computed in the following way:

(1) The total potential, $U - W$, [strain energy minus the work done by the applied load set (N_x, N_y, N_{xy})], is written in terms of f and m.
(2) This total potential is minimized with respect to f and m.
(3) In the resulting two equations, all terms with f^2 are neglected, since the amplitude of the bifurcation buckling mode f is infinitesimal.
(4) The equation resulting from $\partial(U-W)/\partial f = 0$ yields an expression for the eigenvalue EKOITR in terms of m, the slope of the buckling nodal lines. This expression is "plugged into" the equation resulting from $\partial(U - W)/\partial m = 0$.
(5) The nonlinear equation for m resulting from step (4) is solved by Newton's method.
(6) The value of m determined in Step (5) is "plugged into" the expression for EKOITR derived in Step (4).

(e) The locally post-buckled state is calculated through solution of three simultaneous nonlinear algebraic equations for f^2, the square of the amplitude of the local buckles; a, the measure of the flattening of the bifurcation buckling mode midway between stringers; and

m, the slope of the buckling nodal lines (nonzero due to in-plane shear and/or unbalanced laminate). These equations are easy to solve because both a and m can be expressed in terms of f^2. The resulting two simultaneous nonlinear algebraic equations are solved by Newton's method in SUBROUTINE NEWTON.

(f) The average strains, e_1, e_2, e_{12}, and average stress resultants, N_1, N_2, N_{12}, in the panel skin are computed in SUBROUTINE NEWTON. These quantities are needed for computation of the tangent stiffness matrix of the locally post-buckled skin. Both the thin and thick portions of the panel skin are included.

(g) The tangent membrane stiffness of the locally post buckled skin is computed. This 3 x 3 matrix called C_{TAN} is needed for later calculation of general instability and wide column buckling of the locally post-buckled panel. This computation takes place in SUBROUTINE KOIT2. Each of the applied resultants, N_x, N_y, N_{xy}, is perturbed in turn, and new values for e_1, e_2, e_{12} and N_1, N_2, N_{12} are recomputed. The tangent stiffness matrix C_{TAN} is calculated knowing the rates of change of N_1, N_2, and N_{12} with respect to e_1, e_2, and e_{12}.

(h) Local membrane strain components, e_x, e_y, e_{xy}, and stress resultants, N_{1var}, N_{2var}, N_{12var}, are next calculated in SUBROUTINE STRMID. These quantities are calculated for all segments in the x-cross section of the single panel module. Particularly important is the accurate computation of the new axial load distribution, since this of course affects the predicted load factors for crippling of the various segments of the stringer cross section. Also, new computations of the stress resultants in the ring cross section are performed.

(i) The stresses in material coordinates are computed in all the layers and at the midwidth and end points of all the segments in the discretized panel module. The stresses are calculated for both sine and cosine amplitudes of the locally post buckled panel. Stress constraint conditions are set up based on the minimum margins for each type of failure in each type of material. The stress failure criteria used in PANDA2 are:

  (1) maximum tension along fibers
  (2) maximum compression along fibers
  (3) maximum tension transverse to fibers
  (4) maximum compression transverse to fibers
  (5) maximum in-plane shear stress

If the user has indicated in BEGIN that certain material types are composite material unidirectional tape, then for these layers the failure criterion (3) maximum tension transverse to fibers, is ignored. Instead, if transverse failure (cracking) has been detected at certain points in the panel module, at those points the panel is not considered to have failed. However, The allowable in compression along the fibers of cracked layers is reduced by as much as 50 per cent, depending upon by what margin the transverse tensile stress exceeds the threshold value.

The stress constraints of the locally post-buckled panel are calculated in SUBROUTINE STRTHK, which is the last subroutine called in the KOITER $=$ 1 branch of SUBROUTINE STRUCT.

(j) a stringer popoff constraint is also calculated in SUBROUTINE STRTHK. This constraint is based on tensile forces that develop in parts of the stringer web adjacent to the flanges. These tensile forces tend to peel the flanges from the panel skin and stringer web(s) to which they are attached. Results from a peel test may be necessary in order to establish an allowable value for the maximum web force permitted before peeling occurs. This maximum permitted force/(axial length) is required as input in BEGIN. The phenomenon and appropriate peel test specimen are shown in Figs. 5-7.

(k) If rings are present the stresses in the various parts of the "ring panel module" (module cross section that is normal to the y-axis) are calculated. This calculation is performed in SUBROUTINE STRCON.

13.3 EXAMPLE: THE HAT-STIFFENED PANEL

Corresponding to $N = 8$ waves from the skin buckling and local postbuckling analysis above, the distributions of N_{1var}, N_{2var}, and N_{12var} in the locally postbuckled panel are next calculated. The maximum stress components in the buckled skin as well as in the stiffener segments are also computed. In addition, the tangent membrane stiffness C_{TAN} in the locally buckled skin is calculated. C_{TAN} is needed for subsequent calculation of the load factor corresponding to wide column panel buckling.

Local bifurcation buckling load factor estimates: No. of axial half-waves= 8; Load Factor from Koiter Theory= 4.08E-01; Load Factor from BOSOR4-type panel module model= 3.80E-01 NOTE: The load factor from Koiter theory is computed for a flat panel. If the actual panel is curved, or if normal pressure is present, or if there exist significant prescribed in-plane resultants N_{xo}, N_{yo} from Load Set B, or if there is significant applied in-plane shear, N_{xy}, the load factor computed from Koiter theory will not necessarily agree with that computed from the BOSOR4-type module model.

```
    RESULTS FOR  8  AXIAL WAVES...POSTBUCKLING PARAMETERS:
      SLOPE, a, f =  6.6238E-01 -2.3679E-01  1.8972E-01
    APPLIED STRESS RESULTANTS (Load set A):
      Nx, Ny, Nxy = -3.0000E+03  0.0000E+00  1.0000E+03
    STRESS RESULTANTS GENERATED BY NORMAL PRESSURE (Load set B):
      Nxo,Nyo,Nxyo=  5.2143E+01 -4.9619E+01  0.0000E+00
    STRAIN AND STRESS FROM APPLIED LOADS (curing not included):
    AVERAGE STRAIN COMPONENTS :
      EPS1,   EPS2,   EPS12   = -3.10E-03 -6.67E-04  5.75E-03
    AVERAGE RESULTANTS IN SKIN:
      N1SKIN, N2SKIN, N12SKIN = -2.34E+03 -4.96E+01  1.00E+03
    TANGENT STIFFNESS MATRIX, CTAN...
        7.9790E+05  -4.0594E+04  0.0000E+00
       -4.0594E+04   4.1972E+05  0.0000E+00
        0.0000E+00   0.0000E+00  1.4111E+05
**** END OF POSTBUCKLING EQUILIBRIUM CALCULATIONS****
```

14.0 CALCULATION OF MAXIMUM STRESSES
IN EACH LAMINA OF EACH SEGMENT
AND CALCULATION OF THE STRINGER POP-OFF FORCE

14.1 GEOMETRY OF THIS CASE, SHOWING (SEGMENT, NODE) AND LAYER NUMBERING

INTERNAL STIFFENER
MODULE WITH HAT-SHAPED (TRAPEZOIDAL) STIFFENER...
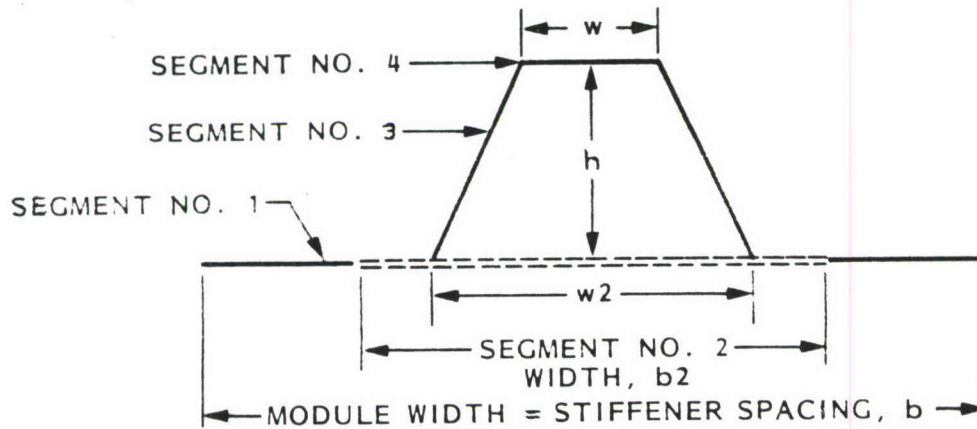
Fig. 16 Segment numbering in this sketch corresponds to numbering used for purposes of providing input data. The number of discretized BOSOR4-type segments into which the panel module is divided depends on whether or not the length b_2 is greater than w_2.

Fig. 17 Segment numbering for discretized single module models of the hat-stiffened panel for the case for which $b_2 > w_2$.

71
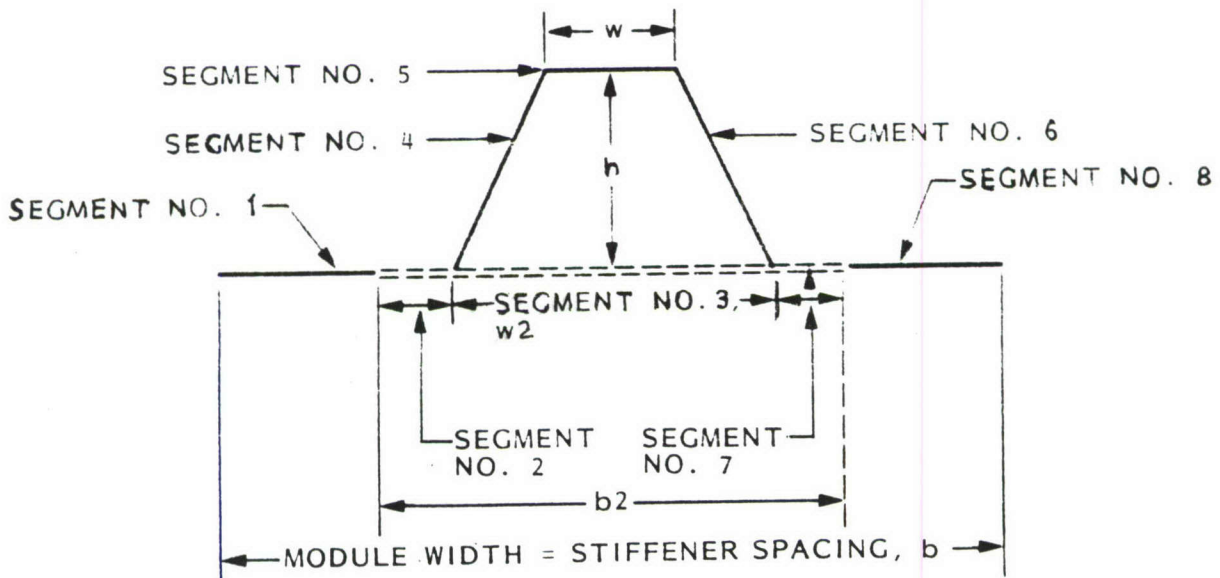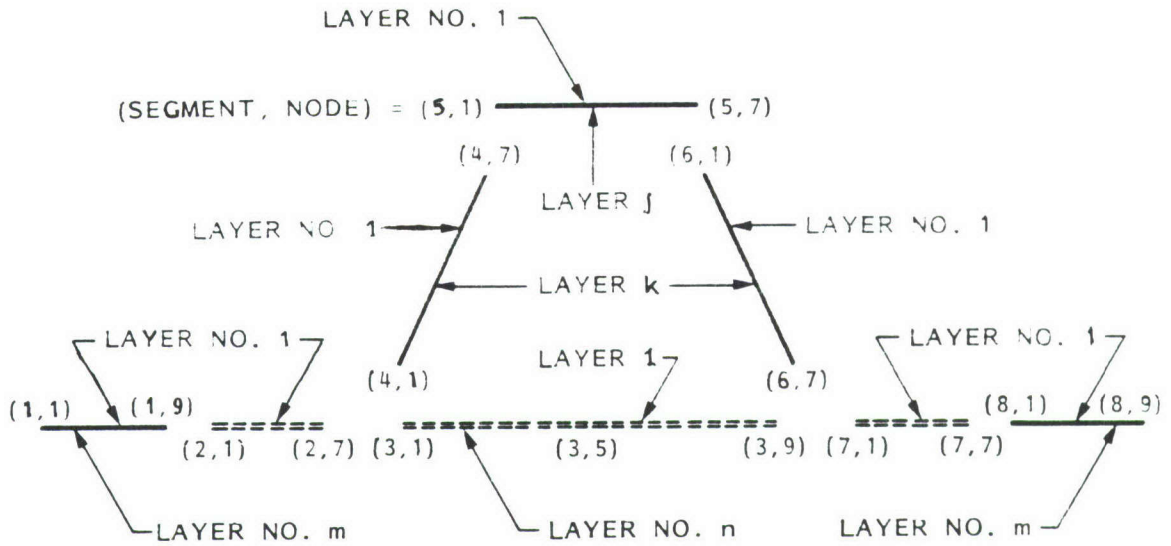
Fig. 18 (Segment, Node) pairs for stress output for hat–stiffened panel module for the case for which $b_2 > w_2$.

14.2 POST–LOCAL–BUCKLING STRESSES IN THE PANEL MODULE

Start calculation of stresses in the panel module depicted above... (Segment numbering below refers to that shown in Fig. 18.) Stresses are calculated in each of the lamina through the thickness only at the nodes shown in Fig. 18 because computation of these stresses requires quite a bit of computer time, especially if there are many layers. The critical stresses are most likely to be at these points in the panel module cross section because these points correspond to the maximum skin buckling amplitude or bending stress concentrations which occur where the thickness changes or where the webs intersect the panel skin or the stringer flange.

There are components of stress that vary in the axial direction as $\sin n\pi x/L$ as well as those that vary as $\cos n\pi x/L$. The values of stress corresponding to the axial locations where $\sin n\pi x/L = 1$ are listed in the rows of the following table in which the leftmost entry is SIN. Those corresponding to axial locations where $\cos n\pi x/L = 1$ are listed in the rows in which the leftmost entry is COS.

Sometimes four entries are given for each layer, two for SIN and two for COS. Notice that each (SIN,COS) pair is for a different value of the coordinate, Z, through the thickness. These two pairs of entries correspond to the stresses at the extreme fibers of the layer. Only one pair is given for any layer that was originally designated by the user as being composite tape. This is because composite tape layers are usually very thin, and it is not necessary to compute the stresses at more than one location through the thickness of a thin layer. Sometimes layers are missing from the list. These are layers the thicknesses of which either the user or PANDA2 has set equal to zero.

72

STRESS COMPONENTS IN THE POST-LOCALLY BUCKLED PANEL MODULE

BUCK. MODE	SEG.	NODE	LAYER	Z	WINDING ANGLE	SIG1	SIG2	SIG12	MODE OF FAILURE	TRANSVERSE CRACKING (1.0 means inactive)	ALLOWABLE STRESS	MATERIAL TYPE
SIN	1	1	1	-4.06E-02	45.0	-4.0459E+04	-2.6136E+04	6.0694E+02	no failure	1.0000E+00		2
COS	1	1	1	-4.06E-02	45.0	2.0488E+04	-1.8483E+04	-9.4879E+02	no failure	1.0000E+00		2
SIN	1	1	1	-3.46E-02	45.0	-3.0952E+04	-2.4504E+04	4.4046E+02	no failure	1.0000E+00		2
SIN	1	1	2	-3.46E-02	-45.0	-2.4504E+04	-3.0952E+04	-4.4046E+02	no failure	1.0000E+00		2
COS	1	1	1	-3.46E-02	45.0	2.0342E+04	-1.8629E+04	-9.6503E+02	no failure	1.0000E+00		2
COS	1	1	2	-3.46E-02	-45.0	-1.8629E+04	2.0342E+04	9.6503E+02	no failure	1.0000E+00		2
SIN	1	1	2	-2.86E-02	-45.0	-2.2873E+04	-2.1446E+04	-2.7399E+02	no failure	1.0000E+00		2
SIN	1	1	3	-2.86E-02	90.0	-4.2404E+04	1.6192E+03	-1.0246E+02	no failure	1.0000E+00		1
COS	1	1	2	-2.86E-02	-45.0	-1.8776E+04	2.0195E+04	9.8127E+02	no failure	1.0000E+00		2
COS	1	1	3	-2.86E-02	90.0	-1.8812E+04	6.1677E+03	-2.7981E+03	no failure	1.0000E+00		1
SIN	1	1	4	-2.34E-02	45.0	-2.9197E+04	2.1628E+03	1.2959E+02	no failure	1.0000E+00		1
COS	1	1	4	-2.34E-02	45.0	3.4167E+04	3.4482E+03	-9.9536E+02	no failure	1.0000E+00		1
SIN	1	1	6	-1.82E-02	-45.0	-4.4082E+04	4.1306E+03	1.4690E+01	no failure	1.0000E+00		1
COS	1	1	6	-1.82E-02	-45.0	-4.4848E+04	7.4248E+03	1.0094E+03	no failure	1.0000E+00		1
SIN	1	1	7	-1.30E-02	0.0	-1.7888E+04	4.0144E+03	1.5730E+03	no failure	1.0000E+00		1
COS	1	1	7	-1.30E-02	0.0	8.7254E+03	4.6751E+03	2.7981E+03	no failure	1.0000E+00		1
SIN	1	1	8	-2.60E-03	90.0	-9.0084E+03	5.9891E+03	-2.5531E+03	no failure	1.0000E+00		1
COS	1	1	8	-2.60E-03	90.0	-2.0948E+04	6.1166E+03	-2.7981E+03	no failure	1.0000E+00		1
SIN	1	1	9	2.56E-09	90.0	-5.6694E+03	6.4260E+03	-2.7981E+03	no failure	1.0000E+00		1
COS	1	1	9	2.56E-09	90.0	-2.1162E+04	6.1115E+03	-2.7981E+03	no failure	1.0000E+00		1
SIN	1	1	10	2.60E-03	0.0	1.4333E+04	6.0176E+03	3.0431E+03	no failure	1.0000E+00		1
COS	1	1	10	2.60E-03	0.0	8.6328E+03	4.5841E+03	2.7981E+03	no failure	1.0000E+00		1
SIN	1	1	11	1.30E-02	-45.0	-3.3221E+04	1.0855E+04	8.8035E+02	90 deg. tension	7.2223E-01	7.8400E+03	1
COS	1	1	11	1.30E-02	-45.0	-4.6223E+04	7.3031E+03	1.0939E+03	no failure	1.0000E+00		1
SIN	1	1	13	1.82E-02	45.0	9.5669E+04	5.5293E+03	-1.0246E+03	no failure	1.0000E+00		1
COS	1	1	13	1.82E-02	45.0	3.2335E+04	3.2860E+03	-1.1080E+03	no failure	1.0000E+00		1
SIN	1	1	14	2.34E-02	90.0	2.4381E+04	1.0358E+04	-5.0033E+03	90 deg. tension	9.4610E-01	9.8000E+03	1
COS	1	1	14	2.34E-02	90.0	-2.3084E+04	6.0655E+03	-2.7981E+03	no failure	1.0000E+00		1
SIN	1	1	15	2.86E-02	-45.0	-7.3151E+03	6.9199E+04	1.3133E+03	no failure	1.0000E+00		2
COS	1	1	15	2.86E-02	-45.0	-2.0172E+04	1.8799E+04	1.1361E+03	no failure	1.0000E+00		2
SIN	1	1	15	3.46E-02	-45.0	-5.6835E+03	7.8706E+04	1.4798E+03	no failure	1.0000E+00		2
SIN	1	1	16	3.46E-02	45.0	7.8706E+04	-5.6835E+03	-1.4798E+03	no failure	1.0000E+00		2
COS	1	1	15	3.46E-02	-45.0	-2.0319E+04	1.8652E+04	1.1524E+03	no failure	1.0000E+00		2
COS	1	1	16	3.46E-02	45.0	1.8652E+04	-2.0319E+04	-1.1524E+03	no failure	1.0000E+00		2
SIN	1	1	16	4.06E-02	45.0	8.8213E+04	-4.0519E+03	-1.6463E+03	no failure	1.0000E+00		2
COS	1	1	16	4.06E-02	45.0	1.8506E+04	-2.0465E+04	-1.1686E+03	no failure	1.0000E+00		2
SIN	1	9	1	-4.06E-02	45.0	3.3996E+04	5.2255E+02	6.7438E+03	no failure	1.0000E+00		2
COS	1	9	1	-4.06E-02	45.0	2.8493E+04	-3.3119E+04	3.7392E+03	no failure	1.0000E+00		2
SIN	1	9	1	-3.46E-02	45.0	3.0166E+04	-4.1194E+03	6.1363E+03	no failure	1.0000E+00		2
SIN	1	9	2	-3.46E-02	-45.0	-4.1194E+03	3.0166E+04	-6.1363E+03	no failure	1.0000E+00		2
COS	1	9	1	-3.46E-02	45.0	2.5683E+04	-3.2584E+04	3.6011E+03	no failure	1.0000E+00		2

-------- MORE RESULTS GIVEN BY PANDA2 BUT NOT LISTED IN ORDER TO SAVE SPACE -------

MAXIMUM STRESS COMPONENTS AND LOCATIONS OF THEM

ALLOWABLE STRESS	MAXIMUM STRESS	STRESS MARGIN	THRU THICKNESS LOCATION, Z	TYPE OF STRESS	LOCATION IN PANEL MODULE
9.1100E+04	-7.6675E+04	1.9205E-01	-6.6004E-02	compression along fiber	seg=2 , node=1 , layer=3 , matl=1
8.0000E+03	4.9272E+03	6.2365E-01	-6.6004E-02	in-plane shear stress	seg=2 , node=1 , layer=3 , matl=1
5.0000E+01	4.2354E+01	1.8053E-01	-1.2000E-02	stringer popoff stress margin	seg=4 , node=1 , layer=1 , matl=AD
5.0000E+01	5.0534E+01	-1.0569E-02	-1.2000E-02	stringer popoff stress margin	seg=6 , node=7 , layer=1 , matl=AD
1.0500E+05	-6.4406E+04	6.3028E-01	-4.0604E-02	compression transverse to fiber	seg=8 , node=1 , layer=1 , matl=2
1.0385E+05	-5.9454E+04	7.4666E-01	-3.4604E-02	compression along fiber	seg=8 , node=1 , layer=2 , matl=2
2.5060E+04	-1.4603E+03	1.6161E+01	-2.3400E-02	compression transverse to fiber	seg=8 , node=1 , layer=4 , matl=1
7.0000E+03	7.0264E+03	-3.7616E-03	4.0605E-02	in-plane shear stress	seg=8 , node=1 , layer=16, matl=2
9.1035E+04	9.0205E+04	9.1990E-03	-4.0604E-02	tension along fiber	seg=8 , node=9 , layer=1 , matl=2
8.9880E+04	8.0404E+04	1.1785E-01	-3.4604E-02	tension transverse to fiber	seg=8 , node=9 , layer=2 , matl=2
1.9000E+05	1.1335E+05	6.7624E-01	-2.3400E-02	tension along fiber	seg=8 , node=9 , layer=4 , matl=1

14.3 RESULTS OF STRINGER POPOFF CALCULATIONS

```
*** STRINGER POPOFF MARGIN FOR FIRST WEB OF HAT ****
Maximum in-plane tensile force in stringer web
tending to peel the faying flange from the skin:
  Peel force that varies axially as cos(nx)=   4.101
  Peel force that varies axially as sin(nx)=  42.35
  Peel force used in popoff constraint,FPOP=  42.35
Maximum allowable peel force, FPOPMAX    =  50.00
Stringer popoff margin=FPOP/FPOPMAX - 1.0 =   0.1805


*** STRINGER POPOFF MARGIN FOR SECOND WEB OF HAT ***
Maximum in-plane tensile force in stringer web
tending to peel the faying flange from the skin:
  Peel force that varies axially as cos(nx)=   4.101
  Peel force that varies axially as sin(nx)=  50.53
  Peel force used in popoff constraint,FPOP=  50.53
Maximum allowable peel force, FPOPMAX    =  50.00
Stringer popoff margin=FPOP/FPOPMAX - 1.0 =  -0.0106
******* END OF STRINGER POPOFF CALCULATIONS *******
***** END OF POSTBUCKLING STRESS CALCULATIONS *****
```

14.4 SOME MISCELLANEOUS DATA ABOUT THE HAT-STIFFENED PANEL

```
BOWING DUE TO CURING, WRESID= -1.1147E-03
BOWING DUE TO NORMAL PRESSURE (GLOBAL MODEL), -1.938E-02
DEPTH OF LOCAL BUCKLE =   0.1897
```

15.0 CRIPPLING OF STIFFENER PARTS

Crippling of stiffener parts is calculated next in SUBROUTINE STFEIG. Proper account is of course made here for redistribution of the applied in-plane loads, N_x, N_y, N_{xy}, due to post-local buckling. After local skin buckling less load is carried by the skin and more by the stringers. The coding in SUBROUTINE STFEIG is essentially the same as that in the original PANDA code [1],[8]. There are two types of crippling:

(a) crippling of so-called "internal" segments, that is stiffener segments that do not have free edges. Crippling loads for these interior segments are calculated as if they are infinitely long axially compressed plates simply supported along their two opposite long edges.

(b) crippling of so-called "end" segments, that is stiffener segments with one free edge. Crippling loads are computed assuming that the stiffener end cross section does not deform and the number of axial half-waves is the same as that for the interior segment to which the end segment is attached.

```
           *** CRIPPLING (short wavelength buckling) ***
            *** of parts of the panel module cross section ***
               *** perpendicular to the panel generator  ***
```

STIFF. TYPE	MODULE SEG.	PRELOAD RESULTANT (from curing and load set B)	APPLIED RESULTANT	CRIPPLING LOAD FACTOR (no transverse shear deformation)	CRIPPLING LOAD FACTOR (with transverse shear deformation)	HALFWAVES BETWEEN RINGS
stringer	2	-1.3970E+02	-5.9489E+03	5.7673E+00	3.6002E+00	14
stringer	3	2.0020E+01	-1.4371E+02	2.2645E+00	2.1380E+00	23
stringer	4	3.8675E+02	-3.7912E+03	6.0272E+00	3.9549E+00	19

```
              *** END OF CRIPPLING CALCULATIONS ***
```

RECENT MODIFICATION IN STIFFENER CRIPPLING CALCULATIONS

Two-Segment Crippling of Stiffeners Just above is described the crippling analysis of stiffener parts. Two kinds of stiffener parts are identified: "internal" segments and "end" segments. In the paragraph on crippling of "end" segments, that is, stiffener segments with one free edge, the following statement is made: "Crippling loads are computed assuming that the stiffener end cross section does not deform and the number of axial half-waves is the same as that for the interior segment to which the end segment is attached." In the recently modified PANDA2 program the number of axial half-waves is no longer thus restricted. Instead, a search over the number of axial half-waves is conducted to find the lowest crippling load factor. In many cases it turns out that the search over the number of axial half-waves is not necessary, but there are cases, such as that shown in Fig. A13 (Appendix A), for which the new search yields a lower crippling load factor.

16.0 WIDE COLUMN BUCKLING

16.1 PANDA2 MODEL AND PHILOSOPHY

Next, the wide column buckling load (an approximation of the panel instability load, that is, buckling between rings) is calculated. The proper tangent stiffness of the locally post-buckled skin is included in this model. Also, redistribution of the axial load due to local buckling of the skin between stringers is accounted for. The wide column load factor is computed by SUBROUTINE BUCKLE. It is called "wide column" because instability of only a single panel module is considered. Therefore, the boundary conditions along the two edges of the complete panel normal to the screen are not considered. Instead, symmetry conditions are imposed along the analogous two edges of the single panel module.

The number of axial halfwaves is restricted to one. The length of panel normal to the screen depends on whether or not there are stiffeners in the transverse direction (rings). If there are not, this length is taken as the length of the entire panel multiplied by a factor that is unity if the actual panel is simply supported along the two edges that lie in the plane of the screen and parallel to it. If the actual panel is clamped along these two edges, the length of panel normal to the screen is taken as the length of the actual panel divided by $3.85^{1/2}$. If the panel is stiffened by transverse stiffeners (called "rings" in PANDA2) the length normal to the screen is taken to be the spacing between ring attachment lines and the panel is assumed to be simply supported along these attachment lines and the rings are neglected in the stability phase of the calculations.

Wide column buckling with use of the discretized single panel module model is included as a constraint because it accounts for local deformations of the stiffener whose axis is normal to the screen in the panel (inter-ring) buckling mode, and it accounts for local deformation of the skin between stringers. In contrast, the PANDA-type of panel instability calculation with the smeared stiffeners does not include these local deformations. The local deformation of the stringer cross section is particularly significant in the case of J-shaped stiffeners and sometimes in the case of hat-shaped stiffeners. Some examples given later show the importance of local deformation of the skin between stringers in the wide column buckling mode.

The wide column buckling model uses the same discretized single panel module as does the local skin buckling model. However, in the case of wide column buckling the number of axial half waves between rings is unity, and the normal modal deflection at the right-hand symmetry plane in the single module model is constrained to be equal to that at the left-hand symmetry plane. In contrast, in the local skin buckling model the number of axial halfwaves between rings varies until a minimum buckling load factor has been found, and the normal modal deflection at the right-hand symmetry plane is constrained to be equal to minus that at the left-hand symmetry plane.

The wide column buckling analysis takes into account the reduced effective stiffness of the panel skin due to local postbuckling of the skin between stringers if you have chosen KOITER = Y. The applied average axial load N_x is assumed to be uniform (equal to N_1), even if you provided for N_x varying in the L2 (circum.) direction.

16.2 RESULTS FROM THE HAT-STIFFENED PANEL EXAMPLE

Next, PANDA2 calculates the wide column buckling factor from a discretized model of a single panel module for design iteration no. 0, load set no. 1, material iteration no. 0. This load factor includes the knockdown factor, 9.158E-01 that accounts for the effect of in-plane shear loading. The effective axial length of the wide column is 1.5289E+01. Resultants are uniform and given by:

```
        LOAD SET A: axial, Nx = -3.00E+03; circ., Ny =  0.00E+00;
           in-plane shear, Nxy =  1.00E+03
        LOAD SET B: axial, Nxo=  0.00E+00; circ., Nyo=  0.00E+00;
           in-plane shear, Nxyo=  0.00E+00 (Not from pressure)
        LOAD SET B: Uniform normal pressure, P =    1.0000E+00
           Resultants from global (smeared stiffener) model:
             Nxo(p)= 57.5  Nyo(p)= -34.2,  Nxyo(p)= 0.0
           Resultants from local (discrete stiffener) model:
             Nxo(p)=-5.36  Nyo(p)= -15.4,  Nxyo(p)= 0.0 :


        WIDE COLUMN PANEL BUCKLING LOAD FACTOR =        3.078E+00


        ISKIN = 0. (WIDE COLUMN BUCKLING IS IGNORED IF ISKIN = 1.)
        IWIDE = 1. (WIDE COLUMN BUCKLING IS IGNORED IF IWIDE = 0.)
        ITIP  = 0. (MODE OF BUCKLING IS STRINGER SIDESWAY IF ITIP = 1.)
           *** END OF WIDE COLUMN BUCKLING CALCULATIONS ***
```

17.0 PANDA[1]-TYPE BUCKLING ANALYSIS

17.1 INTRODUCTION

Next, local, panel, and general instability load factors and load factors corresponding to rolling of the stiffeners with and without participation of the skin are calculated in SUB-ROUTINE BUCPAN. (Calculations including rolling of the stiffeners are not performed for hat-stiffened panels. However, the torsional rigidity derived from the area enclosed within the hat is accounted for correctly, as previously described in the section of smeared stiffener analysis.) If KOITER = 1 (local post buckling effects included in the analysis) the proper constitutive law for the locally post buckled skin is used in generation of panel and general instability load factors. The following represents a PANDA-type of buckling analysis of the entire panel. It does not involve the discretized model of the panel module.

17.2 EXPLANATION AND RESULTS FOR THE HAT–STIFFENED PANEL

Next, various types of buckling (general, panel, local, rolling) are calculated with use of subroutines from the original PANDA program. See Refs. [1] and [8] for details on methods used.

In the list below, "simp-support" means that the region of the panel being considered is assumed to be simply-supported along all four edges and there are no stiffeners along these edges; "local buck." indicates the region being considered is that bounded by adjacent rings and stringers; "smear string" indicates the region is that bounded axially by adjacent rings and bounded circumferentially by the panel longitudinal edges, with stringers smeared out; "smear rings" indicates the region is that bounded axially by the panel lateral edges and circumferentially by adjacent stringers, with rings smeared out in the model; "rolling with" means that both stiffeners and skin participate in the buckling deflections; "rolling only" means that only the stiffener cross sections deform–the panel skin does not participate; M is the number of axial half-waves in the region being considered; N is the number of circumferential half-waves in the region being considered; and "slope" is the slope of the nodal lines in the buckling modal pattern (non-zero for panels with unbalanced laminates and panels with applied in-plane shear loading). Loading is assumed to be uniform (N_1, N_2, N_{12}) even if you provided for N_x varying in the L2 (circumferential) direction. Clamping is taken into account by doing the analysis for a panel that is shorter in the axial direction by the factor $3.85^{1/2}$ than the dimension that you originally provided as input.

Buckling load factors from PANDA-type models for design iteration no. 0, load set no. 1, material iteration no. 0. These load factors include the effect of in-plane shear loading. M = axial half-waves; N = circ. half-waves. Loading is uniform, with resultants given by:

```
LOAD SET A: axial, Nx = -3.00E+03; circ., Ny =  0.00E+00;
   in-plane shear, Nxy =  1.00E+03
LOAD SET B: axial, Nxo=  0.00E+00; circ., Nyo=  0.00E+00;
   in-plane shear, Nxyo=  0.00E+00 (Not from pressure)
LOAD SET B: Uniform normal pressure, P =    1.0000E+00
   Resultants from global (smeared stiffener) model:
```

78

```
      Nxo(p)= 57.5   Nyo(p)= -34.2,   Nxyo(p)= 0.0
   Resultants from local (discrete stiffener) model:
      Nxo(p)=-5.36   Nyo(p)= -15.4,   Nxyo(p)= 0.0 :
```

We are now in SUBROUTINE GENSTB, which is called from SUBROUTINE BUCPAN.
PANDA-type "closed form" analysis. In this particular call to SUBROUTINE GENSTB
we obtain a buckling load factor for buckling of the following type:

General buckling (simple support at all boundaries). Rolling of non-smeared stiffeners is
not included.

```
   Axial, circumferential lengths, this buckling model=
      1.5289E+01   2.4000E+01
   Eigenvalue in-plane loads/length of edge,
      Nx,Ny,Nxy= -3.0000E+03 -3.1623E+00  1.0000E+03
   Fixed       in-plane loads/length of edge,
      Nxo, Nyo =  5.2143E+01 -4.9620E+01
   Effective thick, x-face, transverse shearing = 1.437E+00
   Effective thick, y-face, transverse shearing = 8.1209E-02
   Transverse shear stiffness components =
      G13, G23 =  3.3717E+04  3.4233E+05
   Is transverse shear deformation weakening included?=  YES

   Buckling load factors, no. of halfwaves, nodal line slope
      (M = axial, N = circumferential):
   Neglecting transverse shear deformation weakening=
      Buckling load factor = 4.7826E+00 (M =  1, N =  1)
      Nodal line slope     = 7.0000E-02
   Including   transverse shear deformation weakening=
      Buckling load factor = 3.2853E+00 (M =  1, N =  1)
      Nodal line slope     = 7.0000E-02
    **** END OF PANDA-TYPE (CLOSED FORM) *****
    *** CALCS. FOR A VARIETY OF BUCKLING MODES ***
```

18.0 FINAL LISTING OF WEIGHT, DESIGN MARGINS, AND DESIGN FOR THE HAT–STIFFENED PANEL

After all behavioral constraints (buckling load factors and stresses) have been calculated in SUBROUTINE STRUCT, the objective function, which in this case is the weight of the panel, is computed in SUBROUTINE OBJECT.

```
***************************************************************
************************* PANEL WEIGHT *************************
****************                         *********************


     CURRENT VALUE OF THE OBJECTIVE FUNCTION:  WEIGHT OF PANEL
VAR.  STR/  SEG.  LAYER  CURRENT
NO.   RNG   NO.   NO.    VALUE               DEFINITION

                         5.239E+00   WEIGHT OF THE ENTIRE PANEL

*****************                         *****************
************************* PANEL WEIGHT *************************
```

Next are listed the design margins, the values of current design parameters with an indication of the role of these parameters in an optimization process and lower and upper bounds of the decision variables, fixed parameters, and allowables. Finally, the thicknesses and winding angles of each layer of each segment in the panel module are listed. The sample case ends with a list of files used and generated during execution of the PANDA2 mainprocessor.

```
          CURRENT VALUES OF MARGINS CORRESPONDING TO CURRENT DESIGN
     SEG. CURRENT
     NO.   VALUE                      DEFINITION
          6.762E-01  tensile fiber: (allowable stress)/(actual stress)-1, matl 1
          1.921E-01  compressive fiber: (allowable stress)/actual-1, matl type 1
          1.616E+01  compres. transverse stress margin: (allow./actual)-1,matl 1
          6.237E-01  in-plane shear stress margin: (allowable/actual)-1,  matl 1
          1.805E-01  stringer popoff stress margin:(allowable/actual)-1, web   1
          9.199E-03  tensile fiber: (allowable stress)/(actual stress)-1, matl 2
          7.467E-01  compressive fiber: (allowable stress)/actual-1, matl type 2
          1.179E-01  tensile transverse stress marg.:(allowable/actual)-1,matl 2
          6.303E-01  compres. transverse stress margin: (allow./actual)-1,matl 2
         -3.762E-03  in-plane shear stress margin: (allowable/actual)-1,  matl 2
         -1.057E-02  stringer popoff stress margin:(allowable/actual)-1, web   2
       2  2.600E+00  crippling margin for stringer segment. 14   local halfwaves
       3  1.138E+00  crippling margin for stringer segment. 23   local halfwaves
       4  2.955E+00  crippling margin for stringer segment. 19   local halfwaves
          2.078E+00  (Wide column panel buck. load factor)/(factor of safety)-1
          2.134E-01  buck.margin simp-support web buckling;M=20;N=1; slope=-0.57
               **********  ALL 1 LOAD SETS PROCESSED  **********
          ***********************************************************
```

SUMMARY OF INFORMATION FROM OPTIMIZATION ANALYSIS

VAR. NO.	DEC. VAR.	ESCAPE VAR.	LINK. VAR.	LINKED TO	LINKING CONSTANT	LOWER BOUND	CURRENT VALUE	UPPER BOUND	DEFINITION
1	N	N	N	0	0.00E+00	0.00E+00	8.0000E+00	0.00E+00	stiffener spacing, b
2	Y	N	N	0	0.00E+00	1.50E+00	2.5000E+00	2.50E+00	width of stiffener base, b2
3	Y	N	N	0	0.00E+00	8.00E-01	1.2434E+00	1.50E+00	height of stiffener (type H to see sketch), h
4	N	N	Y	5	8.00E-01	0.00E+00	1.3129E+00	0.00E+00	width of outer flange of stiffener, w
5	Y	N	N	0	0.00E+00	8.00E-01	1.6411E+00	2.00E+00	width of hat base, w2
6	N	N	N	0	0.00E+00	0.00E+00	6.0000E-03	0.00E+00	thickness for layer index no.(1)
7	N	N	N	0	0.00E+00	0.00E+00	6.0000E-03	0.00E+00	thickness for layer index no.(2)
8	N	N	N	0	0.00E+00	0.00E+00	5.2045E-03	0.00E+00	thickness for layer index no.(3)
9	N	N	N	0	0.00E+00	0.00E+00	5.2000E-03	0.00E+00	thickness for layer index no.(4)
10	N	N	N	0	0.00E+00	0.00E+00	0.0000E+00	0.00E+00	thickness for layer index no.(5)
11	N	N	N	0	0.00E+00	0.00E+00	5.2000E-03	0.00E+00	thickness for layer index no.(6)
12	N	N	N	0	0.00E+00	0.00E+00	1.0400E-02	0.00E+00	thickness for layer index no.(7)
13	N	N	N	0	0.00E+00	0.00E+00	2.6000E-03	0.00E+00	thickness for layer index no.(8)
14	N	N	N	0	0.00E+00	0.00E+00	1.5600E-02	0.00E+00	thickness for layer index no.(9)
15	N	N	N	0	0.00E+00	0.00E+00	5.2000E-03	0.00E+00	thickness for layer index no.(10)
16	N	N	N	0	0.00E+00	0.00E+00	1.0400E-02	0.00E+00	thickness for layer index no.(11)

PARAMETERS WHICH ARE ALWAYS FIXED.   NONE CAN BE DECISION VARIAB.

VAR. NO.	STR/ RNG	SEG. NO.	LAYER NO.	CURRENT VALUE	DEFINITION
1		0	0	3.000E+01	Panel length normal to the plane of the screen, L1
2		0	0	2.400E+01	Panel length in the plane of the screen, L2
3	STR	0	0	HAT	Identify type of stiffener along L1 (N, T, J, R, A)
4	STR	0	0	1.000E+00	Are the stringers cocured with the skin?
5	STR	1	1	4.500E+01	winding angle (deg.) for layer index no.(1)
6	STR	1	2	-4.500E+01	winding angle (deg.) for layer index no.(2)
7	STR	1	3	9.000E+01	winding angle (deg.) for layer index no.(3)
8	STR	1	4	4.500E+01	winding angle (deg.) for layer index no.(4)
9	STR	1	5	0.000E+00	winding angle (deg.) for layer index no.(5)
10	STR	1	6	-4.500E+01	winding angle (deg.) for layer index no.(6)
11	STR	1	7	0.000E+00	winding angle (deg.) for layer index no.(7)
12	STR	1	8	9.000E+01	winding angle (deg.) for layer index no.(8)
13	STR	2	3	0.000E+00	winding angle (deg.) for layer index no.(9)
14	STR	2	4	9.000E+01	winding angle (deg.) for layer index no.(10)
15	STR	4	3	0.000E+00	winding angle (deg.) for layer index no.(11)
16	STR	0	0	1.000E+00	choose external (0) or internal (1) stiffeners
17	RNG	0	0	NONE	Identify type of stiffener along L2 (N, T, J, R, A)
18		0	0	-1.940E+02	Radius of curvature in the plane of screen, R
19		0	0	3.842E+05	Radius of curvature normal to plane of screen, R2
20		0	0	2.000E+07	modulus in the fiber direction, E1(1)
21		0	0	1.400E+06	modulus transverse to fibers, E2(1)
22		0	0	7.000E+05	in-plane shear modulus, G(1)
23		0	0	2.030E-02	small Poisson's ratio, NU(1)
24		0	0	7.000E+05	out-of-plane shear modulus, G13(1)
25		0	0	4.000E+05	out-of-plane shear modulus, G23(1)
26		0	0	5.000E-08	thermal expansion along fibers, A1(1)
27		0	0	1.600E-05	transverse thermal expansion, A2(1)
28		0	0	2.700E+02	residual stress temperature (positive),TEMPTUR(1)
29		0	0	5.600E-02	weight density (gtr than 0!) of material type(1)
30		0	0	5.200E-03	Thickness of a single lamina of matl type(1)

81

```
31        0    0    1.050E+07    modulus in the fiber direction, E1(2 )
32        0    0    1.050E+07    modulus transverse to fibers,   E2(2 )
33        0    0    7.000E+05    in-plane shear modulus,          G(2 )
34        0    0    7.700E-02    small Poisson's ratio,          NU(2 )
35        0    0    7.000E+05    out-of-plane shear modulus,    G13(2 )
36        0    0    4.000E+05    out-of-plane shear modulus,    G23(2 )
37        0    0    1.500E-06    thermal expansion along fibers, A1(2 )
38        0    0    1.500E-06    transverse thermal expansion,   A2(2 )
39        0    0    2.700E+02    residual stress temperature (positive),TEMPTUR(2 )
40        0    0    5.600E-02    weight density (gtr than 0!) of material type(2 )
41        0    0    0.000E+00    Thickness of a single lamina of matl type(2 )
42        0    0    1.000E+00    Choose 0=simple support or 1=clamping
```

PARAMETERS WHICH ARE CLASSIFIED AS ALLOWABLES (e.g. max. stress)

VAR. NO.	STR/ RNG	SEG. NO.	LAYER NO.	CURRENT VALUE	DEFINITION
1	STR	0	0	5.000E+01	What force/(axial length) will cause web peel-off?
2		0	0	2.000E+07	Maximum allowable stress in material type(1)
3		0	0	1.900E+05	maximum tensile stress along fibers, matl(1)
4		0	0	1.828E+05	max compressive stress along fibers, matl(1)
5		0	0	9.800E+03	max tensile stress normal to fibers, matl(1)
6		0	0	2.506E+04	max compress stress normal to fibers,matl(1)
7		0	0	1.000E+04	maximum shear stress in material type(1)
8		0	0	1.050E+07	Maximum allowable stress in material type(2)
9		0	0	9.104E+04	maximum tensile stress along fibers, matl(2)
10		0	0	1.038E+05	max compressive stress along fibers, matl(2)
11		0	0	8.988E+04	max tensile stress normal to fibers, matl(2)
12		0	0	1.050E+05	max compress stress normal to fibers,matl(2)
13		0	0	7.000E+03	maximum shear stress in material type(2)
14		0	0	1.000E+00	maximum value of local/general buckling

PANEL GEOMETRY IN THE AXIAL (L1) DIRECTION
MODULE WITH HAT-SHAPED (TRAPEZOIDAL) STIFFENER
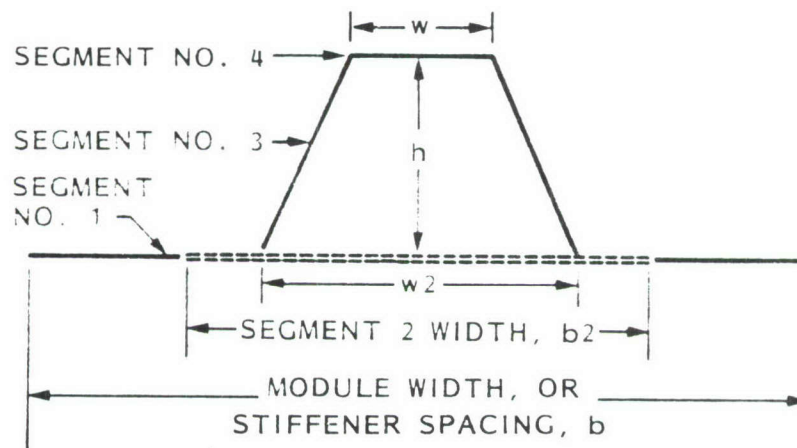
Fig. 19 Segment numbering for wall construction list that follows.

STR/ RNG	TYPE	SEG. NO.	LAYER NO.	LAYER TYPE	THICKNESS	WINDING ANGLE	MATERAL TYPE	CRACKING RATIO
STR	HAT	1	1	1	6.0000E-03	4.5000E+01	2	1.0000E+00
STR	HAT	1	2	2	6.0000E-03	-4.5000E+01	2	1.0000E+00
STR	HAT	1	3	3	5.2045E-03	9.0000E+01	1	1.0000E+00
STR	HAT	1	4	4	5.2000E-03	4.5000E+01	1	1.0000E+00
STR	HAT	1	5	5	0.0000E+00	0.0000E+00	1	1.0000E+00
STR	HAT	1	6	6	5.2000E-03	-4.5000E+01	1	1.0000E+00
STR	HAT	1	7	7	1.0400E-02	0.0000E+00	1	1.0000E+00
STR	HAT	1	8	8	2.6000E-03	9.0000E+01	1	1.0000E+00
STR	HAT	1	9	8	2.6000E-03	9.0000E+01	1	1.0000E+00
STR	HAT	1	10	7	1.0400E-02	0.0000E+00	1	1.0000E+00
STR	HAT	1	11	6	5.2000E-03	-4.5000E+01	1	1.0000E+00
STR	HAT	1	12	5	0.0000E+00	0.0000E+00	1	1.0000E+00
STR	HAT	1	13	4	5.2000E-03	4.5000E+01	1	1.0000E+00
STR	HAT	1	14	3	5.2045E-03	9.0000E+01	1	1.0000E+00
STR	HAT	1	15	2	6.0000E-03	-4.5000E+01	2	1.0000E+00
STR	HAT	1	16	1	6.0000E-03	4.5000E+01	2	1.0000E+00
STR	HAT	2	1	1	6.0000E-03	4.5000E+01	2	1.0000E+00
STR	HAT	2	2	2	6.0000E-03	-4.5000E+01	2	1.0000E+00
STR	HAT	2	3	9	1.5600E-02	0.0000E+00	1	1.0000E+00
STR	HAT	2	4	10	5.2000E-03	9.0000E+01	1	1.0000E+00
STR	HAT	2	5	9	1.5600E-02	0.0000E+00	1	1.0000E+00
STR	HAT	2	6	3	5.2045E-03	9.0000E+01	1	1.0000E+00
STR	HAT	2	7	4	5.2000E-03	4.5000E+01	1	1.0000E+00
STR	HAT	2	8	5	0.0000E+00	0.0000E+00	1	1.0000E+00
STR	HAT	2	9	6	5.2000E-03	-4.5000E+01	1	1.0000E+00
STR	HAT	2	10	7	1.0400E-02	0.0000E+00	1	1.0000E+00
STR	HAT	2	11	8	2.6000E-03	9.0000E+01	1	1.0000E+00
STR	HAT	2	12	8	2.6000E-03	9.0000E+01	1	1.0000E+00
STR	HAT	2	13	7	1.0400E-02	0.0000E+00	1	1.0000E+00
STR	HAT	2	14	6	5.2000E-03	-4.5000E+01	1	1.0000E+00
STR	HAT	2	15	5	0.0000E+00	0.0000E+00	1	1.0000E+00
STR	HAT	2	16	4	5.2000E-03	4.5000E+01	1	1.0000E+00
STR	HAT	2	17	3	5.2045E-03	9.0000E+01	1	1.0000E+00
STR	HAT	2	18	9	1.5600E-02	0.0000E+00	1	1.0000E+00
STR	HAT	2	19	10	5.2000E-03	9.0000E+01	1	1.0000E+00
STR	HAT	2	20	9	1.5600E-02	0.0000E+00	1	1.0000E+00
STR	HAT	2	21	2	6.0000E-03	-4.5000E+01	2	1.0000E+00
STR	HAT	2	22	1	6.0000E-03	4.5000E+01	2	1.0000E+00
STR	HAT	3	1	1	6.0000E-03	4.5000E+01	2	1.0000E+00
STR	HAT	3	2	2	6.0000E-03	-4.5000E+01	2	1.0000E+00
STR	HAT	3	3	2	6.0000E-03	-4.5000E+01	2	1.0000E+00
STR	HAT	3	4	1	6.0000E-03	4.5000E+01	2	1.0000E+00

```
STR   HAT   4      1      1    6.0000E-03   4.5000E+01      2              1.0000E+00
STR   HAT   4      2      2    6.0000E-03  -4.5000E+01      2              1.0000E+00
STR   HAT   4      3     11    1.5600E-02   0.0000E+00      1              1.0000E+00
STR   HAT   4      4     10    5.2000E-03   9.0000E+01      1              1.0000E+00
STR   HAT   4      5     11    1.5600E-02   0.0000E+00      1              1.0000E+00
STR   HAT   4      6     10    5.2000E-03   9.0000E+01      1              1.0000E+00
STR   HAT   4      7     11    1.5600E-02   0.0000E+00      1              1.0000E+00
STR   HAT   4      8     10    5.2000E-03   9.0000E+01      1              1.0000E+00
STR   HAT   4      9     11    1.5600E-02   0.0000E+00      1              1.0000E+00
STR   HAT   4     10     10    5.2000E-03   9.0000E+01      1              1.0000E+00
STR   HAT   4     11     11    1.5600E-02   0.0000E+00      1              1.0000E+00
STR   HAT   4     12     10    5.2000E-03   9.0000E+01      1              1.0000E+00
STR   HAT   4     13     11    1.5600E-02   0.0000E+00      1              1.0000E+00
STR   HAT   4     14      2    6.0000E-03  -4.5000E+01      2              1.0000E+00
STR   HAT   4     15      1    6.0000E-03   4.5000E+01      2              1.0000E+00
```

DESCRIPTION OF FILES USED AND GENERATED IN THIS RUN:
 HAT.NAM = This file contains only the name of the case.
 HAT.OPT = Input data generated by MAINSETUP.
 HAT.OPM = Output data. Please list this file and inspect
           carefully before proceeding.
 HAT.CBL = Labelled common blocks for PANDA2 analysis.
           (This is an unformatted sequential file.)
 HAT.BL1 = Labelled common blocks for BOSOR4-type discretized
           model of single panel module.
           (This is an unformatted sequential file.)
 HAT.BL2 = Labelled common blocks for BOSOR4-type discretized
           model of entire panel with smeared stiffeners.
           (This is an unformatted sequential file.)
 HAT.RN1 = Direct access file for data base pertaining to
           BOSOR4-type discretized model of single module.
           (This is an unformatted direct access file.)
 HAT.RN2 = Direct access file for data base pertaining to
           BOSOR4-type discretized model of entire panel
           with smeared stiffeners.
           (This is an unformatted direct access file.)
 HAT.OO3 = Scratch file similar to the .OPT file.
 PROMPT.DAT = Prompt file for interactive input for PANDA2.
 TUTORMAIN.DAT = File containing rather detailed explanations
                 of theories on which PANDA2 is based.

For further information about files used and generated
during operation of PANDA2, give the command HELPAN FILES.

Menu of commands: PANDAOPT, PLOTTER, MAINSETUP, CHANGE,
                  DECIDE, PANEL

18.1 PLOTS OF DISCRETIZED, SEGMENTED PANEL MODULE MODEL

Figure 20(b) shows a discretized model of a single module of the hat-stiffened panel. This module consists of eight segments, each of which is discretized via the BOSOR4-type of finite-difference element [2]. Figure 20(a) shows the predicted bifurcation buckling mode corresponding to local buckling of the skin between stiffeners, and Fig. 20(c) shows the predicted wide-column buckling mode. These plots were obtained via execution of the PANDA2 processor called PLOTTER.

18.2 BOSOR4 RUN OF ENTIRE PANEL
WITH ALL SKIN AND STRINGER SEGMENTS MODELED
AS DISCRETIZED BRANCHES

Figure 21 shows the discretized model and the six lowest eigenvalues and eigenmodes. These plots were generated after the optimum design of the hat-stiffened panel had been obtained, and after PLOTTER hand been executed to obtain plots of the single module models of local and wide-column buckling. The results shown in Fig. 21 were obtained by means of the following runstream:

PANEL   (The user first answers a few simple questions. Then the PANDA2
                    system sets up a BOSOR4 input file for a multi–module panel.)
BOSOR4LOG   (You activate the BOSOR4 command set.)
BOSORALL   (You launch a batch run of BOSOR4 to get general bifurcation
                    buckling of the multi–module model.)
BOSORPLOT   (The BOSOR4 system generates a multi–module panel plot file.)
PLOT   (You give a command that generates plots at your facility.)

The PANDA2 processor called PANEL uses current dimensions, properties, and loading of the single panel module model to set up a multi–segment model of the entire panel. The processor PANEL asks the user how wide the panel is, whether or not there are stringers at the edges (or are the edges midway between stringers?), and whether or not the boundaries of the panel normal to the screen are constrained other than by stringers, and if they are constrained, are they simply-supported or is there a symmetry condition there?

Given the output from this short interactive session, and given the current state of the panel module, including any variation of load due to post-local buckling of the skin, PANDA2 sets up a file called NAME.ALL which is suitable without modification for use as input to BOSOR4.

The discretized model shown in Fig. 21(a) was generated after the user responded to PANEL that the panel is 24 inches wide, has stringers at the edges, and is not further supported there. This discretized model has 27 shell segments, 6 in each of the hat stiffeners [Segments 2–7 in Fig. 20(b)], and three skin segments forming the bays between the stringers. The model is subjected to axial load that varies across the panel in a periodic fashion because the skin is in its post-locally-buckled state and has therefore shed axial load to the stringers. The stiffness of the skin between stringers is the tangent stiffness

C_{TAN} determined as described above. The stiffness of the stringer segments is $Cx(i,j,k)$, $k = 2, 3, 4$, where k is the segment number in Fig 3.

The length of the panel normal to the plane of the paper is equal to the length between adjacent rings. If there are no rings, the length is equal to the "effective" length of the panel provided by PANDA2. (This "effective" length is either the user-provided length L if the panel is simply–supported along the edges at $x = 0$ and at $x = L$, or it is $L/3.85^1/2$ if the panel is clamped along these two edges.

To be able to analyze this complex structure with BOSOR4 requires treating it as a shell of revolution. This is done using the "trick" described in detail in Chapter 7 of Ref. [30]: essentially the axial and circumferential coordinates are interchanged; the panel is treated as a section of a torus of large diameter. The coordinate along the axis of the panel is the same as the coordinate around the circumference of the torus; the coordinate along the circumference of the panel (transverse to the stringers) is the same as the coordinate along the meridian of the torus. In applying the PANEL and BOSOR4 processors as described above, the user does not need to worry about coordinates, however. This is taken care of internally.

It is important to remember at this point that BOSOR4 does not have the capability to predict buckling in the presence of in-plane shear loading. Therefore, the applied in-plane shear load of 1000 lb/in is ignored in the BOSOR4 analysis. One must multiply all load factors obtained with BOSOR4 by the knockdown factor FKNOCK(4) pertaining to inter-ring buckling and given by PANDA2.

Figures 21(b-g) show bifurcation buckling modes predicted by BOSOR4. It is clear that the first four modes represent skin buckling, and therefore are not of much interest. The fifth and sixth modes, however, represent general instability of at least one stringer. The buckling load factor, $\lambda_5 = 2.912$ multiplied by the knockdown factor for in-plane shear loading, FKNOCK(4) = 0.916 (from the final PANDA2 run), should be compared with the PANDA2 prediction of wide column buckling and/or general instability.

****************** END OF SAMPLE CASE ********************

86

19.0 COMPARISONS BETWEEN TESTS, PANDA2, AND RESULTS FROM OTHER SOURCES

19.1 Comparison with Results from PANDA

PANDA2 has been exercised for most of the cases given in Ref. [1]. Since much of the coding in PANDA2 is taken directly from PANDA [1], agreement with PANDA is good.

19.2 Axially Compressed, Graphite-Epoxy, TEE-Stiffened Panel

Figure 22 shows the geometry and local and wide-column bifurcation buckling modes predicted by PANDA2. Graphite- epoxy, flat panels 32 inches long and 24 inches wide were tested under pure axial compression at the NASA Langley Research Center. Complete descriptions of the panels and test and computer models and results are presented by Starnes, Knight, and Rouse [5].

The panel to which Fig. 22 corresponds carried an ultimate axial load about three times the local bifurcation buckling load, P(cr). Figure 23 shows back-to-back axial strains at the peak of a local buckle. Figure 24 demonstrates the load redistribution that occurs from the skin to the stringers as the panel is loaded further into the post-local-buckling region. In view of the approximate nature of the PANDA2 analysis, it is felt that the agreement between PANDA2 results and STAGSC-1 [17] results is reasonably good.

19.3 Predictions of Bifurcation Buckling of Isotropic and Orthotropic Plates Under Various Combinations of N_x, N_y, and N_{xy}

Leissa [6] has written a long survey on buckling of laminated composite plates and shells. Some results presented in [6] are compared with PANDA2 results in the following paragraphs.

Table 1 lists comparisons between PANDA2 and the results of calculations by Chamis [7], who used a trigonometric series and the Galerkin method to compute buckling loads of isotropic and orthotropic plates under combined N_x, N_y and N_{xy}. Inspection of Table 1 reveals that the agreement between PANDA2 and Chamis' results is excellent if no in-plane shear load is present, is good if N_{xy} is considerably less than N_x or N_y, and in every case underestimates the buckling load factor in instances in which the agreement with Chamis' results is not very good: PANDA2 errs on the safe side.

The theory by which buckling load factors are obtained for cases involving in-plane shear and/or unbalanced laminates is explained on pages 40 and 41 and in Fig. 14 of Ref. [8]. PANDA2 uses a one-term Rayleigh-Ritz method, rather than a trigonometric series expansion, as did Chamis. It appears that the quality of the results obtained justifies the greatly improved efficiency on the computer. This efficiency is required for the practical solution of optimization problems of the complex sort solved by PANDA2. Anderson and Stroud [9] and Stroud and Anderson [10] use a strategy that is similar to that used in PANDA2 for obtaining improved results with their optimization code, PASCO, for cases involving in-plane shear loading.

Table 1   BUCKLING LOAD FACTORS Ncr FOR SIMPLY SUPPORTED PLATES
Matl Props:Orthotropic: E11, E12, G = 32.9, 1.8, 0.88 x 10**6 psi
large nu = 0.24; fibers along E11
Isotropic: E = 10.0 x 10**6 psi, nu = 0.3
Plate thickness, t = 0.096 in.; B.C.s: all edges simply supported

Plate Dim. X x Y (in.)	Nx	Ny (lb/in)	Nxy	Fibers along x PANDA2	Chamis	Fibers along y PANDA2	Chamis	Isotropic PANDA2	Chamis
5x10	-1	0	0	996	998	145	145	499	500
"	0	-1	0	578	581	576	581	1278	1279
"	-1	-1	0	463	465	116	116	400	400
"	-1	0	1	949	948	132	114	466	479
"	0	-1	1	532	619	300	395	940	998
"	-1	-1	1	437	446	109	113	383	389
"	-.001	0	1	1949	2185	487	700	1858	2104
10x10	-1	0	0	285	286	145	145	320	320
"	0	-1	0	145	145	285	286	320	320
"	-1	-1	0	116	116	116	116	160	160
"	-1	0	1	239	246	133	136	214	277
"	0	-1	1	133	136	239	246	235	277
"	-1	-1	1	109	111	109	136	140	153
"	-.001	0	1	487	531	487	531	464	752
"	-1	-0.75	0	145	145	122	122	183	183
"	-1	-0.50	0	190	191	129	129	213	213
"	-1	-0.25	0	228	229	136	137	256	256
"	-1	+0.25	0	378	381	154	155	427	426
"	-1	+0.50	0	570	572	165	166	571	571
"	-1	+1.00	0	1328	1330	193	194	666	666
"	-1	-0.50	0.25	189	190	128	129	209	212
"	-1	+0.50	0.25	532	549	164	165	482	562
"	-1	-0.50	0.50	190	187	126	127	199	209
"	-1	+0.50	0.50	470	496	161	163	384	539
20x10	-1	0	0	144	145	145	145	320	320
"	0	-1	0	36.4	36	249	249	125	125
"	-1	-1	0	29.1	29	116	116	100	100
"	-1	0	1	74.9	99	133	155	235	250
"	0	-1	1	33.6	35	237	237	117	120
"	-1	-1	1	27.4	28	109	111	96	97
"	-.001	0	1	122	175	487	491	464	528

88

19.4 Transverse Shear Deformation Effects

Leissa [6] includes examples originally presented in Refs [11-13]. Figure 25 shows PANDA2 results compared with results from classical plate theory and results obtained by Whitney [12] for a uniformly axially compressed plate with an infinite number of layers with fibers at plus and minus 45 degrees. Whitney's theory represents an extension of Ambartsumyan's [11] valid for angle-ply laminates. Table 2 lists comparisons of PANDA2 results with results from a theory for orthotropic plates given by Vinson and Smith [13]. In both cases PANDA2, which is based on Timoshenko beam theory, yields conservative buckling loads when transverse shear deformation is taken into account.

```
       Table 2   BUCKLING LOAD FACTORS (Nx*pi**2/G13*h)
                 FOR SIMPLY SUPPORTED, ORTHOTROPIC PLATES
    Material Properties:
     E1, E2, G12, G13, G23 = 32.5, 1.84, 0.642, 0.642, 0.361 x 10**6 psi
                 large nu = 0.256
     Geometry:  Axial length  a;   Width b;   Thickness h;   h/a = 0.1
===================================================================

    Plate Aspect     Classical Plate Theory      Including Transverse
    Ratio   a/b                                   Shear Deformation

                     PANDA2    REF. [13]        PANDA2    REF. [13]
-------------------------------------------------------------------


       0.33          4.18       4.15             2.77      2.76
       0.50          4.25       4.22             2.80      2.80
       1.00          4.80       4.78             3.03      3.32
       1.50          6.27       6.28             3.56      4.95
       2.00          9.56       9.60             4.41      9.20

===================================================================
```

19.5 Nonuniformly Axially Compressed Orthotropic Plates

Table 3 lists results from PANDA2 and from a theory given by Brunelle and Oyibo in Ref. [14] for orthotropic flat plates subjected to a membrane stress field corresponding to pure in-plane axial bending in the prebuckling phase, and simply supported on all four edges in the buckling phase. The buckling load factor,

$$k_o = N_x b^2 / [\pi^2 (D_{11} D_{22})^{1/2}] \tag{19.1}$$

is determined by a single parameter,

$$D = (D_{12} + 2D_{66})/(D_{11} D_{22})^{1/2} \tag{19.2}$$

in which b is the panel width and D_{11}, D_{12}, D_{22}, D_{66} are the bending and twisting stiffnesses previously called C_{44}, C_{55}, C_{45} and C_{66} in the sections on PANDA2 theory.

The PANDA2 results, which are conservative, are computed from a BOSOR4-type of model in which the panel width b is discretized and buckling modal displacements are assumed to vary harmonically in the axial direction.

89

Table 3   BUCKLING LOAD FACTORS ko FOR ORTHOTROPIC PLATES
SUBJECTED TO PURE IN-PLANE BENDING

Stiffness Ratio, D	Buckling Load Factor ko	
	PANDA2	REF. [14]
0.0	12.11	12.87
0.4	15.89	17.39
1.0	23.68	23.90

19.6 Stiffened Panels Under Combined Axial Compression and In-Plane Shear

Figures 26 through 29 pertain to 6 stiffened panels analyzed by Stroud, Greene and Anderson [15]. They obtained results using PASCO [10], EAL [16], and STAGS [17]. Figure 26 gives the properties of the four panels stiffened by blades. The sketches in Fig. 26 show a single module only. All of the panels had six equally spaced stiffeners and were 30 inches square. They were simply supported on all four edges.

In Fig. 27 results from PANDA2 are compared with those from EAL. In the EAL model the panel and stringers were discretized into a rather fine grid of finite elements. The EAL results agreed very well with those obtained with STAGS. Therefore, these results are regarded here as the correct, converged standard with which to compare the results obtained with PANDA2.

The coordinates in each of the four frames in Fig. 27 are the ratios of the applied loads to critical loads calculated by the EAL program for pure axial compression $[N_{xcr}(N_{xy} = 0)]$ and pure in-plane shear $[N_{xycr}(N_x = 0)]$.

Interaction curves for several PANDA2 models are plotted in each frame of Fig. 27. In Example 1 the local buckling load factor far exceeds that for general buckling; in Examples 2 and 3 local and general buckling load factors are fairly close to eachother; and in Example 4 the local buckling load factor is much smaller than that for general buckling.

In PANDA2 general or panel (between rings) buckling load factors are calculated with use of three models:

1.   a wide column model, based on results obtained with use of a single discretized panel module. Examples of buckling modes obtained with this model are shown in Figs. 20(c) and 22(c). The wide column model simulates panel buckling, that is buckling between rings in which both panel skin and stringers participate in the buckling mode. If there are no rings, the wide column model simulates general instability.

2.   a smeared stiffener model, based on the closed form theory used in PANDA [1] and based on the assumption that the panel skin between stringers is fully effective in resisting buckling. Panel instability is predicted by a model in which the stringers are smeared out and buckling occurs between rings, with simple support boundary conditions being applied

at the ring lines of attachment and rings neglected. General instability is predicted by a model in which both stringers and rings are smeared out, with simple support boundary conditions being applied on all four edges of the panel and the axial length of the panel being modified as previously described to simulate clamping.

3. a smeared stiffener model, based on the closed form theory used in PANDA [1] and based on the assumption that the skin is only partially effective in resisting buckling (called "reduced skin stiffness" in Fig. 27). In this model the reduced skin stiffness is used for both panel (between rings) and general (overall) instability predictions.

During optimization runs with PANDA2, buckling constraint conditions corresponding to general or panel instability are generated with use of the wide column criterion because it is generally conservative. However, there are two circumstances in which the wide column buckling load factor does not constrain the design:

1. if the user indicates that he or she does not want it to constrain the design; and

2. if the wide column buckling mode resembles a local skin buckling mode. To identify precisely what is meant by "resembles": if the amplitude of the wide column buckling modal normal deflection midway between stiffeners is more than 10 times the normal deflection directly under a stiffener, then this mode is rejected by PANDA2 as an indicator of wide column buckling. For example, the buckling modes in Figs. 20(c) and 22(c) were both accepted by PANDA2 as indicators of panel instability because the normal deflection of the panel skin where the stiffener is attached is about 25 per cent of the maximum normal deflection shown in Fig. 20(c) and is about 50 per cent of the maximum normal deflection shown in Fig. 22(c). An example is given later of a "wide column" buckling mode that was rejected by PANDA2 as an indicator of panel instability.

If either circumstance 1 or 2 pertains, PANDA2 uses as a constraint condition in the optimization process, the buckling load factor from the closed form PANDA analysis with skin stiffness reduced as discribed in Section 8.5.

An important observation from Fig. 27 is that the wide column buckling load factor does not necessarily yield a conservative estimate of the general instability load. Wide column buckling loads overestimate the general instability load as predicted from EAL when the loading is predominantly in-plane shear and local and general buckling occur at loads that are fairly close to eachother. This result is most noticeable in Fig. 27(c), NASA Example 3.

Figure 28 depicts two additional panel modules treated in the NASA paper [15], and Fig. 29 shows the corresponding load interaction curves. The statement just made with regard to conservativeness of buckling load factors obtained for panels loaded predominantly in shear holds in these cases also, the more noticeable being NASA Example 7.

In view of these results, the user should probably apply a factor of safety of something like 1.5 to load factors for general instability in cases when the loading is predominantly in-plane shear and local and general instability loads factors are fairly close to eachother.

Figure 30 shows interaction curves obtained for two optimized designs. The starting design corresponding to Fig. 30(a) was the NASA Example 2 shown in Fig. 26(b). The

starting design corresponding to Fig. 30(b) was the final design in Fig. 30(a). The decision variables during optimization were the skin thickness, stiffener thickness, and stiffener height. In each case the panel was considered to be subjected to 5 independent combinations of axial load N_x and in-plane shear load N_{xy}:

$$(N_x, N_{xy}) = (-1000, 0), (-866, 500), (-707, 707), (-500, 866), (-100, 950)$$

in which the units of N_x and N_{xy} are lb/in. In each case five design iterations were used. Approximately 14 minutes of VAX 11/780 (VMS operating system version 4.2) were required for the five iterations. The option IQUICK = 0 was used, that is, the optimum designs were obtained with use of discretized single panel module models as well as PANDA closed-form models.

The results in Fig. 30(a) were obtained via a strategy that required the use of the wide column buckling load factor as a design constraint. Therefore, the smeared stringer model with skin stiffness reduced as described in Section 8.5 was not active in this run. The load-interaction curve for the reduced skin stiffness model is shown in Fig. 30(a) so that it can be compared to that for the wide column model, which was active during the optimization process.

The results in Fig. 30(b) were obtained via a strategy that ignored the wide column buckling load factor but used the smeared stringer model with reduced skin stiffness instead.

In this case there is very little difference between the results. It is slightly more conservative to use the reduced skin stiffness model rather than the wide column buckling model in this case, but the difference is insignificant. As a general rule, it is probably good practice to run cases of particular importance both ways and choose the more conservative design.

19.7 Optimization, Tests, and Comparison of Test and Theory for Axially Compressed, Graphite-Epoxy, Hat-Stiffened Panels

PANDA2 was used to find the minimum weight design of a graphite-epoxy curved panel, 30 inches long, 24 inches wide, with a radius of curvature of 194 inches (hat stiffeners on the inside), and clamped along the curved edges. The panel was optimized for 3000 lb/in uniform axial compression. All factors of safety were set equal to unity.

Local skin buckling did not constrain the design. That is, the panel was designed so that the skin was permitted to go far into its postbuckled state. Rather than the load factor corresponding to local bifurcation of the panel skin constraining the design, the maximum stresses generated in certain of the laminae as the skin stretches, compresses, and bends in its locally postbuckled state constrained the design instead.

The procedure for optimization was as follows:

1. A starting design was established via the BEGIN processor. This design is listed in the section on BEGIN. Notice that the force/(axial length) required to cause web peel-off is given as 50 lb/in. This number was used after some peel tests had been conducted

92

on graphite-epoxy samples with thicknesses and fiber angles similar to those obtained in previously optimized designs. In these T-tests, peeling occurred between 50 and 100 lb/in. tension. One of the peel text specimens after failure is shown in Fig. 7, and the origin of the stiffener "pop-off" constraint used in PANDA2 is illustrated in Figs. 5 and 6.

2. Decision variables, linked variables, and escape variables were initially selected as listed in the section on DECIDE.

3. Loading was initially selected as listed in the section, ESTABLISHING LOADS AND STRATEGY IN PANDA2, except that there was no pressure loading and the type of analysis selected was optimization (analysis type 1) rather than fixed design (analysis type 2). Note that even though we wished to load the panel only in axial compression in the test with which the results obtained with PANDA2 were to be compared, a combination of axial compression of 3000 lb/in and in-plane shear of 1000 lb/in was initially selected during the first interactive session in MAINSETUP. There is an interesting reason for initially using combined axial compression and in-plane shear rather than axial compression alone, a reason that becomes obvious only after trying to optimize an axially stiffened panel under pure axial compression: The optimum design of an axially stiffened panel with no applied in-plane shear load is a panel with no skin at all, just an array of columns that support the axial load! The writer has fallen into this trap more than once in giving demonstrations of PANDA2.

4. The main processor PANDAOPT was executed several times. Each time it performed 5 design iterations. A minimum weight design was obtained.

5. Next, DECIDE was used again. Certain of the layers in the panel skin, in particular those with plus and minus 45-degree fiber angles, were assigned minimum thicknesses close to those determined previously. This was done so that in optimization runs performed for axial compression only, the skin would not disappear entirely and the panel to be tested would be capable of supporting considerable in-plane shear if required.

6. MAINSETUP was used again. This time the in-plane shear load was dropped. The panel was loaded by 3000 lb/in axial compression only.

7. PANDAOPT was exercised several times again in order to obtain a new minimum weight under the less severe loading.

8. The processor CHANGE was used in order to change thicknesses of certain of the laminae so that all laminae represented integral numbers of layers of graphite-epoxy tape of thickness 0.0052 inch or graphite-epoxy cloth of thickness 0.006 inch, where appropriate (Fig. 31). The total thicknesses of all laminae were kept as close as possible to those obtained via the PANDA2 optimization in Step 7.

8. DECIDE was exercised again. This time no thicknesses were chosen as decision variables. Only the height and width of the hat and the width of the base under the hat were chosen as decision variables.

9. PANDAOPT was exercised again to obtain a final optimum design. This design is shown in Fig. 31.

The predicted failure load is, of course, 3000 lb/in pure axial compression, and the predicted failure mode is maximum shear strain in the outermost cloth layers at the twelve points shown in Fig. 32. According to PANDA2 predictions, the failure mode should be characterized by vertical tears through the wall adjacent to the stiffeners where the skin is thin.

Notice that PANDA2 causes a rather thick base to be built up under each hat stiffener. This base appears to perform three functions:

(a) It causes reduction in the forces tending to peel the hat webs from the panel skin by reducing the amplitude of the local skin buckling pattern at the lines of attachment of the hat webs to the panel skin. This reduced amplitude of the local skin buckling mode can be seen in Fig. 20(a).

(b) It maximizes the bending moment of inertia of each hat by balancing the material in the crown of the hat, thereby maximizing the wide column buckling load factor.

(c) It minimizes the amount of axial bowing in the panel due to curing.

The predicted failure load of 3000 lb/in corresponds to a model in which the panel is assumed to be infinitely wide with stringers spaced at 8-inch intervals. The actual test panels were 27.25 inches wide and had stringers near each edge. Hence, the actual panel is axially stiffer than the theoretical model of it because there are 4 stiffeners in 27.25 inches, whereas in the theoretical model there are 3 stiffeners in 24 inches. If the PANDA2 prediction of 3000 lb/in is multiplied by the ratio of the axial stiffness of the test panel to the axial stiffness of the theoretical panel (1.17), a new prediction of failure of the test article at an axial load/(circumferential arclength) of 3510 lb/in is obtained.

Before any large panels were fabricated, several tests were conducted on small, flat panels, an example of which is shown in Fig. 33. The small panels were about 18 inches long and 11 inches wide. They had two stringers, one near each edge. The vertical edges were clamped lightly together to prevent delaminations from propagating in from a free edge. Many small C-clamps were applied to short aluminum tabs. Small axial gaps between each aluminum tab prevented this edge support from accepting significant axial load. The C-clamps and aluminum tabs are visible in Fig. 33, with some of the small axial gaps visible near the bottom of the panel where the failure occurred.

The purpose of testing several small panels first was to learn how best to fabricate the large panel. Should kevlar stitching be used near the hats in order to postpone stringer pop-off, a failure mode frequently encountered by other investigators? Should adhesive be used in addition to the basic epoxy? Six of the small panels were tested with various combinations of stitching and adhesive. As a result of these tests, it was found best to use adhesive alone, as specified in Fig. 31. (An interesting finding is that stitching plus adhesive seems to be worse than adhesive alone.)

Figure 34 shows one of the large, curved panels installed in a testing machine especially built for axial compression tests of panels of this type. Details about the testing machine are given by Holmes in Ref. [18]. The top head of the machine can rotate and translate as a rigid body in order to accommodate any linear errors in the trim of the panel to

be tested. Axial strain measurements from crown and base of each of the four stringers at their midlengths inform the operator of the test machine how to actuate the head in order to make the axial load as uniform as possible across the panel width and to minimize bending of the stringers at low load levels. The placement of the eight strain gages is indicated in Fig. 35.

Three large hat stiffened panels were tested. Figure 34 shows Panel No. 1 installed in the test fixture. Notice the C-clamps along the vertical edges. The purpose of these clamps, described previously in connection with tests on small panels, is to prevent early delaminations from propagating inward from the free edges of the panel.

The following test procedure was used for all three panels:

1. Strain gages were attached to the crown and opposite sides of each of the four stringers at the midlength of the panel, the curved ends of which had previously been carefully trimmed potted, and attached to aluminum plates.

2. The panel was installed in the test fixture.

3. Axial compression was applied, and the top head of the machine tilted front and back and side to side in order to obtain the smallest differences in the readings of front and back and side to side load cells. The eight strain gages on the stringers were carefully monitored, the goal being to minimize the differences in the strains measured by these gages, especially at low load levels.

4. The panel was loaded well into the local-post-buckling regime. For all panels, local buckling occurred at about 8000 lbs total axial compression [Nxcr(local) = 294 lb/in]. The panels were loaded in this preliminary phase to about 35000 lbs, at which load the local buckling pattern was clearly visible. This local buckling pattern was carefully inspected. Based on the location of the maximum buckling displacement in the middle bay of the panel, nearest the midlength, marks were made on the panel to identify locations of strain gages to be attached. Ten channels were available, and it was decided to attach gages at the following locations:

   a. back-to-back axial and hoop gages at the buckle inward peak nearest the center of the panel (4 channels);

   b. back-to-back axial gages at the buckle outward peak nearest the inward peak and above it. (Panels 1 and 3 only) (2 channels);

   c. hoop gages on the outer (convex) and inner (concave) surfaces at the same axial station as the gages in a., but located where the sharpest curvature is observed in the local inward buckle. These gages should be located where the material in the stiffener base tapers down to the skin thickness in the center bay of the panel. The positions of them are called out in Fig. 32 (4 channels). These gages are important because they are located at positions where PANDA2 predicts maximum stress and failure.

   d. hoop gages on the outer (convex) surface at the same axial location as b, located as described in c. (Panel 2 only) (2 channels).

95

5. The panel was unloaded and the ten gages identified in a.-d. above were attached.

6. The panel was reinstalled in the test fixture and loaded to failure. Strain and load data were recorded by a computerized data acquisition system.

Figures 35 through 45 give test and theoretical results for these three large panels.

Figure 35 displays Southwell plots for the three panels. The average axial strain difference between axial strain in the skin opposite the stringers and axial strain in the crown of the stringers, $\triangle \bar{e} = (\bar{e}_1 - \bar{e}_2)$, essentially represents the axial bowing of the panel. The Southwell plots, $\triangle \bar{e}/P$ vs. $\triangle \bar{e}$, yield estimates of the wide-column buckling loads of the panels: the slope of the plot for each panel represents the inverse of the wide-column buckling load of that panel. (An explanation of the Southwell method with a discussion of its limitations is given in pages 357-367 of Ref.[30].)

From Fig. 35 it is seen that the wide-column buckling loads of Panel 1 and Panel 3 are within 10 per cent of eachother and are much higher than that of Panel 2. Yet all three panels were nominally identical. Since each Southwell plot represents behavior averaged over an entire panel, it is unlikely that this rather dramatic difference is caused by local flaws in any of the panels. It is much more likely to be caused by a difference in restraint at the boundaries.

In the tests Panel 1 failed at about 86,000 lbs, Panel 2 at 70,000 lbs, and Panel 3 at 83,000 lbs. The Southwell plot of Panel 2 behavior indicates that its failure was due to wide-column buckling, since the inverse of the slope of the Southwell plot, $P_{southwell}(2)$ = 71,800 lbs, is not far above the load, $P_{test}(2)$ = 70,000 lbs, at failure in the test. The Southwell plots of Panel 1 and 3 behavior indicate that their failure was not due to wide column buckling, since the inverses of the slopes of the Southwell plots for these two panels, $P_{southwell}(1)$ = 123,000 lbs for Panel 1 and $P_{southwell}(3)$ = 110,500 lbs for Panel 3, are far above the loads, $P_{test}(1)$ = 86,000 lbs and $P_{test}(3)$ = 86,000 lbs, respectively, at which Panels 1 and 3 failed in the tests.

Figure 36 is analogous to Fig. 21. It corresponds to the design actually tested. This model yields a prediction of general instability (similar to wide-column buckling) at P_{cr} = 125,000 lbs. Clamped boundaries at the loaded ends of the panel were assumed in this model. The critical general instability load, P_{cr}(BOSOR4) = 125,000 lbs, corresponding to clamped ends, is not very far above the values P_{cr}(test)=123,000 lbs for Panel 1 and P_{cr}(test) = 110,500 lbs for Panel 3 obtained from the Southwell plots of Fig. 35. Since wide-column buckling of axially stiffened panels is sensitive to the rotational restraint at the boundaries, it appears that in the tests Panels 1 and 3 were very nearly clamped at the loaded edges, but that Panel 2 was not.

After the tests on all three panels, it was determined that because of mislabelled aluminum stock, Panel 2 was mounted on 6061/T4 (26 ksi yield) aluminum end plates, whereas Panels 1 and 3 were mounted on significantly harder 6061/T6 (56 ksi yield) aluminum end plates. Figure 37 shows part of one of the end plates of Panel 2 after its test. There is significant "print-through" caused by local plastic flow directly over the stringers.

This "print-through" cannot be seen in the end plates of Panels 1 and 3. It indicates that Panel 2 was freer to rotate at its loaded ends than were Panels 1 and 3.

Figure 38 shows load-axial strain curves from test, from PANDA2 predictions, and from PANDA2 predictions multiplied by a factor 1.17 to account for the fact that the test panel had 4 stringers in a width of 27.25 inches, whereas the PANDA2 theory applies to a panel with 3 stringers in a width of 24 inches. There is some bending in the stringers from the beginning, bending which is not predicted in the PANDA2 analysis. (Bending from axial bowing of the panel caused by curing, which is predicted by PANDA2, is not significant in this case.)

In the PANDA2 model of the panel, one extra "fake" layer was added to each side of each wall in the multi–segment model. These layers were very thin (0.0001 in.), had a modulus of unity and a Poisson ratio of zero, and a very small density. The purpose of these fake layers was to obtain strain in the panel coordinate system (x, y) directly, rather than have to convert stresses in the material coordinate system to strains in the panel coordinate system. This "trick" does not affect the panel behavior. It was also used in the analysis of the NASA T-stiffened panel described in the discussion associated with Figs. 22–24.

The local buckling pattern observed in the test agreed qualitatively with that predicted by PANDA2 (seven axial half waves in the test, 8 axial half waves predicted by PANDA2, but the predicted bifurcation buckling loads for 7 and 8 waves are within one per cent of eachother). The test panel failed at about 13 per cent below what one might expect from the PANDA2 predictions as modified by the factor of 1.17. However, Fig. 39, which shows the failed panel removed from the test machine, indicates that the mode of failure is in agreement with that predicted by PANDA2: Vertical tears exist at locations where the hat base has tapered to the thickness of the panel skin. (See Fig. 32). There was no evidence of skin-stringer separation. No secondary bifurcation, described below, was observed during the test of this panel. The post-local-buckling axial wave pattern remained qualitatively constant throughout the test.

Figures 38, 40 and 41 show the axial strains at the 4 stringer locations for Panels 1, 2, and 3, respectively. The following observations apply to these three figures:

1. There is rather a lot of bending in the stringers, especially in Panel No. 1 and Panel No. 2, even at fairly low loads. Much of this may be generated by axially nonuniform Poisson-ratio expansion of the radius of the panel as the load is increased. While Poisson ratio expansion is, of course, included in the PANDA2 theory, it is assumed to occur in the plane of the panel and not normal to it: the prebuckling state of the panel in this case (no normal pressure and insignficant axial bowing) is assumed to be uniform: it does not vary in the axial direction due to edge restraint. It is as if there were no edge restraint in the prebuckling phase, simple support or clamping conditions being applied only in the bifurcation buckling analyses.

2. It is possible (although unlikely because of the evidence supplied by the Southwell plots in Fig. 35 and the BOSOR4 prediction in Fig. 36) that all three panels failed via

general instability rather than maximum stress. The PANDA2 calculations were conducted with the assumption that the curved edges of the panel were clamped, whereas in the test the support is not as rigid as clamping: in the test the zero rotation constraint is enforced only by a natural feedback mechanism: as the curved edges rotate the load shifts so as to counteract this rotation. PANDA2 predicts wide column buckling of the clamped panel at a load factor of only 1.36 times the imposed axial load of 3000 lb/in. Wide column buckling loads of panels such as these, with stringers that are very strong compared to the skin, are very sensitive to the nature of the rotational restraint at the edge. It could be that all of the test panels, bearing as they do on aluminum end plates, have end constraints weak enough to lead to wide column instability prior to or combined with material failure. As discussed above in connection with the Southwell plots, it is very likely that Panel 2 failed in general instability, but that Panels 1 and 3, because of their harder aluminum end plates, did not.

Figures 42 through 45 show various strain components from test and theory. The following observations apply:

1. The axial strains at the peaks of the inward and outward buckles are quite different (Fig. 42). PANDA2 is based on a theory that neglects this difference. While this might appear to be a serious omission at first, it is not very critical because these strains are much smaller than strains predicted elsewhere which cause material failure.

2. There is a great deal of scatter in the behavior of hoop strain, as can be seen from a comparison of Figs. 43 and 44. In both figures the hoop strains are generally greater than those predicted by PANDA2. However, the comment given in 1. applies here also: These strains do not come close to generating material failure, and so do not govern the evolution of the optimum design.

3. The comparison between test and theory for the most important strain, the hoop strain at the interface between the thickened stringer base and the thin skin, indicates reasonably good agreement (Fig. 45).

4. Panel No. 2 exhibited a sudden change in the buckle pattern at a load of about 35000 lbs. The change was accompanied by a rather loud noise. The redistribution of energy caused the applied load to decrease abruptly to about 29000 lbs. It appeared that the number of axial half-waves in the center bay of the panel increased from 7 to 8. (8 agrees with the PANDA2 prediction, although the critical bifurcation buckling loads corresponding to 7 waves and 8 waves are within one percent of eachother.) While the strain gages were located based on the 7-wave pattern, it seems that fortuitously, the gage locations remained appropriate for the 8-wave pattern: the gages initially located at the peak of an inward buckle in the 7-wave pattern, became located at the peak of an outward buckle in the 8-wave pattern. Hence, in Figs. 44 and 45, the locations of the gages are called out as if they were in different bays of the panel. Actually, only the middle bay had gages and it was the buckle pattern that changed during loading. As seen from Fig. 45, curves 2 and 4 and 5 and 7, the continuity of strain measurement in the neighborhood of the load at which the buckle pattern changed is extroadinarily good.

Unfortunately, only in Panel 2 were the hoop gages located properly to catch the maximum strains. In Panel 1 they were located too far away from the tapered section to capture the very sharp, local change in circumferential curvature of the locally buckled skin of the middle bay. In Panel 3 the gages were applied in the correct positions according to observations during the preliminary loading phase, but when the panel was reinstalled in the test machine and reloaded, the local buckle pattern shifted enough to destroy completely the usefulness of these as well as the other strain gages placed on the panel skin! Apparently the local buckle pattern can rather freely "slide" in the axial direction, and the locations of peak buckling displacements depend on very small load eccentricity effects.

It is clear that more tests of this type should be conducted and that there should be many more gages applied to a panel in order to ensure capture of the peak strains. The conclusion from tests conducted so far is that PANDA2 agrees reasonably well with test results. The difficulty seems to lie mainly in obtaining repeatablility in tests with regard to uniformity of load and determination of proper locations for strain gages. There may also be considerable scatter in the quality of composite panels of this type with rather complex cross sections.

20.0 INVESTIGATION OF BLADE-STIFFENED PANEL WITH AXIAL COMPRESSION, PRESSURE, AND THERMAL LOADING

20.1 Introduction

In this section is described a variety of phenomena for a stiffened elastic plate with geometry and linear material shown in Fig. 46. The plate is designed so that it buckles locally between the stringers at an axial load well below the wide column buckling load. This case does not represent a good engineering design. Its purpose is to demonstrate many interesting and sometimes rather subtle and complex phenomena that occur when the plate is loaded in pure axial compression far into its locally postbuckled regime, when it is loaded by pure normal pressure far into the nonlinear regime (geometric, not material nonlinearity), and when it is loaded by combinations of axial compression and normal pressure or axial compression and nonuniform temperature that simulates curing of a composite panel.

20.2 Summary of this section

Figures 48 through 54 pertain to the case of pure axial compression with neither pressure nor thermal effects. The main purpose of this section is to obtain comparisons with results from a new version of the STAGSC-1 program [19] which contains a new algorithm called the "Thurston Processor", or "TP" for short [20]. This algorithm mitigates difficulties encountered during a nonlinear process when load-deflection curves are tracked in the neighborhood of single or multiple bifurcation points. Through certain transformations, the Thurston Process eases the transition from prebuckling to postbuckling load-deflection curves, and from primary postbuckling to secondary postbuckling load-deflection curves, etc.

Figures 55 through 64 pertain to the case of pure normal pressure, with neither axial compression nor thermal effects. The purposes here are

1. to demonstrate the approximate method used in PANDA2 to obtain reasonably accurate predictions for nonlinear behavior of a stiffened panel under uniform normal pressure;

2. to obtain comparisons with results from STAGSC-1; and

3. to describe some interesting phenomena.

Figures 65 through 71 pertain to the case of axial compression combined with normal pressure. The purpose is to describe some interesting phenomena.

Figures 72 through 77 pertain to the case of axial compression combined with thermal loading that simulates curing of a composite panel. The purpose is to describe some interesting phenomena.

20.3 Computer models

Figure 46(b) shows the discretized panel module used in the PANDA2 analysis throughout. Fig. 46(c) shows the local buckling mode and Fig. 46(d) shows the wide column buckling mode. In PANDA2 both local and wide column buckling load factors are obtained with use of the same discretized model. The local mode is singled out by enforcing equal and opposite normal displacements at the symmetry planes at either end of the single module model depicted in Fig. 46(b). The wide column mode is singled out by imposing equal normal displacements at either end of the single module model. As mentioned previously, the wide column mode is rejected by PANDA2 as an indicator of general instability if the normal displacement under the stiffener is less than 10 per cent of that midway between stiffeners.

Figure 47 shows the STAGS finite element model used for the study of the behavior of the panel under normal pressure. One fourth of the plate is included, with symmetry planes at midlength and midwidth. The STAGS model for pure axial compression is twice as large: the symmetry plane at the panel midwidth is retained, but the entire length of 30 inches is included for two reasons:

1. It is not known a priori (except from PANDA2 results, which are being checked!) whether the local skin bifurcation buckling pattern has an odd or an even number of axial halfwaves.

2. It is possible that the number of axial halfwaves in the local buckling pattern will change by one as the panel is loaded far into the post-local-buckling regime. A symmetry plane introduced at the panel midlength would artificially preclude this from happening. Recall that in the test of hat-stiffened Panel No. 2, described in the previous section, the number of axial halfwaves in the local skin buckling pattern increased from 7 to 8 at an axial load somewhat less than half of that for which the panel was optimally designed. (See Fig. 45).

In addition, the STAGS finite element model for the case of pure axial compression contained additional rather small elements near the stringer not at the panel edge in order better to capture the fairly localized inflection behavior of the local buckling mode seen in Fig. 46(c).

The boundary conditions in the STAGS model for pure axial compression differed from that in the STAGS model for pure normal pressure:

1. In the axial compression case the stiffened edges were free, except for the presence of the stiffener, of course, and the loaded edges were subjected to uniform end shortening with no rotation allowed.

2. In the normal pressure case the three displacement components u, v, w were restrained at the stiffened edge and at the other edge not at a symmetry plane, and the edge rotation was free. The other two edges were symmetry planes.

20.4 Results for Pure Axial Compression

Figure 48 shows load-axial strain curves from PANDA2 and STAGS. The STAGS model shows higher axial stiffness at low axial load because there are four stringers in 24 inches in the STAGS model, whereas there are only three in the PANDA2 model. (Recall the similar difference in the case of the hat-stiffened test panels and the PANDA2 models of them; see Fig. 38, for example.) The slope of the post-local buckling curve is essentially constant in the PANDA2 model because the number of axial half waves is fixed at that predicted for the critical bifurcation buckling mode. Changes in the number of axial halfwaves after primary bifurcation are not accounted for by PANDA2. This slope decreases slightly in the STAGS model because the post-buckling mode of deformation changes during loading, as will be described later.

The load coordinate in Fig. 48 is normalized by the local bifurcation buckling load predicted by PANDA2. This normalizing factor is used throughout this study.

Figure 49 depicts the normal deflection at the center of the panel as a function of normalized axial load. The STAGS and PANDA2 models agree extraordinarily well up to a load factor $N_x/N_{xcr} = 5.22$. At an axial load slightly higher than that, STAGS has difficulty converging. Use of the Thurston processor, however, aids convergence. As the axial load is further increased, STAGS predicts maximum normal displacements that exceed those predicted with PANDA2. The number of axial waves in the post-locally buckled panel does not change throughout the load range, but the distribution of displacments changes. For axial loads that are less than $N_x/N_{xcr} = 5.22$ both STAGS and PANDA2 predict normal displacements that have equal inward and outward maxima and uniform wavelengths. For higher axial loads, however, the waviness predicted by STAGS becomes more nonuniform. STAGS and PANDA2 predictions of normal displacement distributions at the maximum axial load, which corresponds to an imposed average axial compression of 3000 lb/in, are plotted in Figs. 50 and 51. The STAGS results indicate a kind of alternating discrepancy with PANDA2 results, in which the maximum normal deflection in one buckle is more than that predicted by PANDA2, whereas that in a neighboring buckle is less than than predicted by PANDA2.

Figure 52 shows a plot of the largest strain anywhere in the panel. STAGS predicts considerably more strain than does PANDA2, possibly because the STAGS model is a bit freer in the y-direction than is the PANDA2 model. In the PANDA2 model symmetry conditions are imposed midway between stringers in the local buckling mode [Fig. 46(c)]. Since the postbuckling behavior is represented in the PANDA2 model as a series expansion of the local buckling mode, the entire panel is not free to become narrower as the skin goes deeper into its postbuckled regime. Possibly this restraint prevents bending about each stringer to the degree that STAGS predicts. However, note that according to STAGS the maximum normal deflection in some of the buckles in the edge bay is considerably less than that predicted by PANDA2, a result that argues against this reasoning. Note also that STAGS predicts some overall axial bowing of the panel which PANDA2 cannot predict in this case (zero pressure, zero curing deformations) because PANDA2 is based on the assumption that the post-local buckling pattern is antisymmetric about all lines of attachment of stringers to the panel skin.

102

Figure 53 shows that the STAGS and PANDA2 predictions of midbay axial strain at the midlength of the panel agree very well for the entire axial load range.

Figure 54 demonstrates the redistribution of axial load from skin to stiffeners as the panel is loaded into the post-local buckling regime. For high axial compression, STAGS predicts that N_{xloc} falls off more steeply with distance from a stringer than does N_{xloc} predicted by PANDA2.

The main conclusion from the results shown in Figs. 49 through 54 is that, with the possible exception of prediction of maximum transverse strain in the immediate neighborhood of a stringer, PANDA2 agrees well enough with STAGS to ensure that it can be used to generate reasonably good minimum weight designs of panels in which the skin is permitted to buckle during service. The discrepancy in maximum hoop strain can be compensated by application of a suitable factor of safety, FSSTR.

20.5 Results for Pure Uniform Normal Pressure

As described in the analysis section, nonlinear theory is used in the PANDA2 analysis. It is well known that monocoque flat plates exhibit a nonlinear stiffening effect under pressure, and that even for rather low design pressures one must account for the membrane stretching that builds up as the plate deflects. Boitnott, Johnson, and Starnes [21] demonstrate that nonlinearities significantly affect the behavior of curved, internally pressurized panels clamped along their straight edges. In this section, which deals with a more complex problem, a stiffened panel, it is shown that geometric nonlinearities must be included in the model.

Stiffened panels under normal pressure exhibit two types of response, identified here and in the following paragraphs as Problem 1 and Problem 2:

Problem 1. The panel bends overall, as shown in Fig. 55. This behavior can be captured with a model in which the stiffeners are smeared out.

Problem 2. The panel bends locally around each stringer, as shown in Fig. 56. This behavior can be captured with a single module model of the type shown in Fig. 46(b).

As described in the analysis section, the strategy in PANDA2 is to obtain a reasonably good solution with little computer time by separation of these two behaviors and analysis of each as a nonlinear problem. The total state of the pressurized panel is obtained by adding the results of the two separate analyses.

Immediately one might object that since the problem is nonlinear, one cannot superpose these results. The PANDA2 strategy would be incorrect if it were not for the fact that the membrane stresses obtained from Problem 1, the overall bending model, occur as prestresses in Problem 2, the local "wrap-around" problem. In this way the essential nonlinear contribution of the first problem to the second is included. As shown in the following, this strategy leads to reasonably good agreement with a rigorous nonlinear finite element solution [19] in the only case explored as of this writing.

103

Figure 55 shows the results from Problem 1, overall bending, obtained with PANDA2 for a range of pressures from +20 psi to -20 psi. The stringers are smeared out and the panel is assumed to be supported in the plane of the skin. For positive pressures the panel continuously stiffens as the pressure increases. This is because both the induced axial forces and transverse (hoop) forces are tensile and monotonically increase with increasing pressure. For positive pressures, therefore, the stiffened panel behaves in a manner qualitatively similar to that of a monocoque panel.

For negative pressures the panel initially softens and then stiffens. The initial softening is caused by induced axial compressive forces that initially increase. For negative pressures greater than about five psi, however, the induced axial compression decreases. At a negative pressure above 12.5 psi the induced axial force becomes tensile and increases at an increasing rate as the negative pressure is further increased. (The behavior of the induced axial force is shown in Fig. 66, which is used later to discuss wide column buckling as a function of pressure.)

Figure 56 shows results from Problem 2, local bending around a stringer. The results are not skew symmetric for plus and minus pressures because the prestress in the panel skin obtained from the solution of Problem 1 is not symmetric. (See Fig. 66). Notice the small range of applicability of linear theory.

Figure 57 shows the total displacement from the solutions of Problem 1 plus Problem 2 compared with the results from the STAGS finite element model depicted in Fig. 47. STAGS predicts a somewhat stiffer behavior, both in the linear and nonlinear range, probably because the STAGS model contains four stringers in the 24-inch panel width, whereas the PANDA2 model contains three.

Figures 58 and 59 show the distributions of normal displacement across the panel width at the midlength symmetry line and along the length at the midwidth symmetry line. Agreement between STAGS and PANDA2 seems good enough to justify the use of PANDA2 for preliminary design optimization.

Figure 60 shows the largest strains anywhere in the panel predicted by PANDA2 and by STAGS. PANDA2 indicates that the largest strains are in the y-direction in the panel skin at the attachment line of any stringer at the midlength of the panel. They are due mostly to local bending of the panel skin around the hard stiffener. STAGS gives a similar result, except that at high pressures these transverse "wrap-around" strains are greater at about one quarter of the way along the panel than they are at the midlength line of symmetry. This is probably because there is less transverse (hoop) tension in the panel skin one quarter of the way along the panel than there is at the midlength plane of symmetry. Therefore, the skin between stringers is freer to deflect more before large local tensile forces build up in it.

Figure 61 demonstrates this effect. The top frame shows the distributions of normal displacement across half of the panel width at various nodal lines in the STAGS model shown in Fig. 47. The bottom frame shows the lengthwise distribution of axial (N_x) and hoop (N_y) resultants in the panel skin at the midwidth line of symmetry. It is clear that in the STAGS model the amount of local "wrap-around" transverse bending decreases

104

as N_y increases. The maximum extreme fiber transverse strain is a sum of membrane plus bending contributions which turns out to be maximum at about nodal line 4 in the STAGS model. In the PANDA model only the prestress at the midlength of the panel from Problem 1 is used in the solution of Problem 2, since in Problem 2 it is assumed that there is no variation in behavior along the length of the panel module. Perhaps it is only fortuitous that the maximum strains anywhere in the panel predicted by PANDA2 are in reasonably good agreement with those predicted by STAGS, even though the locations of them are different. One would need to run more cases to find out.

Figures 62 through 64 show certain stress resultants predicted by PANDA2 and by STAGS. These are important because they affect the local bifurcation buckling and post-local-buckling behavior, to be described next.

20.6 Results for Combined Axial Compression and Normal Pressure

Figures 65 through 71 pertain to this section. The behavioral characteristics of primary importance arise from the following:

1. The normal pressure bows the panel, and a bowed panel under axial compression behaves differently from a straight panel.

2. The normal pressure prestresses the panel skin and stiffeners, which affects the local bifurcation buckling load factor, mode shape, and postbuckling behavior.

3. The change in postbuckling behavior due to pressure, especially the change in postbuckling skin stiffness and the change in the share of total axial load carried by the skin cause changes in the wide column buckling load factor and mode shape.

Figure 65 demonstrates the effect of pressure on the share of unit axial load carried by the panel skin and the local bifurcation buckling load factor and mode shape. For positive and increasing pressure the panel bows upward to an increasing degree. Hence, an increasing share of the applied axial load passes through the skin. By itself, this trend would lead to decreasing load factors for local buckling. However, the skin also becomes prestressed by the pressure, especially in the direction transverse to the stringers. This by itself would postpone local buckling and would cause the critical buckling mode to have more halfwaves in the axial direction than the critical mode for the unpressurized panel. A membrane tensile stress field also develops in the stringers. This effect postpones local buckling because the pretensioned stringer, especially the fibers of it farthest from the skin, will not want to rotate in the local buckling mode. Therefore, the pretensioned stringer will act more like a line along which the panel is clamped that it would if it were not pretensioned. The bowing and the prestressing therefore have opposite effects. In this case, the tensile prestress field predominates, so that for positive and increasing pressure the local bifurcation buckling load factor increases even though the skin carries an increasing percentage of the applied axial load.

For increasingly negative pressure, bowing leads to a smaller share of applied load going through the panel skin, which by itself would lead to higher bifurcation buckling load factors than that for the unpressurized panel. Negative pressure also generates a

tensile stress field in the panel skin, which additionally postpones local bifurcation buckling. Therefore, unlike the case of positive pressure, for negative pressure these two factors have the same effect. However, the extreme fibers of the stringer become compressed, a factor that would by itself reduce the local bifurcation buckling load factor because it tends to make the stringer want to roll over. This tendency is small for small negative pressures, but predominates for large negative pressures, as seen from the change in direction of curve (2) in Fig. 65 and the change in the local buckling mode shape as the negative pressure increases above 10 psi.

Whereas Figure 65 demonstrates the effect of pressure on local bifurcation buckling behavior, Figs. 66 and 67 demonstrate the effect of pressure on wide column and general instability. There is much information in Figs. 66 and 67. It may help to list items of primary importance:

1.   For increasing positive pressure the overall axial tension induced by the pressure increases, as seen from Curve (1). This increase gives rise to the slopes of curves (2a), (2b) and (3).

2.   The wide column buckling load factor is very sensitive to the amount of skin deformation present in the wide column buckling mode, as seen from the sketches in Fig. 67. The more skin deformation, the lower is the wide column buckling mode.

3.   If there is little or no local skin deformation in the wide column buckling mode, as is the case in Fig. 67, bottom left, then the wide column buckling load factor should be approximately equal to the load factor from the PANDA-type closed form analysis corresponding to zero pressure.

The fact that for positive pressure the curve for N_{xcr} neglecting local postbuckling (Curve 2a) lies to the left of that for N_{xcr} including local postbuckling (Curve 2b) requires explanation because this result at first runs counter to intuition. One would think that including local postbuckling effects means using reduced axial skin stiffness in the buckling analysis, which would naturally lead to reduced wide column buckling load factors.

However, one must remember that the prebuckling loads in the skin are much smaller in the theory that includes local postbuckling than they are in the theory that neglects local postbuckling. This difference in load distribution over the cross section of the wide column causes the differences in the wide column buckling modes and load factors listed in the top part of Fig. 67. Notice that for all pressures greater than p = -3 there is much more movement of the relatively heavy stiffener in the buckling modes corresponding to "local postbuckling included" than there is for those corresponding to "local postbuckling neglected". This is because relatively more axial load passes through the stringer in the "local postbuckling included" case, giving rise to buckling modes that reflect general instability behavior rather than local skin buckling. In fact, the mode corresponding to p = 0 on the left-hand side of Fig. 67 was rejected by PANDA2 as an indicator of general instability. Therefore, the eigenvalue of 0.306 would not have represented a violated constraint in an optimization analysis of this panel. The mode shape just above the rejected mode was barely accepted. (It is felt that the acceptance of such modes, which actually

106

represent local skin buckling more than general instability, is a good practice, since it helps to yield conservative results for general instability, a mode of failure that is more likely to be sensitive to unknown imperfections than is the local instability mode of failure.)

Figure 68 shows the effect of pressure on (axial load) - (axial strain) curves. Those for positive pressure lie to the right of those for negative pressure for two reasons:

1. The axial bowing induced by pressure increases as the axial load increases, and if the pressure is positive this bowing is of such a sign as to give rise to average decreases in distance between the two loaded ends of the panel skin reference surface, at which the average axial end shortening is measured.

2. As seen from Fig. 65, positive pressure leads to local bifurcation buckling modes that have more axial halfwaves than is the case for no pressure or negative pressure. The tangent stiffness of postbuckled panel skin decreases with increasing number of axial halfwaves in the postbuckled modal pattern.

Figures 69 and 70 show the effect of pressure on postbuckling normal deflection and maximum strain in the panel. From Fig. 69 one can see that negative pressure leads to a higher local bifurcation load than does a positive pressure. This is for the reasons explained in connection with Fig. 65. The growth of the local buckles is faster with increasing axial load in the case of positive pressure than it is with negative pressure. This is because a relatively larger share of axial compression passes through the skin, as shown in Fig. 65.

From Fig. 70 one can see that positive pressure leads to much higher strains than negative pressure. This is obviously related to the much faster growth of the local buckles in the case of positive pressure.

Figure 71 shows the effect of pressure on the pre- and post-local- buckling axial strain in the panel skin midway between stringers. The PANDA2 results are explained by the faster growth of local buckles in the case of positive pressure.

20.7 Results for Combined Axial Compression and Simulated Curing

In panels similar to the isotropic blade stiffened panel being studied here, but fabricated from composite materials, optimum designs would be characterized by stringers with predominantly axial fibers and a skin which may be predominantly plus and minus 45- degree fibers. If the skin and stiffeners are cocured, thermal stresses and deformations build up as the panel cools from the temperature at which the composite material sets to ambient temperature. If the stringers have mostly zero fibers while the skin has mostly plus and minus 45-degree fibers, the skin will try to shrink more than the stringers, and the panel will bow axially so that the side of the skin farthest from the stringers is concave. This thermally induced residual state can be predicted with PANDA2.

In the case of the isotropic material of this example, there would not be any overall residual stresses or deformations in an actual case because the stringers and skin would shrink equally during post-cure cool-down from a uniform temperature. However, this

rather unrealistic example involving skin and stringers at different temperatures is introduced for demonstration purposes. The phenomena described next would occur in realistic cases also, although they probably would be a lot less pronounced, even in a non-optimally designed panel.

The results are shown in Figs. 72 through 77. The axial load-strain curves in Fig. 72 have qualitatively the same shape as those in Fig. 68 for plus and minus pressure, respectively, because the important effect, axial bowing of the panel, has the same sign and approximately the same amplitude, as seen from comparison of Figs. 57 and 76.

Figure 73 demonstrates that following local bifurcation buckling, the amplitude of the local buckles increases at the fastest rate when the panel bows so that the side of the skin away from the stringers becomes concave (curve labelled $T = -290$). This happens because a higher share of the axial load goes through the skin, as shown in Fig. 77, than is the case with bowing of the opposite sign. The same effect was obtained with positive pressure. (See Figs. 65 and 69.) The bifurcation buckling load is higher than those for $T = 0$ and $T = +290$ because the residual resultant is tensile in the skin. The local bifurcation buckling load factor is nearly zero for the panel with the heated skin because the residual state of the "cured" panel almost causes local buckling by itself.

The maximum transverse strains in the locally postbuckled panel, shown in Fig. 74, exhibit behavior analogous to that in the pressurized axially compressed panel for the same reason: the local buckles grow faster for the panel bowed so that the highest percentage of applied axial load is absorbed by the skin. However, the effect is much less dramatic in the case of thermal residual strains than it is for strains due to pressure because there is no thermal strain concentration in the prebuckling phase analogous to the "wrap-around" strain concentration described in the section on panels subjected to normal pressure alone.

Figure 75 shows the extreme fiber axial strain in the panel skin midway between stringers. This behavior is also explained by the later bifurcation of the panel in which the residual axial resultant is tensile but the buckles of this panel grow faster than do those in the panel that is thermally bowed the opposite way.

Figure 76 shows the linear dependence of axial bowing and axial residual stress resultant on temperature. Figure 77 shows the effect of temperature on share of axial load carried by the skin and on the local bifurcation buckling load factor. In this case the local bifurcation buckling load factor is influenced by two counteracting factors:

1. For increasing skin temperature (Note: positive temperatures are plotted downward to preserve the analogy with the normal pressure case!) the smaller share of axial load carried by the panel skin would lead to higher bifurcation load factors if there were no residual stress resultant in the skin.

2. For increasing skin temperature there is increasing compressive residual stress resultant in the skin, which would lead to lower bifurcation load factors. This is the dominant effect.

108

21.0 OPTIMUM DESIGN OF ARIANE4 INTERSTAGE

21.1 Procedure for Designing with PANDA2

Section 19.7 contains a brief description of the steps leading to an optimum design of a graphite-epoxy, hat-stiffened panel loaded in axial compression. That panel is subjected to only one set of loads, and results are not given for the evolution of the design during iterations.

In this section the design procedure is explained more fully. Minimum weight designs are obtained for the ARIANE4 interstage between the second and third stages of the ARIANE4 booster. Blaas and Wiggenraad call it "Interstage 2/3" [31]. This example is employed to illustrate a typical use of PANDA2 to solve a practical, rather large, design problem. Two design concepts are explored: (1) T-shaped stringers for which two "sub-concepts" are investigated: (1.1) all-graphite-epoxy and (1.2) graphite-epoxy with an aluminum insert inside the stringers and stringer bases, and (2) Hat-shaped stringers.

Table 4 lists the tasks required during the design process.

21.1.1 Step 1: Identify the structure to be optimized
Step 1 is to identify the structure to be optimized. Figure 78 shows the ARIANE4 2/3-interstage, which is initially assumed to be a cylindrical shell reinforced by external T-shaped stringers and internal rectangular rings. (In the PANDA2 analysis special end fittings and doublers are of course neglected. The weights of the panels designed by PANDA2 do not include any structure, such as large end rings, that would be required to provide end support for the interstage.)

21.1.2 Steps 2 and 3: How much and what load sets?
Steps 2 and 3 are to decide how much of the structure to include in the optimization analysis and how many and what load sets to optimize this portion to withstand. The very important decisions that the user makes in Steps 2 and 3 depend on whether or not the loading varies along the length and around the circumference of the structure selected in Step 1.

In this case the cylindrical shell is subjected to overall bending, axial compression, and shear loads, **M**, **P**, and **S**, as shown in the top part of Fig. 79. The bending moment **M** is assumed to be represented by an axial line load load $N_x(\theta)$ that is distributed around the circumference of the cylindrical shell as $\cos\theta$, and the shear load **S** is represented by a shear line load $N_{xy}(\theta)$ distributed as $\sin\theta$. In order to determine the in-plane shear N_{xy} at $\theta = 90$ degrees generated by the cosinusoidally varying axial load $N_x(\theta)$, an initial run was made with BOSOR4 with use of its INDIC = 3 analysis branch [2]. The design used for this preliminary analysis was that obtained by Blaas and Wiggenraad [31]. This shear line load plus that generated from the applied shear load **S** constitute the total maximum N_{xy}. In this analysis it is assumed that the maximum axial compression from bending **M** is $N_x(\text{from M}) = 2000$ lb/in.; the uniform axial compression from **P** is $N_x(\text{from P}) = 1000$ lb/in.; and the maximum in-plane shear at $\theta = 90$ degrees from both **M** and **S** is $N_{xy} = 1000$ lb/in.

The actual problem is to find the minimum weight of a complete cylindrical shell with axial line load N_x and shear line load N_{xy} both varying around the circumference.

PANDA2 allows only N_x to vary along the panel edge. Therefore, this problem was approached by assuming that the complete cylindrical shell is divided into identical panels, each spanning 40 inches of circumference and each subjected to uniform loads. Three such panels are depicted in the bottom of Fig. 79. The optimum design of the complete cylindrical shell with loads varying over its surface can be determined by optimizing one of the identical 40-inch-wide panels subjected to multiple sets of uniform loads. Initially the three load sets shown at the bottom of Fig. 79 were chosen. However, it was soon determined that the uniform tension load, $N_x = 2000$ lb/in, did not generate any critical behavioral constraint conditions. Therefore, this load set was dropped.

21.1.3 Step 4: Decide what design concept to use Step 4 is to decide what design concept to use. In this case the skin and stringers are initially assumed to be fabricated of graphite-epoxy cloth and tape, as depicted in Fig. 80. The spacing of the stringers is to be determined. The internal rings are of aluminum and are equally spaced 26.75 inches apart.

Details of the design concept with the T-shaped stringers appear in Fig. 80. The graphite-epoxy cloth and tape (Material types 1 and 3) have the same properties as those listed in the file HAT.BEG given at the end of Section 3. The Default Group of 12 layers of graphite-epoxy tape has layup angles fixed but thicknesses to be determined during optimization. The graphite-epoxy cloth has the same modulus along the fibers in the two orthogonal directions ("pseudo-isotropic") but low shear modulus. The fiber directions are oriented at plus and minus 45 degrees from the axis of the stringers. Only one layer is given because this cloth is considered to be homogeneous material with the same properties in the plus and minus 45-degree directions. The thickness of this cloth is a decision variable.

Both tape and cloth are made in certain ply thicknesses. It is not possible to fabricate a structure with layer thicknesses that are not integral numbers of plies of this tape or cloth. However, PANDA2 treats all decision variables as continuous. If the user indicates that a certain material is composite tape, then PANDA2 sets the thickness of any layer of this material that is less than a quarter of the thickness of a single ply of the tape equal to zero. Hence, if the user indicates that Material Type 1 is composite tape with ply thickness of 0.005 in., then any layer consisting of this material becoming less than 0.00125 inches in thickness during optimization iterations is dropped from further consideration unless the user reinserts it via the CHANGE processor. PANDA2 does not eliminate any layers not designated by the user as being made of composite tape.

After several sets of design iterations are performed, a panel will doubtless consist of many layers that are not integral numbers of plies of tape or cloth. It is up to the user to decide which layers to eliminate, which to increase in thickness, and which to decrease in thickness in order to make them integral numbers of plies of tape or cloth. These changes can be made via the CHANGE processor. Lower and upper bounds should then be reset at values equal to integral numbers of plies, and certain of the thickness variables should doubtless be eliminated as decision variables. Then more design iterations should be made. The user should continue this cycle until all thicknesses in the panel and stiffeners are integral numbers of plies of tape or cloth. The examples given here demonstrate this strategy.

Note that the design concept drawn in Fig. 80 allows for three extra layers $[0_{m_2}/90/0_{m_2}]$ in the base under the stringer. The role of the extra 0-degree layers is described in Section 19.7. The 0-degree layers are divided into two groups separated by a 90-degree layer in both the stringer base and in the stringer flange because tests have shown that large numbers of uniaxially oriented layers have less ultimate strength than do small numbers of such layers. Hence, it is wise to break up these "blocks" of material by inserting 90-degree layers of a single thickness of tape.

Note that although the aluminum rings indicated in Fig. 80 have T-shaped cross sections, they are considered to be rectangular by PANDA2. This is because the faying flanges of the rings (flanges next to the panel skin) are considered by PANDA2 to be part of the skin, not part of the stiffener. These flanges are one of the layers in Segment 2 of the ring module. The outstanding leg of the ring is Segment 3 of the ring module.

21.1.4 Steps 5–8: Starting design, Optimization parameters, Optimization strategy, Final evaluation Table 4 lists the remaining steps (Steps 5–8) in the design procedure. Once the starting design is selected and decision, linked, and escape variables are chosen, a certain design strategy or sequence of design strategies are pursued. The final optimum design is partially checked via the PANEL processor, which sets up a BOSOR4 model of the entire panel width with all stringers treated as shell branches. The BOSOR4 model considers only buckling between rings in modes with one half axial wave between rings. In an actual design process, the user should of course fully check the optimum design obtained with PANDA2 by performing detailed multidimensional finite element analyses and tests.

21.2 Starting Design with All-Composite, T-Shaped Stringers (Step 5)

Table 5 lists the input data for the BEGIN processor. Note that as input for Segment 2 of the ring module (Table 5 following the entries "R" and 26.75) there are several new layer types, 11, 12, 13, 14, and 15. Layer index 15 really does represent a new layer type, the faying flange of the aluminum ring, but layer types 11, 12, 13, and 14 are simply layer types 2, 4, 6 and 7 for the stringer module as seen from the perspective of a ring cross section. They must be introduced as new layer types because the 90-degree layup angle for layer type 2 of the stringer module becomes a 0-degree layup angle from the perspective of a ring module; the 0-degree layup angle for layer type 4 of the stringer module becomes a 90-degree layup angle for the ring module, and so on. Later, in DECIDE, the thicknesses of these new layer types must be linked to the thicknesses of layer types 2, 4, 6, and 7, respectively.

Note also, that layer type 1 of the stringer module remains layer type 1 in the ring module. Although the +45-degree layup angle in the stringer module becomes a -45-degree layup angle from the perspective of the ring module, since the properties of this cloth layer are the same in both the + and - 45-degree directions, it is not necessary to introduce a new layer type. Note that the third layer in the stringer module (+45-degree tape) becomes -45-degree tape from the perspective of the ring module. Hence, one must either introduce a new layer type in the ring module or see if some other layer type in the stringer module will suffice. Since the thickness of the -45-degree layer (layer no. 5) in the stringer module

111

will be constrained later to be equal to that of the +45-degree layer in the stringer module, this layer type can be used for the third layer of the ring module. Similarly, the fifth layer in the ring module can be designated layer type 3.

21.3 Selection of Decision, Linked, Escape Variables (Step 6)

Tables 6 and 7 list the input to the DECIDE processor and part of the output from DECIDE. We see from these tables the linking of the thicknesses of certain of the layers in the ring module to those in the stringer module. The thicknesses of layer types 1 through 8 and layer type 10 were chosen as decision variables by use of a default option in DECIDE, as seen from the second input entry in Table 6. The thickness of layer type 9 is not a decision variable because this 90-degree layer is simply intended to prevent the buildup of thick blocks of 0-degree layers in the stringer base and flange.

21.4 Optimization Strategy (Step 7)

Figures 81 and 82 show the overall architecture of the PANDA2 mainprocessor, which is invoked via the command PANDAOPT. With the rather large number of decision variables indicated in Table 7, particularly if there are multiple sets of combined loads and if highly nonlinear, post-local buckling behavior is allowed to occur, the design of a complex panel with use of discretized models may require quite a bit of computer time. It is best therefore to begin by using the IQUICK = 1 option. The meaning of IQUICK was introduced in Section 6.2. With this option only the closed-form PANDA [1] type of analysis is used and local postbuckling behavior is not investigated. Following MAINSETUP, sample input for which is listed in Table 8, the user should give the command PANDAOPT several times, each time allowing PANDA2 to perform from 5 to 10 design iterations with IQUICK = 1. In the current example there were three sets of 5 iterations each and a fourth with 10 iterations.

Why take several sets of 5 iterations each, instead of just one set with 15 or 20 iterations? There are two reasons. The first is that it is always a good idea for the user to monitor carefully the output as the design is evolving. Hence, after each set of 5 iterations the user should inspect the file NAME.OPM (in this case NAME = ARIANE) to ensure that the intermediate results seem correct and that each design looks reasonable. The second reason has to do with how the optimizer CONMIN works. Figure 83 illustrates for the case of two decision variables. Given the user's lower and upper bounds of the decision variables, CONMIN establishes a more restrictive "window" within which the decision variables are allowed to vary in any given iteration. The size of this window decreases with each design iteration. (In PANDA2 the dimensions of the window decrease by a factor 0.8 with each iteration.) These restrictions are placed upon the permitted excursions of the decision variables in order to prevent wild swings in the design as it evolves. The example shown in Fig. 83 shows eight iterations, and the last design point is labeled "FINAL DESIGN." Note, however, that the "window" of permitted excursions is rather small. To the user it may appear that design iterations have converged, whereas actually they may not have. On the other hand, they really may have converged. This can easily be checked simply by executing PANDAOPT again. When this is done, the "window" of permitted

excursions is re-expanded to its original size, the new starting design is the last design obtained in the previous set of iterations, and new iterations proceed as before. The user should keep executing PANDAOPT until the objective does not change very much. When the user is satisfied with the current design, he or she should then take one additional set of design iterations in which the number of iterations is larger than the number used previously, say twice or three times as many.

After the user is satified with the preliminary design obtained with the IQUICK = 1 option, he or she should pursue further design iterations with IQUICK = 0. Lower factors of safety can generally be used with the IQUICK = 0 option, expecially for buckling between rings, because the wide column buckling model is used with this option. This model is more conservative than the smeared-stringer model used with the IQUICK = 1 option, since it neglects the curvature of the panel and it accounts for local deformations of the panel module cross section as it buckles in the wide-column mode. However, note that some factor greater than unity should generally be used because PANDA2 does not account for local initial imperfections and the important effect of these on overall buckling, particularly for cases in which local and general buckling occur at loads that are close.

21.5 Results with IQUICK = 1 (Step 7.1)

The leftmost portions of Figs. 84 through 89 give results obtained with IQUICK = 1. The 25 iterations are performed in three sets of 5 each followed by one set of 10. A total of about 8 minutes of CPU time on the VAX 11/785 with the VMS 4.2 operating system are required for execution of the 25 iterations. For the first load set (pure axial compression of 3000 lb/in) a factor of safety of 2.0 is used for general instability. For the second load set (axial compression of 1000 lb/in combined with in-plane shear of 1000 lb/in) a factor of safety of 1.5 is used. The behavior of the decision variables and design margins is reasonably smooth.

21.6 Results with IQUICK = 0, Post-Local Buckling Permitted (Step 7.2)

The remaining portions of Figs. 84 through 89, Tables 9 through 11, and Figures 90 and 91 pertain to optimization with use of the discretized panel module models and with local buckling of the panel skin permitted. The factors of safety for general instability are now 1.5 for load set 1 and 1.2 for load set 2. The computer time required for 5 design iterations varied from 15 minutes to half an hour of VAX 11/785 time, depending on how much local postbuckling analysis was required. (The PANDA2 system decides this, not the user!)

Note that the decision variables and the design margins no longer vary smoothly with design iterations, as they did with the IQUICK = 1 option. It appears that an optimum design corresponds to early postbuckling, a domain in which the state of the panel is very sensitive to small changes in stringer spacing and thickness. From Fig. 88, which corresponds to load set 1, one can see that the behavioral constraints most often violated (violated behavioral constraint = negative design margin) are the stringer pop-off constraint and the wide column buckling constraint. Also violated is the "long wavelength local buckling" constraint, the purpose of which is described in Section 12.1(b), where it is called "low axial wavenumber" local buckling. From Fig. 89, which corresponds to load set

113

2, one can see that the constraints most often violated are stringer pop-off, wide column buckling, and maximum tensile stress in the cloth. (This maximum tensile stress occurs at the peaks of the buckles midway between stringers.)

In Fig. 84 five of the points are blackened. These 5 designs, all quite different, correspond to feasible designs, or designs that are almost feasible. (Check the margins in Figs. 88 and 89!) Points at the corresponding iterations are also blackened in Figs. 85 and 87. (This code is NOT used in Figs. 86, 88, or 89, in which blackened points have different meanings.) Although these feasible designs are all quite different, they all correspond to weights that are close to 33 lbs. There are other feasible designs encountered during the approximately 100 iterations, but these correspond to somewhat heavier panels. The designs corresponding to iterations 32 and 59 are not in their locally postbuckled states for either of the two load sets; that at iteration 70 is not in its locally postbuckled state for load set 1 but is for load set 2; and those at iterations 79 and 86 are in their locally postbuckled states for both load sets.

Figures 85, 86 and 87 illustrate the use of the PANDA2 processors CHANGE and DECIDE in the midst of design iterations. These figures show that the design was "bobbing around" during iterations 35 through 45. At iteration 45 it was decided to increase the stringer spacing and drop and combine certain layer types, as depicted in Fig. 85. At iteration 60 it was observed that a pre-established upper bound of 2.0 in. on the width of the stringer base was limiting design opportunities, and this upper bound was increased to 3.0 in. Also, it was judged beneficial to remove layer type 6 as a decision variable.

After 100 iterations a decision was made to use the design at iteration 70 as a starting design, to change the thicknesses so that all thicknesses represented integral numbers of plies of cloth or tape (the cloth is 0.006 inch per ply and the tape is 0.0052 inch per ply), to eliminate all thicknesses as decision variables, and to perform more design iterations. The results after 15 iterations performed in a single set are listed in Tables 9, 10 and 11. It turns out that the panel is not in its post-locally-buckled state for either of the two load sets. Figure 90 gives plots of the discretized optimum panel module and the local and wide column buckling modes and load factors λ_{LOCAL} and $\lambda_{WIDECOLUMN}$ corresponding to load set 1, pure axial compression of 3000 lb/in. Please note that the BOSOR4-type of analysis yields a local buckling load factor $\lambda_{LOCAL} = 0.9151$, indicating that the panel is in its early post-locally-buckled state. However, in this case the Koiter post- buckling analysis yields an eigenvalue for local buckling that is slightly greater than unity, and therefore no post-buckling calculations are performed by PANDA2; the panel is assumed to remain in its unbuckled state. The eigenvalue for local buckling obtained from the Koiter analysis is different from that obtained from the BOSOR4 analysis because the two theories are different.

Figure 91 shows the results of using the PANEL processor followed by a BOSOR4 run. This represents Step 8 in Table 4. The use of BOSOR4 to treat prismatic structures such as stiffened panels is described in Chapter 7 of [30]. The multi-segment BOSOR4 model is depicted in Fig. 91(a) and the two lowest buckling load factors are given in Figs. 91(b) and (c). The buckling modal displacements vary sinusoidally in the x-direction (normal to the plane of the page), with a half-wavelength equal to the ring spacing of 26.75 inches.

The buckling mode shown in Fig. 91(b) is simply another form of skin buckling because the intersections of the stringer webs with the panel skin move only slightly. It is the load factor and mode shape in Fig. 91(c) that should be compared to the wide-column buckling load factor $\lambda_{WIDECOLUMN} = 1.528$ given in Fig. 90(c).

21.7 Results with IQUICK = 0, Post-Local Buckling NOT Permitted (Step 7.3)

Figures 92 through 96 and Tables 12, 13 and 14 give results that are analogous to those already given in Section 21.6, but with post-local buckling not permitted. The panel weight again approaches 33 lbs, but the stringers are closer together in this case than they were in the case for which local postbuckling is permitted. From Fig. 93 it is seen that the critical buckling mode for load set 1 is wide column buckling, and from Fig. 94 it is seen that the critical buckling mode for load set 2 is local buckling. After several iterations and repeated use of CHANGE and DECIDE the results become better behaved, settling down to a stable pattern as iterations proceed. This is because there is no sensitive behavior associated with the early postbuckling regime, as was the case for the optimization described in Section 21.6.

Figure 95 shows the optimized panel module (a), the local buckling mode and load factor λ_{LOCAL} (b), and another buckling mode and load factor (c) corresponding to load set 1. Notice in Fig. 95(c) that the load factor $\lambda_{WIDECOL.} = 1.482$ does not correspond to a wide column buckling mode, which would resemble the mode shown in Fig. 90(c), but rather a long-wavelength side-sway of the stringer. However, the load factor λ associated with this side-sway mode is retained as a constraint for wide column buckling because it represents a lower bound to the wide column buckling load. We know it is a lower bound because the eigenvalue extraction routine used in PANDA2 (same as the routine used in BOSOR4) calculates eigenvalues in increasing order. Therefore, we know that λ corresponding to a mode similar to that depicted in Fig. 90(c) is higher than 1.482.

Figure 96 shows the multisegment model generated by the processor PANEL and the three lowest eigenmodes and load factors from the BOSOR4 analysis of this model. All of the modes correspond to side-sway of one or more of the stringers. The wide-column eigenvalue must be greater than 1.309, which is the highest mode calculated in the BOSOR4 run, for which only the three lowest eigenvalues were requested by the user.

Tables 12, 13 and 14 list the final design, weight, and design margins corresponding to load set 1 and load set 2.

21.8 Conclusions from the Results Given in Sections 21.6 and 21.7

Apparently in this case designing the panel to permit local buckling between the stringers does not lead to any reduction in weight. However, it does permit panels with stringers farther apart than is the case in which local buckling is not permitted. Another point should also be made. Since the same factors of safety were used to generate the results in both Sections 21.6 and 21.7, it might be argued that the panels operating in their locally postbuckled states are more reliable than are those in which local buckling is not permitted. This is because the former will be less sensitive in initial imperfections than

the latter. In the former case the reduction in panel skin stiffness due to local buckling is accounted for when general instability load factors are computed. In the latter case there is no such reduction in skin stiffness. However, actual panels have local imperfections that reduce the effective stiffness of the skin much as if it were buckled. Since PANDA2 does not include the effect of initial imperfections, it may overestimate general instability load factors in cases for which the skin is not in its postbuckled state.

Another conclusion that might be drawn, especially from the results in Figs. 88 and 89 which show that the most critical behavioral constraint is stringer pop-off, is that if the design could be revised in some way as to increase dramatically the allowable peel force in the web (the present value is 100 lb/in), then significant reduction in weight might be attained by permitting local buckling to occur. The results given in the next section qualify this hypothesis.

21.9 Optimum Designs with Increased Allowable Web Peel Force

In the analyses reported in Sections 21.6 and 21.7 the allowable web peel force (see Figs. 5 - 7) was set at 100 lb/in, a value close to what has been observed in tests of graphite-epoxy cloth bonded to graphite-epoxy tape. This value can be greatly increased if a metal I-shaped insert can be included as a core element in the stringer, as shown in Fig. 97. The loads from web to faying flange and from web to outstanding flange can then be carried through generous fillets machined at the junctions between web and flanges of the insert.

The analyses reported in Sections 21.6 and 21.7 were repeated for the configuration shown in Fig. 97. The maximum allowable web peel force was increased to 1000 lb/in. Two new decision variables were introduced: the thickness of the flanges of the aluminum insert (faying flange thickness equal to outstanding flange thickness) and the thickness of the web of the aluminum insert.

The minimum weight designs are listed in Table 15. A weight reduction of about 10 per cent is obtained when local buckling is allowed compared to the minimum weight for the same design concept when local buckling is not permitted. Figure 98(a) shows the optimized design for the case in which local buckling is permitted, and Fig. 98(b) gives the local buckling mode and load factor λ_{LOCAL} corresponding to load set 1. Since the local buckling load factor, λ_{LOCAL} equals 0.339, the axial compression supported by the optimum design, $N_x = 3000$ lb/in., is about three times the local buckling load. Therefore the panel is loaded rather far into the post-local-buckling regime. Note, however, that the weight saved is not significant when compared with the minimum weight designs obtained without the aluminum insert. These designs weigh about 33 lbs. Also, the concept with the aluminum insert would doubtless be significantly more expensive than the all-composite concepts.

It is concluded from these results and from the results presented in Sections 21.6 and 21.7 that without additional convincing proof that the optimum designs with local buckling permitted are more reliable than those in which local buckling is not permitted, we cannot affirm that there is much to be gained in this particular case by designing to allow local buckling.

116

21.10 Optimum Designs with Hat-Shaped Stringers

Lighter designs should be possible for panels with stringers that enclose area, since the torsional stiffness of the stringer is thereby greatly increased without much increase in weight. Table 16 lists results for optimum designs with local buckling permitted and with local buckling prohibited. There is very little reduction in weight afforded by a design that permits local buckling. For this design the panel fails under load set 1 at only 10 per cent above the local buckling load and under load set 2 at about 31 per cent above the local buckling load. Designs with stringers further apart are feasible and fail at a load that may be many times the local buckling load, but these designs are heavier than those listed in Table 16.

Figure 99 depicts the discretized model and the local and wide column buckling modes and load factors corresponding to load set 1 for the panel designed not to buckle locally. For the same panel Fig. 100 shows the discretized model and several inter-ring buckling modes predicted with use of PANEL and BOSOR4. The load factors for these inter-ring modes are close and agree reasonably well with the load factor calculated from the PANDA-type closed form analysis for a panel simply supported at the ring stations with stringers smeared out.

22.0 SUMMARY, CONCLUSIONS, PITFALLS AND LIMITATIONS AND SUGGESTIONS FOR FURTHER WORK

22.1 Summary and Conclusions

The purpose, scope and operation of the PANDA2 system of programs has been explained through a sample case run with use of a tutorial option. Several examples are given with results compared with those in the literature and those obtained by other computer programs such as EAL and STAGS. It is concluded that the agreement between predictions from PANDA2 with those from general purpose programs justifies the use of PANDA2 for preliminary design. An interstage for the ARIANE4 booster is designed both allowing and prohibiting local buckling. Various design concepts are tried, and it is concluded that in this case little is gained by allowing local buckling during service.

Because of the inclusion of initial local geometric impefections in the form of the local buckling mode (See Appendix A), PANDA2 can predict the nonlinear modal interaction effects described by Koiter, Hutchinson, Tvergaard, Thompson, van der Neut, and others. In Appendix A good agreement is displayed between results obtained by PANDA2 and theoretical and experimental results obtained previously by others.

PANDA2 is similar to other sizing codes for stiffened panels, such as PASCO [10], developed at NASA Langley Research Center by Anderson and Stroud, and POSTOP [22]-[24], developed at Lockheed-Georgia by Dickson, Biggers, and Wang. However, PANDA2 will in certain branches of its operation handle rings as well as stringers, will allow normal pressure as one of the loads, and is constructed with rather extensive interactive aids for users. The post-local-buckling analysis used in PANDA2 is based upon a modified form of Koiter's theory [4] which probably yields more accurate strains than those obtained by POSTOP because the local buckling mode is derived from a discretized model of the panel module cross section, rather than from an assumed shape function with only two or three coefficients. Also, PANDA2 includes the effects of overall (bowing) imperfections as well as local imperfections in the analyses performed within the optimization loop. The popoff constraint used in PANDA2 is different from that used in POSTOP. From the very limited experience of the few tests on the hat-stiffened panels (Fig. 31), this popoff constraint, which requires results of standard peel tests, seems to work.

22.2 Pitfalls and Limitations

PANDA2 is aimed at very difficult, complex, nonlinear structural problems, and because the goal is to obtain reasonable preliminary (and even, perhaps, final) designs in a short time, there are many assumptions and approximations used in the theories on which it is based. Therefore, any designs produced by PANDA2 should be thoroughly evaluated by application of rigorous nonlinear finite element models and tests. There is much that is unknown about the behavior of composite materials, and the user should realize that the failure criteria that he or she enter as input data affect the final outcome.

The following is a list of pitfalls the user should be aware of. They are not listed in order of importance, but rather in the order that the writer happened to think of them.

118

1. PANDA2 is intended to be used for the analysis of uniform panels, in the sense that the panel contains regular arrays of stringers and or rings. It is not meant for use in cases in which there is only one stringer, for example.

2. In PANDA2 rings are sort of "second-class citizens". For example, the local postbuckling analysis is conducted only for a single panel module that represents one stringer with the panel skin and stringer base between adjacent stringers. No analogous treatment is included for local postbuckling of panels with rings only, for example. Also, local buckling load factors for panels stiffened by rings only are not calculated by means of any models in which the ring cross sections are discretized, as the the case for stringers.

3. The effect of imperfections in panels and shells stiffened by BOTH rings and stringers is included explicitly as described in Appendix A ONLY for the portion between adjacent rings. The conservative wide column buckling model applies ONLY to the portion between adjacent rings, not to the entire ring and stringer-stiffened structure. Therefore, if one is designing a ring and stringer-stiffened cylindrical panel or shell, one must provide a sufficient factor of safety FSGEN to generate a reliable margin for general instability. (Note, however, that the reduction in skin and stringer stiffnesses caused by local deformation of these parts IS INCLUDED in the general instability model.)

4. The material behavior is linear. There is no plasticity.

5. In the postbuckling analysis the axial wavelength of the local buckles is assumed to be constant. There is no theory in PANDA2 allowing secondary bifurcations, that is bifurcations from the locally postbuckled state. Secondary bifurcations are frequently observed in tests.

6. Only simple failure criteria are used in PANDA2. An attempt is made to account for the fact that cracking due to tension normal to the fibers does not necessarily lead to failure of the structure but does lead to decrease in stiffness and decrease in the allowable compression along the fiber, but these portions of PANDA2 should be regarded, if not with paranoia, at least with a certain healthy skepticism.

7. Boundary conditions are rather inflexible in PANDA2. The edges normal to the screen (generators of a cylindrical panel) are always assumed to be simply supported. The other two edges (curved edges in a cylindrical panel) can be either simply supported or clamped, but clamping is simulated by analyzing a simply supported panel the length of which is $L/(3.85)^{1/2}$, where L is the actual length of the panel.

8. It is possible that PANDA2 will lead to designs that are feasible in the sense that all design margins are positive, but that are unreasonable because of other considerations not formally introduced by the user, either through oversight or because of limitations in PANDA2. The user should always monitor carefully the design process to make sure that he or she has introduced sufficient lower and upper bounds, and has accounted for practical items such as possibility of fabrication, cost, clearance of parts, etc.

9. There is no guarantee that PANDA2 will find a minimum weight design in the global sense. From Figs. 84 – 89 we see several feasible designs many of which correspond to local minima in the surface of weight as a function of decision variables. Before the user decides

to accept a design, he or she must use the CHANGE processor, alter one or more of the decision variables, and perform more design iterations. When in doubt always perform more design iterations! They are cheap compared to building and testing something and then finding out later that much better possibilities exist. Varying the stiffener spacing is perhaps the best way to search for other minimum weight designs.

10. In designing panels that are allowed to buckle locally in service, it may frequently happen that optimum designs correspond to the early postbuckling regime. This is because maximum stresses and stringer pop-off forces increase steeply in design space in the early postbuckling regime and therefore are likely to encounter maximum allowable values in this regime. Design iterations may not converge in this regime due to the discontinuity in behavior of the panel just before local buckling and just after local buckling. The user will find that it helps to allow more iterations in each iteration set in cases such as this.

11. The post-local-buckling analysis performed with PANDA2 is based on the assumption that the local buckling deformations are antisymmetric with respect to the stringer line of attachment to the panel skin. This assumption is not as good for curved panels as it is for flat panels.

12. The user should not be fooled by spurious convergence of the design due to a restricted "window" of permitted excursion of decision variables, a property of PANDA2 described in Section 21.4. When in doubt perform another (and yet another!) set of design iterations.

13. Composite material is made in certain ply thicknesses. The user must ensure that his final design consists of integral numbers of ply thicknesses for every layup angle.

14. In the final stages of a design process most or all thickness variables may have been eliminated as decision variables. In such cases there may not be enough escape variables to avoid CONMIN's inability to generate moves in design space if more constraints are violated than there are decision variables remaining in the problem. In such cases the user may have to do some "optimization by hand", that is, he or she may have to "jiggle" one or more of the decision variables in a sequence of fixed design runs. This kind of problem only seems to arise when the design is very close to being feasible. Therefore, it can be handled in an alternative way simply by allowing slightly increased factors of safety.

22.3 Suggestions for Further Work

Perhaps the weakest part of the PANDA2 post-local buckling analysis is the assumption that the number of axial halfwaves at bifurcation remains constant as the load increases beyond the bifurcation load. Koiter proved that for infinitely long, axially compressed flat plates the postbuckling axial wavelength becomes shorter as the load increases beyond the bifurcation load. In tests on finite panels the axial wavelength stays approximately constant for rather large load ranges, but then the buckle pattern may change abruptly into another similar pattern but with more axial waves. There is probably some complicated transition pattern or series of patterns that governs this secondary bifurcation or series of closely related bifurcations. Whether and at what axial load the secondary bifurcation or bifurcations occur seems to depend on small, perhaps unavoidable imperfections in uniformity of load and panel properties. Whatever actually occurs, it would be a good

idea to allow the axial length of the local buckling pattern to be variable in the postbuckling analysis in PANDA2.

It has been beneficial to include local imperfections in the panel skin in the PANDA2 analysis. Details are given in Appendix A. The imperfection is assumed to have the form of the critical local bifurcation buckling mode of the perfect panel. This additional capability is especially useful in cases for which the optimum design yields local and general buckling loads that are close. In such cases, van der Neut [25], Thompson, Tulk, and Walker [26], Tvergaard [27], Byskov and Hutchinson [28], Koiter [29], and others referenced in [30] have shown that the interaction between local and general buckling may cause significant reduction of the load-carrying capability below that of the perfect panel. Inclusion of initial local imperfections also serves to smooth the transition from prebuckling to postbuckling regimes, which is likely to eliminate much of the jumpiness of behavior during design iterations for panels the optimum designs of which correspond to the early postbuckling regime.

The postbuckling analysis in PANDA2 is based on the treatment of a single panel module, which is assumed to be flat. The postbuckling pattern is a two-term series expansion of the local bifurcation buckling mode:

$$w(x,y) = f\left(\phi + a\,\phi^3\right) \sin[(\pi/L)(x - my)] \tag{22.1}$$

in which ϕ is the bifurcation buckling mode. If ϕ is antisymmetric about the stiffener line of attachment, as it is in Figs. 20(a), 22(a), and 46(c), for examples, then $w(x,y)$ will always be antisymmetrical. However, if the panel is curved $w(x,y)$ observed in tests will not be antisymmetrical: outward buckles will differ from inward buckles. To predict this behavior, terms with even powers of ϕ would be required in the series expansion for $w(x,y)$.

It would be beneficial to expand the PANDA2 capability to include nonlinear material behavior.

Inclusion of a discretization of the entire panel width inside the optimization loop, at least as a user-chosen option, would be a good idea. This would eliminate much of the difficulty associated with use of the wide column buckling load as an indicator of general instability. Of course optimization runs would take much more computer time. However, the user could choose this more elaborate model only after a reasonably good optimum design had already been obtained with use of the wide column model described in this paper.

121

23.0 ACKNOWLEDGMENTS

24.0 REFERENCES

[1] Bushnell, D., "PANDA–Interactive program for minimum weight design of stiffened cylindrical panels and shells," Computers and Structures, Vol. 16, pp. 167-185, 1983

[2] Bushnell, D., "BOSOR4: Program for stress, buckling, and vibration of complex shells of revolution," Structural Mechanics Software Series - Vol. 1, (N. Perrone and W. Pilkey, editors), University Press of Virginia, pp. 11-131, 1977. See also Computers and Structures, Vol. 4, pp. 399-435, 1974, AIAA J, Vol. 9, No. 10, pp. 2004-2013, 1971, and Pergamon Press Software Guide, 1986

[3] Vanderplaats, G. N., "CONMIN–a FORTRAN program for constrained funcion minimization," NASA TM X 62-282, version updated in March, 1975, Ames Research Center, Moffett Field, CA (Aug.1973) See also, Vanderplaats, G. N. and Moses, F., "Structural optimization by methods of feasible directions," Computers and Structures, Vol. 3, pp 739-755, 1973

[4] Koiter, W. T., "Het Schuifplooiveld by Grote Overshrijdingen van de Knikspanning," Nationaal Luchtvaart Laboratorium, Report X295, November 1946 (in Dutch)

[5] Starnes, J. H.,Jr., Knight, N. F.,Jr., and Rouse, M., "Postbuckling behavior of selected flat stiffened graphite- epoxy panels loaded in compression," AIAA Paper 82-0777, presented at AIAA 23rd Structures, Structural Dynamics, and Materials Conference, New Orleans, May, 1982. See also, AIAA J., Vol. 23, No. 8, pp.1236-1246, (Aug. 1985)

[6] Leissa, A. W., "Buckling of laminated composite plates and shell panels," AFWAL-TR-85-3069, Air Force Wright Aeronautical Laboratories, Wright-Patterson AFB, Ohio 45433, June, 1985

[7] Chamis, C.C., "Buckling of anisotropic composite plates," Proc. ASCE, Journal of the Structural Division, Vol. 95 (ST 10), pp. 2119-2139 (1969). Also see Chamis, C.C., "Buckling of Anisotropic Plates, Closure and Errata," Proc. ASCE, Journal of the Structural Division, Vol. 97, pp. 960-962 (1971)

[8] Bushnell, D., "Panel optimization with integrated software (POIS), Panda–Interactive program for preliminary minimum weight design," AFWAL-TR-81-3073, vol. 1, Air Force Wright Aeronautical Laboratories, Wright-Patterson AFB, Ohio 45433, July 1981

[9] Anderson, M. S. and Stroud, W. J., "General panel sizing computer code and its application to composite structural panels," AIAA Journal, Vol. 17, No. 8, pp. 892-897 (1979)

[10] Stroud, W. J. and Anderson, M. S., "PASCO: Structural panel analysis and sizing code, capability and analytical foundations," NASA TM-80181 (1981)

[11] Ambartsumyan, S. A., THEORY OF ANISOTROPIC PLATES, Technomic Publishing Co., Stamford, CT (1970)

[12] Whitney, J. M., "The effect of transverse shear deformation on the bending of laminated plates," Journal of Composite Materials, Vol. 3, pp. 534-547 (1969)

[13] Vinson, J. and Smith, A. P. Jr., "The effect of transverse shear deformation on the elastic stability of plates of composite materials," AFOSR TR-75-1628, March 1975

[14] Brunelle, E. J. and Oyibo, G. A., "Generic buckling curves for specially orthotropic rectangular plates," AIAA J., Aug. 1983

[15] Stroud, W. J., Greene, W. H., and Anderson, M. S., "Buckling loads of stiffened panels subjected to combined longitudinal compression and shear: Results obtained with PASCO, EAL, and STAGS computer programs," NASA TP 2215, Nasa Langley Research Center, January 1984

[16] Whetstone, W. D., "EISI-EAL, Engineering Analysis Language," Proceedings of the Second Conference on Computing in Civil Engineering, ASCE, pp. 276-285 (1980)

[17] Almroth, B. O. and Brogan, F. A., "The STAGS Computer Code", NASA CR-2950, Nasa Langley Research Center, (1978)

[18] Bushnell, D., Holmes, A. M. C., Flaggs, D., and McCormick, P. "Fabrication and Test of Large Stiffened Graphite-Epoxy Curved Panels in Axial Compression,"

[19] Rankin, C. C., Stehlin, P. and Brogan, F. A., "Enhancements to the STAGS computer code", Lockheed Missiles and Space Co., Inc., Palo Alto, CA., LMSC-D060755, November 1985

[20] Thurston, G. A., Brogan, F. A., and Stehlin, P., "Postbuckling analysis using a general purpose code", AIAA Paper No. 85-0719-CP, AIAA 26th Structures, Structural Dynamics, and Materials Conference, Orlando, Florida, April 15-17, 1985

[21] Boitnott, R. L., Johnson, E. R., and Starnes, J. H.,Jr., "A nonlinear analysis of infinitely long graphite-epoxy cylindrical panels loaded with internal pressure", AIAA 26th Structures, Structural Dynamics, and Materials Conference, Orlando, Florida, April 15-17, 1985

[22] Dickson, J. N., Cole, R. T., and Wang, J. T. S., "Design of stiffened composite panels in the post-buckling range," FIBROUS COMPOSITES IN STRUCTURAL DESIGN, edited by E. M. Lenoe, D. W. Oplinger, and J. J. Burke, Plenum Press, New York, pp 313-327 (1980)

[23] Dickson, J. N., Biggers, S. B., and Wang, J. T. S., "Preliminary design procedure for composite panels with open-section stiffeners loaded in the post-buckling range," ADVANCES IN COMPOSITE MATERIALS, edited by A. R. Bunsell, et al, Pergamon Press Ltd., Oxford, England, pp 812-825 (1980)

[24] Dickson, J. N. and Biggers, S. B., "POSTOP: Postbuckled open- stiffened optimum panels, theory and capability", NASA Langley Research Center, NASA Contractor Report from NASA Contract NAS1 - 15949, May 1982

[25] van der Neut, A., "The interaction of local buckling and column failure of thin-walled comporession members", Proceedings of the Twelfth International Congress of

Applied MEchanics, edited by M. Hetenyi and W. G. Vincenti, Springer, Berlin, pp 389-399 (1969)

[26] Thompson, J. M. T., Tulk, J. D. and Walker, A. C., "An experimental study of imperfection-sensitivity in the interactive buckling of stiffened plates", BUCKLING OF STRUCTURES, edited by B. Budiansky, Springer-Verlag, pp 149-159 (1976)

[27] Tvergaard, V., "Influence of post-buckling behavior on optimum design of stiffened panels", International Journal of Solids and Structures, Vol. 9, pp 1519-1534 (1973)

[28] Byskov, E. and Hutchinson, J. W., "Mode interaction in axially stiffened cylindrical shells", AIAA J., Vol. 15, No. 7, pp 941-948 (1977)

[29] Koiter, W. T. and Pignataro, M., "An alternative approach to the interaction between local and overall buckling in stiffened panels", BUCKLING OF STRUCTURES, edited by B. Budiansky, Springer-Verlag, pp 133-148 (1976)

[30] Bushnell, D. COMPUTERIZED BUCKLING ANALYSIS OF SHELLS , Nijhoff, The Netherlands, (1985)

[31] Blaas, C. and Wiggenraad, J. F. M., "Development and test verification of the ARIANE 4 interstage 2/3 in CFRP", Proceedings of the AIAA/ASME 27th Structures, Structural Dynamics and Materials Conference, Part 1, pp. 307–313, May, 1986

Table 1 BUCKLING LOAD FACTORS Ncr FOR SIMPLY SUPPORTED PLATES

Matl Props:Orthotropic: E11, E12, G = 32.9, 1.8, 0.88 x 10**6 psi
large nu = 0.24; fibers along E11
Isotropic: E = 10.0 x 10**6 psi, nu = 0.3
Plate thickness, t = 0.096 in.; B.C.s: all edges simply supported

Plate Dim. X x Y (in.)	Loading Combination Nx	Ny (lb/in)	Nxy	Orthotropic Fibers along x PANDA2	Chamis	Fibers along y PANDA2	Chamis	Isotropic PANDA2	Chamis
5x10	-1	0	0	996	998	145	145	499	500
"	0	-1	0	578	581	576	581	1278	1279
"	-1	-1	0	463	465	116	116	400	400
"	-1	0	1	949	948	132	114	466	479
"	0	-1	1	532	619	300	395	940	998
"	-1	-1	1	437	446	109	113	383	389
"	-.001	0	1	1949	2185	487	700	1858	2104
10x10	-1	0	0	285	286	145	145	320	320
"	0	-1	0	145	145	285	286	320	320
"	-1	-1	0	116	116	116	116	160	160
"	-1	0	1	239	246	133	136	214	277
"	0	-1	1	133	136	239	246	235	277
"	-1	-1	1	109	111	109	136	140	153
"	-.001	0	1	487	531	487	531	464	752
"	-1	-0.75	0	145	145	122	122	183	183
"	-1	-0.50	0	190	191	129	129	213	213
"	-1	-0.25	0	228	229	136	137	256	256
"	-1	+0.25	Q	378	381	154	155	427	426
"	-1	+0.50	0	570	572	165	166	571	571
"	-1	+1.00	0	1328	1330	193	194	666	666
"	-1	-0.50	0.25	189	190	128	129	209	212
"	-1	+0.50	0.25	532	549	164	165	482	562
"	-1	-0.50	0.50	190	187	126	127	199	209
"	-1	+0.50	0.50	470	496	161	163	384	539
20x10	-1	0	0	144	145	145	145	320	320
"	0	-1	0	36.4	36	249	249	125	125
"	-1	-1	0	29.1	29	116	116	100	100
"	-1	0	1	74.9	99	133	155	235	250
"	0	-1	1	33.6	35	237	237	117	120
"	-1	-1	1	27.4	28	109	111	96	97
"	-.001	0	1	122	175	487	491	464	528

Table 2   BUCKLING LOAD FACTORS (Nx*pi2/G13*h)**
FOR SIMPLY SUPPORTED, ORTHOTROPIC PLATES

Material Properties:
  E1, E2, G12, G13, G23 = 32.5, 1.84, 0.642, 0.642, 0.361 x 10**6 psi
           large nu = 0.256
  Geometry: Axial length a;   Width b;   Thickness h;   h/a = 0.1

Plate Aspect Ratio a/b	Classical Plate Theory		Including Transverse Shear Deformation	
	PANDA2	REF. [13]	PANDA2	REF. [13]
0.33	4.18	4.15	2.77	2.76
0.50	4.25	4.22	2.80	2.80
1.00	4.80	4.78	3.03	3.32
1.50	6.27	6.28	3.56	4.95
2.00	9.56	9.60	4.41	9.20

Table 3   BUCKLING LOAD FACTORS ko FOR ORTHOTROPIC PLATES
SUBJECTED TO PURE IN-PLANE BENDING

Stiffness Ratio, D	Buckling Load Factor ko	
	PANDA2	REF. [14]
0.0	12.11	12.87
0.4	15.89	17.39
1.0	23.68	23.90

TABLE 4 (2 pages)

PROCEDURE FOR DESIGNING A STIFFENED SHELL WITH PANDA2
===
TASK	EXAMPLE

1. Decide what part of a structure to optimize.

ARIANE4 2/3 interstage (Fig. 78).

2. Decide how to model the part.

Entire cylindrical shell with spatially varying loads is modeled as a 40-inch-wide panel with multiple sets of uniform loads (Fig. 79).

3. Decide what load sets to use.

Load sets are shown in Fig. 79:
  3.1. Uniform axial compression of 3000 lb/in.
  3.2. Uniform axial compression of 1000 lb/in. combined with uniform in-plane shear of 1000 lb/in.
  3.3. Uniform axial tension of 2000 lb/in.

4. Decide what design concept to use.

Concept is shown in Fig. 80:
  4.1. Graphite-epoxy (GR/EP), external, T-shaped, stringers.
  4.2. Aluminum, internal, rectangular rings spaced 26.75 inches apart.
  4.3. Balanced laminates throughout.
  4.4. 45-degree, GR/EP "isotropic" cloth outer layers (layer type 1 in Fig. 80).
  4.5. Web of stringer formed by extension of top cloth layer.
  4.6. In addition to the outer cloth layers, default group of 12 GR/EP tape layers for panel skin: [90/45/0/-45/0/90]s
  4.7. 3-layer insert [0(m2)/90/0(m2)] within stringer base.
  4.8. 3-layer insert [0(m4)/90/0(m4)] within stringer flange.

5. Choose starting design and material properties

Starting design and material properties are listed in Table 5, which represents input for the BEGIN processor.

Table 4 (continued and concluded)

6. Choose decision, linked, escape variables, and lower and upper bounds of decision variables.

Decision variables, linked variables, escape variables and lower and upper bounds of decision variables are listed in Table 7. Table 6 represents input for the DECIDE processor.

7. Decide what optimization strategy to use, and whether or not to permit local buckling. Choose factors of safety.

Sequence of optimization runs:

7.1. Several runs with IQUICK=1 in order to get approximate approximate design quickly. (Figs. 84-89). Factor of safety for general and panel buckling = 2.0 for Load Set 1 (pure axial compression); F.S. = 1.5 for general and panel buckling for Load Set 2 (combined axial compression and in-plane shear). All other F.S.'s = 1.0.

7.2. Several runs with IQUICK=0 and with KOITER=1 (local buckling allowed). Factors of safety for general and panel buckling that were 2.0 and 1.5 in the IQUICK=1 runs are reduced to 1.5 and 1.2, respectively (Figs. 84-90).

7.3. Several runs with IQUICK=0 and with KOITER=0 (no local buckling permitted). Factors of safety remain as in 2 (Figs. 92-95).

8. Evaluate final design by running PANEL followed by BOSOR4LOG and BOSORALL.

Results from the KOITER = 1 design are shown in Fig. 91. Results from KOITER = 0 design are shown in Fig. 96.

===

129

TABLE 5 (6 pages)
INPUT DATA FOR STARTING DESIGN
OF ARIANE4 2/3 INTERSTAGE
This file is called ARIANE.BEG

```
N                 $ Do you want a tutorial session and tutorial output?
        107       $ Panel length normal to the plane of the screen, L1
         40       $ Panel length in the plane of the screen, L2
T                 $ Identify type of stiffener along L1    (N, T, J, R, A)
          5       $ stiffener spacing, b
          1       $ width of stiffener base, b2 (must be > 0, see Help)
          1       $ height of stiffener (type H to see sketch), h
          1       $ width of outer flange of stiffener, w
N                 $ Are the stringers cocured with the skin?
        100       $ What force/(axial length) will cause web peel-off?
N                 $ Is the next group of layers to be a "default group"?
          1       $ number of layers in the next group in Segment no.( 1)
N                 $ Can winding (layup) angles ever be decision variables?
          1       $ layer index (1,2,...), for layer no.( 1)
Y                 $ Is this a new layer type?
0.1200000E-01     $ thickness for layer index no.( 1)
         45       $ winding angle (deg.) for layer index no.( 1)
          3       $ material index (1,2,...) for layer index no.( 1)
Y                 $ Any more layers or groups of layers in Segment no.( 1)
Y                 $ Is the next group of layers to be a "default group"?
N                 $ Is this default group identical to a previous group?
0.5200000E-02     $ thickness of each layer of the default group
          1       $ material type in the default group
Y                 $ Any more layers or groups of layers in Segment no.( 1)
N                 $ Is the next group of layers to be a "default group"?
          1       $ number of layers in the next group in Segment no.( 1)
N                 $ Can winding (layup) angles ever be decision variables?
          1       $ layer index (1,2,...), for layer no.(14)
N                 $ Is this a new layer type?
N                 $ Any more layers or groups of layers in Segment no.( 1)
N                 $ Is the next group of layers to be a "default group"?
          7       $ number of layers in the next group in Segment no.( 2)
N                 $ Can winding (layup) angles ever be decision variables?
          1       $ layer index (1,2,...), for layer no.( 1)
N                 $ Is this a new layer type?
          2       $ layer index (1,2,...), for layer no.( 2)
N                 $ Is this a new layer type?
          3       $ layer index (1,2,...), for layer no.( 3)
N                 $ Is this a new layer type?
          4       $ layer index (1,2,...), for layer no.( 4)
N                 $ Is this a new layer type?
          5       $ layer index (1,2,...), for layer no.( 5)
N                 $ Is this a new layer type?
```

```
          6         $ layer index (1,2,...), for layer no.( 6)
     N              $ Is this a new layer type?
          7         $ layer index (1,2,...), for layer no.( 7)
     N              $ Is this a new layer type?
     Y              $ Any more layers or groups of layers in Segment no.( 2)
     N              $ Is the next group of layers to be a "default group"?
          3         $ number of layers in the next group in Segment no.( 2)
     N              $ Can winding (layup) angles ever be decision variables?
          8         $ layer index (1,2,...), for layer no.( 8)
     Y              $ Is this a new layer type?
 0.1040000E-01      $ thickness for layer index no.( 8)
          0         $ winding angle (deg.) for layer index no.( 8)
          1         $ material index (1,2,...) for layer index no.( 8)
          9         $ layer index (1,2,...), for layer no.( 9)
     Y              $ Is this a new layer type?
 0.5200000E-02      $ thickness for layer index no.( 9)
         90         $ winding angle (deg.) for layer index no.( 9)
          1         $ material index (1,2,...) for layer index no.( 9)
          8         $ layer index (1,2,...), for layer no.(10)
     N              $ Is this a new layer type?
     Y              $ Any more layers or groups of layers in Segment no.( 2)
     N              $ Is the next group of layers to be a "default group"?
          7         $ number of layers in the next group in Segment no.( 2)
     N              $ Can winding (layup) angles ever be decision variables?
          7         $ layer index (1,2,...), for layer no.(11)
     N              $ Is this a new layer type?
          6         $ layer index (1,2,...), for layer no.(12)
     N              $ Is this a new layer type?
          5         $ layer index (1,2,...), for layer no.(13)
     N              $ Is this a new layer type?
          4         $ layer index (1,2,...), for layer no.(14)
     N              $ Is this a new layer type?
          3         $ layer index (1,2,...), for layer no.(15)
     N              $ Is this a new layer type?
          2         $ layer index (1,2,...), for layer no.(16)
     N              $ Is this a new layer type?
          1         $ layer index (1,2,...), for layer no.(17)
     N              $ Is this a new layer type?
     N              $ Any more layers or groups of layers in Segment no.( 2)
     N              $ Is the next group of layers to be a "default group"?
          2         $ number of layers in the next group in Segment no.( 3)
     N              $ Can winding (layup) angles ever be decision variables?
          1         $ layer index (1,2,...), for layer no.( 1)
     N              $ Is this a new layer type?
          1         $ layer index (1,2,...), for layer no.( 2)
     N              $ Is this a new layer type?
     N              $ Any more layers or groups of layers in Segment no.( 3)
     N              $ Is the next group of layers to be a "default group"?
```

131

Table 5, p3

```
        1           $ number of layers in the next group in Segment no.( 4)
        N           $ Can winding (layup) angles ever be decision variables?
        1           $ layer index (1,2,...), for layer no.( 1)
        N           $ Is this a new layer type?
        Y           $ Any more layers or groups of layers in Segment no.( 4)
        N           $ Is the next group of layers to be a "default group"?
        3           $ number of layers in the next group in Segment no.( 4)
        N           $ Can winding (layup) angles ever be decision variables?
       10           $ layer index (1,2,...), for layer no.( 2)
        Y           $ Is this a new layer type?
 0.1040000E-01      $ thickness for layer index no.(10)
        0           $ winding angle (deg.) for layer index no.(10)
        1           $ material index (1,2,...) for layer index no.(10)
        9           $ layer index (1,2,...), for layer no.( 3)
        N           $ Is this a new layer type?
       10           $ layer index (1,2,...), for layer no.( 4)
        N           $ Is this a new layer type?
        Y           $ Any more layers or groups of layers in Segment no.( 4)
        N           $ Is the next group of layers to be a "default group"?
        1           $ number of layers in the next group in Segment no.( 4)
        N           $ Can winding (layup) angles ever be decision variables?
        1           $ layer index (1,2,...), for layer no.( 5)
        N           $ Is this a new layer type?
        N           $ Any more layers or groups of layers in Segment no.( 4)
        0           $ choose external (0) or internal (1) stringers
        R           $ Identify type of stiffener along L2  (N, T, J, R, A)
 26.75000           $ stiffener spacing, b
        1           $ width of stiffener base, b2 (must be > 0, see Help)
        1           $ height of stiffener (type H to see sketch), h
        N           $ Are the rings cocured with the skin?
        N           $ Is the next group of layers to be a "default group"?
        7           $ number of layers in the next group in Segment no.( 2)
        N           $ Can winding (layup) angles ever be decision variables?
        1           $ layer index (1,2,...), for layer no.( 1)
        N           $ Is this a new layer type?
       11           $ layer index (1,2,...), for layer no.( 2)
        Y           $ Is this a new layer type?
 0.5200000E-02      $ thickness for layer index no.(11)
        0           $ winding angle (deg.) for layer index no.(11)
        1           $ material index (1,2,...) for layer index no.(11)
        5           $ layer index (1,2,...), for layer no.( 3)
        N           $ Is this a new layer type?
       12           $ layer index (1,2,...), for layer no.( 4)
        Y           $ Is this a new layer type?
 0.5200000E-02      $ thickness for layer index no.(12)
       90           $ winding angle (deg.) for layer index no.(12)
        1           $ material index (1,2,...) for layer index no.(12)
        3           $ layer index (1,2,...), for layer no.( 5)
```

132

```
        N              $ Is this a new layer type?
           13          $ layer index (1,2,...), for layer no.( 6)
        Y              $ Is this a new layer type?
0.5200000E-02          $ thickness for layer index no.(13)
           90          $ winding angle (deg.) for layer index no.(13)
            1          $ material index (1,2,...) for layer index no.(13)
           14          $ layer index (1,2,...), for layer no.( 7)
        Y              $ Is this a new layer type?
0.5200000E-02          $ thickness for layer index no.(14)
            0          $ winding angle (deg.) for layer index no.(14)
            1          $ material index (1,2,...) for layer index no.(14)
        Y              $ Any more layers or groups of layers in Segment no.( 2)
        N              $ Is the next group of layers to be a "default group"?
            7          $ number of layers in the next group in Segment no.( 2)
        N              $ Can winding (layup) angles ever be decision variables?
           14          $ layer index (1,2,...), for layer no.( 8)
        N              $ Is this a new layer type?
           13          $ layer index (1,2,...), for layer no.( 9)
        N              $ Is this a new layer type?
            3          $ layer index (1,2,...), for layer no.(10)
        N              $ Is this a new layer type?
           12          $ layer index (1,2,...), for layer no.(11)
        N              $ Is this a new layer type?
            5          $ layer index (1,2,...), for layer no.(12)
        N              $ Is this a new layer type?
           11          $ layer index (1,2,...), for layer no.(13)
        N              $ Is this a new layer type?
            1          $ layer index (1,2,...), for layer no.(14)
        N              $ Is this a new layer type?
        Y              $ Any more layers or groups of layers in Segment no.( 2)
        N              $ Is the next group of layers to be a "default group"?
            1          $ number of layers in the next group in Segment no.( 2)
        N              $ Can winding (layup) angles ever be decision variables?
           15          $ layer index (1,2,...), for layer no.(15)
        Y              $ Is this a new layer type?
    0.1000000          $ thickness for layer index no.(15)
            0          $ winding angle (deg.) for layer index no.(15)
            2          $ material index (1,2,...) for layer index no.(15)
        N              $ Any more layers or groups of layers in Segment no.( 2)
        N              $ Is the next group of layers to be a "default group"?
            1          $ number of layers in the next group in Segment no.( 3)
        N              $ Can winding (layup) angles ever be decision variables?
           15          $ layer index (1,2,...), for layer no.( 1)
        N              $ Is this a new layer type?
        N              $ Any more layers or groups of layers in Segment no.( 3)
            1          $ choose external (0) or internal (1) rings
        Y              $ Is the panel curved in the plane of the screen (Y for cyls.)?
           51          $ Radius of curvature (cyl. rad.) in the plane of screen, R
```

```
      N            $ Is panel curved normal to plane of screen? (answer N)
      N            $ Is this material isotropic (Y or N)?
0.2000000E+08 $ modulus in the fiber direction, E1( 1)
 1400000.      $ modulus transverse to fibers,    E2( 1)
 700000.0      $ in-plane shear modulus,          G( 1)
0.2030000E-01 $ small Poisson's ratio,           NU( 1)
 700000.0      $ out-of-plane shear modulus,      G13( 1)
 400000.0      $ out-of-plane shear modulus,      G23( 1)
0.5000000E-07 $ thermal expansion along fibers, A1( 1)
0.1600000E-04 $ transverse thermal expansion,    A2( 1)
 270.0000      $ residual stress temperature (positive),TEMPTUR( 1)
      N            $ Want to specify  maximum effective stress (N)?
 190000.0      $ maximum tensile stress along fibers, matl( 1)
 182800        $ max compressive stress along fibers, matl( 1)
 9800          $ max tensile stress normal to fibers, matl( 1)
 25060         $ max compress stress normal to fibers,matl( 1)
 10000         $ maximum  shear  stress  in  material type( 1)
0.5600000E-01 $ weight density (greater than 0!) of material type( 1)
      Y            $ Is this unidirectional composite material (tape) ?
0.5200000E-02 $ Thickness of a single lamina of matl type( 1)
      Y            $ Does max. allowable stress decrease for more layers?
         0       $ Degradation (%) in max. sig1(tension) for n layers, n=( 2)
         0       $ Degradation (%) in max. sig1(comp.)   for n layers, n=( 2)
        20       $ Degradation (%) in max. sig2(tension) for n layers, n=( 2)
         0       $ Degradation (%) in max. sig2(comp.)   for n layers, n=( 2)
         0       $ Degradation (%) in max. sig12         for n layers, n=( 2)
      Y            $ Any further degradation with more layers of matl type( 1)
         0       $ Degradation (%) in max. sig1(tension) for n layers, n=( 3)
         0       $ Degradation (%) in max. sig1(comp.)   for n layers, n=( 3)
        30       $ Degradation (%) in max. sig2(tension) for n layers, n=( 3)
         0       $ Degradation (%) in max. sig2(comp.)   for n layers, n=( 3)
         0       $ Degradation (%) in max. sig12         for n layers, n=( 3)
      Y            $ Any further degradation with more layers of matl type( 1)
         0       $ Degradation (%) in max. sig1(tension) for n layers, n=( 4)
         0       $ Degradation (%) in max. sig1(comp.)   for n layers, n=( 4)
        37       $ Degradation (%) in max. sig2(tension) for n layers, n=( 4)
         0       $ Degradation (%) in max. sig2(comp.)   for n layers, n=( 4)
         0       $ Degradation (%) in max. sig12         for n layers, n=( 4)
      N            $ Any further degradation with more layers of matl type( 1)
      Y            $ Is this material isotropic (Y or N)?
0.1000000E+08 $ Young's modulus,                  E( 2)
0.3200000      $ small Poisson's ratio,           NU( 2)
 3846000.      $ transverse shear modulus,        G13( 2)
         0       $ Thermal expansion coeff.,        ALPHA( 2)
         0       $ residual stress temperature (positive),TEMPTUR( 2)
      N            $ Want to supply a stress-strain "curve" for this mat'l? (N)
      Y            $ Want to specify  maximum effective stress (N)?
 50000.00      $ Maximum allowable effective stress in material type( 2)
```

```
0.1000000        $ weight density (greater than 0!) of material type( 2)
   N             $ Is this unidirectional composite material (tape) ?
   N             $ Is this material isotropic (Y or N)?
0.1050000E+08    $ modulus in the fiber direction, E1( 3)
0.1050000E+08    $ modulus transverse to fibers,   E2( 3)
 700000.0        $ in-plane shear modulus,          G( 3)
0.7700000E-01    $ small Poisson's ratio,          NU( 3)
 700000.0        $ out-of-plane shear modulus,     G13( 3)
 400000.0        $ out-of-plane shear modulus,     G23( 3)
0.1500000E-05    $ thermal expansion along fibers, A1( 3)
0.1500000E-05    $ transverse thermal expansion,   A2( 3)
 270.0000        $ residual stress temperature (positive),TEMPTUR( 3)
   N             $ Want to specify  maximum effective stress (N)?
   91035         $ maximum tensile stress along fibers, matl( 3)
  103845         $ max compressive stress along fibers, matl( 3)
   89880         $ max tensile stress normal to fibers, matl( 3)
  105000         $ max compress stress normal to fibers,matl( 3)
    7000         $ maximum  shear  stress  in  material type( 3)
0.5600000E-01    $ weight density (greater than 0!) of material type( 3)
   N             $ Is this unidirectional composite material (tape) ?
       0         $ Choose 0=simple support or 1=clamping
```

TABLE 6
INPUT DATA FOR SELECTION OF
DECISION, LINKED, AND ESCAPE VARIABLES
FOR MINIMUM WEIGHT DESIGN OF ARIANE4 2/3 INTERSTAGE
This file is called ARIANE.DEC

```
N           $ Do you want a tutorial session and tutorial output?
Y           $ Want to use default for thickness decision variables?
      1     $ Lowest layer index for default decision variable
      8     $ Highest layer index for default decision variable
Y           $ Any more ranges of layer types for default dec. var.?
     10     $ Lowest layer index for default decision variable
     10     $ Highest layer index for default decision variable
N           $ Any more ranges of layer types for default dec. var.?
Y           $ Any more decision variables (Y or N) ?
      1     $ Choose a decision variable (1,2,3,...)
2.500000    $ Lower bound of variable no.( 1)
     10     $ Upper bound of variable no.( 1)
Y           $ Any more decision variables (Y or N) ?
      2     $ Choose a decision variable (1,2,3,...)
0.5000000   $ Lower bound of variable no.( 2)
      3     $ Upper bound of variable no.( 2)
Y           $ Any more decision variables (Y or N) ?
      3     $ Choose a decision variable (1,2,3,...)
0.2000000   $ Lower bound of variable no.( 3)
      2     $ Upper bound of variable no.( 3)
Y           $ Any more decision variables (Y or N) ?
      4     $ Choose a decision variable (1,2,3,...)
0.1000000   $ Lower bound of variable no.( 4)
      2     $ Upper bound of variable no.( 4)
Y           $ Any more decision variables (Y or N) ?
     17     $ Choose a decision variable (1,2,3,...)
      1     $ Lower bound of variable no.(17)
      2     $ Upper bound of variable no.(17)
N           $ Any more decision variables (Y or N) ?
Y           $ Any linked variables (Y or N) ?
     18     $ Choose a linked variable (1,2,3,...)
      6     $ To which variable is this variable linked?
      1     $ Assign a value to the linking constant, C(18)
Y           $ Any more linked variables (Y or N) ?
     19     $ Choose a linked variable (1,2,3,...)
      8     $ To which variable is this variable linked?
      1     $ Assign a value to the linking constant, C(19)
Y           $ Any more linked variables (Y or N) ?
     20     $ Choose a linked variable (1,2,3,...)
     10     $ To which variable is this variable linked?
      1     $ Assign a value to the linking constant, C(20)
Y           $ Any more linked variables (Y or N) ?
     21     $ Choose a linked variable (1,2,3,...)
     11     $ To which variable is this variable linked?
      1     $ Assign a value to the linking constant, C(21)
N           $ Any more linked variables (Y or N) ?
Y           $ Any escape variables (Y or N) ?
Y           $ Want to have escape variables chosen by default?
```

136

TABLE 7

PART OF OUTPUT FROM THE PROCESSOR "DECIDE"

DECISION, LINKED, AND ESCAPE VARIABLES

FOR MINIMUM WEIGHT DESIGN OF ARIANE4 2/3 INTERSTAGE

This list is part of the file called ARIANE.OPD

SUMMARY OF INFORMATION FOR OPTIMIZATION ANALYSIS

VAR. NO.	DEC. VAR.	ESCAPE VAR.	LINK. VAR.	LINKED TO	LINKING CONSTANT	LOWER BOUND	CURRENT VALUE	UPPER BOUND	DEFINITION
1	Y	N	N	0	0.00E+00	2.50E+00	5.0000E+00	1.00E+01	stiffener spacing, b
2	Y	N	N	0	0.00E+00	5.00E-01	1.0000E+00	2.00E+00	width of stiffener base, b2
3	Y	N	N	0	0.00E+00	2.00E-01	1.0000E+00	2.00E+00	height of stiffener, h
4	Y	N	N	0	0.00E+00	1.00E-01	1.0000E+00	2.00E+00	width of outer flange of stiffener, w
5	Y	Y	N	0	0.00E+00	1.20E-04	1.2000E-02	1.20E+00	thickness for layer index no. (1)
6	Y	Y	N	0	0.00E+00	5.20E-05	5.2000E-03	5.20E-01	thickness for layer index no. (2)
7	Y	Y	N	0	0.00E+00	5.20E-05	5.2000E-03	5.20E-01	thickness for layer index no. (3)
8	Y	Y	N	0	0.00E+00	5.20E-05	5.2000E-03	5.20E-01	thickness for layer index no. (4)
9	N	Y	Y	7	1.00E+00	0.00E+00	5.2000E-03	0.00E+00	thickness for layer index no. (5)
10	Y	Y	N	0	0.00E+00	5.20E-05	5.2000E-03	5.20E-01	thickness for layer index no. (6)
11	Y	Y	N	0	0.00E+00	5.20E-05	5.2000E-03	5.20E-01	thickness for layer index no. (7)
12	Y	Y	N	0	0.00E+00	1.04E-04	1.0400E-02	1.04E+00	thickness for layer index no. (8)
13	N	Y	N	0	0.00E+00	0.00E+00	5.2000E-03	0.00E+00	thickness for layer index no. (9)
14	Y	Y	N	0	0.00E+00	1.04E-04	1.0400E-02	1.04E+00	thickness for layer index no. (10)
15	N	N	N	0	0.00E+00	0.00E+00	2.6750E+01	0.00E+00	stiffener spacing, b
16	N	N	N	0	0.00E+00	0.00E+00	1.0000E+00	0.00E+00	width of stiffener base, b2
17	Y	N	N	0	0.00E+00	1.00E+00	1.0000E+00	2.00E+00	height of stiffener, h
18	N	N	Y	6	1.00E+00	0.00E+00	5.2000E-03	0.00E+00	thickness for layer index no. (11)
19	N	N	Y	8	1.00E+00	0.00E+00	5.2000E-03	0.00E+00	thickness for layer index no. (12)
20	N	N	Y	10	1.00E+00	0.00E+00	5.2000E-03	0.00E+00	thickness for layer index no. (13)
21	N	N	Y	11	1.00E+00	0.00E+00	5.2000E-03	0.00E+00	thickness for layer index no. (14)
22	N	N	N	0	0.00E+00	0.00E+00	1.0000E-01	0.00E+00	thickness for layer index no. (15)

TABLE 8
INPUT DATA FOR PANDA2 PROCESSOR "MAINSETUP"
FOR OPTIMIZATION OF ARIANE4 2/3 INTERSTAGE
There are two load sets, and IQUICK=1
This file is called ARIANE.OPT

```
N              $ Do you want a tutorial session and tutorial output?
-3000          $ Resultant normal to the plane of screen, N1( 1)
    0          $ Resultant in the plane of the screen,    N2( 1)
    0          $ In-plane shear in load set A,            N12( 1)
N              $ Does the axial load vary in the L2 direction?
    2.0        $ Factor of safety for general instability, FSGEN( 1)
    1          $ Factor of safety for local instability, FSLOC( 1)
    0          $ Resultant normal to the plane of screen, N10( 1)
    0          $ Resultant in the plane of the screen,    N20( 1)
    0          $ Uniform applied pressure (positive upward), p( 1)
Y              $ Want to provide another load set (N1,N2,N12,N10,N20, p)?
-1000          $ Resultant normal to the plane of screen, N1( 2)
    0          $ Resultant in the plane of the screen,    N2( 2)
 1000          $ In-plane shear in load set A,            N12( 2)
N              $ Does the axial load vary in the L2 direction?
1.500000       $ Factor of safety for general instability, FSGEN( 2)
    1          $ Factor of safety for local instability, FSLOC( 2)
    0          $ Resultant normal to the plane of screen, N10( 2)
    0          $ Resultant in the plane of the screen,    N20( 2)
    0          $ Uniform applied pressure (positive upward), p( 2)
N              $ Want to provide another load set (N1,N2,N12,N10,N20, p)?
Y              $ Want to include effect of transverse shear deformation?
    1          $ IQUICK = quick analysis indicator (0 or 1)
    1          $ NPRINT= output index (1=good, 2=debug, 3=too much)
    1          $ Choose type of analysis (1=opt., 2=fixed design)
    5          $ How many design iterations in this run (3 to 10)?
    1          $ Index for objective (1=min. weight, 2=min. distortion)
```

Table 9   FINAL DESIGN OF ARIANE 4 2/3-INTERSTAGE WITH T-SHAPED STRINGERS
           IN WHICH LOCAL POST-BUCKLING IS PERMITTED

SUMMARY OF INFORMATION FROM OPTIMIZATION ANALYSIS

VAR. NO.	DEC. VAR.	ESCAPE VAR.	LINK. VAR.	LINKED TO	LINKING CONSTANT	LOWER BOUND	CURRENT VALUE	UPPER BOUND	DEFINITION
1	Y	N	N	0	0.00E+00	2.50E+00	4.5539E+00	5.00E+00	stiffener spacing, b
2	Y	N	N	0	0.00E+00	3.00E-01	2.3235E+00	3.00E+00	width of stringer base, b2
3	Y	N	N	0	0.00E+00	5.00E-01	1.1855E+00	2.00E+00	height of stringer, h
4	Y	N	N	0	0.00E+00	2.00E-01	1.4022E+00	2.00E+00	width of outer flange of stiffener, w
5	N	N	N	0	0.00E+00	0.00E+00	1.8000E-02	0.00E+00	thickness for layer index no.(1)
6	N	N	N	0	0.00E+00	0.00E+00	0.0000E+00	0.00E+00	thickness for layer index no.(2)
7	N	N	N	0	0.00E+00	0.00E+00	0.0000E+00	0.00E+00	thickness for layer index no.(3)
8	N	N	N	0	0.00E+00	0.00E+00	0.0000E+00	0.00E+00	thickness for layer index no.(4)
9	N	N	N	0	0.00E+00	0.00E+00	0.0000E+00	0.00E+00	thickness for layer index no.(5)
10	N	N	N	0	0.00E+00	0.00E+00	5.2000E-03	0.00E+00	thickness for layer index no.(6)
11	N	N	N	0	0.00E+00	0.00E+00	0.0000E+00	0.00E+00	thickness for layer index no.(7)
12	N	N	N	0	0.00E+00	0.00E+00	4.1600E-02	0.00E+00	thickness for layer index no.(8)
13	N	N	N	0	0.00E+00	0.00E+00	5.2000E-03	0.00E+00	thickness for layer index no.(9)
14	Y	Y	N	0	0.00E+00	2.08E-02	2.2954E-02	2.60E-02	thickness for layer index no.(10)
15	N	N	N	0	0.00E+00	0.00E+00	2.6750E+01	0.00E+00	stiffener spacing, b
16	N	N	N	0	0.00E+00	0.00E+00	1.0000E+00	0.00E+00	width of ring base, b2
17	N	N	N	0	0.00E+00	0.00E+00	1.0000E+00	0.00E+00	height of ring, h
18	N	N	N	0	0.00E+00	0.00E+00	0.0000E+00	0.00E+00	thickness for layer index no.(11)
19	N	N	N	0	0.00E+00	0.00E+00	0.0000E+00	0.00E+00	thickness for layer index no.(12)
20	N	N	N	0	0.00E+00	0.00E+00	5.2000E-03	0.00E+00	thickness for layer index no.(13)
21	N	N	N	0	0.00E+00	0.00E+00	0.0000E+00	0.00E+00	thickness for layer index no.(14)
22	N	N	N	0	0.00E+00	0.00E+00	1.0000E-01	0.00E+00	thickness for layer index no.(15)

****
****
*********** DESIGN OBJECTIVE ****************************
****
*********** CURRENT VALUE OF THE OBJECTIVE FUNCTION:

VAR. NO.	STR/ RNG	SEG. NO.	LAYER NO.	CURRENT VALUE	DEFINITION
0	0			3.381E+01	WEIGHT OF THE ENTIRE PANEL

****
*********** DESIGN OBJECTIVE ****************************
****
****

139

Table 10   MARGINS CORRESPONDING TO LOAD SET 1 APPLIED TO THE FINAL DESIGN
OF ARIANE 4 2/3-INTERSTAGE WITH T-SHAPED STRINGERS
IN WHICH LOCAL POST-BUCKLING IS PERMITTED

********** LOAD SET NO. 1 **********

APPLIED LOADS IN LOAD SET A ("eigenvalue" loads):
Applied axial   stress resultant, N1= -3.0000E+03
Applied circumferential stress resultant, N2= -3.0000E+00
Applied in-plane   shear resultant, N12= 1.5000E+01

APPLIED LOADS IN LOAD SET B (fixed uniform loads):
Applied axial   stress resultant, N10= 0.0000E+00
Applied circumferential stress resultant, N20= 0.0000E+00
Applied in-plane   shear resultant, N120= 0.0000E+00
Applied pressure (positive for internal), P = 0.0000E+00

CURRENT VALUES OF MARGINS CORRESPONDING TO CURRENT DESIGN

VAR. NO.	STR/RNG	SEG. NO.	LAYER NO.	CURRENT VALUE	DEFINITION
		0	0	3.722E+00	compressive fiber: (allowable stress)/actual-1, matl type 1
		0	0	1.731E+02	in-plane shear stress margin: (allowable/actual)-1, matl 1
		0	0	9.131E+00	compressive fiber: (allowable stress)/actual-1, matl type 3
		0	0	8.679E+00	compres. transverse stress margin: (allow./actual)-1, matl 3
		0	0	2.450E+00	in-plane shear stress margin: (allowable/actual)-1, matl 3
	RNG	2	1	3.680E+02	compressive transverse stress margin: (allowable/actual) - 1
	RNG	2	1	1.896E+02	compressive fiber stress margin: (allowable/actual) - 1
	RNG	2	1	2.924E+00	in-plane shear margin: (allowable stress)/(actual stress) - 1
	RNG	2	6	4.687E+00	compressive fiber stress margin: (allowable/actual) - 1
	RNG	2	6	5.338E+02	in-plane shear margin: (allowable stress)/(actual stress) - 1
	RNG	2	15	2.097E+00	compressive transverse stress margin: (allowable/actual) - 1
	RNG	2	15	1.481E+01	tensile fiber margin: (allowable stress)/(actual stress) - 1
	RNG	2	15	2.843E+02	in-plane shear margin: (allowable stress)/(actual stress) - 1
	RNG	3	1	2.070E+01	tensile fiber margin: (allowable stress)/(actual stress) - 1
	STR	3	0	4.923E+00	crippling margin for stringer segment. 22 local halfwaves
	STR	4	0	9.753E-01	crippling margin for stringer segment. 22 local halfwaves
		0	0	1.869E-02	(Wide column panel buck. factor)/(factor of safety) - 1
		0	0	2.668E-01	buck.margin simp-support smear string;M=1 ; N=9 ; slope= 0.00
		0	0	4.484E-01	buck.margin simp-support general buck;M=2 ; N=2 ; slope= 0.00
		0	0	2.641E-01	buck.margin rolling with smear string;M=1 ; N=9 ; slope= 0.00
		0	0	1.020E+00	buck.margin rolling only of stringers;M=4 ; N=0 ; slope= 0.00

Table 11   MARGINS CORRESPONDING TO LOAD SET 2 APPLIED TO THE FINAL DESIGN
            OF ARIANE 4 2/3-INTERSTAGE WITH T-SHAPED STRINGERS
            IN WHICH LOCAL POST-BUCKLING IS PERMITTED

*********** LOAD SET NO. 2 ***************

APPLIED LOADS IN LOAD SET A ("eigenvalue" loads):
    Applied   axial   stress resultant, N1= -1.0000E+03
    Applied circumferential stress resultant, N2= -1.4142E+00
    Applied   in-plane   shear resultant,N12= 1.0000E+03

APPLIED LOADS IN LOAD SET B (fixed uniform loads):
    Applied   axial   stress resultant,N10= 0.0000E+00
    Applied circumferential stress resultant,N20= 0.0000E+00
    Applied   in-plane   shear resultant,N120= 0.0000E+00
    Applied pressure (positive for internal), P = 0.0000E+00

CURRENT VALUES OF MARGINS CORRESPONDING TO CURRENT DESIGN

VAR. NO.	STR/ RNG	SEG. NO.	LAYER NO.	CURRENT VALUE	DEFINITION
	0	0	0	6.533E+00	compressive fiber: (allowable stress)/actual-1, matl type 1
	0	0	0	1.611E+00	in-plane shear stress margin: (allowable/actual)-1, matl 1
	0	0	0	2.661E+00	tensile fiber: (allowable stress)/(actual stress)-1, matl 3
	0	0	0	2.527E+01	compressive fiber: (allowable stress)/actual-1, matl type 3
	0	0	0	2.687E+00	compres. transverse stress margin: (allow./actual)-1, matl 3
	0	0	0	1.499E+01	in-plane shear stress margin: (allowable/actual)-1, matl 3
	RNG	2	1	7.448E+00	tensile transverse stress margin: (allowable/actual) - 1
	RNG	2	1	1.445E+01	compressive fiber stress margin: (allowable/actual) - 1
	RNG	2	1	1.249E+01	in-plane shear margin: (allowable stress)/(actual stress) - 1
	RNG	2	6	1.719E+01	compressive fiber stress margin: (allowable/actual) - 1
	RNG	2	6	7.022E+00	in-plane shear margin: (allowable stress)/(actual stress) - 1
	RNG	2	15	7.023E+00	compressive transverse stress margin: (allowable/actual) - 1
	RNG	2	15	8.027E+01	compressive fiber stress margin: (allowable/actual) - 1
	RNG	2	15	3.280E+00	in-plane shear margin: (allowable stress)/(actual stress) - 1
	RNG	3	1	6.501E+01	tensile fiber margin: (allowable stress)/(actual stress) - 1
	STR	3	0	1.677E+01	crippling margin for stringer segment. 22 local halfwaves
	STR	4	0	4.926E+00	crippling margin for stringer segment. 22 local halfwaves
	0	0	0	3.931E-01	(Wide column panel buck. factor)/(factor of safety) - 1
	0	0	0	7.214E-01	buck.margin simp-support smear string;M=1 ; N=12 ; slope= 0.05
	0	0	0	1.849E-01	buck.margin simp-support general buck;M=1 ; N=2 ; slope= 0.27
	0	0	0	7.267E-01	buck.margin rolling with smear string;M=1 ; N=12 ; slope= 0.05
	0	0	0	5.059E+00	buck.margin rolling only of stringers;M=4 ; N=0 ; slope= 0.00

141

Table 12   FINAL DESIGN OF ARIANE 4 2/3-INTERSTAGE WITH T-SHAPED STRINGERS
           IN WHICH LOCAL POST-BUCKLING IS NOT PERMITTED

SUMMARY OF INFORMATION FROM OPTIMIZATION ANALYSIS

VAR. NO.	DEC. VAR.	ESCAPE VAR.	LINK. VAR.	LINKED TO	LINKING CONSTANT	LOWER BOUND	CURRENT VALUE	UPPER BOUND	DEFINITION
1	Y	N	N	0	0.00E+00	2.50E+00	3.2761E+00	2.00E+01	stiffener spacing, b
2	Y	N	N	0	0.00E+00	5.00E-01	1.0547E+00	3.00E+00	width of stringer base, b2
3	Y	N	N	0	0.00E+00	1.00E-01	1.0654E+00	2.00E+00	height of stringer, h
4	Y	N	N	0	0.00E+00	1.00E-01	1.4693E+00	3.00E+00	width of outer flange of stiffener, w
5	N	N	N	0	0.00E+00	0.00E+00	1.2000E-02	0.00E+00	thickness for layer index no. (1)
6	N	N	N	0	0.00E+00	0.00E+00	5.2000E-03	0.00E+00	thickness for layer index no. (2)
7	N	N	N	0	0.00E+00	0.00E+00	0.0000E+00	0.00E+00	thickness for layer index no. (3)
8	N	N	N	0	0.00E+00	0.00E+00	0.0000E+00	0.00E+00	thickness for layer index no. (4)
9	N	N	N	0	0.00E+00	0.00E+00	0.0000E+00	0.00E+00	thickness for layer index no. (5)
10	N	N	N	0	0.00E+00	0.00E+00	5.2000E-03	0.00E+00	thickness for layer index no. (6)
11	N	N	N	0	0.00E+00	0.00E+00	5.2000E-03	0.00E+00	thickness for layer index no. (7)
12	N	N	N	0	0.00E+00	0.00E+00	3.6400E-02	0.00E+00	thickness for layer index no. (8)
13	N	N	N	0	0.00E+00	0.00E+00	5.2000E-03	0.00E+00	thickness for layer index no. (9)
14	N	N	N	0	0.00E+00	0.00E+00	2.6000E-02	0.00E+00	thickness for layer index no. (10)
15	N	N	N	0	0.00E+00	0.00E+00	2.6750E+01	0.00E+00	stiffener spacing, b
16	N	N	N	0	0.00E+00	0.00E+00	1.0000E+00	0.00E+00	width of ring base, b2
17	Y	N	N	0	0.00E+00	1.00E+00	1.0000E+00	2.00E+00	height of ring, h
18	N	N	N	0	0.00E+00	0.00E+00	5.2000E-03	0.00E+00	thickness for layer index no. (11)
19	N	N	N	0	0.00E+00	0.00E+00	0.0000E+00	0.00E+00	thickness for layer index no. (12)
20	N	N	N	0	0.00E+00	0.00E+00	5.2000E-03	0.00E+00	thickness for layer index no. (13)
21	N	N	N	0	0.00E+00	0.00E+00	5.2000E-03	0.00E+00	thickness for layer index no. (14)
22	N	N	N	0	0.00E+00	0.00E+00	1.0000E-01	0.00E+00	thickness for layer index no. (15)

```
********************* DESIGN OBJECTIVE *********************
*****                                                  *****
*****     CURRENT VALUE OF THE OBJECTIVE FUNCTION:      *****
*****   VAR. STR/ SEG. LAYER  CURRENT                   *****
*****   NO.  RNG  NO.   NO.    VALUE        DEFINITION  *****
*****    0    0               3.305E+01   WEIGHT OF THE ENTIRE PANEL
*****                                                  *****
********************* DESIGN OBJECTIVE *********************
```

Table 13   MARGINS CORRESPONDING TO LOAD SET 1 APPLIED TO THE FINAL DESIGN
OF ARIANE 4 2/3-INTERSTAGE WITH T-SHAPED STRINGERS
IN WHICH LOCAL POST-BUCKLING IS NOT PERMITTED

```
*********** LOAD SET NO. 1  ***********
APPLIED LOADS IN LOAD SET A ("eigenvalue" loads):
   Applied   axial          stress resultant, N1= -3.0000E+03
   Applied circumferential stress resultant, N2= -3.0000E+00
   Applied   in-plane       shear  resultant,N12=  1.5000E+01

APPLIED LOADS IN LOAD SET B ( fixed uniform loads):
   Applied   axial          stress resultant,N10=  0.0000E+00
   Applied circumferential stress resultant,N20=  0.0000E+00
   Applied   in-plane       shear  resultant,N120=  0.0000E+00
   Applied pressure (positive for internal), P =  0.0000E+00
```

CURRENT VALUES OF MARGINS CORRESPONDING TO CURRENT DESIGN

VAR. NO.	STR/ RNG	SEG. NO.	LAYER NO.	CURRENT VALUE	DEFINITION
	0	0	0	2.868E-01	Local buckling from discrete model-1.,M=10 axial waves
STR	3	0	0	2.187E+00	crippling margin for stringer segment. 25 local halfwaves
STR	4	0	0	8.047E-01	crippling margin for stringer segment. 25 local halfwaves
	0	0	0	-4.323E-03	(Wide column panel buck. factor)/(factor of safety) - 1
	0	0	0	6.800E-01	buck.margin simp-support smear string;M=1 ; N=4 ; slope= 0.00
	0	0	0	1.999E+00	buck.margin simp-support smear rings; M=124; N=1 ; slope= 0.00
	0	0	0	4.832E-01	buck.margin simp-support general buck.;M=2 ; N=2 ; slope= 0.00
	0	0	0	6.779E-01	buck.margin rolling with smear string;M=1 ; N=4 , slope= 0.00
	0	0	0	1.256E+01	buck.margin rolling with smear rings; M=21 ; N=1 ; slope= 0.00
	0	0	0	1.212E-01	buck.margin rolling only of stringers;M=3 ; N=0 ; slope= 0.00

Table 14   MARGINS CORRESPONDING TO LOAD SET 2 APPLIED TO THE FINAL DESIGN
OF ARIANE 4 2/3-INTERSTAGE WITH T-SHAPED STRINGERS
IN WHICH LOCAL POST-BUCKLING IS NOT PERMITTED

```
********* LOAD SET NO. 2  *********

APPLIED LOADS IN LOAD SET A ("eigenvalue" loads):

    Applied  axial          stress resultant, N1= -1.0000E+03
    Applied  circumferential stress resultant, N2= -1.4142E+00
    Applied  in-plane       shear  resultant,N12=  1.0000E+03

APPLIED LOADS IN LOAD SET B ( fixed uniform loads):

    Applied  axial          stress resultant,N10=  0.0000E+00
    Applied  circumferential stress resultant,N20=  0.0000E+00
    Applied  in-plane       shear  resultant,N120=  0.0000E+00
    Applied  pressure (positive for internal),  P =  0.0000E+00

********* NOTE   NOTE   NOTE  *********
          WIDE COLUMN BUCKLING LOAD FACTOR
CORRESPONDS TO SIDESWAY (ROLLING) OF THE STRINGER BY ITSELF.
*****************************************************************
```

CURRENT VALUES OF MARGINS CORRESPONDING TO CURRENT DESIGN

VAR. NO.	STR/RNG	SEG. NO.	LAYER NO.	CURRENT VALUE	DEFINITION
	STR	3	0	1.042E-02	Local buckling from discrete model-1.,M=10 axial waves
	STR	4	0	8.562E+00	crippling margin for stringer segment. 25 local halfwaves
	STR	1	0	4.414E+00	crippling margin for stringer segment. 25 local halfwaves
			2	9.833E-01	in-plane shear margin: (allowable stress)/(actual stress) - 1
			0	3.898E-01	(Wide column panel buck. factor)/(factor of safety) - 1
			0	1.359E+00	buck.margin simp-support smear string;M=1 ; N=10 ; slope= 0.07
			0	3.935E+00	buck.margin simp-support smear rings; M=124; N=1 ; slope= 0.07
			0	2.441E-01	buck.margin simp-support general buck.;M=1 ; N=2 ; slope= 0.27
			0	1.362E+00	buck.margin rolling with smear string;M=1 ; N=10 ; slope= 0.07
			0	5.269E-01	buck.margin rolling with smear rings; M=21 ; N=1 ; slope= 0.57
			0	2.364E+00	buck.margin rolling only of stringers;M=3 ; N=0 ; slope= 0.00

144

TABLE 15(2 pages)

OPTIMUM DESIGNS OF ARIANE4 2/3 INTERSTAGE
WITH ALUMINUM I-SHAPED INSERT INSIDE STRINGERS

| | | LOCAL BUCKLING: | |
		PERMITTED	NOT PERMITTED
FINAL DIMENSIONS (inches)...			
Stringer spacing,	b =	5.57	4.04
Stringer base width,	b2 =	0.804	0.832
Stringer height,	h =	1.54	1.21
Stringer flange width,	w =	0.896	0.671
Thicknesses:			
layer type 1, 45 deg. cloth	t(1) =	0.018	0.006
layer type 2, 90 deg. tape	t(2) =	0.0052	0.0052
layer type 3, 45 deg. tape	t(3) =	0.0000	0.0052
layer type 4, 0 deg. tape	t(4) =	0.0000	0.0000
layer type 5,-45 deg. tape	t(5) =	0.0000	0.0052
layer type 6, 0 deg. tape	t(6) =	0.0052	0.0000
layer type 7, 90 deg. tape	t(7) =	0.0052	0.0104
layer type 8, 0 deg. tape in base	t(8) =	0.0260	0.0468
layer type 9, AL in base & flange	t(9) =	0.0200	0.0200
layer type 10, AL in web	t(10) =	0.0201	0.0275
layer type 11,0 deg. tape in flange	t(11) =	0.0260	0.0468
PANEL WEIGHT (lbs)....		31.9	34.9
DESIGN MARGINS.....			
LOAD SET 1 (Nx = -3000 lb/in, Nxy = 0)....			
Local buckling		-----	0.501
Wide column buckling between rings		-0.0207	0.0000
Rolling of stringers without skin motion		0.0000	0.0000
General instability		0.257	0.657
Buckling between rings, smeared stringers		0.669	0.853
Crippling of stringer web		0.863	0.682
Crippling of stringer flange		0.521	2.391
Stringer popoff		0.257	-----
In-plane shear stress, GR/EP cloth, Segment 3 (web), Node 1, layer 1		-0.003	-----
Compression in aluminum insert		0.099	-----
Compression in aluminum insert, Segment 2 (stringer base)		-----	0.540
Compression in aluminum insert, Segment 4 (flange)		-----	0.594

Table 15 (continued and concluded)

```
LOAD SET 2   (Nx = -1000 lb/in, Nxy = 1000 lb/in)....
    Local buckling                                -----      0.0000
    Wide column buckling between rings            0.100      0.463
    General instability                           0.134      0.353
    Stringer popoff                               0.418      -----
    Tension along fibers, GR/EP cloth,
        Seg. 5 (panel skin), node 9, layer 1   -0.0038      -----
    In-plane shear stress, GR/EP cloth,
        Seg. 1 (panel skin), node 9, layer 1     0.621      -----
    In-plane shear stress, aluminum insert,
        Seg. 2 (stringer base), node 1           0.912      -----
==========================================================================
```

TABLE 16 (2 pages)

OPTIMUM DESIGNS OF ARIANE4 2/3 INTERSTAGE
WITH HAT-SHAPED STRINGERS

			LOCAL BUCKLING:	
			PERMITTED	NOT PERMITTED
FINAL DIMENSIONS (inches)...				
Stringer spacing,	b	=	5.07	4.20
Stringer base width,	b2	=	2.50	2.50
Stringer height,	h	=	1.42	1.34
Stringer outer flange width,	w	=	1.20	1.20
Stringer hat base width,	w2	=	1.50	1.50
Thicknesses:				
layer type 1, 45 deg. cloth	t(1)	=	0.012	0.012
layer type 2, 90 deg. tape	t(2)	=	0.0000	0.0052
layer type 3, 45 deg. tape	t(3)	=	0.0052	0.0000
layer type 4, 0 deg. tape	t(4)	=	0.0000	0.0000
layer type 5,-45 deg. tape	t(5)	=	0.0052	0.0000
layer type 6, 0 deg. tape	t(6)	=	0.0000	0.0052
layer type 7, 90 deg. tape	t(7)	=	0.0052	0.0052
layer type 8, 0 deg. tape in base	t(8)	=	0.0052	0.0104
layer type 9, 90 in base & flange	t(9)	=	0.0052	0.0052
layer type 11,0 deg. tape in flange	t(11)	=	0.0416	0.0208

PANEL WEIGHT (lbs)....	27.9	28.7

DESIGN MARGINS.....		
LOAD SET 1 (Nx = -3000 lb/in, Nxy = 0)....		
Local buckling	-----	0.0000
Wide column buckling between rings	-0.0400	0.0116
General instability	0.558	0.292
Buckling between rings, smeared stringers	1.22	0.694
Crippling of stringer webs	0.0697	0.410
Crippling of stringer flange	1.38	0.940
Crippling under hat	1.47	1.23
Stringer popoff	3.11	-----
In-plane shear stress, GR/EP cloth, Segment 1 (skin), Node 9, Layer 1	0.256	1.32
Compression along fibers, Seg. 1, Layer 6	-----	1.43
In-plane shear stress, tape, Segment 1 (skin), Node 9, Layer 3	0.951	-----
Compression along fibers, tape, Segment 2 (base), Node 1, Layer 8	1.06	-----

Table 16 (continued and concluded)

LOAD SET 2   (Nx = -1000 lb/in, Nxy = 1000 lb/in)....

Local buckling	-----	0.108
Wide column buckling between rings	0.654	0.919
General instability	0.176	0.138
Stringer popoff	0.898	-----
Tension along fibers, GR/EP cloth, Seg. 1 (skin), Node 1, Layer 14	0.0202	-----
In-plane shear stress, GR/EP cloth, Seg. 2 (base), Node 7, Layer 1	0.621	-----
In-plane shear stress, tape, Seg. 1, Layer 2	-----	0.983

===
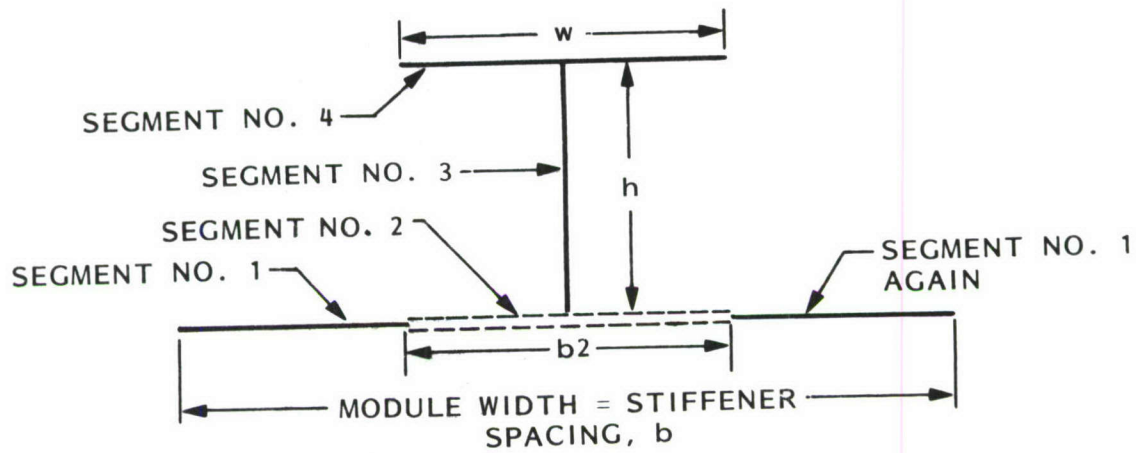
Fig. 1 Single module of a panel with T–shaped stringer. (Axial load N_x acts normal to the screen).
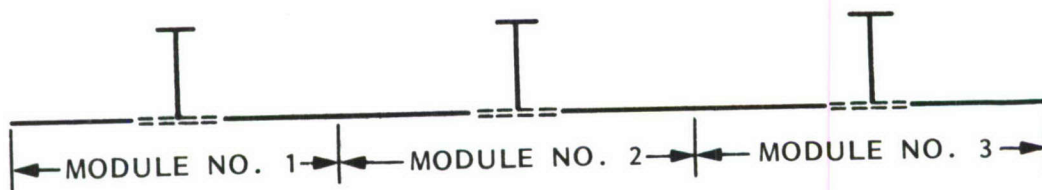
Fig. 2 Panel with T–shaped stringers. There are three modules in this example.
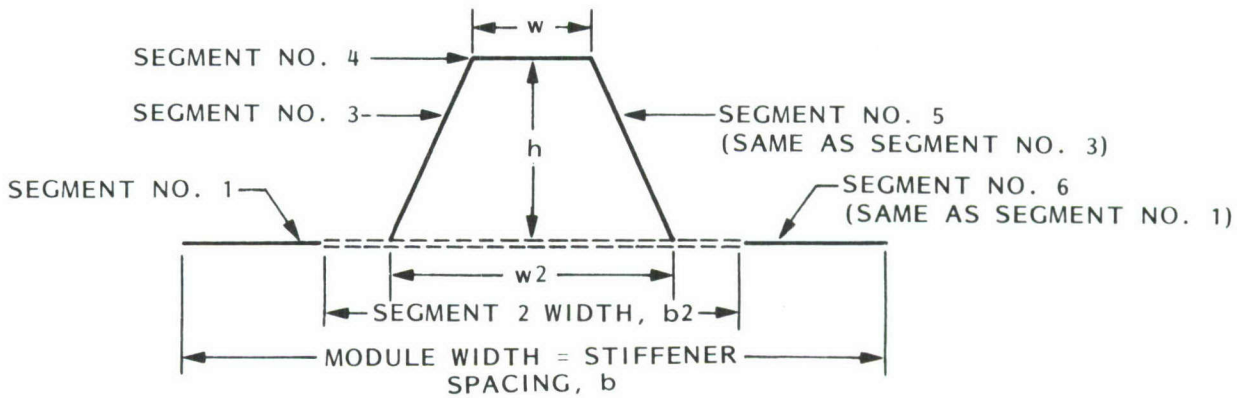
Fig. 3   Panel module with hat-shaped stiffener.
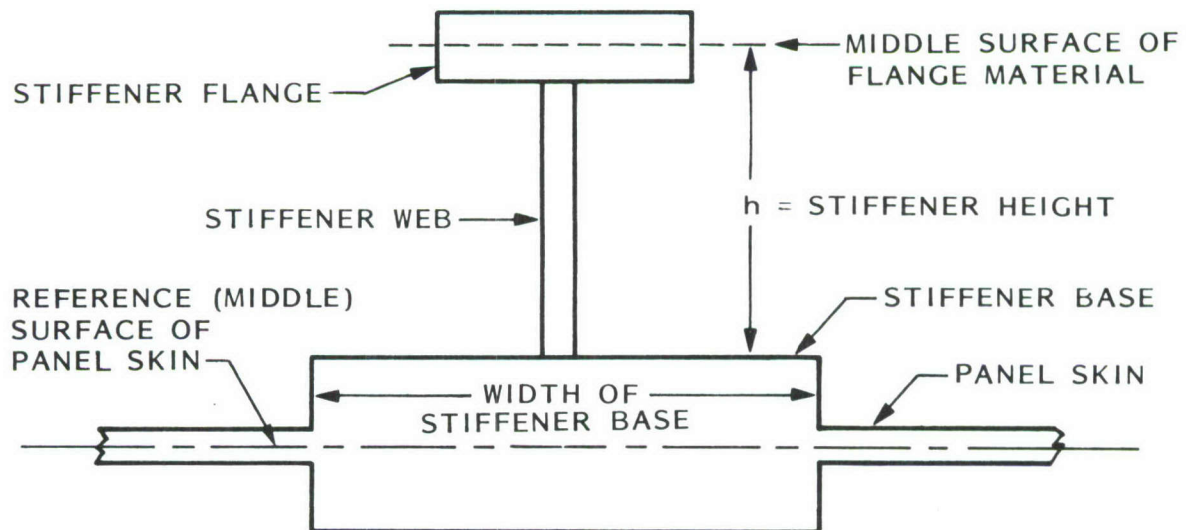
Fig. 4   Height of the stiffener is measured from the top of the stiffener base to the middle surface of the flange.
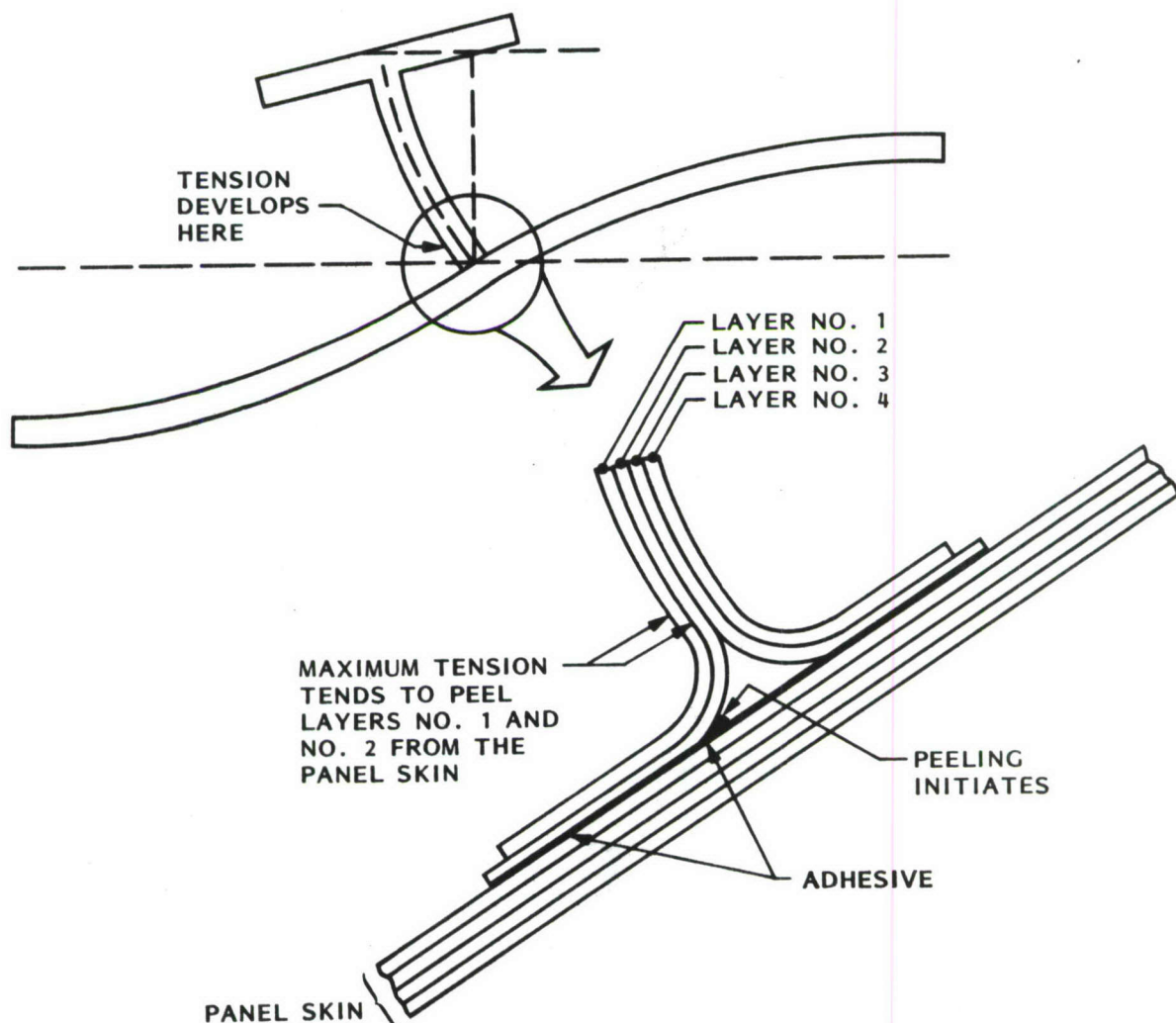
Fig. 5 Schematic of locally buckled panel, showing how bending of the stringer web gives rise to local tension in the plane of the web normal to the panel skin at the stringer line of attachment. This tension tends to peel the web from the panel skin, causing stiffener pop-off.

ADHESIVE

F_p

F_p

HALF OF STRINGER WEB

PANEL SKIN

c. PEEL TEST SPECIMEN

STRINGER FLANGE

STRINGER WEB

LOCALLY BUCKLED PANEL SKIN

STRINGER WEB

ADHESIVE

PANEL SKIN

a. LOCALLY BUCKLED PANEL

b. DETAIL NEAR WEB-SKIN JOINT
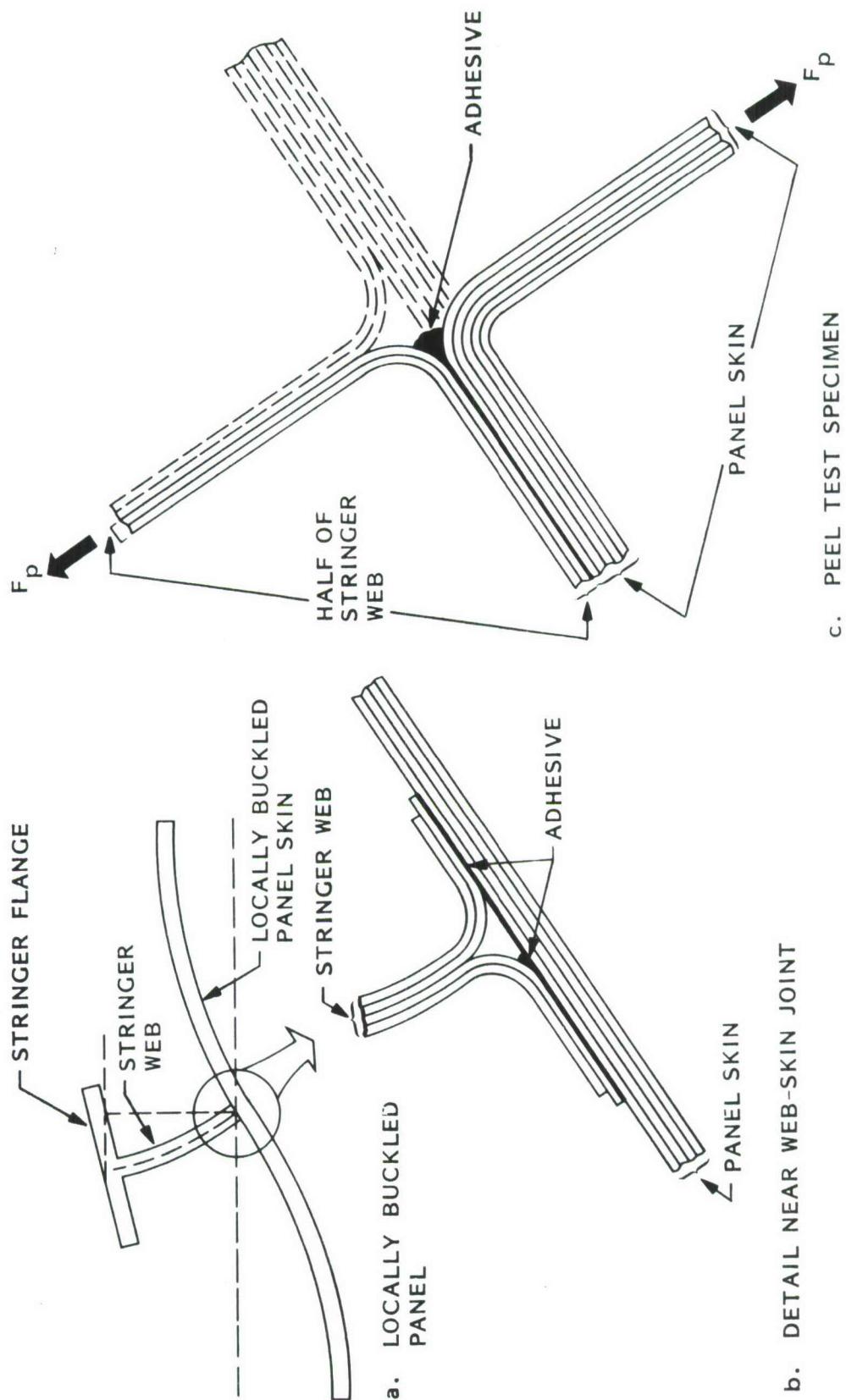
Fig. 6 Proper design of a T-peel test specimen that reproduces the local behavior near the root of the web of a stringer of a locally buckled panel that leads to stringer pop-off.

152

Fig. 7 Failed T-peel test specimen. In this case graphite-epoxy cloth is bonded to graphite-epoxy tape. The peel test simulates the behavior near the root of one of the webs of a hat-stiffened panel buckling locally is shown in Fig. 20(a).

PANEL MODULE

STRINGER

POSITIVE PRESSURE

NEGATIVE PRESSURE

POSITIVE PRESSURE

NEGATIVE PRESSURE

a. FLAT PANEL

b. CURVED PANEL,
   EXTERNAL STRINGER
   (POSITIVE CURVATURE)

c. CURVED PANEL,
   INTERNAL STRINGER
   (NEGATIVE CURVATURE)

d. CURVED PANEL,
   NO STRINGER
   (POSITIVE CURVATURE)
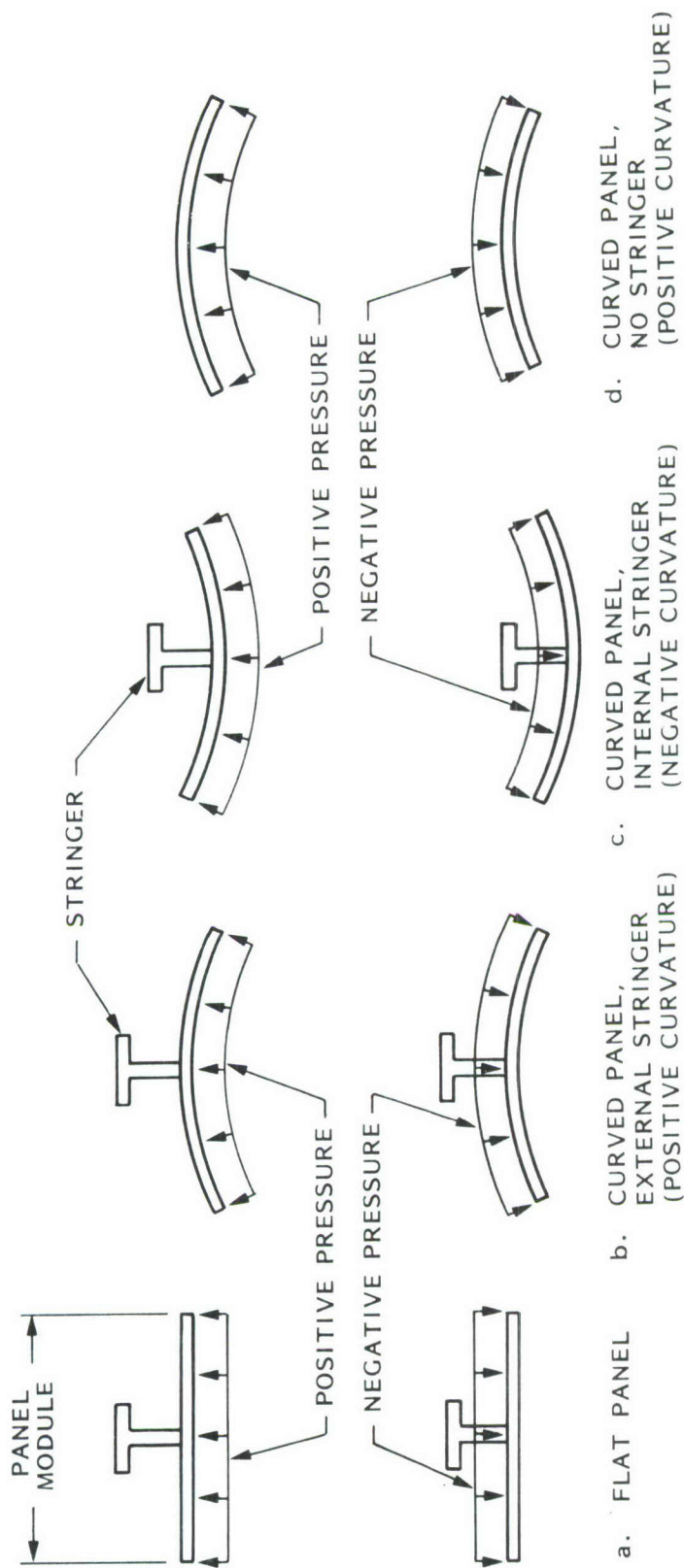
Fig. 8   Sign convention for pressure and curvature. In PANDA2 the following rules hold:

(1) The stringer is always "on top" of the panel skin;

(2) If the panel is curved the user always supplies a positive number for the radius of curvature;

(3) If the user specifies "external stringer" the panel curvature will be positive, as shown in (b);

(4) If the user specifies "internal stringer" the panel curvature will be negative, as shown in (c);

(5) If there are no stringers the curvature will be positive, as in (d);

(6) Positive pressure always pushes downward, no matter what the curvature is or where the stiffeners are.

154
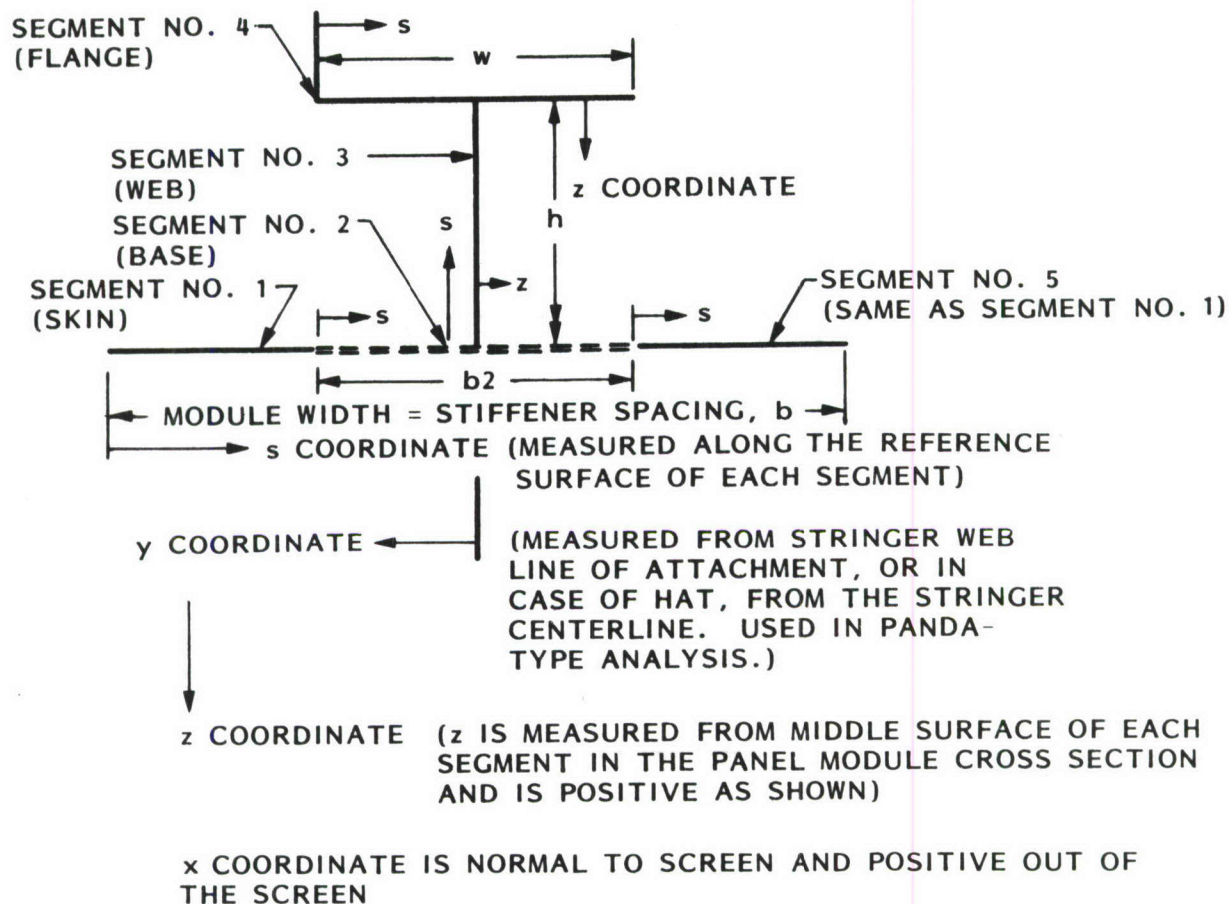
Fig. 9   Typical panel module cross section, coordinates, segments, nomenclature.
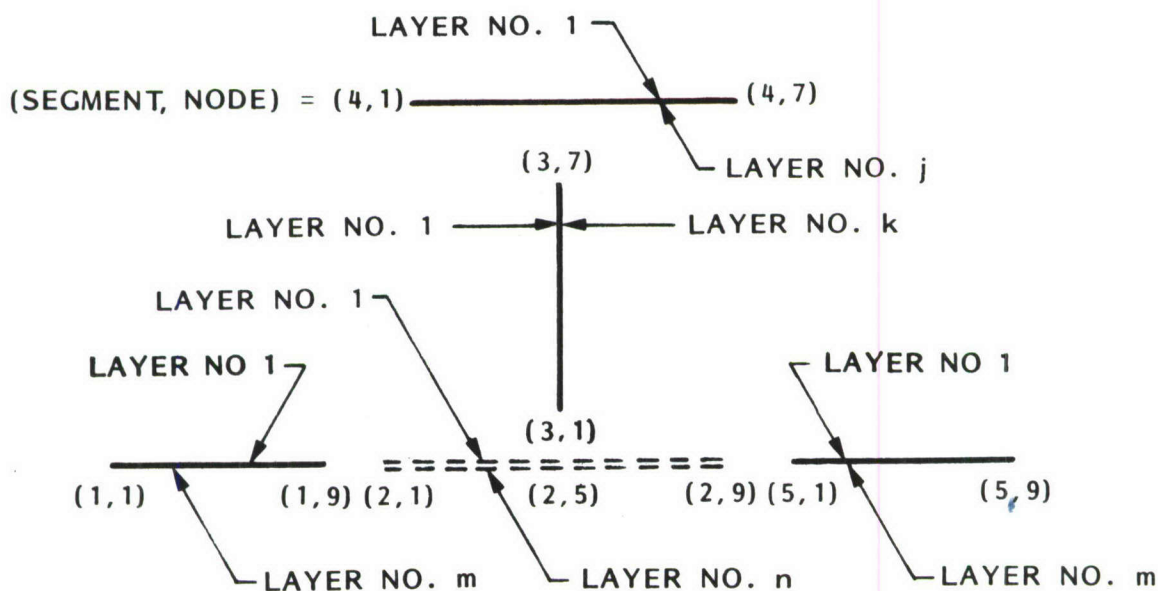
Fig. 10 Exploded view, showing layers and (Segment, Node) numbers.
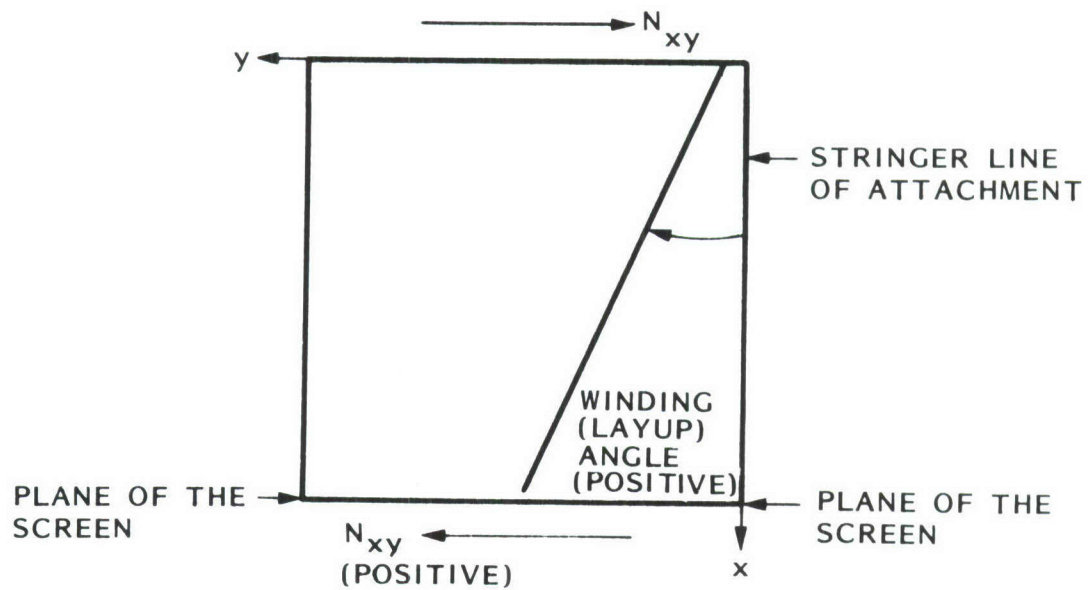
Fig. 11 Positive in-plane shear, winding (layup) angle.
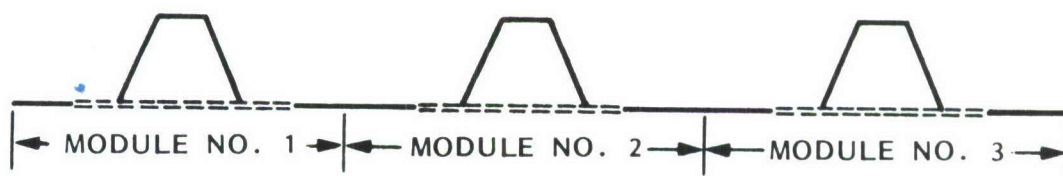
Fig. 12 Panel with three hat modules.

THIS ANALYSIS IS FOR A MODULE WITH HAT-SHAPED (TRAPEZOIDAL) STIFFENER...
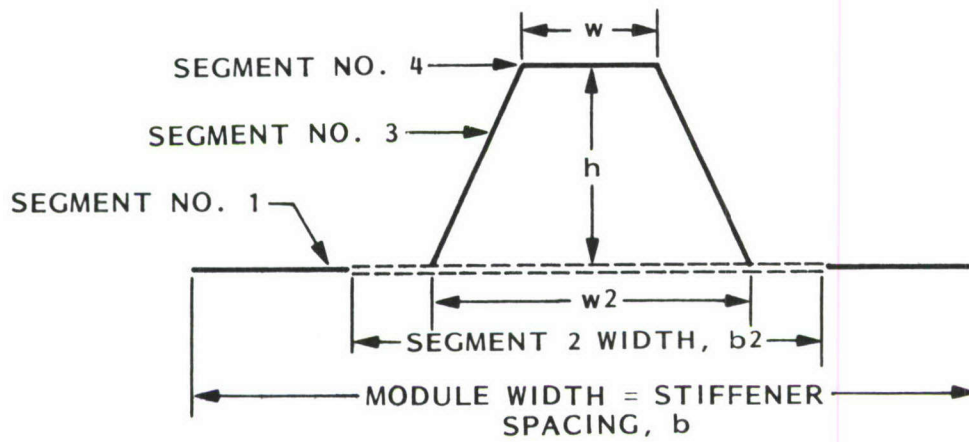
Fig. 13 Single panel module with hat stiffener.

Fig. 14 Plan view of a single panel module used in the development of the integrated constitutive law C_{ij} for the panel with smeared stringers and rings.

SKIN MIDDLE SURFACE, USED
AS THE REFERENCE
SURFACE FOR THE OLD
CONSTITUTIVE MATRIX, C
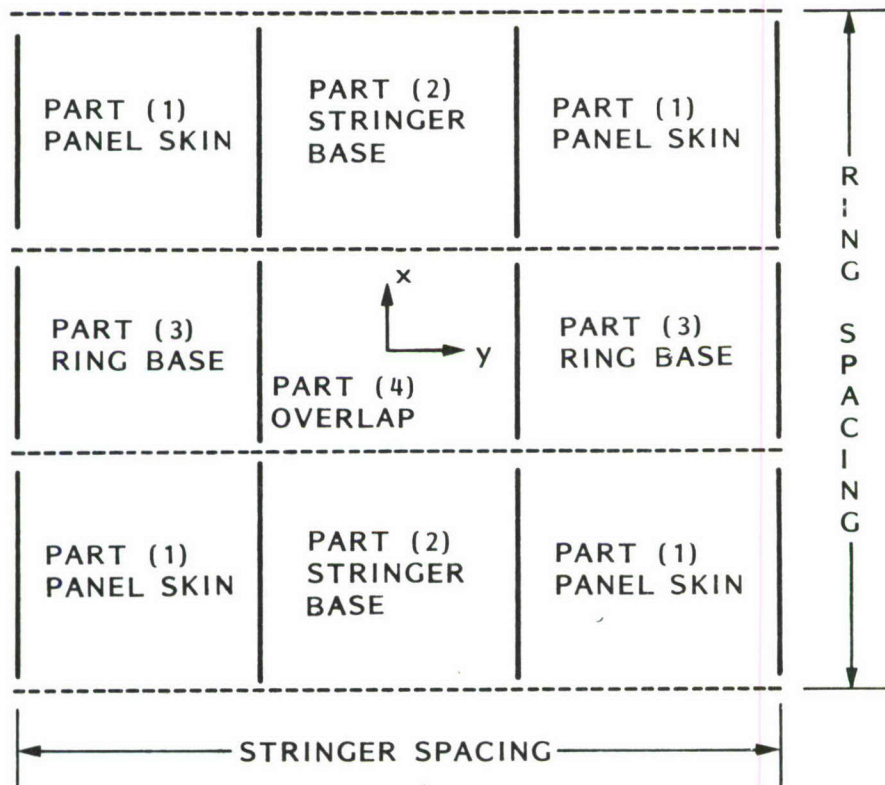
NEW REFERENCE SURFACE,
LOCATED DISTANCE
$D = -C(1,4)/C(1,1)$
BELOW THE SKIN
MIDDLE SURFACE
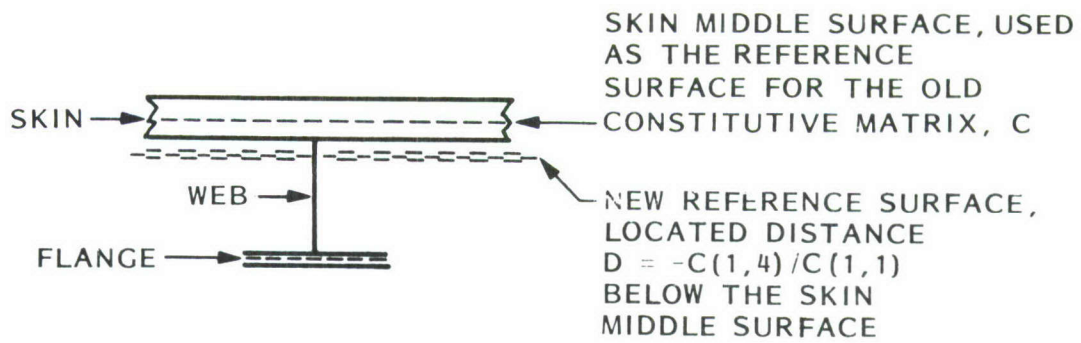
Fig. 15 a) View of a panel module cross section, showing the old reference surface located at the skin middle surface, and the new reference surface located a distance D below the skin middle surface. (D will be positive in the figure above.)
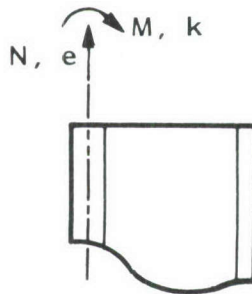
Fig. 15 b) Elevation of panel, showing reference surface at skin middle surface, axial resultant N, moment M, strain e, and curvature change k.
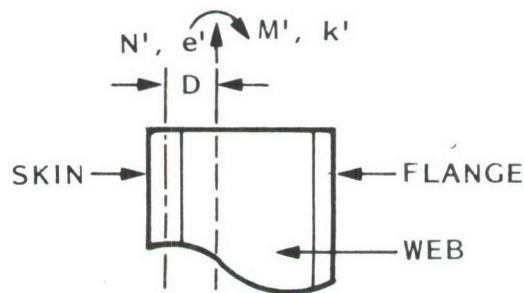
Fig. 15 c) Elevation of panel, showing reference surface near the neutral plane, shift D, axial resultant N', moment M', strain e', and curvature change k'.

158

INTERNAL STIFFENER
MODULE WITH HAT-SHAPED (TRAPEZOIDAL) STIFFENER...
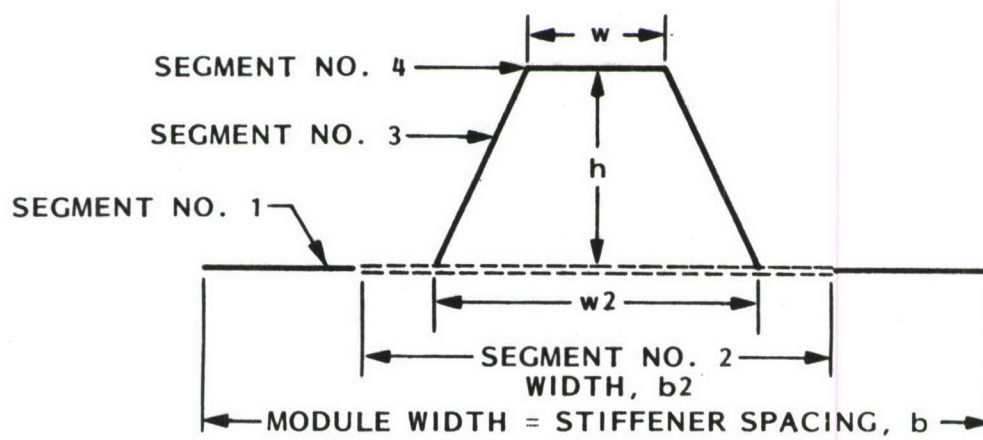
Fig. 16 Segment numbering in this sketch corresponds to numbering used for purposes of providing input data. The number of discretized BOSOR4-type segments into which the panel module is divided depends on whether or not the length b_2 is greater than w_2.

MODULE WITH b2 > w2
MODULE WITH HAT-SHAPED (TRAPEZOIDAL) STIFFENER ...
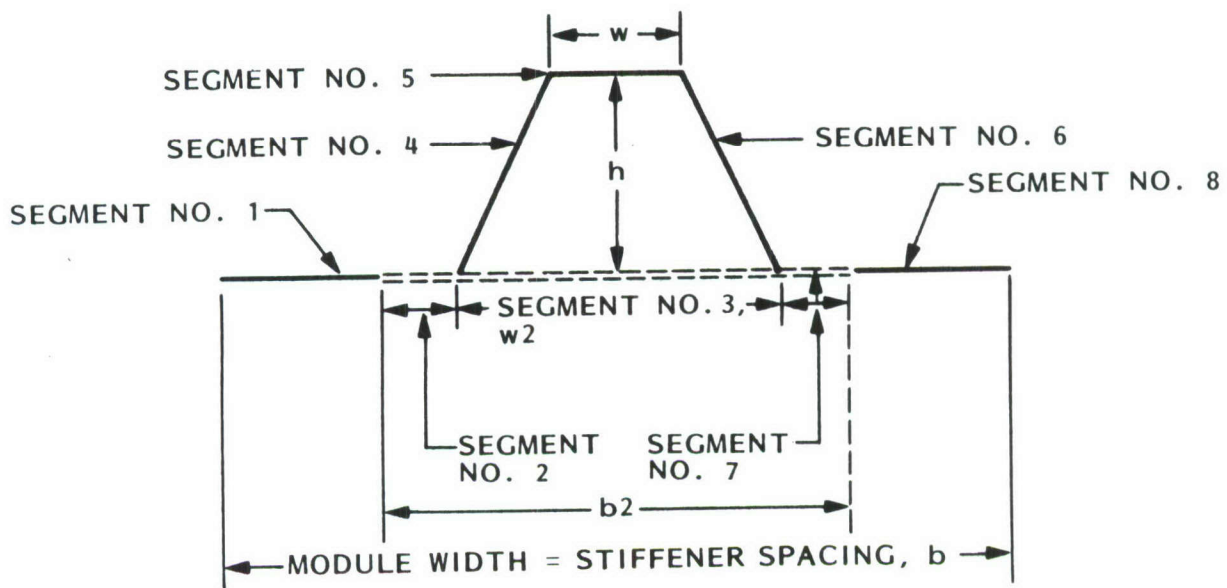
Fig. 17 Segment numbering for discretized single module models of the hat–stiffened panel for the case for which $b_2 > w_2$.

Fig. 18 (Segment, Node) pairs for stress output for hat–stiffened panel module for the case for which $b_2 > w_2$.

161

PANEL GEOMETRY IN THE AXIAL (L1) DIRECTION
MODULE WITH HAT-SHAPED (TRAPEZOIDAL) STIFFENER

Fig. 19 Segment numbering for wall construction list that follows.

(a) LOCAL BUCKLING AT LOAD FACTOR = 0.380
n = 7 HALFWAVES NORMAL TO THE PLANE OF
THE PAPER
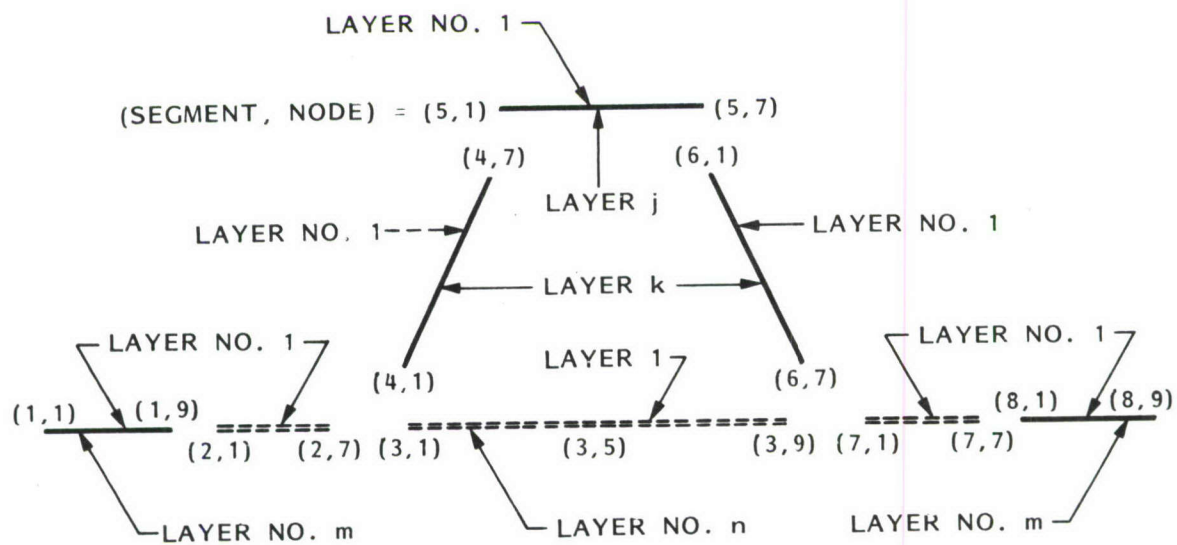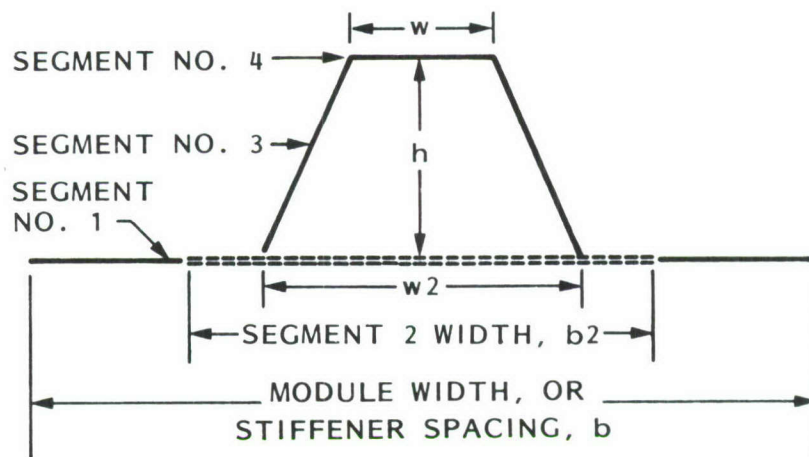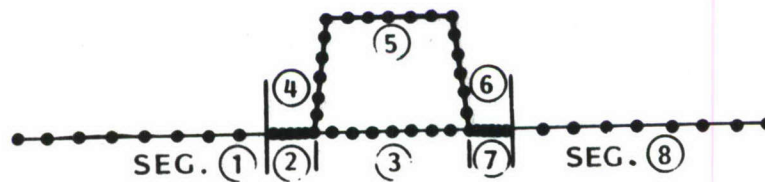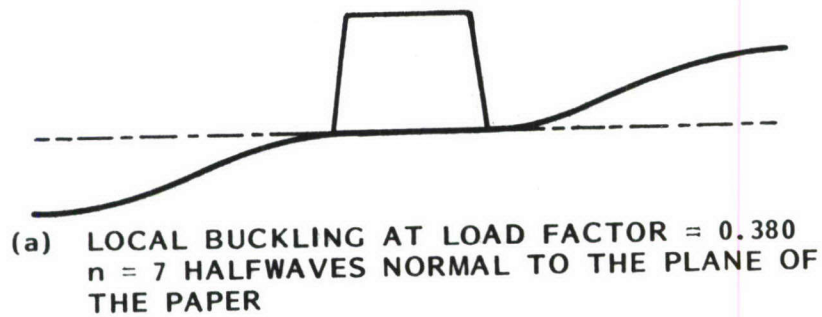
(b) DISCRETIZED CROSS SECTION OF PANEL
MODULE

(c) WIDE COLUMN BUCKLING AT LOAD FACTOR
= 2.65
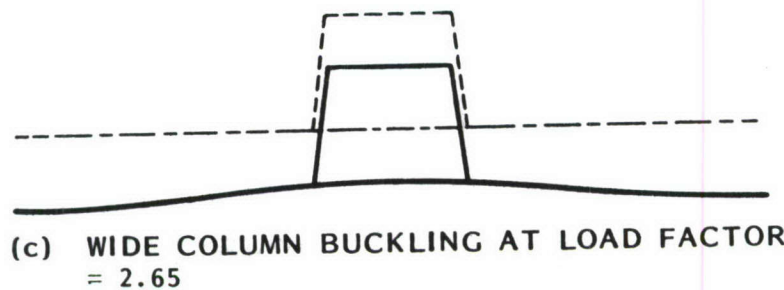
Fig. 20 Discretized model of hat-stiffened module with local bifurcation buckling mode and wide column buckling mode.

163

(a) Discretized 27-SEGMENT BOSOR4 MODEL

(b) MODE 1: $\lambda = 1.801$

(e) MODE 4: $\lambda = 2.488$

(c) MODE 2: $\lambda = 1.996$

(f) MODE 5: $\lambda = 2.912$

(d) MODE 3: $\lambda = 2.298$

(g) MODE 6: $\lambda = 2.991$
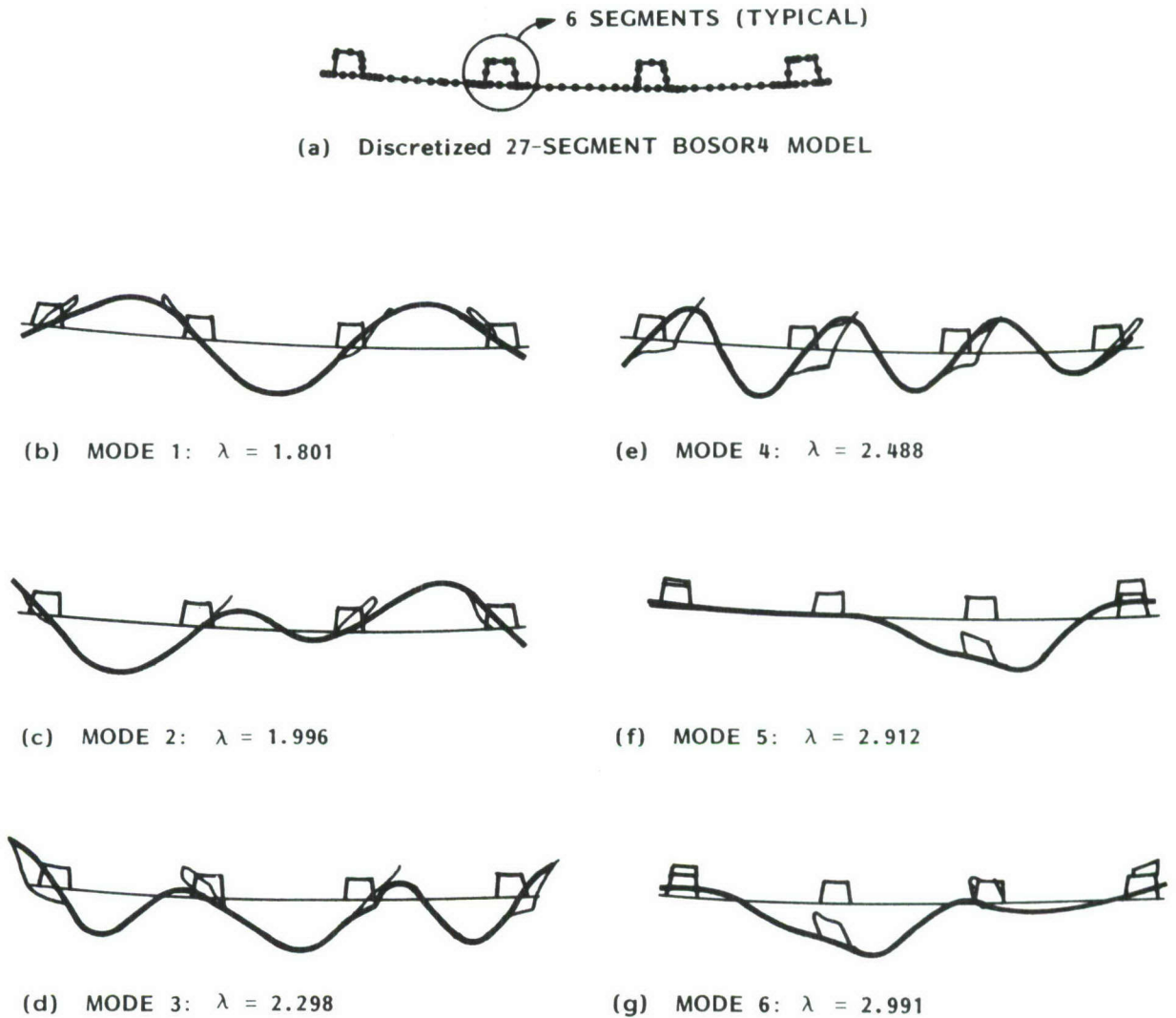
Fig. 21 (a) 27–segment BOSOR4 model of the entire hat– stiffened panel. This
model was automatically generated with use of the PANEL processor. (b–g)
Buckling modes and load factors λ corresponding to buckling between rings
(in this case buckling over the entire length of the panel, since there are no
rings.) Only the fifth and sixth modes represent general instability. The in–
plane shear load of 1000 lb/in is neglected in the calculation of these buckling
load factors and modes. The fifth mode load factor, $\lambda = 2.912$, times the
knockdown factor for in-plane shear, FKNOCK(4)=0.916, should be com-
pared to the wide–column buckling load predicted by PANDA2: $\lambda_{wide\,column}$
$= 2.61$.

(a) LOCAL BUCKLING MODE

(b) DISCRETIZED PANEL MODULE

(c) WIDE COLUMN BUCKLING MODE
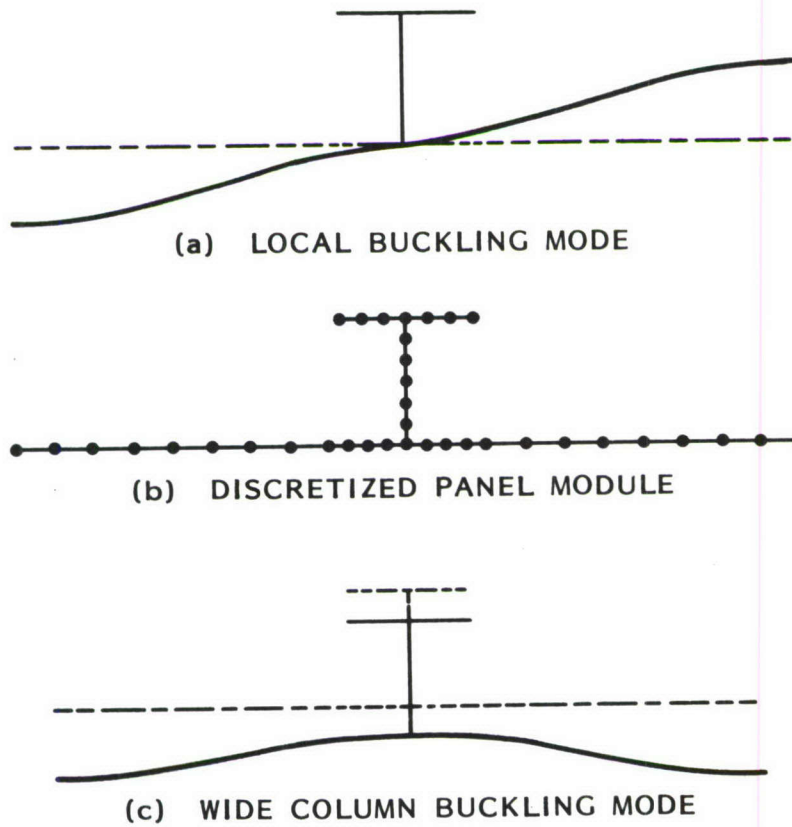
Fig. 22 Discretized model of tee-stiffened module with (a) local bifurcation buckling mode and (c) wide column buckling mode. These results correspond to a test performed at NASA [5] on a flat, graphite-epoxy panel under pure axial compression.
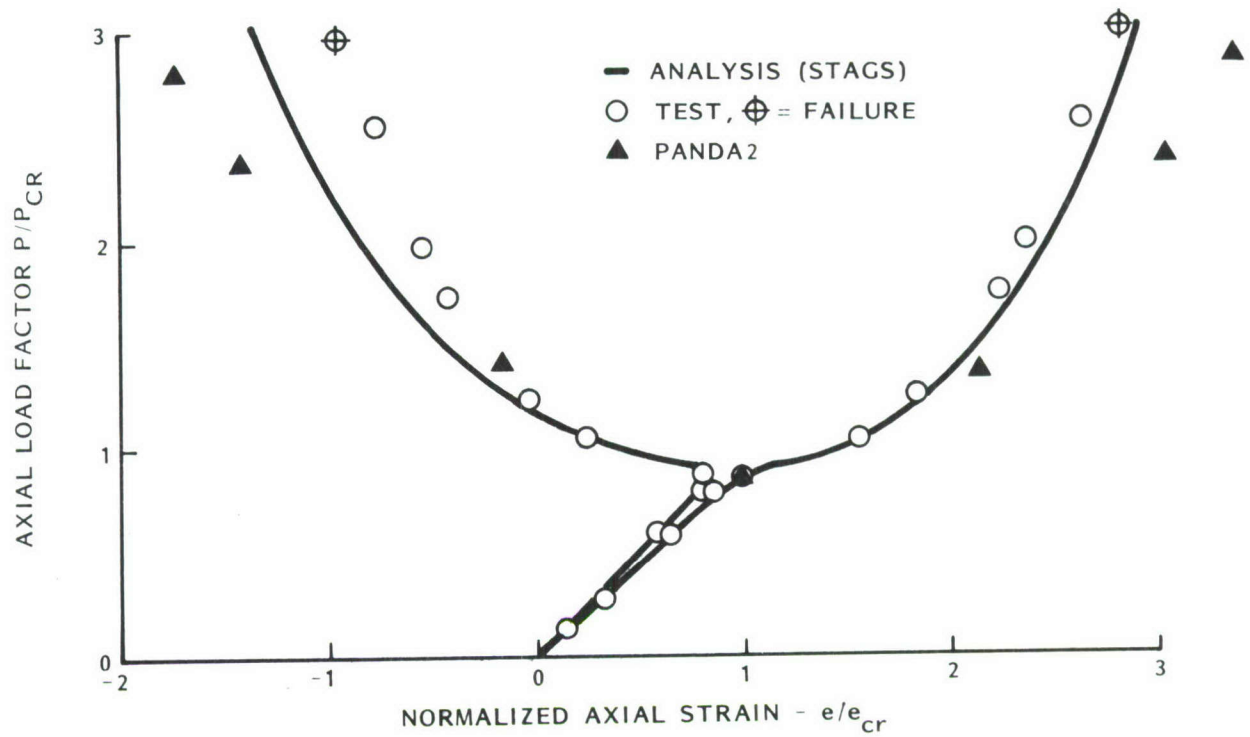
Fig. 23 Comparison of axial strain at a local buckle peak from test [5], STAGSC-1 analysis [5], and PANDA2 analysis for axially compressed, Tee-stiffened, graphite-epoxy flat panel. (adapted from Fig. 13c of [5])
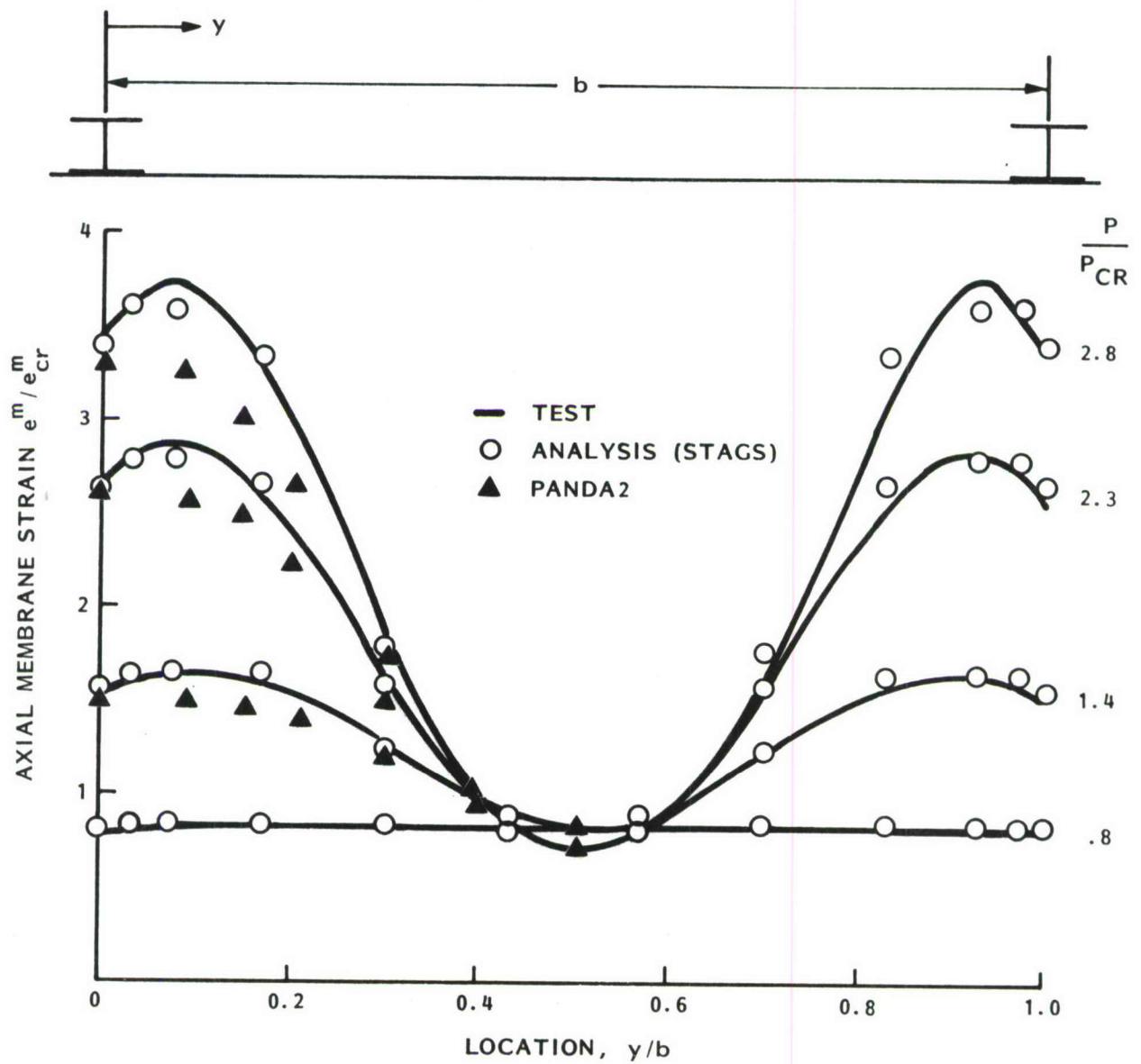
Fig. 24 Comparison of membrane axial strain from test [5], STAGSC-1 analysis [5], and PANDA2 analysis for axially compressed, tee-stiffened, graphite-epoxy flat panel. (adapted from Fig. 14 of [5])
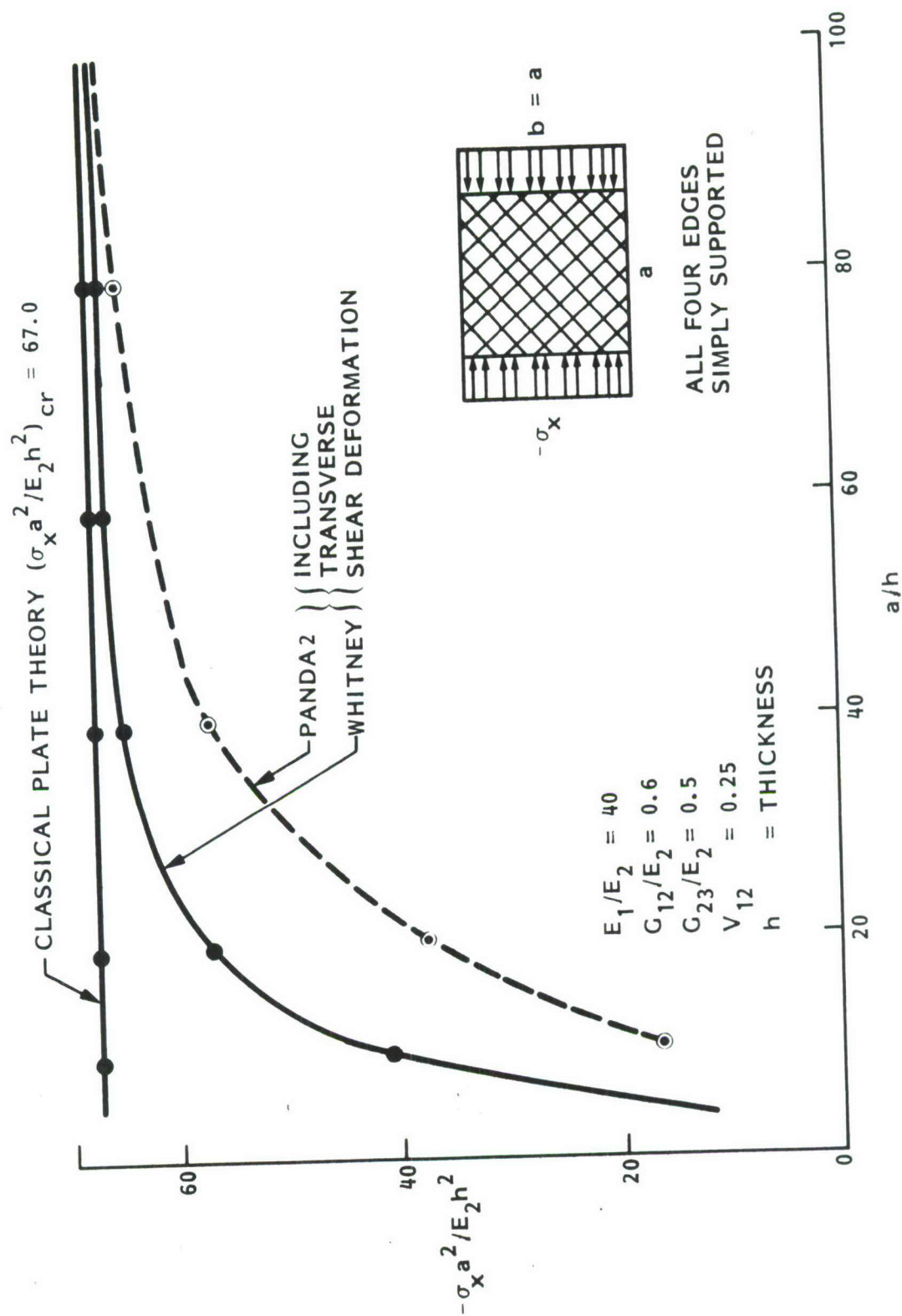
Fig. 25 Buckling of uniformly axially compressed, simply supported, plus-and-minus 45-degree angle-ply square plate with an infinite number of layers, with and without accounting for transverse shear deformation.

168

(a) COMPOSITE

WINDING ANGLE (deg) [45, -45, -45, 45, 0, 90]$_s$
THICKNESS (mil) [5.5, 5.5, 5.5, 5.5, 5.5, 49.5]$_s$

WINDING ANGLE (deg) [45, -45, -45, 45, 0]$_s$
THICKNESS (mil) [5.5, 5.5, 5.5, 5.5, 11.0]$_s$

5.0 in.
1.275

$E_1 = 19 \times 10^6$ psi $G/E_1 = 0.0489$
$E_2/E_1 = 0.0995$ ν (SMALL) $= 0.0378$
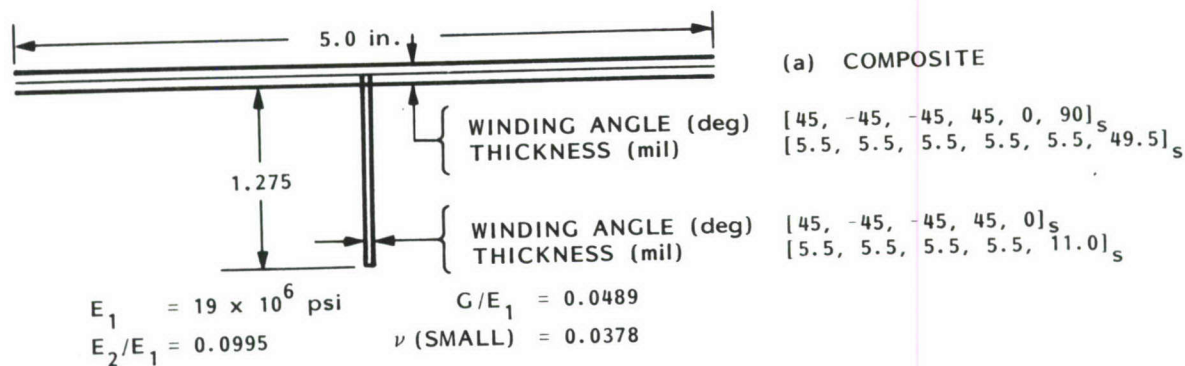
ENTIRE PANEL: SIX STRINGERS, LENGTH L = 30 in.; WIDTH = 30 in.
SIMPLE SUPPORT ON ALL FOUR EDGES

(b) METAL (ALUMINUM)

5.0 in.
0.084 in.
1.31 in.
0.058 in.

$E = 10.5 \times 10^6$ psi
$\nu = 0.32$

(c) COMPOSITE

E_1, E_2, G, ν
SAME AS IN (a)

WINDING ANGLE (deg) [45, -45, -45, 45, 0, 90]$_s$
THICKNESS (mil) [6.37, 6.37, 6.37, 6.37, 24.9, 41.6]$_s$

WINDING ANGLE (deg) [45, -45, -45, 45, 0]$_s$
THICKNESS (mil) [8.23, 8.23, 8.23, 8.23, 67.5]$_s$

5.0 in.
1.878 in.

(d) METAL

5.0 in.
0.050 in.
0.058 in.
1.327 in.

$E = 10.5 \times 10^6$ psi
$\nu = 0.32$
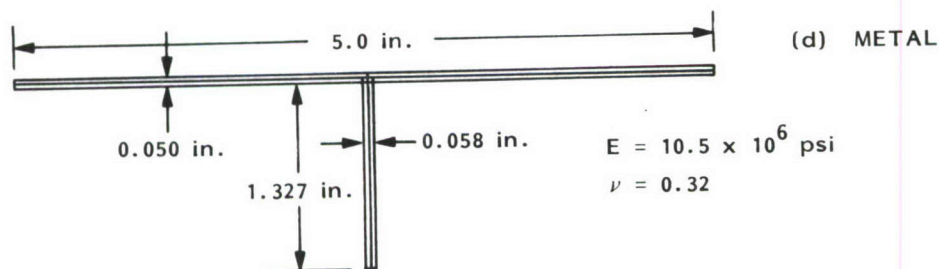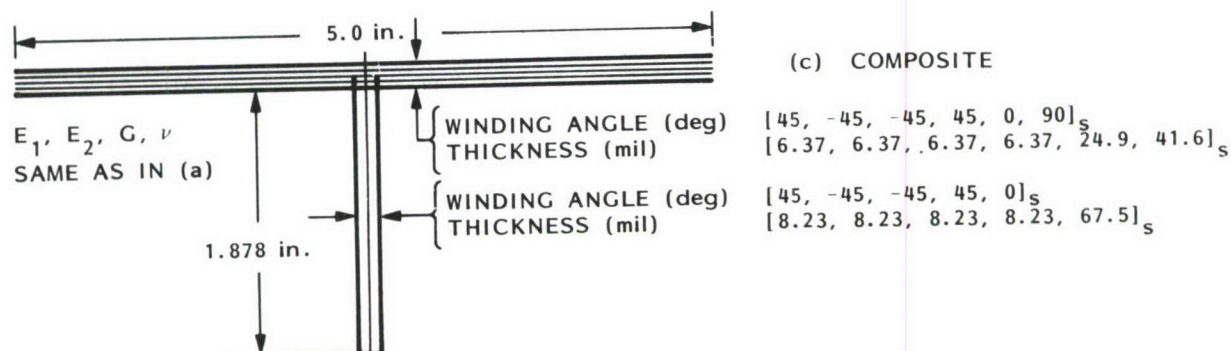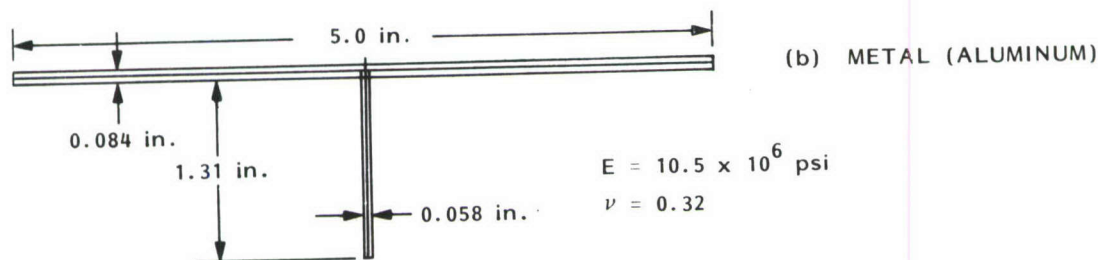
Fig. 26 Blade stiffened panel modules that comprise the 30-in.-square simply supported panels under axial compression and in-plane shear analyzed by Stroud, Greene and Anderson at NASA Langley [15].

169
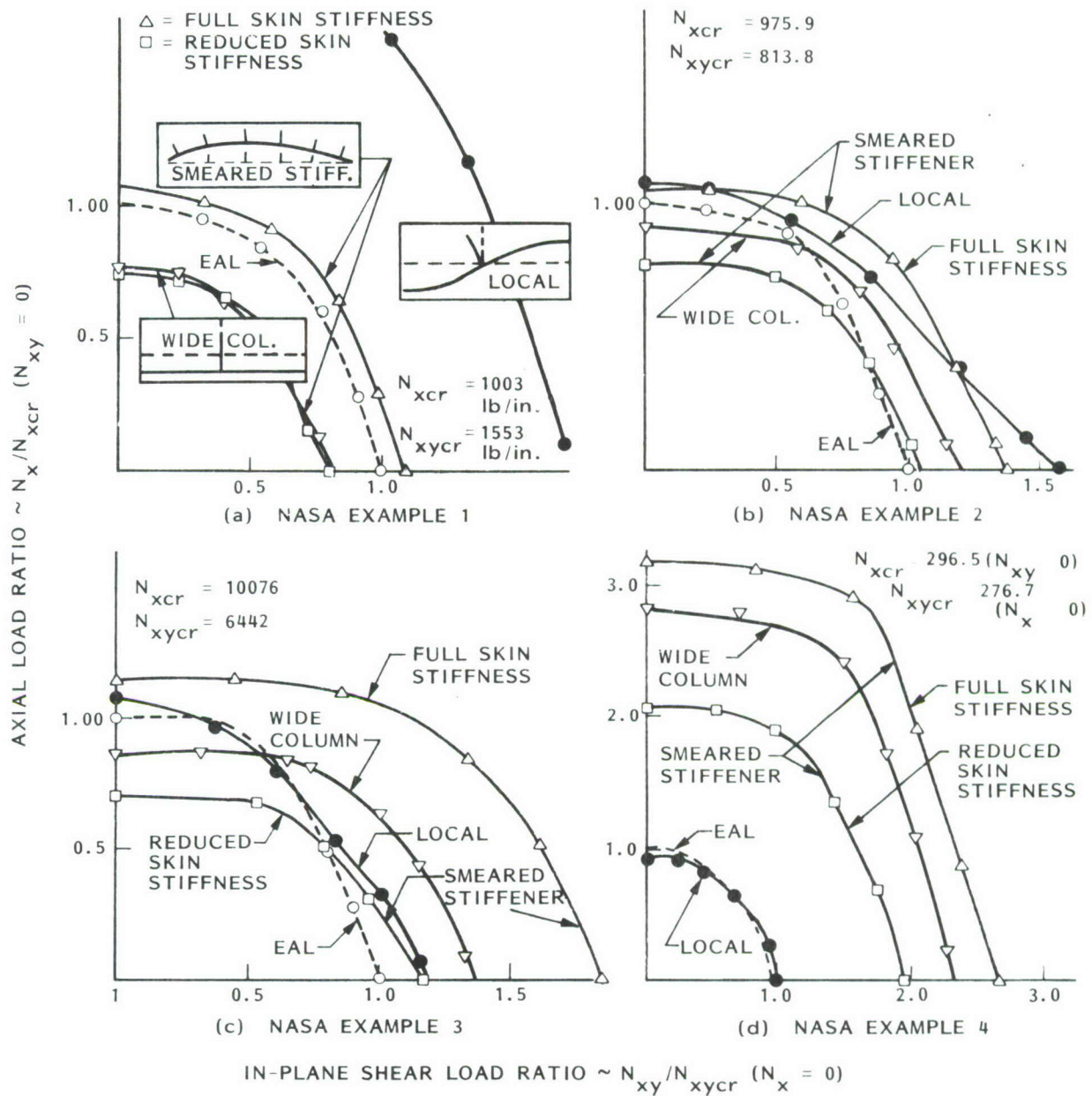
Fig. 27 Bifurcation buckling load-interaction curves obtained from PANDA2 and from a finite element model (EAL) for the four blade stiffened panels identified in the previous figure.

170
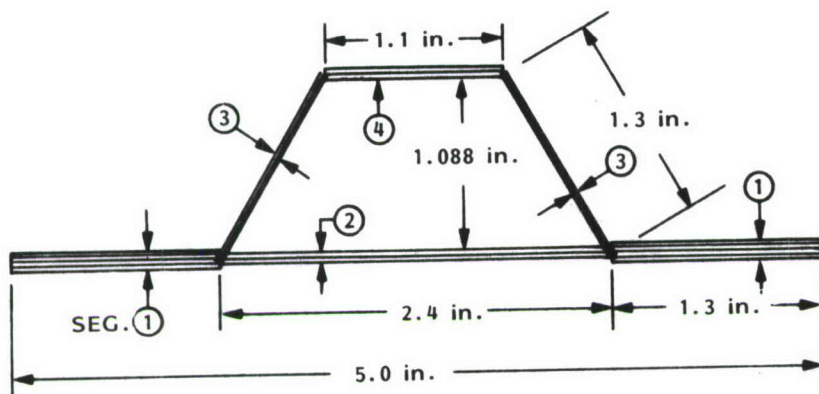
SEG. ① WINDING ANGLES (deg)   [45, -45, -45, 45, 0]ₛ
THICKNESS (mil)   [10.315, 10.315, 10.315, 10.315, 9.953]ₛ

SEG. ② WINDING ANGLES (deg)   [45, -45, 0]ₛ
THICKNESS (mil)   [10.315, 10.315, 16.955]ₛ

SEG. ③ WINDING ANGLES (deg)   [45, -45]ₛ
THICKNESS (mil)   [10.315, 10.315]ₛ

SEG. ④ WINDING ANGLES (deg)   [45, -45, 0]ₛ
THICKNESS (mil)   [10.315, 10.315, 25.383]ₛ
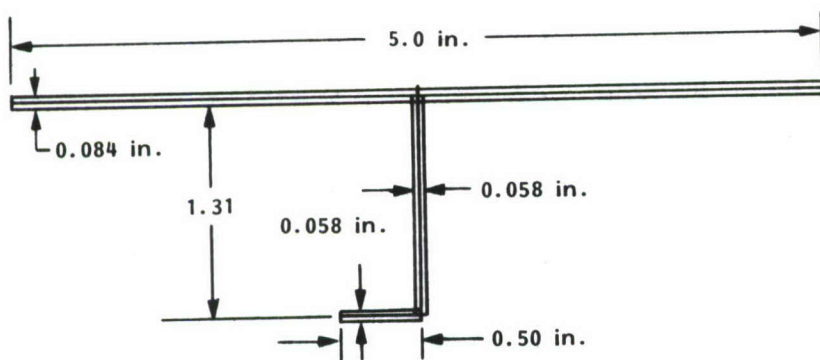
Fig. 28 Hat and J stiffened panel modules that comprise the 30-in.-square simply supported panels under axial compression and in-plane shear analyzed by Stroud, Greene and Anderson at NASA Langley [15].

171
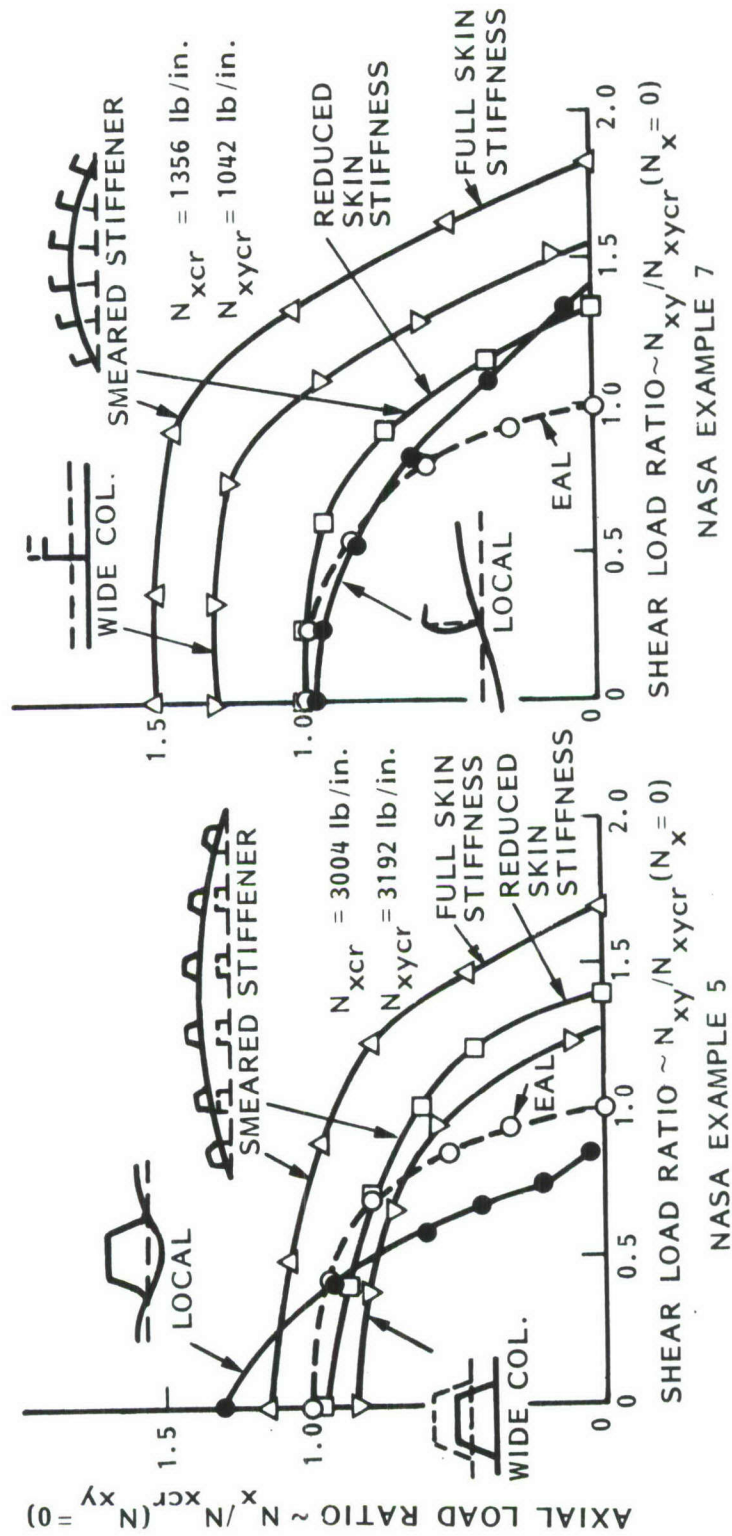
Fig. 29 Bifurcation buckling load-interaction curves obtained from PANDA2 and from a finite element model (EAL) for the hat and J stiffened panels identified in the previous figure.

172
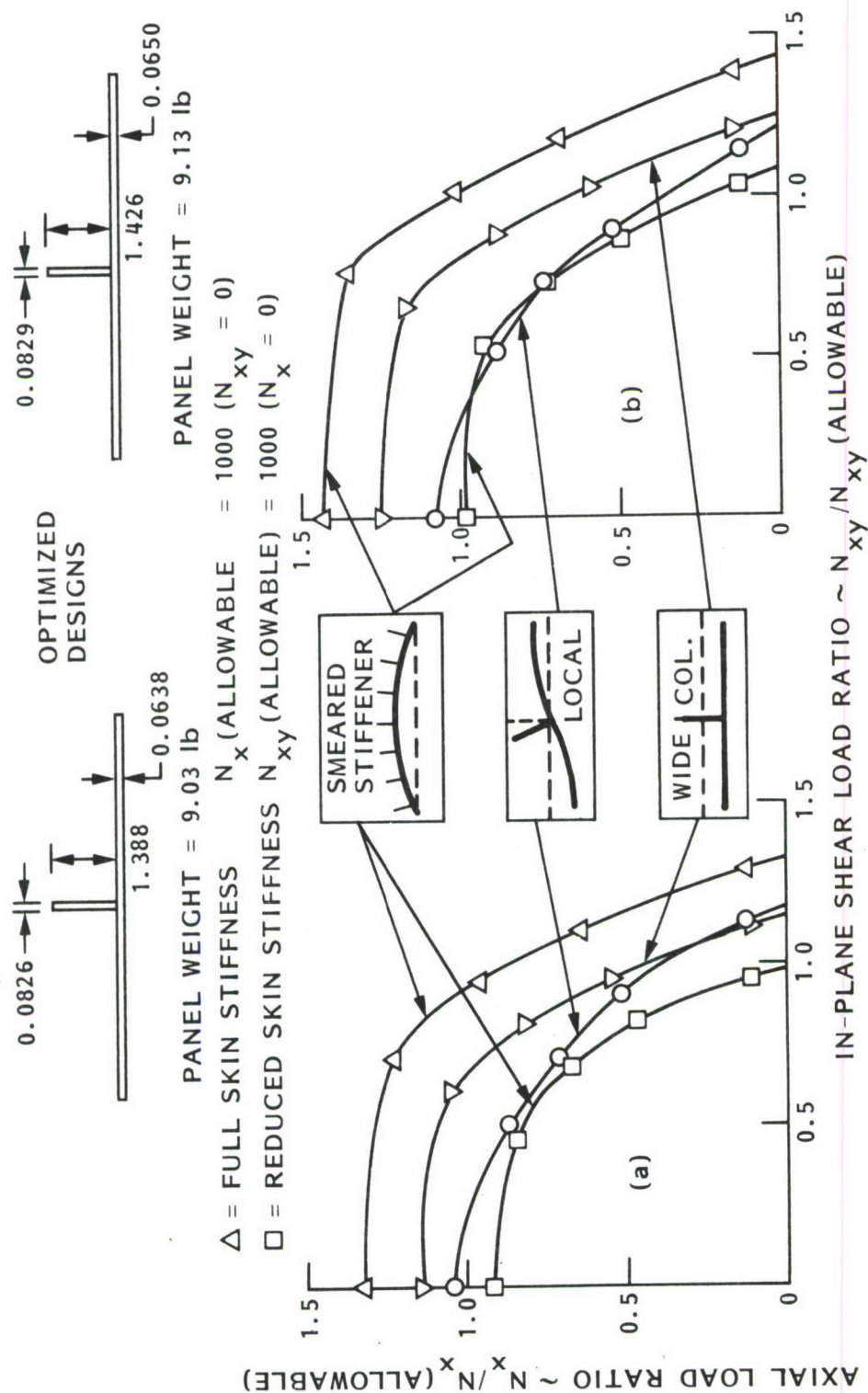
Fig. 30 Bifurcation buckling load-interaction curves obtained from designs optimized with use of PANDA2: (a) Optimum design with use of the wide column buckling load factor as a design constraint; (b) Optimum design with neglect of the wide column buckling load factor as a design constraint.

173

Fig. 31 Optimum design of hat-stiffened, graphite-epoxy panel designed to survive 3000 lb/in uniform axial compression. Several panels were fabricated to this specification and tested.

174

HOOP STRAIN GAGES LOCATED TO CAPTURE
MAXIMUM STRAIN ——
(4 PLACES)

PREDICTED FAILURE DUE TO EXCESSIVE
IN-PLANE SHEAR STRESS IN OUTERMOST
CLOTH LAYER (12 PLACES)
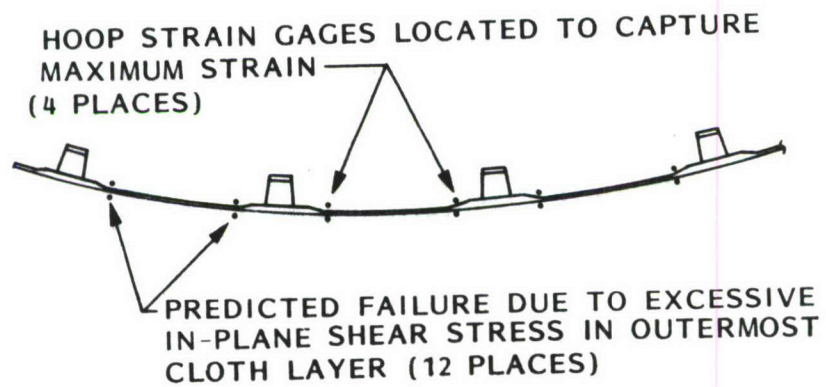
Fig. 32 Predicted locations of critical stresses in the locally postbuckled, axially com-
pressed, hat-stiffened, graphite-epoxy panel.
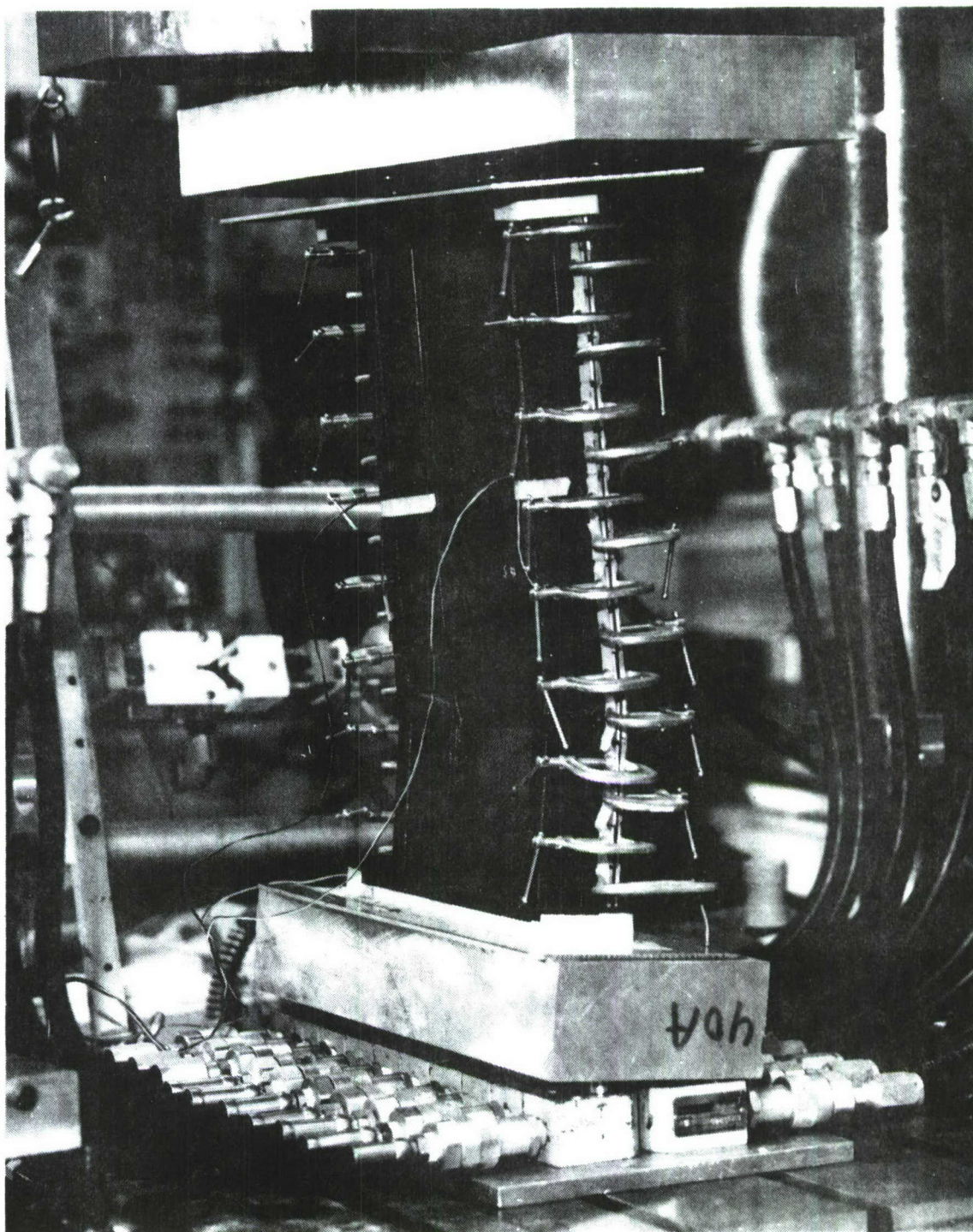
Fig. 33 Test setup for buckling of small (18 x 11 inch) flat panel under axial compression.
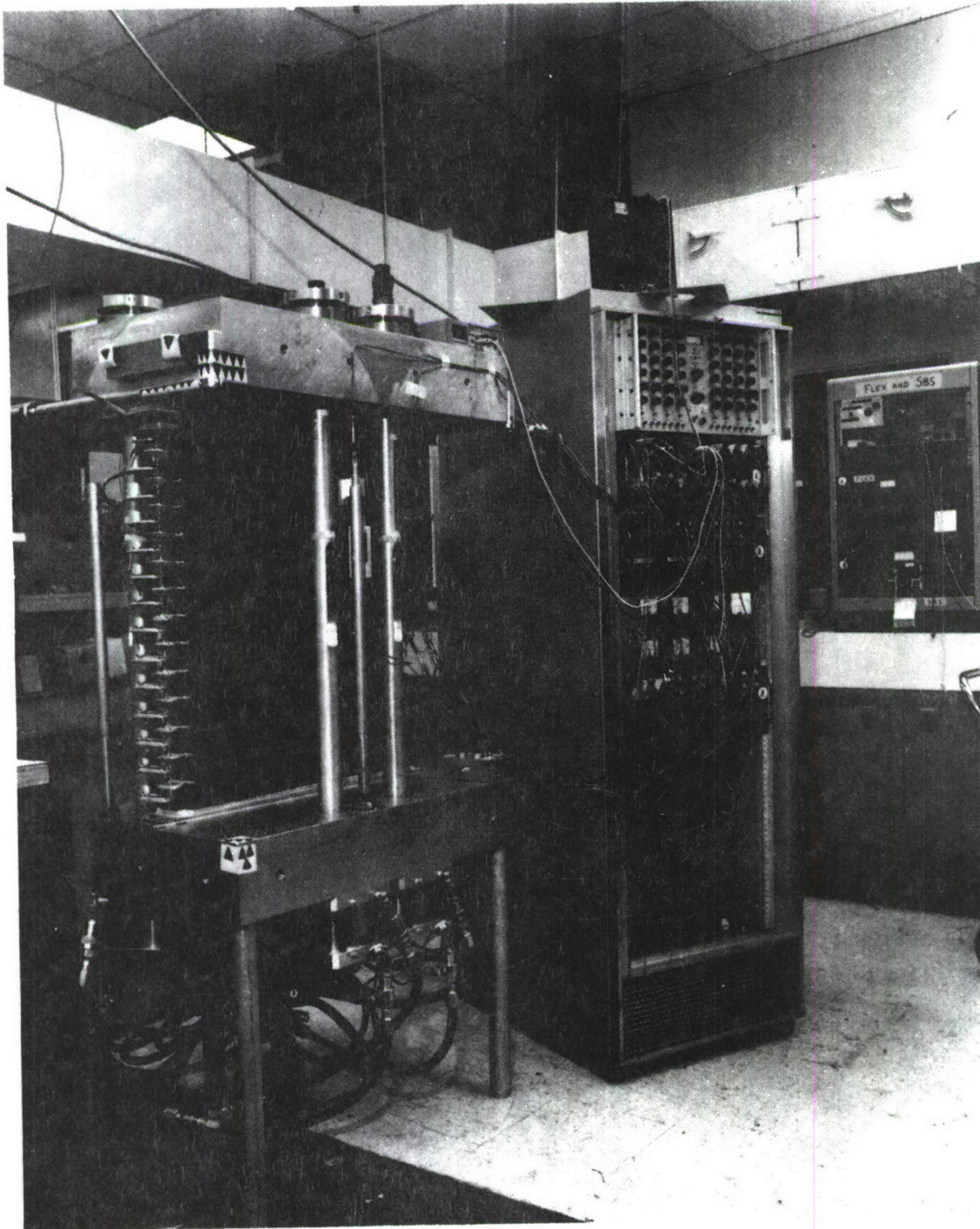
Fig. 34 Test setup for buckling of large (30 x 27 inch) curved panels under axial compression.
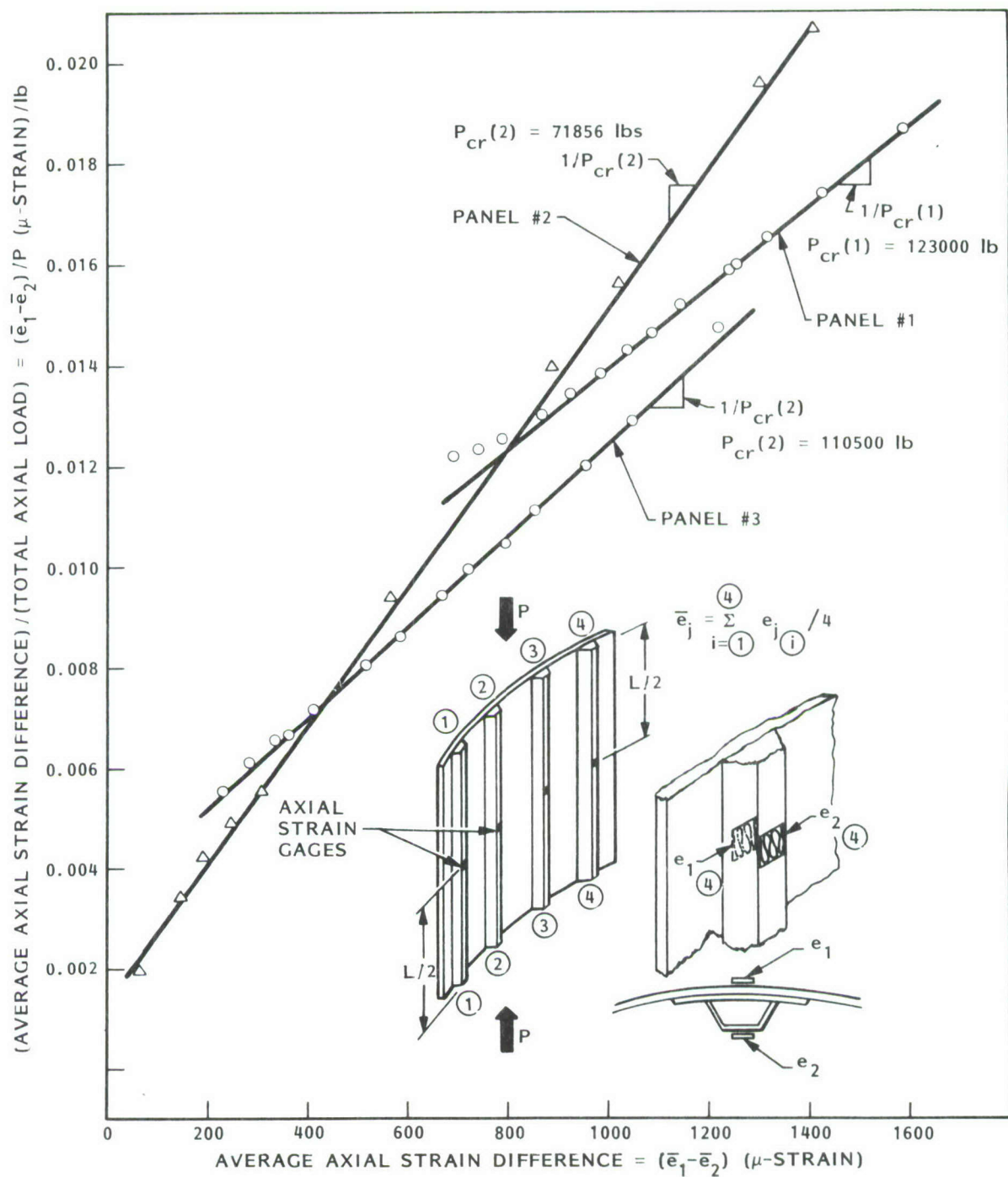
Fig. 35 Southwell plots for the three large panels tested to failure under pure axial compression.

178

a.

b.

Fig. 36 (a) 27–segment BOSOR4 model of the panels that were tested and (b) predicted general instability mode shape. The predicted critical total axial load, $P_{cr} = 125000$ lbs compression. This prediction should be compared with the predictions shown on the previous figure from the inverse of the slopes of the Southwell plots.

179
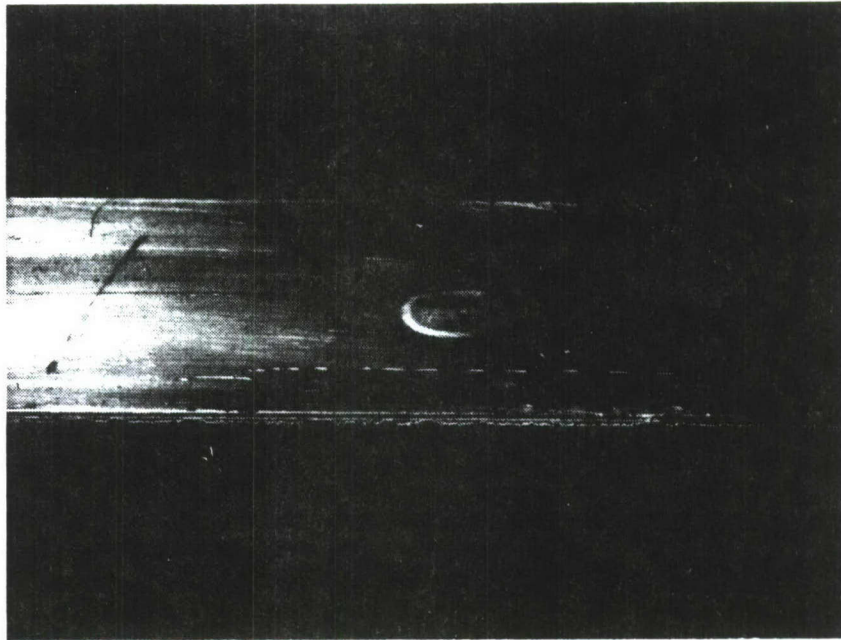
Fig. 37 Photograph of the local deformation of one of the soft aluminum end plates that occurred directly over one of the stringers in Panel 2. This end plate was fabricated from 6061T4 aluminum stock, which had a 26 ksi yield stress. No such deformations were observed in the end plates of Panels 1 and 3. These other harder end plates were fabricated from 6061T6 aluminum stock, which had a 56 ksi yield stress.
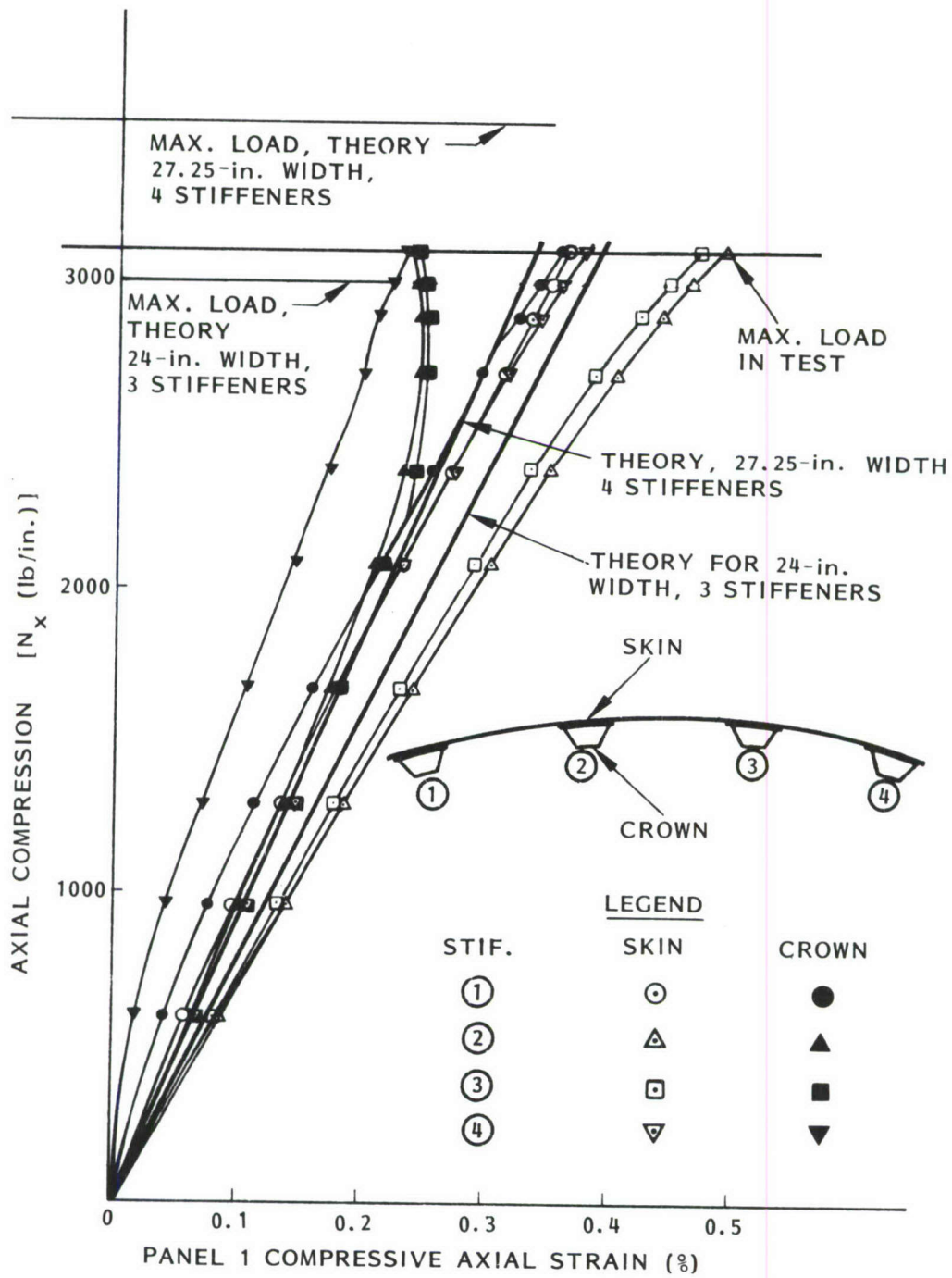
Fig. 38 Load-strain curves for axially compressed large Panel No. 1.
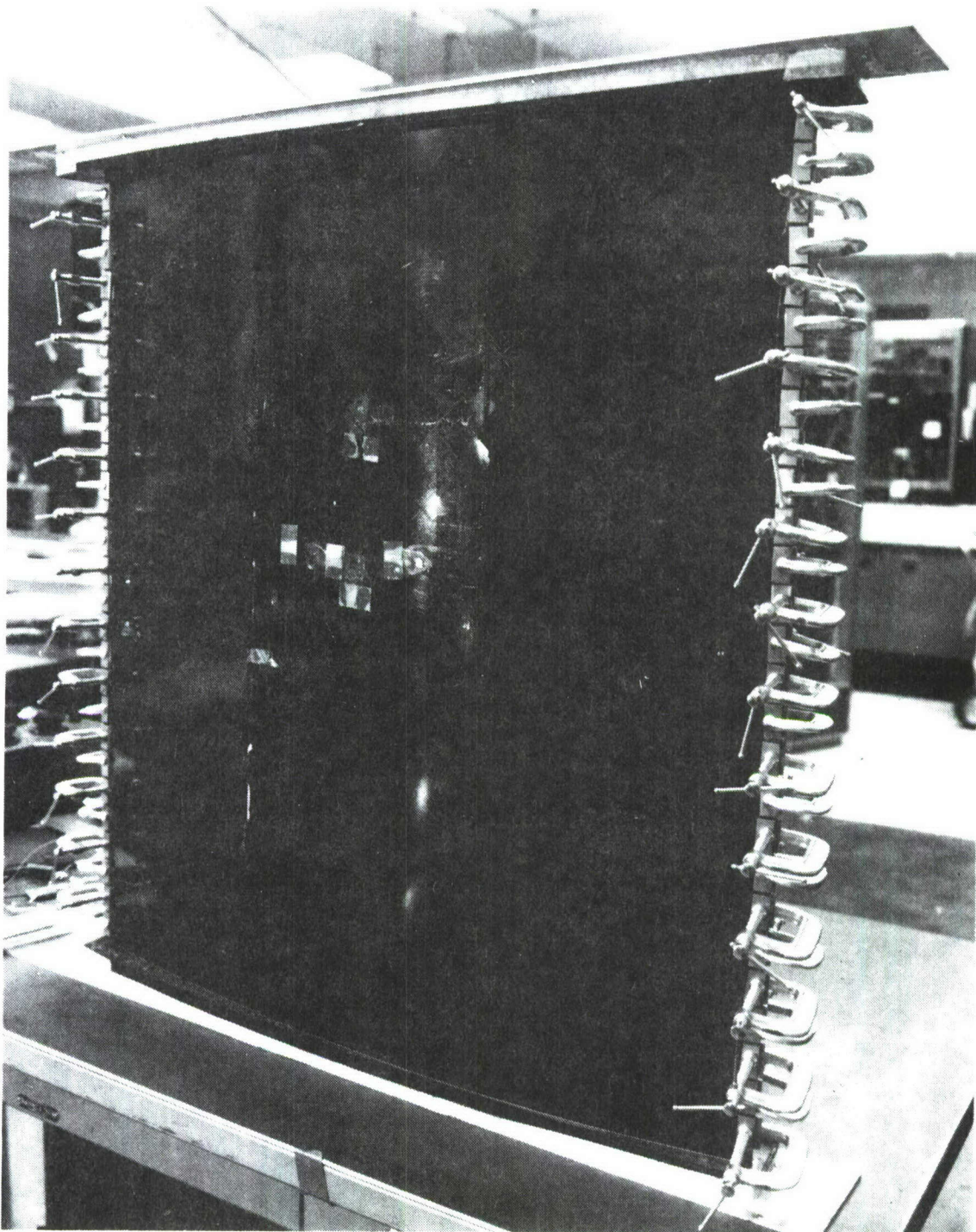
Fig. 39 Panel No. 1 after testing. The failure mode consists of vertical fractures that occur where the thickened base under the hat stiffeners tapers down to the skin thickness. Failure is due to excessive stresses caused by sharp changes in skin curvature that occur in the locally postbuckled panel. These large stresses are predicted by PANDA2.
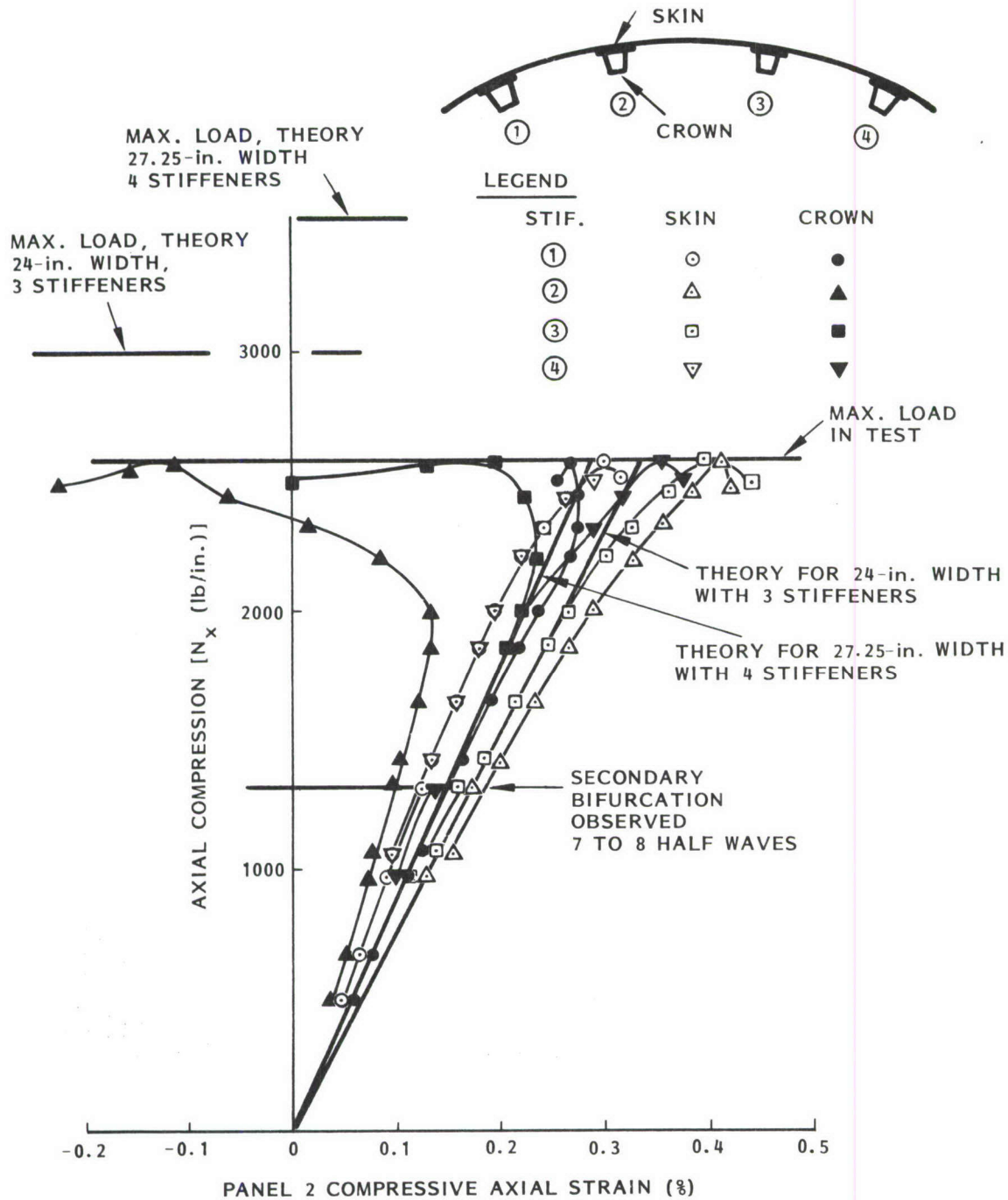
Fig. 40 Load-strain curves for axially compressed large Panel No. 2.
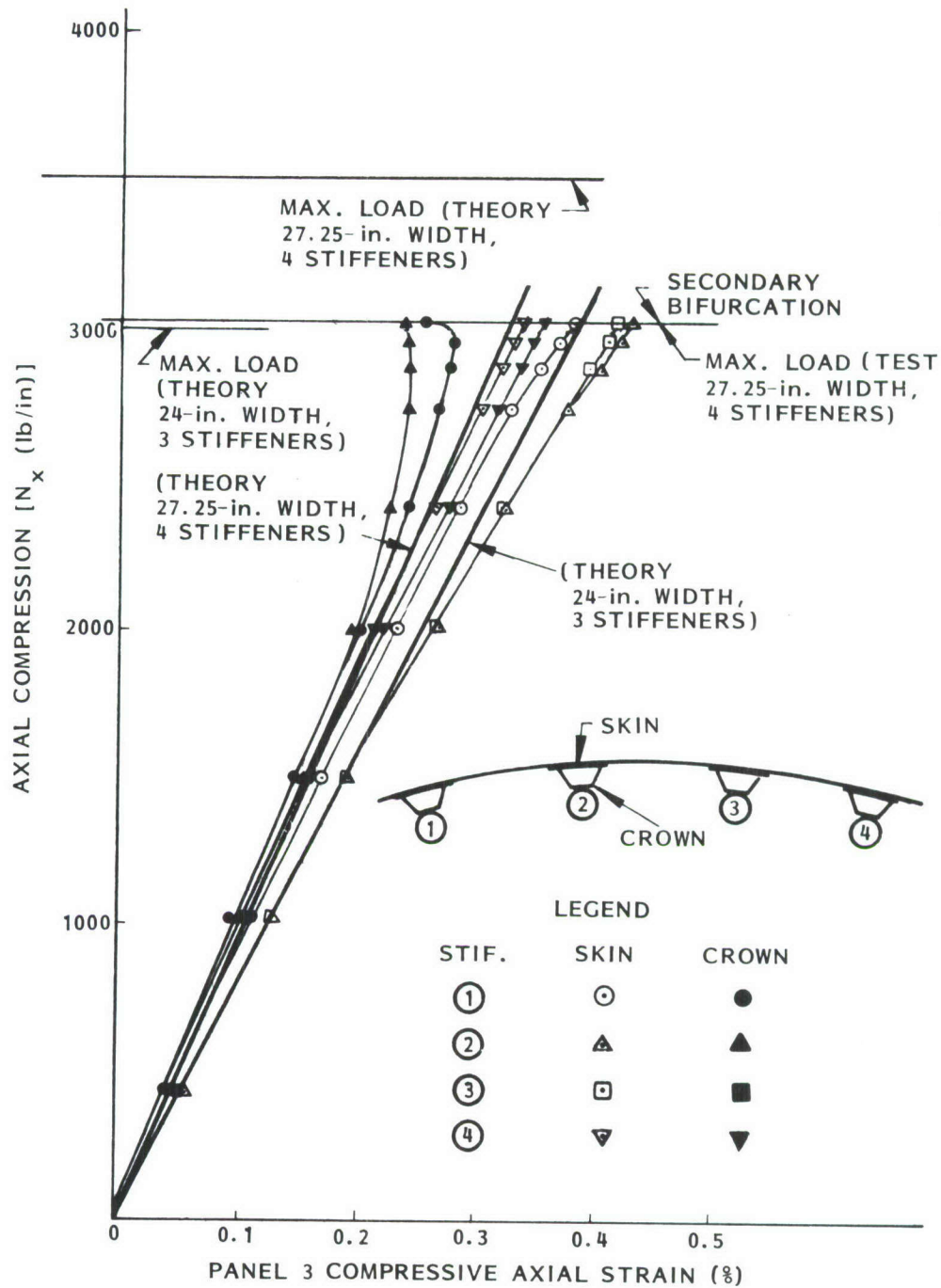
Fig. 41 Load-strain curves for axially compressed large Panel No. 3.

184
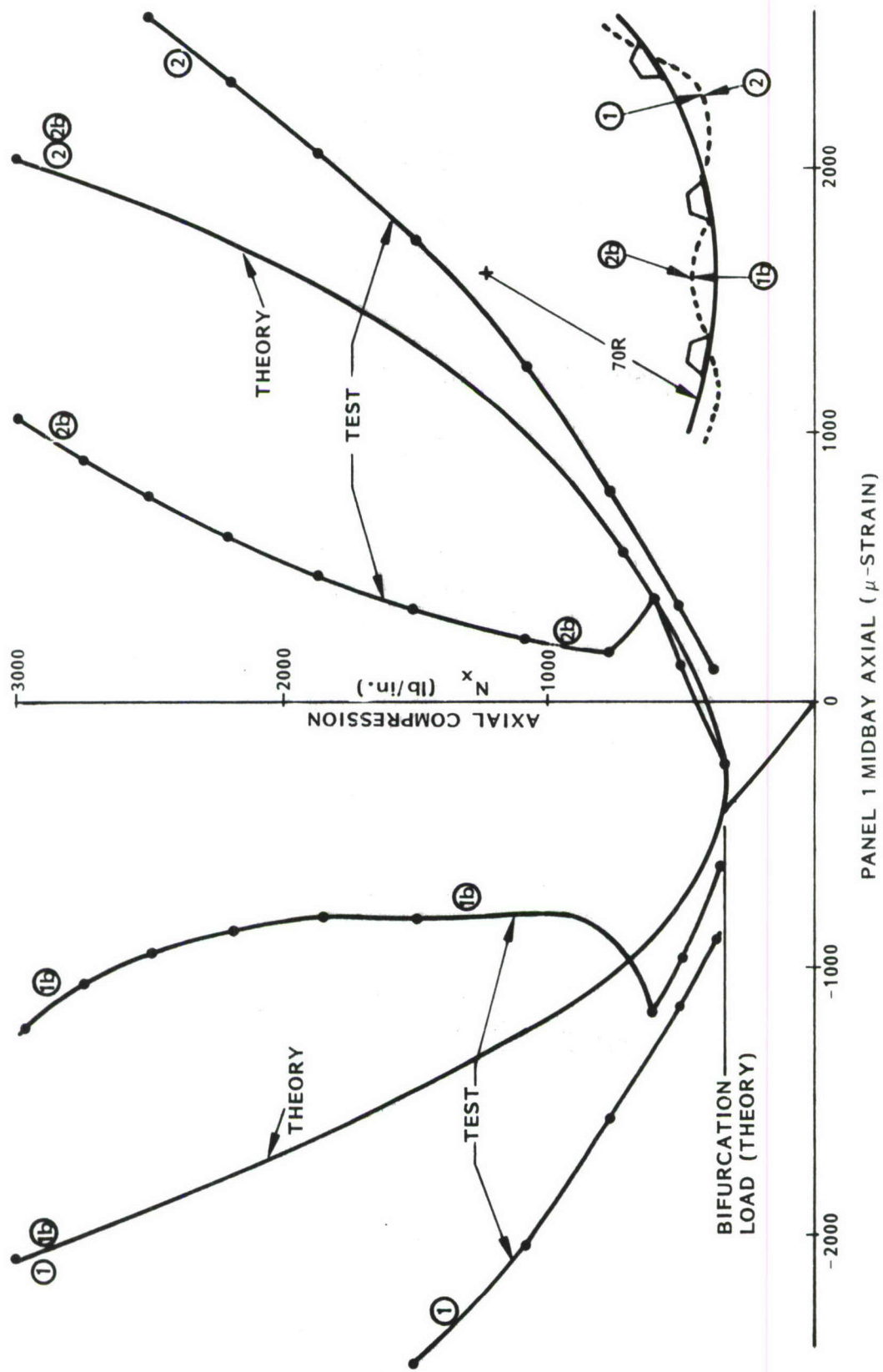
Fig. 42 Axial strain at inward and outward buckles midway between stringers 2 and 3 in Panel No. 1.

185
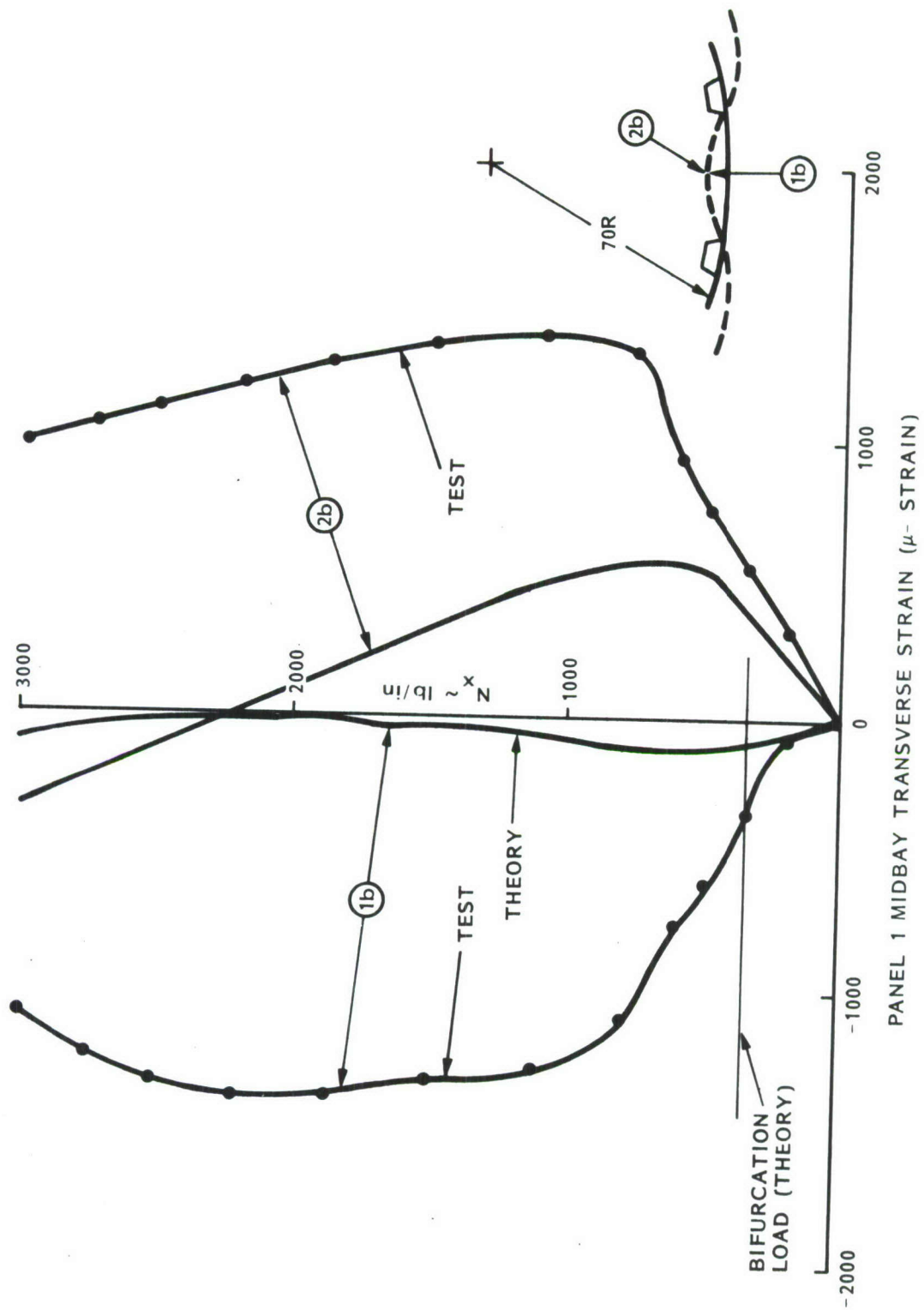
Fig. 43 Hoop strain at an inward buckle midway between stringers 2 and 3 in Panel No. 1.
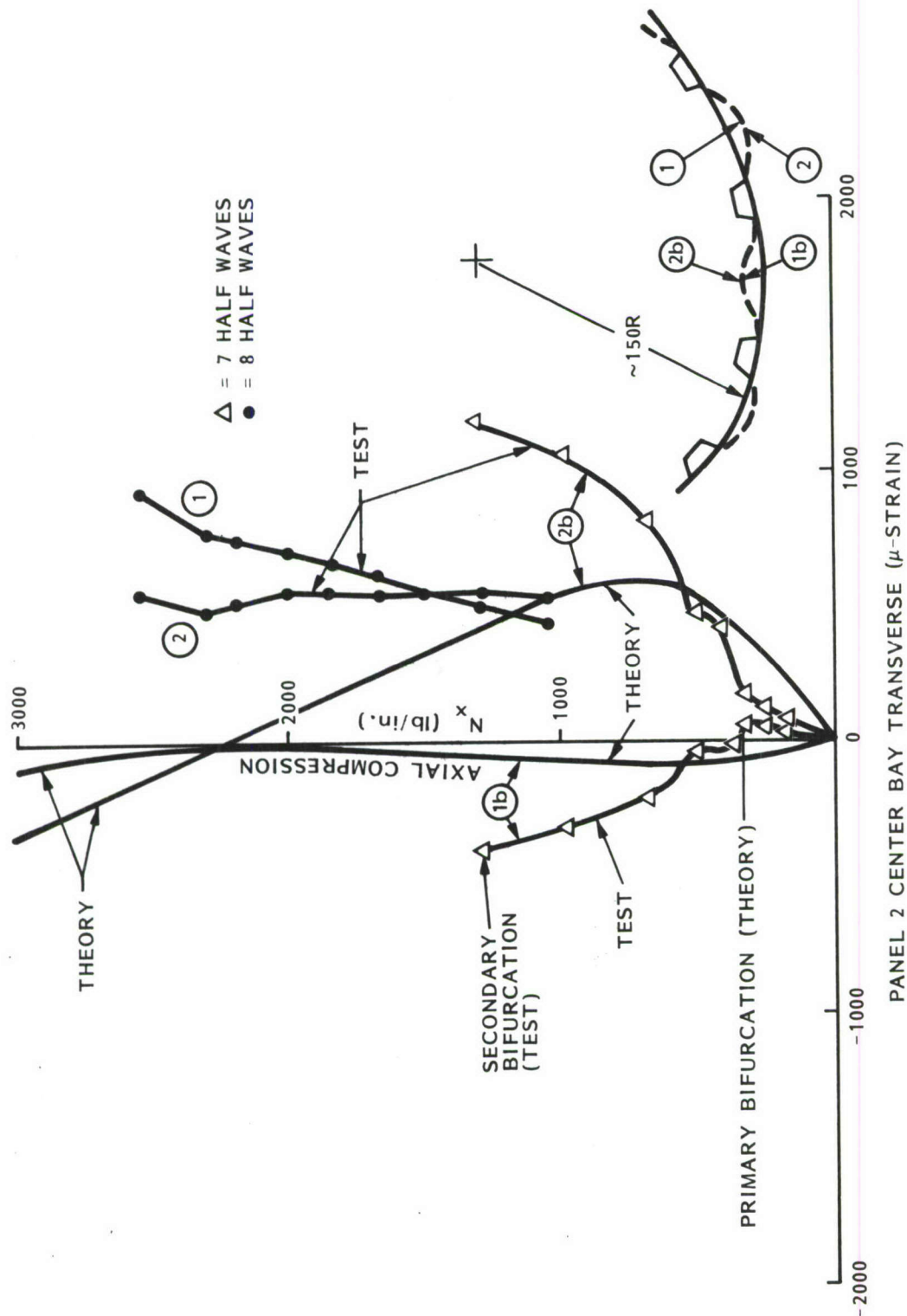
Fig. 44 Hoop strain at an inward buckle midway between stringers 2 and 3 prior to secondary bifurcation and at an outward buckle at the same location after secondary bifurcation, Panel No. 2.

187
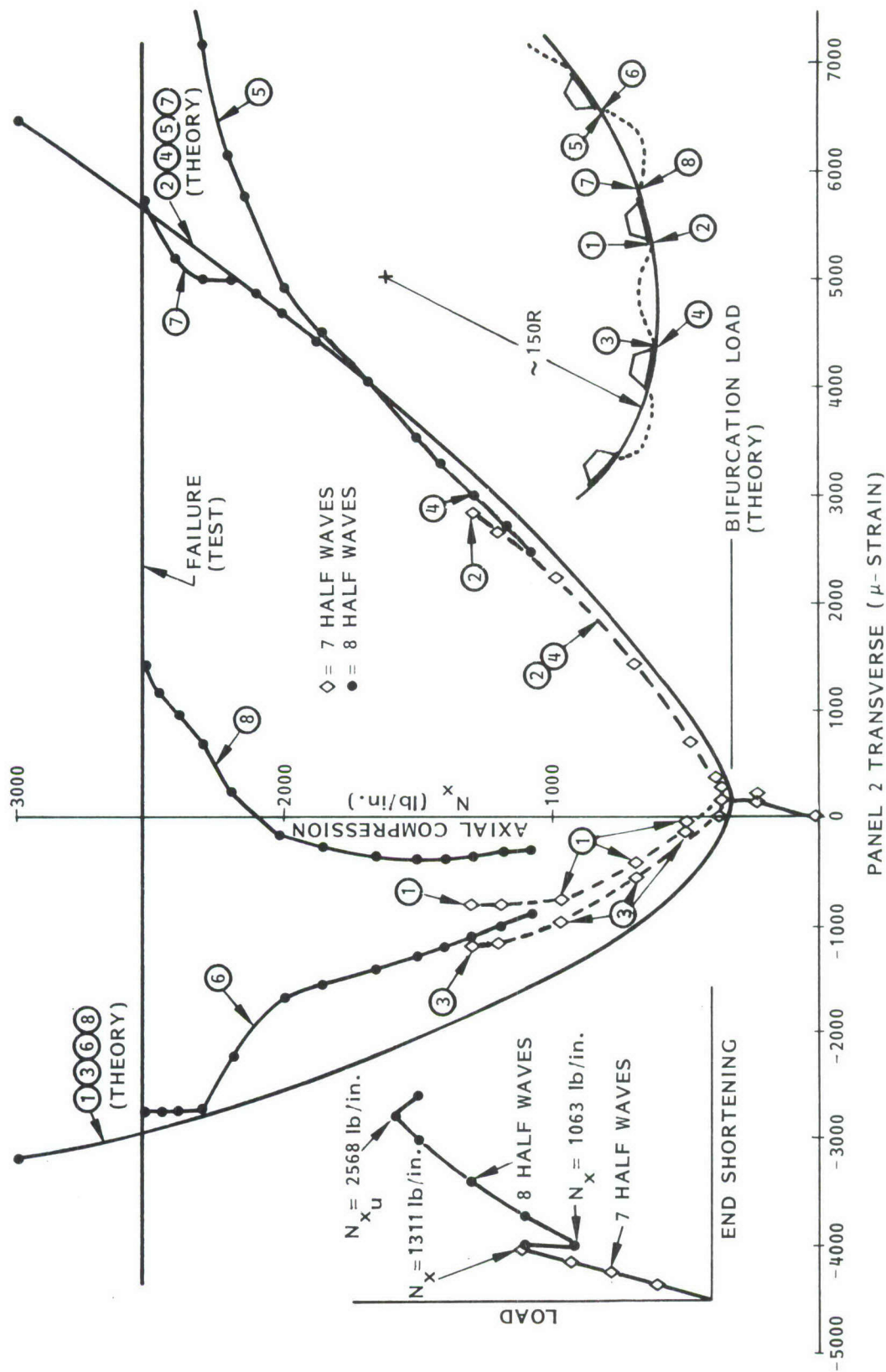
Fig. 45 Hoop strain next to the stringer bases in the middle bay at an inward buckle prior to secondary bifurcation and at an outward buckle after secondary bifurcation, Panel No. 2.
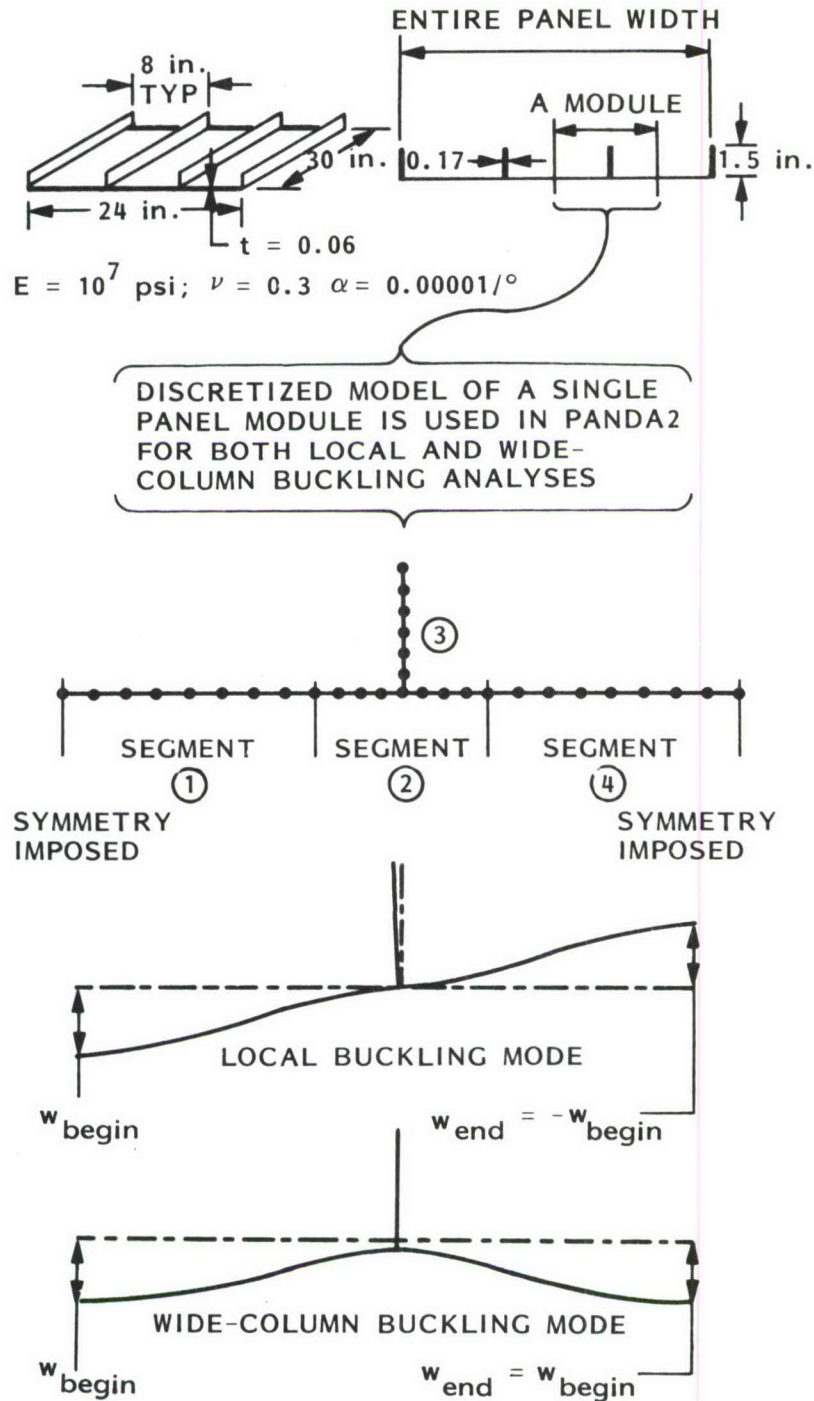
Fig. 46 (a) Blade stiffened aluminum panel. Loading is uniform axial compression N_x or uniform pressure p or combinations of axial compression and pressure.
(b) Discretized model of a single panel module.
(c) Local buckling mode is induced by imposing antisymmetrical normal displacement w about the attachment line of the stringer to the panel skin.
(d) Wide column (general) instability is induced by imposing symmetrical w about the attachment line of the stringer to the panel skin.

189

FOR $p \neq 0$ $\begin{cases} u = v = w = o \\ \text{ROT. FREE} \end{cases}$

FOR $N_x \neq 0$ {FREE EDGE

SYMMETRY

10
9
8
7
6
5
4
3
2
1

$\mathbb{C}$

$\mathbb{C}$

SYMMETRY

$L/2 = 15$ in.

$t = 0.06$ in.

AXIAL NODE 0
NUMBER

y

x

FOR $p \neq 0$ $\begin{cases} u = v = w = 0 \\ \text{ROT. FREE} \end{cases}$

$N_x \neq 0$ $\begin{cases} \text{CLAMPED WITH} \\ \text{IMPOSED END} \\ \text{SHORTENING} \end{cases}$

DETAIL

t
t
t
t

{ PURPOSE OF NARROW FINITE
ELEMENTS IS TO CAPTURE
LOCAL STRAIN PEAK UNDER
STRINGER
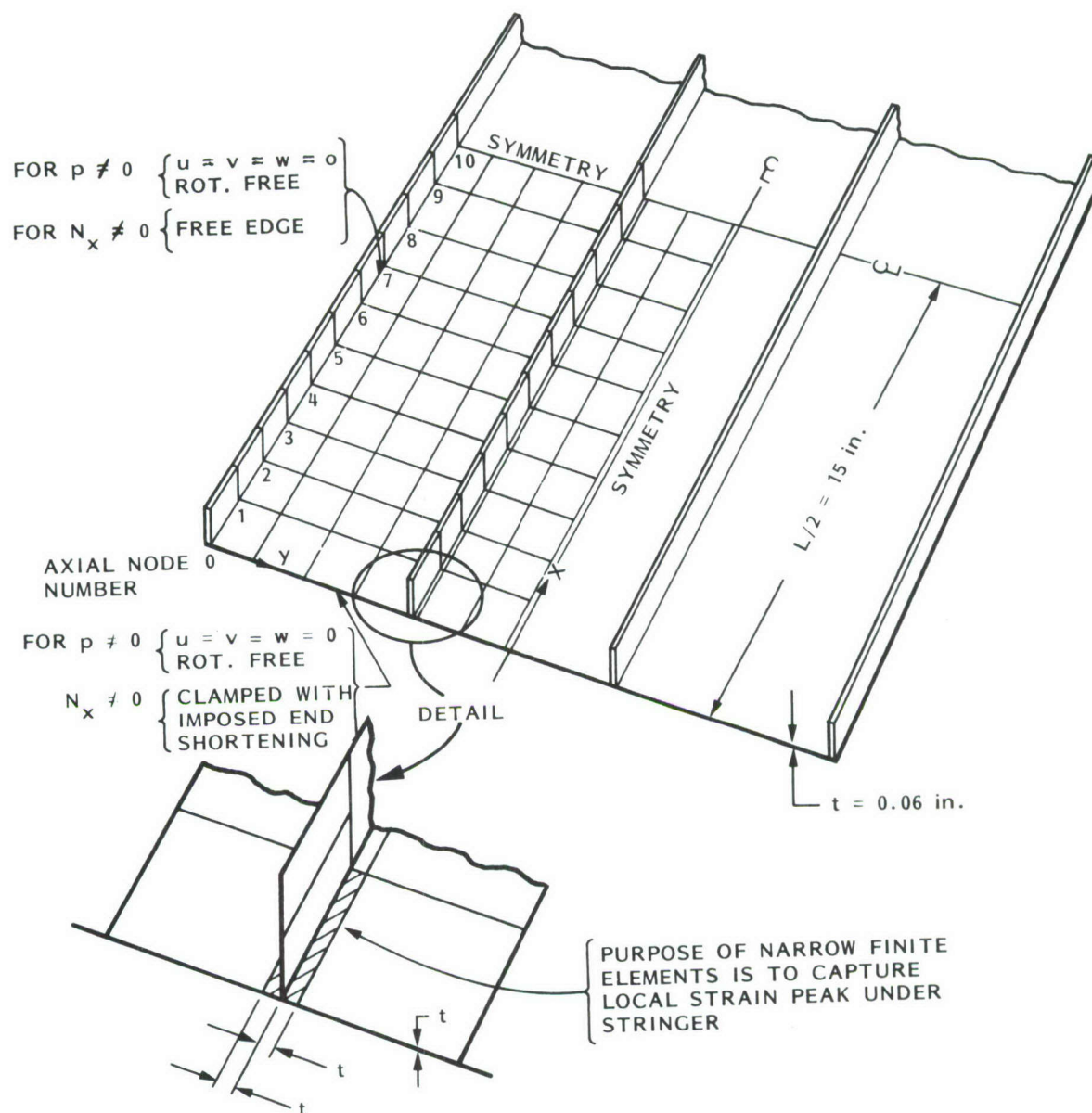
Fig. 47 Discretized model used for the STAGSC-1 analysis of the panel under uniform normal pressure p. The STAGSC-1 model for the case with uniform axial compression N_x is analogous, although the compression model has an extra finite element on either side of the stringer not at the edge and runs the entire 30–inch length rather than having a symmetry plane at midlength.

190
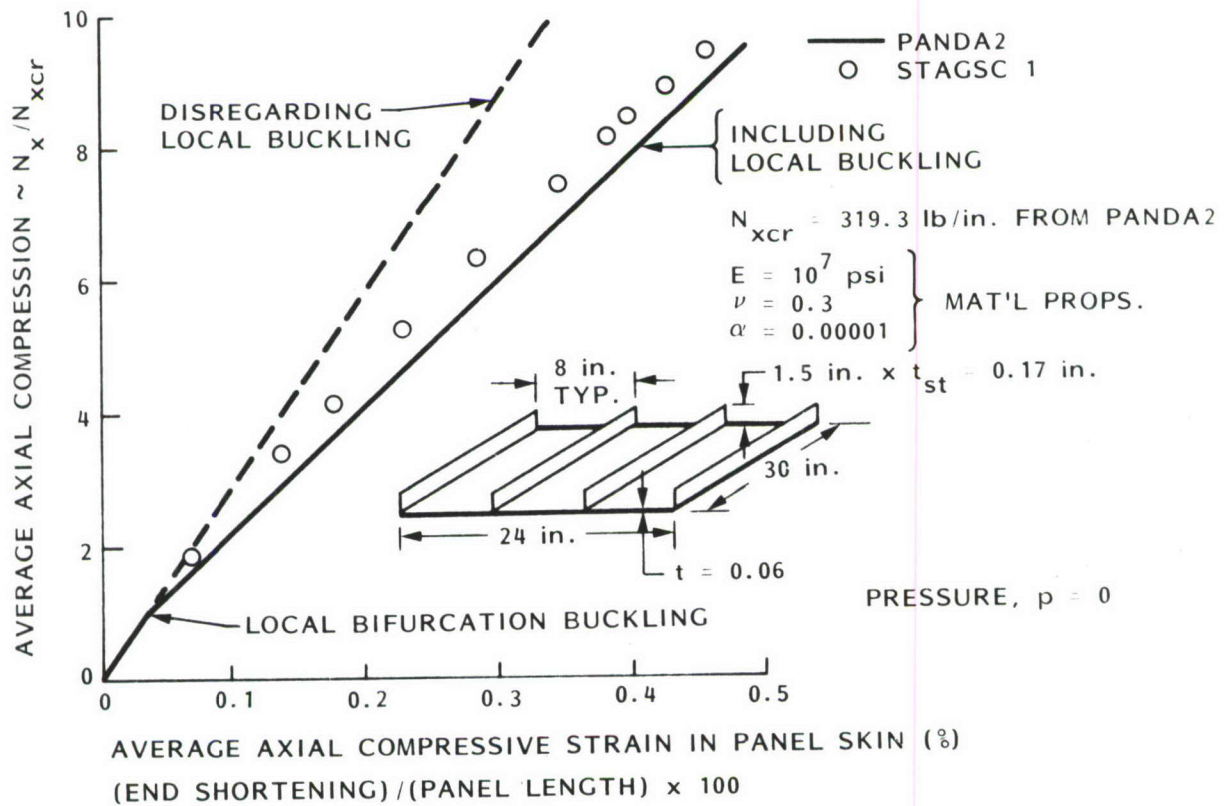
Fig. 48 Load–end–shortening for uniformly axially compressed panel. Local buckling pattern has five axial half-waves. The STAGS result shows more axial stiffness because the STAGS model has stringers at each edge (4 stringers in a width of 24 inches), whereas the PANDA2 model has 3 stringers in the width of 24 inches.
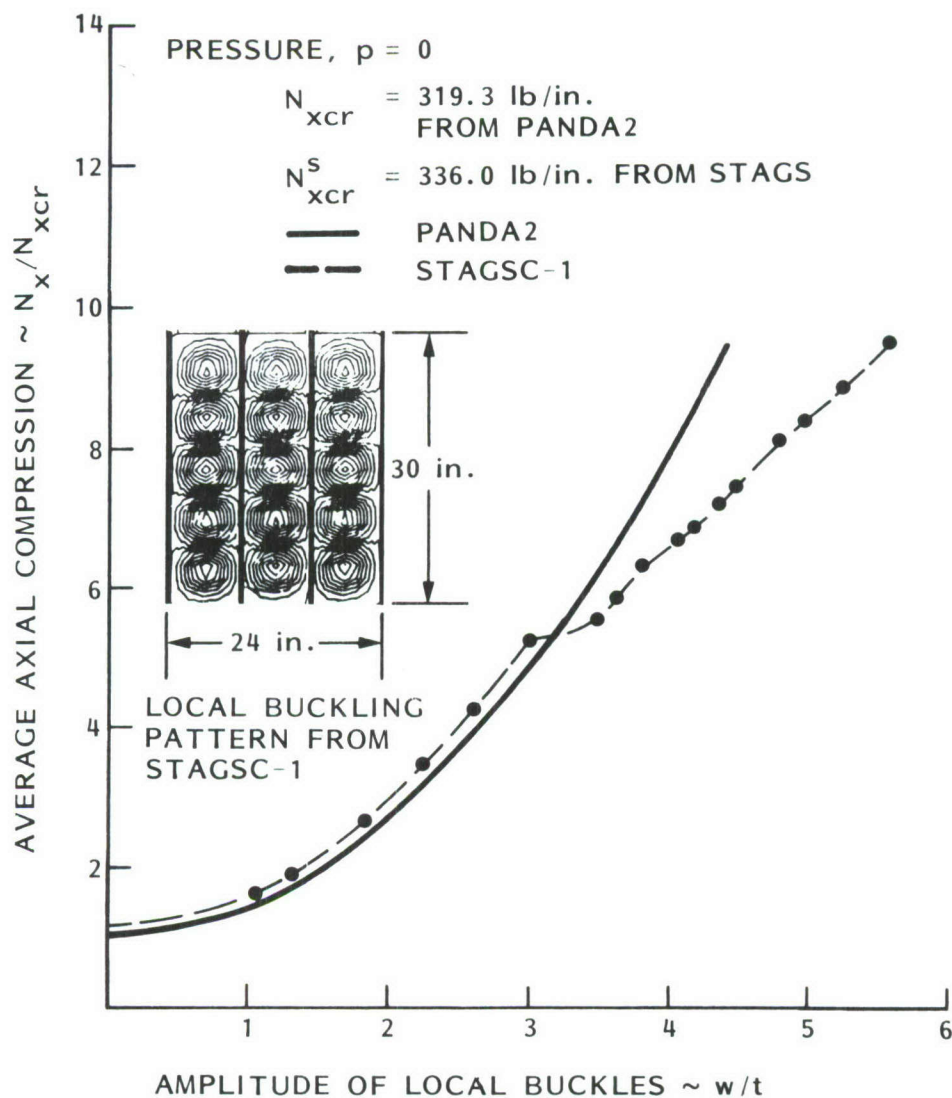
Fig. 49 Normal deflection w at the center of the panel. The bifurcation buckling load factor predicted from **STAGSC-1** is 336 lb/in., compared with PANDA2's prediction of 319 lb/in.. The difference is due to the axial restraint at the loaded end of the panel, present in the local bifurcation buckling problem in the **STAGS** model but absent in the local bifurcation buckling problem in the **PANDA2** model.
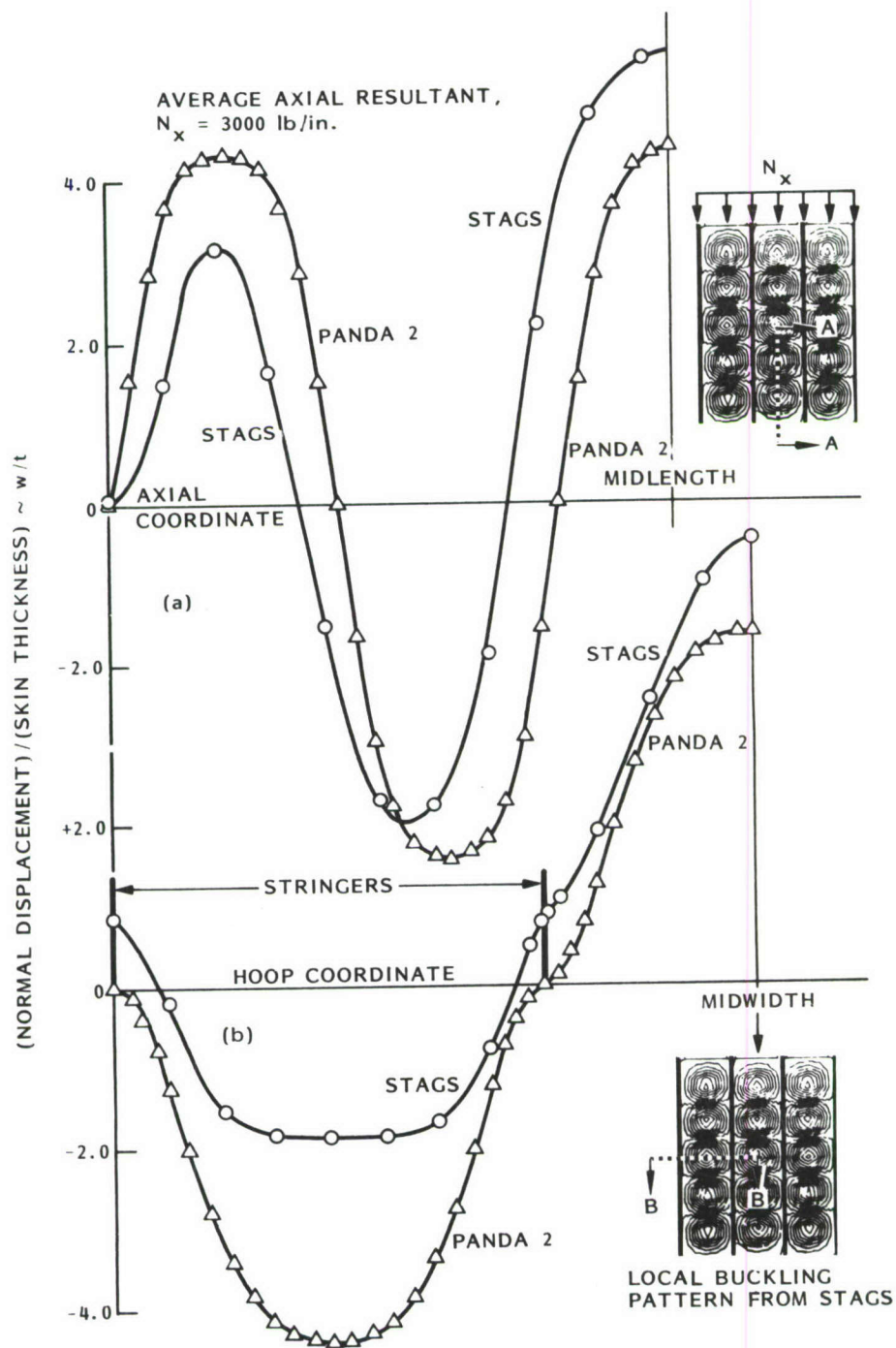
Fig. 50 Normal deflection w as predicted by STAGS and PANDA2 (a) along half the length of the panel in the middle bay and (b) across half the width at the midlength symmetry plane.
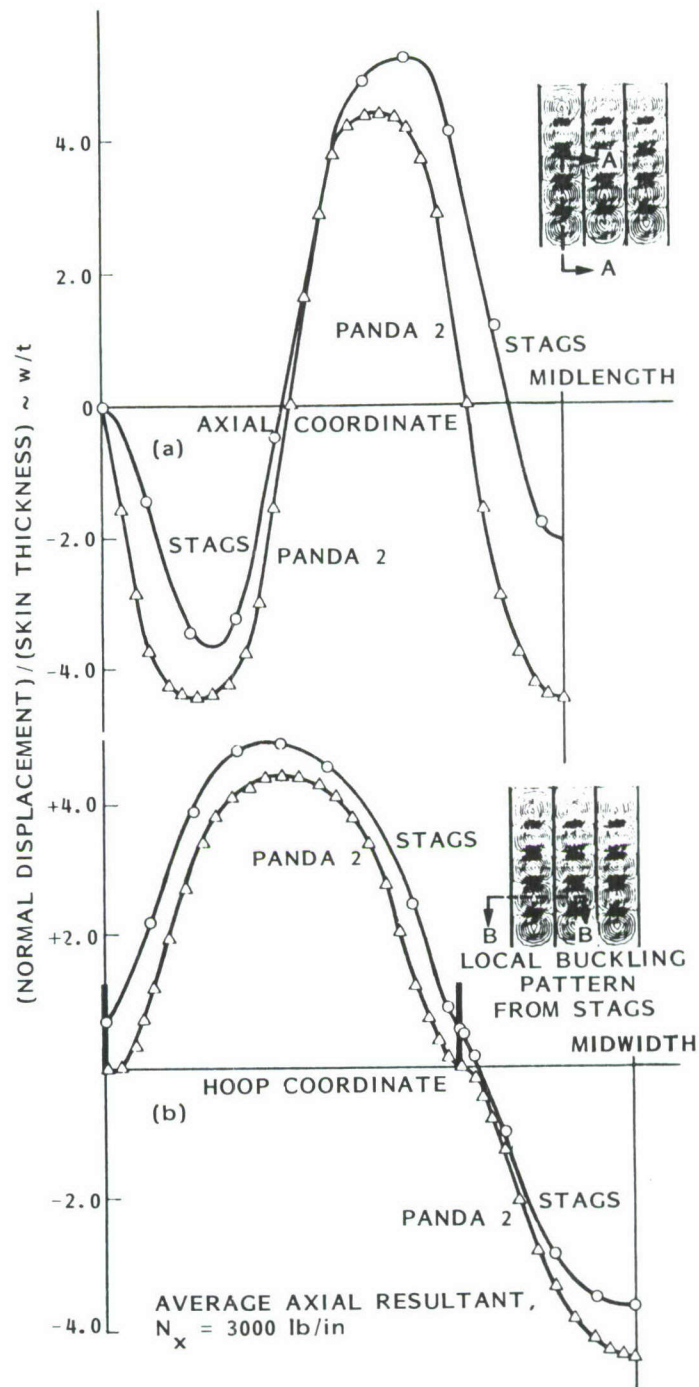
Fig. 51 Normal deflection w as predicted by STAGS and PANDA2 (a) along half the length of the panel in one of the side bays and (b) across half the width at one quarter of the length.

194
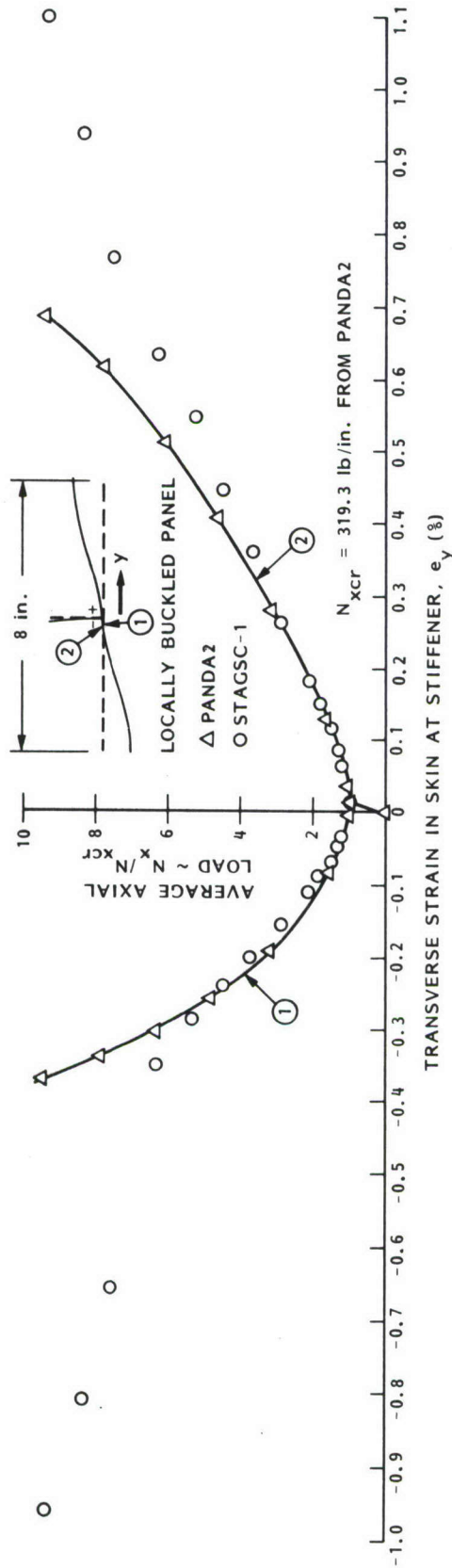
Fig. 52 Maximum transverse ("hoop") strain in the panel skin under the stringer that is not at the edge of the panel, at axial node no. 10. The strains plotted here correspond to the "minus" side of the stringer. These include the largest strain anywhere in the panel.

195
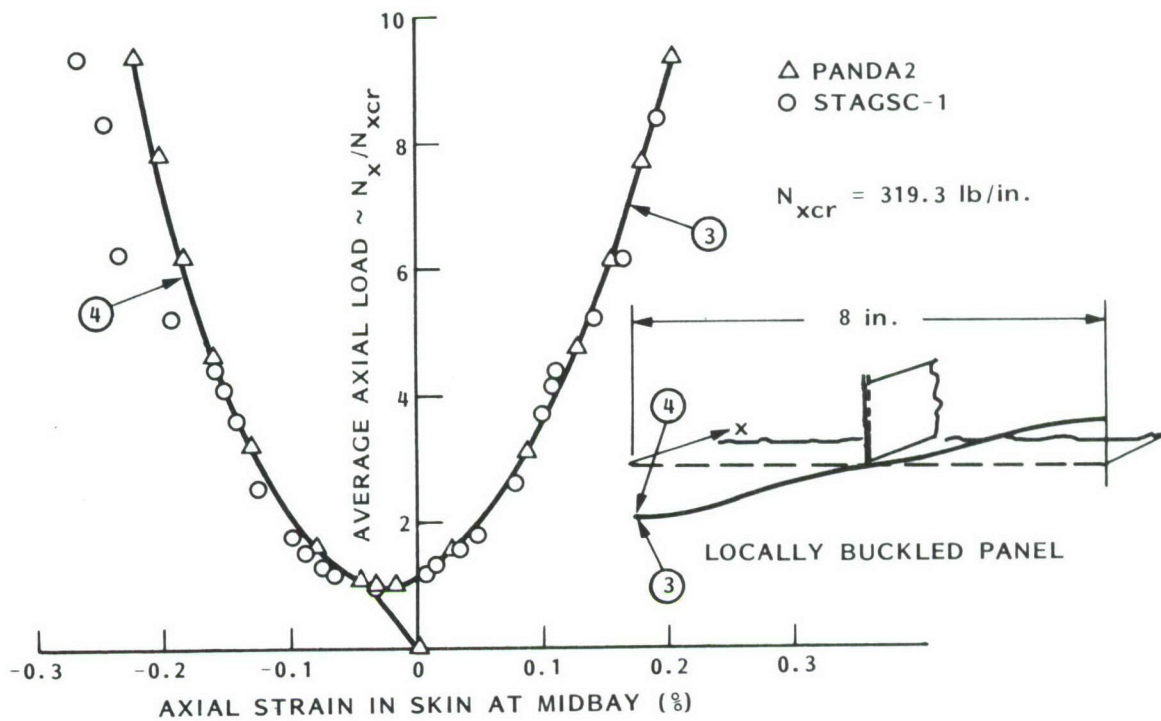
Fig. 53 Maximum axial strain in the panel skin at the midwidth of the panel. The STAGSC-1 results correspond to a point at axial node no. 10.
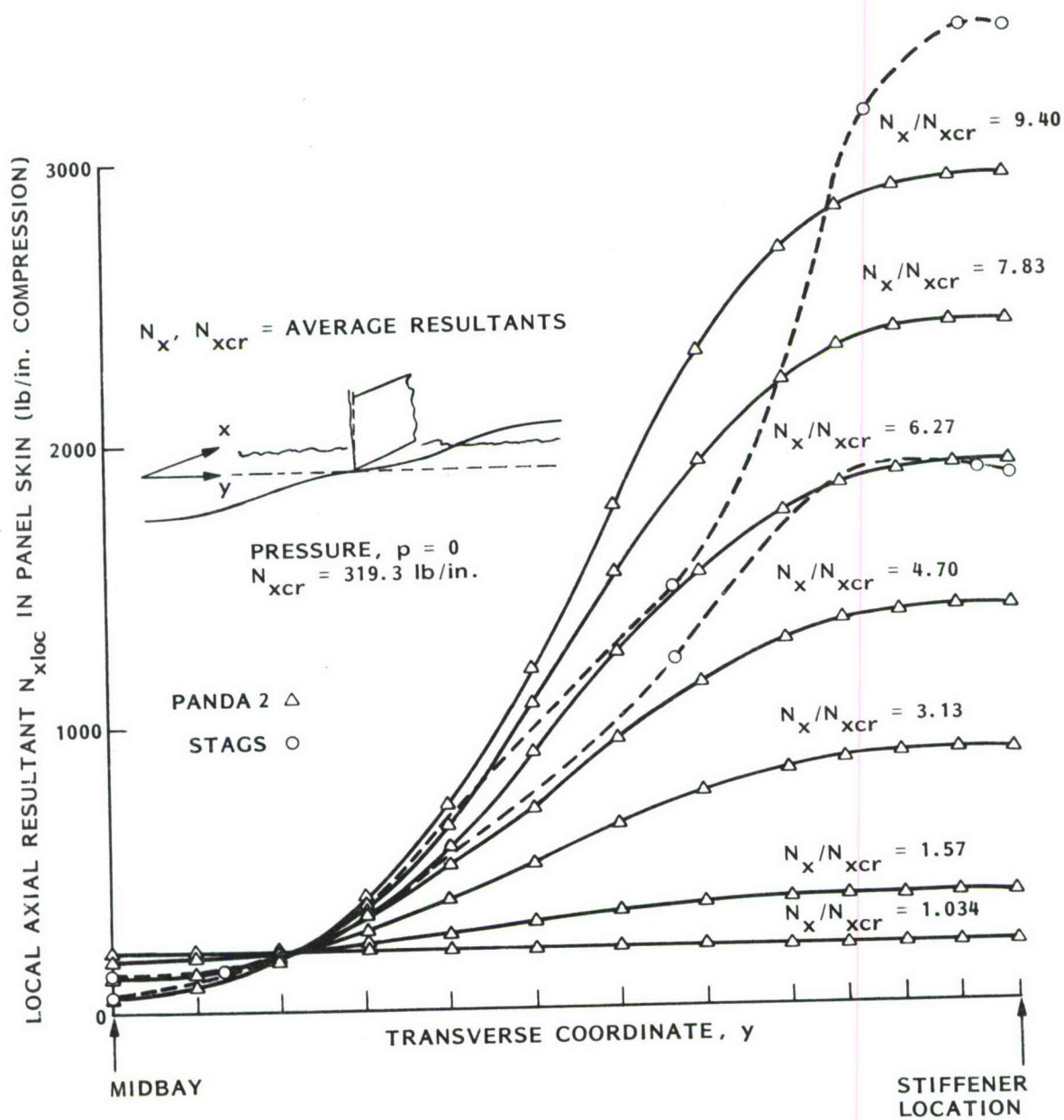
Fig. 54 Local axial resultant, N_x(local), in panel skin for various average axial loads N_x/N_{xcr}. **STAGS** results correspond to values at the axial symmetry line in the bay that includes the center of the panel.

197
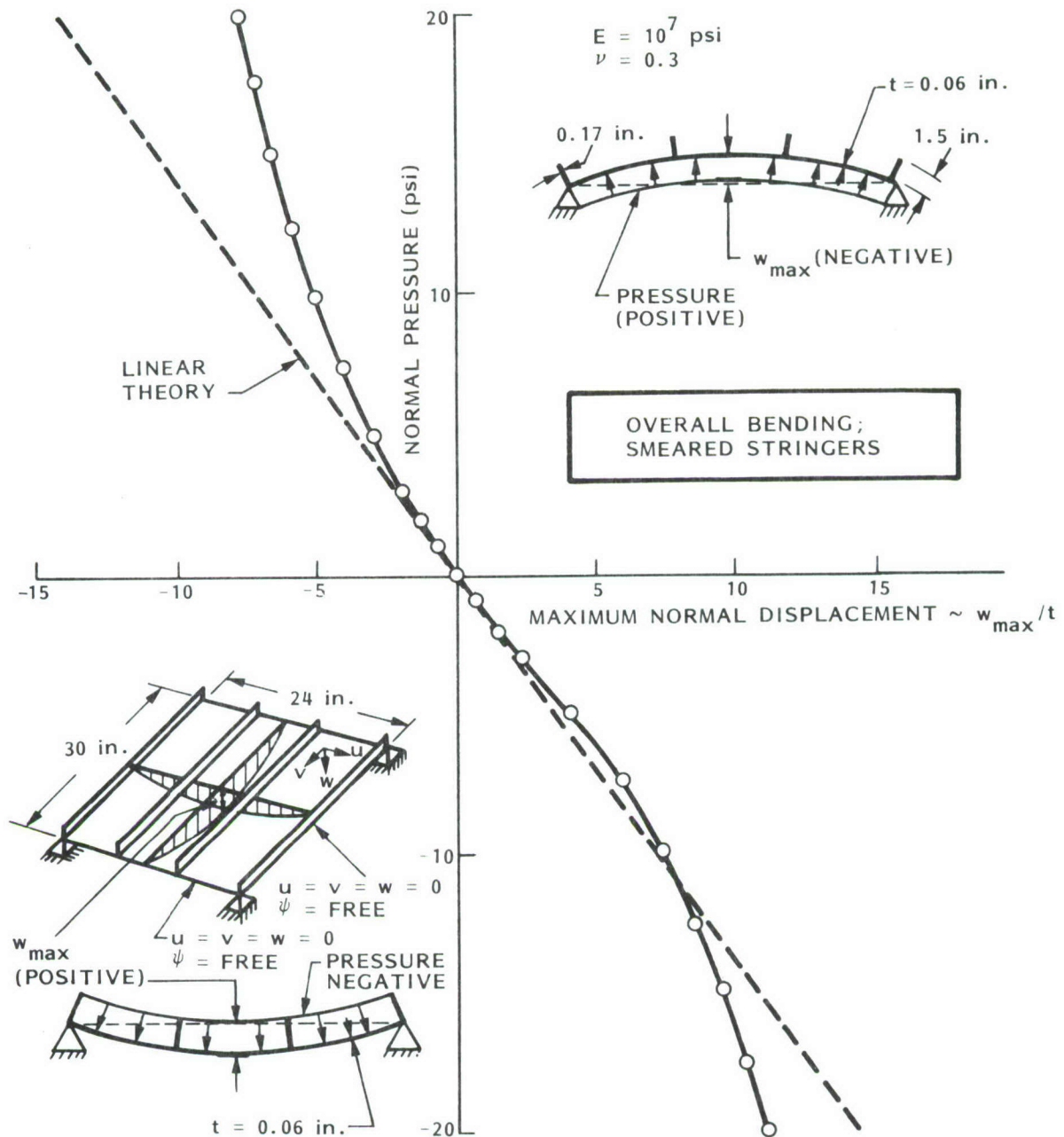
Fig. 55 PANDA2 prediction for the normal deflection w at the center of the panel loaded only by uniform pressure p. In this PANDA2 model the stringers are smeared out, the panel width (y coord.) is discretized with 36 nodes, and displacements are assumed to vary along the length (x coord.) as follows:

$$U(x,y) = u(y)\sin(n\pi x/L), \quad V(x,y) = v(y)\sin(2n\pi x/L), \quad W(x,y) = w(y)\sin(n\pi x/L).$$
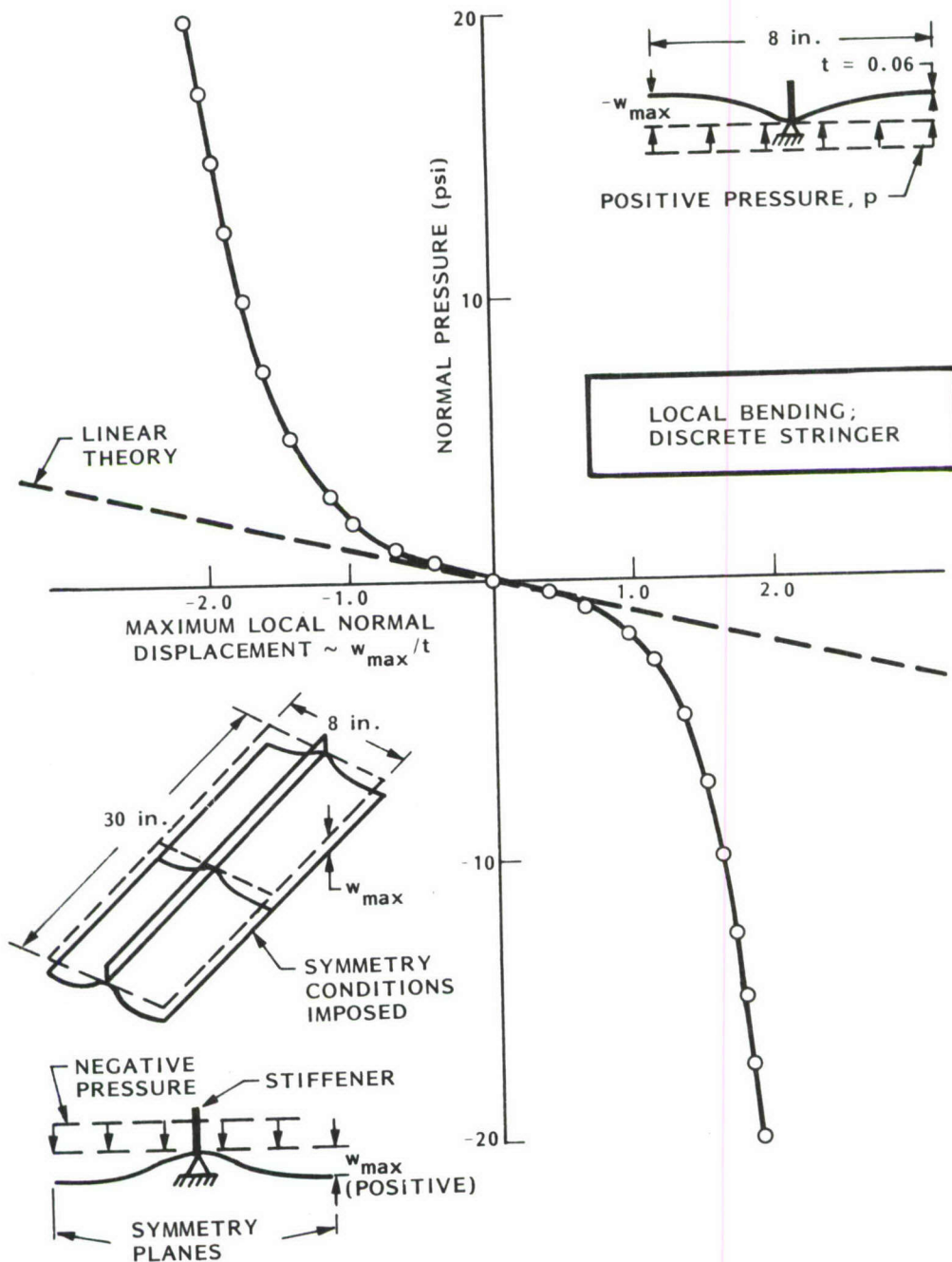
Fig. 56 PANDA2 prediction for the normal deflection w at the symmetry plane midway between stringers for a single-module (discrete stringer) model of a panel loaded only by uniform pressure. In this model the single panel module is discretized as shown in Fig. 46(b); bending of the stringer in its plane is prevented; the panel module is assumed to be infinitely long normal to the plane of the paper; and the membrane prestress state at the center of the panel calculated from the model shown in the previous figure is included in the nonlinear equilibrium analysis.

199
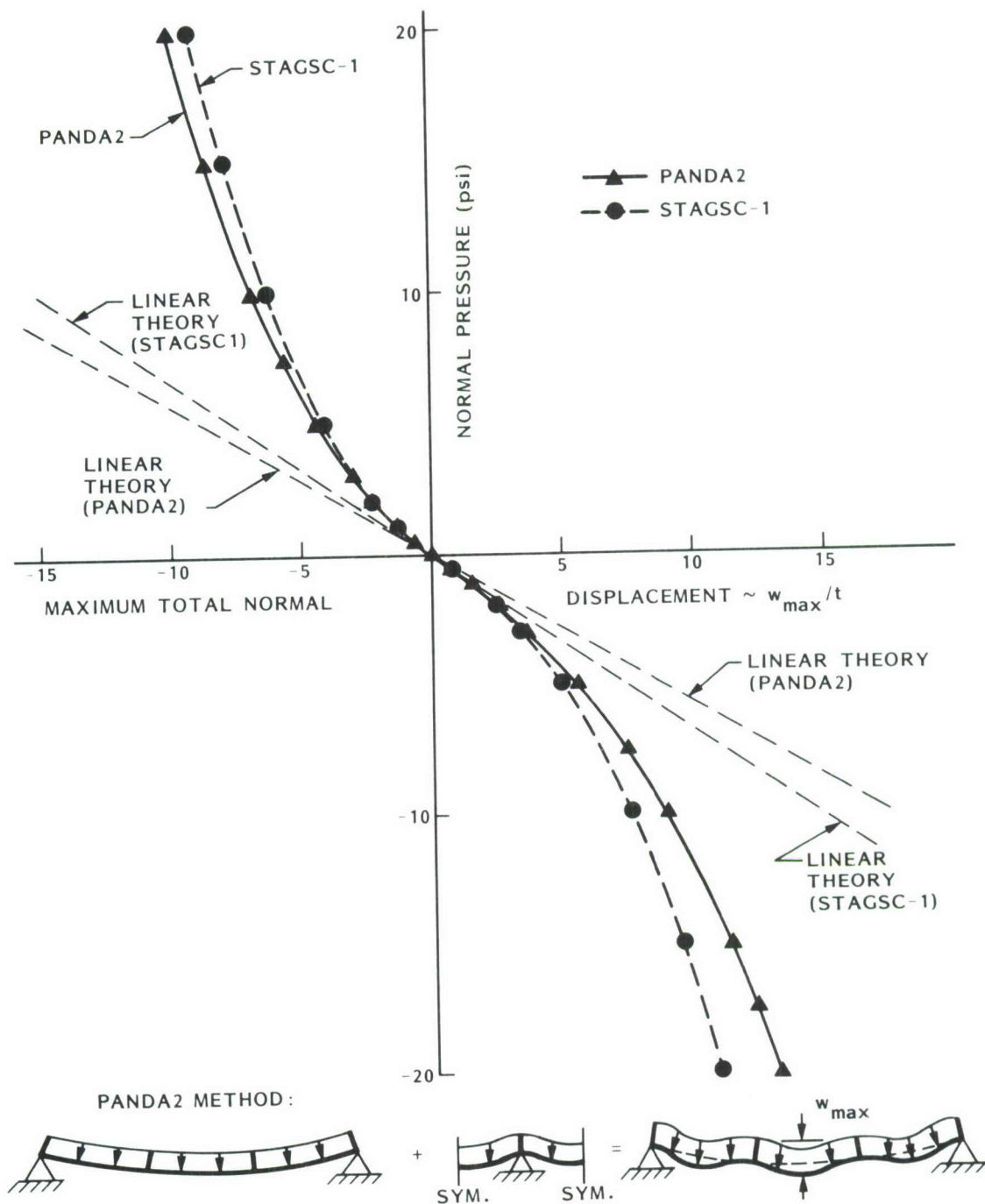
Fig. 57 PANDA2 and STAGS predictions of the normal displacement w at the center of the panel. The PANDA2 prediction is obtained by adding results shown in the previous two figures.

200
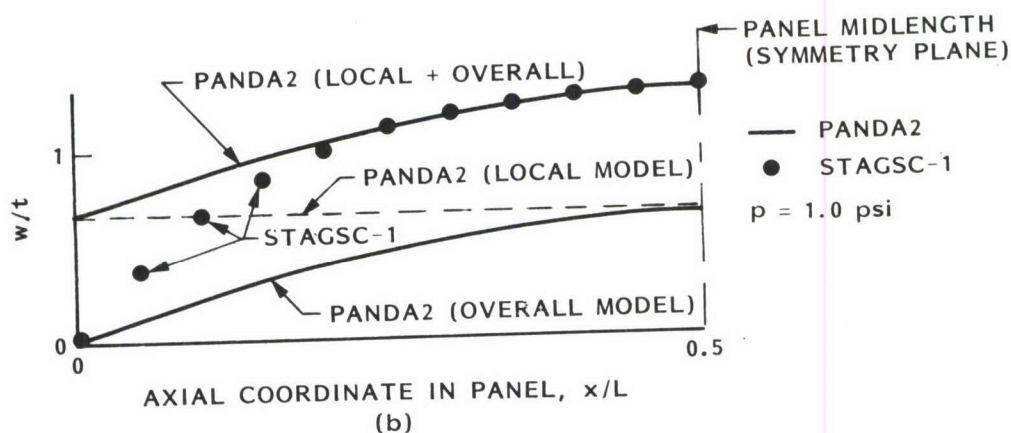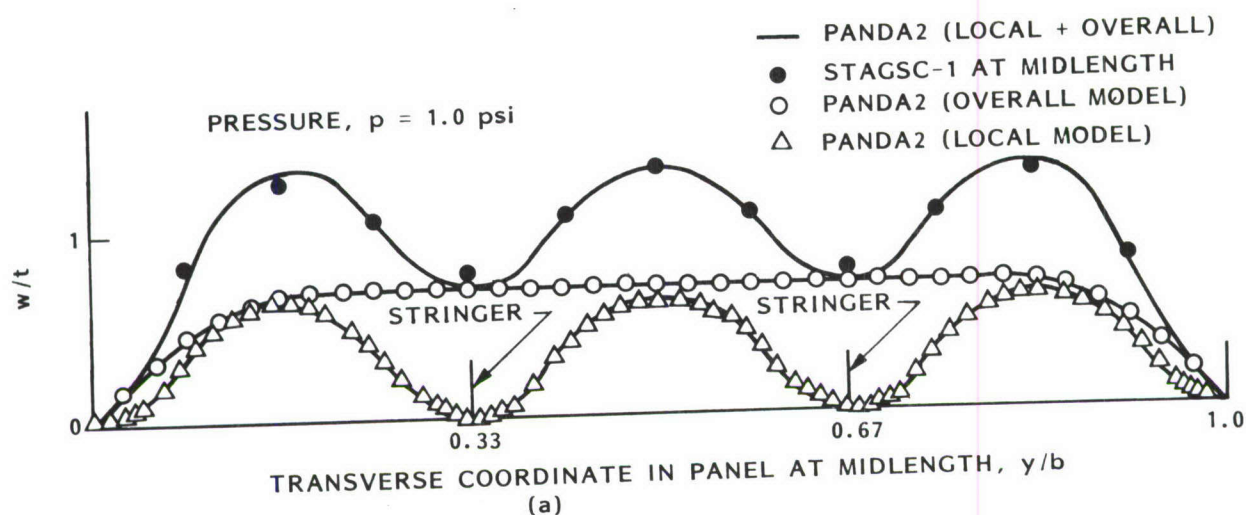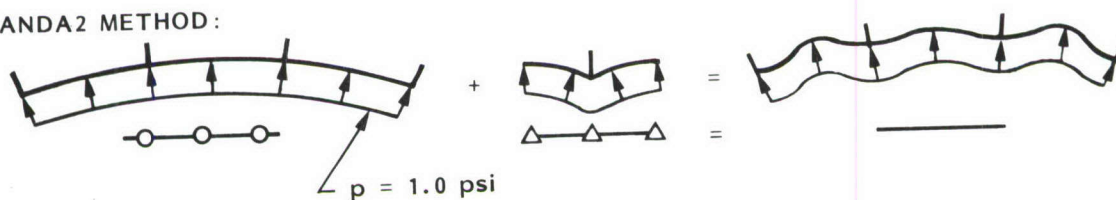
Fig. 58 Comparison between predictions of PANDA2 and STAGS for the normal displacement w (a) across the panel at the axial symmetry plane and (b) along the panel at its midwidth at a pressure, $p = 1.0$ psi.

201
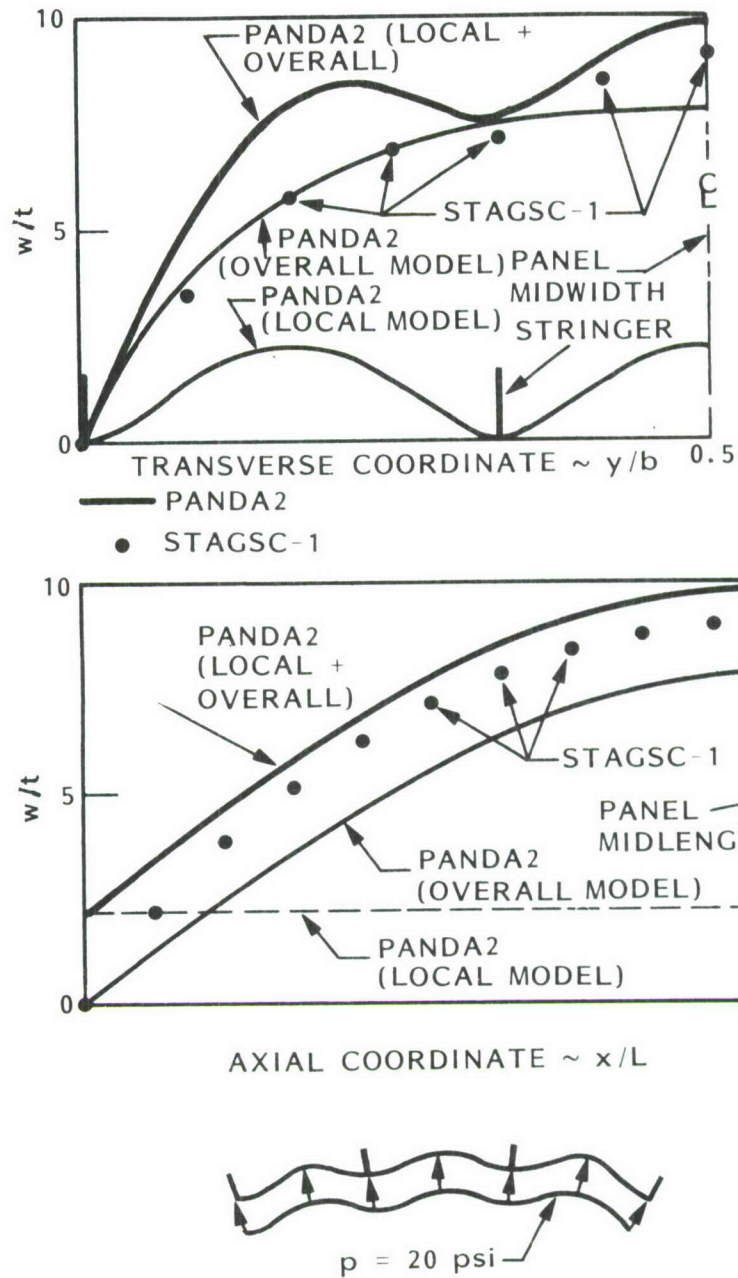
Fig. 59 Comparison between predictions of PANDA2 and STAGS for the normal displacement w (a) across the panel at the axial symmetry plane and (b) along the panel at its midwidth at a pressure, $p = 20.0$ psi.

202
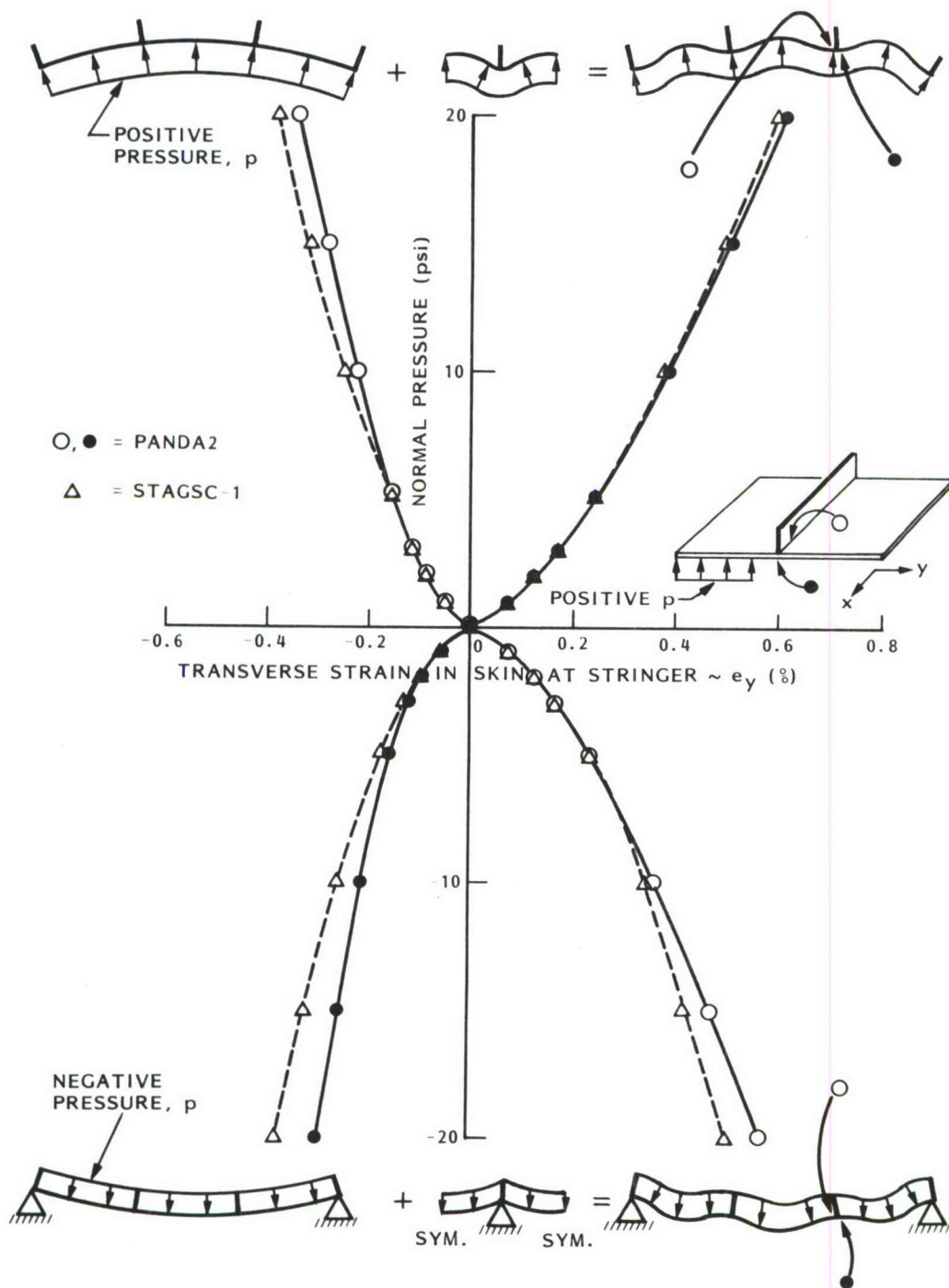
Fig. 60 Comparison of the maximum strains in the panel predicted by PANDA2 and STAGS

203
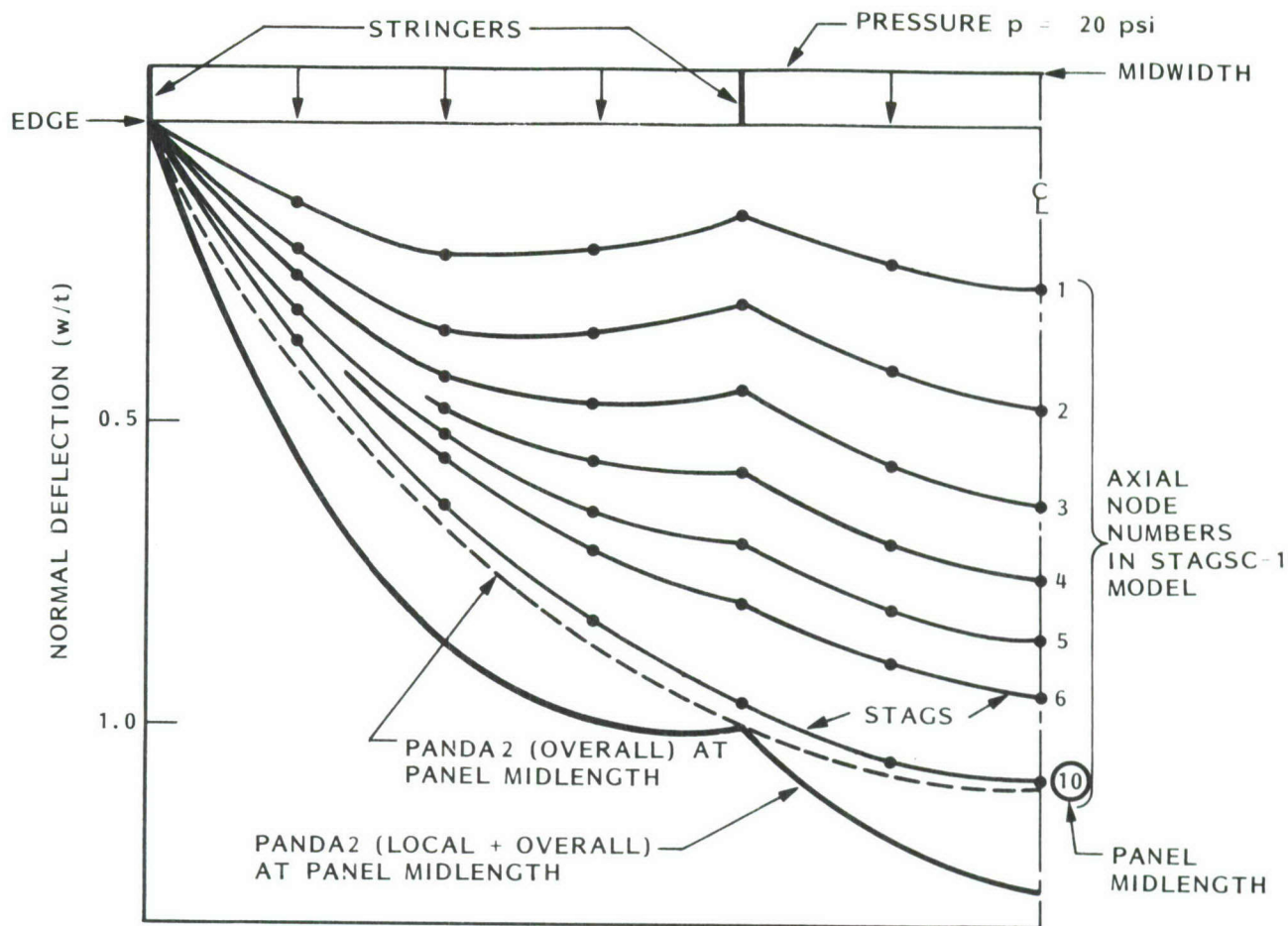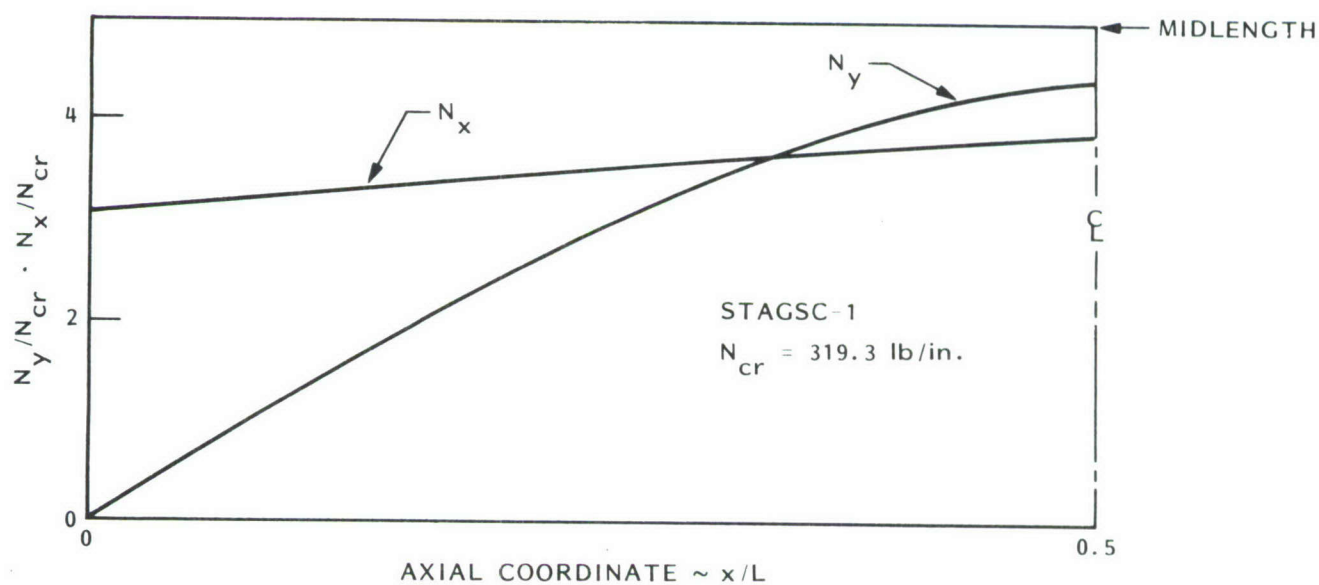
Fig. 61 (a) Distribution of normal displacement w across the width of the panel for pressure, $p = -20$ psi;
(b) STAGS prediction of axial distributions of axial resultant N_x and hoop resultant N_y at the panel midwidth.

204
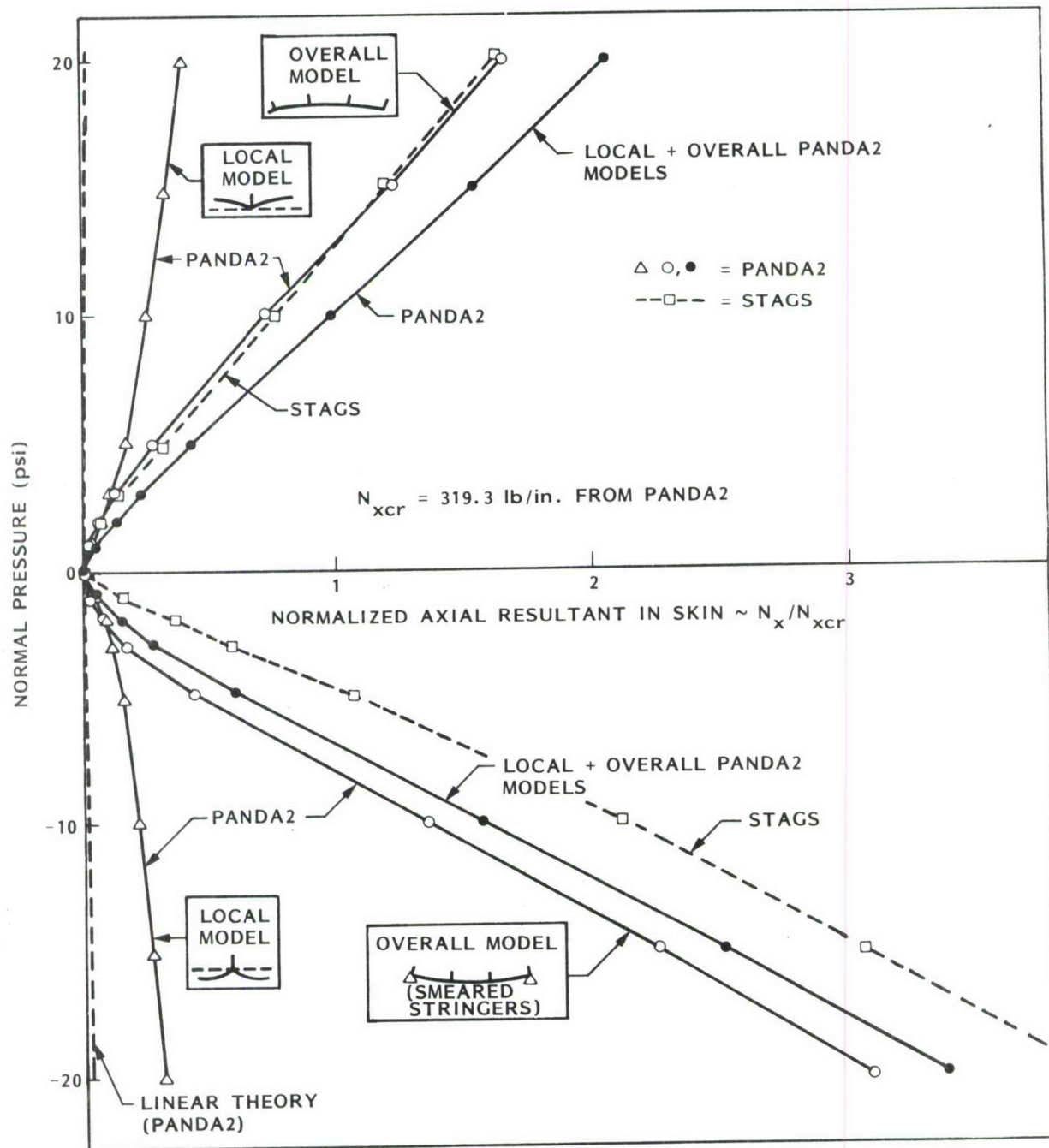
Fig. 62 PANDA2 and STAGS predictions of the axial resultant N_x at the center of the panel.
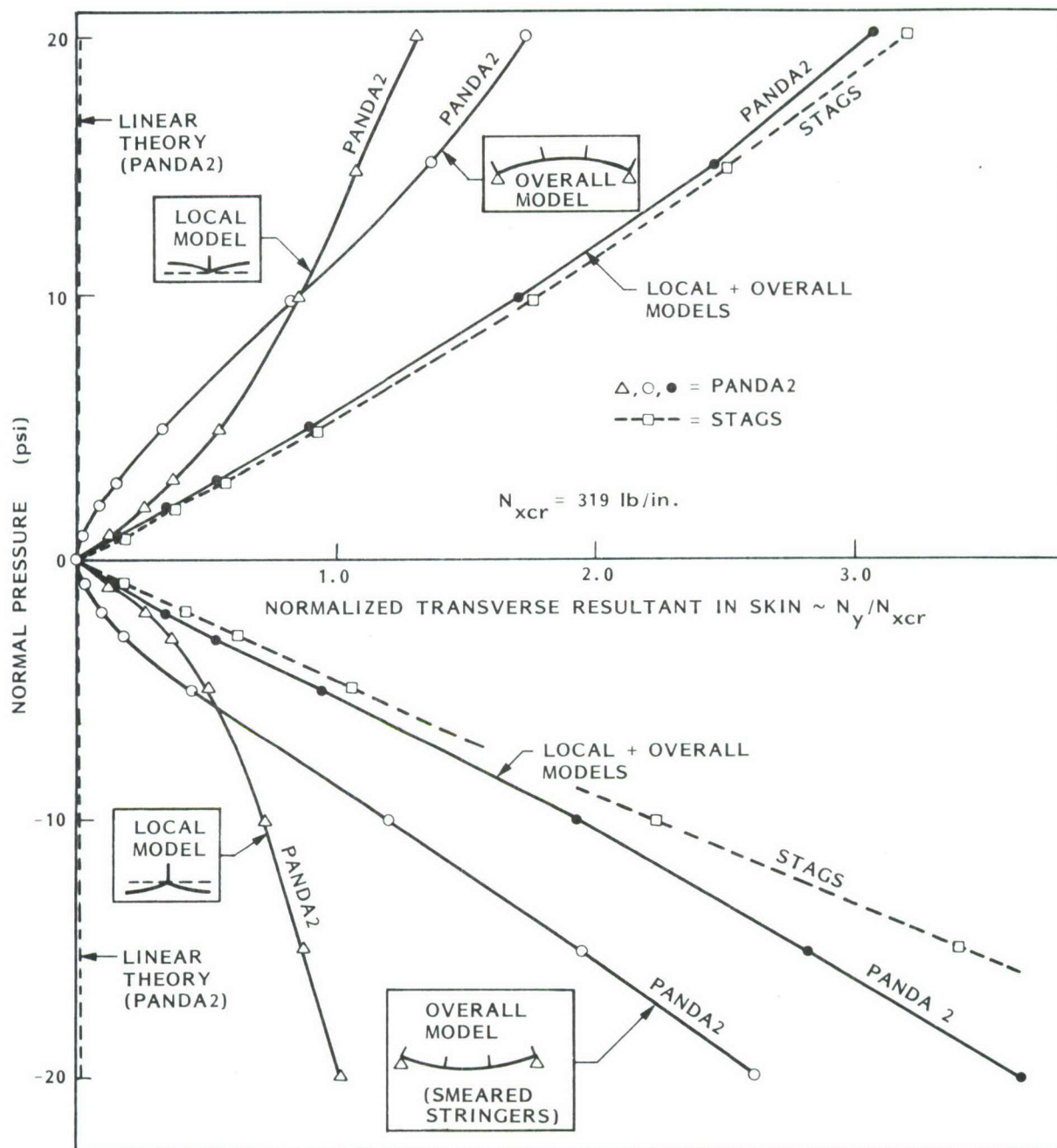
Fig. 63 PANDA2 and STAGS predictions of the transverse ("hoop") resultant N_y at the center of the panel.

206
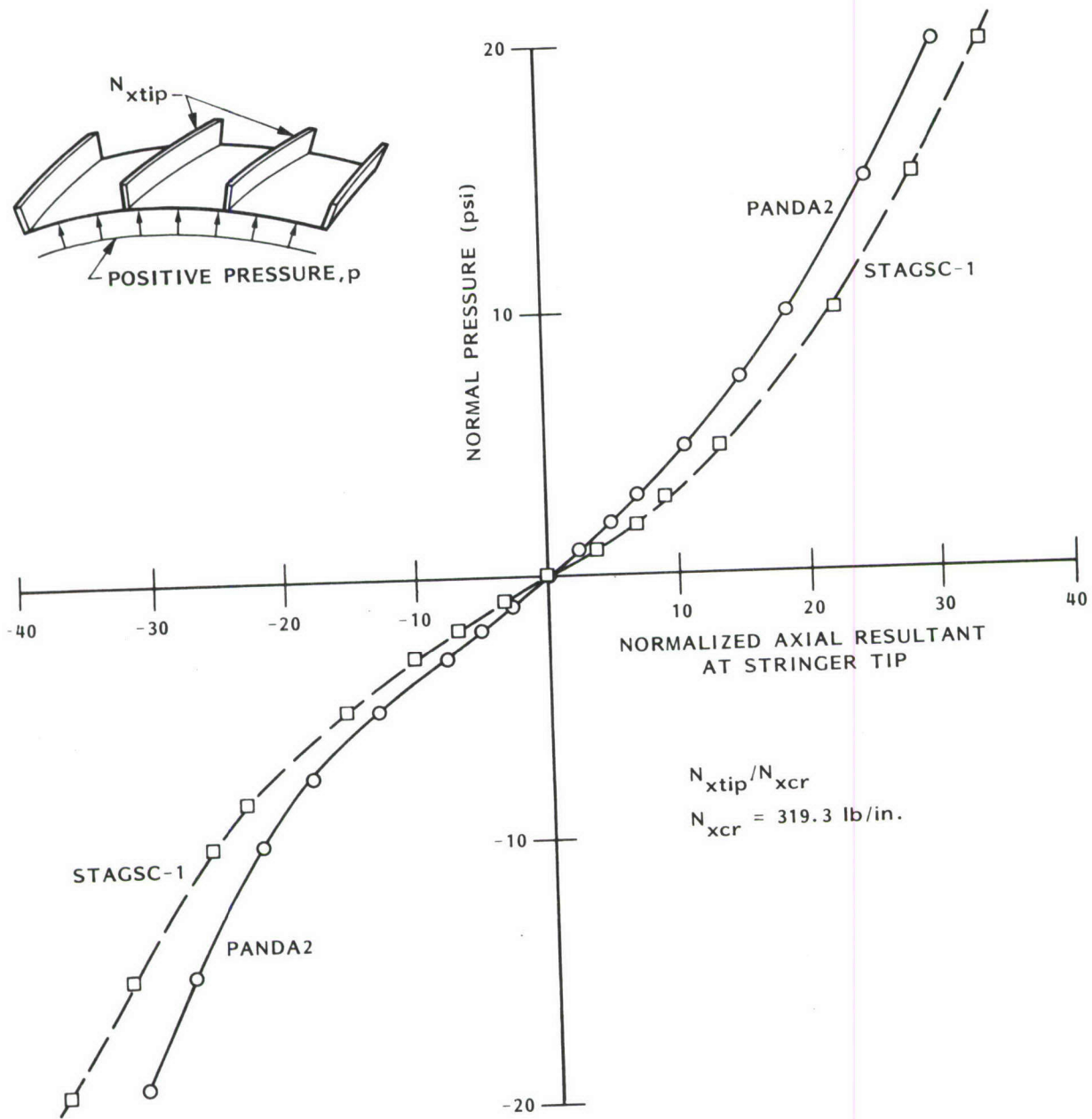
Fig. 64 PANDA2 and STAGS predictions of the axial resultant N_{xtip} at the tips of the stringers that are not at the panel edges, at the midlength of the panel.
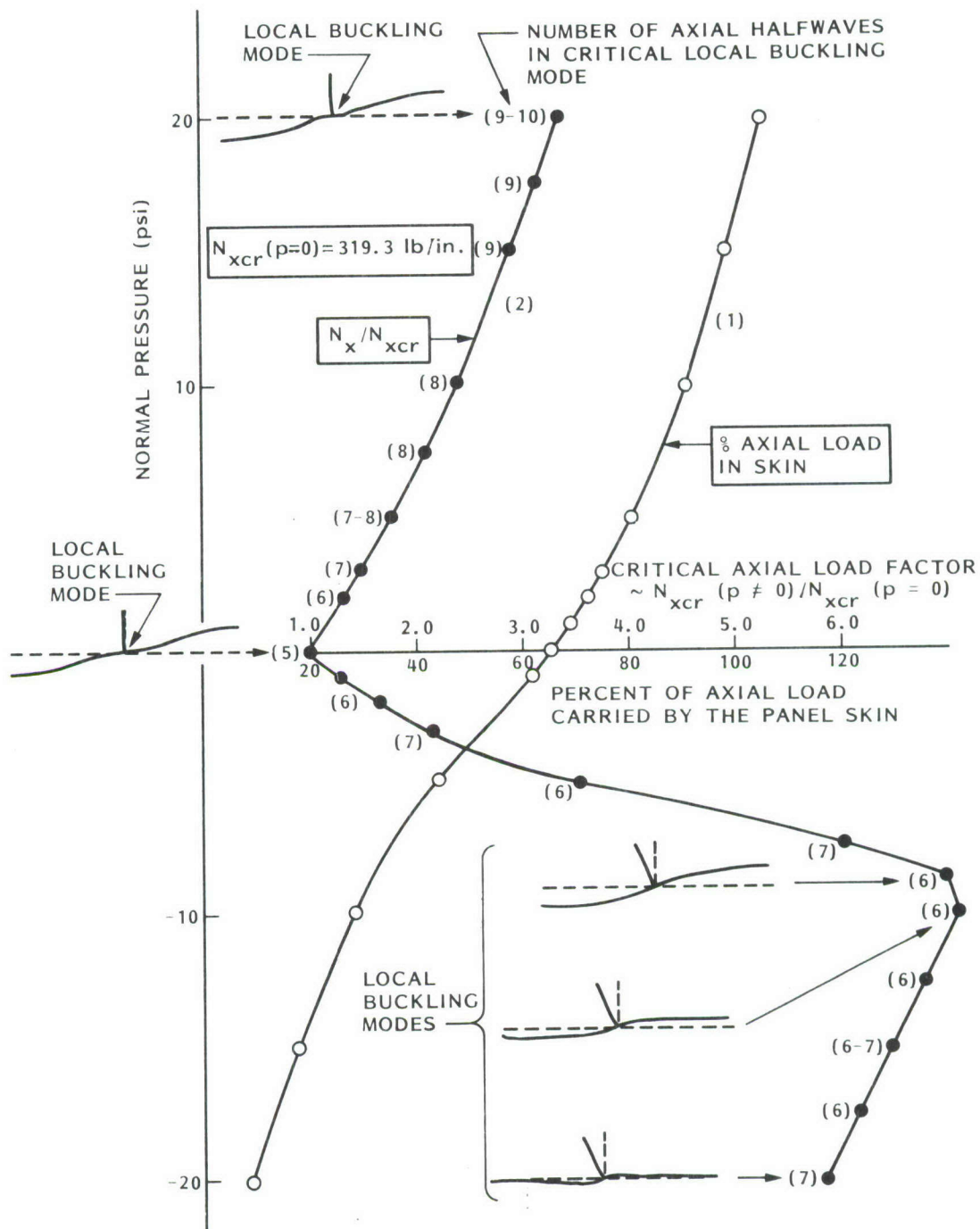
Fig. 65 PANDA2 predictions of the effect of pressure p on:

    (1) how much of the average applied axial load N_x is carried by the skin, and

    (2) local bifurcation buckling load factor and number of axial half waves
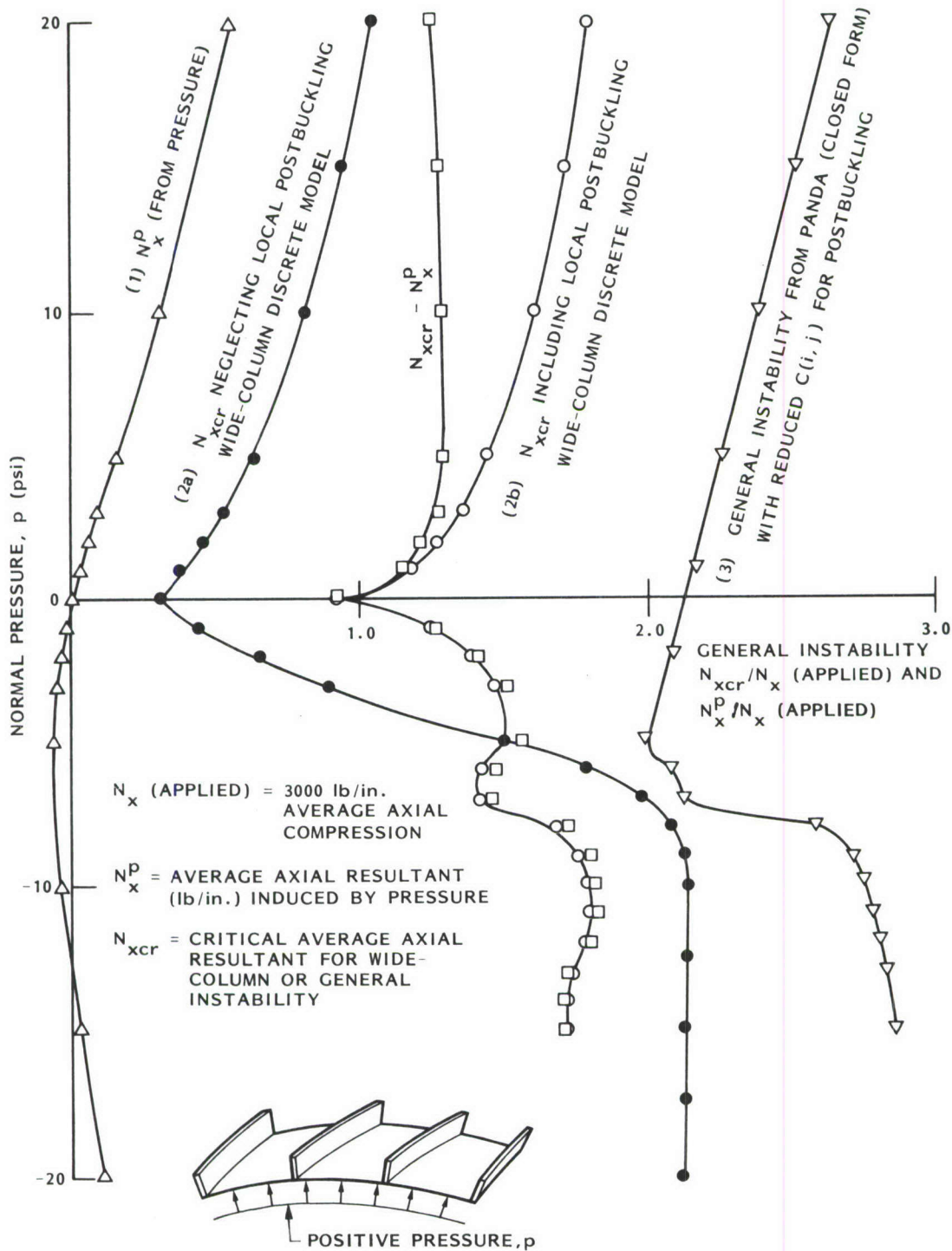
Fig. 66 PANDA2 predictions of the effect of pressure p on:
(1) average axial membrane prestress, N_x^p
(2) wide column buckling load factors N_{xcr} obtained from theories in which:
(a) local postbuckling of the skin is neglected,
(b) local postbuckling of the skin is included,
(3) general instability as predicted by a PANDA-type (closed form) analysis.

209
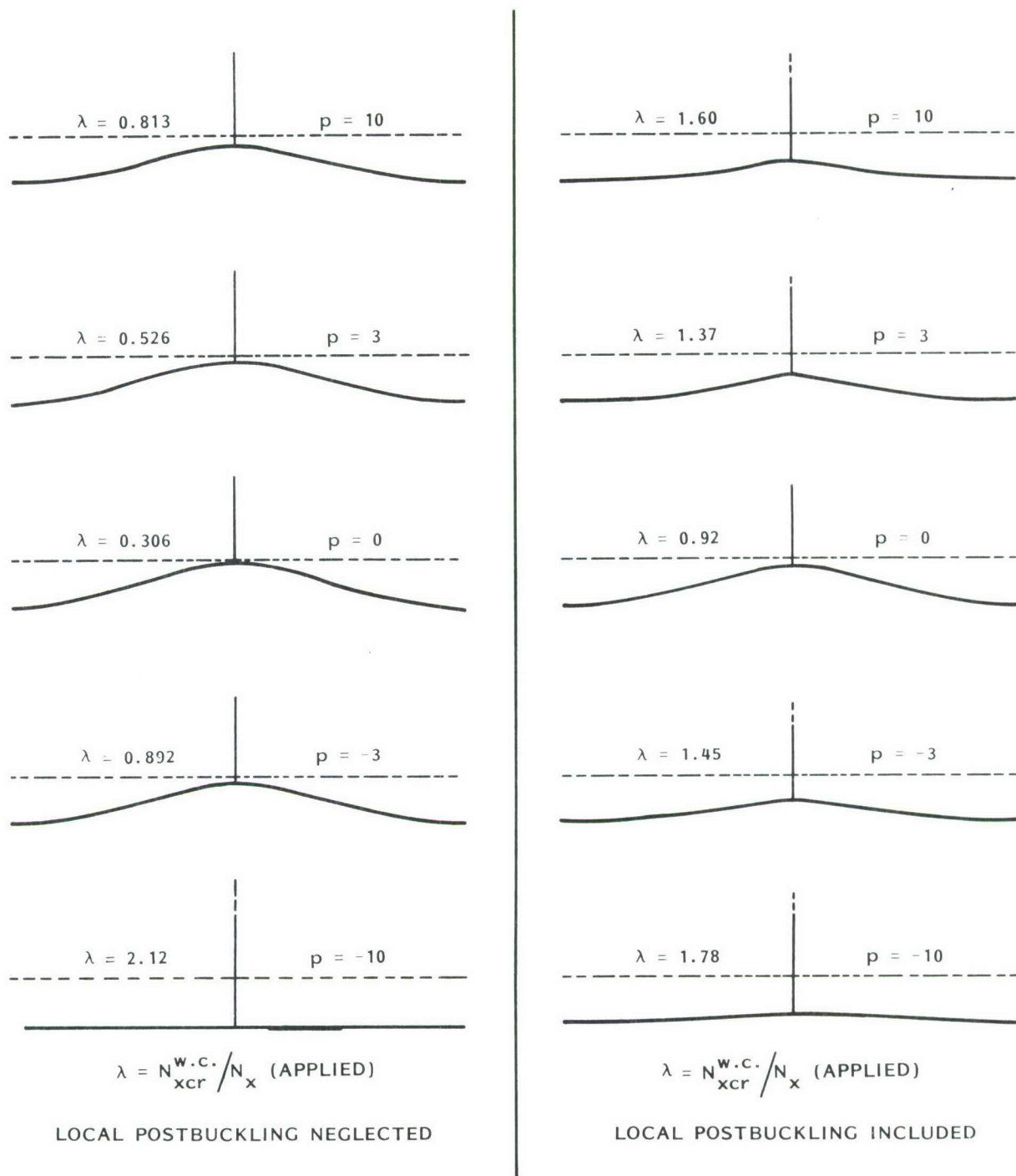
Fig. 67 PANDA2 predictions of the effect of pressure on the wide column buckling modes and load factors obtained with use of the discretized model of the single panel module.

N_{xcr} (p = 0) = 319.3 lb/in.
△ = p = -5.0 psi
○ = p = +5.0 psi
--- = NO POSTBUCKLING THEORY
——— = YES POSTBUCKLING THEORY
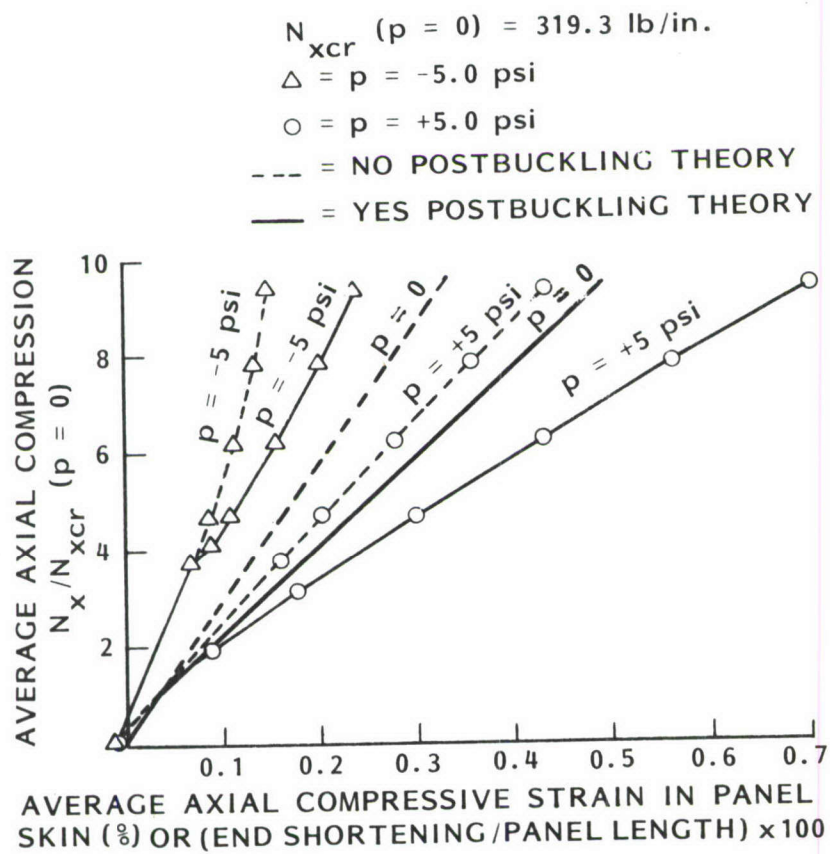
Fig. 68 PANDA2 predictions of the effect of pressure on load-end-shortening curves for the uniformly axially compressed blade-stiffened panel.
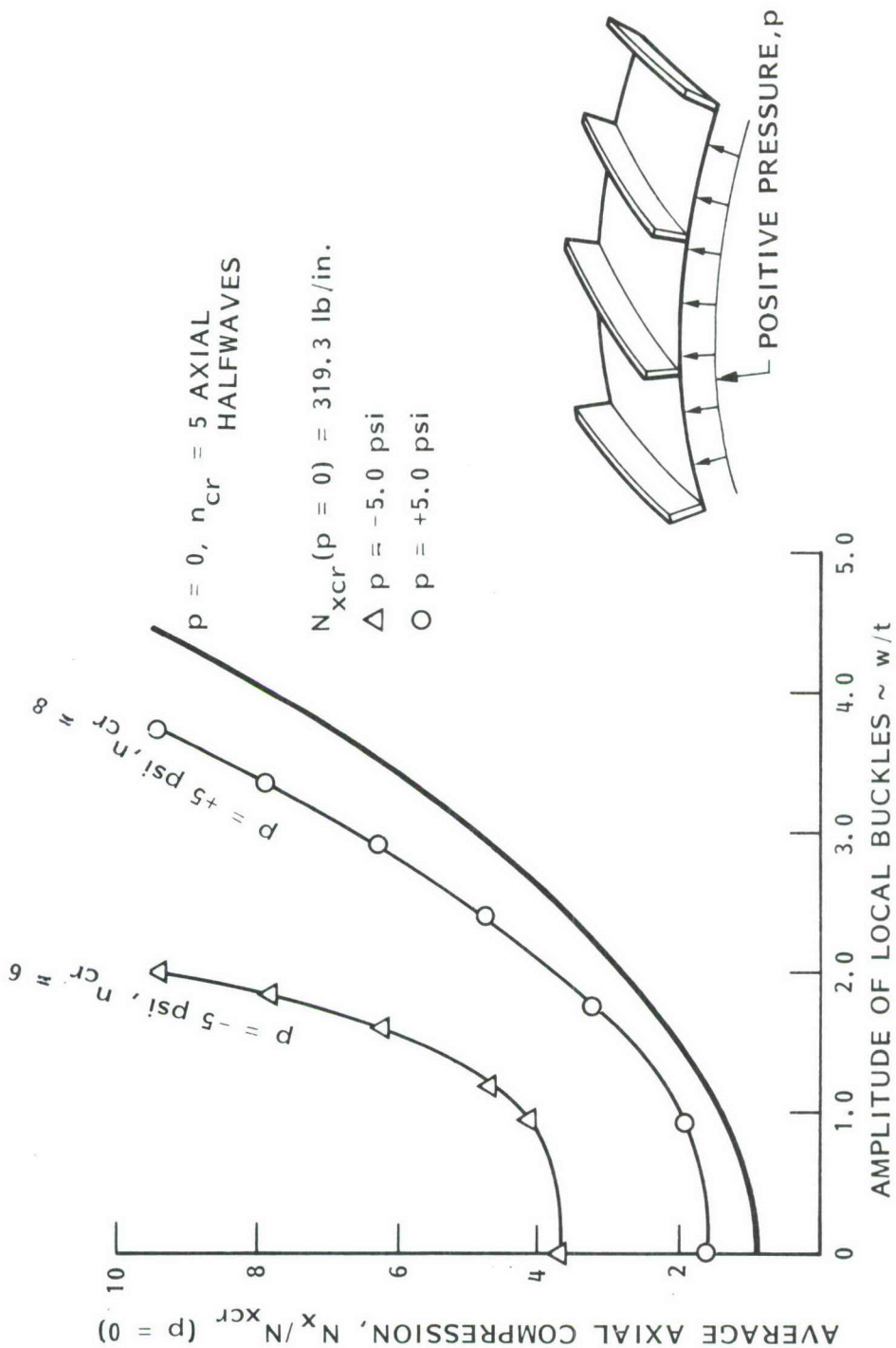
211

Fig. 69 PANDA2 predictions of the effect of pressure on local bifurcation and growth of the local normal displacement pattern in the postbuckling regime.
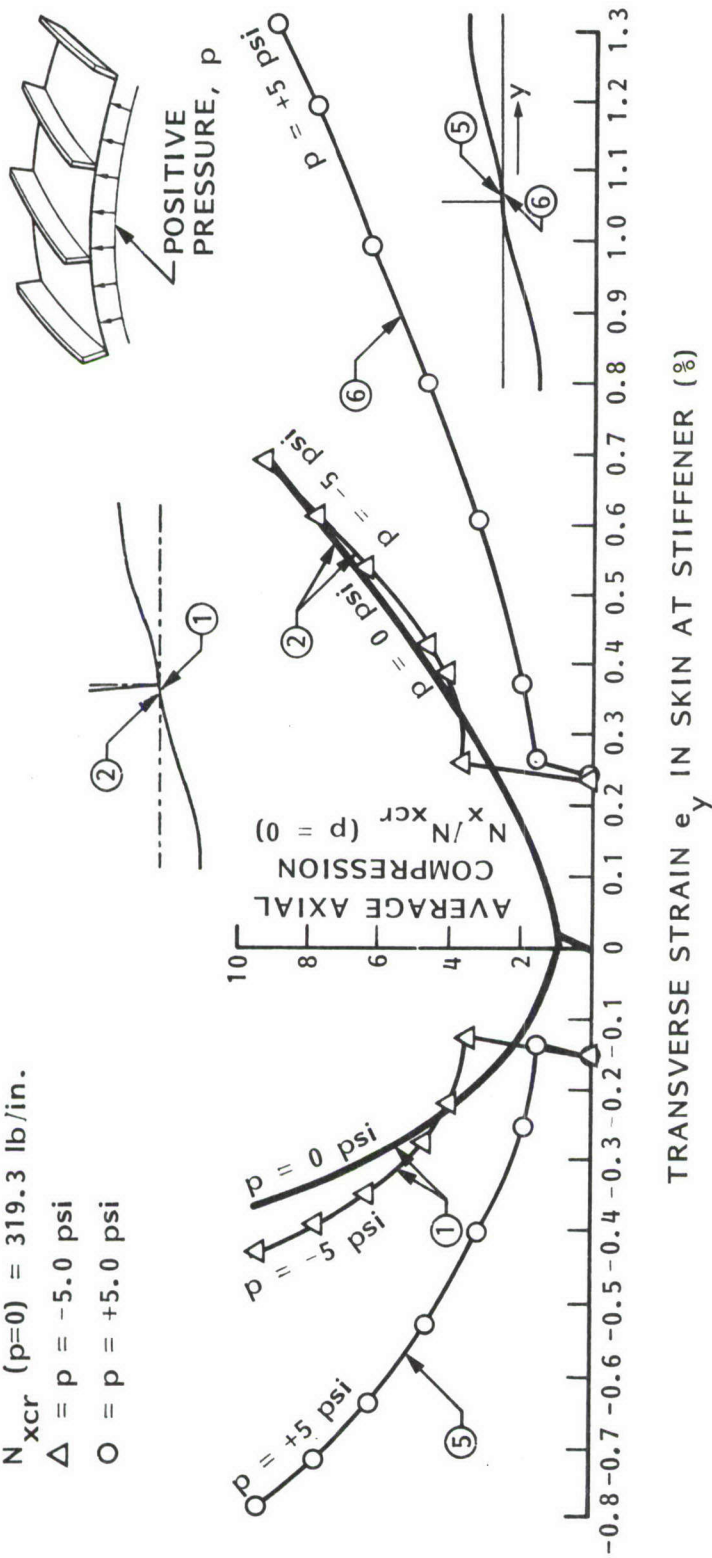
Fig. 70 PANDA2 predictions of the effect of pressure on the maximum transverse strain e_y in the panel skin next to the stringer.
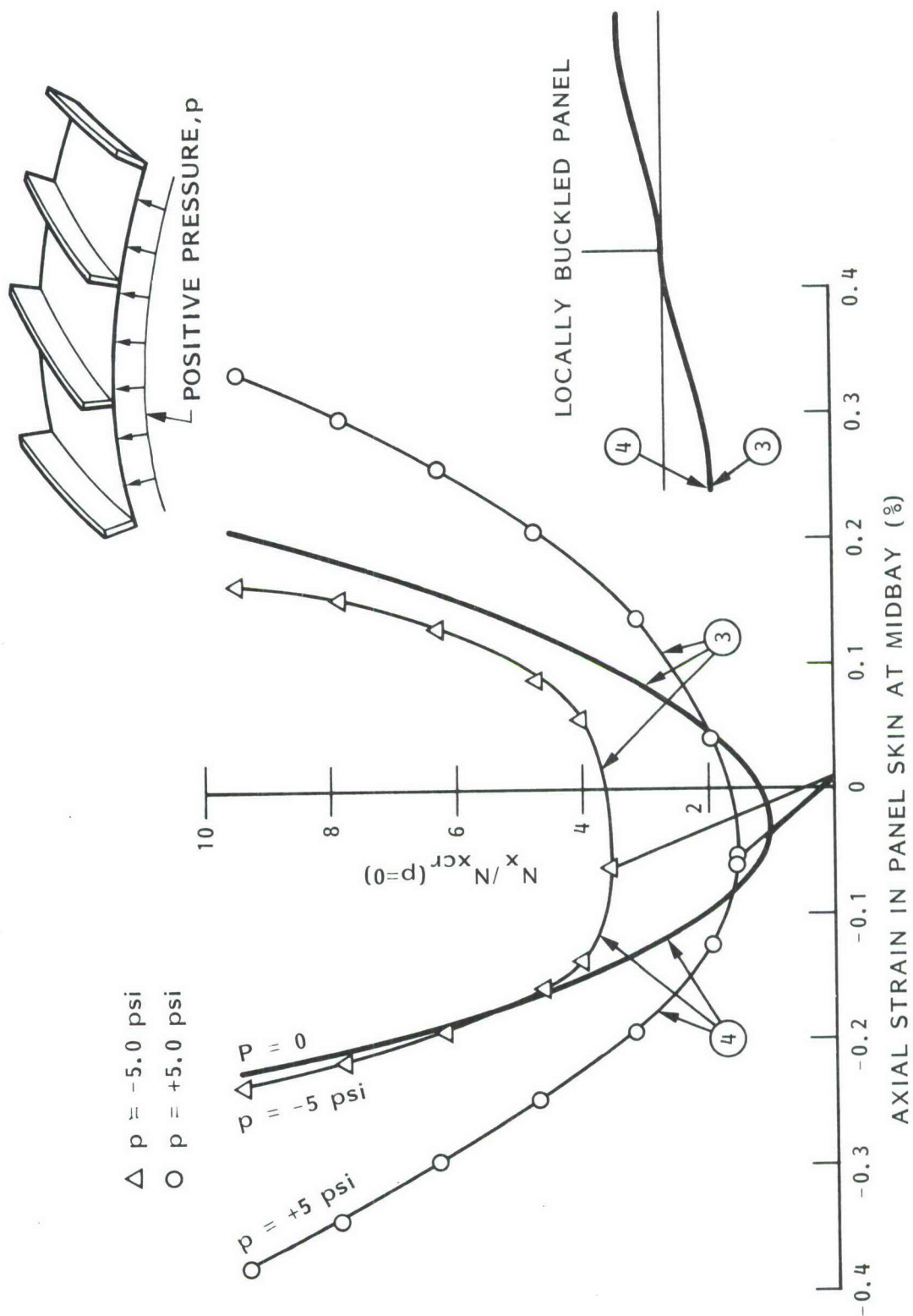
213

Fig. 71 PANDA2 predictions of the effect of pressure on the maximum axial strain e_z in the panel skin midway between stringers.
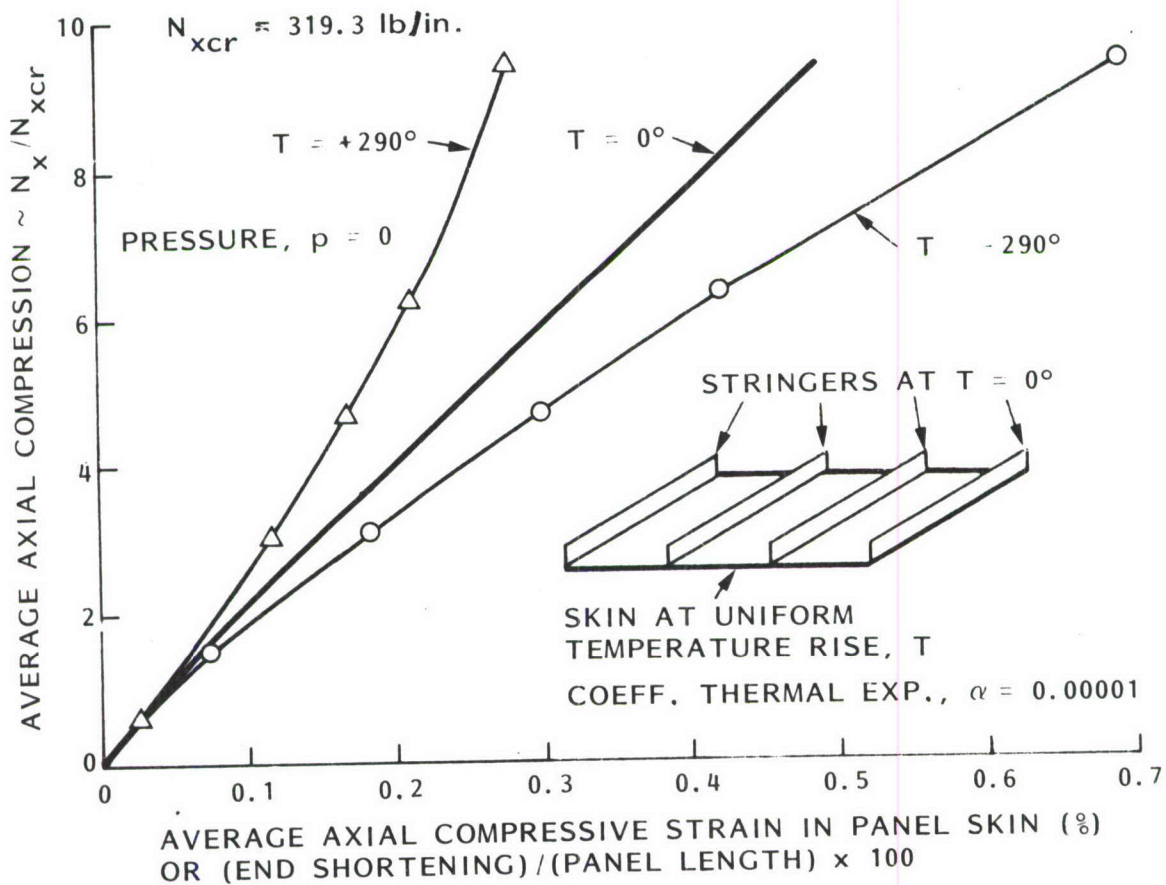
214

Fig. 72 PANDA2 predictions of the effect of curing on load-end-shortening curves for the uniformly axially compressed blade-stiffened panel. Curing is simulated by heating or cooling the panel skin relative to the stringers, which in this example are kept at ambient temperature (T=0).
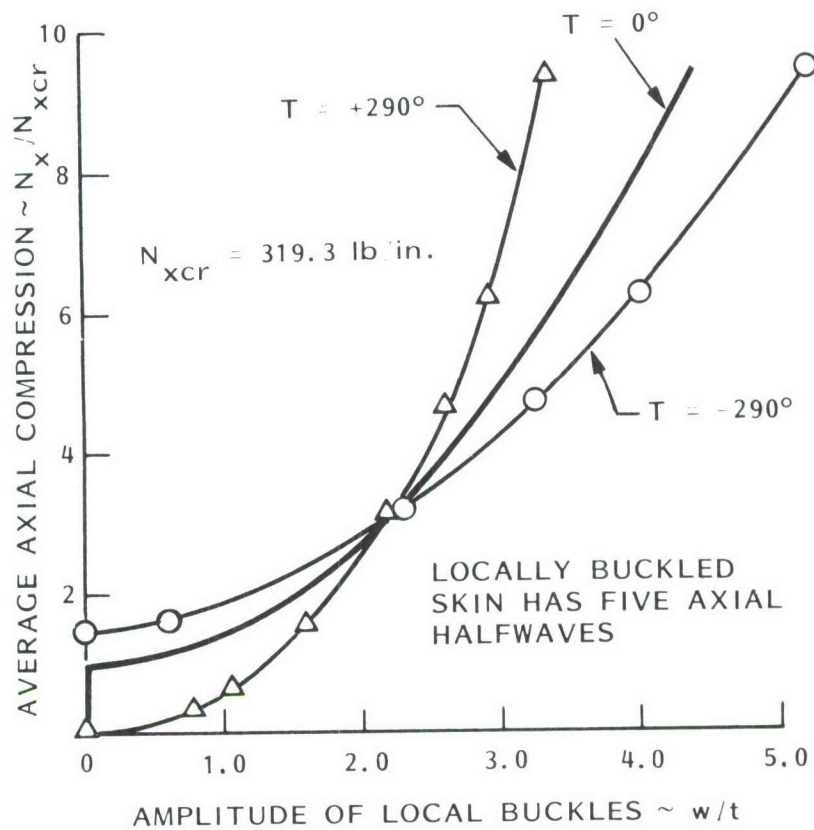
215

Fig. 73 PANDA2 predictions of the effect of curing on local bifurcation and growth of the local normal displacement pattern in the postbuckling regime.
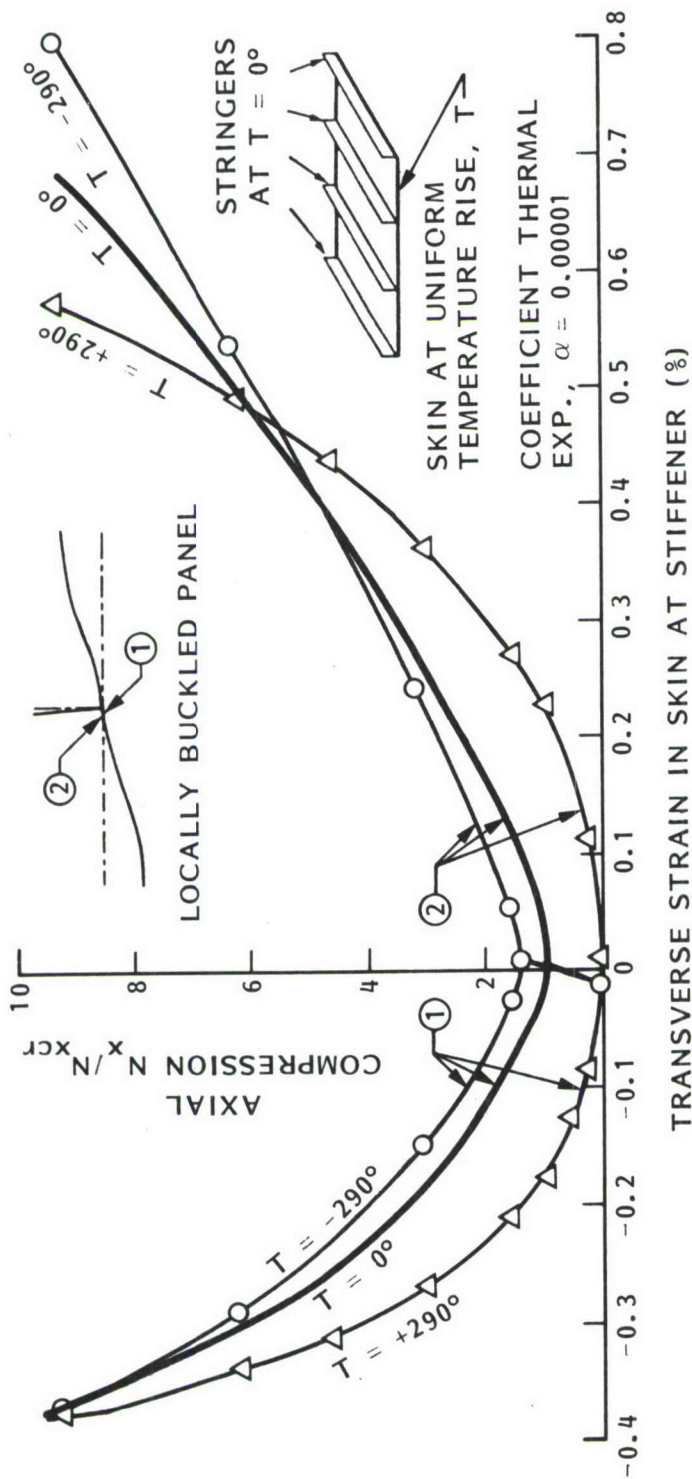
Fig. 74 PANDA2 predictions of the effect of curing on the maximum transverse strain e_y in the panel skin next to the stringer.
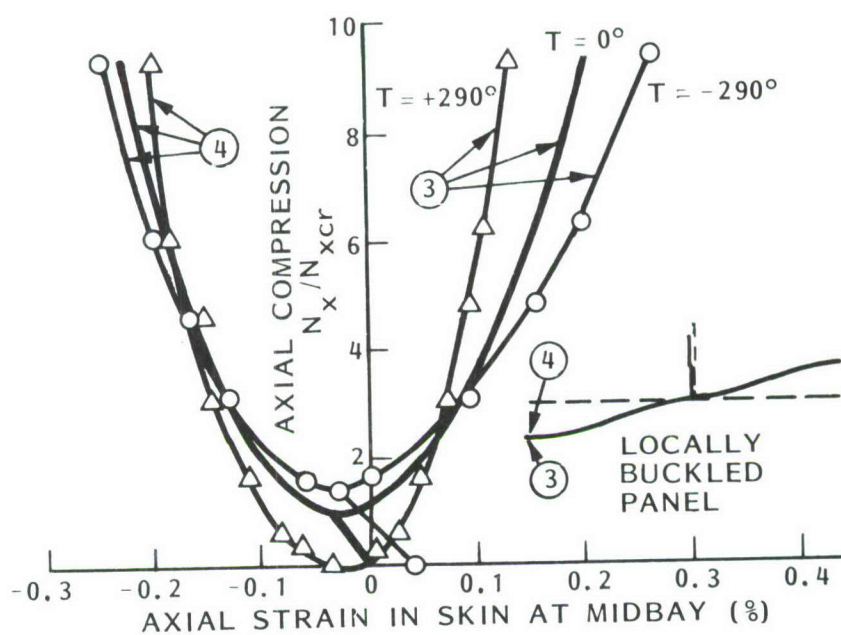
Fig. 75 PANDA2 predictions of the effect of curing on the maximum axial strain e_x in the panel skin midway between stringers.
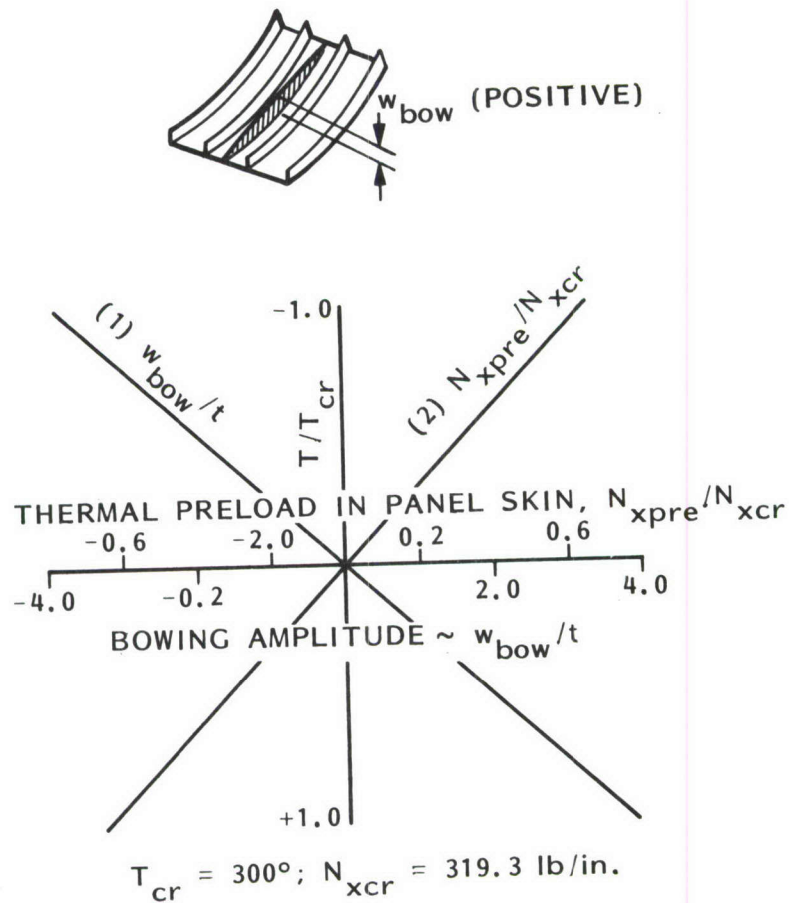
Fig. 76 PANDA2 predictions of the effect of curing temperature on:
(1) the amount of axial bowing
(2) the average thermal resultant in the panel skin
Note that the temperature scale is inverted: minus at the top.
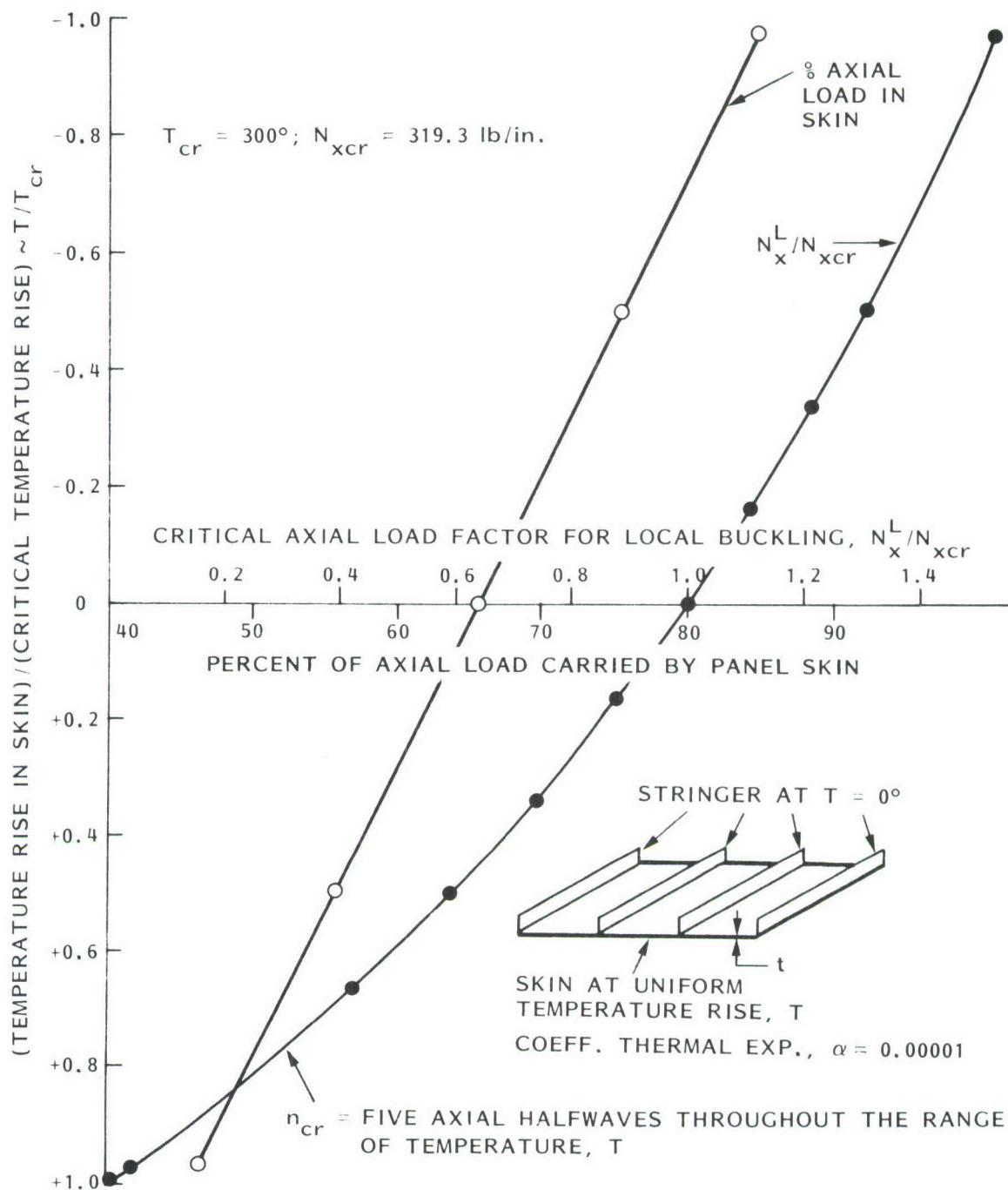
Fig. 77 PANDA2 predictions of the effect of curing temperature on:
(1) the percentage of applied axial load carried by the panel skin,
(2) the bifurcation buckling load factor for local buckling of the bowed, thermally prestressed panel.
Note that the temperature scale is inverted: minus at the top.

ARIANE 4

RING

102 in.

26.75 in.

107 in.

INTERSTAGE 2/3

STRINGER

SKIN
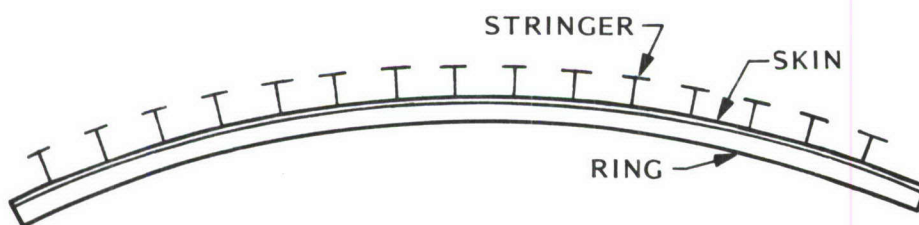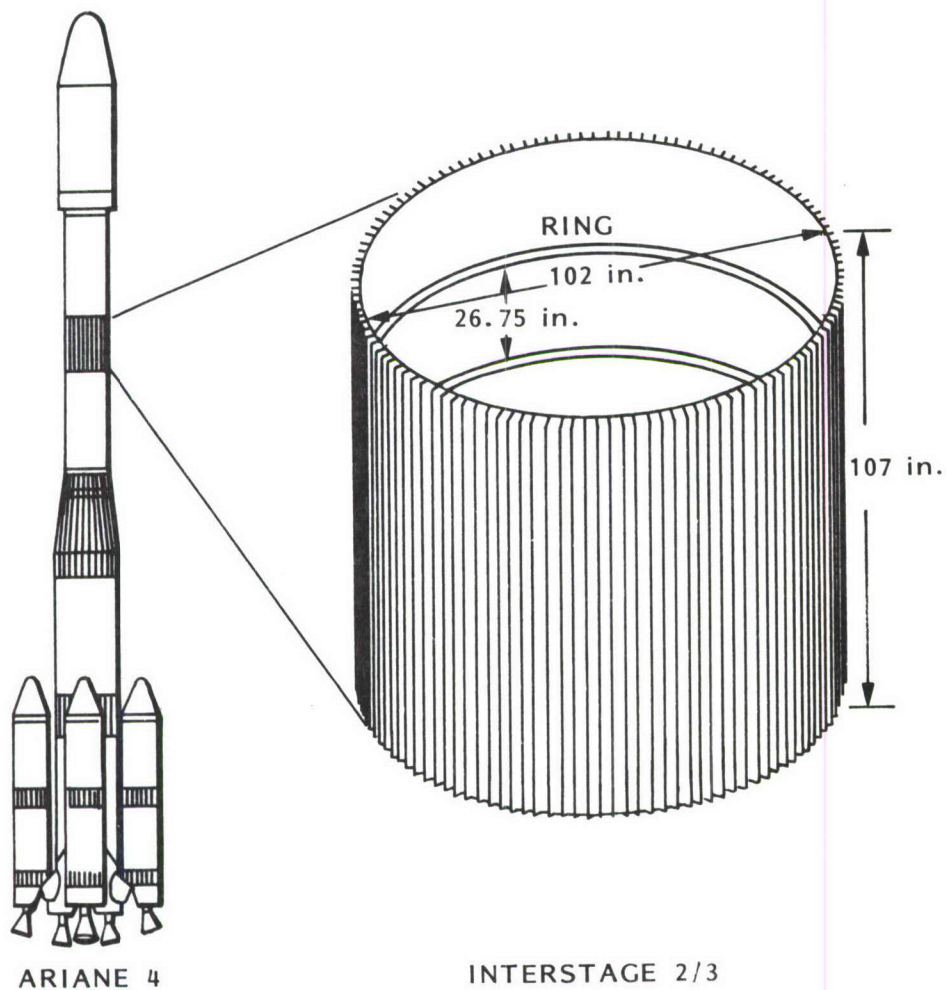
RING

Fig. 78 ARIANE4 interstage between stage 2 and stage 3. The cylindrical shell is reinforced by external stringers and internal rings.
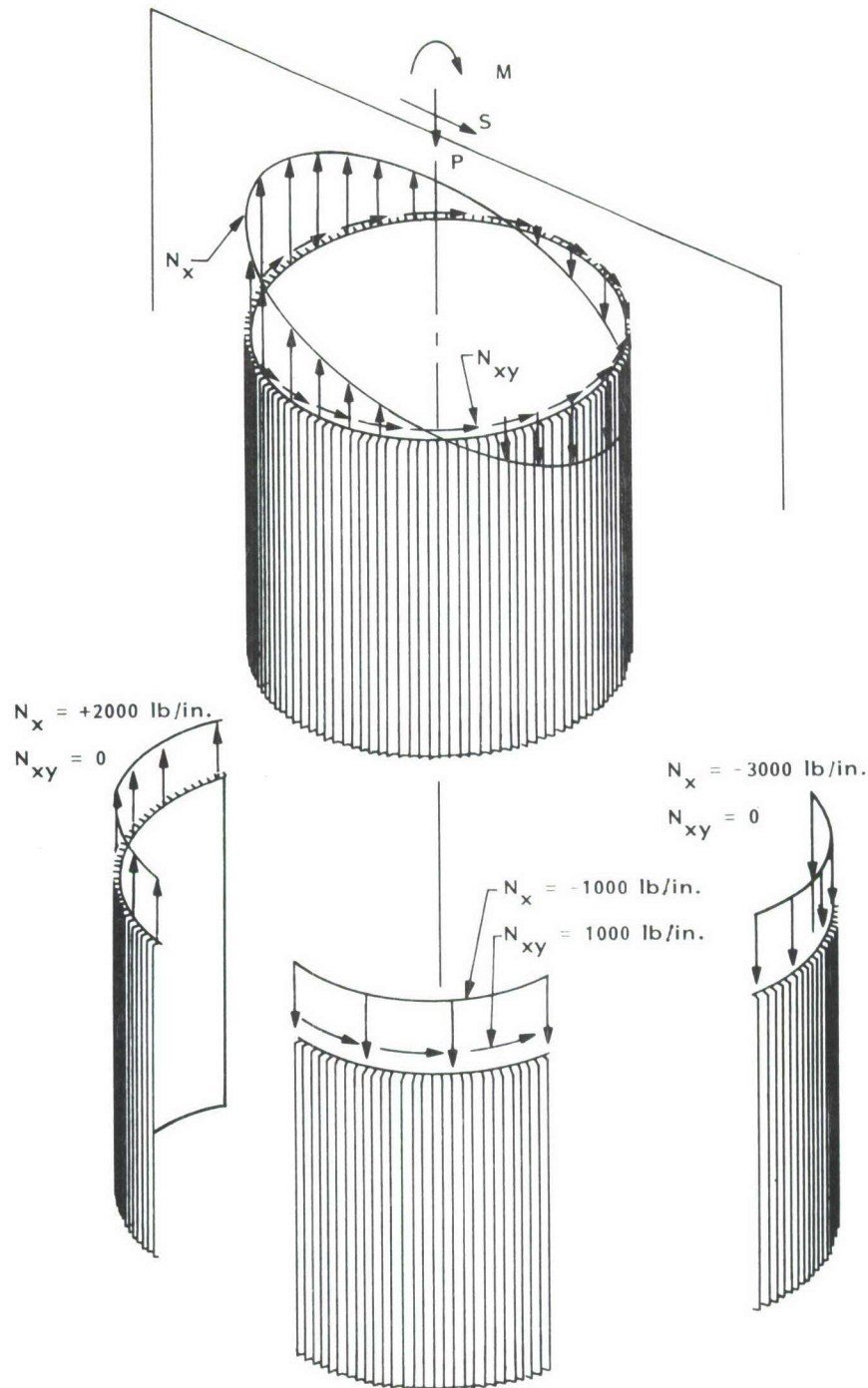
Fig. 79 Applied moment M, axial compression P, and shear S; assumed resulting distribution of line loads N_x and N_{xy} in the shell; and replacement of the actual complete cylindrical shell with circumferentially varying line loads by a single cylindrical panel spanning 40 inches of circumference with three separate load sets, each of which acts alone and each of which has uniform line loads N_x and N_{xy}

Fig. 80 Design concept to be optimized: External T-shaped stringers made of graphite-epoxy cloth and tape with thickened areas under the stringer web, and internal aluminum rings with spacing fixed at 26.75 inches. The spacing of the stringers is to be determined, as well as the cross section dimensions and thicknesses of the various composite laminae.

223
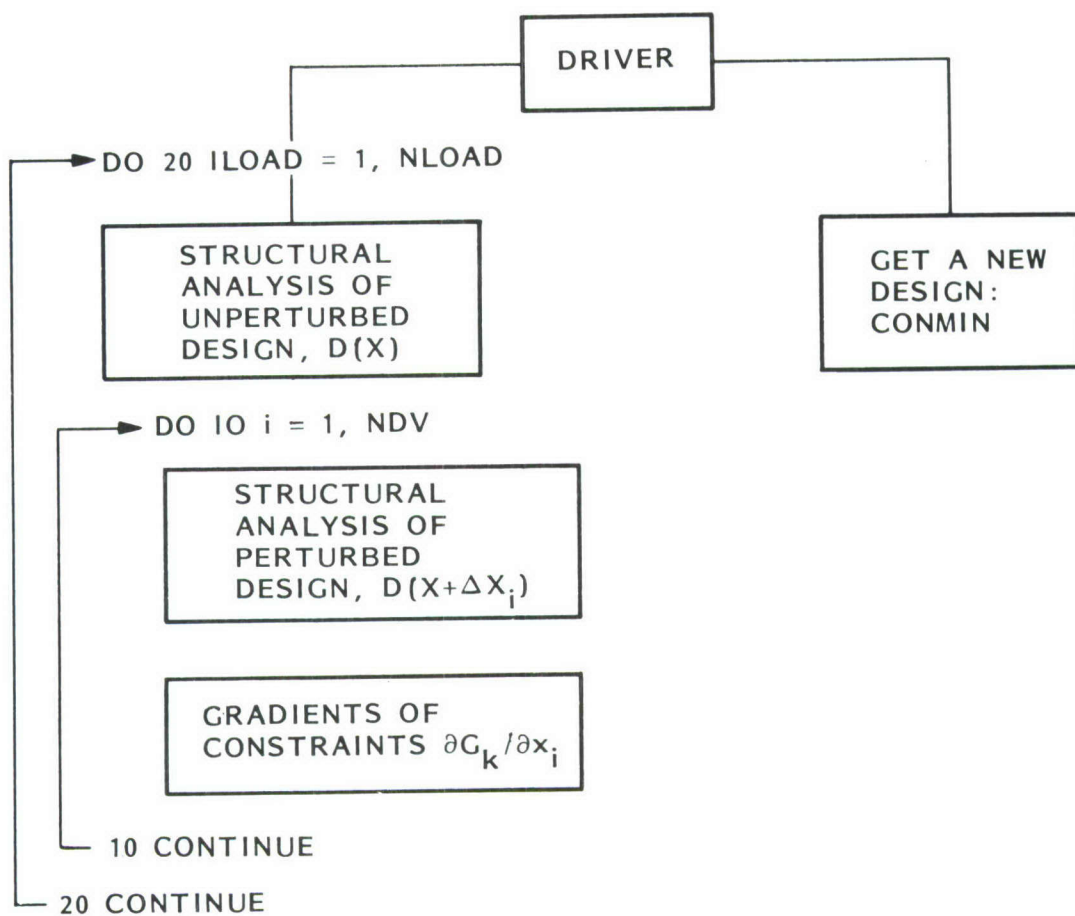
Fig. 81 Architecture of the PANDA2 mainprocessor.
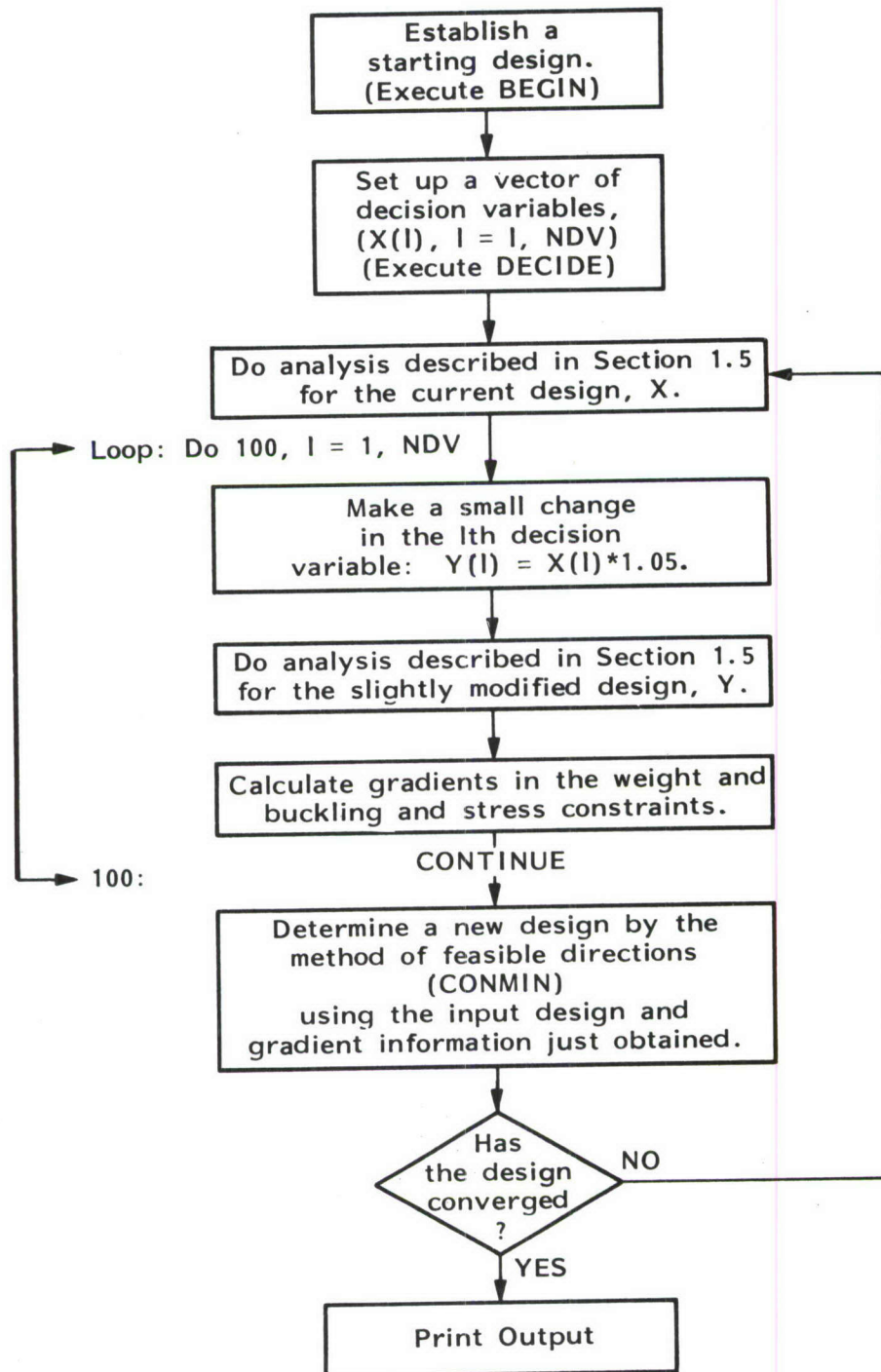
Fig. 82 Flow of calculations in the PANDA2 mainprocessor for an optimization analysis.
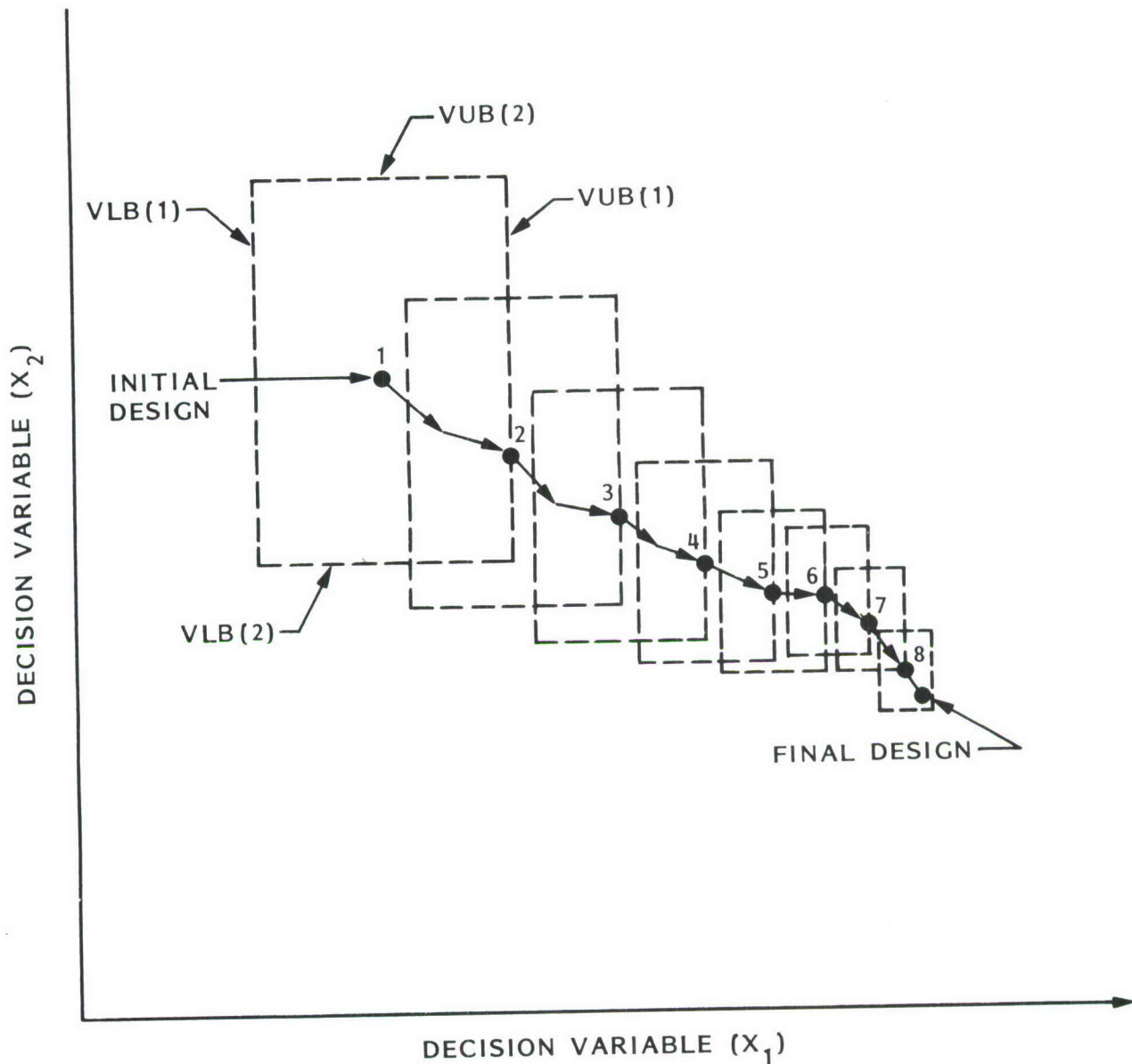
Fig. 83 Schematic of the evolution of a design with two decision variables, X_1 and X_2. With each iteration, the optimizer, CONMIN, establishes a "window" of permitted excursion of the decision variables. In PANDA2 this "window" shrinks by a factor of 0.8 for each design iteration. Upon re-execution of PANDAOPT the "window" is re-expanded to its original size, which depends upon lower and upper bounds supplied by the user and certain strategies used by CONMIN.

226
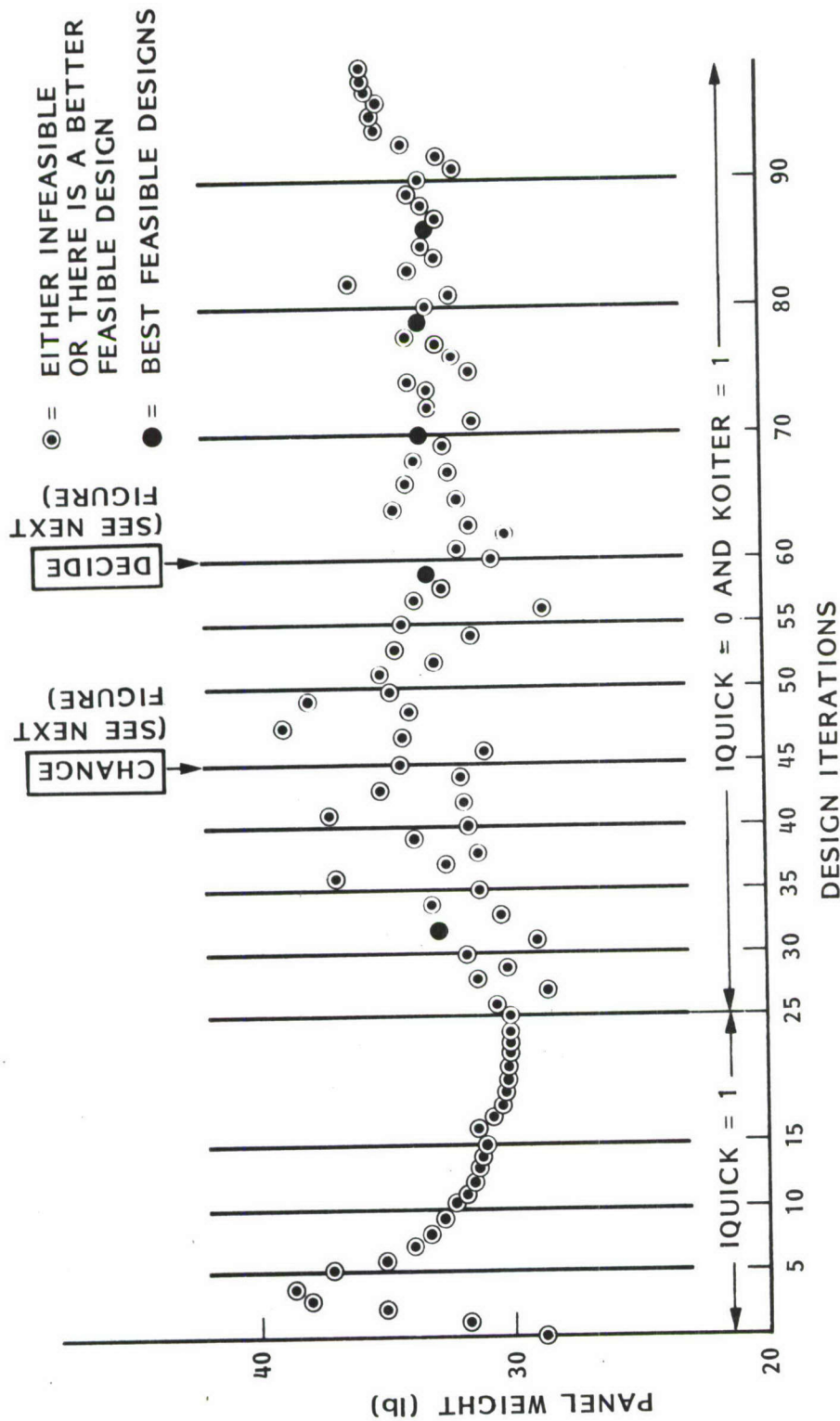
Fig. 84 Evolution of the panel weight during design iterations. There are 25 iterations with use of the closed-form PANDA-type [1] models (IQUICK = 1), followed by 75 iterations with use of the discretized BOSOR4-type panel module models plus the PANDA-type models (IQUICK = 0). In these latter iterations local postbuckling IS permitted (KOITER = 1).

227
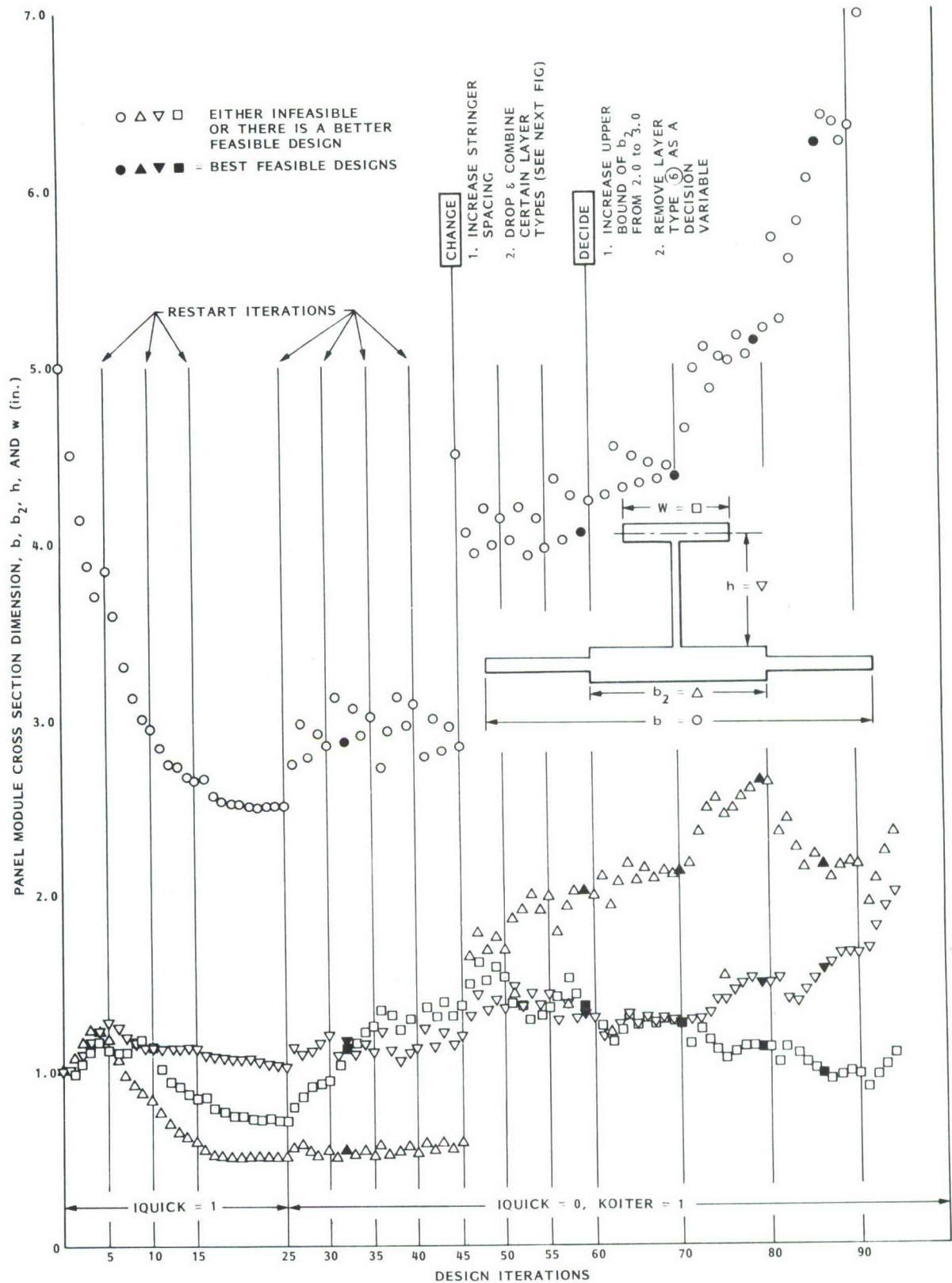
Fig. 85 Evolution of the cross section dimensions in the all-composite T-shaped stringers during design iterations. Local postbuckling IS permitted (KOITER = 1). The rather unstable behavior in the IQUICK=0 regime results from optimum designs being sought in the early postbuckling regime, in which the behavior of the panel (stress, internal load distribution) changes steeply with change in panel dimensions.

228
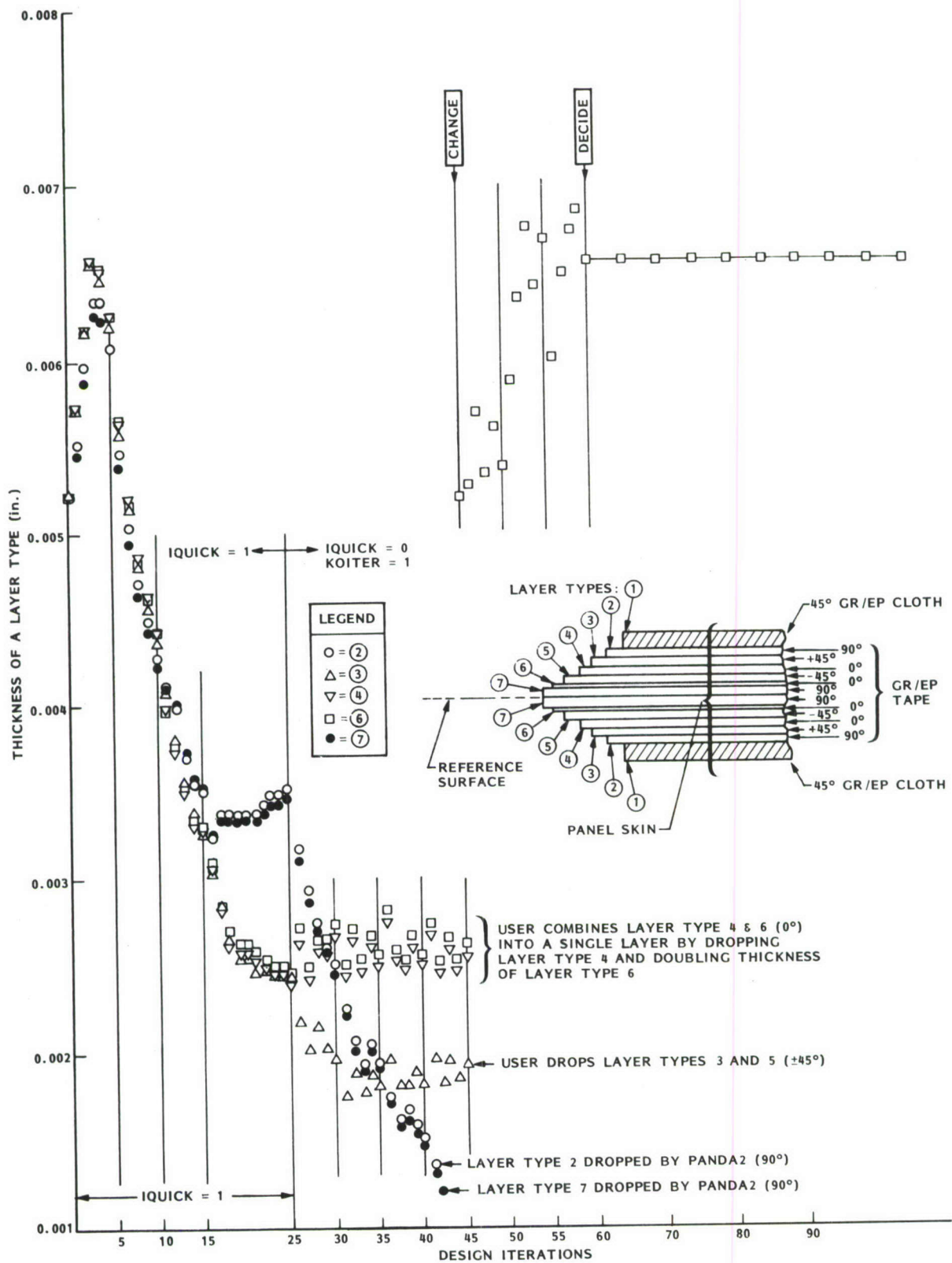
Fig. 86 Evolution of the thicknesses of the 12-layer default stacking sequence $[90/45/0/-45/0/90]_s$ during design iterations. Local postbuckling IS permitted (KOITER = 1).
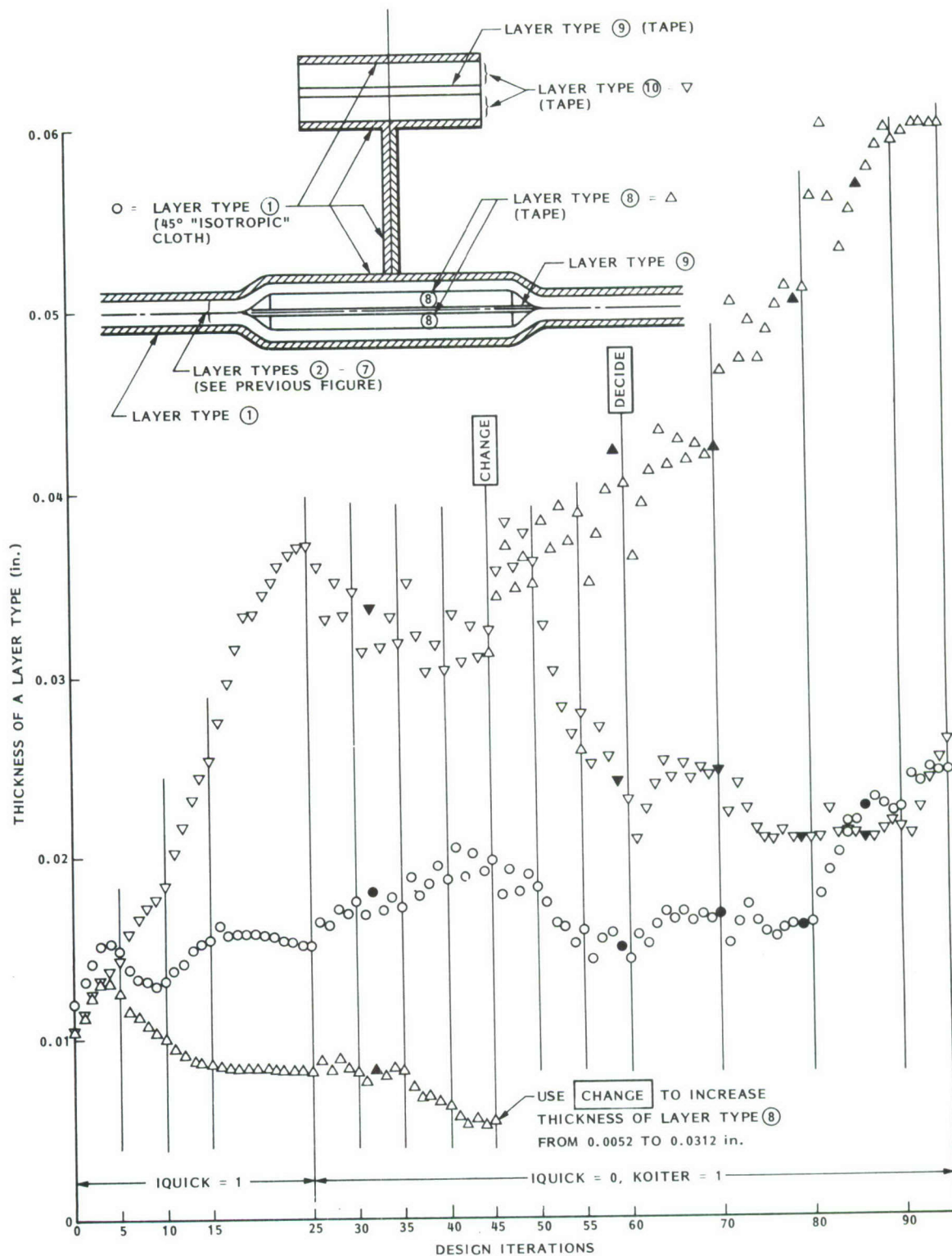
Fig. 87 Evolution of the thickness of the graphite-epoxy cloth and of the 0-degree layers in the stringer base and in the flange during design iterations. Local postbuckling IS permitted (KOITER = 1). Blackened points represent feasible or almost feasible designs.

230

Fig. 88 Evolution of design margins corresponding to Load Set 1 ($N_x = -3000$ lb/in, $N_{xy} = 0$) during iterations. Local postbuckling IS permitted. The most critical margins are wide column buckling and stringer pop-off.

The legend on the figure:

O = GENERAL INSTABILITY
△ = WIDE COLUMN BUCKLING BETWEEN RINGS
▽ = SMEARED STRINGER BUCKLING BETWEEN RINGS
□ = ROLLING OF STRINGERS, NO SKIN PARTICIPATION
● = LOCAL BUCKLING
◀ = CRIPPLING OF FLANGE
■ = STRINGER "POP-OFF"
X = MAX. SHEAR STRESS IN MATL #3
▶ = LONG WAVELENGTH LOCAL BUCKLING

Vertical axis: DESIGN MARGINS FOR LOAD SET NO. 1: PURE AXIAL COMPRESSION

Horizontal axis: DESIGN ITERATIONS

IQUICK = 1

Fig. 89 Evolution of design margins corresponding to Load Set 2 ($N_z = -1000$ lb/in, $N_{xy} = 1000$ lb/in) during iterations. Local postbuckling IS permitted. The most critical margins are wide column buckling, stringer pop-off, and maximum tensile stress in the cloth in the peaks of the local buckles midway between stringers.

232

(a)

SEG. ④
w = 1.402

SEG. ③

h = 1.186

SEG. ①

SEGMENT ②

SEG. ⑤

DIMENSIONS
IN INCHES

STRINGER BASE,
$b_2 = 2.324$

STRINGER SPACING, b = 4.554

(b)

$\lambda_{LOCAL} = 0.9151$

M = 4 AXIAL HALF WAVES BETWEEN RINGS

(c)

$\lambda_{WIDE\ COLUMN} = 1.528$

M = 1 AXIAL HALF WAVES BETWEEN RINGS
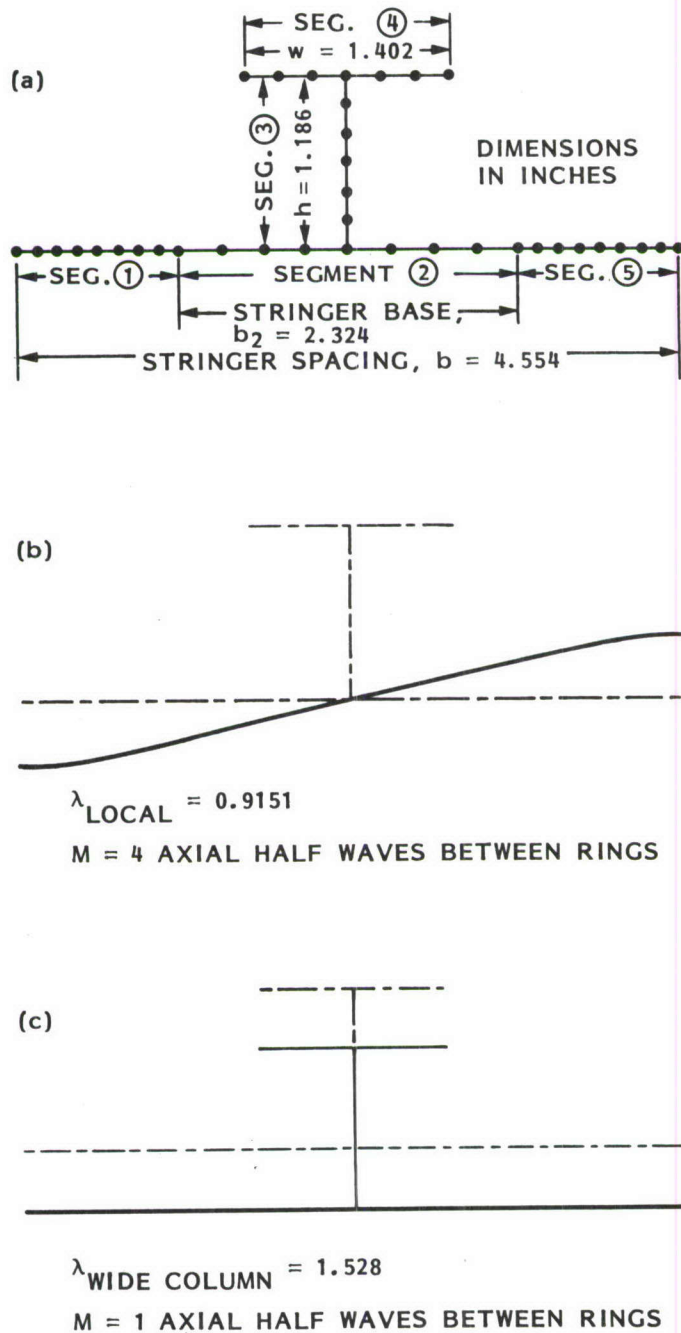
Fig. 90 Selected optimum design for the case in which local postbuckling IS permit-
ted, showing (a) discretized panel module model, and (b,c) buckling modes
and load factors corresponding to Load Set 1. (b) local buckling mode and
load factor, and (c) wide column buckling mode and load factor. The mode
shapes vary as $\sin(M\pi x/L)$ along the axis of the panel, where L is the ring
spacing.

233

4.554 in.

40.986 in.

(a)

(b) $\lambda_1 = 1.423$

M = 1 AXIAL HALF WAVE BETWEEN RINGS

(c) $\lambda_2 = 1.515$
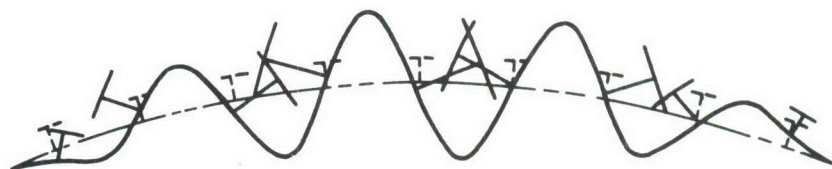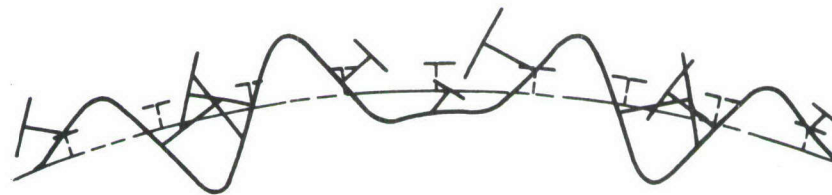
M = 1 AXIAL HALF WAVE BETWEEN RINGS

Fig. 91 (a) Multi-segment, branched BOSOR4 model of the optimized panel gener-
ated by the PANEL processor (local buckling IS permitted), and (b,c) buckling
modes corresponding to Load Set 1. (b) Lowest buckling mode represents
a kind of local buckling because the stringer web lines of attachment to the
panel skin do not move very much. (c) Second buckling mode represents a
form of general instability. The load factor, $\lambda_2 = 1.515$ should be compared
with the wide column buckling load factor $\lambda_{WIDE COLUMN} = 1.528$ given
in the previous figure. In (b) and (c) the mode shapes vary as $\sin(M\pi x/L)$
along the axis of the panel, where L is the ring spacing.

234
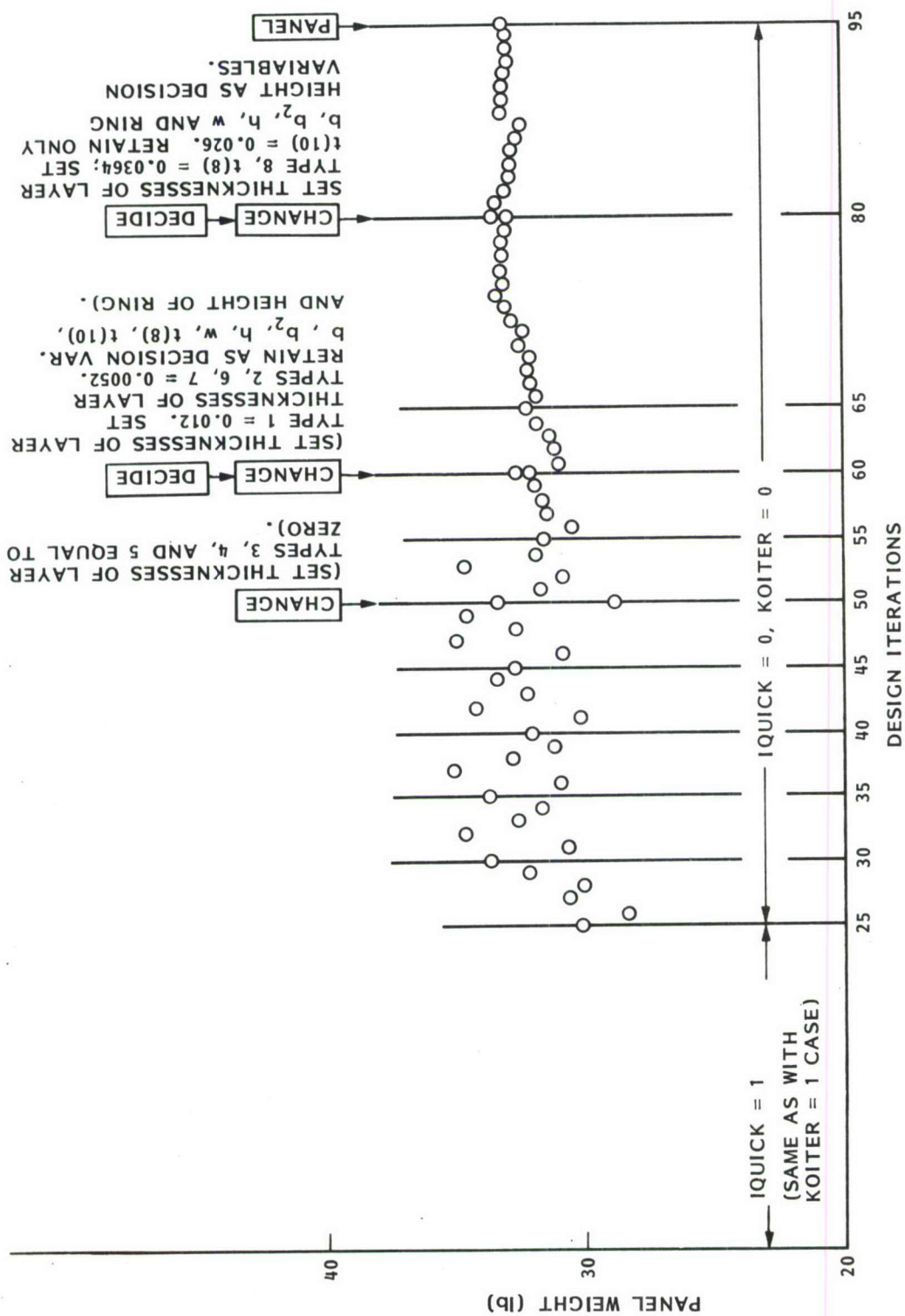
Fig. 92 Evolution of the panel weight during design iterations. Local postbuckling is NOT permitted (KOITER = 0).
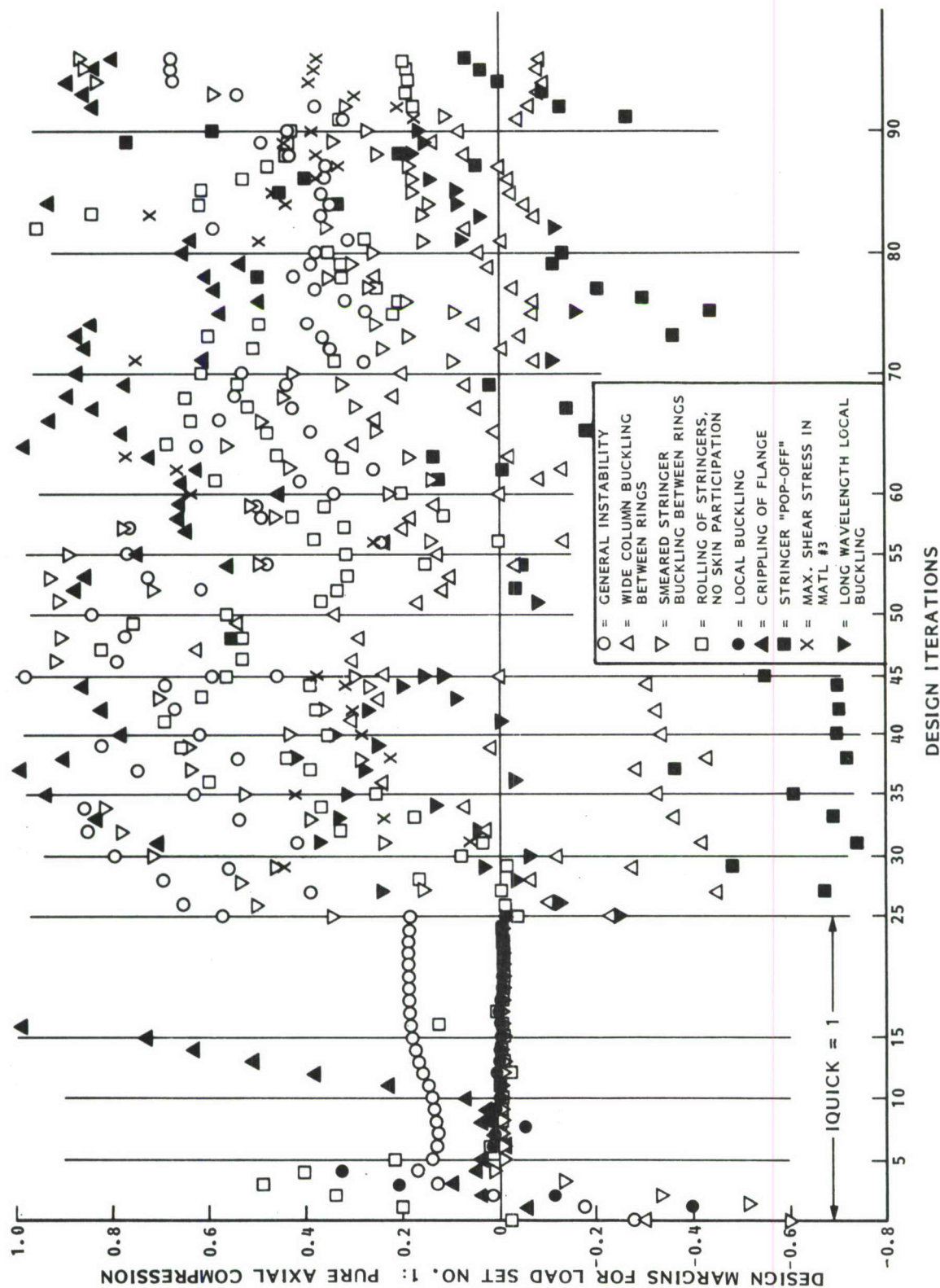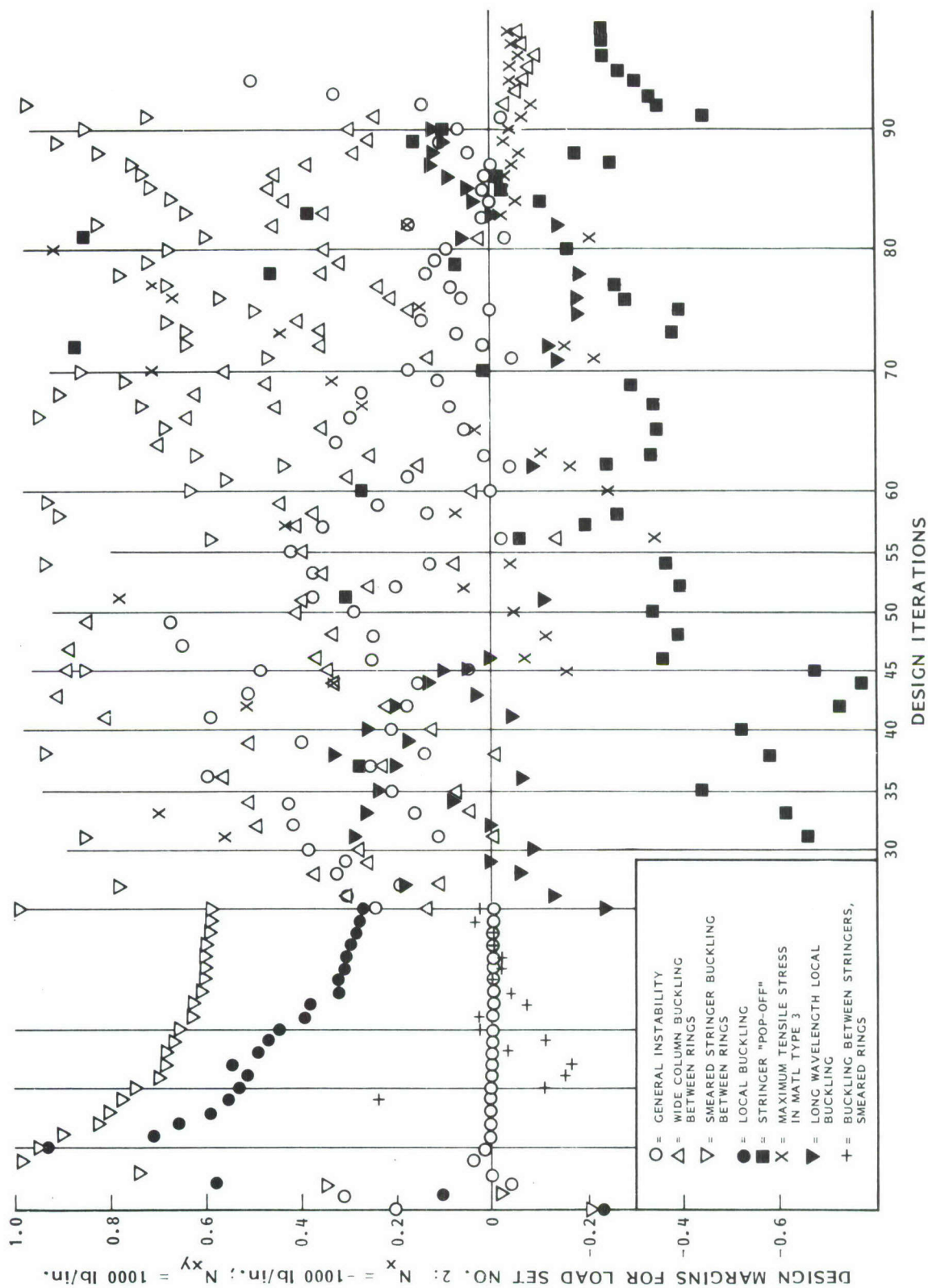
235
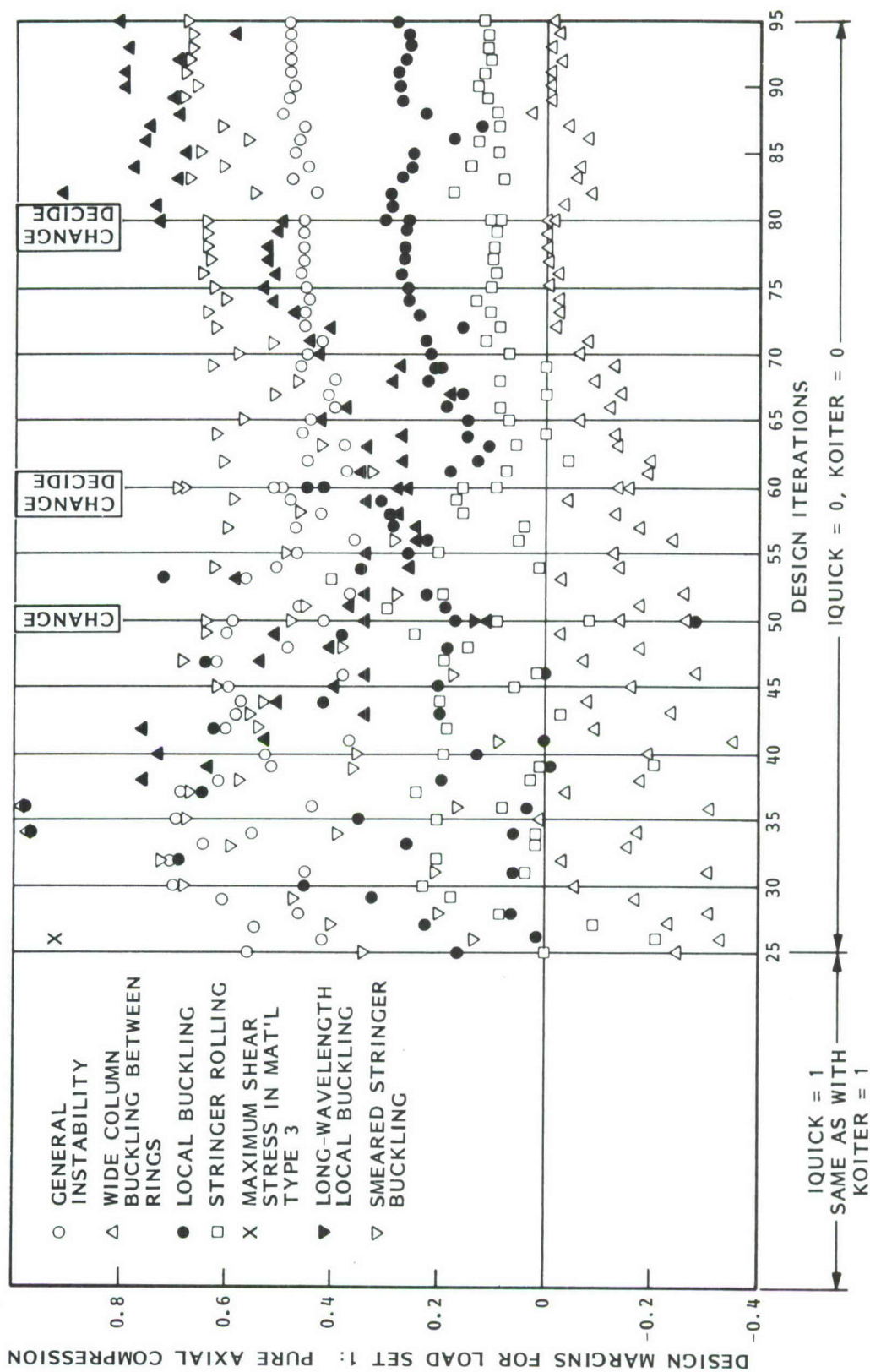
Fig. 93 Evolution of design margins corresponding to Load Set 1 ($N_x = -3000$ lb/in, $N_{xy} = 0$) during iterations. Local postbuckling is NOT permitted. The most critical margin is wide column buckling.
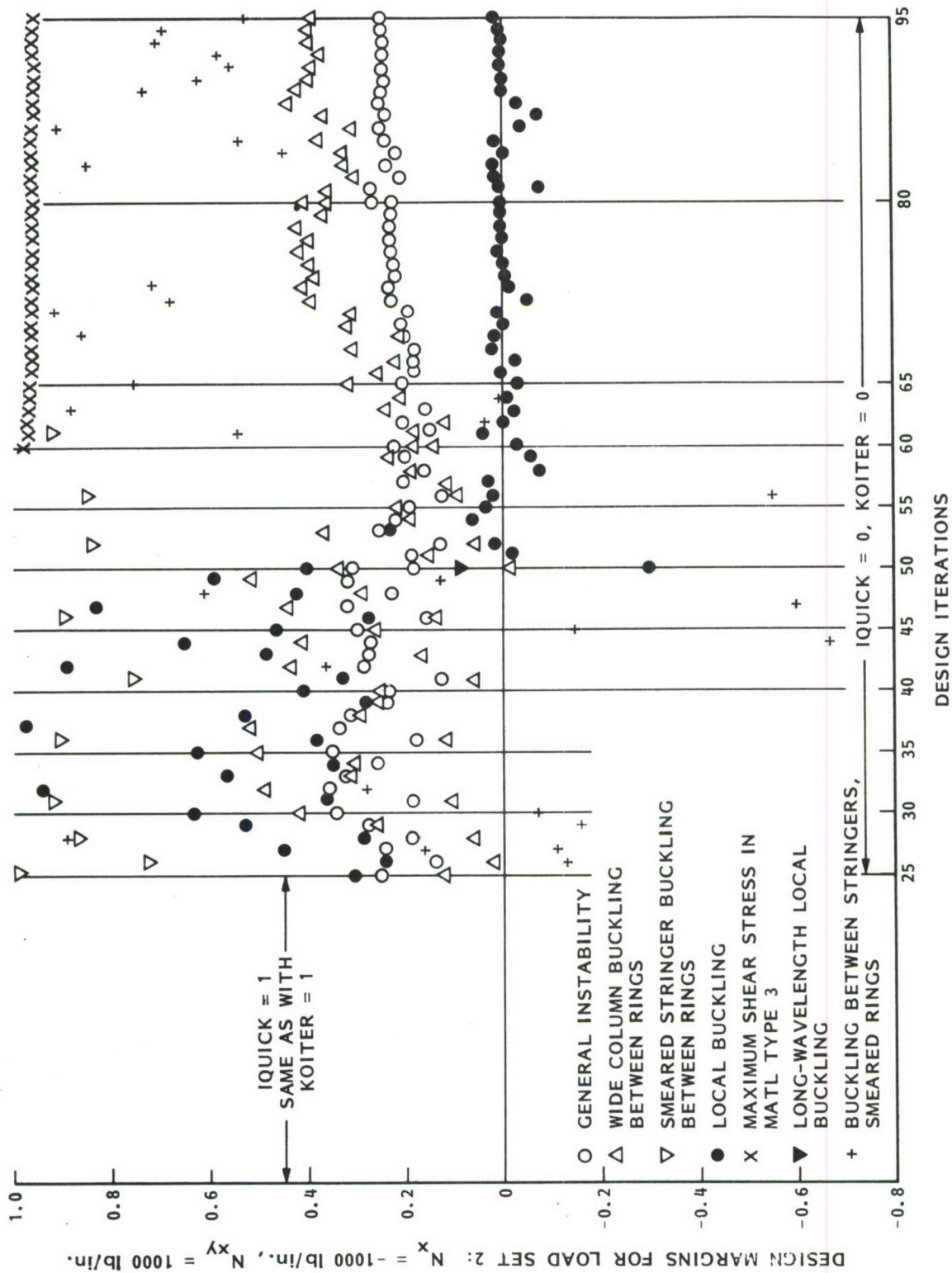
Fig. 94 Evolution of design margins corresponding to Load Set 2 ($N_x = -1000$ lb/in, $N_{xy} = 1000$ lb/in) during iterations. Local postbuckling is NOT permitted. The most critical margin is local buckling.

DESIGN ITERATIONS

DESIGN MARGINS FOR LOAD SET 2: $N_x = -1000$ lb/in., $N_{xy} = 1000$ lb/in.

IQUICK = 1
SAME AS WITH
KOITER = 1

IQUICK = 0, KOITER = 0

O GENERAL INSTABILITY
△ WIDE COLUMN BUCKLING BETWEEN RINGS
▽ SMEARED STRINGER BUCKLING BETWEEN RINGS
● LOCAL BUCKLING
X MAXIMUM SHEAR STRESS IN MATL TYPE 3
▶ LONG-WAVELENGTH LOCAL BUCKLING
+ BUCKLING BETWEEN STRINGERS, SMEARED RINGS

237

(a)

SEG.④

w = 1.469

h = 1.065

SEG.③

DIMENSIONS
IN INCHES

SEG.① SEG.② SEG.⑤

b_2 = 1.055

STRINGER SPACING, b = 3.276

(b)

λ_{LOCAL} = 1.287

m = 10 AXIAL HALF WAVES
BETWEEN RINGS

(c)

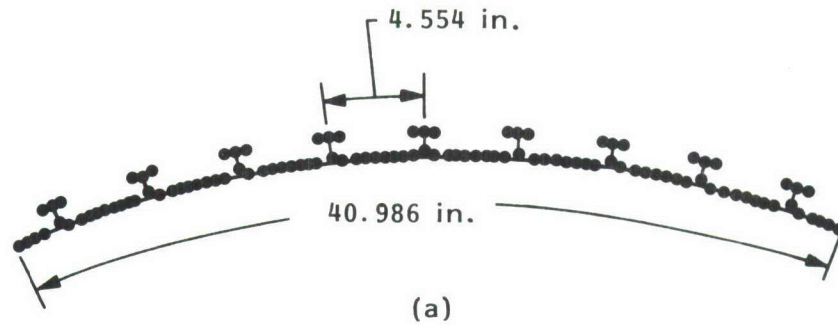$\lambda_{WIDE\ COL.}$ = 1.482

m = 1 AXIAL HALF WAVE
BETWEEN RINGS

Fig. 95 Final optimum design for the case in which local postbuckling is NOT permitted, showing (a) discretized panel module model, and (b,c) buckling modes and load factors corresponding to Load Set 1. (b) local buckling mode and load factor, and (c) stringer side-sway buckling mode and load factor. The mode shapes vary as $\sin(m\pi x/L)$ along the axis of the panel, where L is the ring spacing.

(a)

$\lambda_1 = 1.293$

(b)

m = 1 AXIAL HALF WAVE
BETWEEN RINGS

$\lambda_2 = 1.307$

(c)

m = 1 AXIAL HALF WAVE
BETWEEN RINGS

$\lambda_3 = 1.309$

(d)

m = 1 AXIAL HALF WAVE
BETWEEN RINGS
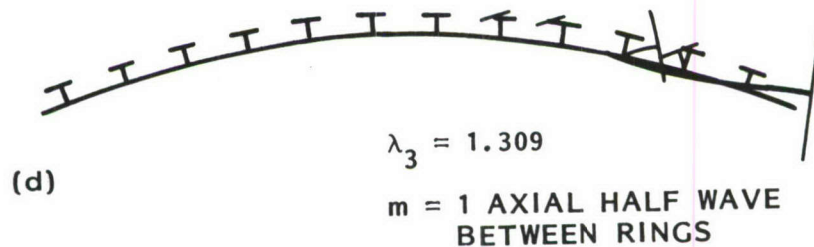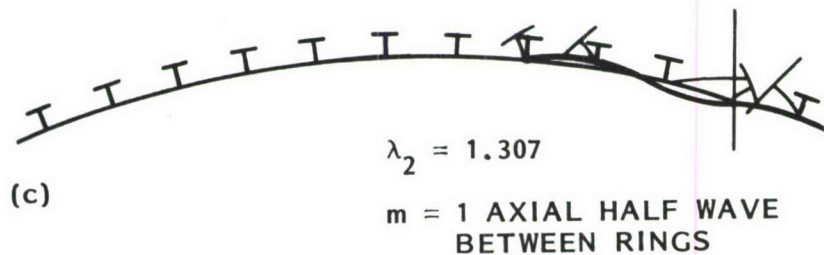
**Fig. 96 (a) Multi-segment, branched BOSOR4 model of the optimized panel gener-
ated by the PANEL processor (local buckling NOT permitted, and (b,c,d)
buckling modes corresponding to Load Set 1. All three buckling modes rep-
resent side-sway of the T-shaped stringers, and not wide column buckling.
The mode shapes vary as $\sin(m\pi x/L)$ along the axis of the panel, where L is
the ring spacing.**

239
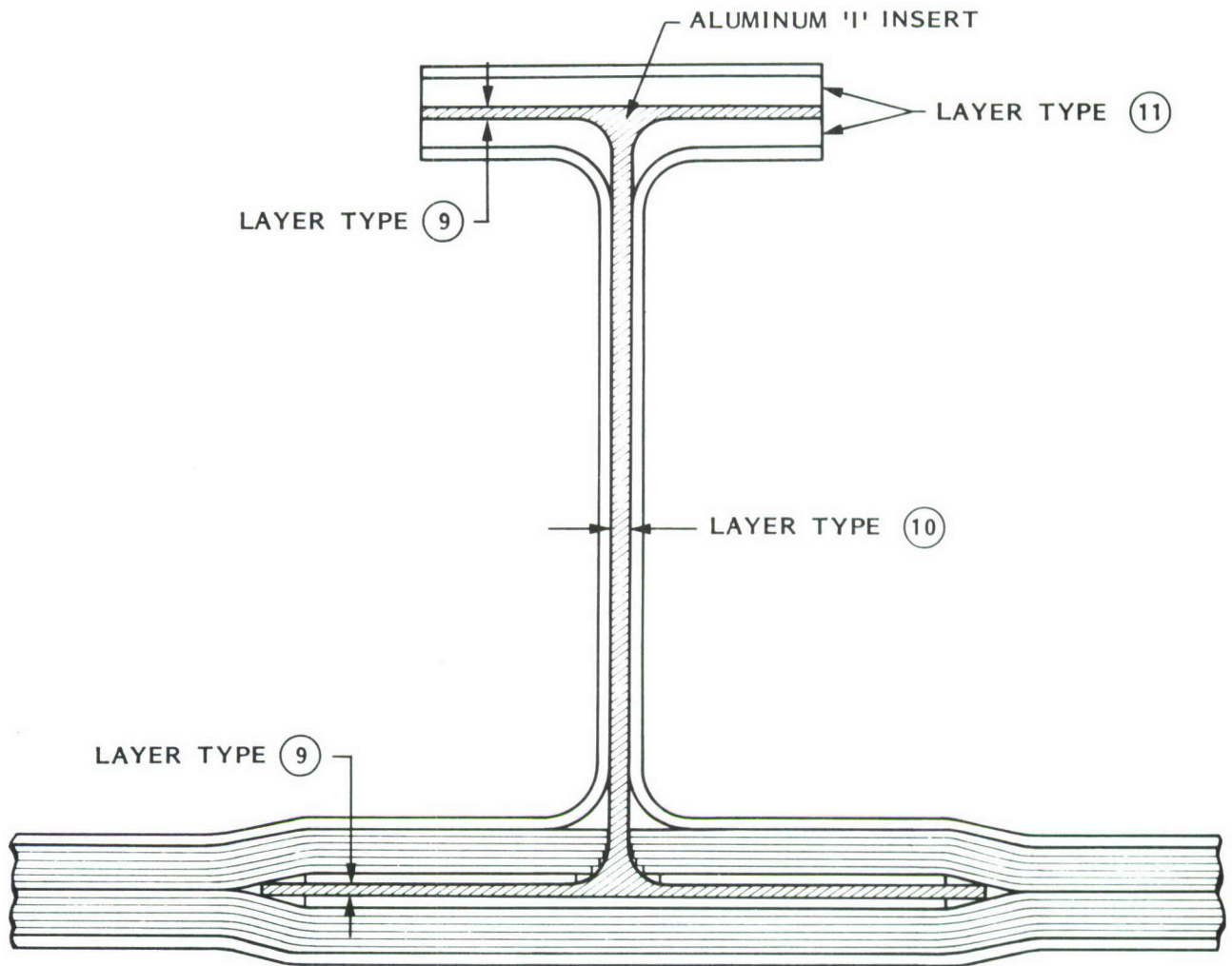
Fig. 97 Graphite-epoxy cloth and tape T-shaped stringer with aluminum insert. The purpose of the aluminum insert is to greatly increase the maximum allowable web peel force, which was only 100 lb/in in the previous design and is 1000 lb/in in this design. It was initially conjectured that such a concept will lead to greater weight reduction for panels designed to operate in the locally postbuckled regime. Results, however, show that although optimized designs of the panel can operate in the far−locally−postbuckled regime, these designs are not significantly lighter than those obtained without the aluminum insert.

(a)

0.896

DIMENSIONS
IN INCHES

1.54

0.804

b — 5.57

(b)

$\lambda_{LOCAL} = 0.339$
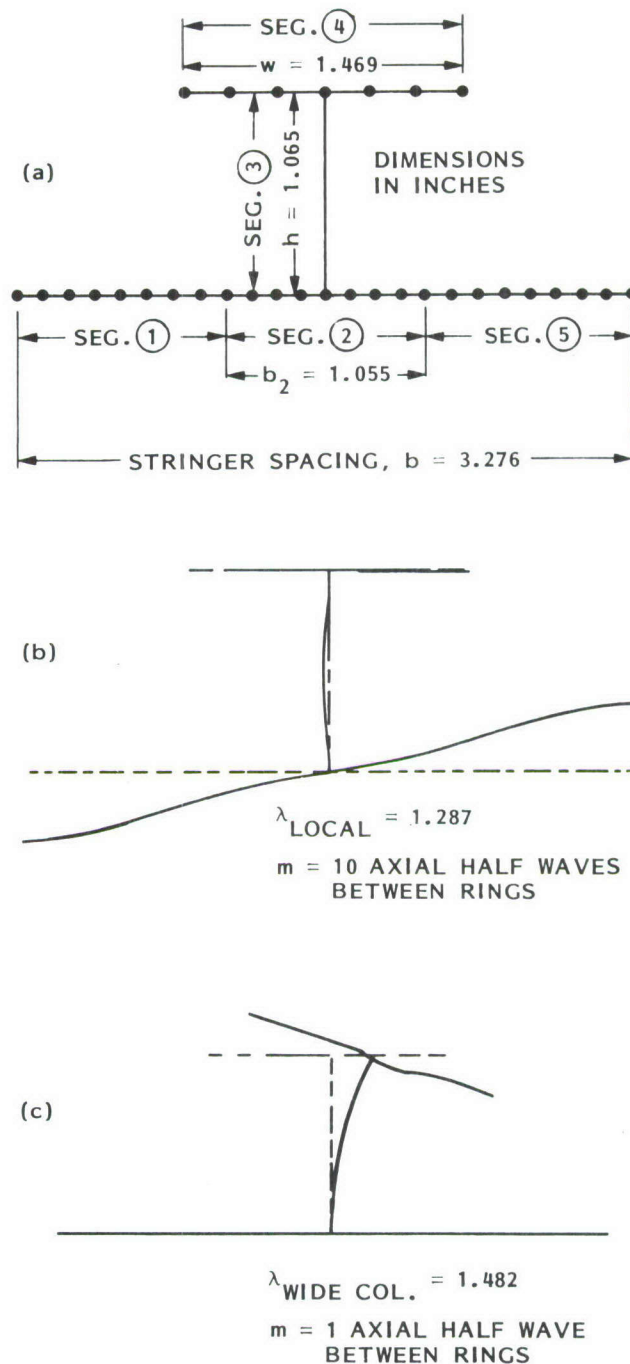
M = 6 HALF WAVES
BETWEEN RINGS
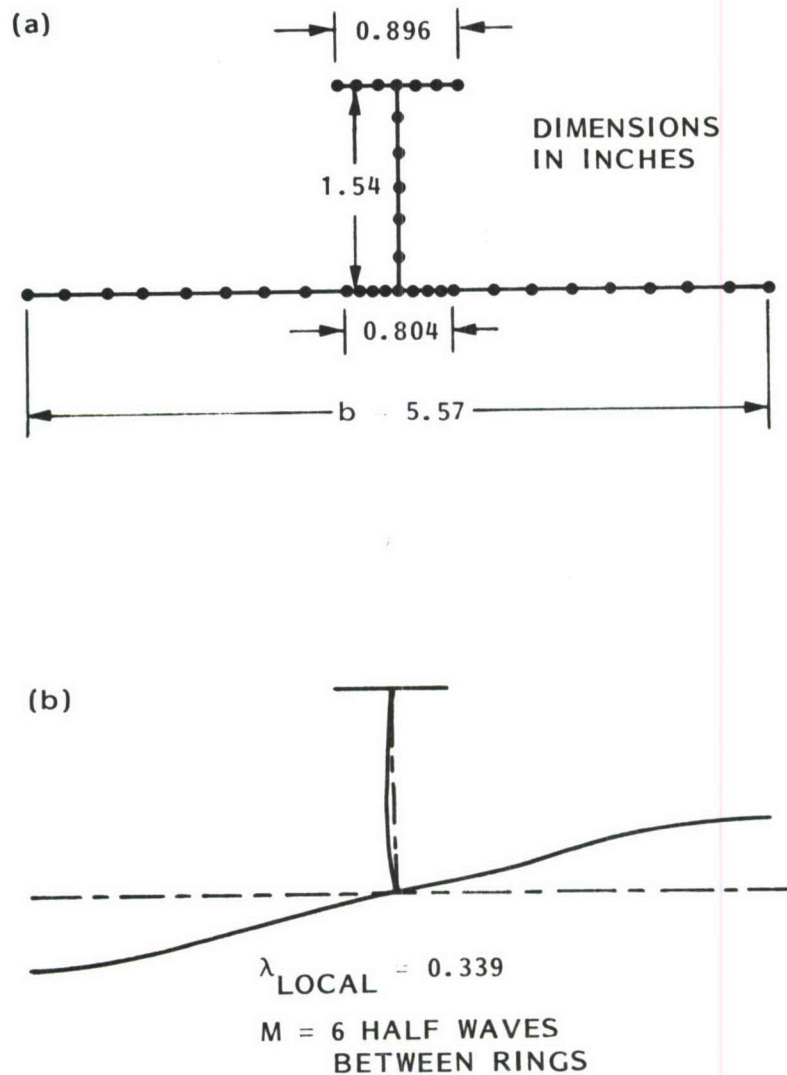
Fig. 98 Final optimum design for the case in which local postbuckling IS permitted,
showing (a) discretized panel module model, and (b) local buckling mode
and load factor corresponding to Load Set 1. The mode shape varies as
$\sin(M\pi x/L)$ along the axis of the panel, where L is the ring spacing. Since
the load factor for local buckling is λ_{LOCAL} equals 0.339, the optimum panel
is designed to operate at an axial load close to three times the local buckling
load.

241

(a)

DIMENSIONS
IN INCHES

w = 1.2

SEG. ⑤

SEG. ④

SEG. ⑥

h = 1.34

SEG. ①

SEG. ②

SEG. ③

SEG. ⑦

SEG. ⑧

$b_2 = 2.5$

b = 4.2

(b)

$\lambda_{LOCAL} = 0.9997$

M = 15 HALF WAVES
BETWEEN RINGS

(c)

$\lambda_{WIDE\ COL} = 1.517$

M = 1 HALF WAVE
BETWEEN RINGS

Fig. 99 Final optimum design for the hat-stiffened panel for the case in which local postbuckling is NOT permitted, showing (a) discretized panel module model, and (b,c) buckling modes and load factors corresponding to Load Set 1. (b) local buckling mode and load factor, and (c) wide column buckling mode and load factor. The mode shapes vary as $\sin(M\pi x/L)$ along the axis of the panel, where L is the ring spacing.

242

(a) DISCRETIZED BOSOR4 MODEL

(b) $\lambda_1 = 2.419$

(c) $\lambda_2 = 2.459$

(d) $\lambda_3 = 2.481$
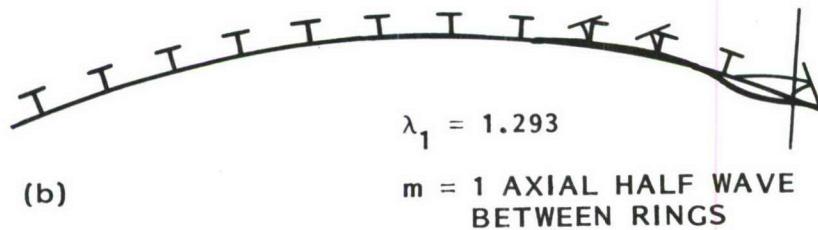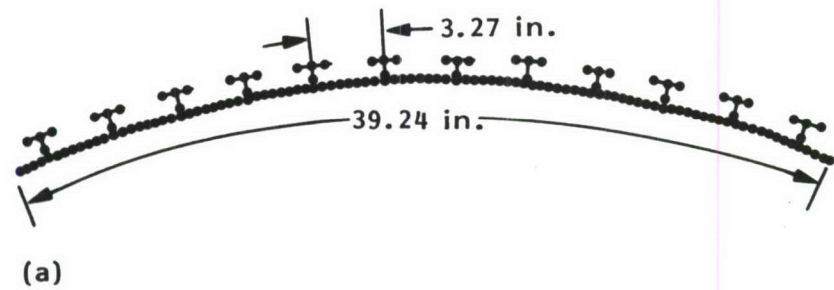
(e) $\lambda_4 = 2.604$

(f) $\lambda_5 = 2.705$

Fig. 100 (a) Multi-segment, branched BOSOR4 model of the optimized panel generated by the PANEL processor (local buckling NOT permitted, and (b,c,d,e,f) buckling modes corresponding to Load Set 1. All five buckling modes represent panel buckling between rings in which stringers and panel skin participate. The load factors are close to that predicted from the PANDA-type model for buckling between rings with smeared stringers. The mode shapes vary as $\sin(\pi x/L)$ along the axis of the panel, where L is the ring spacing.

243

APPENDIX A: NONLINEAR EQUILIBRIUM OF IMPERFECT, LOCALLY DEFORMED STRINGER-STIFFENED PANELS UNDER COMBINED IN-PLANE LOADS

ABSTRACT

A theory based on minimum potential energy for the nonlinear equilibrium of composite, stringer-stiffened, imperfect panels subjected to combined in-plane loads is derived. The normal displacement $w(x,y)$ is assumed to have the form $W(y)\sin[\pi(x - my)/L]$ in which x is the coordinate along the axis of the stringers, y is the coordinate in the plane of the panel skin and normal to x, m is the slope of the nodal lines in the local buckling pattern in the panel skin, and L is the half- wavelength of the local bifurcation buckling mode. The function $W(y)$ is obtained from a series expansion of the buckling modal normal displacement field obtained from a model in which the cross section of a panel module is discretized as in the BOSOR4 analysis of shells of revolution. Nonlinear strain-displacement relations analogous to those developed in 1946 by Koiter for perfect panels are extended to handle panels with imperfections in the form of the critical local bifurcation buckling mode. The theory is incorporated into the PANDA2 computer program for minimum weight design. The nonlinear theory for the prediction of behavior of locally imperfect panels appears to be properly implemented in PANDA2, since there is excellent agreement between PANDA2 and STAGS for the case of a uniformly axially compressed, imperfect, rectangular, isotropic panel loaded to four times the local bifurcation buckling load. The theory captures reasonably well the nonlinear modal interaction effect described in many papers published by Koiter, Hutchinson, Thompson, Tvergaard and others in the 1970's. There is good agreement between these previous theories, PANDA2 results, and tests. Locally and globally imperfect panels can be automatically optimized with PANDA2, as demonstrated for the case of a blade-stiffened, imperfect, aluminum panel. The inclusion of local and global imperfections with amplitudes likely to occur in practice does not appear to affect dramatically the behavior nor the optimum design of axially stiffened panels that behave approximately as wide columns in the general instability mode of failure. Optimum designs of imperfect blade, tee, and hat-stiffened panels are compared. Some recent modifications to the PANDA2 computer program are briefly described.

1. Introduction

The theory sketched in Section 13 of Ref. [A1] for equilibrium of locally postbuckled stiffened panels is valid only for perfect panels. The purposes of this discussion are to provide more details of the theory and to extend it to handle nonlinear behavior of a panel with an imperfection in the form of the local buckling mode. (Overall bowing imperfections are handled in a manner to be described later.)

If an axially stiffened panel has a finite imperfection in the form of the local buckling mode, there are no longer any distinct "prebuckling" and "postbuckling" phases of behavior. Rather, the panel deforms in a continuous manner as the external loads are increased. This difference in behavior for perfect and imperfect panels is illustrated in Fig. A1. An unstiffened, isotropic panel is subjected to uniform end shortening up to an average axial load four times the load at which the perfect panel buckles locally. The imperfection, in the form of the bifurcation buckling mode of the perfect panel, has five halfwaves along the length and one half wave across the width. Two cases are shown: an almost perfect panel, with normalized imperfection amplitude $w_0/t = 0.001$, and a panel with $w_0/t = 0.1$.

The almost perfect panel (imperfection amplitude $w_o/t = 0.001$) exhibits an almost discontinuous behavior at the bifurcation load, whereas the panel with larger imperfection amplitude, $w_o/t = 0.1$, exhibits a continuous softening followed by stiffening behavior.

Two computational advantages result from the inclusion of local imperfections:

1. The behavior of stiffened panels that have been optimized is often sensitive to imperfections. If imperfections are neglected in the theory, the program user must provide a significant factor of safety to compensate for random geometric imperfections that are always present in practical structures. It is difficult to choose an appropriate factor of safety. Introduction of an imperfection in the form of the local buckling mode of the perfect structure partially eliminates this difficulty. While it may still be necessary to introduce a factor of safety larger than unity, the factor can be much closer to unity and can be thought of as a factor to compensate for uncertainties in load, material properties, and failure criteria rather than as a factor to compensate for uncertainty in geometry. Uncertainties in load, material properties, and failure criteria generally do not affect the behavior with increasing severity, as does uncertainty in geometry, as the structure approaches its optimum configuration. Therefore it is particularly advantageous to include the effect of uncertainty in geometry in the structural analysis rather than compensate for it by use of a large, rather arbitrary, factor of safety.

2. Because of discontinuous behavior such as that exhibited in Fig. A1 for the almost perfect panel, design iterations often lead to designs and margins that jump around. For example, this behavior occurred during optimization of the ARIANE interstage, and is evident in Figs. 88 and 89 of Ref. [A1]. Introduction of a local imperfection smooths the behavior, as displayed in Fig. A1 for the panel with the larger imperfection amplitude. Therefore, gradients of behavior of imperfect panels with respect to design perturbations are generally smooth. They do not ordinarily lead to erratic swings in design or in design margins as the optimum state is sought.

245

2. Components of Strain Energy and External Work

The following derivation applies to panels that consist of segments each of which has a balanced laminate. Most of the derivation involves the extensional strain energy of the panel skin and stringer web(s) and flange. Rings are ignored, as this section is concerned only with the portion of the structure between adjacent rings, that is, the panel skin and stringers. The relevant geometry is shown in Fig. 9 or Fig. 13 of Ref. [A1]: a single panel module including one stringer and a width of panel skin that represents the spacing b of the stringers. Equilibrium equations are derived from the principle of virtual work and the first variation of the total potential, $U - W$, in which U is the strain energy and W is the work done by average prescribed external loads, N_1, N_2, N_{12}.

For balanced laminates the components of strain energy are:

1. First variation of extensional energy in panel skin (including stringer base):

$$U'_{ext}(skin) = \int_0^{2L} \int_0^b (N_x e'_x + N_y e'_y + N_{xy} e'_{xy}) dy dx \qquad (1)$$

2. First variation of extensional energy in stringer web(s) and flange:

$$U'_{ext}(stringer) = \int_0^{2L} \sum_{i=3}^4 \int_0^{width_i} (N_x^i e_x^{i\prime} + N_s^i e_s^{i\prime} + N_{xs}^i e_{xs}^{i\prime}) ds dx \qquad (2)$$

3. Bending and twisting strain energy in the panel skin (including the stringer base):

$$U_{bend}(skin) = \frac{1}{2} \int_0^{2L} \int_0^b [C_{44} w_{,xx}^2 + 2C_{45} w_{,xx} w_{,yy} + C_{55} w_{,yy}^2$$
$$+ 4w_{,xy}(C_{46} w_{,xx} + C_{56} w_{,yy} + C_{66} w_{,xy})] dy dx \qquad (3)$$

4. Bending and twisting strain energy in the stringer web and flange:

$$U_{bend}(stringer) = \frac{1}{2} \int_0^{2L} \sum_{i=3}^4 \int_0^{width_i} [C_{44}^i w_{,xx}^2 + 2C_{45}^i w_{,xx} w_{,ss} + C_{55}^i w_{,ss}^2$$
$$+ 4w_{,xs}(C_{46}^i w_{,xx} + C_{56}^i w_{,ss} + C_{66}^i w_{,xs})] ds dx \qquad (4)$$

In Eqs. (1-4) $()'$ denotes "derivative with respect to a degree of freedom"; $()_{,xx}$ means $\partial^2()/\partial x^2$; b is the stringer spacing; L is the axial length of one half wave of the local buckling pattern; x is the axial coordinate; y is the transverse coordinate, measured from the left-hand side of the panel module shown in Fig. 9 in Ref. [A1] (not from the attachment line of the stringer web to the panel skin, as shown there); $i = 3$ denotes stringer web (Segment 3 in Fig. 9 of [A1]); $i = 4$ denotes outstanding stringer flange (Segment 4 in Fig. 9 of [A1]); $width_i$ means width of the ith stringer part (e.g. height h for the web and width

w for the flange); and s is the local segment coordinate shown in Fig. 9 of [A1]. The C_{ij} in Eqs. (3) and (4) are the coefficients of the integrated constitutive relationship that appear in Eq. (8.1) of Ref. [A1]. The quantities N_x, N_y, N_{xy} are the stress resultants at x, y in the panel skin, and N_x^i, N_s^i, N_{xs}^i are the stress resultants at x, s in the stringer web ($i = 3$) and stringer flange ($i = 4$). The quantities $e_x, e_y, e_{xy}, e_s, e_{xs}$ are the strain components in the reference surface, which herein is the middle surface, of the various segments of the panel module.

The first variation of the work done by the uniform external in-plane loads, N_1, N_2, N_{12}, is given by

$$W' = 2Lb(N_1 e_1' + N_2 e_2' + N_{12} e_{12}') \tag{5}$$

in which e_1, e_2, e_{12} are the average in-plane strains of the reference surface of the panel skin, and

$$N_1 = \frac{1}{b}\left\{ \int_0^b N_x dy + \sum_{i=3}^4 \int_0^{width_i} N_x^i ds \right\} \tag{6}$$

and

$$N_2 = \frac{1}{2L} \int_0^{2L} N_y dx \tag{7}$$

The in-plane shear resultant N_{12} is constant and equal to N_{xy}. The axial resultant N_x is assumed to be constant in the x-direction, and the hoop resultant N_y is assumed to be constant in the y-direction. Therefore, we can write:

$$N_1 = \frac{1}{2L} \int_0^{2L} \frac{1}{b}\left\{ \int_0^b N_x dy + \sum_{i=3}^4 \int_0^{width_i} N_x^i ds \right\} dx \tag{8}$$

and

$$N_2 = \frac{1}{2L}\frac{1}{b} \int_0^{2L} \int_0^b N_y dy dx \tag{9}$$

The derivatives of the strains with respect to the degrees of freedom (as yet unspecified) of the problem can be expressed as derivatives of uniform average strains and increments, thus:

$$\begin{aligned} e_x' &= e_1' + \Delta e_x' \\ e_y' &= e_2' + \Delta e_y' \\ e_{xy}' &= e_{12}' + \Delta e_{xy}' \end{aligned} \tag{10}$$

From Eqs. (1), (2), and (5), the assumption of uniform in-plane shear resultant N_{xy}, and with use of Eqs. (8) and (9), it follows that the first variation of the extensional energy of skin and stringers minus the first variation of the work done by the prescribed uniform external in-plane loads N_1, N_2, N_{12} is given by:

$$\begin{aligned} (U_{ext} - W)' = \int_0^{2L} &\left\{ \int_0^b (N_x \Delta e_x' + N_y \Delta e_y' + N_{xy} \Delta e_{xy}') dy \right. \\ &\left. \sum_{i=3}^4 \int_0^{width_i} (N_x^i \Delta e_x^{i'} + N_s^i \Delta e_s^{i'} + N_{xs}^i \Delta e_{xs}^{i'}) ds \right\} dx \end{aligned} \tag{11}$$

3. $\Delta e_x, \Delta e_y, \Delta e_{xy}$ in the Panel Skin

In the following development it is assumed that the undeformed, perfect panel skin is flat. The formulas in this section, valid for imperfect panels, are analogous to those derived by Koiter [A2], who analyzed perfect panels.

The normal displacement $w(x,y)$ in the panel skin is assumed to have the form

$$w(x,y) = W(y) \sin[\pi(x - my)/L] \tag{12}$$

in which $W(y)$ is given later [Eq. (24b)], and m is the slope of the local buckling nodal lines. The initial imperfection is assumed to have a similar form

$$w_0(x,y) = W_0(y) \sin[\pi(x - my)/L] \tag{13}$$

in which $W_0(y)$ is given later [Eq. (24a)]. In a lengthy derivation, Koiter [A2] establishes formulas for perfect panels analogous to the following, which apply to locally imperfect panels:

Axial strain increment:

$$\Delta e_x = N(W^2 + 2W_0 W) \tag{14}$$

Hoop strain increment:

$$\Delta e_y = -\nu \Delta e_x + C + \frac{1}{8}(WW_{,yy} - W_{,y}^2 + WW_{0,yy} + W_0 W_{,yy} - 2W_{,y} W_{0,y}) \cos[2\pi(x - my)/L] \tag{15}$$

In-plane shear strain increment:

$$\Delta e_{xy} = -2Nm\frac{1}{b}\int_0^b (W^2 + 2W_0 W)dy \tag{16}$$

in which

$$N = \pi^2/(4L^2); \qquad \nu = C_{12}/C_{22} \tag{17}$$

and

$$C = \frac{1}{b}\int_0^b [N(\nu + m^2)(W^2 + 2W_0 W) + \frac{1}{4}(W_{,y}^2 + 2W_{0,y} W_{,y})]dy \tag{18}$$

Notice that in the Koiter theory Δe_x is a function of y only and Δe_{xy} is uniform throughout the entire panel skin.

4. $\Delta e_x, \Delta e_s, \Delta e_{xs}$ in the Stringer Web and Flange

We assume that in the stringer web and flange the slope of the local buckling nodal lines is zero. The displacement components have the form:

$$\begin{aligned}
u(x,s) &= U(s) \sin(\pi x/L) \\
v(x,s) &= V(s) \cos(\pi x/L) \\
w(x,s) &= W(s) \sin(\pi x/L)
\end{aligned} \tag{19}$$

248

in which $U(s), V(s), W(s)$ have the same form as the local buckling modal displacement components. The total strain components at any location (x, s) in the stringer web or flange (neglecting thermal strains, which are not functions of the degrees of freedom and therefore do not appear in the derivatives $()'$), are given by

Axial strain:

$$e_x^i = e_1 - Z\kappa_x + v_{,x} + \frac{1}{2}(u_{,x}^2 + w_{,x}^2 + 2u_{0,x}u_{,x} + 2w_{0,x}w_{,x}) \tag{20}$$

Strain in width direction, s:

$$e_s^i = -\nu e_x^i \tag{21}$$

In-plane shear strain:

$$e_{xs}^i = v_{,s} + u_{,x} + w_{,x}w_{,s} + w_{,x}w_{0,s} + w_{0,x}w_{,s} \tag{22}$$

in which Z is the coordinate normal to the panel skin and positive as shown for Segment 1 in Fig. 9 of Ref. [A1]; κ_x is the change in overall axial bowing due to the applied loads, positive in the sense that the lower surface of the panel skin portrayed in Fig. 9 of [A1] becomes concave; and ν is defined as in Eq. (17b) with the C_{ij} being the constitutive coefficients for the appropriate stringer segment, either web ($i = 3$) or flange ($i = 4$).

The derivatives of the strain increments with respect to the as yet unspecified degrees of freedom appear in the second line of Eq. (11). They are given by

$$\begin{aligned}
\Delta e_x^{i\prime} &= v_{,x}' + \frac{1}{2}(u_{,x}^2 + w_{,x}^2 + 2u_{0,x}u_{,x} + 2w_{0,x}w_{,x})' \\
\Delta e_s^{i\prime} &= -\nu \Delta e_x^{i\prime} \\
\Delta e_{xs}^{i\prime} &= v_{,s}' + u_{,x}' + (w_{,x}w_{,s} + w_{,x}w_{0,s} + w_{0,x}w_{,s})'
\end{aligned} \tag{23}$$

The κ_x term is absent from Eq. (23a) because κ_x is not considered to be a function of any of the degrees of freedom of the nonlinear equilibrium problem. Instead, κ_x is assumed to grow hyperbolically as axial compression increases. An amplitude factor for any initial axial bowing, whether it be caused by an initial geometric imperfection, applied pressure, residual deformation due to curing the panel, axial load eccentricity, or any combination of these effects, is calculated based on a preliminary estimate of the general instability load factor. The overall axial curvature change, κ_x is assumed to be equal to the axial bowing caused by the effects just listed multiplied by the amplitude factor, which is a number between one and ten, depending on how close the applied axial load is to the estimated critical load factor. This amplitude factor is derived in Section 16 below.

5. Initial Local Imperfection and Modal Displacements

The local imperfection causes no residual stresses, but simply represents modification of the shape of the panel. In the panel skin the initial local imperfection W_0 and additional displacement W caused by loading are assumed to be given by

$$\begin{aligned}
W_0(y) &= w_0\phi(y) \\
W(y) &= f(\phi + a\phi^3)
\end{aligned} \tag{24}$$

in which w_0 is a PANDA2-user-supplied amplitude, and $\phi = \phi(y)$ is the critical local buckling mode obtained from the single panel module discretized model, such as shown in Fig. 20 a and b and in Fig. 22 a and b of Ref. [A1]. Note that the local buckling mode $\phi(y)$ contains in general not only normal modal displacements W, but also in-plane modal displacements U and V. However, for a flat panel skin, to which this section applies, the in-plane modal displacement components U and V are zero. In the PANDA2 program ϕ is a vector containing displacements at the nodal points in the discretized panel module model.

In the stringer web and flange the initial local imperfection U_0, V_0, W_0 and additional displacement U, V, W caused by loading are taken as

$$
\begin{aligned}
U_0(s), V_0(s), W_0(s) &= w_0 \phi(s) \\
U(s), V(s), W(s) &= f\phi(s)
\end{aligned}
\tag{25}
$$

Note that in the case of the stringer web and flange in in-plane modal displacement components U and V are not always zero, especially in the flange.

The amplitude f, the "mode shape modification parameter" a, and the slope of the local buckling nodal lines m, are the three degrees of freedom of the nonlinear equilibrium problem established by minimization of the total potential energy, $U - W$, with respect to these degrees of freedom.

6. Stress Resultants N_x, N_y, N_{xy}

For a balanced laminate, the stress resultants that appear in Eq. (11) have the form

$$
\begin{aligned}
N_x &= C_{11}e_x + C_{12}e_y + N_{x0} \\
N_y &= C_{12}e_x + C_{22}e_y + N_{y0} \\
N_{xy} &= C_{33}e_{xy}
\end{aligned}
\tag{26}
$$

in which N_{x0} and N_{y0} are initial resultants from curing the panel, and the reference surface strains are given by

$$
\begin{aligned}
e_x &= e_1 + \Delta e_x \\
e_y &= e_2 + \Delta e_y \\
e_{xy} &= e_{12} + \Delta e_{xy}
\end{aligned}
\tag{27}
$$

With subscript y replaced by subscript s, Eqs. (26) and (27) apply to the stringer web and flange also.

7. Extensional Strain Energy in the Panel Skin

In this section we are concerned only with the first line of Eq. (11). Insertion of Eqs. (14) - (16) into Eqs. (27), and Eqs. (27) thus modified into Eqs. (26), and Eqs. (26) thus

modified into the first line of Eq. (11), followed by integration over x and some algebra yields

$$\frac{(U_{ext} - W)'}{2Lb} = \frac{1}{b} \int_0^b \left\{ (C_{11}^* e_1 + N_{x0}^*) N(W^2 + 2W_0 W)' + \frac{1}{2} C_{11}^* [(W^2 + 2W_0 W)^2 N^2]' \right.$$

$$+ \frac{C_{22}}{256} [(WW_{,yy} - W_{,y}^2 + WW_{0,yy} + W_0 W_{,yy} - 2W_{,y} W_{0,y})^2]' \bigg\} dy$$

$$+ (\bar{C}_{12} e_1 + \bar{C}_{22} e_2^* + \bar{N}_{y0}) C' + N_{xy} \Delta e_{xy}' \tag{28}$$

in which

$$C_{11}^* = C_{11} - C_{12}^2 / C_{22} \qquad N_{x0}^* = N_{x0} - \nu N_{y0}$$

$$\bar{C}_{ij} = \sum_{i=1}^2 B_{1i} C_{ij}^i \qquad \bar{N}_{y0} = \sum_{i=1}^2 B_{1i} N_{y0}^i = 0 \tag{29}$$

$$B_{11} = (b - b_2)/b; \qquad B_{12} = b_2/b$$

$$e_2^* = e_2 + C$$

with N and ν given by Eq. (17), and C given by Eq. (18). The quantity b_2 is the width of the base under the stringer. It is assumed herein that the rings are far enough apart so that $\bar{N}_{y0}$, the residual hoop resultant between rings due to curing the panel, equals zero. In Eq. (28) $()'$ denotes "derivative with respect to a degree of freedom". The degrees of freedom are:

1. The amplitude factor f given in Eqs. (24b) and (25b);
2. The coefficient a that appears in Eq. (24b);
3. The slope m of the buckling nodal lines [Eqs. (12),(13)].

8. Evaluating e_1 and e_2^*

Equation (28) contains the average strain quantities, e_1 and e_2^*, which must be expressed in terms of the degrees of freedom and other parameters of the equilibrium problem such as the known, prescribed applied average loads, N_1 and N_2. In this section we will derive expressions for e_1 and e_2^*.

Use of the right-hand-sides of Eqs. (26a,b) in Eqs. (8) and (9) gives

$$N_1 = \frac{1}{2L} \int_0^{2L} \frac{1}{b} \left\{ \int_0^b (C_{11} e_x + C_{12} e_y + N_{x0}) dy \right.$$

$$\left. + \sum_{i=3}^4 \int_0^{width_i} (C_{11}^i e_x^i + C_{12}^i e_s^i + N_{x0}^i) ds \right\} dx \tag{30}$$

$$N_2 = \frac{1}{2L} \int_0^{2L} \frac{1}{b} \int_0^b (C_{12} e_x + C_{22} e_y + N_{y0}) dy dx$$

Insertion of the right-hand-sides of Eqs. (27) into Eqs. (26), use of Eqs. (14), (15), (20), and (21), and integration over x leads to an expression for the average axial resultant N_1:

$$
N_1 = \frac{1}{b} \int_0^b [C_{11}e_1 + C_{12}e_2^* + C_{11}^* N(W^2 + 2W_0 W) + N_{x0}] dy
$$
$$
+ \frac{1}{b} \sum_{i=3}^4 \int_0^{width_i} \left\{ C_{11}^{*i}[e_1 - Z\kappa_x + N(U^2 + W^2 + 2U_0 U + 2W_0 W)] + N_{x0}^i \right\} ds \quad (31)
$$

and for the average hoop resultant N_2:

$$
N_2 = \bar{C}_{12}e_1 + \bar{C}_{22}e_2^* + \bar{N}_{y0} = \bar{C}_{12}e_1 + \bar{C}_{22}e_2^* \quad (32)
$$

In Eq. (31) the quantities U and U_0 are the modal displacement component and initial local imperfection component in the s-direction in the stringer web and flange. Use of Eqs. (24) and integration over y in the first integral of Eq. (31), and use of Eqs. (25) and integration over s in the second integral of Eq. (31) yields

$$
N_1 = \bar{C}_{11}e_1 + \bar{C}_{12}e_2^* + \bar{N}_{x0} + f^2(g_7 + ag_8 + a^2 g_9) + f(g_{w7} + ag_{w8})
$$
$$
+ (STIFL1)e_1 + C_s(1,4)\kappa_x + \frac{1}{b} \sum_{i=3}^4 (width_i) N_{x0}^i + (ASUM6) N(f^2 + 2fw_0) \quad (33)
$$

in which the $\bar{C}_{ij}$ are given by Eq. (29c); e_2^* is given by Eq. (29f); $C_s(1,4)$ is the constitutive coefficient for the panel with smeared stringers (between rings) that relates axial load N_1 to the overall change in curvature κ_x; and

$$
\bar{N}_{x0} = \sum_{i=1}^2 B_{1i} N_{x0}^i
$$

$$
g_7 = N \sum_{i=1}^2 C_{11}^{*i} A_1^i \qquad g_8 = 2N \sum_{i=1}^2 C_{11}^{*i} A_2^i \qquad g_9 = N \sum_{i=1}^2 C_{11}^{*i} A_3^i \qquad (34)
$$

$$
g_{w7} = 2w_0 g_7 \qquad g_{w8} = w_0 g_8
$$

$$
ASUM6 = \sum_{i=3}^4 C_{11}^{*i} A_{21}^i \qquad STIFL1 = \frac{1}{b} \sum_{i=3}^4 (width_i) C_{11}^{*i}.
$$

The quantity C_{11}^* is defined in Eq. (29a) and the A_k^i are integrals of functions of the local buckling modal displacements U, V, W included in Eqs. (35). The A_k that do not appear in Eqs. (34) arise from other integrals that appear in Eq. (28) and that will appear in the expressions for bending energy, to be developed below. The superscript in the terms A_k^i and C_{11}^{*i} pertains to the segment number of the panel module, with $i = 1$ signifying the thin part of the panel skin, $i = 2$ signifying the thickened base under the stringer, $i = 3$ signifying the stringer web, and $i = 4$ signifying the stringer flange. A complete list of

252

the integrals over the cross section of the panel module, required for the entire nonlinear equilibrium analysis follows:

$$A_1 = \frac{1}{b}\int_{y_1}^{y_2} W^2 dy \quad A_2 = \frac{1}{b}\int_{y_1}^{y_2} W^4 dy \quad A_3 = \frac{1}{b}\int_{y_1}^{y_2} W^6 dy \quad A_4 = \frac{1}{b}\int_{y_1}^{y_2} W_{,y}^2 dy$$

$$A_5 = \frac{1}{b}\int_{y_1}^{y_2} W^2 W_{,y}^2 dy \quad A_6 = \frac{1}{b}\int_{y_1}^{y_2} W^4 W_{,y}^2 dy \quad A_7 = \frac{1}{b}\int_{y_1}^{y_2} W W_{,yy} dy$$

$$A_8 = \frac{1}{b}\int_{y_1}^{y_2} W^8 dy \quad A_9 = \frac{1}{b}\int_{y_1}^{y_2} W^{10} dy \quad A_{10} = \frac{1}{b}\int_{y_1}^{y_2} W^{12} dy$$

$$A_{11} = \frac{1}{b}\int_{y_1}^{y_2} (W W_{,yy} - W_{,y}^2) dy \quad A_{12} = \frac{1}{b}\int_{y_1}^{y_2} 8 W^3 W_{,yy}(W W_{,yy} - W_{,y}^2) dy$$

$$A_{13} = \frac{1}{b}\int_{y_1}^{y_2} [16 W^6 W_{,yy}^2 + 6(W W_{,yy} - W_{,y}^2)(W^5 W_{,yy} - W^4 W_{,y}^2)] dy$$

$$A_{14} = \frac{1}{b}\int_{y_1}^{y_2} 24 W^3 W_{,yy}(W^5 W_{,yy} - W^4 W_{,y}^2) dy$$

$$A_{15} = \frac{1}{b}\int_{y_1}^{y_2} 9(W^5 W_{,yy} - W^4 W_{,y}^2)^2] dy \tag{35}$$

$$A_{16} = \frac{1}{b}\int_{y_1}^{y_2} W^3 W_{,yy} dy \quad A_{17} = \frac{1}{b}\int_{y_1}^{y_2} W^5 W_{,yy} dy \quad A_{18} = \frac{1}{b}\int_{y_1}^{y_2} W_{,yy}^2 dy$$

$$A_{19} = \frac{1}{b}\int_{y_1}^{y_2} W_{,yy}(6 W^2 W_{,yy} + 12 W W_{,y}^2) dy$$

$$A_{20} = \frac{1}{b}\int_{y_1}^{y_2} (3 W^2 W_{,yy} + 6 W W_{,y}^2)^2 dy$$

$$A_{21}^i = \frac{1}{b}\int_0^{width_i} (U^2 + W^2) ds \quad A_{22}^i = \frac{1}{b}\int_0^{width_i} (V_{,s} + 2 N^{1/2} U)^2 ds$$

$$A_{23}^i = \frac{1}{b}\int_0^{width_i} V^2 ds \quad A_{24}^i = \frac{1}{b}\int_0^{width_i} (U^2 + W^2) Z ds$$

$$A_{25}^i = \frac{1}{b}\int_0^{width_i} (U^2 + W^2)^2 ds \quad A_{26} = \frac{1}{b}\int_{y_1}^{y_2} 16 W^6 W_{,yy}^2 dy$$

in which the limits y_1 and y_2 depend on which segment of the panel module cross section is involved in the integral. When Eqs. (35) are applied to the stringer web and flange the independent variable y should be understood as the coordinate s along the web or flange, as shown in Fig. 9 of Ref. [A1].

From Eq. (32) we have

$$e_2^* = (N_2 - \bar{C}_{12} e_1)/\bar{C}_{22} \tag{36}$$

Insertion of the right-hand-side of Eq. (36) into Eq. (33) and solution for e_1 yields

$$e_1 = \left\{ N_1 - C_s(1,4)\kappa_x - \bar{\nu} N_2 - f^2(g_7 + N(ASUM6) + a g_8 + a^2 g_9) \right.$$

253

$$-f(g_{w7} + 2w_0 N(ASUM6) + ag_{w8})\}/(\bar{C}_{11} - \bar{\nu}\bar{C}_{12} + STIFL1) \tag{37}$$

It should be emphasized that the residual stress terms that occur in Eq. (33) must add to zero:

$$\bar{N}_{x0} + \frac{1}{b}\sum_{i=3}^{4}(width_i)N_{x0}^i = 0 \tag{38}$$

since the residual stress over the entire panel module cross section must be self-equilibrating.

The average strain components, which appear in Eq. (28), can now be expressed in the form:

$$\begin{aligned} e_1 &= F_1 + f^2(g_{11} + ag_{12} + a^2 g_{13}) + f(g_{w11} + ag_{w12}) \\ e_2^* &= F_2 + f^2(g_{21} + ag_{22} + a^2 g_{23}) + f(g_{w21} + ag_{w22}) \end{aligned} \tag{39}$$

in which

$$\begin{aligned} F_1 &= (N_1 - C_s(1,4)\kappa_x - \bar{\nu}N_2)/A_{x11} \\ F_2 &= N_2/\bar{C}_{22} - \bar{\nu}F_1 \\ \bar{\nu} &= \bar{C}_{12}/\bar{C}_{22} \end{aligned} \tag{40}$$

$$(g_{21}, g_{22}, g_{23}, g_{w21}, g_{w22}) = -\bar{\nu}(g_{11}, g_{12}, g_{13}, g_{w11}, g_{w12})$$

and $g_{11}, g_{12}, g_{13}, g_{w11}, g_{w12}$ are easily derived from Eq. (37). The quantity A_{x11} is the denominator of the right-hand-side of Eq. (37).

9. Extensional Strain Energy in Stringer Web and Flange

The extensional strain energy in the stringer web and flange is expressed in the second line of Eq. (11), with the strain increments given in Eqs. (23) and the stress resultants given by Eqs. (26) (replace y by s in the subscripts). Noting that the resultant $N_s = 0$, we obtain for the derivative of the extensional strain energy density

$$\frac{(U_{ext} - W)'}{2Lb} = \frac{1}{2L}\int_0^{2L}\frac{1}{b}\sum_{i=3}^{4}\int_0^{width_i}\left\{[C_{11}^{*i}(e_1 - Z\kappa_x + \Delta e_x^i) + N_{x0}^{*i}]\Delta e_x^{i\prime} + C_{33}^i e_{xs}^i \Delta e_{xs}^{i\prime}\right\}ds\,dx \tag{41}$$

in which Δe_x and Δe_{xs} are given by Eqs. (23a,c) without the primes, C_{11}^* and N_{x0}^* are given by Eqs. (29a,b), and $()'$ denotes differentiation with respect to the amplitude parameter f. Use of the right-hand-sides of Eqs. (23) with and without the primes, as appropriate, use of Eqs. (25), and integration over x yields

$$\begin{aligned} \frac{(U_{ext} - W)'}{2Lb} = {}& N[e_1(ASUM6) - \kappa_x(ASUM6P) + TSUM6](f^2 + 2fw_0)' \\ & + [N(ASUM7) + (A6SUM2)/4](f^2)' \\ & + [3N^2(ASUM4)/4 + N(A6SM10)/4]((f^2 + 2fw_0)^2)' \end{aligned} \tag{42}$$

in which

$$TSUM6 = \sum_{i=3}^{4} N_{x0}^{*i} A_{21}^i \qquad ASUM6 = \sum_{i=3}^{4} C_{11}^{*i} A_{21}^i \qquad ASUM6P = \sum_{i=3}^{4} C_{11}^{*i} A_{24}^i$$

$$ASUM4 = \sum_{i=3}^{4} C_{11}^{*i} A_{25}^i \qquad ASUM7 = \sum_{i=3}^{4} C_{11}^{*i} A_{23}^i \qquad A6SUM2 = \sum_{i=3}^{4} C_{33}^{i} A_{22}^i \qquad (43)$$

$$A6SM10 = \sum_{i=3}^{4} C_{33}^{i} A_{5}^i$$

10. Further Development of Extensional Strain Energy in Skin

With use of Eqs. (16), (18), (24), (32), and (35) in Eq. (28), and integration over the spacing b between stringers, yields

$$
\begin{aligned}
\frac{(U_{ext} - W)'}{2Lb} = \sum_{i=1}^{2} \Big\{ & NC_{11}^{*i} e_1 \{ f^2(A_1^i + 2aA_2^i + a^2 A_3^i) + fw_0(2A_1^i + 2aA_2^i) \}' \\
& + NN_{x0}^{*i} \{ f^2(A_1^i + 2aA_2^i + a^2 A_3^i) + fw_0(2A_1^i + 2aA_2^i) \}' \\
& + (N_2 + \bar{N}_{y0}) \big[N\nu^i \{ f^2(A_1^i + 2aA_2^i + a^2 A_3^i) + fw_0(2A_1^i + 2aA_2^i) \}' \\
& + \{ f^2(A_4^i + 6aA_5^i + 9a^2 A_6^i) + fw_0(2A_4^i + 6aA_5^i) \}'/4 \big] \\
& + C_{11}^{*i} N^2 \{ f^4(A_2^i + 4aA_3^i + 6a^2 A_8^i + 4a^3 A_9^i + a^4 A_{10}^i) \}'/2 \\
& + \frac{C_{22}^i}{256} \{ f^4(A_{11}^i + aA_{12}^i + a^2 A_{13}^i + a^3 A_{14}^i + a^4 A_{15}^i) \}' \\
& + C_{11}^{*i} N^2 w_0 \{ f^3(2A_2^i + 6aA_3^i + 6a^2 A_8^i + 2a^3 A_9^i) \}' \\
& + \frac{C_{22}^i w_0}{256} \{ f^3(4A_{11}^i + 3aA_{12}^i + 2a^2 A_{13}^i + a^3 A_{14}^i) \}' \\
& + C_{11}^{*i} N^2 w_0^2 \{ f^2(2A_2^i + 4aA_3^i + 2a^2 A_8^i) \}' \\
& + \frac{C_{22}^i w_0^2}{256} \{ f^2(4A_{11}^i + 2aA_{12}^i + a^2 A_{26}^i) \}' \\
& + N \big[[(N_2 + \bar{N}_{y0})m^2 - 2mN_{xy}] \{ f^2(A_1^i + 2aA_2^i + a^2 A_3^i) \\
& + fw_0(2A_1^i + 2aA_2^i) \}' \big]' \Big\}
\end{aligned}
$$

$$(44)$$

in which the A_k^i are integrals of the type listed in Eqs. (35) and e_1 is given by Eq. (37).

11. Bending/Twisting Strain Energy Density of the Panel Skin and Stringer Parts

If Eqs. (12), (13), (24), and (35) are used with Eqs. (3), and integration is performed with respect to x and y, the following expression results for the bending and twisting strain

energy density of the panel skin:

$$\frac{U_{bend}(skin)}{2Lb} = f^2 \sum_{i=1}^{2} \left\{ 4N^2 D_{11}^{*i}(A_1^i + 2aA_2^i + a^2 A_3^i) \right.$$
$$+ ND_{12}^{*i}[A_7^i + a(4A_{16}^i + 6A_5^i) + a^2(3A_{17}^i + 6A_6^i)]$$
$$+ ND_{22}^{*i}(A_4^i + 6aA_5^i + 9a^2 A_6^i)$$
$$\left. + C_{55}^i(A_{18}^i + aA_{19}^i + a^2 A_{20}^i)/4 \right\} \tag{45}$$

in which
$$D_{11}^{*i} = C_{44}^i + 2C_{45}^i m^2 + C_{55}^i m^4 - 4C_{46}^i m - 4C_{56}^i m^3 + 4C_{66}^i m^2$$
$$D_{12}^{*i} = -2C_{45}^i - 2C_{55}^i m^2 + 4C_{56}^i m \tag{46}$$
$$D_{22}^{*i} = 4C_{55}^i m^2 - 8C_{56}^i m + 4C_{66}^i$$

The C_{ij}^i are the bending and twisting components of the thickness-integrated constitutive relationship given by Eq. (8.1) of Ref. [A1]; m is the slope of the local buckling nodal lines; $i = 1$ denotes the part of the panel skin that does not form the stringer base of width b_2; and $i = 2$ denotes the stringer base of width b_2.

The bending/twisting strain energy density of the stringer web and flange are calculated in an analogous manner through use of Eqs. (19b), (25) and (35) in Eq. (4). The final expression is:

$$\frac{U_{bend}(stringer)}{2Lb} = f^2 \sum_{i=3}^{4} \left\{ 4N^2 C_{44}^i A_1^i - 2N C_{45}^i A_7^i + 4N C_{66}^i A_4^i + \frac{1}{4} C_{55}^i A_{18}^i \right\} \tag{47}$$

The stringer bending/twisting energy does not depend on the slope m of the local buckling nodal lines nor on the buckling mode modification parameter, a.

12. Final Equilibrium Equations

The nonlinear equilibrium equations contain contributions from the extensional energy terms, Eqs. (42) and (44), and the bending/twisting energy terms, Eqs. (45) and (47). The average axial strain e_1 that occurs in Eq. (42) is expressed in terms of f and a and stiffness parameters [Eq. (37)], and like powers of the amplitude factor f and the buckling mode shape modification parameter a are appropriately collected. The three nonlinear equilibrium equations are derived from the first variation of the total potential with respect to f or a or m. All three equations are represented by:

$$(U - W)' = \{f^2(C_1 + aC_2 + a^2 C_3) + f(C_4 + aC_5)\}'$$
$$\times [f^2(C_{42} + aC_{43} + a^2 C_{44}) + f(C_{45} + aC_{46})]$$
$$+ \left\{ f^2[(C_6 + aC_7 + a^2 C_8) + m^2(C_9 + aC_{10} + a^2 C_{11}) + SBPB(m,a)] \right.$$
$$+ f[(C_{12} + aC_{13}) + m^2(C_{14} + aC_{15})]$$

$$+ \left[f^2[(C_{16} + aC_{17} + a^2C_{18}) + m(C_{19} + aC_{20} + a^2C_{21}) + m^2(C_{22} + aC_{23} + a^2C_{24})] \right.$$

$$+ \left. f|(C_{25} + aC_{26}) + m(C_{27} + aC_{28}) + m^2(C_{29} + aC_{30})]\right]_{\text{eigenvalue terms}}$$

$$+ f^4[C_{31} + aC_{32} + a^2C_{33} + a^3C_{34} + a^4C_{35}]$$

$$+ \left. f^3[C_{36} + aC_{37} + a^2C_{38} + a^3C_{39}]\right\}' = 0 \tag{48}$$

in which $SBPB(m, a)$ represents the bending/twisting strain energy of the panel skin [Eqs. (45),(46)], and

$$C_1 = N\sum_{i=1}^{2} C_{11}^{*i}A_1^i + N(ASUM6) \qquad C_2 = 2N\sum_{i=1}^{2} C_{11}^{*i}A_2^i \qquad C_3 = N\sum_{i=1}^{2} C_{11}^{*i}A_3^i \tag{49}$$

$$C_4 = 2w_0C_1 \qquad C_5 = w_0C_2$$

$$C_6 = g_{010} + 4w_0^2\sum_{i=1}^{2}(N^2C_{11}^{*i}A_2^i/2 + C_{22}^iA_{11}^i/256) + F_{1B}C_1 - N(ASUM6P)\kappa_{xB}$$

$$+ (USTBPB) + N(TSUM6 + ASUM7) + (A6SUM2)/4$$

$$+ 4w_0^2N[3N(ASUM4)/4 + (A6SM10)/4]$$

$$C_7 = g_{011} + 2w_0^2\sum_{i=1}^{2}(2N^2C_{11}^{*i}A_3^i + C_{22}^iA_{12}^i/256) + F_{1B}C_2 \tag{50}$$

$$C_8 = g_{012} + w_0^2\sum_{i=1}^{2}(2N^2C_{11}^{*i}A_8^i + C_{22}^iA_{26}^i/256) + F_{1B}C_3$$

$$C_9 = g_4N_{2totB} \qquad C_{10} = g_5N_{2totB} \qquad C_{11} = g_6N_{2totB}$$

$$C_{12} = 2w_0g_{010} + F_{1B}C_4 + 2w_0N[(TSUM6) - (ASUM6P)\kappa_{xB}]$$

$$C_{13} = w_0g_{011} + F_{1B}C_5 \qquad C_{14} = 2w_0C_9 \qquad C_{15} = w_0C_{10}$$

$$C_{16} = g_{10} + F_{1A}C_1 - N(ASUM6P)\kappa_{xA}$$

$$C_{17} = g_{11} + F_{1A}C_2 \qquad C_{18} = g_{12} + F_{1A}C_3$$

$$C_{19} = -2g_4N_{xyA} \qquad C_{20} = -2g_5N_{xyA} \qquad C_{21} = -2g_6N_{xyA}$$

$$C_{22} = g_4N_{2A} \qquad C_{23} = g_5N_{2A} \qquad C_{24} = g_6N_{2A} \tag{51}$$

$$C_{25} = 2w_0g_{10} + F_{1A}C_4 - 2w_0N(ASUM6P)\kappa_{xA}$$

$$C_{26} = w_0g_{11} + F_{1A}C_5$$

$$C_{27} = 2w_0C_{19} \qquad C_{28} = w_0C_{20} \qquad C_{29} = 2w_0C_{22} \qquad C_{30} = w_0C_{23}$$

$$C_{31} = \sum_{i=1}^{2}(N^2 C_{11}^{*i} A_2^i/2 + C_{22}^i A_{11}^i/256) + N[3N(ASUM4)/4 + (A6SM10)/4]$$

$$C_{32} = \sum_{i=1}^{2}(2N^2 C_{11}^{*i} A_3^i + C_{22}^i A_{12}^i/256) \qquad C_{33} = \sum_{i=1}^{2}(3N^2 C_{11}^{*i} A_8^i + C_{22}^i A_{13}^i/256)$$

$$C_{34} = \sum_{i=1}^{2}(2N^2 C_{11}^{*i} A_9^i + C_{22}^i A_{14}^i/256) \qquad C_{35} = \sum_{i=1}^{2}(N^2 C_{11}^{*i} A_{10}^i/2 + C_{22}^i A_{15}^i/256) \qquad (52)$$

$$C_{36} = 4w_0 C_{31} \qquad C_{37} = 3w_0 C_{32} \qquad C_{38} = 2w_0 C_{33} \qquad C_{39} = w_0 C_{34}$$

$$C_{40} = \text{not needed} \qquad C_{41} = \text{not needed}$$

$$C_{42} = -C_1/A_{x11} \qquad C_{43} = -C_2/A_{x11} \qquad C_{44} = -C_3/A_{x11}$$

$$C_{45} = 2w_0 C_{42} \qquad C_{46} = w_0 C_{43}$$

In Eqs. (49-52) N is given by Eq. (17a), C_{11}^* by Eq. (29a), A_k^i by Eqs. (35), and $ASUM6, ASUM6P, TSUM6, ASUM7, A6SUM2, ASUM4$ and $A6SM10$ by Eqs. (43). The quantity $USTBPB$ represents the bending/twisting strain energy of the stringer web and flange, and is given by Eq. (47). Subscripts A and B in the quantities F_{1A} and F_{1B}, κ_{xA} and κ_{xB}, N_{2totB} and N_{2A}, and N_{xyA} denote "Load Set A" and "Load Set B", where "Load Set A" means those loads to be multiplied by a load factor (eigenvalue) and "Load Set B" means those loads that are simply parameters of the problem and are not to be multiplied by a load factor. (A buckling quantity would thus be given by $N_{cr} = N_B + \lambda N_A$, in which λ is the load factor or eigenvalue.) The quantities F_{1A} and F_{1B} are given by Eq. (40). Other quantities that appear in Eqs. (49) are

$$g_{010} = \sum_{i=1}^{2}\left\{(N\nu^i A_1^i + A_4^i/4)N_{2totB} + N N_{x0}^{*i} A_1^i\right\}$$

$$g_{011} = \sum_{i=1}^{2}\left\{(2N\nu^i A_2^i + 3A_5^i/2)N_{2totB} + 2N N_{x0}^{*i} A_2^i\right\}$$

$$g_{012} = \sum_{i=1}^{2}\left\{(N\nu^i A_3^i + 9A_6^i/4)N_{2totB} + N N_{x0}^{*i} A_3^i\right\}$$

$$g_{10} = \sum_{i=1}^{2}\left\{(N\nu^i A_1^i + A_4^i/4)N_{2A}\right\} \qquad g_{11} = \sum_{i=1}^{2}\left\{(2N\nu^i A_2^i + 3A_5^i/2)N_{2A}\right\} \qquad (53)$$

$$g_{12} = \sum_{i=1}^{2}\left\{(N\nu^i A_3^i + 9A_6^i/4)N_{2A}\right\}$$

$$g_4 = \sum_{i=1}^{2}N A_1^i \qquad g_5 = \sum_{i=1}^{2}2N A_2^i \qquad g_6 = \sum_{i=1}^{2}N A_3^i$$

$$N_{2totB} = N_{2B} + \bar{N}_{y0} \qquad A_{x11} = \bar{C}_{11} - \bar{\nu}\bar{C}_{12} + STIFL1$$

in which $\bar{N}_{y0}$ and $\bar{C}_{ij}$ are given in Eqs. (29); $\bar{\nu}$ is given in Eq. (40c); and $STIFL1$ is given

in Eqs. (34).

13. Local Buckling Load Factor λ from This Theory

The load factor corresponding to initiation of local buckling is obtained from Eq. (48) modified as follows:

1. Set the initial local imperfection amplitude $w_0 = 0$.
2. Set the mode shape modification parameter $a = 0$.
3. Neglect terms with cubic and quartic powers of f.

The resulting two equilibrium equations corresponding to the variation of the total potential with respect to f and m are represented by:

$$(U - W)' = \left\{ f^2 \{[C_6 + m^2 C_9 + SBPB(m, a)] + \lambda[C_{16} + mC_{19} + m^2 C_{22}]\} \right\} = 0 \quad (54)$$

The "f" equation yields

$$\lambda = -(NUM)/(DEN) \quad (55)$$

in which

$$NUM = C_6 + m^2 C_9 + SBPB(m, a) \qquad DEN = C_{16} + mC_{19} + m^2 C_{22} \quad (56)$$

and the "m" equation yields

$$2mC_9 + (SBPB),_m - \frac{NUM}{DEN}(C_{19} + 2mC_{22}) = 0 \quad (57)$$

where $(),_m$ indicates partial differentiation with respect to m. Equation (57) is solved for the slope of the local buckling nodal lines m by Newton's method, and the result is inserted into the right-hand-side of Eq. (55) to yield the load factor λ for local bifurcation buckling.

All of these calculations as well as the calculations described in previous sections are performed for a local buckling axial half-wavelength L determined from a BOSOR4-type of buckling analysis of the discretized panel module model. The critical local buckling load factor and number of axial halfwaves between rings is determined by performing a search over the number of axial halfwaves until a minimum value is found.

14. Strategies for Solving the Nonlinear Equations

The three nonlinear equilibrium equations represented by Eq. (48) are solved by the Newton-Raphson method. Various strategies are pursued in order to achieve convergence:

1. If the BOSOR4-type local buckling analysis reveals that the applied load exceeds the critical local bifurcation buckling load of the locally perfect shell ($\lambda < 1$), then a solution is first obtained with the local imperfection amplitude w_0 set to zero and with $f = 0$, $a = 0$, and $m = m_0$, where m_0 is the slope of the local buckling nodal lines obtained from the eigenvalue analysis just described. If convergence with $w_0 = 0$ is achieved within 45 iterations the resulting f, a, and m are then used as starting

values for the case with $w_0 > 0$. If convergence is not achieved with $w_0 = 0$ then convergence is attemped with $w_0 > 0$ with zero starting values for f and a and with $m = m_0$.

2. If the BOSOR4-type local buckling analysis reveals that the applied load is less than the critical local bifurcation buckling load of the locally perfect shell ($\lambda > 1$), then convergence is first attempted with $w_0 > 0$, as described in the last sentence of Strategy 1.

3. If convergence fails in Strategy 1 or Strategy 2, then either of two strategies will be chosen:

   a. If optimization is being performed and if more than ten design iterations have been completed in the current set of design iterations, then the converged solution for the previous design iteration will be used as a starting value and convergence will be attempted again.

   b. Strategy 4 will be pursued.

4. If convergence has continued to fail, the slope of the local buckling nodal lines m will be set equal to zero and the "m" equation will be removed from the set of three equations to be solved iteratively, leaving only the "f" and the "a" equations to be solved iteratively, an easier problem for which to find a converged solution. If this reduced problem converges within 45 iterations, then $m = m_0$ will be re-introduced as a starting value, along with the values of f and a determined from the reduced problem, and the full three-variable problem will be attempted again.

5. If convergence has continued to fail, both m and a will be set equal to zero and both the "m" and "a" equations will be removed, leaving only the "f" equation to be solved iteratively. In this case the full three-variable problem is not attempted again.

6. If convergence has continued to fail, f and a are set equal to zero and m is set equal to m_0, the value obtained from solution of the eigenvalue problem described in Section 13 just above.

15. Tangent Stiffness Matrix

The tangent stiffness of the locally deformed panel is required for computation of the wide-column buckling load of the portion of the panel between adjacent rings and of the general instability buckling load. The reduced effective stiffnesses of the panel skin and of the stringer parts are computed by perturbation of each of the prescribed average in-plane load components N_1, N_2, N_{12} in turn, re-solution of the nonlinear equations for f, a, and m, calculation of the average strains from Eqs. (39) and Eq. (27c), and identification of the required tangent stiffness terms with the appropriate rates of change of average in-plane load components with average in-plane strain components.

16. How Global Imperfection (Axial Bowing) is Handled in PANDA2

Equation (20) contains the term κ_x, which is the change in axial curvature between rings due to loading. As discussed earlier, κ_x is assumed to grow hyperbolically as the axial load increases. The rationale for this assumption is given in Ref. [A3], pp 358 and 359, and is repeated here for completeness:

Suppose that an elastic column is not quite straight initially. Let the initial deflection of the neutral axis be denoted by $\bar{w}$. The condition for equilibrium of the bent configuration, based on small deflection theory, is given by

$$\frac{\delta^2 w}{\delta x^2} + \frac{P}{EI}(\bar{w} + w) = 0 \tag{58}$$

in which w is the additional deflection, P is the axial force, and EI is the flexural rigidity of the column. Both $\bar{w}$ and w can be represented by Fourier sine series with coefficients $\bar{w}_n$ and w_n, respectively. Substitution of these series into the equilibrium equation (58) yields, after rearrangement of terms,

$$w_n = \bar{w}_n/(P_n/P - 1) \tag{59}$$

in which P_n is the nth critical load for the perfect column, only the smallest of which, $(P_{cr} = \lambda P)$ is of practical importance. When P approaches its critical value, the first coefficient w_1 becomes the predominant component of the Fourier series expansion of w, and the additional deflection δ of the column at its midlength is approximated by

$$\delta \approx w_1 = \bar{w}_1/(P_{cr}/P - 1) \tag{60}$$

The total deflection, $\bar{w} + w$, is given by

$$\bar{w} + w = \frac{\lambda}{\lambda - 1}\bar{w} \tag{61}$$

where the eigenvalue $\lambda = P_{cr}/P$

The factor, $\lambda/(\lambda - 1)$, represents an amplitude factor which in PANDA2 is multiplied by any axial bowing, whether it be due to an initial imperfection, axial load eccentricity, normal pressure, curing the panel, or any combination of these effects. This amplitude factor is multiplied by the change in axial curvature κ_x computed from small deflection theory for the portion of panel between adjacent rings loaded by a combination of in-plane loads N_1, N_2, N_{12}, temperature cool-down associated with curing, axial load eccentricity, and uniform normal pressure. Therefore, local stress distribution in the various segments of the panel module, deforming as a wide column, accounts for the growth in axial bowing due to axial compression.

In PANDA2 the critical load factor λ in Eq. (61) is calculated from a preliminary estimate of the general instability load for the portion of the panel between rings. In this calculation the effective stiffness of the skin between stringers may or may not be reduced, depending upon whether local postbuckling is to be allowed or whether wide column buckling estimates are to constrain the design. These are user-selected strategies. The amplitude factor $\lambda/(\lambda - 1)$ is constrained to be between one and ten.

17. Numerical Results for Imperfect Panels

17.1 Axial Compression of an Unstiffened Rectangular Plate
Figure A1 has been discussed briefly in order to emphasize the usefulness of the capability of PANDA2 to handle

261

nonlinear behavior of locally imperfect panels. Notice that excellent agreement between PANDA2 and STAGS [A4, A5] is obtained. In the STAGS model there were 24 finite elements in the axial direction and six elements across the width. In PANDA2 the model of the unstiffened panel is analogous to that of a stringer-stiffened panel with a stringer of zero stiffness, that is, anti-symmetry conditions are imposed at the midwidth of the panel by forcing the normal displacement at the leftmost vertical edge to be the negative of that at the rightmost vertical edge, a condition described in Ref. [A1] for the case of the stiffened panel depicted in Figs. 22a and b of Ref. [A1].

Please note that in the PANDA2 computer program, if the user specifies that there is a local imperfection of zero amplitude $w_0 = 0$, the program replaces this with a local imperfection with an amplitude equal to one tenth of the thickness of the panel skin midway between stringers. If the user wishes to explore the behavior with an imperfection smaller than $0.1t$, he or she must specify it during MAINSETUP processing. A perfect structure can be simulated by specification of a very, very small imperfection, such as $w_0 = 0.00001t$.

17.2 Buckling Modal Interaction The problem of interaction between local and overall buckling of stiffened structures was extensively studied in the early 1970's by Koiter, Tvergaard, Hutchinson, van der Neut, Thompson, and others [A6–A10]. Inclusion of both local and overall (bowing) imperfections in PANDA2 permits the inclusion of this effect in the minimum weight design of stiffened panels.

The interaction effect is illustrated in Figs. A2 and A3: The effective axial stiffness of an axially compressed, unstiffened rectangular plate changes rather abruptly at the local buckling load of the plate, as shown in Fig. A2. The reduction in effective axial stiffness is due, of course, to the rapid growth of normal displacements as the local buckling pattern develops for loads slightly in excess of the bifurcation buckling load. This rapid development is demonstrated in Fig. A1 for the almost perfect plate. The development is somewhat more gradual for plates with local imperfections of larger amplitude, as is evident in Fig. A1 for the case with $w_0/t = 0.1$, and as is sketched in Fig. A2.

An axially stiffened plate may be regarded as a series of long rectangular unstiffened plates separated by stringers. At the local buckling load of the long rectangular plates between adjacent stringers, the overall axial stiffness of the stiffened structure is therefore abruptly reduced. This reduction in axial stiffness naturally causes reduction of the axial load at which the stiffened plate buckles in a general instability or wide column mode. The severity of the reduction is maximum if the plate is designed so that local buckling and wide column buckling of the perfect panel occur at the same axial load.

Figure A3 demonstrates the phenomenon of modal interaction. In this figure the critical axial load is plotted versus the stringer spacing. One may assume that all designs represented on the horizontal axis have the same weight. Therefore, the value of stringer spacing b for which the critical axial load is maximum represents the optimum design. This design corresponds to local buckling of the skin between stringers and overall (Euler) buckling at the same load. Also drawn in Fig. A3 is a curve for Euler buckling with axial stiffness of the skin reduced as shown in Fig. A2 because the skin, having been loaded to a state above the curve labelled "Local Buckling", is in its locally postbuckled state. The

dashed curve in Fig. A3 corresponds to a stiffened panel with an imperfection in the form of the local buckling mode. For panels with closely spaced stringers the imperfection has little chance to grow at the low loads associated with Euler buckling because the critical local buckling load is so far above the critical Euler load. For panels with stringers very far apart the skin is in its far postbuckled state, so that any initial imperfection has little impact on the Euler buckling. However, between these two extremes the dashed curve must make the transition from the Euler curve for the locally unbuckled plate to the Euler curve for the locally postbuckled plate. This transition occurs in the neighborhood of the optimum design, as shown in Fig. A3. The behavior of the stiffened plate is "imperfection sensitive" in the sense that the critical load of the locally imperfect plate is somewhat lower than the critical load of the perfect plate.

Figure A4 shows the effect of local and global (bowing) imperfections, w_{loc} and w_{bow}, respectively, on the wide column collapse of an axially compressed, blade stiffened panel with the dimensions shown in the figure. This panel is designed so that local and wide column buckling of the perfect panel occur at the same axial load. The results of three theories are included:

1. An asymptotic theory of Tvergaard [A8] based upon the behavior in the immediate neighborhood of the bifurcation buckling load;

2. An approximate nonlinear theory of Koiter and Pignataro [A10]; and

3. The PANDA2 computer program.

The most important results shown in Fig. A4 are as follows:

1. For panels with local imperfections only, the asymptotic theory is valid only for extremely small imperfections, and the asymptote from Koiter and Pignataro [A10] for large local imperfections, indicated by λ^*, is in good agreement with the PANDA2 result for a wide range of local imperfection amplitudes.

2. For panels with bowing imperfections only, PANDA2 and the asymptotic theory are fairly close and are conservative when compared with the asymptote from Koiter and Pignataro for large bowing imperfections, indicated by λ_{as}.

3. Nothing dramatic happens when local and bowing imperfections are mixed.

4. The asymptotic theory is too conservative for the case of local imperfections of amplitude likely to occur in practice.

Figures A5 – A7 pertain to blade stiffened, axially compressed panels tested by Thompson, Tulk, and Walker [A7], who investigated the interaction between local and overall imperfections experimentally. They fabricated the panels of low–modulus epoxy plastic, cleverly producing local initial imperfections by heating the panels, loading them until a local buckling pattern of the desired amplitude existed, and then cooling the panels so that the local buckling pattern was frozen into them. Thompson, et al, produced global (bowing) imperfections by applying the axial compression with varying amounts of eccentricity. The panels were simply supported at the loaded edges.

Figure A5 pertains to panels with stocky stiffeners, that is, the stiffeners are dimensioned so that there is no possibility of torsional instability. In Fig. A5 the asymptote labelled "Post-buckled limit (P_E^*)" is the wide column buckling load of the panel with post-locally-buckled skin. This buckling load represents a point on the curve in Fig A3 labelled "Euler buckling (locally buckled skin)". The parabola joining the classical Euler load with the limit load P_E^* represents the load at which local buckling would occur in the panel skin if the local imperfection amplitude were zero. Positive bowing is indicated in Fig. A4.

The PANDA2 results indicate somewhat less sensitivity to local imperfections for the case with zero bowing imperfection than do the test results. However, the PANDA2 results are in good agreement with the theoretical results of Koiter and Pignataro [A10], which apply for panels with stiffeners of the geometry indicated in this figure. For larger bowing imperfections the PANDA2 results are in good agreement with the test results and with the theoretical asymptote, P_E^*.

Figures A6 and A7 pertain to an axially compressed panel with thin stiffeners, that is, stiffeners which are of slender enough cross section to produce torsional instability for negative bowing imperfections of sufficient amplitude. Figure A6 shows the PANDA2 discretized panel module model, with typical local and wide column buckling modes. Figure A7 shows theoretical results from PANDA2 and test results from Thompson, Tulk, and Walker [A7]. Three local buckling modes predicted by PANDA2 are also depicted in Fig. A7, one for which the stringers are compressed more than the skin because of negative bowing, one for which there is no bowing, and one for which the stringers are under net tension because of positive bowing. (In PANDA2 the sign convention for bowing is opposite to that used by Thompson, et al. We use Thompson's sign convention here because Figures A5 and A7 represent adaptations taken from Ref. [A7]).

There is reasonably good agreement between test and PANDA2 theory for the entire range of parameters. The test results approach an asymptote that is somewhat lower than the limit load P_E^* probably because the axial wavelength of the local buckles becomes somewhat reduced when the skin is taken into the far-postbuckling regime, an effect that is neglected in PANDA2 and in Thompson's calculation of P_E^*.

Note that in a finite neighborhood of zero bowing imperfection, the Euler collapse of the panel with perfect skin is independent of the initial bowing imperfection. This result is obtained for two reasons:

1. The panel is designed so that with zero local and bowing imperfections the local buckling load is five per cent higher than the Euler buckling load. Therefore, with small but finite positive bowing the skin buckling load is still a bit higher than the Euler load of the perfect panel.

2. With small negative bowing the stiffener, although of slender cross section, is still stocky enough so that it is torsionally unstable only enough to cancel the slightly decreased compression in the skin caused by the negative bow. The dominant role of torsional instability of the stringer, evident in the mode shape depicted on the left

side of the figure, requires a larger amplitude of negative bowing than about $-0.25t$, where t is the panel skin thickness.

18. Optimization of Imperfect and Perfect Axially Stiffened Panels

Figures A8 and A9 show the results of optimization of a blade-stiffened panel with module cross section sketched in Fig. A8. The decision variables are the three thicknesses, t_1, t_2, t_3, and the cross section dimensions, b, b_2, and h. The overall dimensions of the panel are 30 inches long and 56 inches wide. Its radius of curvature is 51 inches and the stringers are external. The panel is simply supported on all edges. It is made entirely of aluminum, with modulus of 10×10^6 psi, Poisson's ratio $\nu = 0.3$, maximum allowable effective (von Mises) stress of 50000 psi, and weight density of 0.1 lb/in^3. The panel is subjected to two sets of combined in-plane loads: Load Set 1 given by $N_1 = $ -3000 lb/in, $N_2 = N_{12} = 0$ lb/in and Load Set 2 given by $N_1 = $ -1000 lb/in, $N_2 = 0$ lb/in, $N_{12} = 1000$ lb/in.

Figure A8 shows the evolution of the design for two cases:

1. An imperfect panel with local imperfection amplitude $w_0/t = 0.1$ and global (bowing) imperfection amplitude $W_0/t = -0.1$ (bowing so that the stringers are compressed more than the skin); the skin is permitted to buckle locally during service.

2. A perfect panel; the skin is not permitted to buckle during service.

The first ten design iterations are performed with the strategy parameter IQUICK = 1, that is, the panel is assumed to be perfect and only the simple PANDA-type closed form solutions are used for the stress and buckling analyses. These ten iterations are performed in two sets of five iterations each. The ten iterations require less than two minutes of CPU time on the VAX ll/785 computer, VMS operating system 4.4. A factor of safety of 2.0 is used for general instability in Load Set 1 (pure axial compression), and a factor of safety of 1.5 is used for general instability in Load Set 2 (combined axial compression and shear).

The next 15 iterations are based on the IQUICK = 0 option, that is, buckling loads and nonlinear postbuckling behavior are determined with use of the discretized panel module model shown in Fig. A10. The panel is both locally and globally imperfect, as described above. The 15 iterations are performed in two sets, a set of five followed by a set of ten. A total of about 45 minutes of VAX 11/785 CPU time is required for execution of the 15 iterations. The factor of safety for Load Set 1 is 1.5 and the factor of safety for Load Set 2 is 1.2. These factors are reduced from those used with the IQUICK = 1 option because the wide column model, which is conservative, governs the design and because initial imperfections are explicitly included.

Fifteen design iterations are then performed, again in a set of five followed by a set of ten, for a panel that is perfect and for which local buckling is not permitted in the skin. The factors of safety for Load Sets 1 and 2 are again taken as 1.5 and 1.2, respectively. Figure A8 shows the evolution of the design. It is not dramatically different from that obtained for the imperfect panel in which skin buckling is permitted.

Figure A9 shows the evolution of design margins during design iterations. At the end of the ten iterations with IQUICK = 1 the critical and near- critical margins include

general instability, local buckling, rolling with local buckling between stringers, and stringer crippling.

At the end of the 15 design iterations for the imperfect panel with IQUICK = 0 the critical and near-critical design margins include maximum allowable effective stress, web crippling, wide column buckling, and stringer popoff. (The allowable stringer popoff force/axial length is 1000 lb/in.) Notice that local buckling does not constrain the design. This is because the iterations were run according to a user-specified directive that local buckling be permitted during service. The maximum stresses in the locally buckled panel occur at the junctions between Segments 1 and 2 and Segments 2 and 4, as indicated in Fig. A10. At these locations there are considerable transverse bending stresses due to the growth of local buckles in the panel skin.

At the end of the 15 design iterations for the perfect panel in which local buckling is not permitted to occur during service, the critical and near-critical design margins include local buckling, wide column buckling, and web crippling. Notice that the maximum effective stress limitation of 50000 psi does not constrain the design in this case. This is because the skin is not permitted to buckle locally, and therefore experiences only the relatively low membrane stresses associated with the uniformly compressed prebuckled state of the panel. The relatively large transverse bending stresses that develop in locally postbuckled panels are absent.

Notice that the weights of the panels designed with and without local and global initial imperfections are nearly the same. However, it is felt that the panel designed accounting for the initial imperfections is probably safer than that designed omitting initial imperfections because the same factors of safety were used in both cases. The strategy in which initial imperfections are included is therefore more conservative than that in which they are omitted.

19. Comparison of Blade, Tee, and Hat Optimum Designs

Figures A10, A11, and A12 show optimum designs of blade, tee, and hat stiffened panels with the same overall dimensions, radius of curvature, material, and loading as that discussed in Section 18. The panels all have local imperfections in the form of the local buckling mode with amplitude $w_0/t = 0.1$. There are no global (bowing) imperfections. The optimum dimensions, weight, local bifurcation buckling load factor λ_{local}, and critical behavioral constraints are indicated in the figures. In all cases the skin is permitted to buckle and the maximum allowable effective stress of 50000 psi constrains the design. Other critical behavioral constraints include wide column buckling and crippling of the stringer web(s).

The most weight-efficient design appears to be the Tee-stiffened panel. This is probably because the stringer popoff allowable force/axial length was set very high (1000 lb/in) and because isotropic material is not very good for use in stringer webs which are not permitted to cripple. Had the popoff allowable been considerably reduced and the webs been constructed primarily of plus and minus 45-degree composite tape or cloth, the hat-stiffened configuration probably would have been the lightest, as was the case for the ARIANE interstage design displayed in Table 16 and Fig. 99 of Ref. [A1].

266

20. Conclusions

The nonlinear theory developed here for the prediction of behavior of locally imperfect panels appears to be properly implemented in PANDA2, since there is excellent agreement between PANDA2 and STAGS, as shown in Fig. A1. The theory captures reasonably well the nonlinear modal interaction effect described in many papers published by Koiter, Hutchinson, Thompson, Tvergaard and others in the 1970's. Results displayed in Figs. A4 – A7 indicate fairly good agreement between these previous theories, PANDA2 results, and tests. Locally and globally imperfect panels can now be automatically optimized, as demonstrated in Figs. A8 – A12. The inclusion of local and global imperfections with amplitudes likely to occur in practice does not appear to affect dramatically the behavior nor the optimum design of axially stiffened panels that behave approximately as wide columns in the general instability mode of failure.

21. Other Recent Changes in PANDA2

21.1 Changes in the Derivation of $C(i,j)$ for Smeared Stiffeners The integrated constitutive law for smeared stiffeners is derived in Section 8 of Ref. [A1]. Since that paper was written the derivation has been modified as follows:

1. Equations (8.7) through (8.10) in Ref. [A1] have been replaced by:

$$N_x(1) = N_x(3) \qquad N_y(1) = N_y(2)$$
$$M_x(1) = M_x(3) \qquad M_y(1) = M_y(2) \tag{62}$$

in which the numbers in parentheses refer to the regions (Parts) indicated in Fig. 14 of Ref. [A1]. Part (4) no longer enters the calculations. Also, the index (i) in Eqs. (8.21–8.24) no longer appears: The strains and changes in curvature in the stiffener webs and flanges are assumed to be equal to the averages over the entire panel. These modifications lead to more consistent results for panels with both stringer bases and ring bases.

21.2 In-Plane Shear in Stiffener Webs Due to Response to Normal Pressure When a stiffened panel is loaded by uniform normal pressure considerable in-plane shear develops in the stiffener webs. These webs can buckle because of this shear. The web shear buckling failure mode is now included in PANDA2.

21.3 Buckling Knockdown Factors Now Include the Effect of Anisotropic C(i,j) In Section 11 of Ref. [A1] a shortcut method is described for including the effect of in-plane shear loads on general, panel, and local instability predictions obtained with use of BOSOR4-type of discretized models, which do not admit the effect of in-plane shear loads directly. The knockdown factors are obtained with PANDA-type analyses and defined in Ref. [A1] by

$$\text{KNOCKDOWN} = \text{EIGENCRIT(with shear)}/\text{EIGENCRIT(no shear)} \tag{11.1}$$

PANDA2 has since been modified to include the effect of anisotropic C(i,j) in the computation of these knockdown factors. They are now calculated from the ratio

$$\text{KNOCKDOWN} = \frac{\text{EIGENCRIT(with shear and fully populated C(i,j))}}{\text{EIGENCRIT(no shear and BOSOR4-type C(i,j)}} \tag{63}$$

The "BOSOR4-type $C(i,j)$" are the constitutive law with $C(1,3)$, $C(1,6)$, $C(2,3)$, $C(2,6)$, $C(3,4)$, $C(3,5)$, $C(4,6)$, $C(5,6)$, and symmetric (j,i) terms set equal to zero. Hence, there may be knockdown factors less than unity even if there is no in-plane shear loading. Knockdown factors are never permitted to be greater than unity, so that "beneficial" anisotropic effects, if any, are not included in the buckling estimates obtained from BOSOR4-type discretized panel module models. However, the effects of anisotropy are usually deleterious, not beneficial.

21.4 Two-Segment Crippling of Stiffeners In Section 15 is described the analysis of crippling of stiffener parts. Two kinds of stiffener parts are identified there, "internal" segments and "end" segments. In the paragraph on crippling of "end" segments, that is, stiffener segments with one free edge, the following statement is made: "Crippling loads are computed assuming that the stiffener end cross section does not deform and the number of axial half-waves is the same as that for the interior segment to which the end segment is attached." In the modified PANDA2 program the number of axial half-waves is no longer thus restricted. Instead, a search over the number of axial half-waves is conducted to find the lowest crippling load factor. In many cases it turns out that the search over the number of axial half-waves is not necessary, but there are cases, such as that shown in Fig. A13, for which the new method yields a much lower crippling load than the old.

21.5 More Extensive Search for Maximum Stringer Popoff Force Previously stringer popoff forces were only computed corresponding to the line of intersection between the stringer web and the panel skin. In the modified PANDA2 program stringer popoff forces are also computed at the line of intersection between the stringer web and the outstanding flange, if any, for Tee-shaped stringers and J-shaped stringers.

Figure A13 shows an example in which popoff is possible at either of the locations. (The loading is uniform axial compression). In the design represented by Fig. A13a the stringer popoff forces were high at the location indicated by σ_A. In the design represented by Fig. A13b the stringer popoff forces were high at the location indicated by $10\sigma_B$ It is interesting that in this case a five-per-cent perturbation of the baseline design caused the popoff forces to change by factors of 10, with a shift in the location of the critical value. It is this sensitive behavior that makes optimization of stiffened structures such as these very difficult indeed.

22. Acknowledgments

23. References

[A1] Bushnell, D., "PANDA2–Program for minimum weight design of stiffened, composite, locally buckled panels", Lockheed Palo Alto Research Laboratories, LMSC-D067175, revised November, 1986; to appear Computers and Structures, 1987.

[A2] Koiter, W. T., "Het Schuifplooiveld by Grote Overshrijdingen van de Knikspanning," Nationaal Luchtvaart Laboratorium, Report X295, November 1946 (in Dutch)

[A3] Bushnell, D. COMPUTERIZED BUCKLING ANALYSIS OF SHELLS", Nijhoff, The Netherlands, (1985)

[A4] Almroth, B. O. and Brogan, F. A., "The STAGS Computer Code", NASA CR-2950, Nasa Langley Research Center, (1978)

[A5] Rankin, C. C., Stehlin, P. and Brogan, F. A., "Enhancements to the STAGS computer code", Lockheed Missiles and Space Co., Inc., Palo Alto, CA., LMSC-D060755, November 1985. See also, Thurston, G. A., Brogan, F. A., and Stehlin, P., "Postbuckling analysis using a general purpose code", AIAA Paper No. 85-0719-CP, AIAA 26th Structures, Structural Dynamics, and Materials Conference, Orlando, Florida, April 15-17, 1985

[A6] van der Neut, A., "The interaction of local buckling and column failure of thin-walled comporession members", Proceedings of the Twelfth International Congress of Applied MEchanics, edited by M. Hetenyi and W. G. Vincenti, Springer, Berlin, pp 389-399 (1969)

[A7] Thompson, J. M. T., Tulk, J. D. and Walker, A. C., "An experimental study of imperfection-sensitivity in the interactive buckling of stiffened plates", BUCKLING OF STRUCTURES, edited by B. Budiansky, Springer-Verlag, pp 149-159 (1976)

[A8] Tvergaard, V., "Influence of post-buckling behavior on optimum design of stiffened panels", International Journal of Solids and Structures, Vol. 9, pp 1519-1534 (1973)

[A9] Byskov, E. and Hutchinson, J. W., "Mode interaction in axially stiffened cylindrical shells", AIAA J., Vol. 15, No. 7, pp 941-948 (1977)

[A10] Koiter, W. T. and Pignataro, M., "An alternative approach to the interaction between local and overall buckling in stiffened panels", BUCKLING OF STRUCTURES, edited by B. Budiansky, Springer-Verlag, pp 133-148 (1976)

LIST OF FIGURES

Fig.A12 Optimum design of hat-stiffened panel with zero bowing imperfection and a local imperfection equal to ten per cent of the thickness of the panel skin midway between stringers. Loading and overall geometry are as specified in the caption of Fig. A8.

Fig. A13 Local buckling modes of an axially compressed panel with tee-shaped stringers, showing two sites at which stiffener debonding is likely to occur. Both of these sites are checked by PANDA2. In this case the local buckling mode shape and therefore the peel stresses tending to cause stiffener popoff is very sensitive to a small change in the width w of the outstanding stiffener flange. This behavior makes it very difficult in this case to find a reliable optimum design.
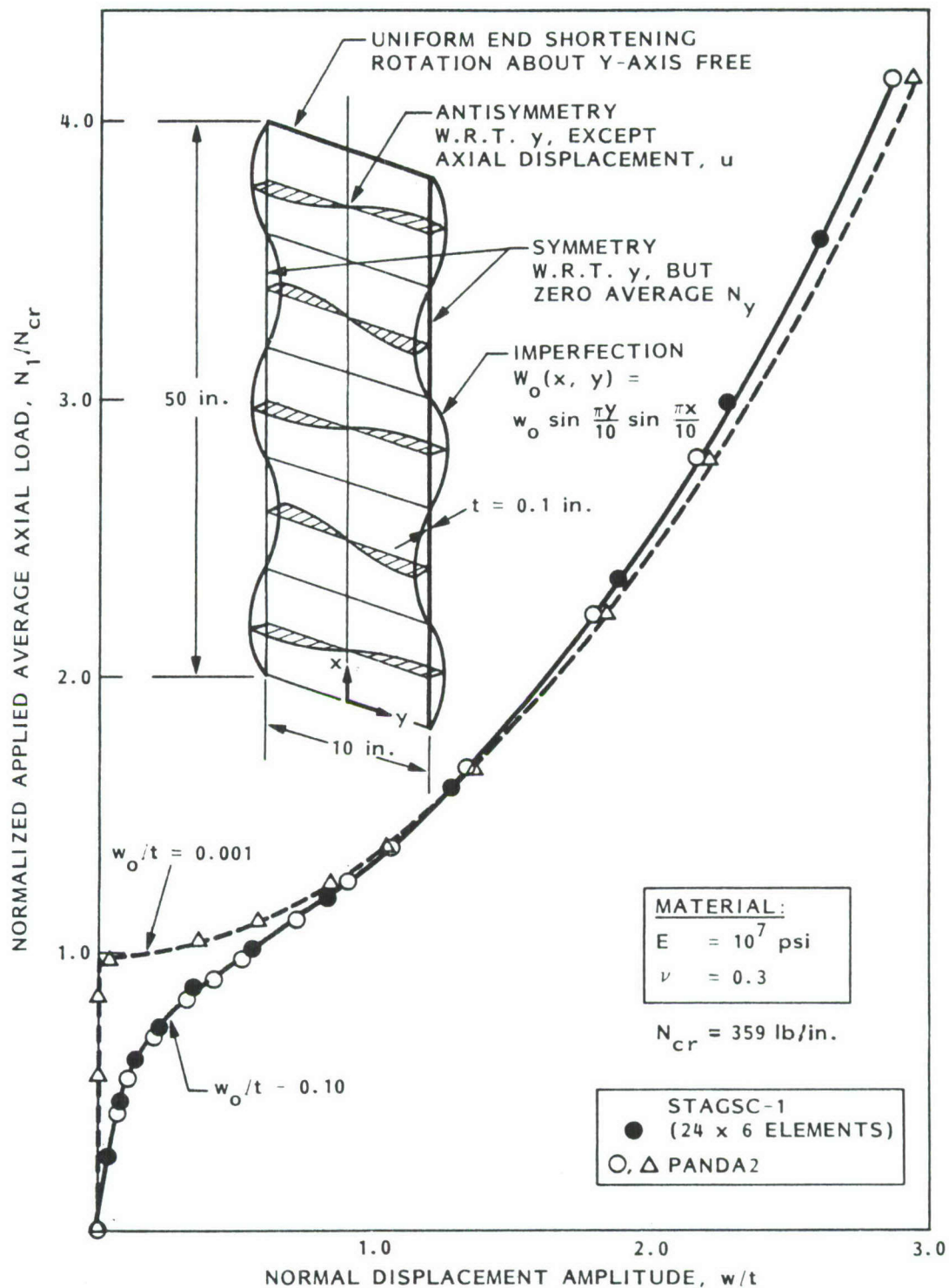
Fig.A1 Axially compressed imperfect flat plate: comparison of results from PANDA2 and STAGSC-1
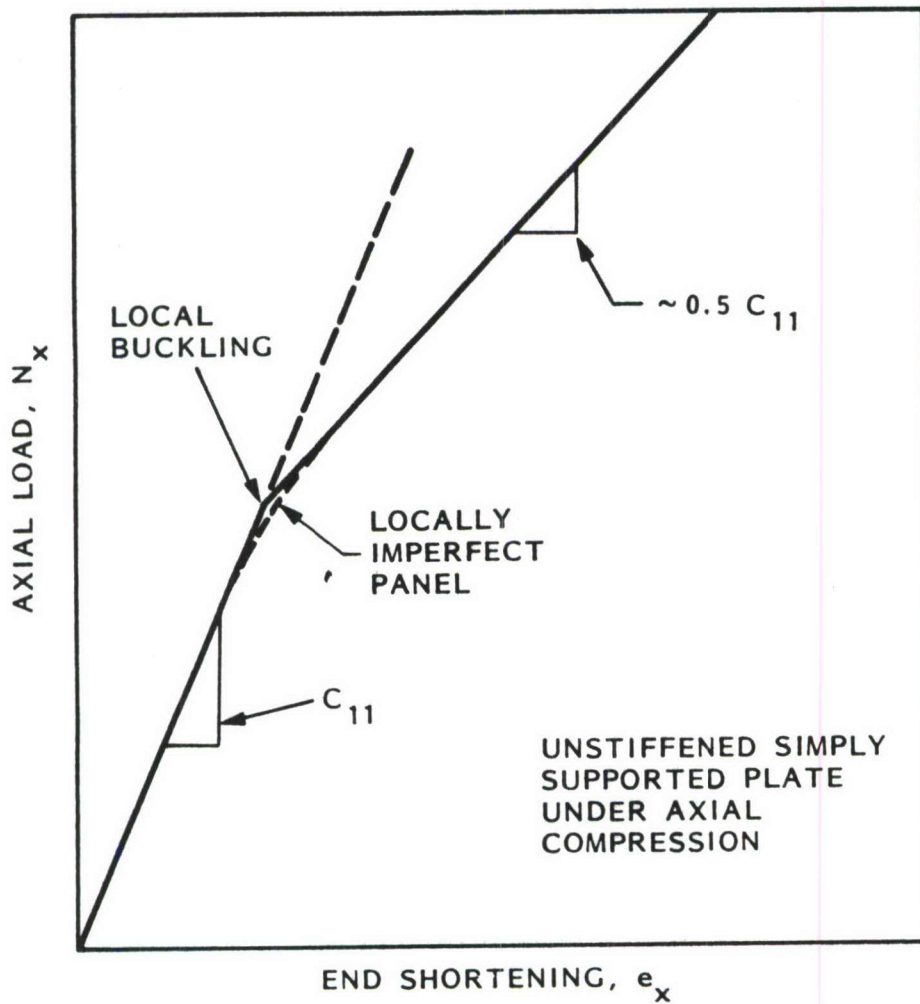
Fig.A2 Typical load-end shortening curve showing abrupt reduction in effective axial stiffness, C_{11}, at the local bifurcation buckling load
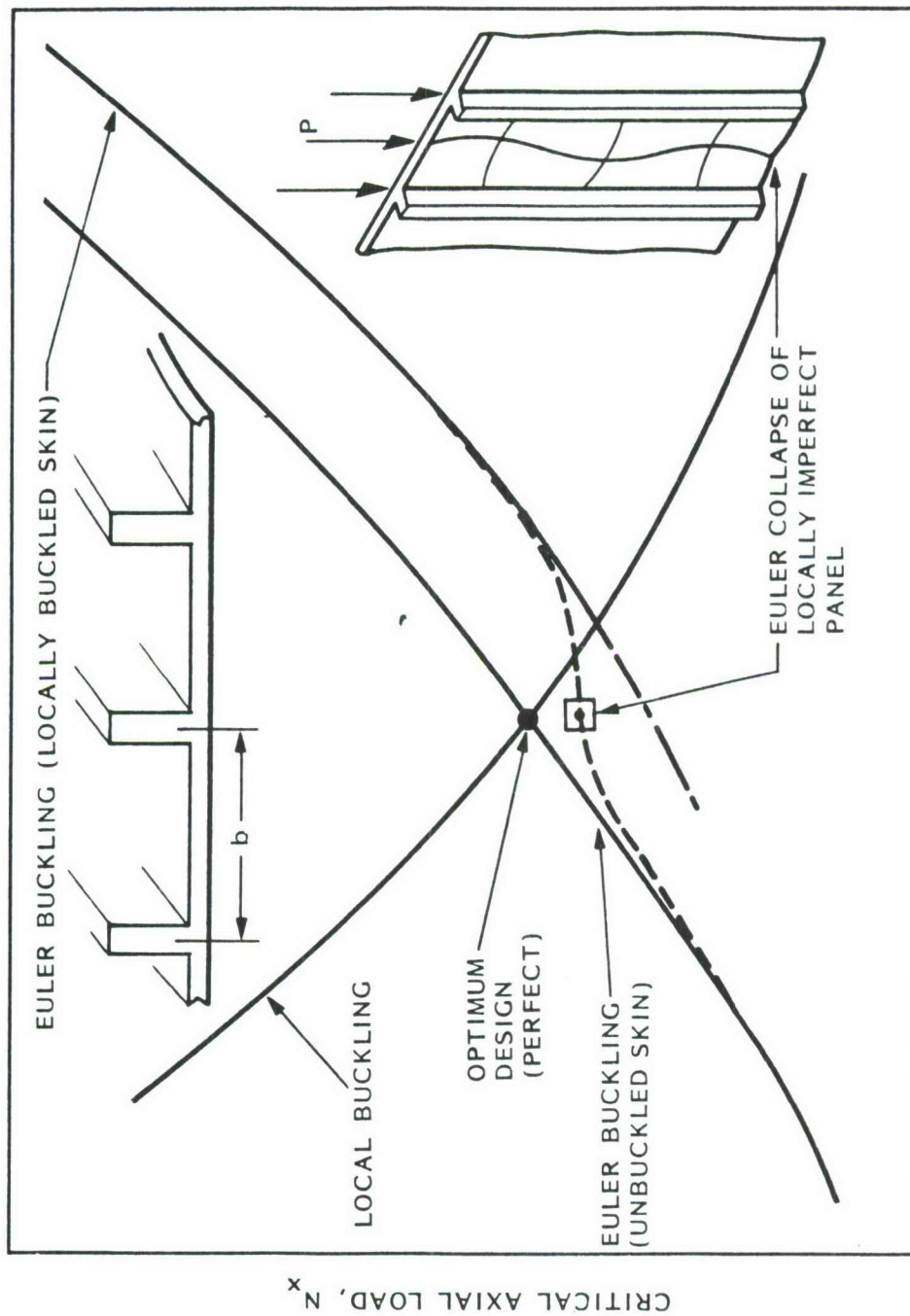
STRINGER SPACING, b → (CONSTANT WEIGHT)

CRITICAL AXIAL LOAD, N_x

Fig.A3 Effect of imperfection in panel skin on Euler buckling of axially stiffened, axially compressed panels. The maximum sensitivity of the buckling load to an initial imperfection in the form of the local buckling mode is in the neighborhood of the optimum design.
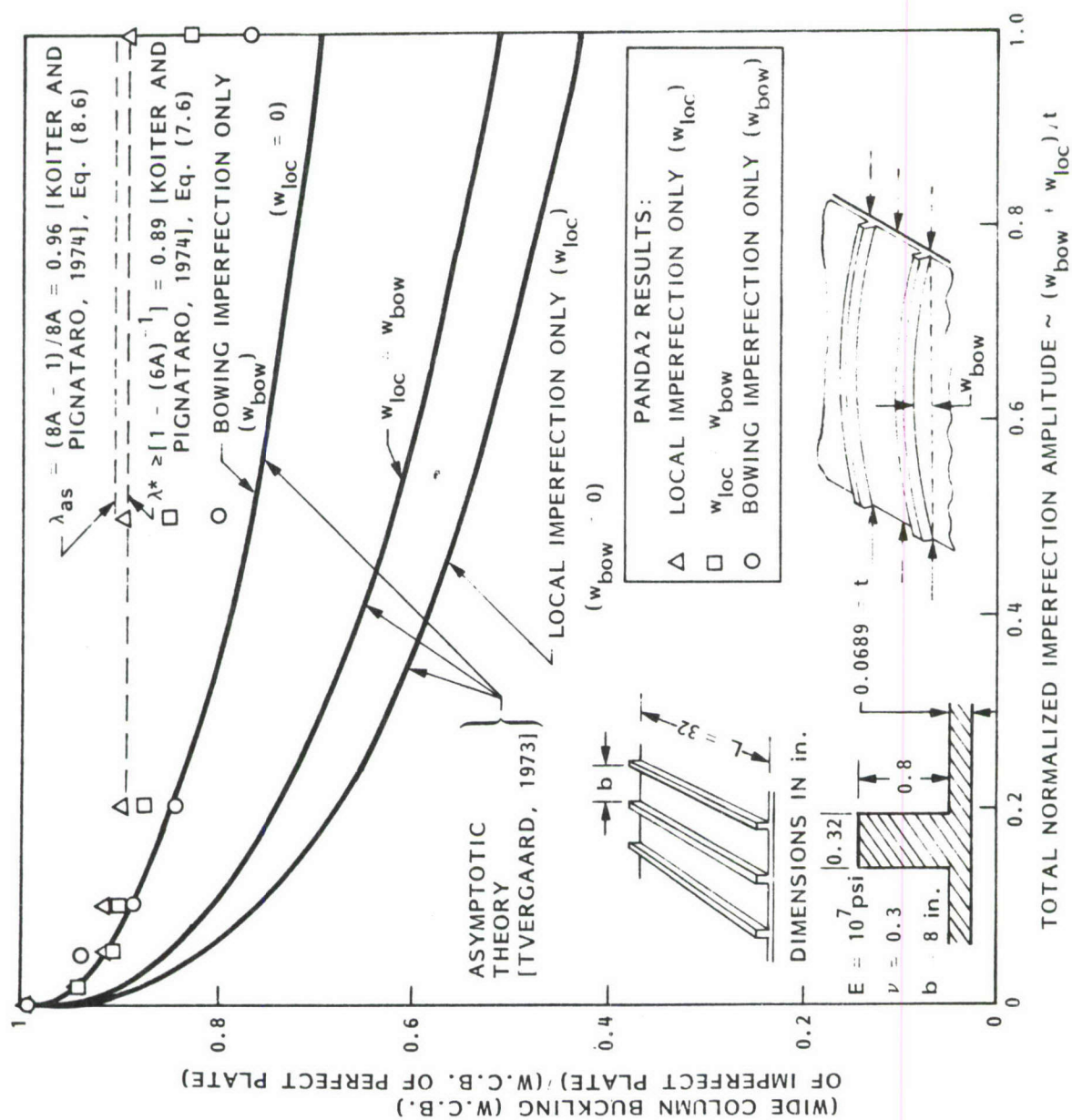
Fig.A4 Comparison of PANDA2 results with theoretical results of Koiter and Pignataro (1974) and Tvergaard (1973) for an imperfect, axially compressed, blade-stiffened panel with stocky stiffeners.
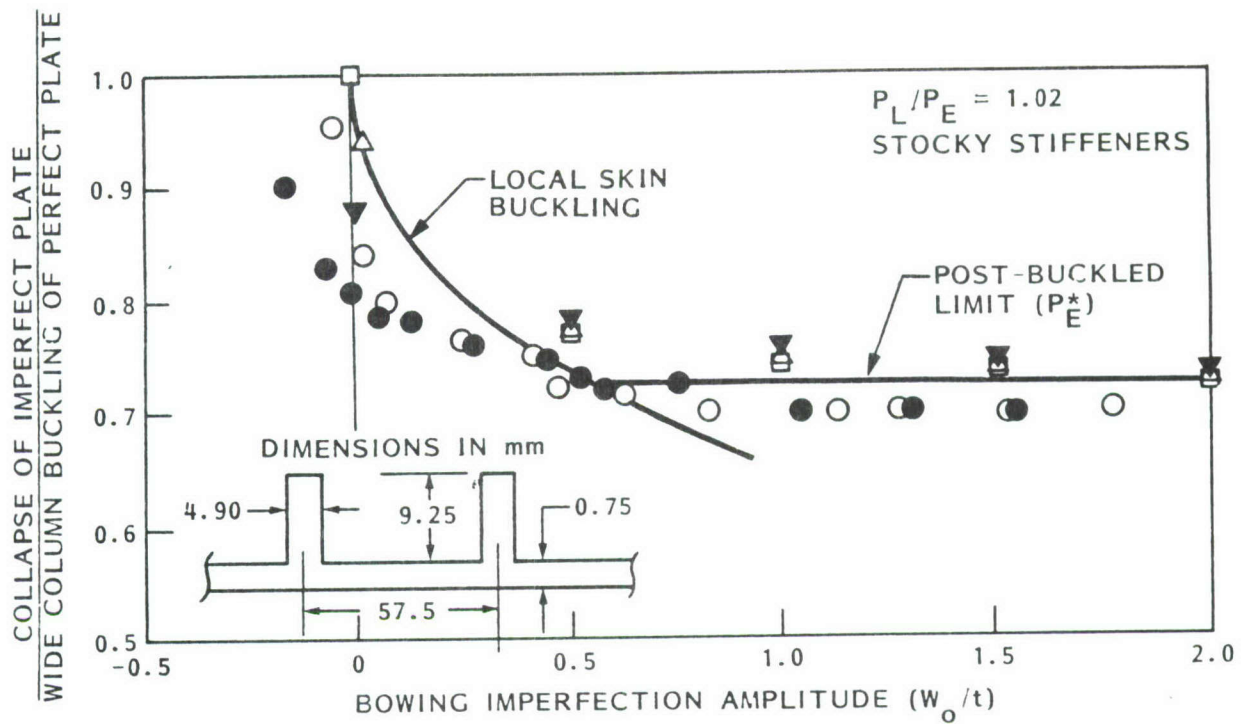
Fig.A5 Comparison of PANDA2 results and test results by Thompson, et al, for axially compressed, imperfect, blade-stiffened panels with stocky stringers. Positive bowing causes tension in the tips of the stringers.
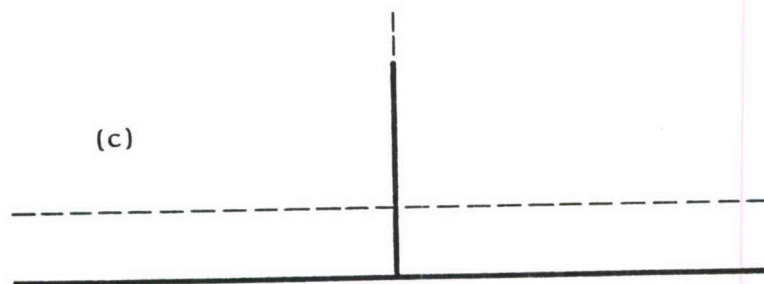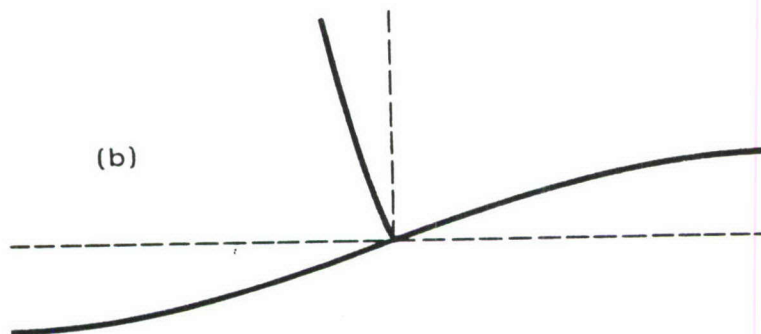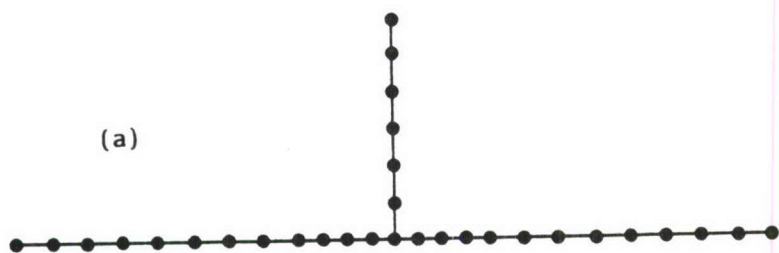
Fig.A6 (a) Discretized panel module, (b) local buckling mode, and (c) wide column buckling mode for an axially compressed, blade-stiffened panel with slender stringers

277
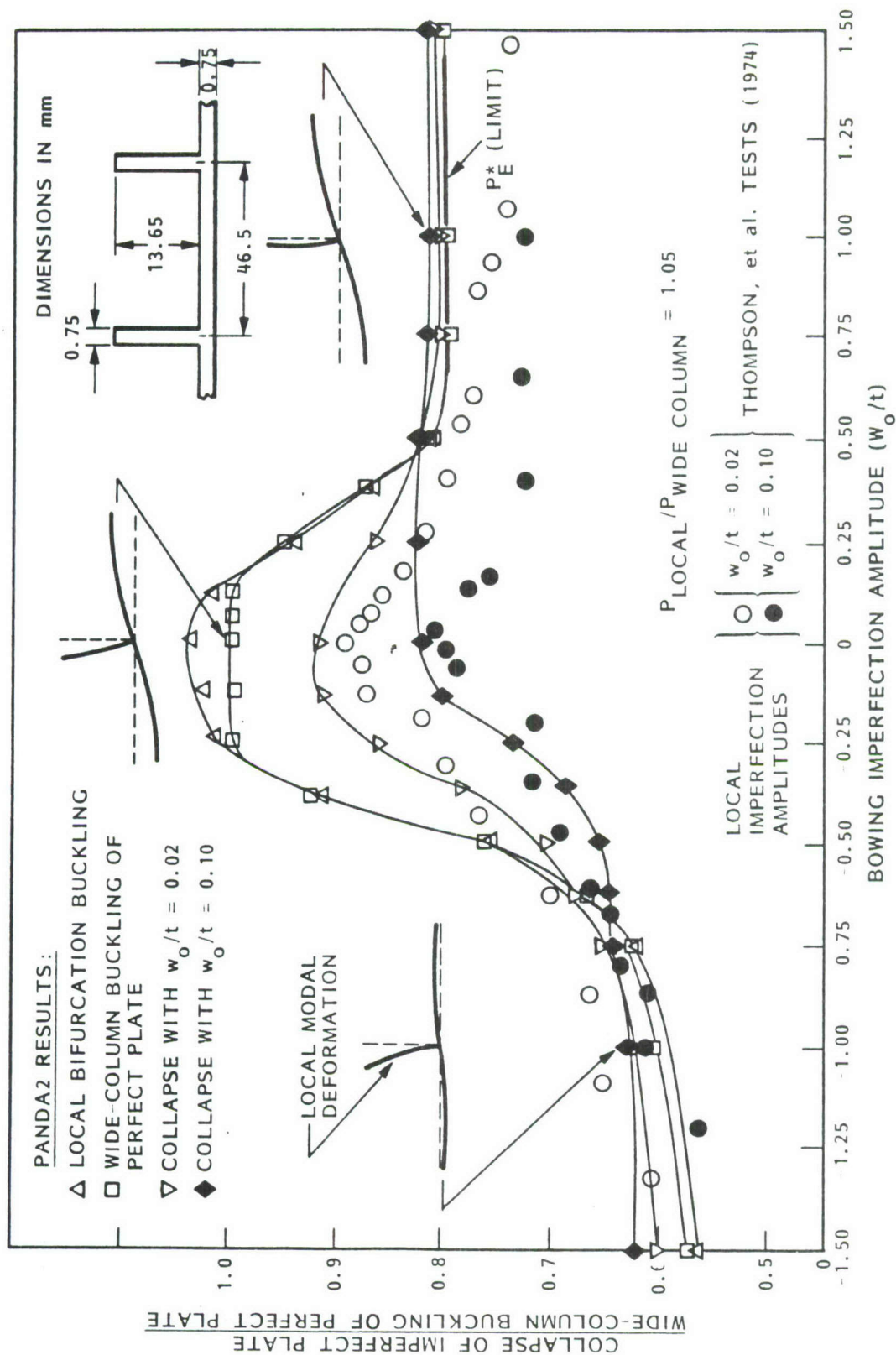
Fig.A7 Comparison of PANDA2 results and test results by Thompson, et al, for axially compressed, imperfect, blade-stiffened panels with slender stringers. Typical local buckling mode shapes predicted by PANDA2 for panels with negative, zero, and positive bowing are also shown.

278
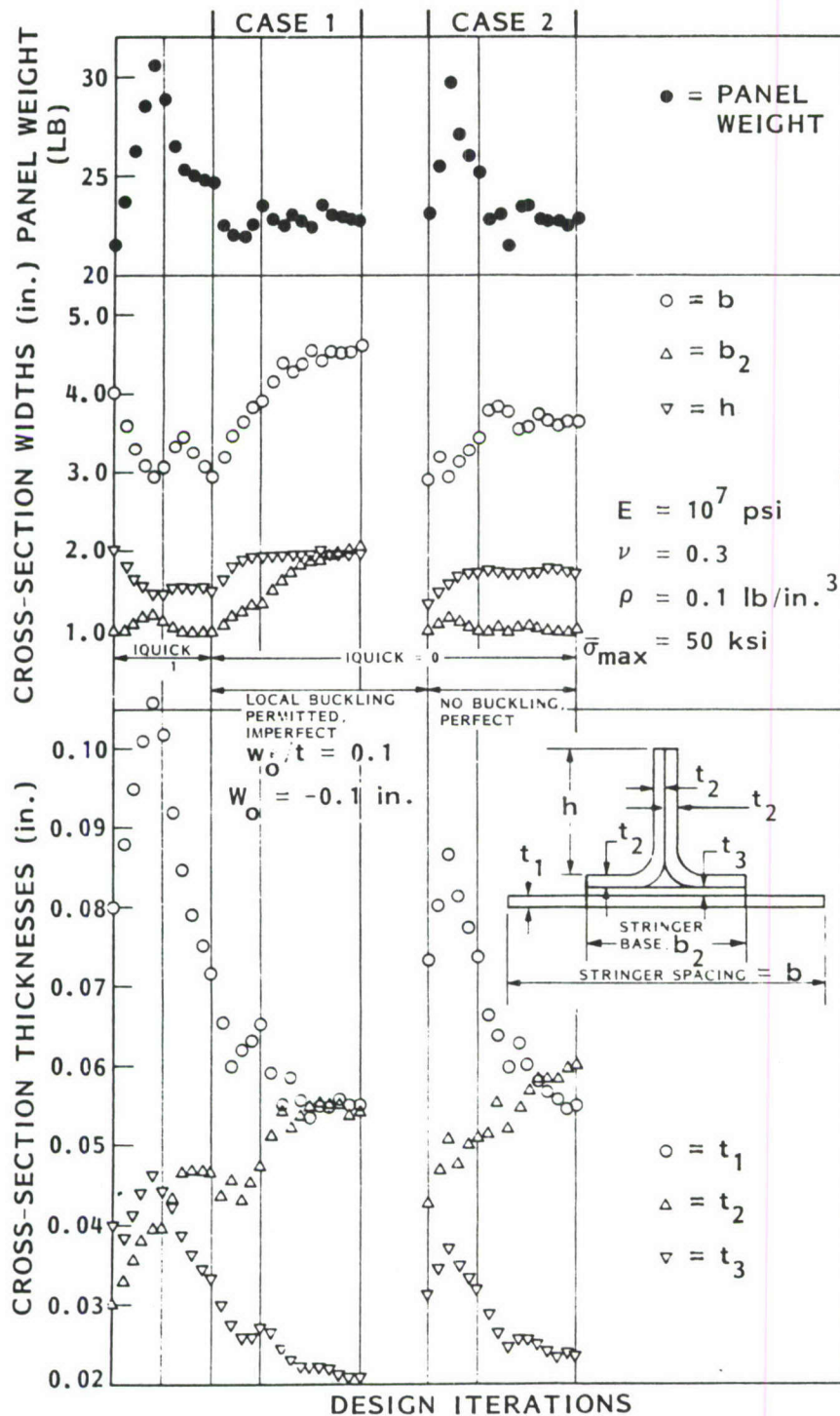
Fig.A8 Evolution of the optimum design of an elastic aluminum cylindrical panel subjected to two load sets: 1. pure axial compression of 3000 lb/in, and 2. combined axial compression of 1000 lb/in and in-plane shear of 1000 lb/in. The overall dimensions of the panel are 30 in. long and 56 in. wide. The radius of curvature is 51 in. and the stringers are external.

279
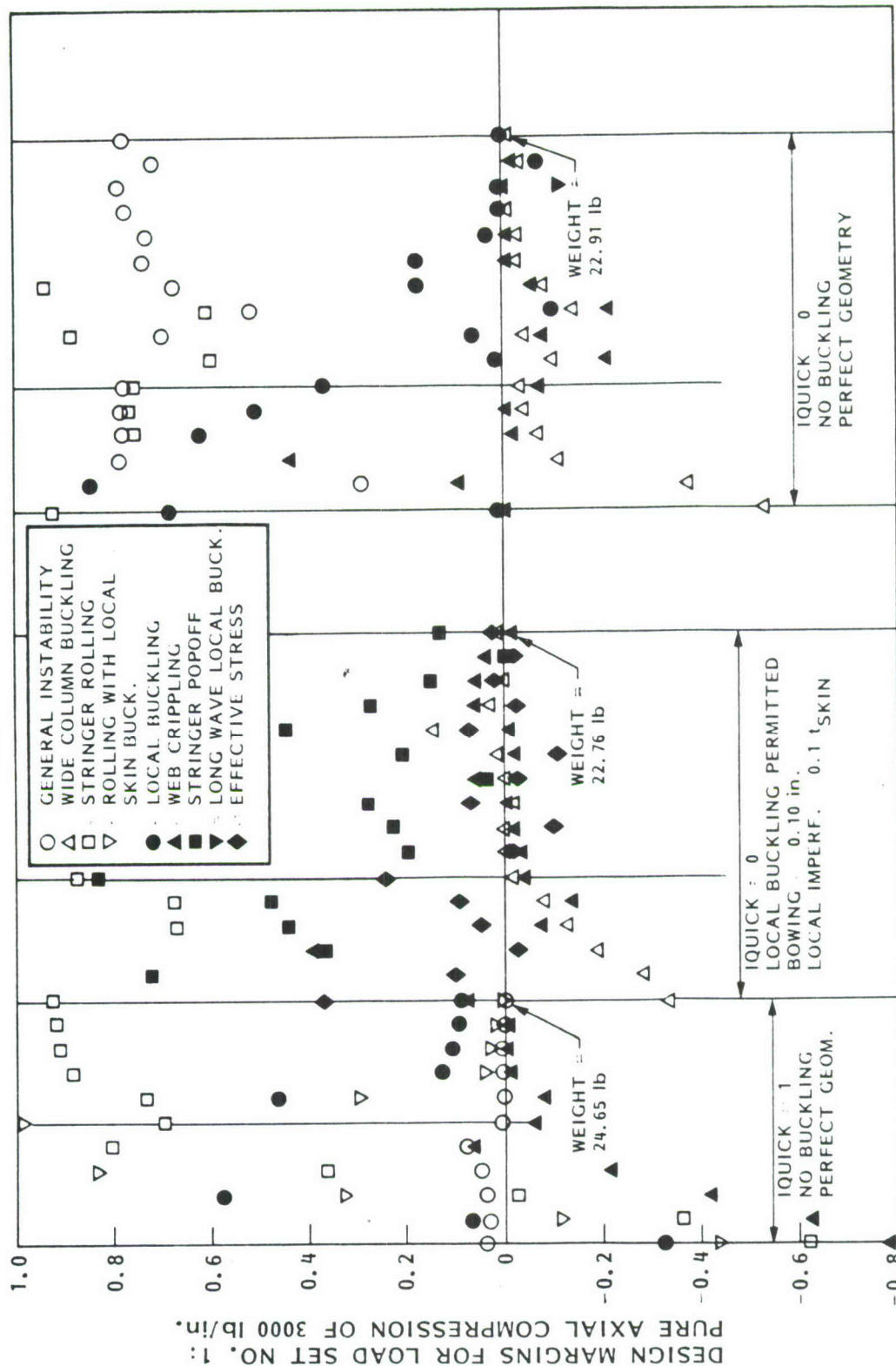
Fig.A9 Evolution of design margins corresponding to the panel of the previous figure. If local buckling is permitted constraints on maximum effective stress and stringer popoff are active, whereas if local buckling is not permitted the local buckling constraint is active.

$0.0728 = t_2$

$0.0685 = t_1$ $0.0239 = t_3$ ③ 1.94

① ② 1.0 ④

5.42 in.

λ_{LOCAL} = 0.57 x 3000 lb/in.

$E = 10^7$ psi

$\nu = 0.3$

$\rho = 0.1$ lb/in.^{3}

$\bar{\sigma}_{max} = 50$ ksi

CRIPPLING

WIDE-COLUMN
BUCKLING IS
CRITICAL

$\bar{\sigma}_{eff}(cr)$

LOCAL BUCKLING

OPTIMUM WEIGHT = 23.29 lb
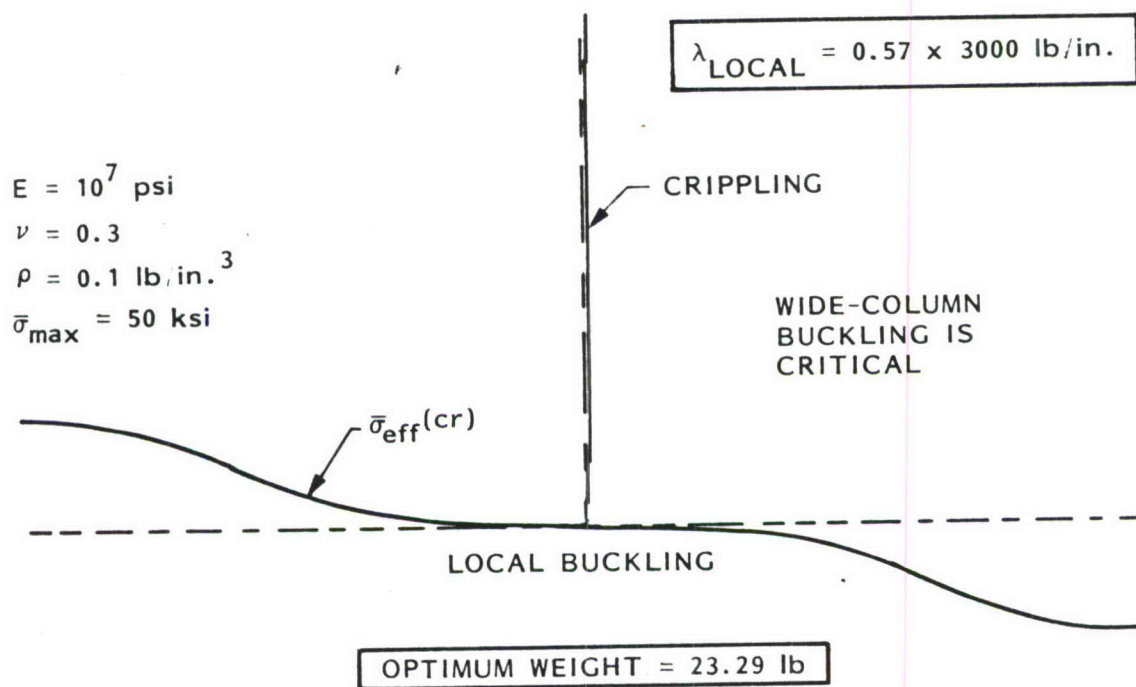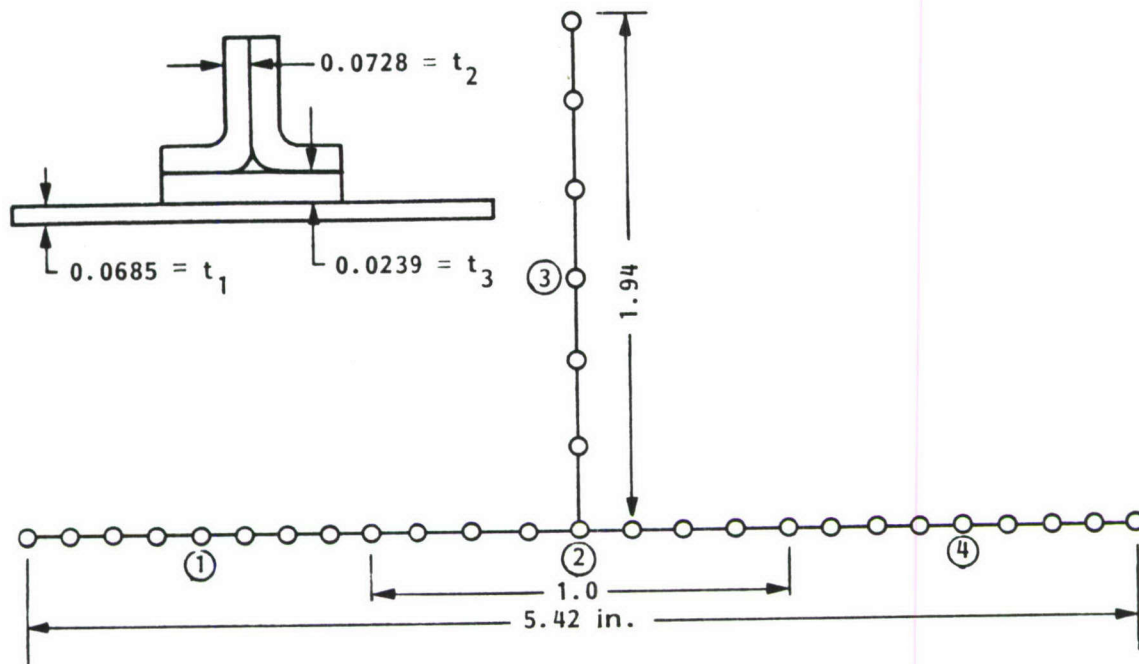
Fig.A10 Optimum design of blade-stiffened panel with zero bowing imperfection and a local imperfection equal to ten per cent of the thickness of the panel skin midway between stringers. Loading and overall geometry are as specified in the caption of Fig. A8.

281

(a) DISCRETIZED MODEL

$$\lambda_{LOCAL} = 0.7 \times 3000$$

$E = 10^7$ psi

$\nu = 0.3$

$\rho = 0.1$ lb/in.

$\bar{\sigma}_{max} = 50$ ksi

$\bar{\sigma}_{eff}(cr)$

CRIPPLING

WIDE
COL. BUCK.
IS CRITICAL
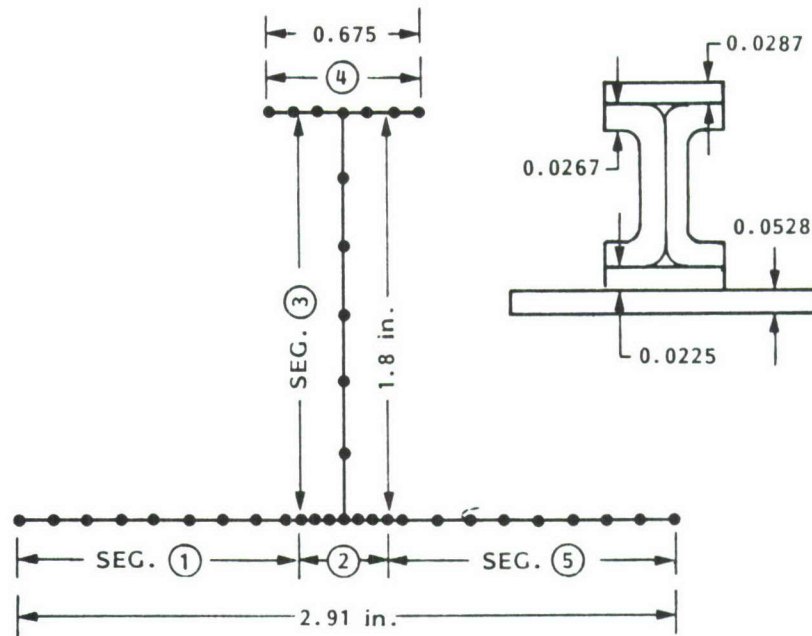
ROLLING ONLY
OF STRINGER
IS CRITICAL

(b) LOCAL BUCKLING MODE

OPTIMUM WEIGHT = 18.00 lb
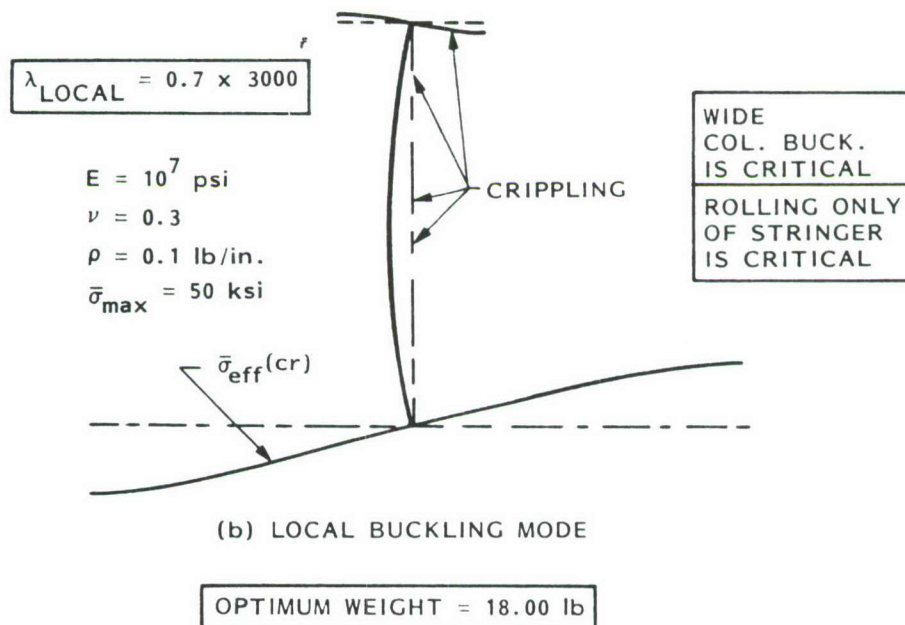
Fig.A11 Optimum design of tee-stiffened panel with zero bowing imperfection and a local imperfection equal to ten per cent of the thickness of the panel skin midway between stringers. Loading and overall geometry are as specified in the caption of Fig. A8.

Fig.A12 Optimum design of hat-stiffened panel with zero bowing imperfection and a local imperfection equal to ten per cent of the thickness of the panel skin midway between stringers. Loading and overall geometry are as specified in the caption of Fig. A8.

a) BASELINE DESIGN

b) PERTURBED DESIGN

Fig. A13Local buckling modes of an axially compressed panel with tee-shaped stringers, showing two sites at which stiffener debonding is likely to occur. Both of these sites are checked by PANDA2. In this case the local buckling mode shape and therefore the peel stresses tending to cause stiffener popoff is very sensitive to a small change in the width w of the outstanding stiffener flange. This behavior makes it very difficult in this case to find a reliable optimum design.

APPENDIX B: BOSOR4 THEORY

In the parts of PANDA2 that have to do with the analysis of discretized models, much of the coding is similar to that in BOSOR4. Therefore, this journal article is included as APPENDIX B.

ANALYSIS OF BUCKLING AND VIBRATION OF RING-STIFFENED, SEGMENTED SHELLS OF REVOLUTION†

DAVID BUSHNELL‡

Lockheed Missiles and Space Company, Palo Alto, California

Abstract—An energy formulation is used in conjunction with the method of finite differences to develop equations leading to buckling loads and vibration frequencies of segmented elastic shells of revolution supported by rings which are treated as discrete elastic structures. A quadratic form for the total potential and kinetic energy is derived through extensive use of matrix methods. The development is similar to that used in the finite element method, and is ideally suited for programming on the digital computer. Numerical results are presented in which two types of finite difference approximations are compared, and convergence properties of eigenvalues and eigenvectors are explored.

NOTATION

A	Beginning of shell meridian
A	Ring cross-section area
B	End of shell meridian
$[B_{i1}], [B_{i2}]$	Equation (14), equation (15)
$[C]$	Constitutive equation coefficients, equation (5)
$\lfloor d \rfloor$	Displacement vector, equation (4e)
d_1, d_2	Figure 1(a)
$[D_i]$	Equation (17)
E	Young's modulus
$[E_1], [E_2]$	Equation (23), equation (24)
e_1, e_2	Figure 1(a)
$[F]$	Equation (42)
G	Shear modulus
$[G_1], [G_2]$	Equation (20), equation (21)
H_n	Hamiltonian corresponding to n-wave pattern
h	Finite difference mesh spacing
I	Ring moment of inertia (subscripted)
J	Ring torsion constant
K	Number of shell segments in shell structure
$[K_1], [K_2]$	Stiffness matrices, equations (2), (45) and (46)
$[K^m]$	Equations (38) and (39)
$K_{A1}, K_{A2}, \ldots$	Boundary condition designators for A end of shell meridian
$K_{B1}, K_{B2}, \ldots$	Boundary condition designators for B end of shell meridian
m	Shell mass/area
$[M]$	Mass matrix, equation (47)
M	Total number of rings
M	Bending moment resultants (subscripted)
n	Number of circumferential waves in buckling or vibration mode
N	Total number of stations at which H_n is evaluated (e.g. 13 in Fig. 1(b))

N	In-plane stress resultants (subscripted)
$[N_o]$	Prestress matrix, equation (4d)
$[P]$	Equation (4f)
p	Normal pressure
$\lfloor q \rfloor$	Displacement vector, equation (10)
$[Q_1], [Q_2]$	Equation (35), equation (36)
r	Parallel circle radius, Fig. 1(a)
R	Radius of curvature (subscripted), Fig. 1(a)
$[R]$	Equation (16)
s	Arc length measured from point A
Δs_i	Weighting factor for numerical integration
$\lfloor S \rfloor$	Stress vector, equation (4a)
t	Shell thickness
$[T]$	Equation (26)
T_s, T_r	Kinetic energy of shell, ring
u, u^*	Meridional, axial displacement, Fig. 1(a)
U_s, U_r	Strain energy of shell, ring
U_c	Constraint "energy"
v, v^*	Circumferential displacement
$\bar{V}$	Axial load applied to ring centroid
w, w^*	Normal, radial displacement, Fig. 1(a)
α	Spherical shell edge angle
γ	Rotation around normal, equation (8c)
δ_i^j	Kronecker delta: $\delta_i^j = 1$ if $i = j$; 0 otherwise
$\lfloor \varepsilon \rfloor$	Strain vector, equations 4(b), (6) and (7)
λ_i^m	Lagrange multipliers for constraint conditions
λ	Eigenvalue
$\varkappa$	Changes in curvature, equation (7)
$\lfloor \omega \rfloor$	Rotation vector, equations (4c) and (8)
Ω	Eigenfrequency
$\dot{\psi}$	Rotation about meridian, equation (8b)
χ	Rotation of meridian, equation (8a)
θ	Circumferential coordinate
v	Poisson's ratio

Subscripts

c	Ring centroid
cr	Critical
i	ith mesh point
j	Mesh point corresponding to ring attachment point
l	Mesh point corresponding to $(\ )^-$ side of juncture
n	Circumferential wave number, also with respect to axis
	Normal to shell meridian (Fig. 1(a))
o	Prebuckling quantity
p	Polar
r	Ring quantity
s	Shell, shear center, or with respect to axis parallel to shell meridian (Fig. 1(a))
t	Twist; $M_t = (M_{12} + M_{21})/2$
x, y, xy	With respect to x–y system (Fig. 1(a))
O	Prebuckling quantity
$1, 2$	Meridional, circumferential directions
12	Shear

Superscripts

k	kth ring support
m	mth set of constraints
T	Transpose
$+, -$	Figure 1(a)
$(\ )'$	Differentiation with respect to s
$*$	Figure 1(a)

INTRODUCTION

RECENT investigations have taken advantage of larger and faster computers to analyze more accurate models of shell structures. Cohen [1], [2] uses a step-by-step numerical integration technique to calculate buckling loads and vibration frequencies of ring-stiffened orthotropic shells of revolution. Kalnins [3] employs a similar method to calculate nonsymmetric deformations of segmented shells of revolution submitted to nonsymmetric loads. In [4] a computer program is described by which buckling loads are calculated for axisymmetrically loaded shells of revolution with general wall construction and with ring supports at the edges.

In this paper the finite difference method is used for the analysis of shells of revolution consisting of elastic shell segments joined by elastic rings. The shell segments may be of various geometries and wall constructions. There are two parts of the analysis: a part in which the axisymmetric state of an axisymmetrically loaded shell is calculated from non-linear theory, and a part in which buckling loads and natural frequencies corresponding to nonsymmetric displacements are calculated. Equilibrium equations similar to those derived by Reissner [5] are used for the prebuckling analysis, and an energy method based on kinematic relations given by Novoshilov [6] is used for the buckling and vibration analysis. The assumptions governing the analysis are:

1. The material is linear–elastic.
2. The Kirchhoff–Love hypothesis holds: normals to the undeformed surface remain unstrained and normal to the deformed middle surface.
3. The structure and loads are axisymmetric, and the prebuckling or prestress deformations are axisymmetric.
4. The prebuckling deflections, while considered finite, are moderate. That is, the square of the meridional rotation can be neglected compared to unity.
5. The ring stiffeners are reasonably "thin". That is, a typical cross-section dimension is small compared to the radius of the ring.
6. The cross-sections of the rings remain undeformed during the deformations of the structure, and the rotation about the ring centroid is equal to the rotation of the shell meridian at the attachment point of the ring.
7. The ring centroids coincide with the ring shear centers.
8. If meridional stiffeners are present, they are numerous enough to include in the analysis by an averaging or "smearing" of their properties over any parallel circle of the shell structure.

For axisymmetrically loaded shells of revolution the partial differential equations governing nonsymmetric buckling and vibration can be reduced to ordinary differential equations through separation of variables. These equations can be solved by application of numerical integration, finite difference, or finite element techniques. With the existence of large computers it is now practical to solve with reasonable accuracy almost any buckling or vibration problem for shells of revolution. It is, for instance, easy to include in the buckling or vibration equations prebuckling quantities as they are obtained from a non-linear analysis. While nonlinear equations were used for instance by Weinitschke [7] and Budiansky [8] for the symmetrical snapping of spherical caps, the influence of the prebuckling displacements and stresses on bifurcation buckling was first recognized by Stein [9] for cylindrical shells and by Huang [10] for spherical caps. In cases such as that treated by

288

Stuhlman *et al.* in [11] with edge moments introducing hoop stresses in the shell, it is imperative that an accurate prebuckling analysis be used.

This paper contains the buckling and vibration analysis only. The nonlinear prebuckling analysis for the axisymmetric prestress is given in [12], in the following it is assumed that this prestress state is known. Some numerical results are given in which two finite-difference schemes are compared, convergence properties are demonstrated, and the effects of round-off errors are revealed. Further numerical results are given in a separate paper [13] in which several comparisons are made between theory and experiment for the buckling of various shells of revolution. Some natural frequencies of an axially compressed, ring and stringer-stiffened cylinder are also given in [13].

It is felt that the major contribution of this paper is the derivation of a practical approach to the solution of a wide class of problems which confront the designer of complex shell structures. The development is similar to that used in the finite element method, and is ideally suited for programming on the digital computer.

The numerical results in this paper and in [12] and [13] were obtained by means of a digital computer code called Bosor 2, which is based on the analyses presented here and in [12]. The Bosor 2 program has a broader capability than its predecessor the Bosor (Buckling of Shells of Revolution) program, which is based on the analysis in [4]. The extensions include:

1. Analysis of segmented (composite) shells, such as cylindercone combinations or joined shells with dissimilar wall characteristics.
2. Analysis of the free vibrations of prestressed, segmented, ring-stiffened shells of revolution.
3. Analysis of shells with discrete rings at a number of stations along the meridian, rather than at the boundaries only.
4. Use of more accurate kinematic relations. The analysis of [4] is based on Donnell-type equations. The analysis which follows is based on Novoshilov-type kinematic relations.
5. Analysis of shells with wall properties which vary along the meridian.
6. Increased generality of the type of axisymmetric loading applied to the shell.

One of the more important extensions of the analysis of [4] is the capability of treating segmented shells. This capability can also be used to advantage in the analysis of simple shells. For instance a rather long cylinder submitted to pressure loading can be divided artificially into three segments: two edge segments in which stresses and displacements vary rapidly over short lengths, and a central segment in which deformations are uniform. The station spacing in the finite difference mesh can be small in the two edge segments and large in the central segment. It has been found from experience that it is better to divide the shell into segments, and thus to maintain uniform station spacing within each segment, rather than to vary the station spacing within any segment.

ANALYSIS FOR BUCKLING AND VIBRATION

The nonlinear analysis for the axisymmetric prestress is given in [12]. In the present paper it is assumed that this prestress state is known. The quantities N_{10}, N_{20}, N_{or}, and χ_0 appear in the buckling and vibration analyses as known variable coefficients.

289

The energy method used in the eigenvalue analysis is based on the definition of the Hamiltonian corresponding to an n-wave deformation pattern:

$$H_n = U_s + \sum_{k=1}^{M} U_r^k - \left(T_s + \sum_{k=1}^{M} T_r^k\right) + \sum_{i=1}^{K+1} U_c^i \tag{1}$$

where

U_s = shell strain energy
U_r^k = strain energy of kth ring stiffener
T_s = shell kinetic energy
T_r^k = kinetic energy of kth ring stiffener
U_c^i = ith set of constraint conditions.

The functional H_n is given in terms of the shell wall displacements and their derivatives. Integration along the shell meridian is performed numerically. The derivatives with respect to the meridional coordinate "s" are simulated by two and three point finite-difference formulas. The derivatives with respect to the circumferential coordinate θ are eliminated because $U = u_n \sin n\theta$, $V = v_n \cos n\theta$, $W = w_n \sin n\theta$. In this way H_n, which is originally an integro-differential quadratic form, becomes an algebraic quadratic form. The constraint conditions are equations of displacement and rotation compatibility at junctures between shell segments and at the shell boundaries.

The algebraic quadratic form H_n is expressed as:

$$H_n = \lfloor q \rfloor [[K_1] + [K_2] + \Omega^2 [M]] \{q\}. \tag{2}$$

The vector $\lfloor q \rfloor$ represents the dependent variables. These include the displacements at the meridional stations in the finite difference mesh and Lagrange multipliers corresponding to the constraint conditions. The matrix $[K_1]$ represents the stiffness matrix (including constraints) of the undeformed and unstressed structure; $[K_2]$ represents the contribution of the prestress terms N_{10}, N_{20}, N_{or}, and χ_0 to the stiffness matrix; and $[M]$ represents the mass matrix. These matrices are symmetric.

The problem is to find the value (eigenvalue) of a parameter which causes H_n to be an extremum. In vibration problems the eigenvalue parameter is the square of the frequency Ω^2. In buckling problems the eigenvalue parameter may be the pressure amplitude p, or any line load or moment $\bar{V}$, $\bar{H}$ or $\bar{M}$ applied to any ring. If some applied load is regarded as the eigenvalue parameter, the kinetic energy terms T_s and T_r^k are zero. The lowest eigenvalue then represents the bifurcation load and the eigenvector represents the mode shape. If, however, the applied load is fixed and Ω^2 is regarded as the eigenvalue parameter, the terms T_s and T_r^k are non-zero. The eigenvalues and eigenvectors then represent frequencies and mode shapes for prestressed shells of revolution. Minimization of H_n with respect to all of the q-components generates a set of simultaneous linear homogeneous algebraic equations, the coefficient matrix of which is symmetric. Nontrivial solutions are obtained for these equations on the digital computer.

Derivation of $[K_1]$, $[K_2]$, *and* $[M]$

In the following derivation variables are used which are defined in Figs. 1(a) and 1(b). These figures show a segmented, ring-stiffened shell supported at the end A by a ring and clamped at B. There are two intermediate rings, one in segment #1 and one between

segments #1 and #2. Fig. 1(a) shows the structure and Fig. 1(b) shows the corresponding finite-difference model.

It is necessary first to define the various components of strain energy and kinetic energy. The shell strain energy U_s can be written as:

$$U_s = \frac{\pi}{2} \int_A^B [\lfloor S \rfloor \{\varepsilon\} + \lfloor \omega \rfloor [N_0] \{\omega\} + \lfloor d \rfloor [P] \{d\}] r \, ds \tag{3}$$
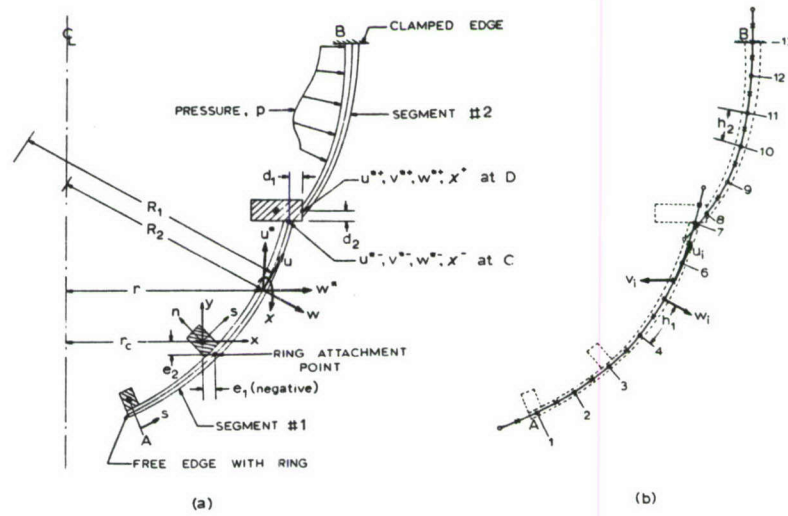
FIG. 1. Ring-stiffened shell with two segments.

where

$$\lfloor S \rfloor \equiv \lfloor N_1, N_2, N_{12}, M_1, M_2, M_t \rfloor$$

$$\lfloor \varepsilon \rfloor \equiv \{\varepsilon\}^T \equiv \lfloor \varepsilon_1, \varepsilon_2, \varepsilon_{12}, \varkappa_1, \varkappa_2, 2\varkappa_{12} \rfloor$$

$$\lfloor \omega \rfloor \equiv \lfloor \chi, \psi, \gamma \rfloor$$

$$[N_0] = \begin{bmatrix} N_{10} & 0 & 0 \\ 0 & N_{20} & 0 \\ 0 & 0 & (N_{10} + N_{20}) \end{bmatrix} \tag{4}$$

$$\lfloor d \rfloor \equiv \lfloor u, v, w \rfloor$$

$$[P] = \begin{bmatrix} -p/R_1 & 0 & -p' \\ 0 & -p/R_2 & 0 \\ -p' & 0 & p(1/R_1 + 1/R_2) \end{bmatrix}$$

291

and

$$
\begin{Bmatrix} N_1 \\ N_2 \\ N_{12} \\ M_1 \\ M_2 \\ M_t \end{Bmatrix} = [C]\{\varepsilon\} = \begin{bmatrix} C_{11} & C_{12} & 0 & C_{14} & C_{15} & 0 \\ C_{12} & C_{22} & 0 & C_{24} & C_{25} & 0 \\ 0 & 0 & C_{33} & 0 & 0 & C_{36} \\ C_{14} & C_{24} & 0 & C_{44} & C_{45} & 0 \\ C_{15} & C_{25} & 0 & C_{45} & C_{55} & 0 \\ 0 & 0 & C_{36} & 0 & 0 & C_{66} \end{bmatrix} \begin{Bmatrix} \varepsilon_1 \\ \varepsilon_2 \\ \varepsilon_{12} \\ \varkappa_1 \\ \varkappa_2 \\ 2\varkappa_{12} \end{Bmatrix} \tag{5}
$$

$$
\varepsilon_1 = u' + w/R_1 + \chi_0\chi
$$
$$
\varepsilon_2 = -nv/r + r'u/r + w/R_2 \tag{6}
$$
$$
\varepsilon_{12} = v' - r'v/r + nu/r + \chi_0\psi
$$

$$
\varkappa_1 = \chi'
$$
$$
\varkappa_2 = -n\psi/r + r'\chi/r \tag{7}
$$
$$
2\varkappa_{12} = 2(-n\chi/r + r'\psi/r + v'/R_2)
$$

$$
\chi = w' - u/R_1
$$
$$
\psi = nw/r - v/R_2 \tag{8}
$$
$$
\gamma = \tfrac{1}{2}(nu/r - rv'/r - r'v/r).
$$

The first term in the integrand of equation (3) is contained in equation (3) of [2]; the second term appears in equation (2) of [14]; and the third term appears in equation (9) of [15]. The coefficients C_{ij} of the constitutive equations (5) are given for various types of shell walls (eccentrically stiffened, layered orthotropic, fiber-wound, corrugated) in [16]. The values of C_{36} and C_{66} in the present analysis are equal to one-half the values given in [16] because of the multiplier 2 in the column vector component $2\varkappa_{12}$. The kinematic relations (6)–(8) which relate infinitesimal buckling strains, changes in curvature, and rotations to infinitesimal buckling displacements are given in equations (4.23) and equations (3.16) of [6] and Equations (7) and (12) of [2].

Figure 1(b) shows the shell meridian with stations $1, 2, 3, 4, \ldots, 13$ identified. The Hamiltonian H_n is expressed at these stations in terms of the displacement components u_i, v_i, and w_i, and the integration in equation (3) is replaced by summation over all stations. The tangential displacement components u_i and v_i occur at stations midway between the stations for w_i and w_{i+1}. A similar arrangement of mesh points was used by Stein in [9]. At the ends of each segment there are "fictitious" points, shown as circles, which correspond to w-values. These points are needed for the expression of the first and second derivatives of w with respect to s at the ends of the segments. The arrangement of mesh points and displacements shown in Fig. 1(b) has been determined to be superior to an arrangement in which u_i, v_i and w_i correspond to displacement components at a single point. More will be said about this in the section on Numerical Results. The station spacing in each segment is constant, but different spacings are used in different segments ($h_1 \neq h_2$

in Fig. 1(b)). The displacements and their derivatives at the ith station are:

$$u = (u_i + u_{i-1})/2 \qquad v = (v_i + v_{i-1})/2 \qquad w = w_i,$$

$$u' = (u_i - u_{i-1})/h \qquad v' = (v_i - v_{i-1})/h \qquad w' = (w_{i+1} - w_{i-1})/2h, \tag{9}$$

$$w'' = (w_{i+1} - 2w_i + w_{i-1})/h^2.$$

It is convenient to define the vector $\lfloor q_i \rfloor$ by

$$\lfloor q_i \rfloor \equiv \{q_i\}^T \equiv \lfloor w_{i-1}, u_{i-1}, v_{i-1}, w_i, u_i, v_i, w_{i+1} \rfloor. \tag{10}$$

From equations (6)–(10) it follows that

$$\{\varepsilon_i\} = [[B_{i1}] + \chi_{oi}[B_{i2}]]\{q_i\} \tag{11}$$

$$\{\omega_i\} = [R_i]\{q_i\} \tag{12}$$

$$\{d\} = [D_i]\{q_i\} \tag{13}$$

in which

$$[B_{i1}] \equiv \begin{bmatrix} 0 & -1/h & 0 & 1/R_1 \\[6pt] 0 & r'/2r & -n/2r & 1/R_2 \\[6pt] 0 & n/2r & \left(-\dfrac{1}{h} - \dfrac{r'}{2r}\right) & 0 \\[10pt] \dfrac{1}{h^2} & \left[\dfrac{1}{hR_1} - \dfrac{(1/R_1)'}{2}\right] & 0 & -\dfrac{2}{h^2} \\[10pt] -r'/2rh & -r'/2rR_1 & n/2rR_2 & -n^2/r^2 \\[10pt] \dfrac{n}{rh} & \dfrac{n}{rR_1} & \left(-\dfrac{r'}{rR_2} - \dfrac{2}{hR_2}\right) & 2\dfrac{nr'}{r^2} \end{bmatrix}$$

$$\begin{matrix} 1/h & 0 & 0 \\[6pt] r'/2r & -n/2r & 0 \\[6pt] n/2r & \left(\dfrac{1}{h} - \dfrac{r'}{2r}\right) & 0 \\[10pt] \left[-\dfrac{1}{hR_1} - \dfrac{(1/R_1)'}{2}\right] & 0 & \dfrac{1}{h^2} \\[10pt] -r'/2rR_1 & n/2rR_2 & r'/2rh \\[10pt] \dfrac{n}{rR_1} & \left(-\dfrac{r'}{rR_2} + \dfrac{2}{hR_2}\right) & -\dfrac{n}{rh} \end{matrix} \tag{14}$$

$$[B_{i2}] \equiv \begin{bmatrix} -1/2h & -1/2R_1 & 0 & 0 & -1/2R_1 & 0 & 1/2h \\ 0 & 0 & 0 & 0 & 0 & 0 & 0 \\ 0 & 0 & -1/2R_2 & n/r & 0 & -1/2R_2 & 0 \\ 0 & 0 & 0 & 0 & 0 & 0 & 0 \\ 0 & 0 & 0 & 0 & 0 & 0 & 0 \\ 0 & 0 & 0 & 0 & 0 & 0 & 0 \end{bmatrix} \tag{15}$$

$$[R_i] \equiv \begin{bmatrix} -1/2h & -1/2R_1 & 0 & 0 & -1/2R_1 & 0 & 1/2h \\ 0 & 0 & -1/2R_2 & n/r & 0 & -1/2R_2 & 0 \\ 0 & n/4r & \left(\dfrac{1}{2h}-\dfrac{r'}{4r}\right) & 0 & n/4r & \left(-\dfrac{1}{2h}-\dfrac{r'}{4r}\right) & 0 \end{bmatrix} \tag{16}$$

$$[D_i] = \begin{bmatrix} 0 & 1/2 & 0 & 0 & 1/2 & 0 & 0 \\ 0 & 0 & 1/2 & 0 & 0 & 1/2 & 0 \\ 0 & 0 & 0 & 1 & 0 & 0 & 0 \end{bmatrix}. \tag{17}$$

For convenience the subscript i has been omitted from the arrays in equations (14)–(16). The geometrical parameters r, r', $1/R_1$, $1/R_2$ and $(1/R_1)'$ are evaluated at every station. The station spacing h should also be subscripted, since it varies from segment to segment.

Insertion of equations (5) and (11)–(16) into equation (3), and replacement of the integral with summation over the number of stations in the finite-difference mesh leads to

$$U_s = \frac{\pi}{2}\sum_{i=1}^{N} r_i \Delta s_i \lfloor q_i \rfloor [[[B_{i1}]^T + \chi_{oi}[B_{i2}]^T][C_i][[B_{i1}] + \chi_{oi}[B_{i2}]]$$
$$+ [R_i]^T[N_{oi}][R_i] + [D_i]^T[P_i][D_i]]\{q_i\}. \tag{18}$$

The integration weights Δs_i are equal to h for all stations except the end stations of each segment, at which $\Delta s_i = h/2$. The strain energy of the kth ring stiffener can be written in the form

$$U_r^k = \frac{\pi}{2}r_c^k \lfloor u_s^*, v_s^*, w_s^*, \chi \rfloor^k [G_1^k + G_2^k]\begin{Bmatrix} u_s^* \\ v_s^* \\ w_s^* \\ \chi \end{Bmatrix}^k \tag{19}$$

in which r_c^k is the radius to the centroid of the kth ring and u_s^*, v_s^*, and w_s^* are the axial, circumferential, and radial displacements of the ring shear center. (In this paper the shear center is assumed to coincide with the centroid.) The quantity G_1 is the stiffness matrix of

294

the unstressed ring, given from [1] by

$$[G_1^k] = \frac{E}{r_c^2} \begin{bmatrix} n^2(n^2 I_x + GJ/E)/r_c^2 & -n^3 I_{xy}/r_c^2 & n^4 I_{xy}/r_c^2 & n^2(I_x + GJ/E)/r_c \\ & n^2(A + I_y/r_c^2) & -n(A + n^2 I_y/r_c^2) & -n I_{xy}/r_c \\ & & A + n^4 I_y/r_c^2 & n^2 I_{xy}/r_c \\ \text{Symmetric} & & & I_x + n^2 GJ/E \end{bmatrix} \tag{20}$$

and G_2^k represents the effect of prestress on the ring stiffness:

$$[G_2^k] = \frac{N_{or}}{r_c^2} \begin{bmatrix} n^2 & 0 & 0 & 0 \\ & 1 & -n & 0 \\ & & n^2 & 0 \\ \text{Symmetric} & & & 0 \end{bmatrix}. \tag{21}$$

The displacements and the rotation of the ring shear center during buckling are related to those of the point on the shell reference surface which corresponds to the attachment point of the ring (see Fig. 1(a)) by

$$\begin{Bmatrix} u_s^* \\ v_s^* \\ w_s^* \\ \chi \end{Bmatrix}^k = [E_i^k + \chi_{oj}^k E_2^k] \begin{Bmatrix} u^* \\ v^* \\ w^* \\ \chi \end{Bmatrix}_j \tag{22}$$

in which $[E_1^k]$ is the transformation matrix for the undeformed shell, given by

$$[E_1^k] = \begin{bmatrix} 1 & 0 & 0 & -e_1 \\ -e_2 n/r & (1 + e_1/r) & -e_1 n/r & 0 \\ 0 & 0 & 1 & e_2 \\ 0 & 0 & 0 & 1 \end{bmatrix} \tag{23}$$

and $[E_2^k]$ represents the effect of "prebuckling" meridional rotation on the transformation (22):

$$[E_2^k] = \begin{bmatrix} 0 & 0 & 0 & -e_2 \\ e_1 n/r & e_2/r & -e_2 n/r & 0 \\ 0 & 0 & 0 & -e_1 \\ 0 & 0 & 0 & 0 \end{bmatrix}. \tag{24}$$

In equations (20)–(24) the superscript k has been omitted from the arrays. The subscript j is the meridional station number corresponding to the ring attachment point. The vector

$[u^*, v^*, w^*, \chi]_j$ is related to the vector $\lfloor q_j \rfloor$ by

$$\begin{Bmatrix} u^* \\ v^* \\ w^* \\ \chi \end{Bmatrix}_j = [T]\{q_j\} \tag{25}$$

where

$$[T] = \begin{bmatrix} 0 & r/2R_2 & 0 & -r' & r/2R_2 & 0 & 0 \\ 0 & 0 & 1/2 & 0 & 0 & 1/2 & 0 \\ 0 & r'/2 & 0 & r/R_2 & r'/2 & 0 & 0 \\ -1/2h & -1/2R_1 & 0 & 0 & -1/2R_1 & 0 & 1/2h \end{bmatrix}. \tag{26}$$

Equations (22) and (25) can be used for determination of U_r^k in equation (19) in terms of $\{q_j\}$:

$$U_r^k = \frac{\pi}{2} r_c^k \lfloor q_j \rfloor [T]^T [E_1^k + \chi_{oj}E_2^k]^T [G_1^k + G_2^k][E_1^k + \chi_{oj}E_2^k][T]\{q_j\}. \tag{27}$$

The kinetic energy of the shell is given by

$$T_s = \frac{\pi}{2}\Omega^2 \int_A^B m(u^2 + v^2 + w^2) r \, \mathrm{d}s \tag{28}$$

which, by use of equations (4e) and (13), and with numerical integration can be written in the form:

$$T_s = \frac{\pi}{2}\Omega^2 \sum_{i=1}^N m_i r_i \Delta s_i \lfloor q_i \rfloor [D]^T [I][D]\{q_i\}. \tag{29}$$

The quantity m_i represents the mass/area at the ith station and $[I]$ is the identity matrix. The kinetic energy of the kth ring is given by

$$T_r^k = \frac{\pi}{2}\Omega^2 \rho_r^k r_c^k [A^k(u_{cj}^{*2} + v_{cj}^{*2} + w_{cj}^{*2}) + I_p^k \chi_j^2 + I_s^k \psi_j^2 + I_n^k \gamma_j^2 - 2I_{sn}^k \psi_j \gamma_j]. \tag{30}$$

Subscript c denotes ring centroid and j denotes meridional station corresponding to the ring attachment point. In this work the centroid is assumed to coincide with the shear center. By use of equations (4c), (12), (22) and (25), equation (30) can be written in the form

$$T_r^k = \frac{\pi}{2}\Omega^2 \rho_r^k r_c^k \lfloor q_j \rfloor [A^k[T]^T [E_1^k + \chi_{oj}E_2^k]^T [T_A^k][E_1^k + \chi_{oj}E_2^k][T] + [R]^T [T_B^k][R]]\{q_j\} \tag{31}$$

where

$$[T_A^k] = \begin{bmatrix} 1 & 0 & 0 & 0 \\ 0 & 1 & 0 & 0 \\ 0 & 0 & 1 & 0 \\ 0 & 0 & 0 & I_p^k/A^k \end{bmatrix} \tag{32}$$

and

$$[T_B^k] = \begin{bmatrix} 0 & 0 & 0 \\ 0 & I_s^k & -I_{sn}^k \\ 0 & -I_{sn}^k & I_n^k \end{bmatrix}$$ (33)

The mth constraint condition U_c^m can be written in the form

$$U_c^m = \lfloor \lambda_1^m, \lambda_2^m, \lambda_3^m, \lambda_4^m \rfloor \left[[I] \begin{Bmatrix} u^{*+} \\ v^{*+} \\ w^{*+} \\ \chi^+ \end{Bmatrix}_l + [Q_1^m + \chi_{0_l} Q_2^m] \begin{Bmatrix} u^{*-} \\ v^{*-} \\ w^{*-} \\ \chi^- \end{Bmatrix}_l \right]$$ (34)

in which subscript l refers to the meridional station corresponding to the mth juncture between segments, and $[Q_1^m]$ and $[Q_2^m]$ are analogous to the negatives of $[E_1^k]$ and $[E_2^k]$:

$$[Q_1^m] = \begin{bmatrix} -1 & 0 & 0 & d_1 \\ nd_2/r & -(1+d_1/r) & nd_1/r & 0 \\ 0 & 0 & -1 & -d_2 \\ 0 & 0 & 0 & -1 \end{bmatrix},$$ (35)

$$[Q_2^m] = \begin{bmatrix} 0 & 0 & 0 & d_2 \\ -nd_1/r & -d_2/r & nd_2/r & 0 \\ 0 & 0 & 0 & d_1 \\ 0 & 0 & 0 & 0 \end{bmatrix}.$$ (36)

In equations (35) and (36) superscript m has been omitted for convenience from the arrays. The λ_1^m, λ_2^m, λ_3^m, and λ_4^m are the mth set of Lagrange multipliers associated with the lth station at which constraints are imposed on the quantities u^*, v^*, w^* and χ. For example, the constraint conditions between Segments #1 and #2 in Fig. 1 ($m = 2, l = 7$) arise from the requirement that the motion during buckling or vibration of point D relative to point C involves no deformation of the ring cross-section. The quantity λ_1^m corresponds to compatibility of axial displacements u^{*-} and u^{*+}; λ_2^m corresponds to compatibility of circumferential displacements v^{*-} and v^{*+}; λ_3^m to compatibility of radial displacements w^{*-} and w^{*+}; and λ_4^m to compatibility of meridional rotations χ^- and χ^+.

Displacement boundary conditions applied at the A and B ends of the meridian (see Fig. 1) take the form

$$U_c^m = [\lambda_1^m, \lambda_2^m, \lambda_3^m, \lambda_4^m][K^m][Q_1^m + \chi_{0_l} Q_2^m] \begin{Bmatrix} u^* \\ v^* \\ w^* \\ \chi \end{Bmatrix}_l$$ (37)

297

in which at the end A of the meridian $m = 1$ with

$$[K^m] = \begin{bmatrix} K_{A1} & 0 & 0 & 0 \\ 0 & K_{A2} & 0 & 0 \\ 0 & 0 & K_{A3} & 0 \\ 0 & 0 & 0 & K_{A4} \end{bmatrix} \tag{38}$$

and at the end B of the meridian $m = K+1$ (K = number of shell segments) with

$$[K^m] = \begin{bmatrix} K_{B1} & 0 & 0 & 0 \\ 0 & K_{B2} & 0 & 0 \\ 0 & 0 & K_{B3} & 0 \\ 0 & 0 & 0 & K_{B4} \end{bmatrix}. \tag{39}$$

The quantities K_{A1}, K_{A2}, etc. and K_{B1}, K_{B2}, etc. are assigned values, either unity if the corresponding displacement component is zero or zero if the corresponding force component is zero. The displacement conditions correspond to a shell which is supported at distances d_1^m and d_2^m from the reference surface. For the shell in Fig. 1(a) the K_{A1}, K_{A2}, etc. would all be zero and the K_{B1}, K_{B2}, etc. would all be unity. The constraint conditions (34) and (37) can be written in terms of the vectors $\lfloor q^+ \rfloor$ and $\lfloor q^- \rfloor$ by introduction of equation (25). The compatibility condition (34) can be written as a symmetric quadratic form in the following way:

$$U_c^m = \lfloor q^-, \lambda, q^+ \rfloor [F] \begin{Bmatrix} q^- \\ \lambda \\ q^+ \end{Bmatrix} \tag{40}$$

with

$$\lambda \equiv \lfloor \lambda_1^m, \lambda_2^m, \lambda_3^m, \lambda_4^m \rfloor \tag{41}$$

$$[F] = \begin{bmatrix} 7 \times 7 & 7 \times 4 & 7 \times 7 \\ [0] & [QT]^T & [0] \\ 4 \times 7 & 4 \times 4 & 4 \times 7 \\ [QT] & [0] & [T] \\ 7 \times 7 & 7 \times 4 & 7 \times 7 \\ [0] & [T]^T & [0] \end{bmatrix} \tag{42}$$

$$Q \equiv [Q_1^m + \chi_{0i} Q_2^m]. \tag{43}$$

The boundary conditions (37) take a similar form:

$$U_c^m = \lfloor q^-, \lambda, q^+ \rfloor \begin{bmatrix} [0] & [KQT]^T & [0] \\ [KQT] & [0] & [0] \\ [0] & [0] & [0] \end{bmatrix} \begin{Bmatrix} q^- \\ \lambda \\ q^+ \end{Bmatrix}. \tag{44}$$

The three coefficient matrices $[K_1]$, $[K_2]$ and $[M]$ in equation (2) can now be written through use of equations (18), (27), (29), (31), (34) and (40). The following expressions are obtained:

$$\lfloor q \rfloor [K_1]\{q\} = \frac{\pi}{2} \sum_{i=1}^{N} \left\{ \lfloor q_i \rfloor [r_i \Delta s_i [B_{i1}]^T[C_i][B_{i1}] + \delta_i^j[T]^T[E_1]^T[G_1][E_1][T]]\{q_i\} \right.$$
$$\left. + \delta_i^l \lfloor q^-, \lambda, q^+ \rfloor [F_1] \begin{Bmatrix} q^- \\ \lambda \\ q^+ \end{Bmatrix} \right\} \tag{45}$$

$$\lfloor q \rfloor [K_2]\{q\} = \frac{\pi}{2} \sum_{i=1}^{N} \left\{ \lfloor q_i \rfloor [r_i \Delta s_i (\chi_{oi}[B_{i1}]^T[C_i][B_{i2}] + \chi_{oi}[B_{i2}]^T[C_i][B_{i1}] \right.$$
$$+ \chi_o^2 [B_{i2}]^T[C_i][B_{i2}] + [R_i]^T[N_{oi}][R_i] + [D_i]^T[P_i][D_i])$$
$$+ \delta_i^j\{[T]^T(\chi_o[E_1]^T[G_1+G_2][E_2] + \chi_o[E_2]^T[G_1+G_2][E_1]$$
$$+ \chi_o^2[E_2]^T[G_1+G_2][E_2] + [E_1]^T[G_2][E_1])[T]\}]\{q_i\} \tag{46}$$
$$\left. + \delta_i^l \lfloor q^-, \lambda, q^+ \rfloor [F_2] \begin{Bmatrix} q^- \\ \lambda \\ q^+ \end{Bmatrix} \right\}$$

$$\lfloor q \rfloor [M]\{q\} = \frac{\pi}{2} \sum_{i=1}^{N} \lfloor q_i \rfloor [m_i r_i \Delta s_i [D]^T[I][D]$$
$$+ \delta_i^j \rho_r r_c (A[T]^T[E_1 + \chi_{oi}E_2]^T[T_A][E_1 + \chi_{oi}E_2][T] + [R]^T[T_B][R])]\{q_i\}. \tag{47}$$

The δ_i^j and δ_i^l are Kronecker deltas, and $[F_1]$ and $[F_2]$ refer to equation (42) with the first and second parts of the matrix Q, respectively [equation (43)].

The coefficient matrices $[K_1]$, $[K_2]$ and $[M]$ have the form shown in Fig. 2. This matrix corresponds to the shell modeled as shown in Fig. 1(b). The boundary conditions at A contribute the elements $[KQT]_1$ and $[KQT]_1^T$; the compatibility conditions for conformity of displacements and rotation at the juncture between Segment #1 and Segment #2 contribute the elements $[QT]_2$, $[QT]_2^T$, $[T]$, and $[T]^T$; and the boundary conditions at B contribute the elements $[KQT]_3$ and $[KQT]_3^T$. Expression of H_n at each of the stations 1 through 13 leads to the sub-arrays of elements so labeled in Fig. 2.

It can be shown that the equations generated by minimization of H_n [equation (48)] with respect to the displacement components u_i, v_i and w_i [indicated in Fig. 1(b)] are the Euler equations of the variational problem in finite difference form. The equations corresponding to $\partial H_n/\partial u_i = 0$ and $\partial H_n/\partial v_i = 0$ represent equilibrium of in-plane forces at the stations where the u_i and v_i are specified; those corresponding to $\partial H_n/\partial w_i = 0$ represent equilibrium of normal forces at the stations where the w_i are specified.

Solution of the eigenvalue problem

The buckling loads or vibration frequencies are calculated from the set of linear, homogeneous, algebraic equations

$$[[K_1]+[K_2]+\Omega^2[M]]\{q\} = 0 \tag{48}$$

299
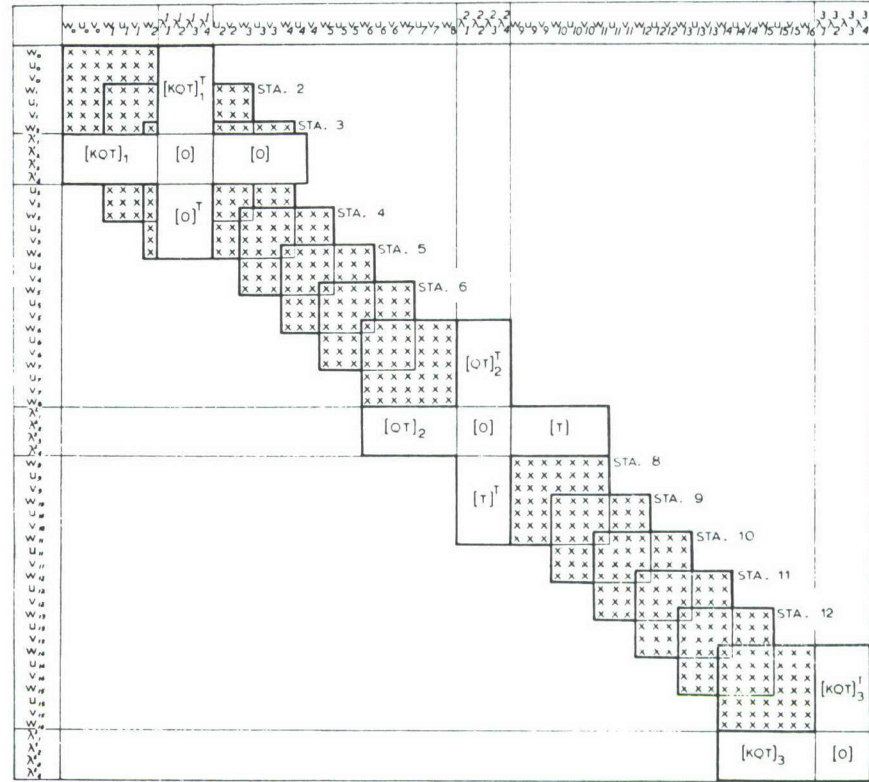
FIG. 2. Form of coefficient matrix with constraint conditions. This matrix corresponds to the model in Fig. 1(b).

for which non-trivial solutions exist if

$$|[K_1]+[K_2]+\Omega^2[M]| = 0. \tag{49}$$

The matrices $[K_1]$, $[K_2]$ and $[M]$ are strongly banded. In vibration problems for prestressed shells calculation of the lowest 5 or so eigenvalues is straightforward. A "classical" eigenvalue problem

$$[K_1 + K_2]q + \Omega^2[M]q = 0 \tag{50}$$

is formulated, and the power method [17], [18] is used for calculation of the lowest few eigenvalues Ω^2 for a particular wave number n. The number of eigenvalues which can be determined accurately depends on the number of mesh points in the finite difference analysis and the complexity ("waviness" in the meridional direction) of the mode shapes.

In buckling problems the eigenvalues of $[K_1 + K_2]$ for given n can be found by "plotting" $|K_1 + K_2|$ versus the eigenvalue parameter λ ($\lambda \equiv p$, N_{10}, or other load) to obtain the load for which $|K_1 + K_2|$ first vanishes. This technique was used in [4] for calculation of bifurcation loads of shells of revolution. On the other hand, a technique of successive approximation, similar to that employed by Cohen [2] for buckling problems can be used. This technique involves the definition of a sequence of "classical" eigenvalue problems which yields a sequence of loads that converges to the load for which $|K_1 + K_2| = 0$. A typical

"classical" eigenvalue problem in the sequence is

$$[K_1 + K_2]q + \lambda_k[K_2]q = 0. \tag{51}$$

Suppose the original load is p_1. The prestress terms N_{10}, N_{20}, N_{or} and χ_o which appear in $[K_2]$ are calculated for this load by means of the nonlinear analysis described in [12]. Then from equation (51) a value λ_1 is obtained. The new load is $p_2 = p_1(1 + \lambda_1)$. New values of N_{10}, N_{20}, etc. corresponding to p_2 are now calculated from the nonlinear analysis of [12] and a new matrix $[K_2]$ is obtained. Then λ_2 is calculated from equation (51). The next value of the load is $p_3 = p_2(1 + \lambda_2)$. The iteration process continues until λ_k, the kth correction, is smaller than some preassigned number. Convergence in some typical cases is discussed in the section on numerical results.

Truncation errors in modal stress resultants

Since a finite number of mesh points is used in the finite difference analysis, truncation errors occur. These errors are particularly large in the evaluation of the modal stress resultants at the boundaries of a shell and at the junctures between shell segments. In the absence of edge displacement constraint conditions and edge rings the natural boundary conditions $N_1 = 0$, $N_{12} = 0$, and $Q_1 = 0$ should be satisfied at the boundaries of the shell. The modal forces N_1, N_{12}, M_1 and Q_1 should be continuous at any juncture between shell segments, provided that the meridian and its slope are continuous and that no ring support exists here. It can be shown that such is the case in the limit $h \to 0$. The equations which correspond to three of the natural boundary conditions at the end "A" of the shell are $\partial H_n/\partial u_o = 0$, $\partial H_n/\partial v_o = 0$, and $\partial H_n/\partial w_o = 0$ (see Figs. 1 and 2). These equations yield, respectively:

$$N_1 + \Delta N_1 = 0, \qquad N_{12} + \Delta N_{12} = 0, \qquad M_1 + \Delta M_1 = 0 \tag{52}$$

where ΔN_1, ΔN_{12} and ΔM_1 are the truncation errors and are given approximately by:

$$\Delta N_1 = -\frac{h}{2r}(N_2 r' + N_{12} n - N_{10}\chi r/R_1)_A,$$

$$\Delta N_{12} = +\frac{h}{2r}(N_{12} r' + N_2 n + N_{20}\psi r/R_2)_A, \tag{53}$$

$$\Delta M_1 = -\frac{h}{2r}(M_2 r' - M_t n + N_1 \chi_o r + N_{10}\chi r)_A.$$

The quantities ΔN_1, ΔN_{12} and ΔM_1 for the end "B" of the shell are given by equation (53) with the opposite signs. For a shell of many segments, equations (53) apply at the ends of each segment, even if rings are present at the junctures between segments. Errors in the modal stresses N_2 and M_2 at the ends of segments are given approximately by:

$$\Delta N_2 = C_{12}\Delta N_1/C_{11}$$
$$\Delta M_2 = C_{45}\Delta M_1/C_{44}. \tag{54}$$

Figure 3 shows the discontinuities in modal stresses occurring between segments of shells. The top three plots give N_1, N_2 and N_{12} for the buckling mode of a shallow spherical cap with an edge ring. The bottom plot gives M_1 for the fundamental vibration mode of a
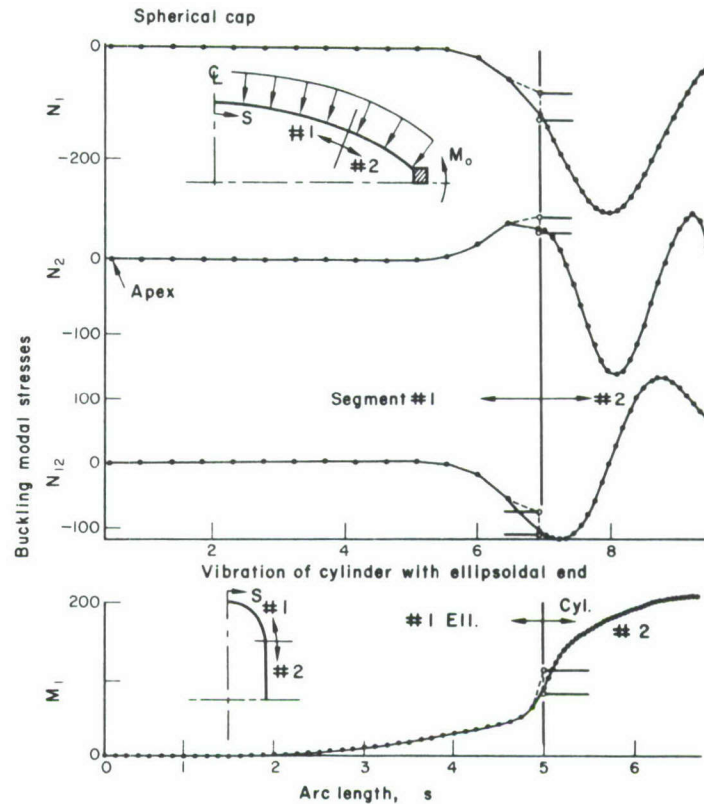
FIG. 3. Buckling and vibration modal stress resultants showing local truncation errors.

cylinder with an ellipsoidal end closure. The circles at the juncture represent the stresses calculated by use of equations (5) and (6)–(9) without correction for the errors ΔN_1, ΔN_2, ΔN_{12} and ΔM_1. Subtraction of the errors (53) and (54) results in modal stresses which are continuous at the juncture. It is evident from Fig. 3 that these errors at the juncture and edge do not "propagate" into the adjacent shell segments. Similar results have been obtained at the boundaries of shells with partially free edges (e.g. simply-supported).

Correction of the modal stresses at shell edges and junctures does not affect the eigen-values, and is therefore not of great significance in buckling and vibration analyses. However, such corrections would have to be made in the finite difference stress analysis of shells. Similar behavior is expected, for example, in the stress analysis of non-symmetrically loaded shells by a two-dimensional finite difference scheme. Since the edge stresses are likely to be the largest, it is important to calculate them as accurately as possible.

NUMERICAL RESULTS

The computer program based on the nonlinear stress analysis of [12] and the linear stability and vibration analysis presented above has been checked through cases for which solutions are known. A rather extensive investigation has been performed of the convergence

302

properties of the eigenvalues with respect to number of points in the finite difference mesh and with respect to number of iterations required for the solution of nonlinear problems. Additional numerical results, including comparisons between test and theory, are given in [13].

Convergence properties

Table 1 gives six examples of the convergence of the sequence of eigenvalue problems as defined by equation (51). The first two examples are for an externally pressurized spherical cap with an edge ring and a constant applied edge moment, M_O (see top of Fig. 3 for geometry). The zeroth iteration represents the program user's initial guess of the critical load. In Example 1 the convergence criterion for the pressure (0·1 %) is satisfied after four iterations. Example 2 represents a problem in which nonlinear effects are dominant because of the large edge moment $M_O = 0·8$ in-lb/in., applied to the spherical cap. Convergence of the pressure is rather slow, and calculations are terminated before the solution has con-

TABLE 1. CONVERGENCE OF SEQUENCE OF EIGENVALUE PROBLEMS $[K_1 + K_2]\{q\} + \lambda_k[K_2]\{q\} = 0$

Iteration number k	Ex. 1† Sph. cap $M_o = 0·2$ p_{cr} (psi)	Ex. 2 Sph. cap $M_o = 0·8$ p_{cr} (psi)	Ex. 3 Cyl. (Fig. 4) 11 points N_{cr} (lb/in.)	Ex. 4 Cyl. (Fig. 4) 41 points N_{cr} (lb/in.)	Ex. 5 Cyl. (Fig. 4) 91 points N_{cr} (lb/in.)	Ex. 6 Cyl. (Fig. 4) 91 pts. D.P. N_{cr} (lb/in.)
0	0·20000	0·1000	7750·0	7750·0	7750·0	7750·0
1	0·65002	0·1407	7960·0	7766·3	7917·8	7775·5
2	0·78577	0·1927	8021·9	7777·7	8098·0	7784·0
3	0·77928	0·2546	8039·6	7781·5	8247·0	7786·8
4	0·77965	0·3221	8044·6	7782·5	8103·4	7787·8
5		0·3883	8046·0	7778·4	8128·1	7788·1
6		0·4462	8046·4	7771·2	8135·2	
7		0·4917		7779·6	8216·1	
8		0·5245		7781·4	8260·4	
9		0·5466			8192·8	
10		0·5609			8009·8	
11		0·5699			8257·6	

† Ex. 1 and 2 are for externally pressurized spherical caps with edge rings (see Fig. 3, top). Ex. 3–6 are for axially compressed, longitudinally stiffened cylinders (see Fig. 4). Ex. 6 calculations in double precision.

verged to the required accuracy of 0·1 %. With a better initial guess for p_{cr} or if iterations are allowed to continue, a solution of $p_{cr} = 0·582$ psi is obtained. Examples 3–6 all apply to the same axially compressed cylindrical shell for which various numbers of mesh points are used (see Fig. 4 for geometry). The first three examples give results from single-precision calculations and the last example gives results from double-precision calculations. The accuracy required for computer "approval" of the solution is 0·01 %. It is seen that round-off errors cause some difficulty in Example 4 and prevent completely convergence in Example 5. It is also clear from Example 5 that a convergence criterion could be chosen (such as 1 %) which would lead to "approval" of the solution 8135·2 lb-in. This load is not within 1 % of the correct load (7788·1 lb/in.). It is evident from the double-precision calculations of Example 6, that round-off errors cause the discrepancy. Figure 4 shows how round-off errors can lead to erroneous results when calculations are performed in single precision. The loads corresponding to 41 and 51 mesh points are "converged" solutions in
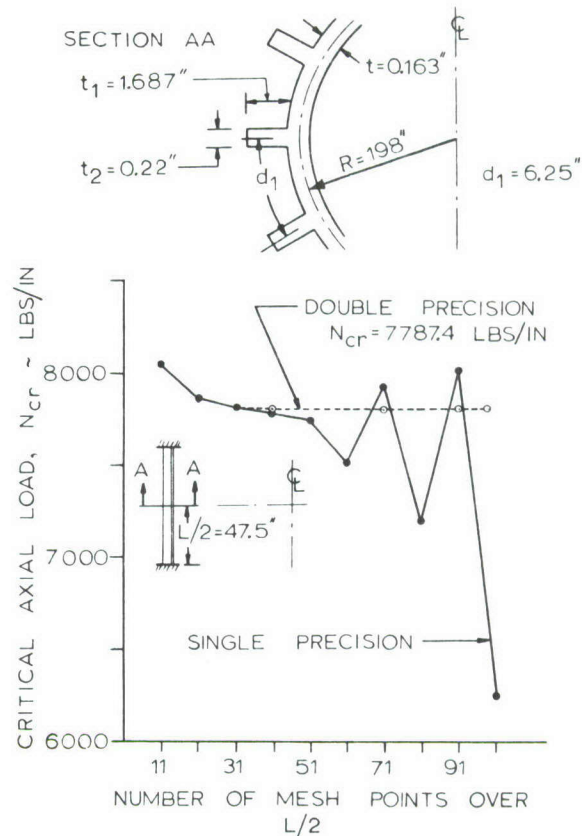
Fig. 4. Convergence of buckling load with increase in number of mesh points.

the sense of Table 1, but they do not have the required accuracy when compared with the solutions labeled "Double Precision". Further increase in the number of mesh points with single-precision calculations leads to further deterioration in the accuracy of the results.

Table 2 gives buckling loads for a spherical shell with an edge angle $\alpha = 160°$ and a free edge. The wave number $n = 2$. Loads are tabulated as a function of the number and the distribution of mesh points. Run times for the Univac 1108 digital computer are also given. These are the times in seconds required for calculation of the buckling load for a single value of the wave number n. Nonlinear prebuckling effects are included. It is seen that much accuracy is gained in this case by division of the shell into two segments. Mesh points are concentrated in the edge region where the modal displacements vary rapidly. For two cases double-precision calculations were made as a check on the single-precision results.

Figure 5 shows a cylindrical shell stiffened by small and large rings. It is desired to find the buckling pressure of this shell. In the analysis the small rings are "smeared out" (see [16]) and the intermittant large rings are treated as discrete elastic structures. The large rings cause significant local disturbances in the prebuckling and buckling modal behavior, as seen in Fig. 6. It is therefore advantageous to analyze the single shell in segments, concentrating mesh points near the large rings where prebuckling and buckling modal displacements vary rapidly.

304

TABLE 2. BUCKLING LOADS OF A SPHERICAL SHELL, $\alpha = 160°$, $A = 0$, $E = 0·91$, $v = 0·3$ CONVERGENCE WITH NUMBER AND DISTRIBUTION OF MESH POINTS; COMPUTER TIME

Number of mesh points	How distributed	Buckling pressure $p_{cr} \times 10^7$ (lb/in²) single precision	Buckling pressure $p_{cr} \times 10^7$ (lb/in²) double precision	Univac 1108 computer time (seconds) single precision
30	1 Segment	19·345		8·511
40	1 Segment	26·978		10·235
50	1 Segment	30·730		10·186
60	1 Segment	32·650		11·794
70	1 Segment	33·761		10·411
80	1 Segment	34·417		11·847
90	1 Segment	34·866		9·614
97	1 Segment	35·056		10·069
10, 10	2 Segments (0°–135°) (135°–160°)	33·594		4·574
15, 15	2 Segments (0°–135°) (135°–160°)	35·405		5·626
20, 20	2 Segments (0°–135°) (135°–160°)	35·872		6·946
25, 25	2 Segments (0°–135°) (135°–160°)	36·039		8·595
30, 30	2 Segments (0°–135°) (135°–160°)	36·090		9·434
35, 35	2 Segments (0°–135°) (135°–160°)	36·160	36·175	10·670
40, 40	2 Segments (0°–135°) (135°–160°)	36·157		11·981
45, 45	2 Segments (0°–135°) (135°–160°)	36·206	36·223	13·223

double
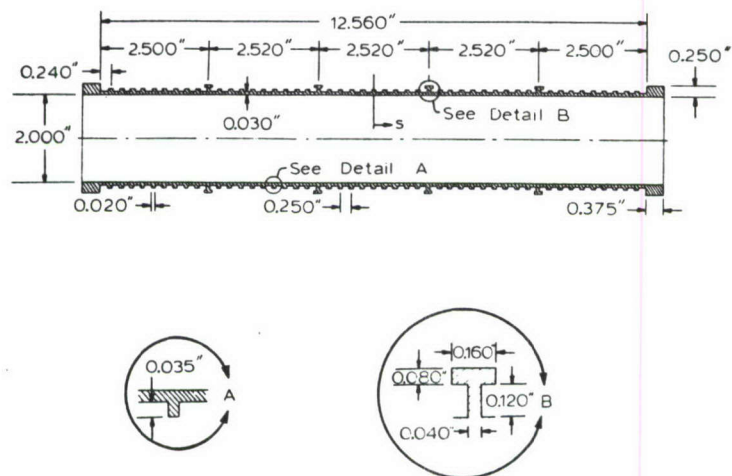
FIG. 5. Geometry of ring-stiffened cylinder submitted to external hydrostatic pressure.
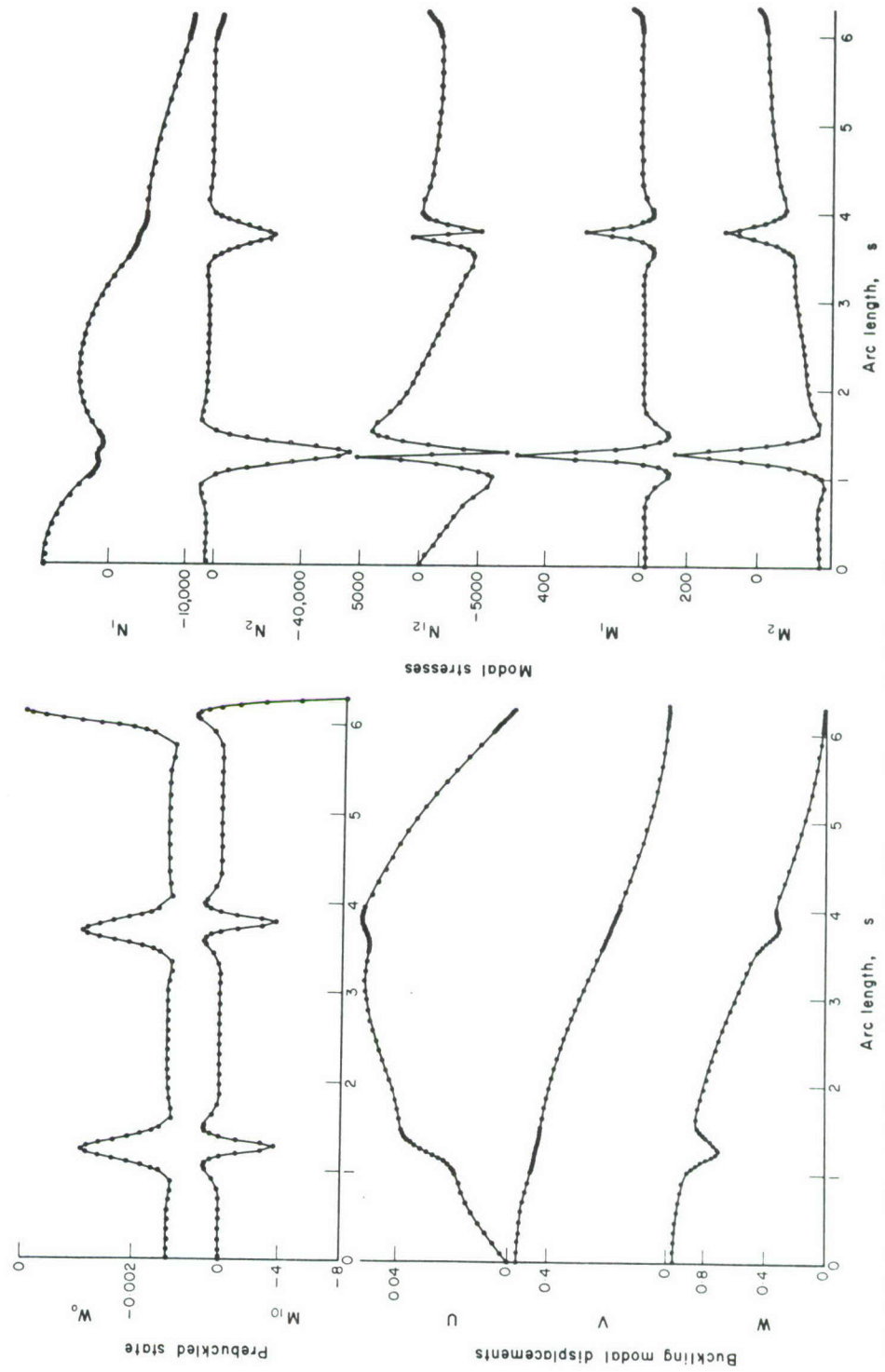
FIG. 6. Prestress state and buckling modal characteristics of the externally pressurized, ring-stiffened cylinder shown in Fig. 5. Single shell analyzed as six segments with mesh points concentrated around large rings.
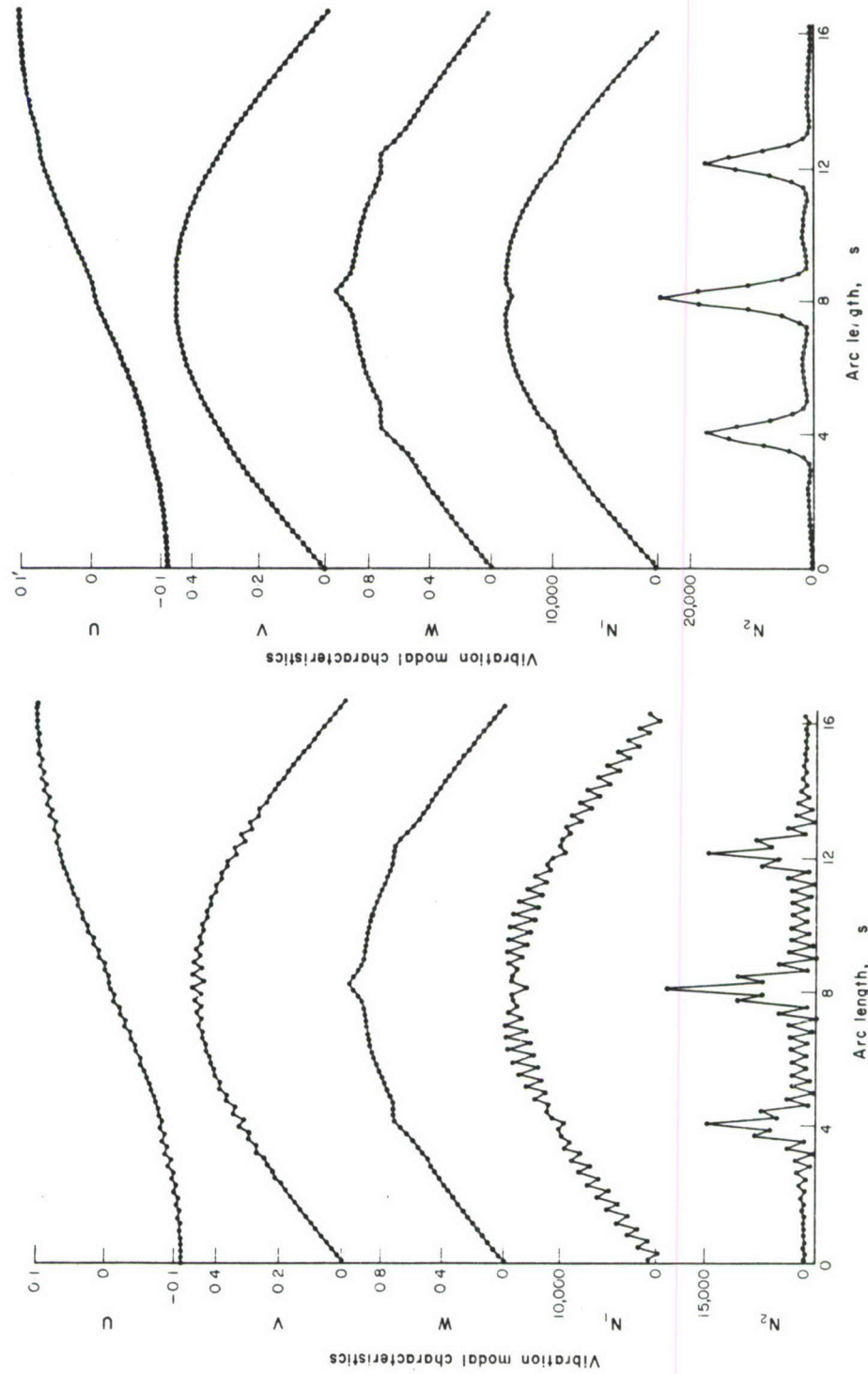
(a) Finite difference scheme #1

(b) Finite difference scheme #2

Fig. 7. Comparison of vibration modal characteristics with finite-difference schemes No. 1 and No. 2 for the ring-stiffened cylinder shown in Fig. 9.

307
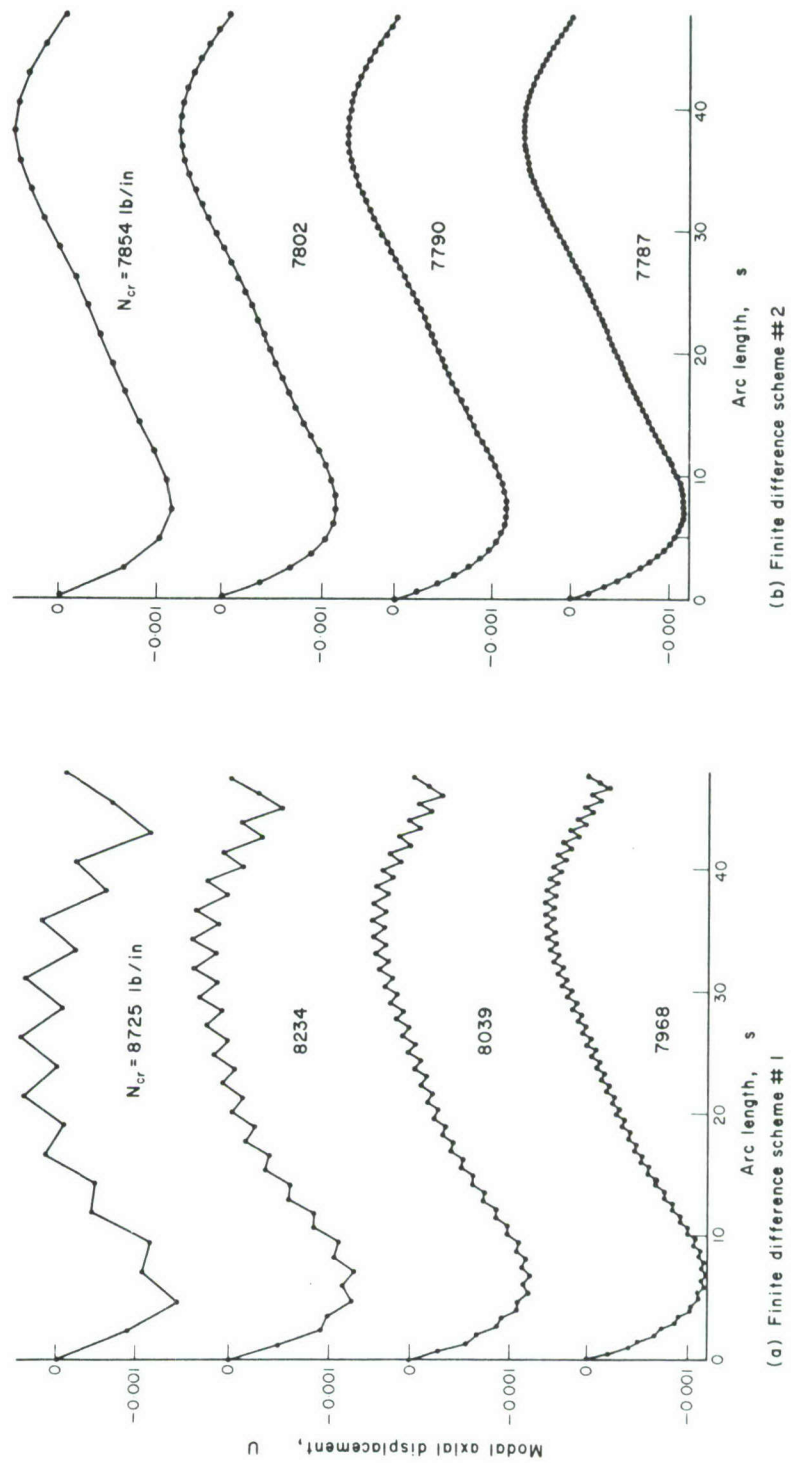
FIG. 8. Comparison of buckling modal displacement u with finite-difference Schemes No. 1 and No. 2 for the axially compressed cylinder shown in Fig. 4.

308

Comparison of two finite difference schemes

Figures 7 and 8 show comparisons between a finite-difference scheme in which all the displacement components u_i, v_i and w_i are specified at the same point (Scheme #1) and the scheme indicated in Fig. 1(b) and equations (9) (Scheme #2). In the Scheme #1 central differences are used everywhere except at the ends "A" and "B" of the shell, where forward and backward differences are used, respectively. With Scheme #1 the coupling between adjacent u_i and v_i values is weak, since no second derivatives of these variables appear in the energy expression. This situation often leads to the "jumpy" behavior of the eigenvector and affects the accuracy of the eigenvalue. Figure 7 shows the fundamental vibration mode of a ring-stiffened cylinder as calculated by the two schemes. The cylinder and ring geometry are shown in Fig. 9. Figure 8 shows the buckling modal displacement u of the axially compressed cylinder depicted in Fig. 4. Convergence of the critical load with number of mesh points is far more rapid with the finite-difference Scheme #2 than with Scheme #1.
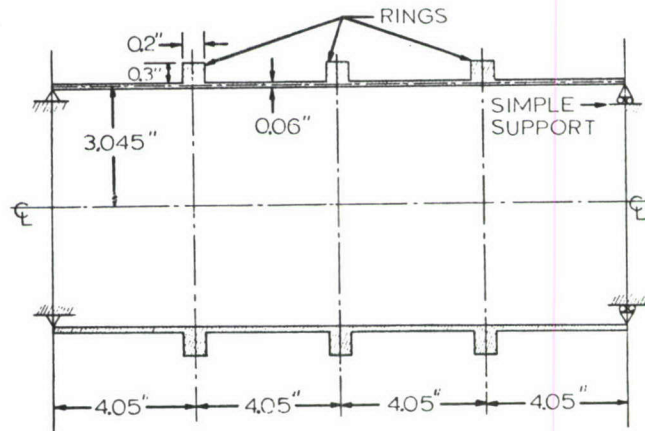
FIG. 9. Geometry of vibrating ring-stiffened cylinder.

REFERENCES

[1] G. A. COHEN, Computer analysis of asymmetric free vibrations of ring-stiffened orthotropic shells of revolution. *AIAA Jnl.* **3**, 2305 (1965).
[2] G. A. COHEN, Computer analysis of asymmetric buckling of ring-stiffened orthotropic shells of revolution. *AIAA Jnl.* **6**, 141 (1968).
[3] A. KALNINS, Analysis of shells of revolution subjected to symmetrical and nonsymmetrical loads. *J. appl. Mech.* 467 (1964).
[4] B. O. ALMROTH and D. BUSHNELL, Computer analysis of various shells of revolution. Presented AIAA 6th Aerospace Sciences Meeting, New York, Jan. 1968, *AIAA Jnl.* **6**, 1848 (1968).
[5] E. REISSNER, On axisymmetrical deformation of thin shells of revolution. *Proc. of Symposia in Applied Mathematics*, Vol. III, p. 27. McGraw-Hill (1950).
[6] V. V. NOVOSHILOV, *The Theory of Thin Shells*, Chapter 1, pp. 18 and 24. Noordhoff (1959).
[7] H. WEINITSCHKE, On the stability problem for shallow spherical shells. *J. Math. Phys.* **38**, 209 (1960).
[8] B. BUDIANSKY, Buckling of clamped shallow spherical shells. *Proc. IUTAM Symp. of Theory of Thin Elastic Shells*, p. 64. North-Holland (1960).
[9] M. STEIN, The effect on the buckling of perfect cylinders of prebuckling deformations and stresses induced by edge support. Collected Papers on Instability of Shell Structures, NASA TN D-1510, p. 217 (1962).
[10] N-C. HUANG, Unsymmetrical buckling of thin shallow spherical shells. *J. appl. Mech.* **31**, 447 (1964).

[11] C. STUHLMAN, A. DELUZIO and B. ALMROTH, Influence of stiffener eccentricity and end moment on stability of cylinders in compression. *AIAA Jnl.* **4**, 872 (1966).
[12] D. BUSHNELL, Nonlinear analysis for axisymmetric elastic stresses in ring-stiffened, segmented shells of revolution. Proceedings ASME/AIAA 10th Structures, Structural Dynamics & Materials Conference, New Orleans, pp. 104–113 (1969).
[13] D. BUSHNELL, Buckling and vibration of ring-stiffened, segmented shells of revolution, Part 2, Numerical results. *Proc. First International Piping and Pressure Vessel Technology Conference*, Delft (1969).
[14] G. A. COHEN, Buckling of axially compressed cylindrical shells with ring-stiffened edges. *AIAA Jnl.* **4**, 1859 (1966).
[15] G. A. COHEN, Conservativeness of a normal pressure field acting on a shell. *AIAA Jnl.* **4**, 1886 (1966).
[16] D. BUSHNELL, B. O. ALMROTH and L. H. SOBEL, Buckling of shells of revolution with various wall constructions, Vol. 2—Basic equations and method of solution. NASA CR-1050 (May 1968).
[17] F. BODEWIG, *Matrix Calculus*. North-Holland (1959).
[18] E. Y. TSUI, F. A. BORGAN and P. STERN, Juncture stress fields in multicellular structures. Lockheed Missiles and Space Co. Report M-77-65-5, Vol. 1 (1965).

Абстракт—Используется энергическая формулировка вместе с методом конечных разностей, с целью выведения уравнений, приводящих к нагрузкам выщучивания и частотам колебаний сегментных упругих оболочек вращения, поддержанных кольцами. Кольца рассматриваются как дискретные упругие конструкции. Дается квадраткая форма для полной потенциальной и кинетической энергии, путем интенсивного применения матричных методов. Разработка оказывается подобна к той, которая используется в методе конечного элемента. Она идеально подходит для программировки на вычислительные машины. Дается численные результаты, в которых сравниваются два типа приближений в конечных разностях. Исследуются свойства сходимости собственных значений и собственных векторов.

310

APPENDIX C: PANDA THEORY

In the parts of PANDA2 that have to do with closed-form PANDA-type models, such as used in the branch of the mainprocessor entered when IQUICK = 1, much of the coding is similar to that in the original PANDA program. Therefore, the following pages from the PANDA report are included as APPENDIX C.

PANDA

PANEL OPTIMIZATION WITH INTEGRATED SOFTWARE (POIS)

PANDA--INTERACTIVE PROGRAM FOR PRELIMINARY MINIMUM WEIGHT DESIGN

DAVID BUSHNELL

LOCKHEED MISSILES AND SPACE COMPANY, INC.
3251 HANOVER STREET
PALO ALTO, CALIFORNIA 94304

JULY 1981

NOMENCLATURE

A	= stiffener cross section area
$\underset{\sim}{A}$	= 3 x 3 integrated constitutive matrix governing extensional (membrane) behavior, Eq. (4)
a_o, b_o	= distances between rings, stringers (Fig. 1)
a, b	= axial, circumferential, dimensions of panel
b_i	= width of ith segment of any stiffener (Fig. 4)
C_{ij}; i=1,6; j=1,6	= 6 x 6 integrated constitutive matrix governing extensional and bending behavior, Eqs. (37) and (40)
c	= slope of buckling nodal lines for panel that is long in the x-direction [Eqs.(51), Fig. 14a]
d	= slope of buckling nodal lines for panel that is long in the y-direction [Eqs.(51), Fig. 14b]
e	= strain or eccentricity, depending on context
$\bar{e}$	= effective strain
E, E_o	= Young's modulus
G, G_o	= shear modulus
$\bar{G}$	= reduced shear modulus, Eq. (41)
g	= plasticity factor, Eq. (30)
I	= stiffener bending moment of inertia
J	= stiffener torsional constant (e.g. $\sum\limits_{i=1}^{N} b_i t_i^3 /3$)
$\bar{n}$, $\bar{m}$	= halfwaves in axial, circumferential directions
n, m	= circumferential, axial wave indices, Eq. (52)
n_1, m_1, n_2, m_2	= wave indices, Eq. (51)
N, M	= stress, moment resultants
p	= pressure

313

R	= radius of cylindrical panel
s	= local coordinate shown in Fig. 18
t	= thickness
u^*, v^*, w^*	= displacement components referred to stiffener coordinates, Figs. 16, 17
u, v, w	= displacement components of panel skin in x, y, z directions, respectively (Fig. 3)
x, y, z	= shell surface coordinates, Fig. 2; or coordinates shown in Fig. 18, depending on context
$\bar{x}_i, \bar{\bar{y}}_i$	= coordinates in the plane of the ith stiffener segment (Fig. 4)
$\bar{x}, \bar{y}, \bar{z}$	= coordinates shown in Fig. 16 and Fig. 17
x_{max}, y_{max}	= defined just after Eq. (49)
β	= rotation of flange, Fig. 18
γ	= stiffener rolling angle, Fig. 17
λ	= eigenvalue or load factor
κ	= change in curvature or twist
ν	= Poisson's ratio
ρ	= density
σ	= stress
$\bar{σ}$	= effective stress
ω	= stiffener rotation components, Figs. 16, 17
φ	= ratio (local buckling load factor)/(general buckling load factor), or angle from material coordinates of a lamina to the axial coordinate (Fig. 2), depending on context

Subscripts

eff   = "effective"

1,2,11,12,22 = pertain to strain components and moduli with respect to the material coordinate directions, 1 and 2, shown in Fig. 2

b   = pertaining to buckling analysis

b   = bending energy [Eqs.(85,88,92,94)]

e   = eigenvalue parameter

f   = flange

i   = stiffener segment number

m   = membrane energy [Eqs.(81-83, 90,91,93]

pl   = material proportional limit

PRE, fixed   = prestress not multiplied by eigenvalue

s   = secant modulus

skin   = pertaining to part of the panel between stiffeners

T   = tangent modulus

w   = web

$\bar{x}$ = $\bar{x}$ – direction (Figs. 16, 17)

x   = x – direction (Fig. 2); or along stiffener axis

y   = y – direction (Fig. 2)

xy   = in-plane shear (Fig. 2), or twist

( ),x   = differentiation with respect to x; Eq. (5)

Superscripts

eff   = "effective"

b   = pertaining to buckling analysis

f   = flange

i   = stiffener segment number

j   = stiffener segment number

k   = layer index

o   = prebuckling condition at design load

r   = ring

s   = stringer

w   = web

SECTION I

INTRODUCTION

Objective

The objective of the development of PANDA has been to cre-
ate an interactive computer program for engineers which derives
minimum weight designs of stiffened cylindrical panels under
combined in-plane loads, N_x , N_y , and N_{xy} . The loading of the
stiffened panel is assumed in most cases to result in uniform
membrane strain components e_x and e_y in both skin and stiffeners
and uniform shear strain e_{xy} in the skin. Meridional bending
between rings in the prebuckling phase is included for shells
without axial stiffeners. Nonlinear material behavior is in-
cluded in the prebuckling analysis if the material is isotropic
or has strength only in one direction (smeared or discrete stif-
feners).

Buckling loads are calculated by use of simple assumed dis-
placement functions. For example, general instability of panels
with balanced laminates and no shear loading is assumed to occur
in the familiar $w(x,y) = C\sin(ny)\sin(mx)$ mode. In the presence
of in-plane shear and/or unbalanced laminates, both local and
general buckling patterns are assumed to have the form

317

$$w(x,y) = C\{ \cos[(n+mc)y - (m+nd)x] - \cos[(n-mc)y + (m-nd)x] \}$$

in which either c or d are zero, depending on the geometry and the stiffness of the entire panel or whatever portion of the panel is under consideration.

The skin is cylindrical with radius R and the stiffeners are composed of assemblages of flat plate segments the lengths of which are large compared to the widths and the widths of which are large compared to the thicknesses. These flat plate segments are oriented either normal or parallel to the plane of the panel skin.

Figure 1 shows an example of the panel geometry. The overall dimensions of the panel are (a,b) and the spacings of the stiffeners are (a_0, b_0).

Material Properties

If the material is orthotropic or anisotropic, buckling is assumed to occur at stress levels for which this material remains elastic. Feasible designs are constrained by maximum stress or strain criteria. Plasticity with arbitrary strain hardening is permitted if the material is isotropic or if it has stiffness in one coordinate direction only, as does the continuum representation of each segment of a smeared stiffener. The cylindrical skin and stiffener segments can be composed of multiple la-

318

yers of isotropic or orthotropic material, as depicted in Fig. 2. Each layer has a unique angle of orthotropy relative in the case of the panel skin to the direction of the generator (x- direction) and in the case of a stiffener segment to the stiffener axis. In the buckling analysis the segments of the stiffeners are assumed to be monocoque and isotropic or orthotropic, not layered anisotropic. Therefore, equivalent orthotropic properties for stiffener segments are calculated from input data for the stiffener segment laminates provided by the program user.

Types of Buckling

Optimum designs with respect to weight are obtained in the presence of constraints due to local and general buckling, maximum tensile and compressive stress or strain, maximum shear strain, and lower and upper bounds on skin layer thicknesses, stiffener cross section dimensions, and stiffener spacings. Design parameters allowed to vary during the optimization phase include panel skin laminae thickness and winding angles, spacings of stiffeners, and thicknesses and widths of the segments of ring and stringer cross sections.

The buckling formulas are derived from Donnell's equations (Reference [1]) with a posteriori application of a reduction factor $(n_c^2 - 1)/n_c^2$ for panels in which the axial half wavelength of the buckling pattern is longer than the panel radius of curvature, R. The circumferential wave index, n_c, equals $n \pi R/b$

319

or $n\pi R/b_o$, with n being the number of half waves in the cir-
cumferential direction over the span b or b_o , respectively.

The many types of buckling included in the PANDA analysis
are summarized in Table 1 and are briefly described next.

Skin Buckling

For the case of balanced laminates and no in-plane shear,
local buckling of the skin is assumed to have the form

$$w_{skin} = C_{skin} \sin\left(\frac{\bar{n}_{skin}\pi y}{b_o}\right) \sin\left(\frac{\bar{m}_{skin}\pi x}{a_o}\right) \tag{1}$$

in which $\bar{n}_{skin}$ and $\bar{m}_{skin}$ are the numbers of half-waves between
stringers with spacing b_o and rings with spacing a_o , respec-
tively. The coordinates and shell wall displacement components
are shown in Fig. 3. Equation(1) implies simple support boun-
dary conditions at stiffener lines of attachment. With shear
present and/or unbalanced laminates the skin buckling pattern
has the form given in the second paragraph under Objective.

General Instability

General instability buckling modes of panels with balanced
laminates and no shear also have the form given in Eq.(1) with
a_o , b_o , $\bar{n}_{skin}$, and $\bar{m}_{skin}$ replaced by quantities appropriate
to the overall dimensions (a,b) of the panel. PANDA also calcu-

320

lates values for "semi-general" instability, that is buckling between rings with smeared stringers and buckling between stringers with smeared rings.

Buckling of Stiffeners

Local buckling of the ith stiffener segment implies

$$w_{stiff}^i = C_{stiff}^i \sin\left(\frac{\pi \bar{\bar{y}}_i}{b_i}\right) \sin\left(\frac{\bar{m}_{stiff}^{-i} \pi \bar{x}}{\ell}\right) \qquad (2)$$

for each stiffener segment with both long edges supported (called "internal" segments in Fig. 4). As shown in Fig. 4 the quantity $\bar{x}$ is the coordinate along the stiffener axis, $\bar{\bar{y}}_i$ is the coordinate perpendicular to $\bar{x}$ in the plane of the ith stiffener segment, b_i is the width of the stiffener segment, and ℓ is the length of the stiffener segment. ($\ell = a_o$ for stringers and $\ell = b_o$ for rings). For stiffener segments with only one long edge supported, (called "end" segments), the local buckling modal displacement is assumed to be in the form

$$w_{stiff}^i = C_{stiff}^i \; \bar{\bar{y}}_i \sin\left(\frac{\bar{m}_{stiff}^{-j} \pi \bar{x}}{\ell}\right) \qquad (3)$$

The stiffener segment buckling analysis is carried out with the assumption that each "internal" segment buckles with its own $\bar{m}^i$. This assumption implies that rotational incompatibility exists at junctions between segments with differing critical values of $\bar{m}^i$. "End" segments are assumed to buckle at the criti-

321

cal $\bar{m}^j$ of the segment to which they are joined. The buckling modes (2) and (3) are shown in Fig. 5.

Rolling Modes

Additional types of panel and stiffener buckling are considered here. These are called "rolling" modes. The first kind of rolling mode involves both skin and stiffeners and is local or "semi-general", the characteristic half-wave-length being integer fractions of the lengths (a_0, b_0), or (a, b_0) or (a_0, b). In these rolling modes the stiffener cross sections rotate about their lines of attachment to the panel skin as shown in Fig. 6a. The cross sections do not deform in the plane of the paper. They do warp, however. The other types of rolling instability do not involve the skin at all. Only the stiffener web deforms, the rest of the stiffener cross section displacing and rotating as a rigid body, as displayed in Fig. 6b. One of these rolling modes (Fig. 6b) occurs in both rings and stringers and in both curved and flat panels. In this mode the buckling deformations are nonuniform (sinusoidal) along the axis of the stiffener. The other rolling mode (Fig. 6c) occurs only in the cases of internal rings on cylindrical panels under external pressure and external rings on cylindrical panels underinternal pressure. In this mode buckling deformations are uniform along the axis of the ring. Stiffener rolling in the more general mode (Fig. 6b) is due to compression along the stiffener and is only weakly dependent on the curvature of this axis. On the other hand, the

322

local ring buckling depicted in Fig. 6c is axisymmetric and arises because of the circumferential curvature of the stiffener axis and prestress in the stiffener segments. It is interesting to note that axisymmetric rolling can occur even if there are no compressive stresses anywhere in the structure, as is the case for internally pressurized cylindrical shells with external rings.

Optimization

The subroutine CONMIN [2,3] is used in PANDA for finding minimum weight designs. This subroutine, written by Vanderplaats in the early 1970's, is based on a nonlinear constrained search algorithm due to Zoutendijk [4]. Briefly, the analytic technique used in CONMIN is to minimize an objective function (panel weight, for example) until one or more constraints, in this case buckling loads, maximum stress or strain, and upper and lower bounds on decision variables, become active. The minimization process then continues by following the constraint boundaries in decision variable space in a direction such that the value of the objective function continues to decrease. When a point is reached where no further decrease in the objective function is obtained, the process is terminated.

Imperfection Sensitivity

It should be emphasized that PANDA does not account expli-

citly for initial structural imperfections. As the code is now written, the user should design a panel to higher loads than those actually to be seen in service; the deleterious effects of initial imperfections can be accounted for in this way.

SECTION II

BRIEF REVIEW OF PREVIOUS WORK ON OPTIMIZATION OF
STIFFENED SHELLS AND PANELS UNDER DESTABILIZING LOADS

This review is concerned with optimization of stiffened shells and panels under destabilizing loads. Optimization techniques per se are not discussed or referenced here. Venkayya [5] has written an excellent survey with an extensive bibliography on this subject.

Most of the work on optimization of stiffened shells and panels under compressive loads has been motivated by the wish to find minimum weight designs of aerospace vehicles. Minimum weight design of ship decks and submarine pressure hulls has also been studied. In recent years computer programs for optimizing aerospace structures have been written for application to laminated wall construction. Design variables include laminae thicknesses and winding angles. Computer programs for optimizing ship structures, especially submarine pressure hulls, have been written to include nonlinear material behavior.

Optimization algorithms have tended to follow either of two strategies: 1. calculation of optimum designs from linear or nonlinear programming techniques created to find minima of an objective function in design space, and 2. calculation of opti-

mum designs from formulas derived from the condition that different types of failures should occur at a given load. (See Venkayya [5] for further details.)

One of the earliest papers on optimum design of stiffened panels is by Catchpole[5a]. Schmit and his colleagues have written several papers on optimization of stiffened plates and cylindrical shells subject to combined in-plane loading [6-10]. Optimization is by various nonlinear programming methods. In an early work, Schmit, Kicher, and Morrow [6] found minimum weight designs of rectangular, simply supported waffle plates. Buckling constraint conditions include general instability, local instability between stiffeners, and stiffener instability. Bronowicki, et al [10] optimized a cylindrical shell with internal T-shaped rings subject to uniform external hydrostatic pressure. They found minimum weight designs with maximum separation of the lowest two frequencies and with maximum separation of the lowest two frequencies with primarily axial content. Gross buckling is prevented by specification of a minimum natural frequency. Additional constraints preclude yielding, buckling of panels between rings, and buckling of stiffeners or stiffener segments. Optimization is by use of a sequential unconstrained minimization technique.

Several papers were written by Burns and his colleagues [11-15]. The primary motivation was to produce minimum weight designs of rocket boosters. The structures were optimized

through application of formulas which dictate that local and general instability occur at the same load.

Many articles and computer programs have been written under the sponsorship of NASA or used by NASA personnel [16-26]. The motivation has been to design minimum weight structures and to provide computer programs for such designs for rocket boosters and airplane fuselages and wings.

The latest in the series of NASA programs for optimization of aerospace structures is the PASCO program [26, 27] written by Anderson, Stroud, and others at NASA. This program calculates minimum weight designs of composite stiffened panels. A panel is considered to be built up of an assemblage of flat plate segments, each of which may have laminated wall construction. The buckling analysis is exact within the limitations of Kirchoff-Love theory. Thus, complex buckling modes are included in the optimization process, modes for example in which general and local waviness are combined. The panels must be simply supported at the top and bottom and be stiffened only in the axial direction. The effect of bow-type imperfections are included, both in the stress and local buckling analyses. PASCO is a combination of a structural program VIPASA written by Wittrick and Williams [23] for the local and general buckling of stiffened flat panels and the previously mentioned optimization routine CONMIN written by Vanderplaats [2].

327

Recent advances in the application of laminated composite materials to aerospace structures has led to many papers on the optimization of stiffened composite panels and wings, among them [28-31].

Several papers on optimization of stiffened cylinders have been written recently by Simitses and his colleagues [32-36]. Their primary motivation has been to produce a computerized capability to design minimum weight fuselages for large aircraft. These structures are subjected to combined axial compression, shear, and internal pres- sure. In the papers by Simitses, et al, the buckling equations are based on Donnell's shell theory [1]. The Galerkin procedure is used to obtain buckling loads. The series expansion for the buckling modal displacement is valid for simply supported panels. Local buckling of stiffener segments is included, and both rings and stringers may be pre- sent. The von Mises yield criterion is used for the maximum stress constraint. Optimization is by a variation of the Sim- plex method.

Papers have been written on the optimization of structures used in ships [39-47]. While recent developments in capabili- ties to create minimum weight designs of aerospace structures have emphasized laminated composites, recent developments of ca- pabilities to create minimum weight designs of ships have in- cluded nonlinear material behavior [44]. Optimization programs for the minimum weight design of submarine pressure hulls (ring

stiffened cylinders) have been written by Pappas and his co-workers [45-47] and by Renzi [44]. Renzi's program, called DAPS3, essentially incorporates the structural analyses and concepts described in [40-43]. Pappas [47] includes in his optimization program general instability, buckling between rings, and crippling of the rings, which have T-shaped cross sections. The design is constrained by a maximum stress criterion and the material must remain elastic. Pappas performs an elaborate search in buckling modal wavelength space (m,n)-space in order to obtain reliably the minimum buckling load corresponding to general instability.

Under the sponsorship of the Air Force Flight Dynamics Laboratory, Almroth, et al [48] have created a system of computer programs that work together to create optimum designs of stiffened cylindrical panels. The PANDA code, based on simple buckling formulas and restricted to simply supported uniform panels, can be used to obtain an initial design. The parameters of this design are stored on a file which can be read by other programs requiring more computer time than PANDA but not restricted as to boundary conditions and uniformity of thickness, stiffener spacing, loading, and buckling mode shapes.

Other papers on optimization subject to constraints other than buckling and stress include Refs. [49] and [50].

SECTION III

FLOW OF CALCULATIONS IN PANDA

Figures 7 and 8 show the flow of calculations in PANDA. Each of
the top two boxes in Figure 7 represents a separate interactive
computer program. In the first program (called BEGIN) the user,
with a specific concept in mind (e.g. knowing in advance that
he wants to find the minimum weight design of a composite cyl-
indrical shell of 7 layers stiffened by T-shaped composite
internal rings and I-shaped aluminum external stringers) pro-
vides the material properties, loads, and starting design in a
"conversational" mode.

In the second program (called DECIDE) the user decides
whether he wants to do simply a buckling analysis of the start-
ing design or whether he wants to do an optimization analysis.
If he wants to do an optimization analysis, the user is then
asked, also in this second program, to identify which of the de-
sign parameters are to be allowed to vary during the optimiza-
tion process, that is which of the design parameters are to be
"decision variables" and what are the lower and upper bounds of
these decision variables. The user can also specify at this
time that certain of the design parameters be "linked" to (to
vary in proportion with) certain of the decision variables. For
example, in laminated composite wall construction the

330

thicknesses of layers with plus winding angles are usually taken to be equal to those with minus the same winding angles; the width of Segment 3 of a T-shaped stiffener is equal to that of Segment 2 (Fig.4a).

When the first two programs have been executed (through commands "RUN BEGIN" and "RUN DECIDE", respectively), the user next executes the main analysis module through the command "RUN PANCON", which performs, with some on-line interaction with the user, the rest of the calculations indicated in Figures 7 and 8.

It is easy to see from Fig. 7 that if there are a large number, NDV, of decision variables (NDV > 6, say) many, many buckling load factors must be computed, especially if the case is complicated so that many different kinds of buckling modes must be considered. For example, in the case displayed in Fig. 9, for which 11 different types of buckling are investigated, as listed in Table 1, there might be as many as 7 decision variables: t, a_o, b_o, t^s, b^s, t^r, and b^r (identified in Figure 9). Thus, each execution of the loop, (I = 1, NDV), in Figure 7 requires calculation of NDV * 11 = 77 critical buckling load factors. Each of the 77 critical buckling load factors represents the results of minimization of the potential energy with respect to the wave indices $\bar{m}$ and $\bar{n}$ and the buckling nodal line slopes c or d. In order to save computer time in PANDA the buckling modal parameters, $\bar{m}(i)$, $\bar{n}(i)$, $c(i)$, and $d(i)$, i = 1, 2 .. 11 corresponding to the 11 critical modes for the current

331

"baseline" design (X(J), J = 1, NDV) are held constant for the slightly perturbed designs Y investigated in the loop over NDV. These perturbed designs must be evaluated with regard to stress and buckling in order to generate gradients of weight and constraint conditions needed by the optimizer CONMIN [2,3].

Simple Example

The PANDA program is completely interactive, with the user's instructions embedded in the three modules, BEGIN, DECIDE, and PANCON. The user has two choices in the preprocessor BEGIN:

(1) The user can choose the long form of the description of the input data, which provides details needed by those who have never before used PANDA or by those who would like to have their memories refreshed; or

(2) The user can choose the short form of the description of the input data, which simply calls for the input data by name, without giving additional description as to what the data are.

Table 2a is a list of a runstream generated with use of the short form for a very simple case with an intuitively obvious answer. The table first illustrates how the three modules of PANDA are exercized simply to calculate a buckling load for a

given design (pages 1-6 of Table 2a). This calculation is followed by an optimization analysis (pages 7-12 of Table 2a). The geometry is for an unstiffened cylinder of radius R = 100 in. and length L = 200 in., with a wall consisting of two layers, each of a different elastic material, loaded in hydrostatic compression with a design pressure of p_o = 20 psi. In the starting design the two layers are of equal thickness and the shell is unnecessarily heavy, that is, the buckling load factor corresponding to the starting design is 3.238 (p. 6 of Table 2a) whereas a load factor of 1.0 would still yield a feasible design.

The material of layer no. 2 (the outer layer) has been deliberately chosen, for the purpose of demonstration, so that its E/ρ is considerably lower than that of the material of layer no. 1. If the decision variables are the thicknesses of the two layers, if these thicknesses are essentially unbounded, and if the effective stress at buckling is less than the maximum specified for either material, then it is known for this simple problem that the optimum design must correspond to the cylinder being made entirely of the material of layer no. 1, with its thickness derived so that the buckling load multiplier (eigenvalue) is equal to unity.

Starting on page 7 of Table 2a are listed the results of a second execution of DECIDE, this for the purpose of choosing decision variables and upper and lower bounds for the optimization

phase of the example. The program module PANCON is subsequently executed again. Results from this second execution of PANCON, this time executed in the optimization mode, begin on page 9 of Table 2a. Design iterations are represented on pages 9 and 10 of Table 2a. Each line "PANEL WEIGHT = ..." corresponds to a trip around the <u>outer</u> loop in Fig. 7. After three sets of five iterations each it appears to the user from successive evaluations of the weight that convergence has been achieved for all practical purposes. The print-out of a summary of design information on page 10 of Table 2a reveals that indeed the outer layer has essentially disappeared and the buckling load factor is very close to unity. Further details of the optimized design can then, at the option of the user, be printed as appears on page 11 of Table 2a.

<u>User's Input Responses Saved on Permanent Files</u>

During executions of BEGIN and DECIDE the user must respond, especially in complex cases, to many requests for input data. It is possible that after he has already spent a considerable amount of time at the terminal he may hit the wrong key, change his mind about some previous input, or be called away from the terminal, or his link with the computer may for some reason be inadvertently destroyed. In order to eliminate the burdon of the user's having to repeat the entire interactive sequence, his responses to requests for input are instantaneously saved on permanent files, one file for BEGIN data and another

(with a different name) for DECIDE data. Examples of these files corresponding to the case in Table 2a are given in Tables 2b-2d. Note that the user can easily investigate cases that represent modifications of his original case by editing these files rather than having to go through the entire interactive sequence repeatedly. Editing the files is easy because each input datum is identified by a short phrase.

It should be emphasized here that during exploration of a given design concept (e.g. cylinder of given materials with two layers and internal T-shaped rings) it is not necessary for the user to execute BEGIN more than once. The user is given the opportunity to modify the design and the loading, as well as to change his mind concerning the choice of decision variables and upper and lower bounds in the program module DECIDE. Note, however, that the user must return to BEGIN if he wishes to change the material properties, the number of layers in the panel skin, or the number or orientation of the segments in either stringers or rings.

Complex Example

The appendix contains output from PANDA corresponding to use of the long form of the description of the input data. This case represents optimization of a composite panel stiffened by both stringers and rings. The stringers are composite. There are two load sets: 1. a combined axial compression and

335

in-plane shear which are eigenvalue parameters, and 2. an internal pressure ($N_{ypre} = 2N_{xpre}$) which represents a fixed load (not an eigenvalue parameter). Figures 10 and 11 show the geometry, stacking sequence, and loading on the panel. There are 11 decision variables, including

1. thickness t_1 of panel skin layer no. 1 (the other layers are linked to layer no. 1);

2. stringer spacing b_o ;

3. thickness t_{s1} of stringer segment no. 1;

4. thickness t_{s2} of stringer segment no. 2;

5. width (height) b_{s1} of stringer segment no. 1;

6. width (height) b_{s2} of stringer segment no. 2;

7. ring spacing a_o ;

8. thickness t_{r1} of ring segment no. 1;

9. thickness t_{r2} of ring segment no. 2;

10. width (height) b_{r1} of ring segment no. 1;

11. width (height) b_{r2} of ring segment no. 2.

One can see from the buckling load factors corresponding to the final design (see p. of the appendix) that three buckling modes are critical: general instability, local skin buckling, and buckling between stringers with smeared rings (a semi-general instability mode). In addition, the mode corresponding to buckling between rings with smeared stringers is close to being critical, exhibiting a margin of only 13 per cent.

SECTION IV

PREBUCKLING AND BUCKLING ANALYSIS ON WHICH PANDA IS BASED

Prebuckling Analysis

The prebuckling analysis is based on the assumption that the panel with smeared stiffeners is in a membrane state of strain $\underset{\sim}{e}^o$. The membrane strain components can be determined from:

$$\underset{\sim}{e}^o \equiv \begin{Bmatrix} e_x^o \\ e_y^o \\ e_{xy}^o \end{Bmatrix} = \begin{bmatrix} & \overset{3 \times 3}{A} & \end{bmatrix}^{-1} \begin{Bmatrix} N_x^o \\ N_y^o \\ N_{xy}^o \end{Bmatrix} \tag{4}$$

in which N_x^o, N_y^o, N_{xy}^o represent the load combination for which the panel is being designed and $\underset{\sim}{A}$ is the 3 x 3 integrated constitutive matrix for extensional deformation of the panel with smeared stiffeners. If the materials of the skin and stiffeners remain elastic at the load level specified by the designer, then the entire prebuckling analysis consists of:

1. an approximate determination of the circumferential strain midway between rings and circumferential strain at ring centroids for panels stiffened by rings only, and

2. a computation from the known strain field and known material properties of how much of the total load N_x^o, N_y^o is carried by the skin and how much is carried by the stiffeners. (The in-plane shear load N_{xy}^o is carried only by the skin.)

Calculation of Midbay Circumferential Strain:

In the case of panels or complete cylindrical shells stiffened by rings and subjected to uniform lateral pressure, the stress in the skin midway between rings can be rather sensitive to the ring cross section area and spacing for

configurations with rather closely spaced rings. Such configurations represent optimum designs of submarine pressure hulls, for example. The buckling pressure corresponding to local instability depends directly on the midbay circumferential stress. When the material behavior is nonlinear, the buckling pressure corresponding to general instability also depends on the state of strain at midbay because the reduced moduli of the skin there naturally act to decrease the coefficients C_{ij} of the integrated constitutive law which appear in the buckling equations.

The differential equation governing the axisymmetric prebuckling behavior of a composite cylindrical shell supported in any way at its ends is derived by Jones and Hennemann [51]:

$$A w,^o_{xxxx} + B w,^o_{xx} + D w^o + E = 0 \tag{5}$$

with the coefficients A, B, D, and E given by:

$$
\begin{aligned}
A &= C_{44} - C_{14}^2 / C_{11} \\
B &= -N_x^o + 2(C_{12}C_{14} - C_{11}C_{15}) / (C_{11}R) \\
D &= (C_{22} - C_{12}^2 / C_{11}) / R^2 \\
E &= C_{12}N_x^o / (C_{11}R) - N_y^o / R
\end{aligned} \tag{6}
$$

in which the C_{ij} are coefficients of the integrated constitutive law relating reference surface strains and changes in curvature of the panel skin to stress and moment resultants in the panel skin (no smeared stiffeners). The homogeneous form of Eq. (5) can be written as:

$$w,^o_{xxxx} + 4S w,^o_{xx} + 4T^2 w^o = 0 \tag{7}$$

where:

$$S = B / (4A) \qquad\qquad T = (D/A)^{\frac{1}{2}} / 2 \qquad\qquad (8)$$

In Eqs. (5) and (7), the axial coordinate x is zero at the mid-length of the cylinder (midbay). The particular solution of Eq. (5) is:

$$w_p^o = -(C_{12}N_x^o - C_{11}N_y^o)R / (C_{11}C_{22} - C_{12}^2) \qquad\qquad (9)$$

Almroth [52] gives the following expression for the axisymmetric normal displacement of a clamped or a simply-supported uniformly loaded cylindrical shell:

$$w^o = w_p^o\left[1 + F_1 \sin(a_1 x)\sinh(a_2 x) + F_2 \cos(a_1 x)\cosh(a_2 x)\right] \qquad (10)$$

in which:

$$a_1 = (T + S)^{\frac{1}{2}} \qquad\qquad a_2 = (T - S)^{\frac{1}{2}} . \qquad\qquad (11)$$

Equation (10) can be applied to the case of a ring stiffened panel. For this configuration Eq. (10) applies to the portion of the panel between adjacent rings. The axial coordinate x is zero midway between rings and equal to $\pm a_o/2$ at the rings. Expression (10) satisfies the symmetry condition at x = 0. The unknown coefficients F_1 and F_2 can be obtained from the two conditions:

340

$$\frac{dw^o}{dx} = 0 \qquad \text{at} \quad x = a_o/2 \tag{12}$$

$$\frac{2}{a_o} \int_0^{(a_o/2)} w^o dx = e_y^o R \tag{13}$$

where e_y^o is the average circumferential strain [Eq.(4)] calculated from the model in which the stiffeners have been smeared out. The first condition is a symmetry condition and the second condition states that the average radial displacement is equal to that calculated from the smeared ring model [Eq. (4)]. Conditions (12) and (13) lead to:

$$F_1 = -B_{22}(a_1^2 + a_2^2)L/\Delta \tag{14}$$

$$F_2 = B_{21}(a_1^2 + a_2^2)L/\Delta$$

with:

$$
\begin{aligned}
L &\equiv a_o/2 \\
\Delta &\equiv B_{11}B_{22} - B_{12}B_{21} \\
B_{11} &= a_2 \sin(a_1 L) \cosh(a_2 L) - a_1 \cos(a_1 L) \sinh(a_2 L) \\
B_{12} &= a_2 \cos(a_1 L) \sinh(a_2 L) + a_1 \sin(a_1 L) \cosh(a_2 L) \\
B_{21} &= a_2 \sin(a_1 L) \cosh(a_2 L) + a_1 \cos(a_1 L) \sinh(a_2 L) \\
B_{22} &= a_2 \cos(a_1 L) \sinh(a_2 L) - a_1 \sin(a_1 L) \cosh(a_2 L)
\end{aligned}
\tag{15}
$$

the prebuckling radial displacements at $x = 0$ (midway between rings) and at the ring attachment stations are :

341

$$w^o(x = 0) = w^o_p + F_2(w^o_p - e^o_y R) \qquad (16)$$

$$w^o(x = L = a_o/2) = w^o_p + (w^o_p - e^o_y R) \left[F_1 \sin(a_1 L) \sinh(a_2 L) \right.$$
$$\left. + F_2 \cos(a_1 L) \cosh(a_2 L) \right] \qquad (17)$$

In certain cases it is important to include the effect of prebuckling axial bending midway between rings. This bending contributes to further plastic straining at the outer fiber of a ring-stiffened, externally pressurized cylindrical shell, leading to a reduction in the instantaneous stiffness coefficients governing stability. The change in axial curvature $w,^o_{xx}$ at $x = 0$ is given by:

$$w,^o_{xx}(x = 0) = (w^o_p - e^o_y R)\left[F_1 2a_1 a_2 + F_2(a_2^2 - a_1^2) \right] \qquad (18)$$

The circumferential strains midway between rings and at ring attachment stations are:

$$e^o_{yskin}(x = 0) = w^o(x = 0)/R$$

$$e^o_{yskin}(x = a_o/2) = w^o(x = a_o/2)/R. \qquad (19)$$

Loads in the Skin and in the Stiffeners: The stress resultants along the axis $\bar{x}$ of each stiffener segment are calculated from the axial strains in these segments, which are available from Eqs. (4) and (19b). Knowing the strains along the axis of each set of stiffeners and the stress-strain curves of the materials from which these segments are fabricated, one can calculate the stress resultants $N^{oi}_{\bar{x}}$ from:

342

$$N\frac{oi}{x} = \sigma\frac{oi}{x}t^i = E_s^i e\frac{oi}{x}t^i \tag{20}$$

in which E_s^i is the secant modulus, $e\frac{i}{x}$ is the strain of the stiffener axis, and t^i is the thickness of the ith stiffener segment.

If local bending of the skin between rings is ignored, the resultants $(N_{xskin}^o, N_{yskin}^o)$ of the skin are given by:

$$N_{xskin}^o = N_x^o - \sum_{i=1}^{N^s} N\frac{oi}{x}(\text{stringer})/b_o \tag{21}$$

$$N_{yskin}^o = N_y^o - \sum_{i=1}^{N^r} N\frac{oi}{x}(\text{ring})/a_o \tag{22}$$

where N^s and N^r are the numbers of stringer segments and ring segments, respectively. If local bending of the skin between rings is accounted for, the circumferential resultant carried by the skin midway between rings is given by:

$$N_{yskin}^o = C_{12}N_{xskin}^o/C_{11} + e_{yskin}^o(x = 0)\left[C_{22} - C_{12}^2/C_{11}\right] \tag{23}$$

with e_{yskin}^o being computed from Eq. (19a).

<u>Inclusion of Plasticity</u>: The flow of calculations in the prebuckling phase is displayed in Fig. 12. As can be seen from this flow, the process is iterative. The objectives of the prebuckling computations are:

1. to compute instantaneous values for the moduli E_{11}^k, E_{12}^k, E_{22}^k, and G^k, $k = 1,2, .. N^L$, where N^L is the number of layers in the panel skin (these

moduli are used in the calculation of the integrated constitutive law governing stability);

2.   to compute instantaneous values for the corresponding moduli of the segments of the rings and stringers;

3.   to compute how much load is carried by the skin and how much is carried by the stiffeners.

These goals are summarized in the two boxes in the lower left-hand corner of Fig. 12.

The contents of the boxes on the right-hand-side of Fig. 12 will next be described.

The strain components in the kth lamina in material coordinates are calculated from:

$$
\left\{ \begin{array}{c} e_1^k \\ e_2^k \\ e_{12}^k \end{array} \right\}
\left[\begin{array}{ccc} c^2 & s^2 & sc \\ s^2 & c^2 & -sc \\ -2sc & 2sc & (c^2-s^2) \end{array} \right]
\left\{ \begin{array}{c} e_x^o - zw^o,_{xx} \\ e_{yskin}^o \\ e_{xy}^o \end{array} \right\}
\tag{24}
$$

in which:

$$
c \equiv \cos\phi \qquad\qquad s \equiv \sin\phi, \text{ (ϕ is shown in Fig. 2)}, \tag{25}
$$

z is the positive outward coordinate normal to the shell reference surface, $w^o,_{xx}$ is given by Eq. (18), and e_{yskin}^o is given by Eq. (19a). The corresponding stress components are:

$$
\begin{aligned}
\sigma_1^k &= E_{11}^k e_1^k + E_{12}^k e_2^k \\
\sigma_2^k &= E_{12}^k e_1^k + E_{22}^k e_2^k \\
\sigma_{12}^k &= G^k e_{12}^k .
\end{aligned}
\tag{26}
$$

344

The moduli E_{11}^k, E_{12}^k, E_{22}^k, and G^k may be reduced from the elastic values because of plastic flow. J_2-deformation theory [53] is used as described next. Hutchinson [53] gives further details.

The effective stress can be calculated from the stress components σ_1^k, σ_2^k, σ_{12}^k:

$$\bar{\sigma}^k = \left[(\sigma_1^k)^2 + (\sigma_2^k)^2 - (\sigma_1^k \sigma_2^k) + 3(\sigma_{12}^k)^2 \right]^{1/2} \tag{27}$$

If $\bar{\sigma}^k$ is less than the proportional limit stress, σ_{pl}^k, no more calculations are performed for the kth layer in this iteration. If $\bar{\sigma}^k > \sigma_{pl}^k$, the effective strain $\bar{e}^k$ is computed from:

$$\bar{e}^k = 0.4714 \left[(e_1^k - e_2^k)^2 + (e_1^k - e_3^k)^2 + (e_2^k - e_3^k)^2 + 3(e_{12}^k)^2/2 \right]^{1/2} \tag{28}$$

The strain e_3^k normal to the reference surface is calculated from:

$$e_3^k = -(e_1^k + e_2^k)(\nu + g/3)(1 - \nu + g/3) \tag{29}$$

in which:

$$g = 1.5(E^k/E_s^k - 1) \tag{30}$$

where E_s^k is the secant modulus obtained from the previous iteration. The effective strain $\bar{e}^k$ is compared with $\bar{e}_I^k$, where:

$$\bar{e}_I^k = e_I^k - (1-2\nu)\sigma_I^k/(3E^k). \tag{31}$$

345

In Eq. (31) e_I and σ_I are coordinates of the stress-strain curve for the material of the kth layer. These are provided by the user of PANDA. The values of e_I^k and σ_I^k that lie on the stress-strain curve and produce $\bar{e}_I^k$ equal to $\bar{e}^k$ from Eq. (28) are used to determine new estimates of the tangent and secant moduli E_T^k and E_S^k, respectively:

$$E_T^k = d\sigma_I^k/de_I^k \; ; \quad E_S^k = \sigma_I^k/e_I^k \tag{32}$$

The new estimate of the effective stress is, of course, σ_I^k. In PANDA the stress-strain curve is represented in a piecewise linear fashion, the linear segments connecting coordinates (e_j, σ_j), $j = 1, 2, \ldots$ that are supplied by the program user. A smoothing technique is used in the determination of E_T^k in order to prevent oscillatory behavior in the optimization phase associated with corners between line segments of the stress-strain curve.

New values of the moduli E_{11}^k, E_{12}^k, E_{22}^k, and G^k are computed from J_2-deformation theory [53]:

$$E_{11}^k = a/\Delta \qquad\qquad E_{12}^k = b/\Delta$$

$$\tag{33}$$

$$E_{22}^k = E_{11}^k \qquad\qquad G^k = G_e^k(1 + \nu)/(1 + \nu + g)$$

in which G_e^k is the elastic shear modulus of the kth layer and

$$a \equiv (1 + 2g/3)/E^k$$

$$b \equiv (\nu + g/3)E^k$$

$$g \equiv 1.5(E^k/E_S^k - 1) \tag{34}$$

$$\Delta \equiv a^2 - b^2 .$$

The above calculations are repeated for every layer in the laminate.

The reduced moduli of the stiffener segments are determined in a completely analogous fashion, except that the effective strain [Eq. (28)] is replaced by:

$$\bar{e} = e_x^o \tag{35}$$

for all stringer segments and:

$$\bar{e} = (R/R_{c.g.})e_{yskin}^o(x = a_o/2) \tag{36}$$

for all ring segments. The quantity $R_{c.g.}$ is the radius to the ring centroid and $e_{yskin}^o(x = a_o/2)$ is the strain in the skin at the ring attachment point [Eq. (19b)].

<u>Integrated Constitutive Law</u>: The integrated constitutive law for the laminated panel skin, for both the prebuckling analysis and the stability analysis, has the form:

$$
\begin{Bmatrix} N_x \\ N_y \\ N_{xy} \\ M_x \\ M_y \\ M_{xy} \end{Bmatrix}
=
\begin{bmatrix}
A_{11} & A_{12} & A_{16} & B_{11} & B_{12} & B_{16} \\
A_{12} & A_{22} & A_{26} & B_{12} & B_{22} & B_{26} \\
A_{16} & A_{26} & A_{66} & B_{16} & B_{26} & B_{66} \\
B_{11} & B_{12} & B_{16} & D_{11} & D_{12} & D_{16} \\
B_{12} & B_{22} & B_{26} & D_{12} & D_{22} & D_{26} \\
B_{16} & B_{26} & B_{66} & D_{16} & D_{26} & D_{66}
\end{bmatrix}
\begin{Bmatrix} e_x \\ e_y \\ e_{xy} \\ \kappa_x \\ \kappa_y \\ 2\kappa_{xy} \end{Bmatrix}
= \underset{\sim}{C}e \tag{37}
$$

in which N_x, N_y, ... M_{xy} are the stress and moment resultants and e_x, e_y, ... κ_{xy} are the reference surface strains, changes in curvature, and twist. The A_{ij}, B_{ij}, and D_{ij} are given by Jones [54]:

$$A_{ij} = \sum_{k=1}^{N^L} (\bar{Q}_{ij})_k (z_k - z_{k-1})$$

$$B_{ij} = \frac{1}{2} \sum_{k=1}^{N^L} (\bar{Q}_{ij})_k (z_k^2 - z_{k-1}^2) \tag{38}$$

$$D_{ij} = \frac{1}{3} \sum_{k=1}^{N^L} (\bar{Q}_{ij})_k (z_k^3 - z_{k-1}^3)$$

in which the z_k are measured from the reference surface. The $\bar{Q}_{ij}$ for each lamina are given by Jones as:

$$\bar{Q}_{11} = E_{11} c^4 + 2(E_{12} + 2G) s^2 c^2 + E_{22} s^4$$

$$\bar{Q}_{12} = (E_{11} + E_{22} - 4G) s^2 c^2 + G(s^4 + c^4)$$

$$\bar{Q}_{22} = E_{11} s^4 + 2(E_{12} + 2G) s^2 c^2 + E_{22} c^4$$

$$\bar{Q}_{16} = (E_{11} - E_{12} - 2G) sc^3 + (E_{12} - E_{22} + 2G) s^3 c \tag{39}$$

$$\bar{Q}_{26} = (E_{11} - E_{12} - 2G) s^3 c + (E_{12} - E_{22} + 2G) sc^3$$

$$\bar{Q}_{66} = (E_{11} + E_{22} - 2E_{12} - 2G) s^2 c^2 + G(s^4 + c^4).$$

For the prebuckling phase, E_{11}, E_{12}, E_{22}, and G are the reduced moduli defined in Eqs. (33), c and s are defined in Eq. (25), and ϕ is the angle from the axial direction to the fiber axis of the lamina (direction in which the modulus E_1 is measured: Fig. 2).

"Smeared" Stiffeners: For the calculation of the average prebuckling strain components from Eq. (4), the stiffeners must be treated as part of the skin, that is, "smeared out" over the panel surface. This

348

"smearing" is accomplished via a theory used by Baruch and Singer [55] as described in the text by Brush and Almroth [56]. To certain of the constitutive coefficients A_{ij}, B_{ij}, and D_{ij} in Eq. (37) are added terms that reflect the extensional, bending, and torsional rigidities of the rings and stringers. For example, with external rings and external stringers (positive eccentricities), all of the segments which are of the same material, new constitutive coefficients C_{ij} are obtained as follows:

$$C_{11} = A_{11} + E_s^s A^s / b_o$$

$$C_{22} = A_{22} + E_s^r A^r / a_o$$

$$C_{14} = B_{11} + e^s E_s^s A^s / b_o$$

$$C_{25} = B_{22} + e^r E_s^r A^r / a_o \qquad\qquad (40)$$

$$C_{44} = D_{11} + E_s^s I^s / b_o$$

$$C_{55} = D_{22} + E_s^r I^r / a_o$$

$$C_{66} = D_{66} + (\overline{G}^s J^s / b_o + \overline{G}^r J^r / a_o)/4$$

in which superscripts s and r denote "stringer" and "ring", respectively; subscript s denotes "secant modulus"; $\overline{G}$ is the effective elastic-plastic shear modulus:

$$\overline{G} = G_e \, (1 + \nu)/(1 + \nu + g) \qquad\qquad (41)$$

with g given by Eq. (34c); and J is the torsion constant for the stiffener cross section. The quantities e^s and e^r are the distances from the skin reference surface to the centroidal axes of the stringers and rings, respectively, positive when these axes lie on the outside of the shell.

The new prebuckling C_{ij} in Eq. (40) are used to calculate new average strain components from Eq. (4), as indicated in Fig. 12. Eqs. (5-41) are solved again. Iterations continue until the prebuckling strain components e_x^o, e_{yskin}^o, e_{xy}^o change no more than 0.01 % from their values as of the previous iteration. Figure 13 shows the results of several prebuckling iterations applied to a ring-stiffened submarine hull subject to uniform external hydrostatic compression. Quadratic extrapolation of the strain components is used every four iterations.

Instantaneous Moduli for Stability Analysis: Once convergence of the prebuckling strain components has been achieved, the instantaneous moduli (tangent moduli) governing stability are calculated. The instantaneous moduli for the kth layer of the panel skin can be calculated with use of J_2-deformation theory [53]:

$$E_{11b}^k = a/\Delta \qquad E_{12b}^k = b/\Delta \qquad E_{22b}^k = c/\Delta$$

$$G_b^k = G_e^k (1+\nu)/\left[1 + \nu + g + 2g'(\sigma_{12}^k)^2\right]$$

(42)

in which:

$$a \equiv (1 + 2g/3 + g's_2^2)/E^k$$

$$b \equiv (\nu + g/3 - g's_1s_2)/E^k$$

$$c \equiv (1 + 2g/3 + g's_1^2)/E^k$$

$$\Delta \equiv ac - b^2$$

(43)

350

with g given by Eq. (34c),

$$g' = 2.25E^k(1/E_T^k - 1/E_s^k)/\overline{\sigma}^2 \tag{44}$$

and the stress deviators s_1 and s_2 given by:

$$s_1 = (2\sigma_1^k - \sigma_2^k)/3 \qquad\qquad s_2 = (2\sigma_2^k - \sigma_1^k)/3. \tag{45}$$

Analogous formulas are used for the instantaneous moduli of the stiffener segments. The instantaneous moduli given in Eq. (42) are used in Eqs. (39), which through Eqs. (38), yield new coefficients A_{ij}^b, B_{ij}^b, and D_{ij}^b in Eq. (37), that apply during the buckling phase of the analysis. Super-script b denotes "value during buckling modal deformation".

For the calculation of general instability and "semi-general" instability, at least one set of stiffeners must be smeared out over whatever domain within the panel $[(a,b), (a_o,b), (a,b_o)]$ is being considered during the current buckling analysis. Formulas for the instantaneous stiffness coefficients C_{ij}^b are similar to those given for C_{ij} in Eq. (40), with the secant moduli E_s^S, E_s^r for the stringers and rings being replaced by the tangent moduli E_T^S, E_T^r; and the A_{ij}, B_{ij}, D_{ij} being replaced by A_{ij}^b, B_{ij}^b, D_{ij}^b.

General, "Semi-General," and Local Instability of Panel

Governing Equations: For layered and stiffened shells with membrane-bending coupling, Eqs. (37), as modified in accordance with Eqs. (40,42), may be written in the form:

$$\left\{ \begin{matrix} N^b \\ M^b \end{matrix} \right\} = \begin{bmatrix} A & B \\ B & D \end{bmatrix} \left\{ \begin{matrix} e^b \\ \kappa^b \end{matrix} \right\} = \underset{\sim}{\overset{6\times6}{C}} \, \underset{\sim}{e}^b \tag{46}$$

where superscript b denotes "value due to buckling modal deformation";

A, B, and D are 3 x 3 symmetric full matrices containing the <u>instantaneous</u> stiffness coefficients just derived (superscript b dropped for convenience); and:

$$\lfloor N^b; M^b \rfloor \equiv \lfloor N^b_x, N^b_y, N^b_{xy}; M^b_x, M^b_y, M^b_{xy} \rfloor$$

$$\lfloor e^b; \kappa^b \rfloor \equiv \lfloor e^b_x, e^b_y, e^b_{xy}; \kappa^b_x, \kappa^b_y, 2\kappa^b_{xy} \rfloor = \underset{\sim}{e}^b \tag{47}$$

The strain energy U and work W done by the prebuckling in-plane loads N^o_x, N^o_y, N^o_{xy} during the buckling process are given by:

$$U = \frac{1}{2} \int_0^{y_{max}} \int_0^{x_{max}} \underset{\sim}{e}^{b^T} \underset{\sim}{C} \underset{\sim}{e}^b dx\, dy \tag{48}$$

$$W = \frac{1}{2} \int_0^{y_{max}} \int_0^{x_{max}} \left(N^o_x w^{b^2}_x + N^o_y w^{b^2}_y + 2N^o_{xy} w^b_x w^b_y \right) dx\, dy \tag{49}$$

in which the upper limits of integration x_{max} and y_{max} depend on what kind of instability is being investigated, general, "semi-general," or local, as follows:

Type of Instability	x_{max}	y_{max}
general	a	b
between rings, smeared stringers	a_o	b
between stringers, smeared rings	a	b_o
local	a_o	b_o

In the domains (x, y) bounded by (a, b) or (a_o, b) or (a, b_o) or (a_o, b_o), the buckling modal displacement components u^b, v^b, w^b are assumed to have the general form:

$$u^b = A(n_2^2 m_1 \sin(n_1 y - m_1 x) + n_1^2 m_2 \sin(n_2 y + m_2 x))$$

$$v^b = B(\quad n_2 \sin(n_1 y - m_1 x) - \quad n_1 \sin(n_2 y + m_2 x)) \qquad (50)$$

$$w^b = C(\quad \cos(n_1 y - m_1 x) - \quad \cos(n_2 y + m_2 x))$$

in which:

$$n_1 = n + mc \qquad\qquad m_1 = m + nd$$
$$\qquad\qquad\qquad\qquad\qquad\qquad\qquad (51)$$
$$n_2 = n - mc \qquad\qquad m_2 = m - nd$$

The displacement functions (50) were chosen to permit nearly inextensional reference surface buckling strain components, e_x^b, e_y^b, and e_{xy}^b, and to allow reasonably accurate determination of buckling loads in the presence of shear and unbalanced laminates without the need for series expansions. The wave indices n and m are:

$$n \equiv \bar{n}\pi/y_{max} \qquad\qquad\qquad m \equiv \bar{m}\,\pi/x_{max} \qquad (52)$$

in which the quantities $\bar{m}$ and $\bar{n}$ are the numbers of half-waves over the arc lengths x_{max} and y_{max}, respectively. The reference surface buckling strains and changes in curvature from Donnell's theory [1] are given by:

$$e_x^b = u^b{,}_x \qquad e_y^b = v^b{,}_y + w^b/R \qquad e_{xy}^b = u^b{,}_y + v^b{,}_x$$
$$\qquad\qquad\qquad\qquad\qquad\qquad\qquad\qquad (53)$$
$$\kappa_x^b = -w^b{,}_{xx} \qquad \kappa_y^b = -w^b{,}_{yy} \qquad \kappa_{xy}^b = -w^b{,}_{xy}$$

where $(\ )_{,x}$ and $(\ )_{,y}$ indicate differentiation.

Insertion of Eqs. (50) into Eqs. (53) and Eqs. (48, 49) leads to an expression for the total potential energy, U-W, of the form:

$$U - W = \begin{bmatrix} A, & B, & C \end{bmatrix} \begin{bmatrix} a_{11} & a_{12} & a_{13} \\ a_{12} & a_{22} & a_{23} \\ a_{13} & a_{23} & a_{33} \end{bmatrix} \begin{Bmatrix} A \\ B \\ C \end{Bmatrix} \tag{54}$$

in which:

$$a_{11} = C_{11}(n_2{}^4 m_1{}^4 + n_1{}^4 m_2{}^4) + C_{33}(n_2{}^4 n_1{}^2 m_1{}^2 + n_1{}^4 n_2{}^2 m_2{}^2)$$
$$+ 2C_{13}(-n_2{}^4 m_1{}^3 n_1 + n_1{}^4 m_2{}^3 n_2)$$

$$a_{12} = -(C_{12} + C_{33})(n_2{}^3 n_1 m_1{}^2 + n_1{}^3 n_2 m_2{}^2) + C_{13}(n_2{}^3 m_1{}^3 - n_1{}^3 m_2{}^3)$$
$$+ C_{23}(n_2{}^3 n_1{}^2 m_1 - n_1{}^3 n_2{}^2 m_2)$$

$$a_{22} = 2C_{22} n_1{}^2 n_2{}^2 + C_{33}(n_2{}^2 m_1{}^2 + n_1{}^2 m_2{}^2) + 2C_{23}(-n_1 n_2{}^2 m_1 + n_1{}^2 n_2 m_2)$$

$$a_{13} = -C_{12}(n_2{}^2 m_1{}^2 + n_1{}^2 m_2{}^2)/R - C_{14}(n_2{}^2 m_1{}^4 + n_1{}^2 m_2{}^4)$$
$$- (C_{15} + 2C_{36}) n_1{}^2 n_2{}^2 (m_1{}^2 + m_2{}^2) + (2C_{16} + C_{34})(n_2{}^2 n_1 m_1{}^3 - n_1{}^2 n_2 m_2{}^3)$$
$$+ C_{23}(n_2{}^2 n_1 m_1 - n_1{}^2 n_2 m_2)/R + C_{35}(n_2{}^2 n_1{}^3 m_1 - n_1{}^2 n_2{}^3 m_2)$$

(55)

$$a_{23} = n_1 n_2 \left[2C_{22}/R + (C_{24} + 2C_{36})(m_1^2 + m_2^2) + C_{25}(n_1^2 + n_2^2) \right]$$

$$+ (2C_{26} + C_{35})(-n_1^2 n_2 m_1 + n_2^2 n_1 m_2) + C_{23}(-n_2 m_1 + n_1 m_2)/R$$

$$+ C_{34}(-n_2 m_1^3 + n_1 m_2^3)$$

(55)

$$a_{33} = 2C_{22}/R^2 + 2C_{24}(m_1^2 + m_2^2)/R + 2C_{25}(n_1^2 + n_2^2)/R$$

$$+ C_{44}(m_1^4 + m_2^4) + C_{55}(n_1^4 + n_2^4) + (2C_{45} + 4C_{66})(n_1^2 m_1^2 + m_2^2 n_2^2)$$

$$+ N_{XPRE}(m_1^2 + m_2^2) + N_{YPRE}(n_1^2 + n_2^2) + 2N_{XYPRE}(n_2 m_2 = n_1 m_1)$$

$$+ 4C_{26}(-n_1 m_1 + n_2 m_2)/R + 4C_{46}(-n_1 m_1^3 + n_2 m_2^3) + 4C_{56}(-n_1^3 m_1 + n_2^3 m_2)$$

In Eqs. (55), the C_{ij} are coefficients of the integrated constitutive law $\underset{\sim}{C}$ relating buckling modal stress and moment resultants to buckling modal reference surface strains and changes in curvature [Eqs. (37,40,46)]. N_{XPRE}, N_{YPRE}, and N_{XYPRE} are in-plane loads that are not multiplied by the load factor (eigenvalue) λ, but represent a fixed prestressed state. The total prebuckling in-plane load components, N_x^o, N_y^o, N_{xy}^o, which appear in Eq. (49) are given by:

$$N_x^o = N_{XPRE} + \lambda N_{xe}$$

$$N_y^o = N_{YPRE} + \lambda N_{ye}$$

(56)

$$N_{xy}^o = N_{XYPRE} + \lambda N_{xye}$$

in which λ is a load factor to be calculated in the buckling analysis and subscript "e" denotes "eigenvalue parameter". One finds the eigenvalue λ by setting the determinant of the a-matrix on the right-hand-side of Eq. (54) equal to zero. The resulting expression for λ is:

$$\lambda = \frac{a_{33} + \dfrac{\left[a_{23}(a_{12}a_{13} - a_{11}a_{23}) + a_{13}(a_{12}a_{23} - a_{13}a_{22})\right]}{\left(a_{11}a_{22} - a_{12}^2\right)}}{-N_{xe}(m_1^2 + m_2^2) - N_{ye}(n_1^2 + n_2^2) - 2N_{xye}(m_2 n_2 - m_1 n_1)} \tag{57}$$

The constraint imposed on the design during the optimization process is that λ should be greater than unity. Equations (46-57) apply to any kind of shell buckling: general, "semi-general", or local. The load factors λ corresponding to the various types of instability are calculated with use of appropriate C_{ij}, x_{max}, and y_{max} pertaining to whatever portion of the structure is being investigated. For general instability both rings and stringers are smeared out; for "semi-general" buckling, either rings or stringers are smeared out; and, for local skin buckling, neither set of stiffeners is smeared out. All buckling load multipliers λ are calculated with the assumption that the boundaries of the portion of the structure under investigation are simply supported. Note that the simple-support condition is violated if either c or d in Eqs. (51) are not equal to zero.

The expression for λ contains unknown quantities m, n, c, and d. When in-plane shear N_{xy}^o is present or when any of the terms A_{i6}, B_{i6}, D_{i6},

356

i ≠ 6 [see Eq. (37)] is non-zero, the minimum value of λ for fixed m and n with respect to the slope, c or d, of the buckling nodal lines is found. In the calculation of this minimum it is always assumed that either c or d is zero. Figure 14 shows the model. For each kind of buckling: general, semi-general, or local, a test is made to see in which coordinate direction the panel is "long". The test is based on the quantity:

$$\bar{L} = \left(x_{max} / y_{max} \right) \left(C_{55} / C_{44} \right)^{1/2} \tag{58}$$

If the panel is shallow ($R/y_{max} > 1.0$) and if $\bar{L} \geq 1.0$, the panel is effectively "long" in the x-direction and the model shown in Fig.14 (a) is used. If the panel is not shallow ($R/y_{max} < 1.0$) or if $\bar{L} < 1$, the opposite is true and the model shown in Fig.14 (b) is used. In this way, the boundary conditions are satisfied along the edges that span the least number of buckling modal half-waves while the correct solution is obtained for buckling of a long cylinder under pure torsion. The boundaries along which the simple support conditions are violated span the largest number of half-waves and hence the conditions there least affect the critical load. The utility of the approximate expressions (50) is thereby maximized. Such a strategy is advantageous because the buckling loads must be calculated very often in the optimization analysis. Since the optimum design is being obtained interactively, it is necessary to avoid discouraging or boring the program user by making him wait a long time at the terminal while elaborate buckling calculations proceed for each new trial design.

To increase the efficiency of the subroutine that calculates buckling loads, the terms in Eqs. (55) are arranged so that those which are often zero (e.g., the terms underlined in Eqs. (55)) are not calculated if it is known in advance that they are zero.

The eigenvalue is modified by a factor "DONNEL" = $(n_c^2 - 1)/n_c^2$ under certain conditions for which the Donnell theory [Eqs. (49, 53)] yields inaccurate results, such as buckling of a complete cylindrical shell under uniform external pressure for which n_{cr} is less than 4 or 5 half-waves over $180°$ of the circumference. The factor "DONNEL" is not applied if $n_c = 1$ or if the axial half-wavelength of the buckling pattern is less than the radius R of the cylinder.

Strategy for finding the minimum buckling load with respect to $\bar{m}$, $\bar{n}$, c, or d: For each wave index combination, $\bar{m}$ and $\bar{n}$, the minimum λ with change in the buckling nodal line slope c or d is found (only in cases for which shear loading is present or any A_{16}, B_{16}, or $D_{16} \neq 0$; $i \neq 6$) by variation of c or d in equal increments or decrements of 0.01 if its absolute value is less than 0.1 and by a factor of 1.2 if its absolute value is greater than 0.1. The buckling nodal line slopes are shown in Fig. 14.

The minimum λ with respect to the wave indices $\bar{m}$ and $\bar{n}$ is found with due attention to the fact that for a given geometry and loading this minimum may be non-unique, as pointed out by Burns [14] and by Pappas and Allentuch [47]. Four regions in $(\bar{m}, \bar{n})$ space are searched for minima in the function $\lambda(\bar{m}, \bar{n})$: low $\bar{m}$, low $\bar{n}$; low $\bar{m}$, high $\bar{n}$; high $\bar{m}$, low $\bar{n}$; and high $\bar{m}$, high $\bar{n}$. Figure 15 shows the results of such a search for an axially compressed composite unstiffened cylindrical shell, the dimensions and properties of which are from Booton and Tennyson's

358

paper [57].

For low $\bar{m}$ ($\bar{m} = 1$), the search begins at:

$$\bar{n}_{start_1} = (y_{max}/x_{max})(C_{44}/C_{55})^{\frac{1}{4}} \quad \text{or} \quad \bar{n}_{start_1} = 1 \quad (59)$$

whichever is larger. With $\bar{m} = 1$, a minimum $\lambda(1, \bar{n})$ is sought. The region in $(\bar{n}, \bar{m})$ space surrounding this minimum is then explored by variation of both $\bar{m}$ and $\bar{n}$. When a local minimum $\lambda_1(\bar{m}_{L1}, \bar{n}_{L1})$ has been found, $\bar{m}$ is reset to unity and a new minimum $\lambda_1(1, \bar{n})$ is sought in whichever region was not covered by the initial search that began at $\bar{n}_{start}$ given by Eq. (59). If the minimum $\bar{n}$ covered in the search for $\lambda_1(\bar{m}_{L1}, \bar{n}_{L1})$ is greater than or equal to 3, the low-$\bar{n}$ range is next covered, starting at $\bar{n} = 1$. If the low-$\bar{n}$ range was covered in the search for $\lambda_1(\bar{m}_{L1}, \bar{n}_{L1})$, the high-$\bar{n}$ range is next covered, starting at:

$$\bar{n}_{start_2} = y_{max}/(0.2R) \quad (60)$$

As before, a minimum $\lambda_2(1, \bar{n})$ is sought, after which the region in $(\bar{m}, \bar{n})$ space about this minimum is explored as before in order to find $\lambda_2(\bar{m}_{L2}, \bar{n}_{L2})$, in which subscript L again denotes "local minimum".

For high $\bar{m}$, low $\bar{n}$, the search for $\lambda_3(\bar{m}_{L3}, \bar{n}_{L3})$ begins at $\bar{n} = 1$ and $\bar{m}$ equal to the larger of the following:

$$\bar{m}_{start} = x_{max}/\left[\pi(R^2 C_{44}/C_{22})^{\frac{1}{4}}\right] \quad (61)$$

or:

$$\bar{m} = (x_{max}/y_{max})(C_{55}/C_{44})^{\frac{1}{4}} \quad (62)$$

Equation (61) yields approximately the number of axial waves in a cylinder of length x_{max} which buckles axisymmetrically and Eq. (62) yields approximately the number of axial waves in an axially compressed flat plate of aspect ratio x_{max}/y_{max}. During the search process $\bar{n}$ is increased monotonically. For each $\bar{n}$ a minimum $\lambda_3(\bar{m}, \bar{n})$ is found, eventually leading to $\lambda_3(\bar{m}_{L3}, \bar{n}_{L3})$. The final region, high $\bar{m}$, high $\bar{n}$, is searched for a local minimum $\lambda_4(\bar{m}_{L4}, \bar{n}_{L4})$ starting with:

$$\bar{m}_{start_2} = \bar{m}_{L3} \qquad\qquad \bar{n}_{start_3} = y_{max}/(0.4R) \qquad (63)$$

In Figure 15, the four regions searched are outlined in dashed boxes. It turns out that in this case each of the four regions contains a local minimum load multiplier λ. PANDA selects the lowest of these minima, as the critical load multiplier. In this case, $\lambda_{cr} = \lambda_2(\bar{m}_{L2}, \bar{n}_{L2}) = \lambda_2(1, 9) = 7.33$. The dotted curve in Fig. 15 represents constant values of the quantity:

$$\left[(\bar{m}\pi R/x_{max})^2 + \bar{n}^2 \right]^2 / (\bar{m}\pi R/x_{max})^2 \qquad (64)$$

which appears in Eqs. (5.50) and (5.51) of Brush and Almroth $\left|56\right|$. In the context of Donnell's theory, minimization of the axial buckling load of an isotropic monocoque cylindrical shell with respect to this quantity yields the formula:

$$\frac{P_{cr}}{2\pi R} = \frac{Et^2/R}{\left[3(1 - v^2)\right]^{\frac{1}{2}}} \qquad (65)$$

in which P_{cr} is the total critical axial load on the cylinder.

If the quantity (64) is set equal to its value corresponding to the minimum $\lambda(\bar{m},\bar{n})$ along the $\bar{m}$-axis in Fig. 15 ($\bar{m} = 9$, $\bar{n} = 0$, value of Quantity (64) = 400) then the dashed curve in Fig. 15 is obtained for the various $(\bar{m}, \bar{n})$ combinations that yield this same value, 400. It is seen that the dashed curve passes close to all of the minima found by PANDA in $(\bar{n}, \bar{m})$ space.

In the optimization analysis it is necessary not only to find the various buckling loads (local, semi-general, general) at a given design point, but to determine how these loads vary with a small change in each decision variable from this design point. In PANDA the small change is equal to 5.0 percent of the current value of the decision variable. Much computer time is saved by use of whatever values of $\bar{m}$, $\bar{n}$, c, and d exist _at_ the design point for calculation of the eigenvalue λ at these neighboring points also. This strategy is indicated in Fig. 7.

Local Buckling (Crippling) of Stiffener Segments

There are two types of stiffeners, those along cylinder generators called stringers and those along circumferences called rings (Fig. 1). Each type of stiffener is assumed to consist of an assemblage of rectangular pieces of width b_i and thickness t_i. The rectangular pieces of each stiffener type are divided into two classes: those that are "internal" or "interior" and those that are "ends". Figure 4 shows examples. "Internal" stiffener segments are those which have both edges connected to other stiffener segments or the panel skin. "Ends" are stiffener segments only one edge of which is connected to another structural part. All stiffener segments are assumed to be flat and long compared to their widths. Thus, for stringers $a_o \gg b_i^s$ and for ring segments $b_o \gg b_i^r$. The curvatures of the ring segments are neglected.

Effective stiffener segment material properties: The theory for crippling of stiffener segments is based on the assumption that these segments are monocoque

361

and orthotropic, not layered anisotropic. Thus, the terms in Eq. (37), A_{16} and D_{16}; $i \neq 6$, are assumed to be zero and all of the B_{ij} are assumed to be zero when applied to the crippling or rolling analyses of stiffener segments. The PANDA program allows the user to provide input as if the stiffener segments were layered anisotropic. From initial values of A_{11}^i, A_{12}^i, A_{22}^i, and A_{66}^i computed from the anisotropic theory for the ith stiffener segment laminate corresponding to the user's starting design, effective moduli and Poisson's ratio are derived from:

$$E_{11}^{i(eff)} = A_{11}^i/t^i; \qquad\qquad E_{22}^{i(eff)} = A_{22}^i/t^i$$

$$\nu_{12}^{i(eff)} = A_{12}^i/A_{22}^i \; ; \qquad\qquad G^{i(eff)} = A_{66}^i/t^i \tag{66}$$

in which:

$$t^i = \sum_{k=1}^{N} t_k^i \tag{67}$$

During the optimization phase the total thickness t^i of the ith stiffener segment laminate may be a decision variable; the thicknesses of each lamina are not decision variables. If the stiffener material is isotropic and if $t^i = t_k^1$ (N = 1 layer), the effect of nonlinear material behavior is included in the analysis. The A_{jk}^i in Eq. (66) are the instantaneous coefficients referred to in the discussion associated with Eqs. (42-45).

Local Buckling of "Internal" Segments: For "internal" segments the critical load factors λ_i can be calculated from Eqs. (55)-(57) with c = d = $N_{xy}^o = N_y^o = 0$, R→∞, and the "anisotropic" $C_{ij}^i = 0$. The axial prebuckling

362

resultant in Eq. (56a) $\left[N_x^o\right]$ is interpreted to mean the prebuckling stress resultant along the axis of the stiffener and the wave index m_i is given by $m_i = \bar{m}_i \pi / \ell$ in which $\bar{m}_i$ is the number of half-waves along ℓ, where ℓ is a_o for a stringer segment and b_o for a ring segment. With these simplifications and definitions the terms a_{13} and a_{23} in Eqs. (55) vanish and Eq. (57) becomes:

$$\lambda_i = \frac{\left[C_{44}^i m_i^2 + C_{55}^i (n_i^4/m_i^2) + (2C_{45}^i + 4C_{66}^i)n_i^2 + N_{XPRE}^i\right]}{-N_{xe}^i} \quad (68)$$

If it is assumed that the internal stiffener segment buckles with one-half wave $(\bar{n}_i = 1)$ across its width b_i, as shown in Fig. 5, then it can be shown that:

$$m_i = n_i (C_{55}^i/C_{44}^i)^{\frac{1}{2}} = (\pi/b_i)(C_{55}^i/C_{44}^i)^{\frac{1}{4}} \quad (69)$$

The quantities C_{44}^i, C_{55}^i, C_{45}^i and C_{66}^i in Eqs. (68, 69) are given by:

$$C_{44}^i = E_{11}^{i(eff)} t^{i^3}/12 \; ; \qquad\qquad C_{55}^i = E_{22}^{i(eff)} t^{i^3}/12 \; ;$$

$$(70)$$

$$C_{45}^i = \nu_{12}^{i(eff)} E_{11}^{i(eff)} t^{i^3}/12 \; ; \qquad C_{66}^i = G^{i(eff)} t^{i^3}/12$$

Use of Eq. (69) with $n_i = \pi/b_i$ in Eq. (68) yields:

$$\lambda_i = \frac{\left\{ 2(\pi/b_i)^2 \left[(C_{44}^i C_{55}^i)^{\frac{1}{2}} + C_{45}^i + 2C_{66}^i \right] + N_{XPRE}^i \right\}}{-N_{xe}^i} \quad (71)$$

in which:

$$N^i_{\overline{XPRE}} \equiv N^i_{\overline{xpre}} \tag{72}$$

$$N^i_{\overline{xe}} = N^{io}_{\overline{x}} - N^i_{\overline{xpre}} \tag{73}$$

where $N^{io}_{\overline{x}}$, given by Eq. (20), is the total prebuckling axial resultant (lb/in) carried by the ith stiffener segment and $N^i_{\overline{xpre}}$ is that portion of the prebuckling axial resultant carried by the ith stiffener segment that is not to be multiplied by the load factor λ_i.

Local Buckling of "end" segments: It is assumed here that the stiffener "end" segment cross-section does not deform in the buckling mode (Fig. 5, Segment 3). The assumed displacement function is:

$$w^i = C\overline{\overline{y}}_i \sin\left[\overline{m}^j \pi \overline{x}/\ell\right] = C\overline{\overline{y}}_i \sin\left[m^j \overline{x}\right]$$

$$u^i = 0 \tag{74}$$

$$v^i = 0$$

Use of Eqs. (74) in Eqs. (48, 49, 53) leads to the following expressions for strain energy of and work done on the ith segment:

$$U^i = C^2 \frac{\ell}{4} \left[C^i_{44} (m^j)^4 b_i^3/3 + 4C^i_{66} (m^j)^2 b_i \right] \tag{75}$$

$$W^i = C^2 \frac{\ell}{4} \left[N^{oi}_{\overline{x}} (m^j)^2 b_i^3/3 \right] \tag{76}$$

364

In Eq. (74), $\bar{\bar{y}}_i$ is the distance along the width of the "end", as shown in Fig. 4, and $\bar{m}^j$ is the number of half-waves in the local critical buckling pattern of the structural segment to which the end segment is attached (Segment j). For example, with reference to Fig. 5, for stiffener Segment 3 (i = 3, j = 2), m^j is given by:

$$m^{(j)} = m^{(2)} = (\pi/b_2)\left[C_{55}^{(2)}/C_{44}^{(2)}\right]^{\frac{1}{4}} \tag{77}$$

For blade stiffeners, such as shown in Fig. (4c):

$$m^j = \bar{m}_{skin}\pi/\ell \tag{78}$$

With the total pre-stress resultant $N_{\bar{x}}^{oi}$ in the end segment defined by Eq. (73), minimization of the total potential energy, $U^i - W^i$, with respect to the undetermined coefficient C in Eqs. (75,76) yields the following equation for the buckling load factor λ_i:

$$\lambda_i = \frac{C_{44}^i(m^j)^2 b_i^3 + 12C_{66}^i b_i + N_{\bar{x}pre}^i b_i^3}{-N_{\bar{x}e}^i b_i^3} \tag{79}$$

If more than one "end" segment is attached to the same "internal" segment or to the skin, the buckling criterion is:

$$-\sum_{k=1}^{K_e} (N_{\bar{x}pre}^k + \lambda N_{\bar{x}e}^k) b_k^3 = \sum_{k=1}^{K_e} \left[(m^j)^2 C_{44k}^k b_k^3 + 12C_{66k}^k b_k\right] \tag{80}$$

in which K_e is the number of "end" segments attached to the jth "internal"

segment or to the panel skin.

Rolling Modes

Three types of rolling modes of instability have been described in the summary and are illustrated in Fig. 6. PANDA accounts for these three types of rolling, one (Fig. 6a) in which the panel skin participates and two (Fig. 6b, c) in which it does not.

Rolling with Participation of the Panel Skin

For panels stiffened by both rings and stringers, there are three eigenvalues (buckling load factors λ) corresponding to the type of rolling in which the panel skin participates. These modes are characterized by (1) local rolling between rings and stringers, with both sets of stiffeners twisting about nodal lines of the buckling pattern; (2) rolling in which the stringers are smeared out and the rings twist about nodal lines of the buckling pattern; and (3) rolling in which the rings are smeared out and the stringers twist about nodal lines in the buckling pattern.

Figures 16 and 17 show in more detail the geometry of the type of rolling deformation depicted in Figure 6a. This deformation is assumed to be either local, that is, the distances x_{max} and y_{max} considered in the rolling instability mode are the spacings a_o and b_o between the rings and stringers, respectively, or "semi-general," that is, the distances x_{max} and y_{max} apply to subdomains of the structure with either rings or stringers smeared and the opposite set of stiffeners twisting along simply-supported boundaries. The widths of the stiffener

segments are assumed to be small compared to the half-wavelength, $\ell/\bar{m}$, of the rolling buckling modes. For local rolling the quantity ℓ is the distance a_0 between rings in the rolling analysis of stringers and ℓ is the distance b_0 between stringers in the rolling analysis of rings. All stiffener segments are assumed to be perpendicular or parallel to the plane of the skin. The effect of curvature of the ring segments on cylindrical panels is neglected.

The assumed deflection field given in Fig. 17 leads to zero in-plane shear of each stiffener segment. **Although Fig. 16 may seem to imply** that the following analysis applies only to stringers, this is not so. It is emphasized that the analysis of this section applies to rings as well. Figure 17 shows the $\bar{x}$, $\bar{y}$, $\bar{z}$ coordinate system and associated displacement components, u^*, v^*, w^*, and rotation components, $\omega_{\bar{y}}$ and $\omega_{\bar{z}}$.

The rolling deformations depicted in Figs. 16 and 17 cause inextensional bending and twisting of the stiffener web and extensional deformation of the flange. The strain energy of the extensional (membrane) deformation of the flange is large compared to its inextensional (bending and twisting) strain energy. Therefore, in the discussion that follows, the inextensional strain energy of the flange is neglected.

Membrane Energy: That portion of the strain energy of the stiffener associated with membrane-type deformations of the ith stiffener segment deforming in the rolling mode is:

$$U_m^i = \frac{1}{2} \int_{\bar{\bar{y}}_i=0}^{b_i} \int_{\bar{x}=0}^{\ell} u^{*2}_{,\bar{x}} \, C_{11}^i \, d\bar{x} d\bar{\bar{y}}_i \qquad (i \neq \text{web}) \qquad (81)$$

367

in which $\bar{\bar{y}}_i$ is the local coordinate shown in Fig. 4, $u,^*_{\bar{x}}$ is the axial strain in this segment, C^i_{11} is the instantaneous stiffness coefficient [same as A^i_{11} in Eq. (66)], b_i is the width of the segment and ℓ is the length of whatever portion of the panel is being investigated, as follows:

Type of Rolling Instability	ℓ	Eq. (81) applies to:
local stringer	a_o	stringer energy
local ring	b_o	ring energy
smeared stringers	b	ring energy
smeared rings	a	stringer energy

The total membrane energy of the stiffener is:

$$U_m = \sum_{\substack{i=1 \\ i \neq web}}^{N} U^i_m \qquad \begin{array}{l} i \neq \text{web or other segments attached} \\ \text{along the line } \bar{y} = \bar{z} = 0. \text{ (Fig. 17)} \end{array}$$

(82)

in which N is the number of segments in the stiffener cross-section.

The corresponding "membrane" work done by the prebuckling stress resultant $N^{oi}_{\bar{x}}$ in the ith segment during rolling deformations is:

$$W^i_m = \frac{1}{2} \int_{\bar{\bar{y}}_i=0}^{b_i} \int_{\bar{x}=0}^{\ell} N^{oi}_{\bar{x}} (\omega_{\bar{z}}^2 + \omega_{\bar{y}}^2) d\bar{x} d\bar{\bar{y}}_i$$

(83)

($i \neq$ web or other segments attached along $\bar{y} = \bar{z} = 0$)

The quantities $\omega_{\bar{z}}$ and $\omega_{\bar{y}}$ are the rotations about the $\bar{z}$ axis and $\bar{y}$ axis,

respectively, and are given by:

$$\omega_{\bar{z}} = \frac{1}{2}\left(\frac{\partial v^*}{\partial \bar{x}} - \frac{\partial u^*}{\partial \bar{y}}\right) \quad ; \quad \omega_{\bar{y}} = \frac{1}{2}\left(\frac{\partial u^*}{\partial \bar{z}} - \frac{\partial w^*}{\partial \bar{x}}\right) \tag{84}$$

Bending and Twisting Energy: In addition to the membrane-energy-related modes just described, the stiffener rolling deformations involve bending and twisting energy, that is, strain energy related to strains which vary through the thickness of each segment, and work done by the prebuckling stress resultant related to out-of-plane rotations of each stiffener segment. Only the bending and twisting energy of the stiffener web and other segments attached along the line $\bar{y} = \bar{z} = 0$ are included, since these components of energy are negligible compared to U_m^i [Eq. (81)] for the remainder of the stiffener cross section. The bending and twisting strain energy of the web shown in Figs. 16 and 17 is given by:

$$U_b^i = \frac{1}{2} \int_{\bar{\bar{y}}_i=0}^{b_i} \int_{\bar{x}=0}^{\ell} \left[\kappa_{\bar{x}}, \kappa_{\bar{z}}, 2\kappa_{\bar{xz}}\right]\left[D^i\right]\left\{\begin{array}{c} \kappa_{\bar{x}} \\ \kappa_{\bar{z}} \\ 2\kappa_{\bar{xz}} \end{array}\right\} d\bar{x}d\bar{\bar{y}}_i \tag{85}$$

(i = web or other segment attached along the line $\bar{y} = \bar{z} = 0$.)

The coefficients of the 3 x 3 flexural rigidity matrix D^i are called c_{44}^i, c_{45}^i, c_{55}^i, c_{66}^i in Eq. (68); they are given by Eqs. (70). Thus:

$$[D^i] \equiv \begin{bmatrix} D^i_{11} & D^i_{12} & 0 \\ D^i_{12} & D^i_{22} & 0 \\ 0 & 0 & D^i_{66} \end{bmatrix} \equiv \begin{bmatrix} C^i_{44} & C^i_{45} & 0 \\ C^i_{45} & C^i_{55} & 0 \\ 0 & 0 & C^i_{66} \end{bmatrix} \qquad (86)$$

These are the instantaneous flexural and twist rigidities of the ith stiffener segment, analogous to those for the panel skin referred to in the discussion associated with Eqs. (42-46). The expressions for changes in curvature and twist of the web are analogous to those for the panel skin:

$$\kappa_{\overline{x}} = -v,^*_{\overline{xx}} \quad ; \qquad \kappa_{\overline{z}} = -v,^*_{\overline{zz}} \quad ; \qquad \kappa_{\overline{xz}} = -v,^*_{\overline{xz}} \qquad (87)$$

where v^* is the displacement in the $\overline{y}$ direction, indicated in Figs. 16 and 17. The work done by the prebuckling stress resultant during buckling of the web is:

$$W^i_b = \frac{1}{2} \int_{\overline{y}_i=0}^{b_i} \int_{x=0}^{\ell} N^{oi}_{\overline{x}} \, v,^{*2}_{\overline{x}} \, d\overline{x} d\overline{y}_i \qquad (88)$$

(i = web or other segments attached along the line $\overline{y} = \overline{z} = 0$)

In PANDA rolling modes are assumed to occur only if the stiffener has a web which is perpendicular to the panel skin. The expressions (81) and (83) apply only to the portion of the stiffener attached to the end of this web. The cross-sections of these flange segments remain undeformed

and initially plane sections of them remain plane during buckling deformations. However, note from Figs. 16 and 17 that this plane rotates about the normal to the shell wall at the web attachment line. Therefore the entire cross-section of the stiffener (web and flange taken together) clearly warps. The expressions (85) and (88) apply only to the web. The bending and twisting energy of the rest of the stiffener cross-section is neglected compared to the membrane energy of the flange represented by Eq. (81). This approximation seems valid as long as the segments are slender (width >> thickness).

<u>Introduction of Displacement Functions</u>: The various components of energy associated with the rolling mode shown in Figs. 6, 16 and 17 are derived from Eqs. (81) to (88) with the assumed displacement field given in Fig. 17 and repeated here:

$$u^* = -m \gamma \bar{y} \bar{z} \cos m \bar{x}$$

$$v^* = +\gamma \bar{z} \sin m \bar{x} \qquad\qquad m = \bar{m} \pi/\ell \qquad (89)$$

$$w^* = -\gamma \bar{y} \sin m \bar{x}$$

If the height (width) of the web is called b_w and one inserts the right-hand side of Eq. (89a) with (with $\bar{z} = b_w$) into Eq. (81), one obtains for the membrane-type energy of each segment of the stiffener attached to the end of the web:

$$U_m^i = \frac{\ell}{4} (\gamma b_w)^2 m^4 \int_{\bar{\bar{y}}_i=0}^{b_i} C_{11}^i \, \bar{\bar{y}}^2 \, d\bar{\bar{y}}_i \qquad (i \neq \text{web}) \qquad (90)$$

U_m^i can be evaluated once $\bar{y}$ as a function of $\bar{\bar{y}}$ is known. For example, in the case of the T-shaped stiffener shown in Fig. (4a), $\bar{y} = \bar{\bar{y}}_2$ in Segment 2 and $\bar{y} = -\bar{\bar{y}}_3$ in Segment 3. Therefore:

$$U_m^i = \frac{\ell}{4} (\gamma b_w)^2 m^4 C_{11}^i b_i^3 / 3 \qquad (i = 2, 3) \qquad (91)$$

If $C_{11}^{(2)} = C_{11}^{(3)}$, the total membrane energy $U_m = 2U_m^{(2)}$. This energy is simply the "EI" bending energy of a beam of depth equal to the width of the flange ($b_2 + b_3$ in Fig. 4a) deforming in its plane in a mode $(\gamma b_w) \sin m\bar{x}$. The bending and twisting energy of the web can be found, with use of Eqs. (85) and (87), to be:

$$U_b^i = \frac{\ell}{4} \left[C_{44}^w m^4 \gamma^2 \frac{b_w^3}{3} + 4C_{66}^w m^2 \gamma^2 b_w \right] \qquad (92)$$
$$(w = \text{"web"})$$
$$(i = \text{"web"})$$

The corresponding "work done" terms, W_m^i and W_b^i, are obtained from Eqs. (83), (84), and (88):

$$W_m^i = \frac{m^2 \ell}{4} (\gamma b_w)^2 \int_{\bar{\bar{y}}=0}^{b_i} N_{\bar{x}}^{oi} \, d\bar{\bar{y}}_i \qquad (i \neq \text{web}) \qquad (93)$$

$$W_b^i = \frac{m^2 \ell}{4} (\gamma b_w)^2 N_{\bar{x}}^{oi} b_w / 3 \qquad (i = \text{web}) \qquad (94)$$

372

Relation to Panel Skin Deformation: With no shear loading and the A_{i6}, B_{i6}, $D_{i6} = 0$ for $i \neq 6$ in Eq. (37), the rotation γ, shown in Fig. 16, is related to the amplitude C of the sinusoidal deformation of the panel skin, $w_{skin} = 2C \sin ny \sin mx$, [Eq. (50c) and Eq. (51) with $c = d = 0$] as follows:

$$\begin{array}{lll} \text{For stringers:} & \gamma = -2Cn \\ \text{For rings:} & \gamma = +2Cm \end{array} \qquad (95)$$

in which n and m are given by Eqs. (52). Through Eqs. (95), the components of rolling mode energy and work done by the prebuckling compression during buckling can be expressed in terms of the undetermined skin buckling amplitude C. The total potential energy U - W has the same form as that given in Eq. (54). The only difference is that the array element a_{33}, given for the panel skin in Eq. (55f), has additional terms associated with stiffener deformations:

$$a_{33} = \left[a_{33}\right]_{skin} + \frac{2m^2n^2}{y_{max}}\left[m^2 b_w^2 \sum_{\substack{i=1 \\ i \neq web}}^{N^s}\left(\int_{\bar{\bar{y}}=0}^{b_i} c_{11}^i\left[\bar{y}(\bar{\bar{y}}_i)\right]^2 d\bar{\bar{y}}_i\right)\right.$$

$$+ \; C_{44}^w m^2 b_w^3/3 \;+\; 4C_{66}^w b_w \;+\; b_w^2 \sum_{\substack{i=1 \\ i \neq web}}^{N^s}\left(\int_{\bar{\bar{y}}=0}^{b_i} N_{\bar{x}pre}^{oi}\, d\bar{\bar{y}}_i\right)$$

$$\left. + \; N_{\bar{x}pre}^{ow}\, b_w^3/3 \right]_{stringer}$$

$$+ \frac{2m^2n^2}{x_{max}}\left[n^2 b_w^2 \sum_{\substack{i=1 \\ i \neq web}}^{N^r}\left(\int_{\bar{\bar{y}}=0}^{b_i} c_{11}^i\left[\bar{y}(\bar{\bar{y}}_i)\right]^2 d\bar{\bar{y}}_i\right)\right. \tag{96}$$

$$+ \; C_{44}^w n^2 b_w^3/3 \;+\; 4C_{66}^w b_w$$

$$\left. + \; b_w^2 \sum_{\substack{i=1 \\ i \neq web}}^{N^r}\left(\int_{\bar{\bar{y}}=0}^{b_i} N_{\bar{x}pre}^{oi}\, d\bar{\bar{y}}_i\right) \;+\; N_{\bar{x}pre}^{ow}\, b_w^3/3 \right]_{ring}$$

in which $\bar{y}(\bar{\bar{y}}_i)$ indicates that $\bar{y}$ is a function of $\bar{\bar{y}}_i$. In Eq. (96), x_{max} and y_{max} have the meanings analogous to those in the discussion following Eq. (49):

Type of Rolling Instability	x_{max}	y_{max}
local	a_o	b_o
smeared stringers	a_o	b
smeared rings	a	b_o

The result in Eq. (96) is obtained after division of both skin and stringer terms, derived from energy expressions, by the quantity $x_{max}y_{max}/4$.

The denominator on the right-hand-side of Eq. (57) must also be modified by addition of the terms:

$$-\frac{2m^2n^2}{y_{max}}\left[b_w^2\sum_{\substack{i=1\\i\neq web}}^{N^s}\left(\int_{\bar{\bar{y}}=0}^{b_i} N_{\underline{xe}}^{oi}\,d\bar{\bar{y}}_i\right) + N_{\underline{xe}}^{ow}b_w^3/3\right]_{stringer}$$

$$\hspace{8cm}(97)$$

$$-\frac{2m^2n^2}{x_{max}}\left[b_w^2\sum_{\substack{i=1\\i\neq web}}^{N^r}\left(\int_{\bar{\bar{y}}=0}^{b_i} N_{\underline{xe}}^{oi}\,d\bar{\bar{y}}_i\right) + N_{\underline{xe}}^{ow}b_w^3/3\right]_{ring}$$

in which $N_{\underline{xe}}^{oi}$ and $N_{\underline{xe}}^{ow}$ are given by Eq. (73). Expressions (95-97) apply only if $c = d = 0$. However, the eigenvalues including stiffener rolling are expected to be reasonably accurate for most practical cases involving combined in-plane loads which include shear.

Rolling of Stiffeners without Participation of Panel Skin

Figure 18 shows the coordinate system and positive displacement components v, u^w, w^w, u^f, w^f in the web and flange. The following

analysis is limited to stiffeners with T-shaped or L-shaped cross-sections. A special case of such a stiffener is a blade, which is a T or L-shaped cross-section with a vanishingly small flange. The analysis is based on treatment of the web as a flexible annulus (a type of shell) and the flange as a very short cylindrical shell. Although Fig. 18 depicts the geometry for a ring, the analysis applies to stringers as well. In that case the radius of the short cylindrical shell that represents the flange is set equal to a very large number in PANDA.

Assumptions: The following assumptions are made with regard to the prebuckling and buckling modal strains and displacements:

1) The prebuckling strains are assumed to be uniform over the web and uniform over the flange (although different prebuckling strain states exist in the web and flange).

2) The buckling modal state is characterized by,

For the web:

$$w_b^w(x, y) = \left[Cx^2 + Dx^2(1 - x/b_w) \right] \sin(\bar{n}\pi y/\ell) \tag{98}$$

$$e_x^b = 0 \tag{99}$$

$$e_{xy}^b = 0 \tag{100}$$

For the Flange:

$$w_b^f(s, y) = u_b^w(x = b_w, y) + s\beta \sin(\bar{n}\pi y/\ell) \tag{101}$$

$$u_b^f(s, y) = \mp \cdot w_b^w(x = b_w, y) = u_b^f(y) \tag{102}$$

376

$$e_s^b = 0; \qquad e_{sy}^b = 0 \tag{103}$$

in which C and D are coefficients to be determined by minimization of the total energy in the rolling stiffener. Quantities such as x, y, s and β and the various web and flange displacement components are indicated in Fig. 18 for both external and internal stiffeners. In terms preceeded with $\pm$ or $\mp$, the top sign corresponds to external stiffening and the bottom to internal stiffening. The quantity $u_b^W(x = b_w, y)$ signifies the value of u^W evaluated at $x = b_w$ (see Fig. 18b, for example).

Strain energy: The total strain energy of the stiffener is:

$$U = \frac{1}{2} \int_{y=0}^{\ell} \left(\sum_{i=1}^{N} \int_{\bar{y}_i=0}^{b_i} (e_{pre} + e^b)^T [C^i] (e_{pre} + e^b) \, d\bar{\bar{y}}_i \right) dy \tag{104}$$

in which N is the number of stiffener segments, $\bar{\bar{y}}_i$ is the local stiffener segment coordinate shown in Fig. 4 ($\bar{\bar{y}}_i = x$ in the web; $\bar{\bar{y}}_i = s$ in the flange), and:

$$(e_{pre})^T = \lfloor 0, \ e_y^o, \ 0, \ 0, \ 0, \ 0 \rfloor \tag{105}$$

$$(e^b)^T = \lfloor 0, \ e_y^b, \ 0, \ \kappa_{\bar{y}}^b, \ \kappa_y^b, \ 2\kappa_{\bar{y}y}^b \rfloor \tag{106}$$

Using Eqs. (104-106), one can write the strain energy of the ith segment of the stiffener in the simpler form:

$$U^i = \frac{1}{2} \int\limits_{y=0}^{\ell} \int\limits_{\bar{\bar{y}}_i=0}^{b_i} \left[C_{22}^i (e_y^o + e_y^b)^2 + C_{44}^i (\kappa_{\bar{y}}^b)^2 + 2C_{45}^i \kappa_{\bar{y}}^b \kappa_y^b \right.$$

(107)

$$\left. + C_{55}^i (\kappa_y^b)^2 + C_{66}^i (2\kappa_{\bar{y}\bar{y}}^b)^2 \right] d\bar{\bar{y}} dy$$

Note that because the web and flange are here being treated as shell components, C_{22}^i and C_{55}^i are identified with the long dimension, ℓ, of the stiffener while C_{44}^i is identified with the width, b_i. This is the opposite nomenclature from that used in the previous section.

<u>Strain-Displacement Relations for Buckling Analysis</u>: The strain displacement relations to be used here are of the Novoshilov-Sanders type. They are the same as those used in BOSOR4 [58] and BOSOR5 [59].

For the web:

$$e_x = u' + (w'^2 + \gamma^2)/2 = 0$$

$$e_y = \dot{v} \pm u/r + (\psi^2 + \gamma^2)/2$$

$$e_{xy} = \dot{u} + r(v/r)' + w'\dot{w} = 0$$

(108)

$$\kappa_x = w''$$

$$\kappa_y = \ddot{w} \pm w'/r$$

$$2\kappa_{xy} = 2(-w'\dot{} \pm \dot{w}/r)$$

378

$$\psi = \overset{\bullet}{w}$$

$$\gamma = (\overset{\bullet}{u} - v' \mp v/r)$$

in which $(\ )' \equiv d(\ )/dx$ and $(\overset{\bullet}{\ }) \equiv d(\ )/dy$.

For the flange:

$$e_s = 0$$

$$e_y = \overset{\bullet}{v} + w/R_f + (\psi^2 + \gamma^2)/2$$

$$e_{sy} = \overset{\bullet}{u} + r(v/r)' + w'(\overset{\bullet}{w} - v/R_f) = 0$$

$$\kappa_s = w''$$

(109)

$$\kappa_y = \overset{\bullet\bullet}{w} - \overset{\bullet}{v}/R_f$$

$$2\kappa_{sy} = 2(-w'^{\bullet} + v'/R_f)$$

$$\psi = \overset{\bullet}{w}$$

$$\gamma = (\overset{\bullet}{u} - v')/2$$

in which $(\ )' \equiv d(\ )/ds$ and $(\overset{\bullet}{\ }) \equiv d(\ )/dy$ and in which superscript b has been dropped for convenience.

Analysis of the Web: The assumptions that $e_x = e_{xy} = 0$ $\Big[$Eqs. (99, 100)$\Big]$ along with Eqs. (108a) and (108c) can be used to determine u^w and v^w, given w^w $\Big[$Eq. (98)$\Big]$. After some algebraic manipulations one obtains:

$$u^w = \left[-2(C+D)^2 x^3/3 \; + \; 3(C+D)Dx^4/(2b_w) \right.$$

$$\left. - \; 9(D/b_w)^2 x^5/10 \right] \sin^2(\bar{n}\pi y/\ell) \tag{110}$$

$$v^w = -(\bar{n}\pi/\ell) \left[(C+D)^2 x^4/6 \; - \; 2(C+D)Dx^5/(5b_w) \right.$$

$$\left. + \; (D/b_w)^2 x^6/5 \right] \sin(\bar{n}\pi y/\ell)\cos(\bar{n}\pi y/\ell) \tag{111}$$

With use of Eqs. (107), (108), (110) and (111), one obtains for the strain energy of the web (including the effect of the prebuckling stress resultant in the y-direction, N^{ow}):

$$U^{web} = \frac{\ell}{4} \left\{ C^2 \left[p_1 + p_2 + 4C_{44}^w b_w + q_1 + q_2 + 4q_3 - s_1 + s_2 \right] \right.$$

$$+ \; CD \left[p_1/5 \; + \; p_2/3 \; - \; 4C_{44}^w b_w + q_1/3 - q_3 + s_1 - s_2 \right]$$

$$\left. + \; D^2 \left[p_1/10 + p_2/21 + 4C_{44}^w b_w + q_1/21 + 2q_3/5 + s_1/5 + s_2/4 \right] \right\} \tag{112}$$

in which:

$$p_1 = \mp N^{ow} b_w^4/(3r_{ave}) \qquad ; \qquad p_2 = n^2 N^{ow} b_w^5/5$$

$$q_1 = b_w^5 (C_{55}^w n^4 + 4C_{66}^w n^2/r_{ave}^2)/5 \quad ; \quad s_1 = 4C_{45} n^2 b_w^3/3$$

$$q_2 = \mp b_w^4 n^2 (C_{55}^w + 4C_{66}^w)/r_{ave} \qquad ; \qquad s_2 = \pm 4C_{45} b_w^2/r_{ave} \tag{113}$$

$$q_3 = b_w^3 (C_{55}^w/r_{ave}^2 + 4C_{66}^w n^2)/3$$

where r_{ave} is the average radius of the web,

$$r_{ave} = (R + R_f)/2 \qquad (114)$$

and n is given by:

$$n = \bar{n}\pi/\ell \qquad (115)$$

In Eq. (113 a, b) the stress resultant in the web N^{ow} is comprised of two parts, a fixed part and a part to be multiplied by the eigenvalue,

$$N^{ow} = N^{ow}_{PRE} + \lambda N^{ow}_e \qquad (116)$$

Analysis of the Flange: From the assumption that $e_{sy} = 0$ [Eq. (103)] along with Eq. (109c) and Eq. (102), an expression for v can be derived. From Eq. (102), it is known that:

$$u^f = \mp Cb_w^{\ 2}\sin(\bar{n}\pi y/\ell) \quad . \qquad (117)$$

Integration of Eq. (109c) yields:

$$v^f = \pm (n\pi/\ell)Cb_w^{\ 2}s \, \cos(\bar{n}\pi y/\ell) + v^w(x = b_w) \qquad (118)$$

in which $v^w(x = b_w)$ signifies the value of v^w evaluated at $x = b_w$ (see Fig. 18). The last term on the right-hand-side of Eq. (118) drops out when integration over y is performed.

With use of Eqs. (107), (109), (117), and (118), one obtains for the strain energy of the flange (including the effect of the prebuckling stress

381

resultant in the y-direction N^{of}):

$$U^f = \frac{\ell}{4}\left\{ C^2\left[f_1c_2 + f_2c_3 + f_3c_4{}^2 + c_5(2 + e)^2 \right]\right.$$

$$+ CD\left[-f_1c_6 - f_3(2e)c_4 - 2(2 + e)c_5 + c_7 \right]$$

$$\left. + D^2\left[f_1c_1 + f_3e^2 + c_5 - .4c_7 \right]\right\}$$

(119)

in which:

$$f_1 = \sum_{\substack{i=1 \\ i\neq web}}^{N} N_i^{of}b_i{}^3/3 \qquad\qquad f_2 = \sum_{\substack{i=1 \\ i\neq web}}^{N} N_i^{of}b_i$$

$$f_3 = \sum_{\substack{i=1 \\ i\neq web}}^{N} C_{22}^i b_i{}^3/3 \qquad\qquad f_4 = \sum_{\substack{i=1 \\ i\neq web}}^{N} C_{55}^i b_i{}^3/3$$

(120)

$$f_5 = \sum_{\substack{i=1 \\ i\neq web}}^{N} C_{66}^i b_i$$

and:

$$c_1 = n^2 b_w{}^2 \qquad\qquad\qquad c_2 = c_1(2 + e)^2$$

$$c_3 = c_1 b_w{}^2 \mp 4b_w{}^3/(3R_f) \qquad c_4 = c_1 + 2e$$

(121)

$$c_5 = c_1(n^2 f_4 + 4f_5) \qquad\qquad c_6 = c_1 2(2 + e)$$

$$c_7 = \pm f_2 b_w{}^3/(3R_f)$$

382

with:

$$e = \mp b_w / R_f \qquad (122)$$

where R_f is the radius of the very short cylindrical shell that represents the flange.

As in the case of the web, the prebuckling stress resultant in the flange is comprised of two parts, a fixed part and a part to be multiplied by the eigenvalue:

$$N_i^{of} = N_{iPRE}^{of} + \lambda N_{ie}^{of} \qquad (123)$$

Lowest Eigenvalue: The lowest eigenvalue λ for stiffener rolling instability without participation of the skin can be obtained by insertion of the right-hand-side of Eq. (116) into Eq. (112), insertion of the right-hand-side of Eq. (123) into Eq. (119), minimization of the sum of U^{web} and U^f with respect to the coefficients C and D, and determination of the lowest root of the quadratic equation in λ that represents the vanishing of the determinant of the coefficient matrix of the two simultaneous homogeneous equations in C and D.

Axisymmetric Rolling Instability: Axisymmetric rolling instability of rings can be calculated by the setting of n in Eqs. (113) and (121) equal to zero. It is interesting to note that rolling instability is possible in the case of internally pressurized cylindrical shells with external rings even though the stresses everywhere in the shell, web, and flange are tensile.

REFERENCES

[1] L. H. Donnell, "A new theory for the buckling of a thin cylinder under axial compression and bending", Trans. ASME Vol. 56, No. 11, 795-806 (1934)

[2] G. N. Vanderplaats, "CONMIN--a FORTRAN program for con- strained function minimization," NASA TM X-62-282, version updated in March 1975, Ames Research Center, Moffett Field, CA (Aug. 1973)

[3] G. N. Vanderplaats and F. Moses, " Structural optimization by methods of feasible directions," Computers and Structures, Vol. 3, pp 739-755 (1973)

[4] Zoutendijk, G., Methods of feasible directions, Elsevier Publishing Company, Amsterdam, 1960.

[5] V. B. Venkayya, "Structural optimization: a review and some recommendations," International Journal of Numerical Methods in Engineering, Vol. 13, pp 203-228 (1978)

[5a] E. J. Catchpole, "The optimum design of compression surfaces having unflanged integral stiffeners," Journal of Royal

Aerospace Society, Vol. 58, p 765 (1954)

[6] L. A. Schmit, T. P. Kicher, and W. M. Morrow, "Structural synthesis capability for integrally stiffened waffle plates," AIAA J, Vol. 1, 2820-2836 (1963)

[7] W. M. Morrow and L. A. Schmit, "Structural synthesis of a stiffened cylinder," NASA CR-1217 (Dec 1968)

[8] T. P. Kicher, "Structural synthesis of integrally stiffened cylinders," Journal of Spacecraft and Rockets, Vol. 5, pp 62-67 (1968)

[9] L. D. Hofmeister and L. P. Felton, "Synthesis of waffle plates with multiple rib sizes," AIAA J, Vol. 5, pp 2193-2199, (1969)

[10] R. J. Bronowicki, R. B. Nelson, L. P. Felton, and L. A. Schmit, Jr., "Optimization of ring stiffened cylindrical shells," AAIA J, Vol. 13, pp 1319-1325 (1975)

[11] R. F. Crawford and A. B. Burns, "Minimum weight potentials for stiffened plates and shells," AAIA J, Vol. 1, pp 879-886 (1963)

[12] A. B. Burns and J. Skogh, "Combined loads minimum weight analysis of stiffened plates and shells," Journal of

Spacecraft and Rockets, Vol. 3, pp 235-240 (1966)

[13] A. B. Burns and B. O. Almroth, "Structural optimization of axially compressed cylinders, considering ring-stringer eccentricity effects," Journal of Spacecraft and Rockets, Vol. 3, pp 1263-1268 (1966)

[14] A. B. Burns, "Optimum stiffened cylinders for combined axial compression and internal or external pressure," Journal of Spacecraft and Rockets, Vol. 5, pp 690-699 (1968)

[15] B. O. Almroth, A. B. Burns, and E. V. Pittner, "Design criteria for axially loaded cylindrical shells," Journal of Spacecraft and Rockets, Vol. 7, pp 714-720 (1970)

[16] G. A. Cohen, "Optimum design of truss-core sandwich cylinders under axial compression," AAIA J, Vol. 1, pp 1626-1630 (1963)

[17] G. Gerard, "Optimum structural design concepts for aerospace vehicles," Journal of Spacecraft and Rockets, Vol. 3, pp 5-18 (1966)

[18] W. J. Stroud and N. P. Sykes, "Minimum-weight stiffened shells with slight meridional curvature designed to support axial compressive loads," AIAA J, Vol. 7, pp 1599-1601 (1969)

[19] C. Lakshmikantham and G. Gerard, "Minimum weight design of stiffened cylinders," Aerospace Quarterly, pp 49-68 (Feb 1970)

[20] D. L. Block, "Minimum weight design of axially compressed ring and stringer stiffened cylindrical shells," NASA CR-1766 (Jul 1971)

[21] J. L. Shideler, M. S. Anderson, and L. R. Jackson, "Optimum mass- strength analysis for orthotropic ring-stiffened cylinders under axial compression," NASA TND-6772 (Jul 1972)

[22] A. V. Viswanathan and M. Tamekuni, "Elastic buckling analysis for composite stiffened panels and other structures subjected to biaxial inplane loads," NASA CR-2216 (Mar 1973)

[23] W. H. Wittrick and F. W. Williams, "Buckling and vibration of anisotropic or isotropic plate assemblies under combined loadings," International Journal of Mechanical Sciences, Vol. 16, pp 209-239 (1974)

[24] J. G. Williams and M. Stein, "Buckling behavior and structural efficiency of open-section stiffened composite compression panels," AIAA J, Vol. 14, pp 1618-1626 (1976)

[25] B. L. Agarwal and L. H. Sobel, "Weight comparisons of optimized stiffened, unstiffened, and sandwich cylindrical shells," Journal of Aircraft, Vol. 14, pp 1000-1008 (1977)

[26] M. S. Anderson and W. J. Stroud, "General panel sizing computer code and its application to composite structural panels," AIAA J, Vol. 17, pp 892-897 (1979)

[27] G. G. Weaver and J. R. Vinson, "Minimum-mass designs of stiffened graphite/polymide compression panels, in Modern Developments in Composite Materials and Structures," ASME 1979 Winter Annual Meeting, pp 215-233 (Dec 1979)

[28] L. A. McCullers, "Automated design of advanced composite structures," ASME AMD, Vol. 7, pp 119-130 (Nov 1974)

[29] T. Hayashi, "Optimization for elastic buckling strength of fiber- reinforced composite structures--columns, plates and cylinders," Proc. Mech. Behavior of Materials, Soc. of Material Science, Japan, pp 399-405 (Aug 1974)

[29a] M. Aswani, "Optimization of stiffened cylinder subject to destabilizing load," Proc. Advances in Civil Eng. Through Engrg. Mech., ASCE, New York, pp 456-459 (May 1977)

[30] N. S. Khot, "Computer Program (OPTCOMP) for optimization of composite structures for minimum weight design,"

[31] J. H. Starnes, Jr., and R. T. Haftka, "Preliminary design of composite wings for buckling strength, and displacement constraints," Journal of Aircraft, Vol. 16, pp 564-570 (1979)

[32] G. J. Simitses and V. Ungbhakorn, "Weight optimization of stiffened cylinders under axial compression," Comp _ Struct, Vol. 5, pp 305-314 (1975)

[33] G. J. Simitses and V. Ungbhakorn, "Minimum-weight design of stiffened cylinders under axial compression," AIAA J, Vol. 13, pp 750-755 (1975)

[34] I. Sheinman and G. J. Simitses, "Buckling analysis of geometrically imperfect stiffened cylinders under axial compression," AIAA J, Vol. 15, pp 374-382 (1977)

[35] G. J. Simitses and J. Giri, "Optimum weight design of stiffened cylinders subjected to torsion combined with axial compression with and without lateral pressure," Comp _ Struct, Vol. 8, pp 19-30 (1978)

[36] G. J. Simitses and I. Sheinman, "Optimization of geometrically imperfect stiffened cylindrical shells under axial compression," Comp. _ Struct, Vol. 9, pp 377-381 (1978)

[37] M. Isreb, "Wing center section optimization with stress and local instability constraints," Comp Struct, Vol. 10, pp 855-861 (1979)

[38] A. Libai, "Optimization of a stiffened square panel subjected to compressive edge loads," AIAA J, Vol. 17, pp 1379-1380 (1979)

[39] J. B. Caldwell and A. D. Hewitt, "Cost effective design of ship structures," Met Constr, Vol. 8, pp 64-67 (1976)

[40] J. G. Pulos and M. A. Krenzke, "Recent developments in pressure hull structures and materials for hydrospace vehicles," David Taylor Model Basin Rep. 2137, Washington, D. C. (Dec 1965)

[41] M. E. Lunchick, "Plastic axisymmetric buckling of ring- stiffened cylindrical shells fabricated from strain-hardening materials and subjected to external hydrostatic pressure," David Taylor Model Basin rep. 1393, Washington, D. C. (Jan 1961)

[42] M. E. Lunchick, "Plastic general-instability pressure of submarine pressure hulls," ASME Paper 62-WA-262 (1962)

[43] L. Boichot and T. E. Reynolds, "Inelastic buckling tests of ring-stiffened cylinders under hydrostatic pressure,"

David Taylor Model Basin rep. 1992, Washington, D. C. (May
1965)

[44] J. R. Renzi, "Optimization of orthotropic,
non-linear, ring- stiffened cylindrical shells under external
hydrostatic pressure as applied to mmc materials," Naval Surface
Weapons Center, NSWC TR 79-305, (Sept. 1979). See also, J. R.
Renzi, "Axisymmetric stresses and deflections, inter-bay buck-
ling, and general instability of orthotropic, hybrid,
ring-stiffened cylindrical shells under external hydrostatic
pressure, Naval Surface Weapons Center, NSWC TR-80-269, April
1981

[45] M. Pappas and C. L. Amba-Rao, "A direct search al-
gorithm for automated optimum structural design," AIAA J, Vol.
9, pp 387-393 (1971)

[46] M. Pappas and A. Allentuch, "Structural synthesis of
frame reinforced submersible circular cylindrical hulls,"
Computers and Structures, Vol. 4, pp 253- 280 (1974)

[47] M. Pappas and A. Allentuch, "Pressure hull optimiza-
tion using general instability equation admitting more than one
longitudinal buckling half-wave," Journal of Ship Research, Vol.
19, pp 18-22 (1975)

[48] B. O. Almroth, P. Stern, and D. Bushnell, "Imper-

fection   sensitivity   of   optimized   structural   panels,"
AFWAL-TR-80-3182, March 1981

[49] S. N. Patnaik and M. Maiti, "Optimum design of
stiffened structures with constraint on the frequency in the
presence of initial stresses," Computer Meth. Appl. Mech.
Eng., Vol. 7, pp 303-322 (1976)

[50] M. W. Dobbs and R. B. Nelson, "Minimum weight de-
sign of stiffened panels with fracture constraints," Computers
and Structures, Vol. 8, pp 753-759 (1978)

[51] R. M. Jones and J. C. F. Hennemann, "Effect of
prebuckling deformations on buckling of laminated composite cir-
cular cylindrical shells," AIAA J, Vol. 18, pp 110-115 (1980),
see also, Proc. AIAA/ASME 19th SDM conf, pp 370-379 (1978)

[52] B. O. Almroth, "Influence of edge conditions on the
stability of axially compressed cylindrical shells," AIAA J,
Vol. 4, pp 134-140 (1966)

[53] J. W. Hutchinson, "Plastic buckling," Advances in
Applied Mechanics, Vol. 14, edited by C. S. Yih, Academic
Press, Inc., pp 69-144 (1974)

[54] R. M. Jones, Mechanics of Composite Materials,
McGraw-Hill Book Co., New York (1975)

[55] M. Baruch and J. Singer, "Effect of eccentricity of stiffeners on the general instability of stiffened cylindrical shells under hydrostatic pressure," J. Mech. Eng. Sci., Vol. 5, No. 1, pp 23-27 (1963)

[56] D. O. Brush and B. O. Almroth, Buckling of Bars, Plates and Shells, McGraw-Hill Book Co., New York (1975)

[57] M. Booton and R. C. Tennyson, "Buckling of imperfect anisotropic circular cylinders under combined loading," AIAA J, Vol. 17, No. 3, pp 278-287 (Mar 1979)

[58] D. Bushnell, "Stress, stability, and vibration of complex, branched shells of revolution," Computers and Structures, Vol. 4, pp. 399-435 (1974)

[59] D. Bushnell, BOSOR5--program for buckling of elastic-plastic complex shells of revolution including large deflections and creep," Computers and Structures, Vol. 6, pp. 221-239 (1976)

[60] G. J. Simitses and I. Sheinman, "Accurate prediction of critical conditions for shear-loaded panels," AIAA J, Vol. 14, No. 5, pp 683-685 (May 1976)

[61] G. J. Simitses, J. Giri and I. Sheinman, "Minimum weight design of stiffened cylinders and cylindrical panels

under combined loads," AFOSR TR-76-0930, Georgia Institute of Technology, Atlanta, GA (1976)

[62] B. O. Almroth and F. A. Brogan, "The STAGS computer code," NASA Langley Research Center, NASA CR 2950, Feb. 1978

[63] G. J. Simitses and J. Giri, "Minimum weight design of stiffened cylinders subjected to pure torsion," Computers and Structures, Vol. 7, pp667-677 (1977)

[64] D. Bushnell, "Evaluation of various analytical models for buckling and vibration of stiffened shells," AIAA Journal, Vol. 11, No. 9, pp. 1283-1291 (1973)

[65] D. W. Block, M. F. Card, and M. F. Mikulas,Jr., "Buckling of eccentrically stiffened orthotropic cylinders," NASA Langley Research Center, NASA TND 2960, Aug. 1965

[66] T. P. Kicher and C-H Wu, "Buckling of anisotropic circular cylindrical shells," AFML Rept. TR-71-260, Nov. 1971

[67] D. Bushnell, "Buckling of shells--pitfall for designers," to appear in AIAA Journal, September or October, 1981

[68] D. Bushnell, "Buckling of elastic-plastic shells of revolution with discrete elastic-plastic ring stiffeners,"

International Journal of Solids and Structures, Vol. 12, pp. 51-66 (1976)

[69] C. D. Miller, Code Case N-284, ASME Boiler and Pressure Vessel Code, 1980 Code Cases, Nuclear Components, American Society of Mechanical Engineers, New York, pp. 633-656 (July 1980)

Table 1 Buckling Modes Included in the PANDA Analysis

TYPE OF BUCKLING	MODEL USED FOR ESTIMATE
1. General instability Fig. 1; Eq. (57)	Buckling of skin and stiffeners together with smeared rings and stringers. Panel is simply supported along the edges $x = y = 0$, $x = a$, and $y = b$.
2. Local instability Fig. 3; Eq. (57)	Buckling of skin between adjacent rings and adjacent stringers. Portion of panel bounded by adjacent stiffeners is simply supported. Stiffeners take their share of the load in the prebuckling analysis but are disregarded in the stability analysis.
3. Panel instability (a) between rings with smeared stringers Fig. 1; Eq. (57)	Buckling of skin and stringers between adjacent rings. Portion of panel bounded by adjacent rings is simply supported. Stringers are smeared. Simple support conditions imposed at $y = 0$ and at $y = b$. Rings take their share of the load in the prebuckling analysis, but are disregarded in the stability analysis.
(b) between stringers with smeared rings Fig. 1; Eq. (57)	Buckling of skin and rings between adjacent stringers. Portion of panel between adjacent stringers is simply supported. Rings are smeared. Simple support conditions imposed at $x = 0$ and at $x = a$. Stringers take their share of the load in the prebuckling analysis, but are disregarded in the stability analysis.
4. Local crippling of stiffener segments (a) "internal" segments Figs. 4,5; Eq. (71)	Individual stiffener segment buckles as if it were a long flat strip simply supported along its two long edges. Loading is compression along the stiffener axis. Curvature of ring segments ignored.
(b) "end" segments Figs. 4,5; Eq. (79)	Individual stiffener segment buckles as if it were a long flat strip simply supported along the long edge at which it is attached to its neighboring segment or to the panel skin and free along the opposite edge. Loading is compression along the stiffener axis. Number of half waves along the stiffener axis is the same as that of the part of the structure to which the "end" is attached. Curvature of ring segments ignored.

Table 1 (continued)

TYPE OF BUCKLING	MODEL USED FOR ESTIMATE
5. Local rolling with skin buckling between stiffeners Fig. 6a; Eqs, (57,96,97)	Same as "Local instability" except that strain energy in stiffeners and work done by prebuckling compression in stiffeners are included in the buckling formula. Stiffener cross sections do not deform as stiffeners twist about their lines of attachment to the panel skin.
6. Rolling instability (a) with smeared stringers Fig. 6a; Eqs. (57,96,97)	Same as "Panel instability", Type (a), except that strain energy of rings and work done by prebuckling compression along the ring centroidal axis are included in the buckling formula. Ring cross section does not deform as ring twists about its line of attachment to the panel skin.
(b) with smeared rings Fig. 6a; Eqs. (57,96,97)	Same as "Panel instability", Type (b), except that strain energy of stringers and work done by prebuckling compression along the stringer centroidal axis are included in the buckling formula. Stringer cross section does not deform as it twists about its line of attachment to the panel skin.
7. Rolling of stringers, no buckling of skin Fig. 6b; Eqs. (112,119)	Stringer web cross section deforms but the flange cross section does not. Buckling mode has waves along stiffener axis.
8. Rolling of rings, no buckling of skin Fig. 6b; Eqs. (112,119)	Ring web cross section deforms but the flange cross section does not. Buckling mode has waves along the ring axis. This mode is sometimes called "frame tripping" by those interested in submarine structures.
9. Axisymmetric rolling of rings, no skin buckling Fig. 6c; Eqs. (112,119)	Same as "Rolling of rings", except that the buckling mode has zero waves around the circumference of the panel.
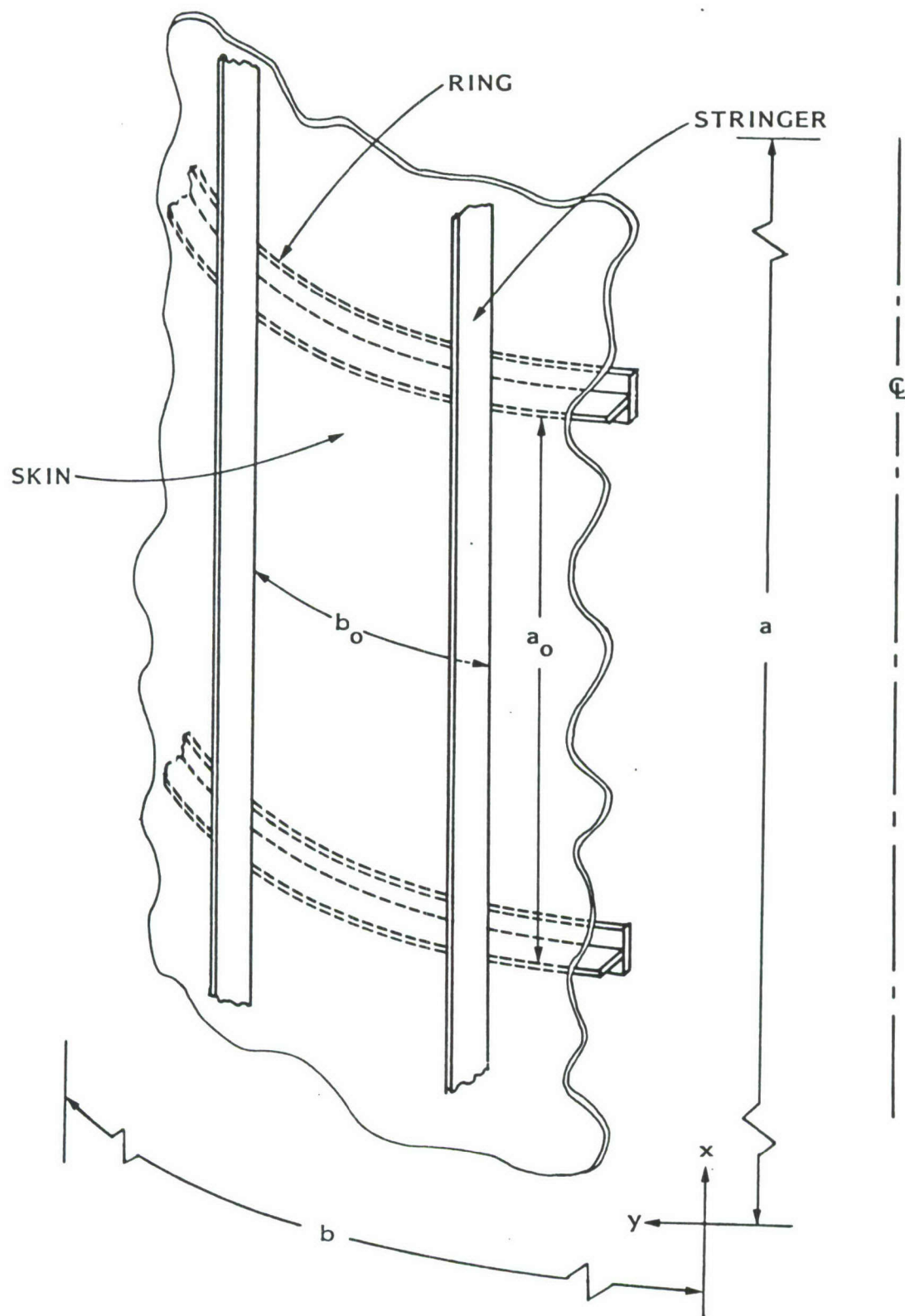
Figure 1.   Stiffened cylindrical panel with overall dimensions (a,b),
             ring spacing (a$_o$), and stringer spacing (b$_e$)
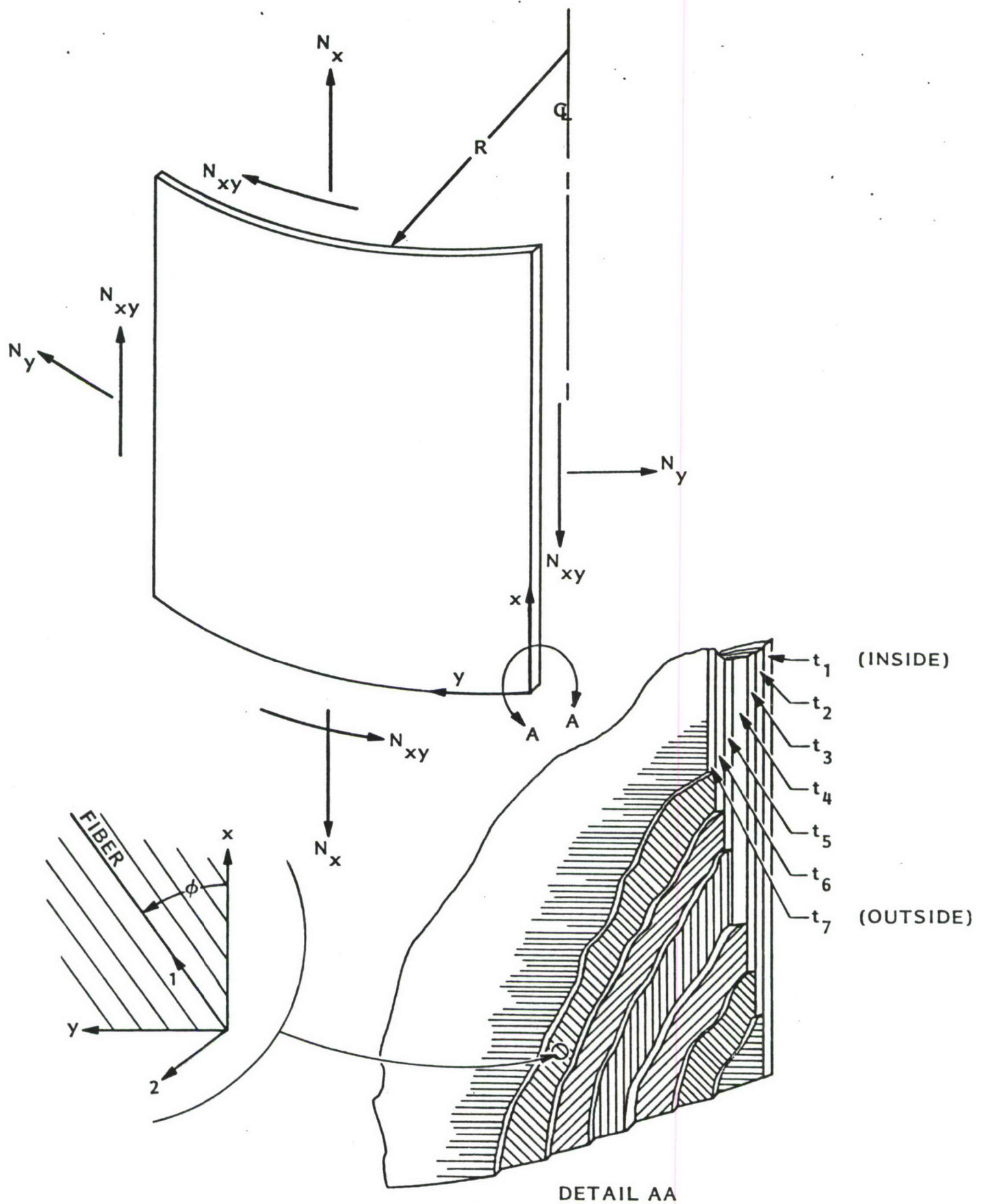
Figure 2.   Coordinates, loading, and wall construction

399
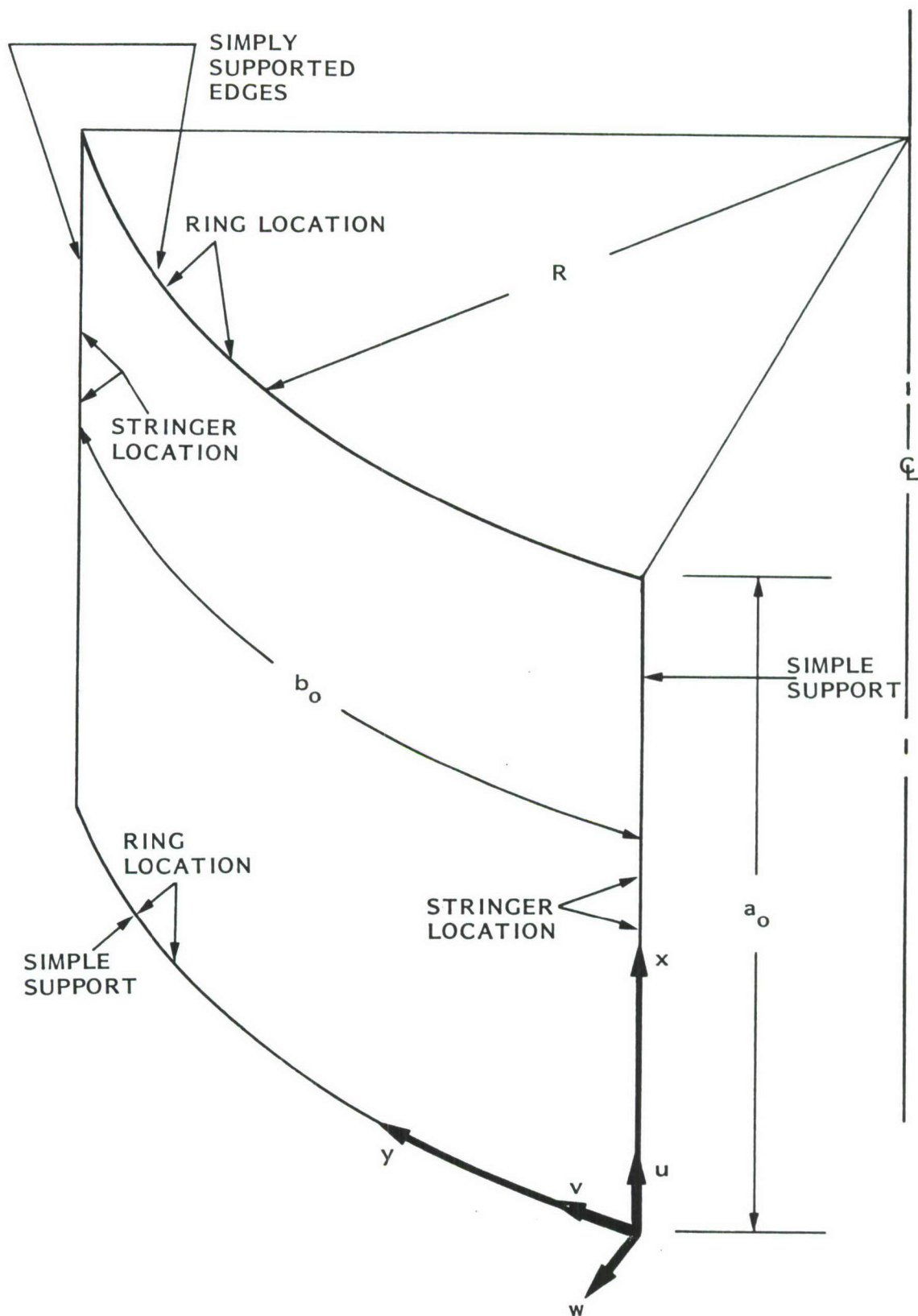
Figure 3.   Cylindrical panel between stiffeners: displacement
components u, v, w, and coordinates for local skin buckling
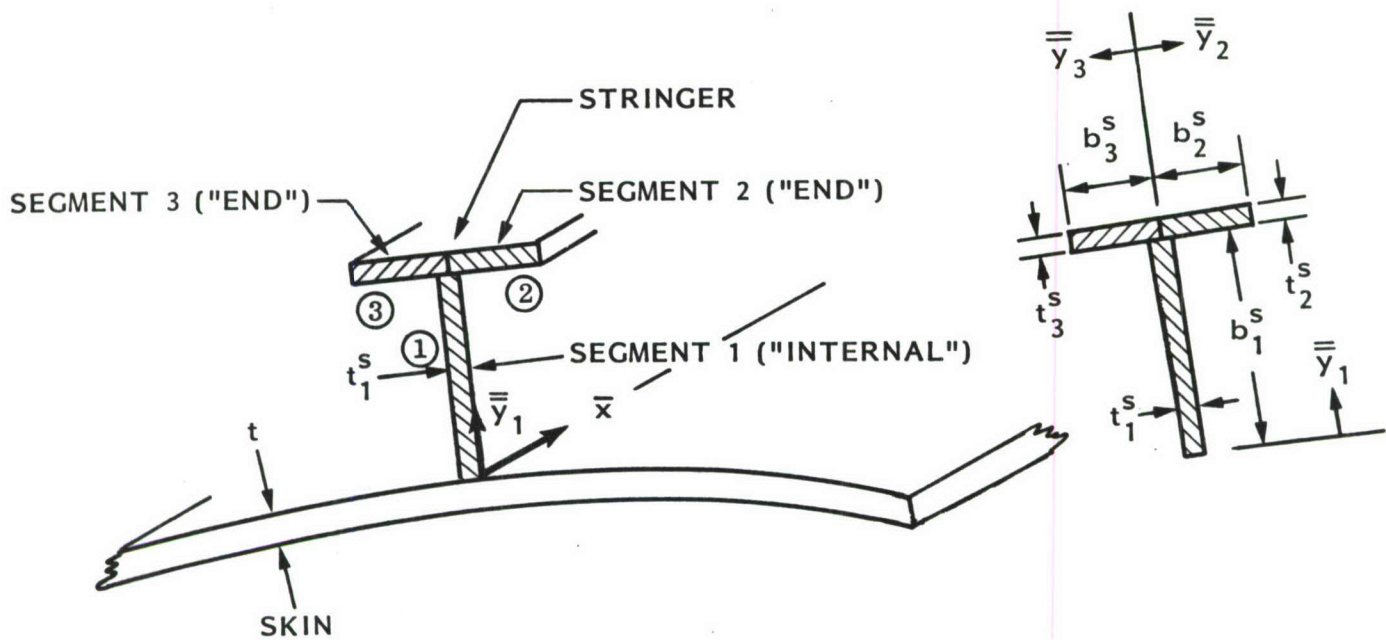
(a) A "T"-shaped stiffener must be treated as if it consists of three segments, one "internal" and two "ends".
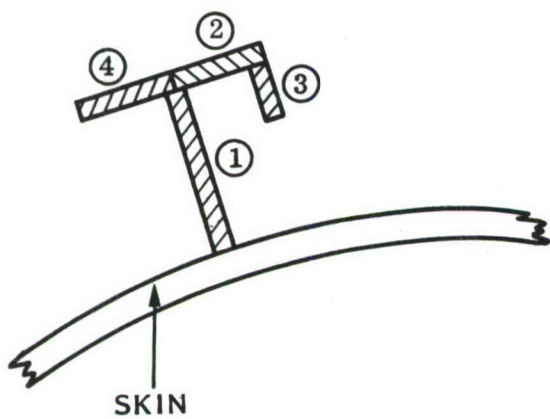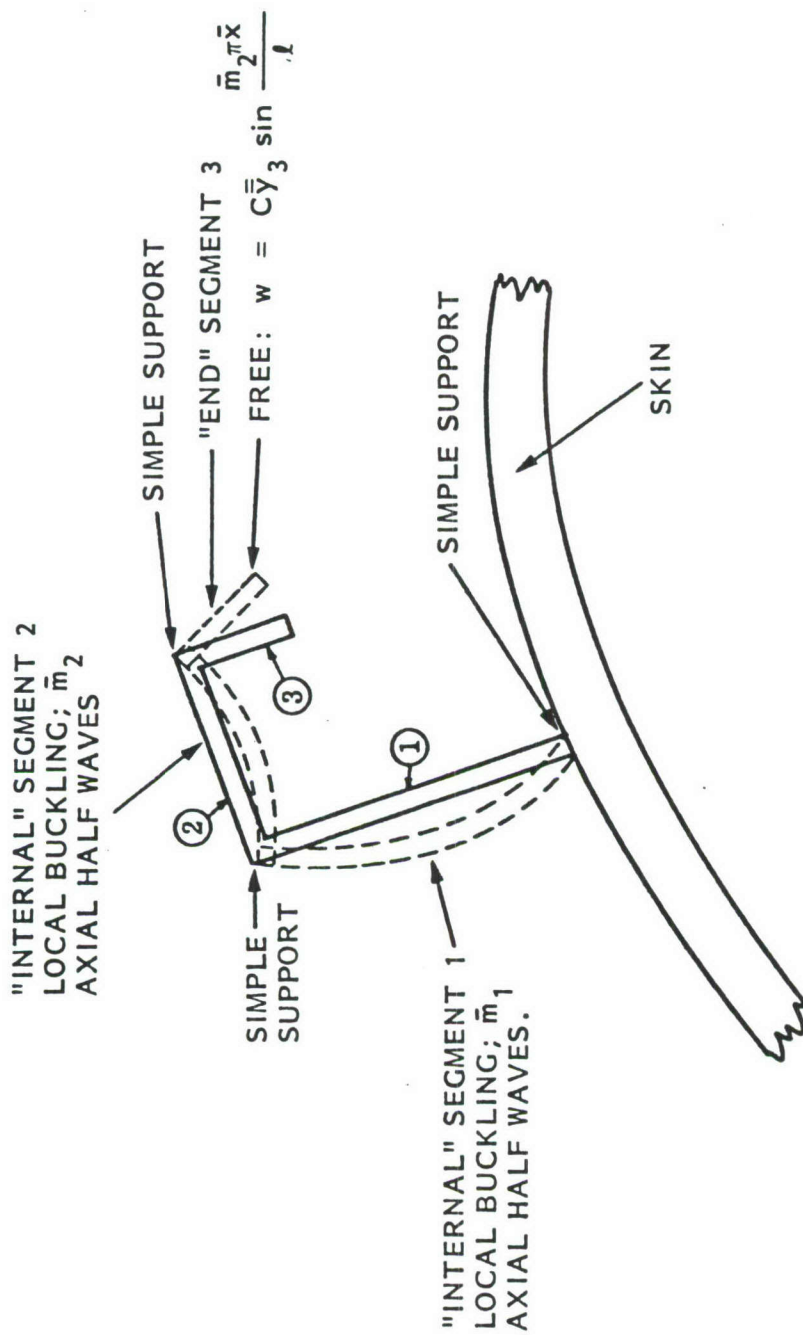

(b) Segments ① and ② are "internal"; ③ and ④ are "ends".
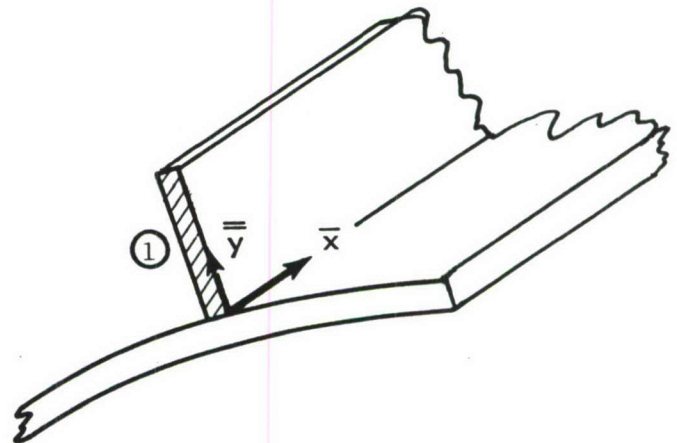
(c) Segment ① is an "end".

Figure 4. Stiffener nomenclature and local coordinates $\bar{x}$ and $\bar{\bar{y}}_i$

401

"INTERNAL" SEGMENT 2
LOCAL BUCKLING; $\bar{m}_2$
AXIAL HALF WAVES

SIMPLE SUPPORT

"END" SEGMENT 3

FREE: $w = C\bar{\bar{y}}_3 \sin \dfrac{\bar{m}_2 \pi \bar{x}}{\ell}$

SIMPLE SUPPORT

SKIN

SIMPLE
SUPPORT

"INTERNAL" SEGMENT 1
LOCAL BUCKLING; $\bar{m}_1$
AXIAL HALF WAVES.

EACH "INTERNAL" STIFFENER SEGMENT IS ASSUMED
TO BE SIMPLY-SUPPORTED AT ITS EDGES. THE "END"
SEGMENT REMAINS STRAIGHT IN THE WIDTH COORDIN-
ATE AS SEGMENTS 2 AND 3 BUCKLE TOGETHER WITH
THE SAME $\bar{m} = \bar{m}_2$.

Figure 5.   Local buckling of stiffener segments

402

(a) Rolling with skin participation.

(b) No skin participation, wavy buckles.

(c) No skin participation; axisymmetric sidesway.
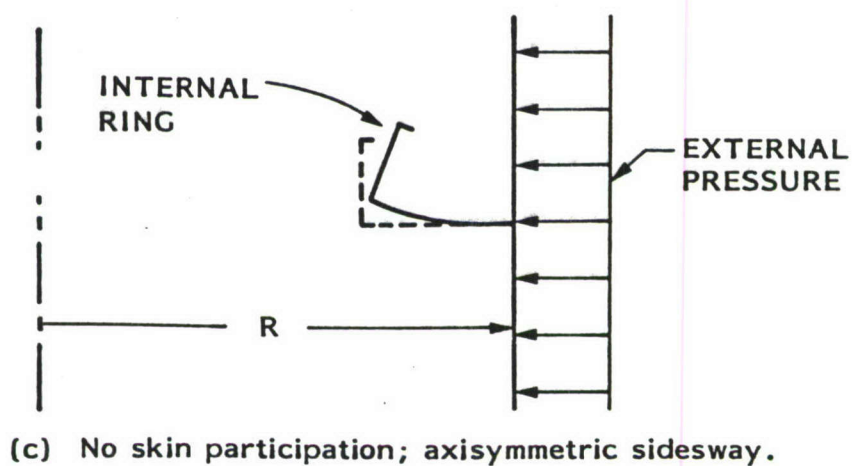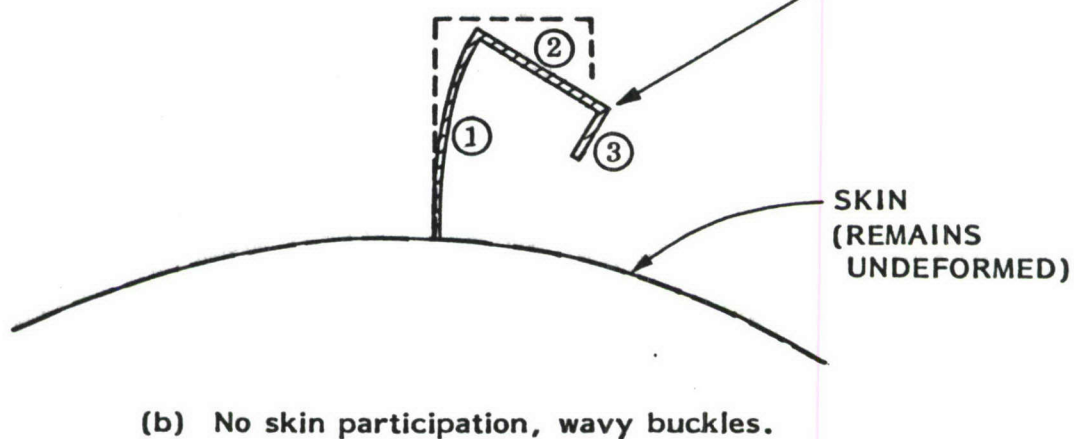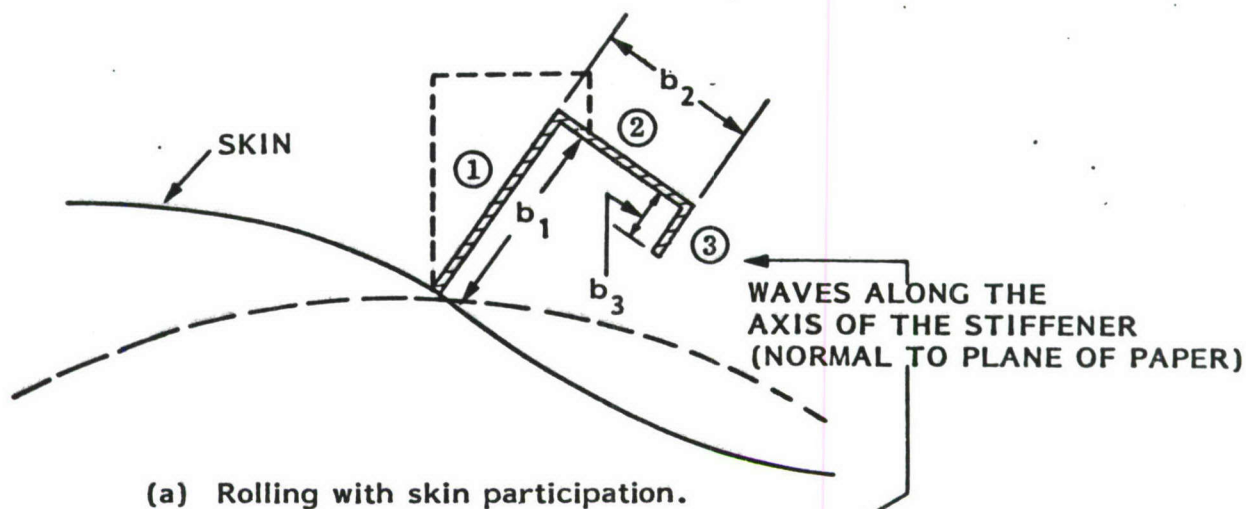
Figure 6.   Three types of "rolling" of a stiffener

403
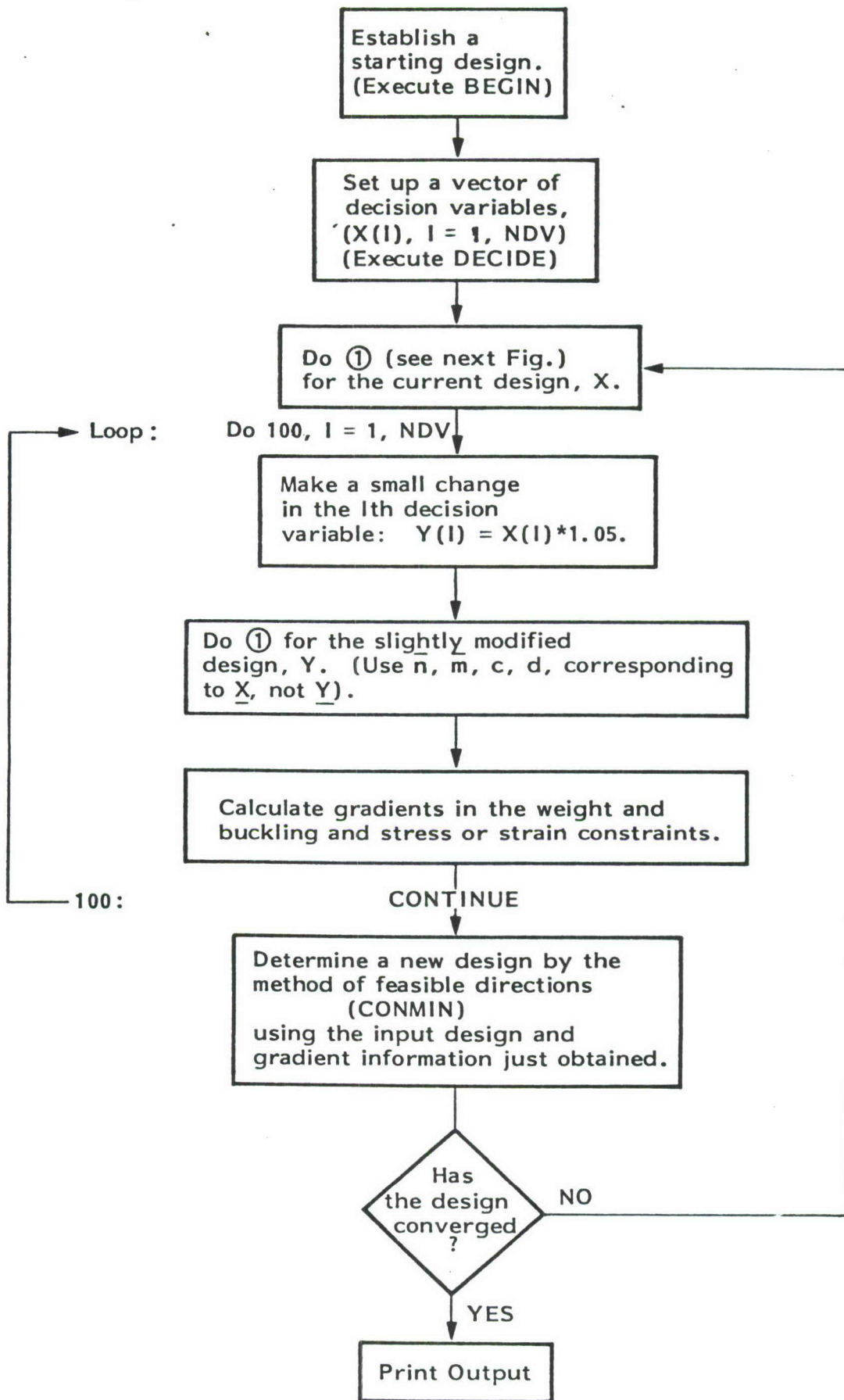
Figure 7.   Flow of calculations in PANDA for an optimization analysis.

1. Calculate prebuckling state, Eqs. (4-41),

2. Calculate constitutive coefficients governing stability for all possible modes of buckling, Eqs. (37-45).

3. Calculate buckling load factors for all possible modes of buckling, Eqs. (46-123):

    (1) shell general, semi-general, and local, Eqs. (46-65).

    (2) stiffener segment crippling, Eqs. (66-80).

    (3) rolling with skin participation, Eqs. (81-97).

    (4) stiffener rolling without skin participation, Eqs. (98-123).

4. Set up a vector of constraint conditions which include:

    (1) buckling margins for all possible modes of buckling.

    (2) stress or strain margins in each shell wall layer and and in each stiffener segment.

5. Calculate weight.

① ≡

Figure 8.   The structural analysis module of PANDA. This module is embedded in the executable processor PANCON.
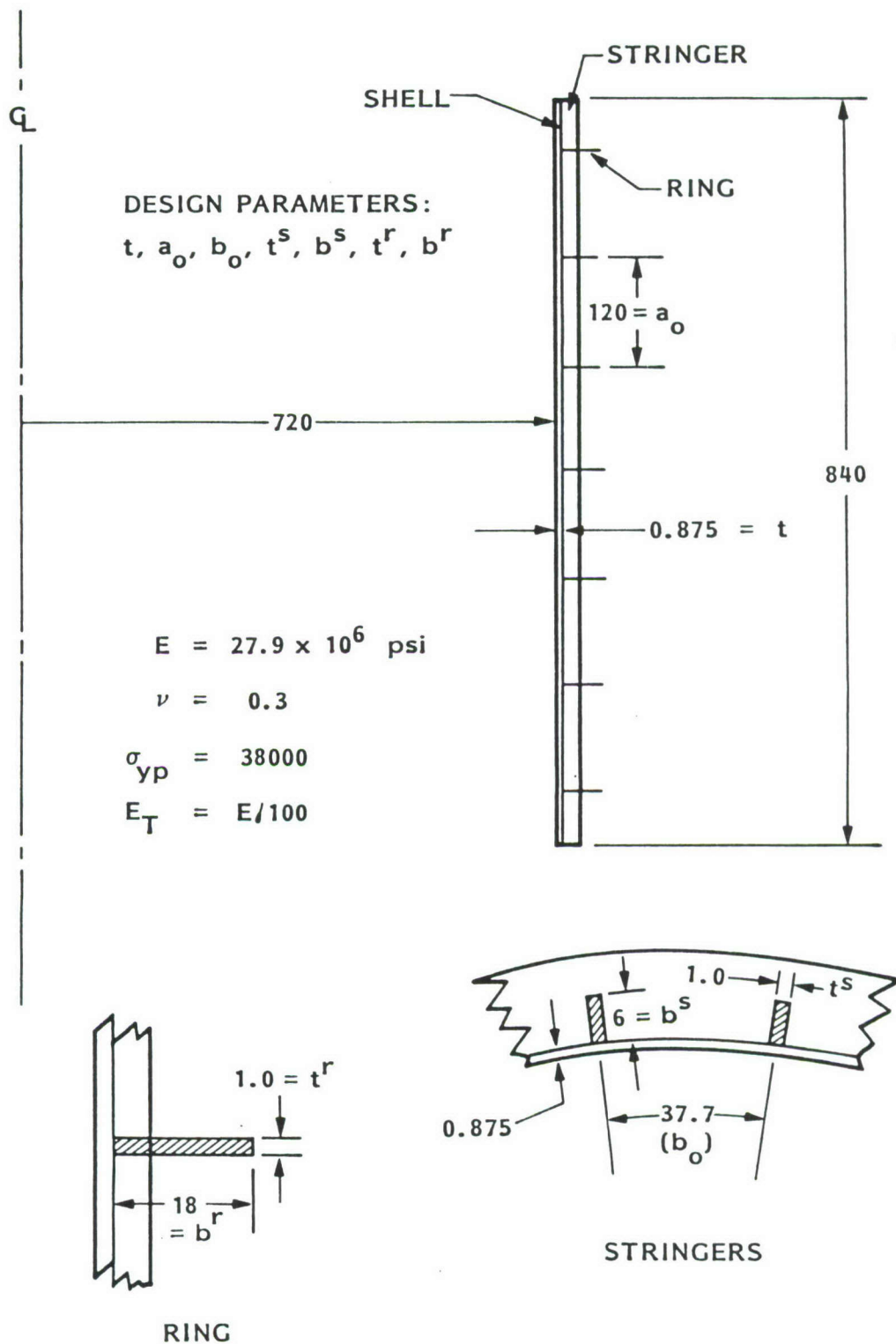
Figure 9. Ring and stringer stiffened cylindrical shell with dimensions typical of a large containment vessel for a nuclear reactor. Buckling load factors from PANDA are listed in Tables 10 and 11.

406

Figure 10.   Composite cylindrical shell (180 deg.) with dimensions
              and loading typical of the fuselage of an air transport.
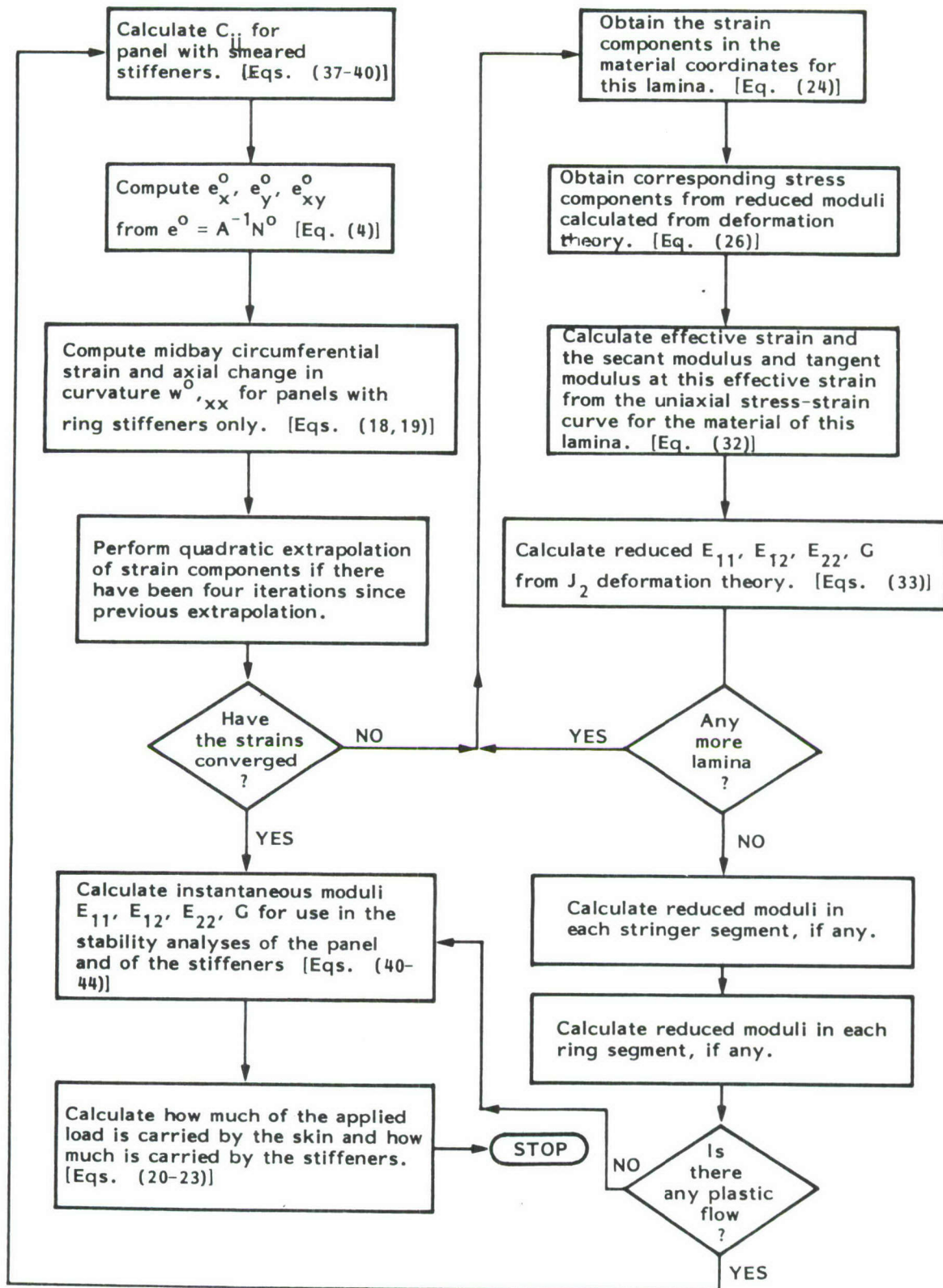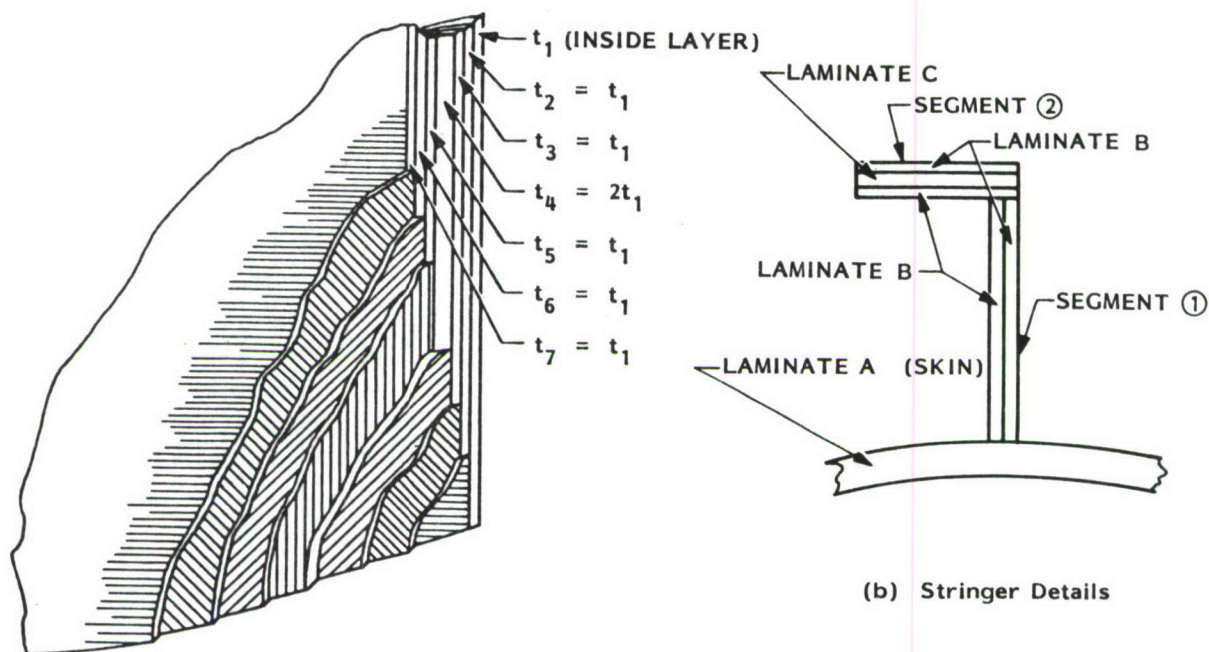   Results from PANDA for this case are listed in the appendix.

407

Figure 12.   Flow of calculations for elastic-plastic prebuckling analysis in PANDA

(a) Detail AA
(Panel Skin = Laminate A)

(b) Stringer Details

STACKING SEQUENCE OF THE PANEL SKIN (LAMINATE A):

$$\phi = (90, \pm45, 0_2, \mp45, 90)$$

STACKING SEQUENCE OF LAMINATE B OF STRINGER:

$$\phi = (90, \pm45, 0)_s$$

STACKING SEQUENCE OF LAMINATE C OF STRINGER

$$\phi = (0_{20})$$

MATERIAL PROPERTIES OF EACH LAMINA OF THE LAMINATES A, B, AND C:

MODULI AND POISSON'S
RATIO IN (1,2) DIRECTIONS:

MAXIMUM STRAINS IN
(1,2) DIRECTIONS:

$E_1 = 23 \times 10^6$ psi

$E_2 = 1.7 \times 10^6$ psi

$G = 0.94 \times 10^6$ psi

$\nu = 0.304$

$\rho' = 0.056$ lb/in.^{3}

e_1 (TENSION) $= .00565$

e_1 (COMPRESSION) $= .00452$

e_2 (TENSION) $= .0032$

e_2 (COMPRESSION) $= .0125$

e_{12} (IN-PLANE SHEAR) $= .0125$

Figure 11.   Wall construction and material properties for the
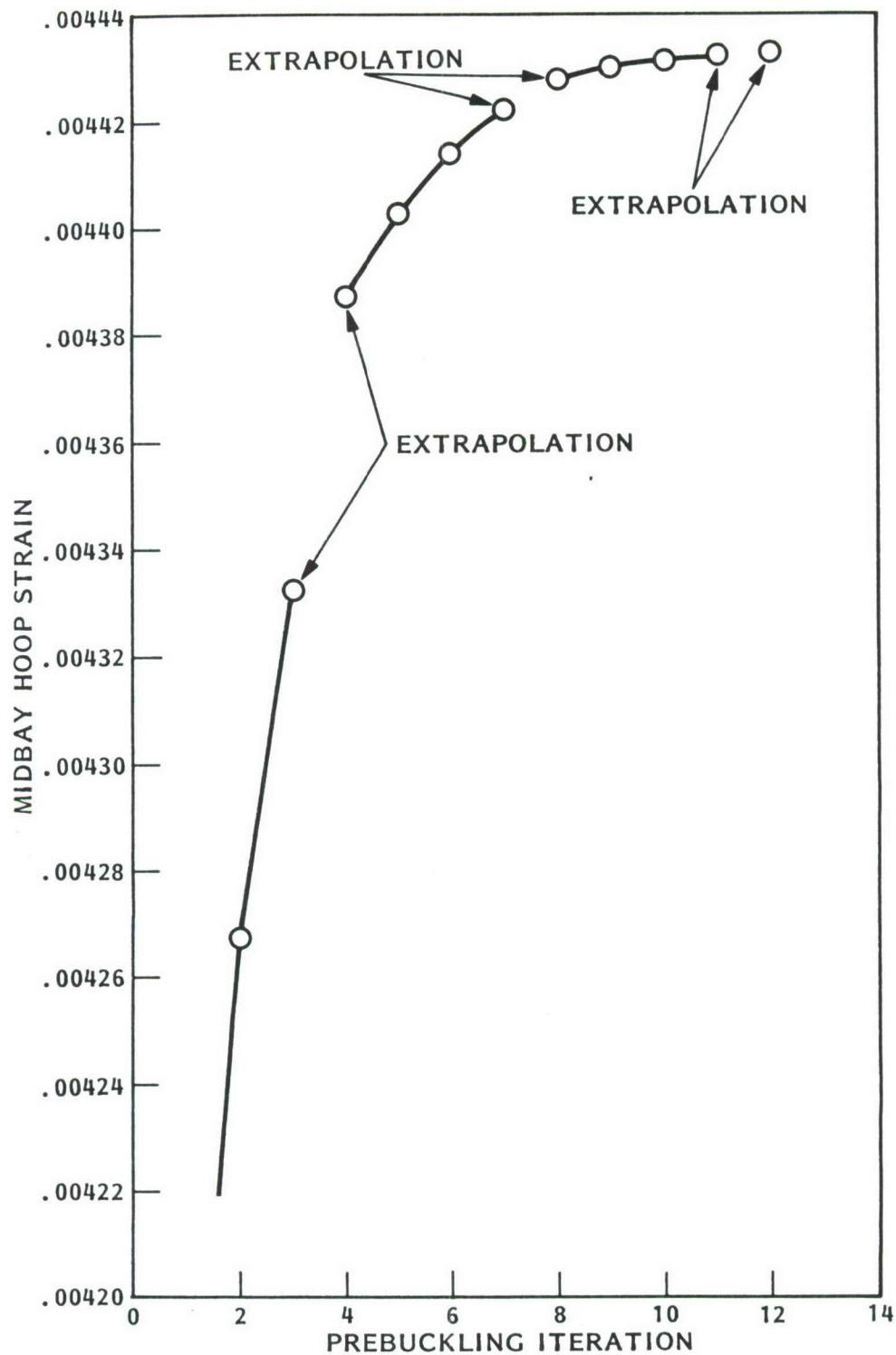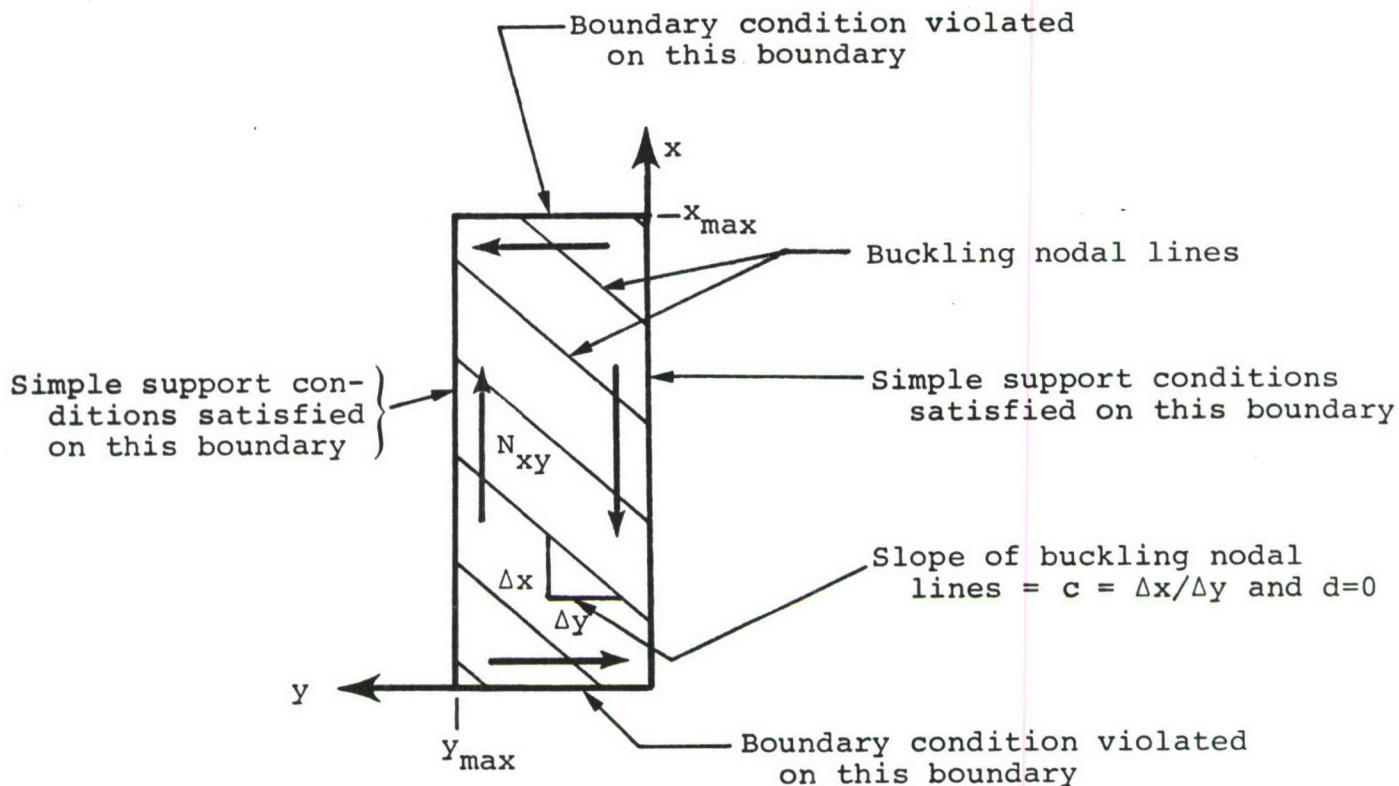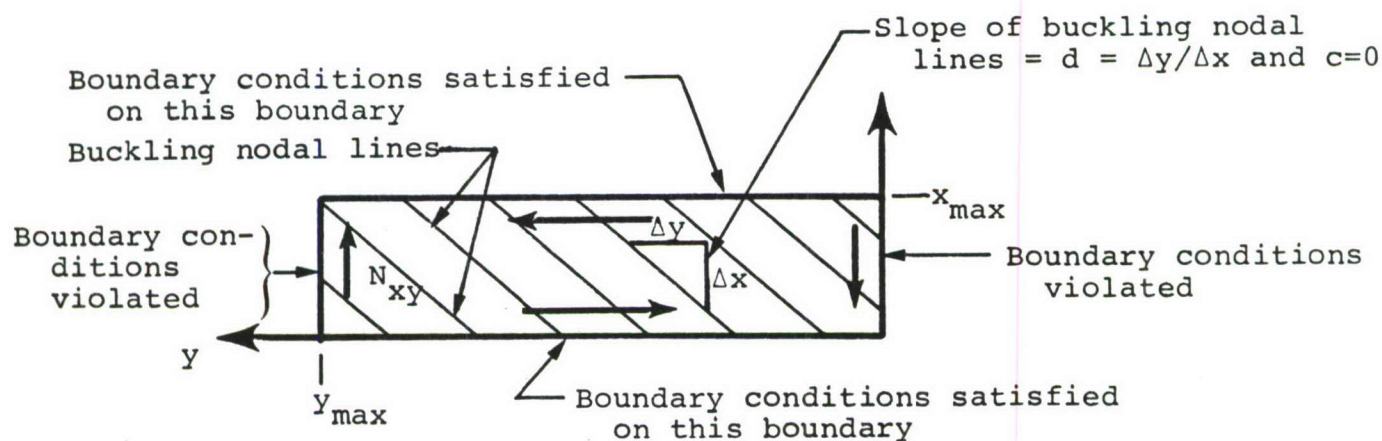stiffened cylindrical shell shown in Fig. 10

Figure 13.   Typical convergence of the prebuckling strain in the plastic region. This case corresponds to a hydrostatically compressed, ring stiffened cylindrical shell.

410

(a) Assumed buckling mode for panel that is
"long" in the x-direction: $w = C \sin(ny)\sin[m(x-cy)]$

(b) Assumed buckling mode for panel that is "long"
in the y-direction: $w = \sin[n(y-dx)]\sin(mx)$

Figure 14. Assumed buckling modal patterns with shear
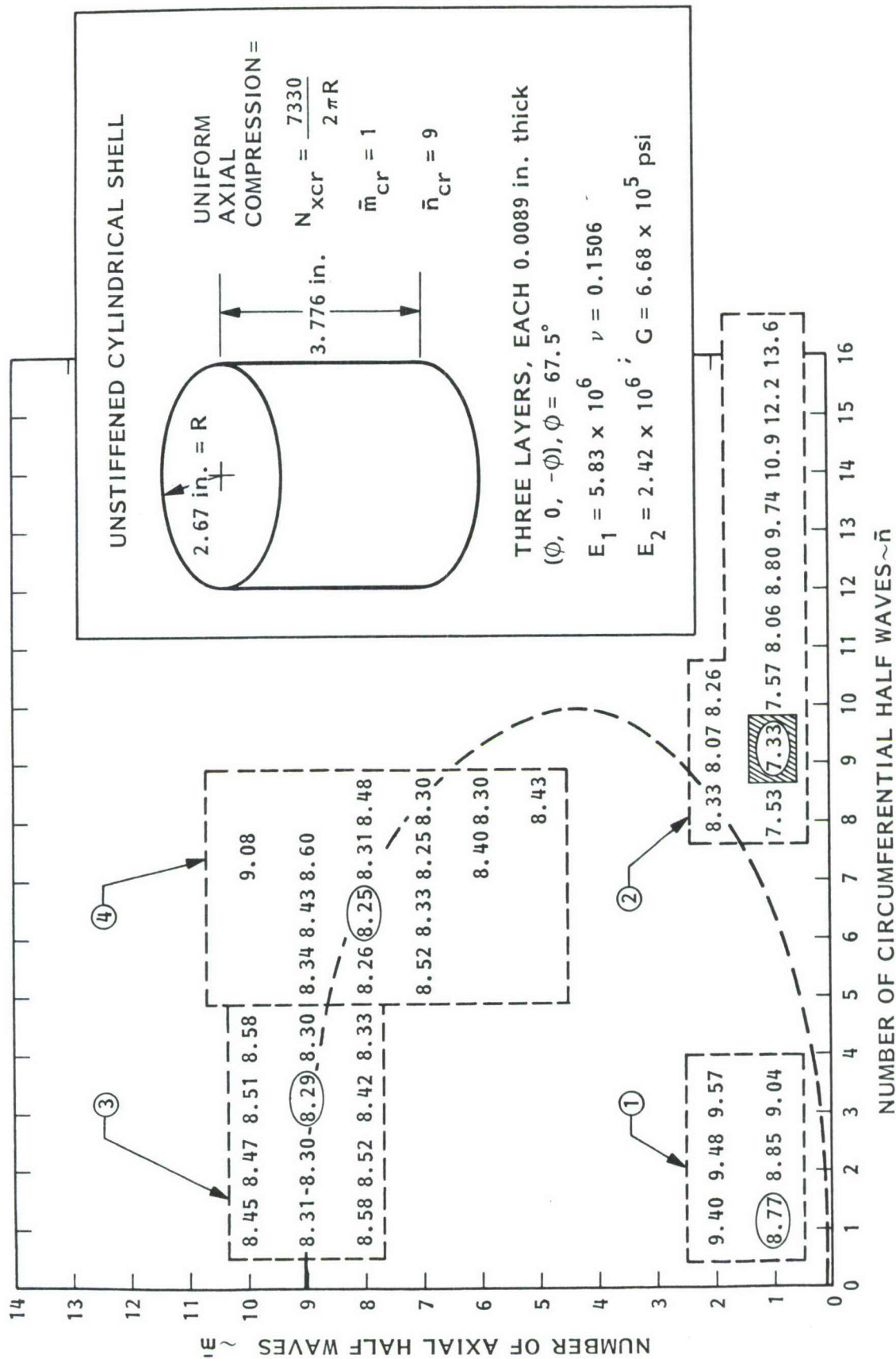and/or unbalanced laminates present

411

Figure 15. Buckling loads for axially compressed composite cylindrical shell with an unbalanced laminate $(\phi, 0, -\phi)$: Four regions, ①②③④ are shown in which minimum critical load multipliers λ_{cr} ($\bar{m}_{cr}$, $\bar{n}_{cr}$) are sought. The numbers in the dashed boxes are buckling loads in thousands of pounds for each ($\bar{m}$, $\bar{n}$) combination investigated by PANDA.
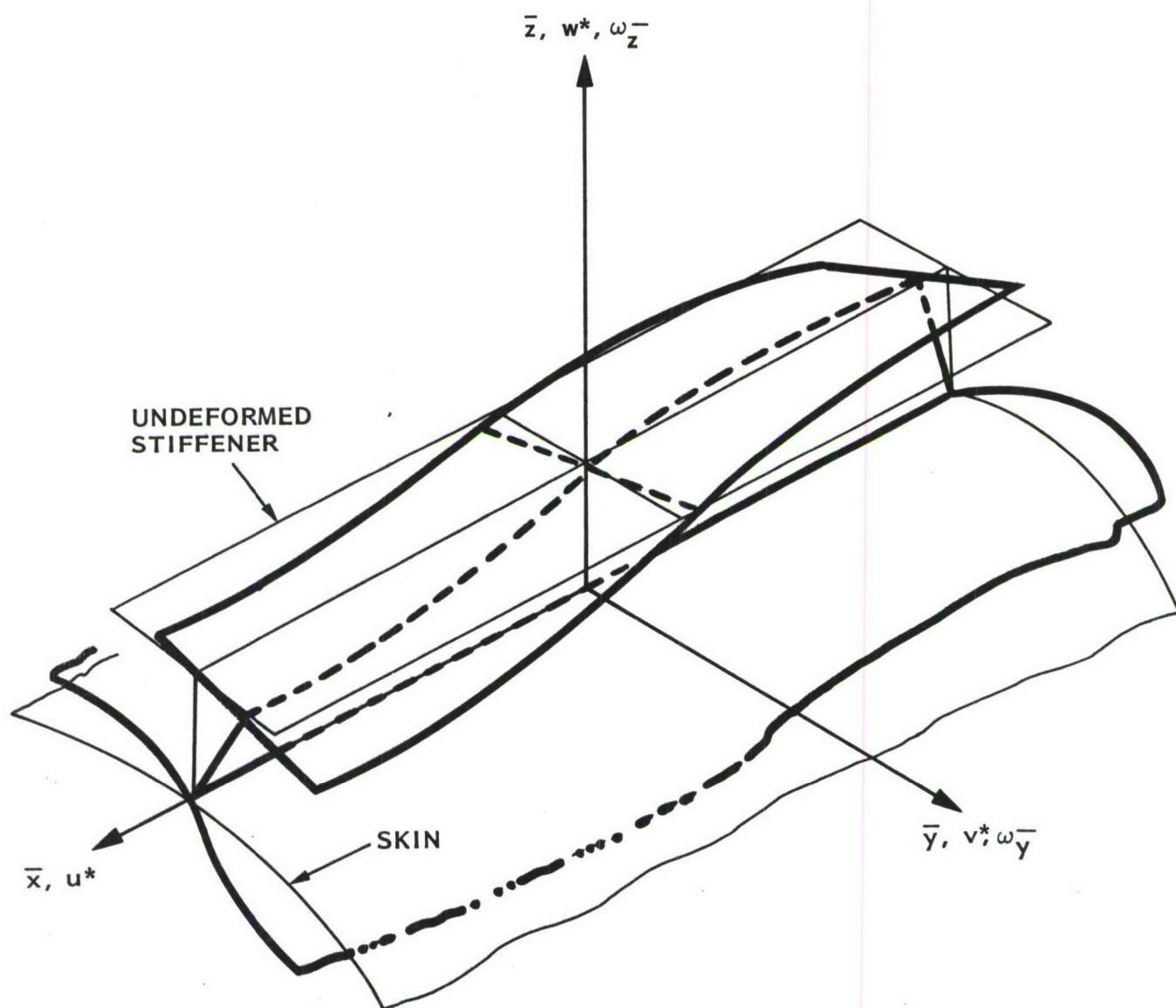
Figure 16.   Rolling of stiffener as in Figure 6a

ASSUMED DISPLACEMENT FIELD DUE TO
ROLLING IN THE MODE SHOWN IN FIG. 6(a):

$$u^* = -m \gamma \bar{y} \bar{z} \cos m \bar{x}$$

$$v^* = \gamma \bar{z} \sin m \bar{x}$$

$$w^* = -\gamma \bar{y} \sin m \bar{x}$$
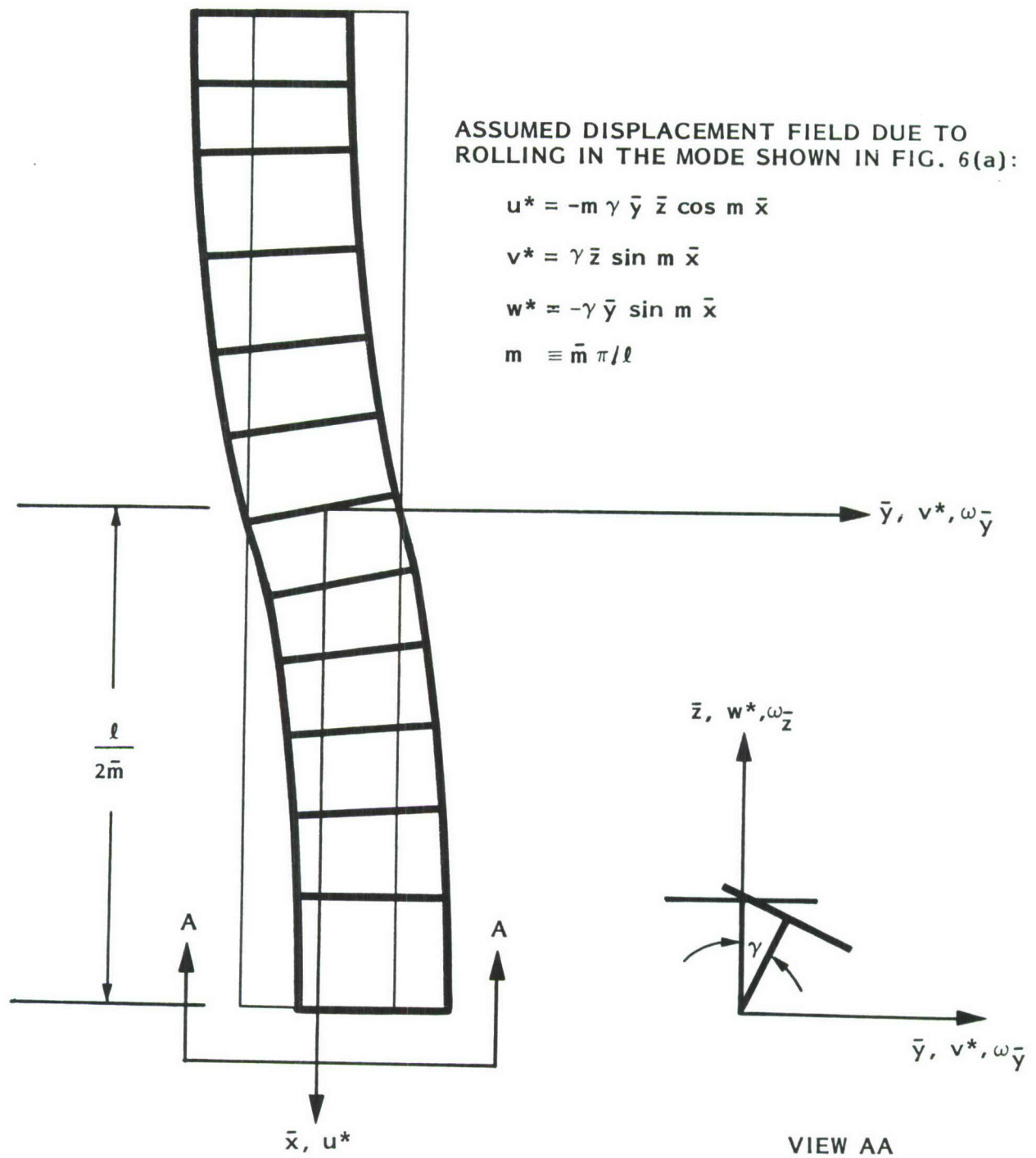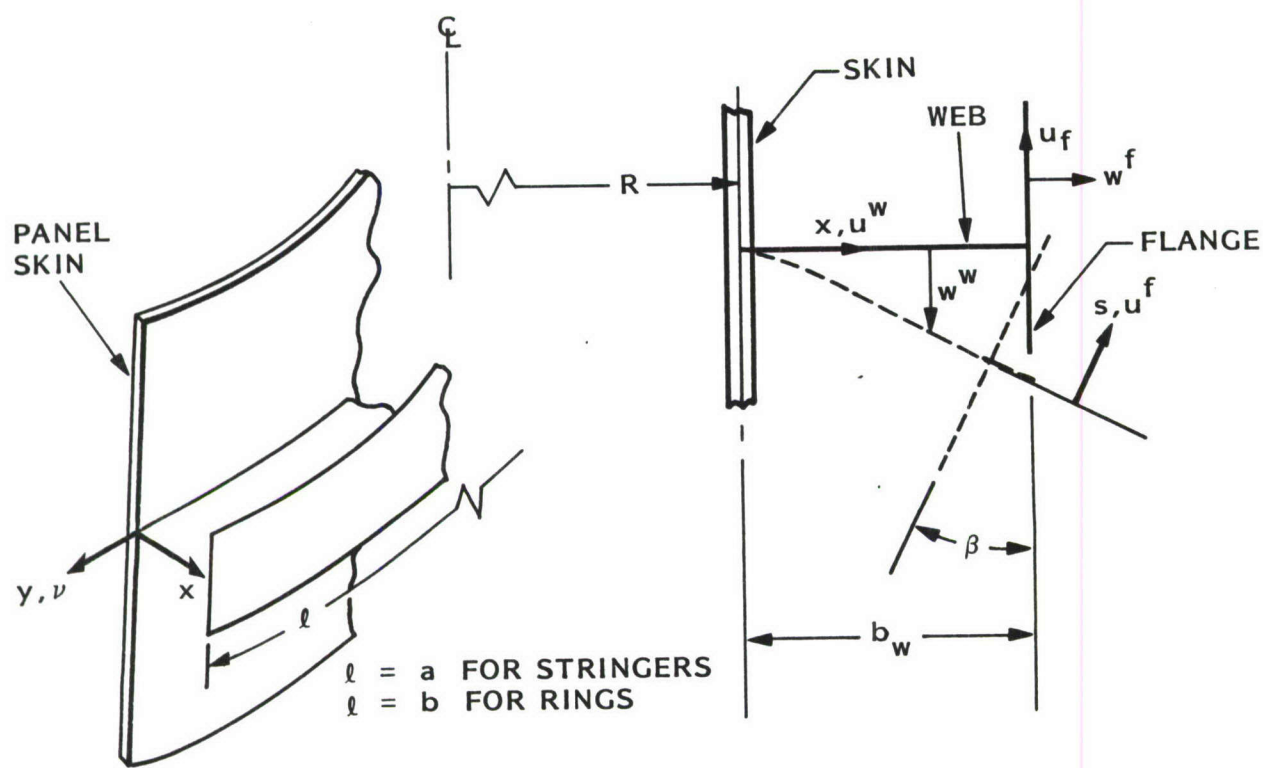
$$m \equiv \bar{m} \pi / \ell$$

Figure 17.   In-plane bending of a flange induced by rolling of the stiffener in the mode shown in Figure 6a

414

(a) T-Shaped Stiffener on Cylindrical Panel

ℓ = a FOR STRINGERS
ℓ = b FOR RINGS

(b) External Stiffener

(c) Internal Stiffener

ASSUMED DISPLACEMENT FUNCTION:

(1) $w^w = \left[Cx^2 + Dx^2 (1 - x/b_w) \right] \sin \dfrac{\bar{n}\pi y}{\ell}$

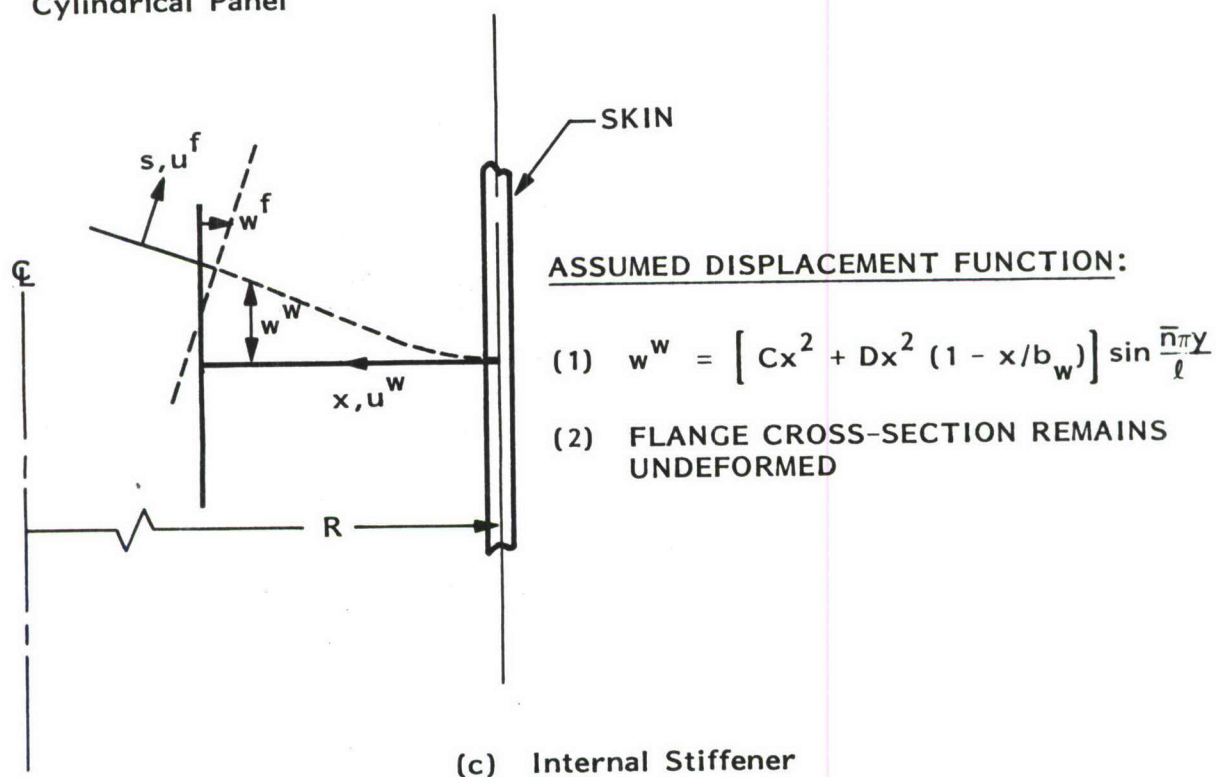(2) FLANGE CROSS-SECTION REMAINS UNDEFORMED

Figure 18. Stiffener coordinates and displacement components for rolling analysis of the types shown in Figs 6b and 6c (no participation of the panel skin)

415